SAPIENZA
UNIVERSITÀ DI ROMA

Faculty of Mathematical, Physical and Natural Sciences

Department of Chemistry

Evaluation of Sustainable-By-Design Organic Materials as Potential Tools for the Development of Green Smart Sensors

PhD in Chemical Sciences

XXXVIII Cycle

PhD Candidate:

Federica Palmeri

Supervisors: Dr. Gloria Zanotti, Dr. Mattea Carmen Castrovilli

Cosupervisor: Prof. Antonella Cartoni

Table of contents

Summary

Growing environmental concerns and the need for responsible technological innovation have increasingly encouraged the scientific community to adopt more sustainable research practices.

In this context, Green Chemistry has emerged as a fundamental framework for designing chemical processes and materials that minimize environmental impact and risks to human health. Its principles promote a holistic perspective that considers the entire lifecycle of materials and technologies, from synthesis and device fabrication to operational use and end-of-life management.

Simultaneously, industrial growth, urbanization, and intensive agriculture have led to widespread contamination of air, water, and soil with pollutants such as heavy metals, pesticides, and pharmaceuticals, highlighting the need for reliable monitoring technologies.

Sensing technologies play a key role in addressing these challenges, enabling rapid, sensitive, and often real-time detection of environmental contaminants. However, conventional sensors frequently rely on hazardous reagents, energy-intensive fabrication, and scarce raw materials, while their limited reusability contributes to electronic and chemical waste. This underscores the urgent need for sustainable approaches that combine high analytical performance with environmental responsibility.

This doctoral thesis focuses on the development of eco-friendly functional organic materials and their integration into sensing devices with reduced environmental footprint. The work was conducted within the Rome Technopole - Innovation Ecosystem, funded by the Italian PNRR and supported by Next Generation EU, under Spoke 1.

A central aspect of the thesis concerns the sustainable synthesis of phthalocyanines, a class of macrocyclic organic compounds widely investigated for their optical, electronic, and sensing properties. Greener synthetic strategies were designed and developed with the aim

of reducing environmental impact through the implementation of pot-economical reactions and the use of environmentally friendly reaction media, to minimize waste and energy demand while preserving functional performance.

These materials were subsequently employed to develop green sensing platforms through eco-friendly fabrication strategies. Drop-casting was used as effective and low-impact technique for immobilizing functional materials onto sensor surfaces. The resulting sensing platform was investigated through parameters such as sensitivity, stability, and reusability, and evaluated for its overall environmental footprint.

During a research period at the University of Edinburgh, the thesis extended these concepts to optical sensor development and sustainable catalysis. A sustainable optical sensor for metal detection was designed and investigated to work both in solution and on paper-based test strips, emphasizing environmentally friendly materials and fabrication processes and enabling simple sensing tools for environmental monitoring.

In addition, the sustainability framework was further extended to the field of sustainable catalysis, exploring catalytic systems based on Earth-abundant elements as alternatives to traditional and toxic precious-metal catalysts for the efficient C–H borylation of arene substrates.

Overall, this research contributes to advancing sustainable materials science and sensor technology by combining green synthesis, environmentally responsible sensor fabrication, and performance evaluation. Furthermore, the results obtained during this work contributed to the development of the European project “Mainstream,” which was successfully funded in Italy with a budget of €241,250 through the National Research Council of Italy (CNR), involving partners from Italy, Spain, Sweden, Germany, and Turkey.

Chapter 1. Introduction

1.1. Green Chemistry

One of the most pressing challenges of the twenty-first century is represented by environmental pollution, with severe implications for ecosystems, human health, and global sustainability.[1] The term Green Chemistry, introduced in the 1990s by researchers at the U.S. Environmental Protection Agency (EPA), contributed to establishing a clear conceptual framework for the growing interest in environmentally sustainable chemical processes and products.

As formalized by the Twelve Principles proposed by Paul T. Anastas and John C. Warner in 1998, Green Chemistry provides a comprehensive framework for minimizing the environmental impact of chemical processes through waste prevention, safer solvents and reagents, energy efficiency, catalysis, and the use of renewable feedstocks (**Figure 1**).[2]

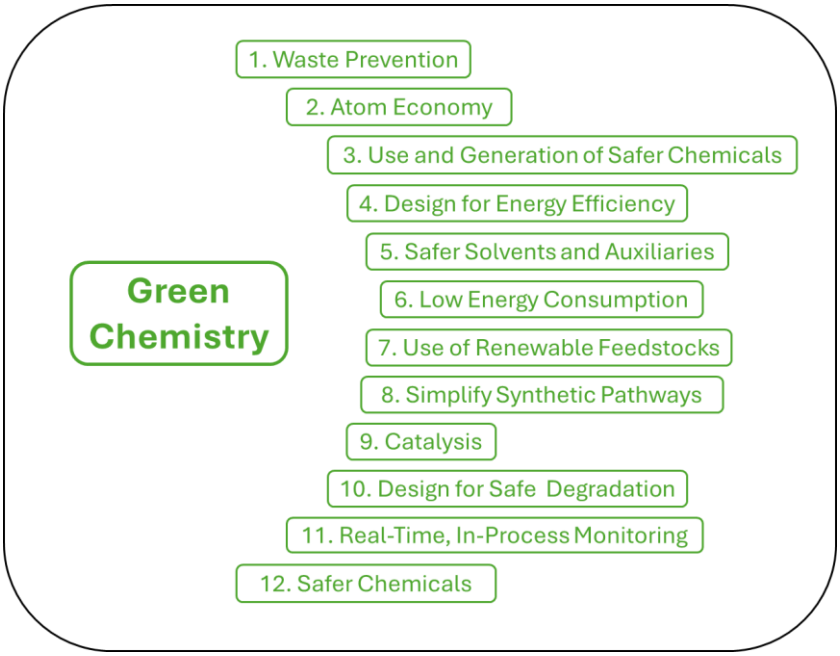

Figure 1. The Twelve Principles of Green Chemistry.

Green Chemistry is now universally recognized as the guiding paradigm for chemists, encompassing education, research, and industrial implementation across the entire chemical supply chain.[3] Often referred to as a "Hyppocratic Oath" for chemists (*First, do not harm*) it emphasizes the ethical responsibility to minimize risks to human health and the environment. This philosophy extends beyond reaction optimization to the entire lifecycle of materials and devices, from material selection and synthesis to device fabrication, operational lifetime, and end-of-life management, encouraging researchers to adopt a holistic, sustainability-driven perspective.

The continuous growth of industrial production, urban expansion, intensive agricultural practices, and the widespread use of synthetic chemicals have led to the accumulation of a wide range of contaminants in air, water, and soil. These pollutants include volatile organic compounds, heavy metals, pesticides, pharmaceuticals, and emerging contaminants, many of which persist in the environment and bioaccumulate along the food chain.[4–6] Furthermore, alterations in temperature and climatic conditions may create favorable environments for pathogen proliferation, potentially leading to the emergence of novel infectious diseases or the resurgence of previously controlled ones.[7,8]

In response to this scenario, the scientific community has devoted increasing attention to the development of technologies aimed at pollution mitigation, early disease detection and diagnosis, and environmental monitoring, to address public health and environmental challenges.

Accurate detection and quantification of pollutants are essential for understanding contamination pathways, assessing environmental risk, enforcing regulatory standards, and supporting remediation strategies. As a result, sensing technologies have invaded our everyday life and become a cornerstone of environmental science, enabling real-time, on-site, and highly sensitive analysis of chemical species in complex matrices.[9,10]

However, despite their undeniable importance in environmental monitoring and protection, many conventional sensing devices suffer from intrinsic sustainability limitations that are frequently overlooked during their design and development. The

fabrication of sensors often relies on multi-step procedures that conflict with several core principles of green chemistry, particularly those related to waste prevention, energy consumption, and the use of safer solvents and auxiliaries.[11] Hazardous organic solvents, toxic reagents and materials are commonly employed, resulting in significant waste generation and increased environmental and safety concerns. Moreover, many sensing platforms depend on critical or scarce raw materials, such as noble metals and rare elements, whose extraction and refinement are associated with intensive production processes, ecosystem degradation, and geopolitical constraints.[12] Furthermore, sensor manufacturing frequently involves high energy demanding techniques, including high-temperature treatments, vacuum-based deposition, and complex lithographic processes, that contradict the green chemistry principles of energy efficiency and inherently safer chemistry.

From a disposal standpoint, in most cases, little attention is devoted to reusability, recyclability, or modular design strategies that would enable material recovery or component reuse, for instance the widespread use of single-use plastic strips and the use of non-recyclable nor bio-degradable materials significantly amplifies electronic waste streams on a global scale.[13–15] This philosophy is in clear contrast with green chemistry and circular economy principles, which advocate durability, material recovery, and waste minimization across the entire lifecycle of chemical products and devices.

Therefore, both the production and disposal of conventional sensor devices pose a significant environmental burden, contributing to widespread ecological damage and underscoring the increasingly urgent need for moving towards greener sensor electronics, by developing sustainable, scalable, and cost-effective alternatives for large-scale environmental monitoring.[16,17]

Consequently, contemporary research in sensor development is increasingly oriented toward the convergence of green chemistry, sustainable materials science, and eco-friendly fabrication methodologies. This convergence not only addresses environmental concerns but also aligns with broader societal and policy-driven objectives aimed at fostering sustainable innovation.

Within this evolving framework, the concept of sustainable-by-design materials has gained significant attention. This approach emphasizes the integration of sustainability considerations from the earliest stages of material development, rather than addressing environmental issues retrospectively. Sustainable-by-design strategies aim to balance performance, functionality, and environmental compatibility by carefully selecting molecular architectures, synthetic pathways, and purification methods with reduced environmental impact.

Functional organic materials are particularly attractive in this regard. Their structural tunability and chemical versatility render them especially promising for sustainable applications. Moreover, these materials can be synthesized and precisely engineered to exhibit tailored specific optical, electronic, or chemical properties, thereby enabling their intentional use and deliberate optimization for specific applications, including sensing.

Nevertheless, the sustainability of such systems cannot be assessed exclusively on the basis of their functional performance. Rather, it necessitates a comprehensive evaluation of the synthetic strategies, resource utilization, waste generation, and overall environmental footprint associated with their production. Only through the integration of material innovation with responsible and sustainability-driven chemical practice can meaningful progress be achieved within the broader framework of environmentally conscious research.

The following chapter addresses these considerations by examining sustainable synthetic strategies for the preparation of functional organic materials, which will subsequently be explored in sensing applications.

1.2. Scope and objectives of the thesis

The present doctoral thesis is conceived within the framework of the PNRR-funded Rome Technopole Innovation Ecosystem, specifically within Spoke 1, Flagship 1 which focuses on the development of sustainable functional materials and their translation into reusable and recyclable green smart devices. The Rome Technopole initiative, established under Mission 4, Component 2 of the Italian National Recovery and Resilience Plan (PNRR), promotes interdisciplinary collaboration between universities, research institutions, and industrial partners to accelerate the transition from fundamental research to technological innovation. Within this ecosystem, Spoke 1, that embraces applied research for technology development and innovation, addresses the challenge of developing materials and devices that combine high technological performance with environmental sustainability, targeting intermediate Technology Readiness Levels and real-world applications.

Aligned with these objectives, the goal of this thesis is to evaluate sustainable-by-design organic materials as enabling tools for the development of green smart sensors, with particular emphasis on environmental monitoring. Rather than focusing exclusively on analytical performance, the thesis adopts a comprehensive perspective in which sustainability considerations permeate all stages of research, from material synthesis to device fabrication and performance assessment, thus aiming at contributing to the advancement of sustainable approaches for environmental sensing.

The **first objective** of this work is to demonstrate how the 12 Green Chemistry Principles can be concretely implemented in the synthesis of functional organic materials. To this end, the thesis develops and evaluates synthetic strategies that prioritize waste minimization, atom economy, and reduced energy demand. One-pot procedures and the use of green reaction media are investigated as means to reduce the environmental footprint associated with material production while preserving functional properties relevant to the desired application.

A **second key objective** is the development of sustainable sensing platforms that challenge conventional fabrication paradigms. Given that many sensor devices are produced using processes that are not environmentally benign,[18] this thesis investigates fabrication techniques that enable efficient material utilization and scalability. In particular, drop-casting is investigated as environmentally friendly, efficient, and easy-to-use deposition technique to achieve sustainable sensor fabrication, offering good sensing performance while minimizing material waste as well as energy consumption. Beyond conventional analytical parameters such as sensitivity, response time, and stability, this work emphasizes reusability considerations. In addition, green electrospray deposition is further explored as an alternative method for the immobilization of functional organic materials.

A **third objective** concerns the systematic evaluation of sustainability metrics. This, in conjunction with the previous two objectives, reflects the necessity of developing sensing technologies that are not only effective but also responsible and aligned with circular economic principles.

Eventually, during the visiting period at the University of Edinburgh in the group of Professor Stephen Thomas, the research also explores the investigation of a sustainable and cost-effective optical sensing platform, intentionally designed and developed from a green perspective for metal environmental monitoring. In parallel, the work extends the sustainability-driven approach to the field of catalysis, acknowledging its central role as a core principle of Green Chemistry. Through the development of innovative catalytic strategies based on Earth-abundant elements, the study contributes to reducing dependence on critical raw materials, such as Platinum Group Metals (PGMs), while highlighting the broader implications of sustainability in chemical process design.

The structure of this thesis will begin with an introduction to phthalocyanines as highly functional molecules with applications across several fields of research. Two different strategies for their low environmental impact synthesis are then presented. Given the strong potential of these molecules in sensing applications, an overview of sensing platforms is

provided, with particular attention to water-soluble PEG-functionalized phthalocyanines designed and synthesized through sustainable approaches. Thanks to their processability in water, these molecules are employed for the green fabrication of sensing devices. A sensor fabricated through the drop-casting technique is presented, and its performance in detecting catechol, a relevant water pollutant, is evaluated. Additional PEGylated phthalocyanines are then explored and evaluated based on the performance of the resulting sensors. The thesis also includes work carried out during the research period abroad, focused on the development of a sustainable optical sensor for metal detection in solution and on paper-based test strips. Finally, the last chapter describes an example of sustainable catalysis, namely the development of a manganese-based catalytic system for C–H borylation reactions leading to boronic esters, key intermediates in organic synthesis.

In summary, this doctoral research seeks to contribute to the cultural and technological transition toward sustainability in applied sciences. By integrating Green Chemistry, sustainable materials, and eco-friendly fabrication sensor techniques, the thesis aligns with the strategic vision of the Rome Technopole ecosystem and addresses the urgent need for sensing technologies capable of monitoring environmental pollution without exacerbating it.

1.3. Bibliography

1. Steffen, W. *et al.* Planetary boundaries : Guiding human development on a changing planet. *Science* **347**, 6223 (2015).

2. Anastas, P. T. & Warner, J. C. Green Chemistry: Theory and Practice. Oxford University Press (1998).

3. Afonso, C. A. M., Crespo, J. G. & Clark, J. H. Green Chemistry for Sustainable Development. in Green Separation Processes, Wiley VCH, (2005).

4. Anderson, M. G. *et al.* The Challenge of Micropollutants. *Science* **313**, 1072–1078 (2006).

5. Graedel, T. E., Harper, E. M., Nassar, N. T., Nuss, P. & Reck, B. K. Criticality of metals and metalloids. *Proc. Natl. Acad. Sci.* **112**, 14, 4257–4262 (2015).

6. Fuller, R. *et al.* Pollution and non-communicable disease : time to end the neglect. *Lancet Planet. Heal.* **2**, e96–e98 (2018).

7. Abbass, K., Zeeshan, M., Huaming, Q., Muntasir, S. & Mahmood, H. A review of the global climate change impacts , adaptation , and sustainable mitigation measures. *Environ. Sci. Pollut. Res.* **29**, 42539–42559 (2022).

8. Semenza, J. C. & Paz, S. Europe Climate change and infectious disease in Europe : Impact , projection and adaptation. *Lancet Reg. Heal. - Eur.* **9**, 100230–100240 (2021).

9. Jornet-Martínez, N., Moliner-Martínez, Y., Molins-Legua, C. & Campíns-Falcó, P. Trends for the Development of In Situ Analysis Devices. *Encycl. Anal. Chem.* 1–23 (2017).

10. Turner, A. P. F. Biosensors: sens and sensibility. *Chem. Soc. Rev.* **42**, 3175–3648 (2013).

11. Kalambate, P. K. *et al.* Electrochemical (bio) sensors go green. *Biosens. Bioelectron.* **163**, 112270–112286 (2020).

12. Enriquez, M. A. *et al.* Mineral supply for sustainable development requires resource governance. *Nature* **543**, 367–372 (2017).

13. Piro, B., Tran, H. V. & Thu, V. T. Sensors Made of Natural Renewable Materials: Efficiency, Recyclability or Biodegradability-The Green Electronics. *Sensors* **20**, 5898–5951 (2020).

14. Ray, P. C., Yu, H. & Fu, P. P. Toxicity and Environmental Risks of Nanomaterials : Challenges and Future Needs. *J. Environ. Sci. Heal. Part C Environ. Carcinog. Ecotoxicol. Rev.* **27**, 1–35 (2009).

15. Zimmerman, J. B., Anastas, P. T., Erythropel, H. C. & Leitner, W. Designing for a green chemistry future. *Science* **367**, 397–400 (2020).

16. Al-amri, A. M. Printed Sensors for Environmental Monitoring : Advancements , Challenges , and Future Directions. *Chemosensors* **13**, 285–322 (2025).

17. Wang, J. Electrochemical Glucose Biosensors. *Chem. Rev.* **108**, 814–825 (2008).

18. Williams, A. *et al.* Biosensors for Public Health and Environmental Monitoring: The Case for Sustainable Biosensing. *ACS Sustain. Chem. Eng.* **12**, 10296–10312 (2024).

Chapter 2. Sustainable synthesis of phthalocyanines

2.1. Introduction

2.1.1. Phthalocyanines as attractive functional organic molecules

The 12 Principles of Green Chemistry can be broadly summarized by the 4Rs of sustainability: Reduce, Reuse, Recycle, and Recover. These concepts provide a simple framework for guiding more sustainable chemical practices across various stages of research and production, promoting chemical recycling after use, efficient waste management, and miniaturization of chemical processes.

As Lutz F. Tietze observed in *Chemical Reviews* (1996, Vol. 96),

"Despite […] the importance of chemistry to our society, its public image has deteriorated. This can be explained by the increasing importance of environmental issues to our society and the fear that chemistry could negatively influence the ecological balance. Today it is not only a question of what we can synthesize, but how we do it. Major problems in chemical production are the handling of waste, the search for environmental tolerable procedures, the preservation of resources, and the increase in efficiency. The solution of these problems would not only be favorable for the environment, but also allow a reduction in production cost.", this insight remains highly relevant today.

In fact, chemistry's societal value is inseparable from its environmental impact, making the true challenge for modern chemistry the promotion of innovation in medicinal and technological applications while ensuring environmental responsibility.

It is precisely within this context that the present chapter explores strategies for environmentally sustainable synthesis, examining approaches that minimize waste, improve efficiency, and integrate resource-conscious design, aligning with the broader goals of green and environmentally mindful chemistry. Particular attention is devoted to the synthesis of molecules, namely phthalocyanines, that combine tailored physicochemical

properties with versatility for a plethora of applications, including sensing. These examples illustrate how sustainability principles can be embedded at the molecular design and synthetic level, providing a foundation for the materials' later use in practical sensing devices investigated in the following chapters.

Within this framework, the choice of solvent in a chemical reaction extends beyond its role as a mere reaction medium, representing a key factor in determining the sustainability and safety profile of a chemical process. This consideration is particularly relevant given that solvents, as well as separating agents, employed in the purification steps of a synthesis often constitute the largest sources of chemical waste, significantly affecting the overall environmental footprint of a synthesis.[1]

The fact that conventionally used organic solvents are toxic, flammable, and non-recoverable has led to the development of two main strategies to minimize solvent-related hazards and reduce their use: one-pot methodologies, that limit solvent consumption by combining multiple reaction steps, and the search for greener solvent alternatives, including bio-based, low-toxicity, and recyclable options. Specifically, both these approaches will be applied in this Chapter to the synthesis of phthalocyanines and will be evaluated and thoroughly discussed, showing how they can allow for enhancing the overall sustainability of synthetic processes under investigation while preserving efficiency, selectivity and versatility.

Phthalocyanines (Pcs) are multifunctional molecular materials belonging to the class of organic dyes, with considerable scientific interest and applicability. They were accidentally discovered as a byproduct in 1907,[2] and Linstead characterized the phthalocyanine structure in 1934.[3]

From a structural point of view, they consist of a planar conjugated system with 18 π-electrons organised in four isoindole units linked through aza-bridges (**Figure 1**). The resulting macrocycle can host up to sixty different metal ions in its core.[4] This very peculiar and highly aromatic structure conveys phthalocyanines unique physical and chemical properties, like high chemical, thermal, and photostability, intense coloration (from blue-

green to blue-black), and high inertness.[5] Their electronic properties are also remarkable, such as high molar absorptivity (>10^5 $mol^{-1}·L·cm^{-1}$), in the red-near infrared range (ca. 600-700 nm), and moderate-to-high fluorescence, phosphorescence, and singlet oxygen generation quantum yields.[6,7]

The phthalocyanine scaffold is a highly versatile platform, allowing extensive functionalization with a plethora of different chemical groups, and the simultaneous use of different substituted precursors may lead to a broad range of structures, including asymmetric derivatives. **Figure 1** shows the peripheral (β-) and non-peripheral (α-) positions on the ring.

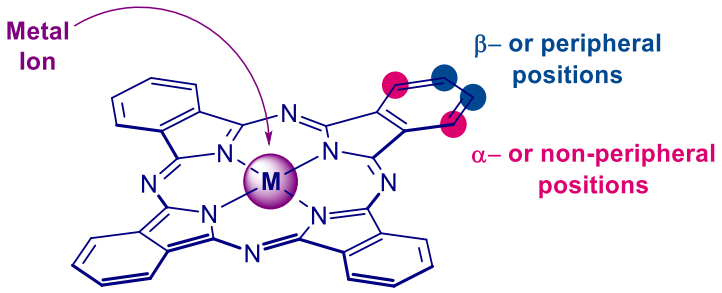

Figure 1. Phthalocyanine chemical structure.

In this work, the discussion is mainly focused on two main categories of peripherally substituted phthalocyanines: phthalocyanine derivatives bearing four substituents at the peripheral positions of the macrocyclic ring are called *tetra*substituted Pcs, while phthalocyanine derivatives functionalized with eight substituents are named *octa*substituted Pcs (**Figure 2**).

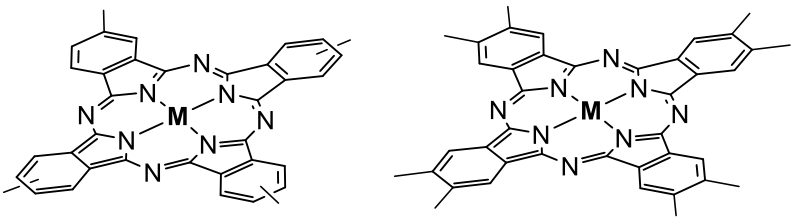

Figure 2. Chemical structure of *tetra*substituted (as a regioisomeric mixture), left, and *octa*substituted, right, Pcs.

Several metal ions can also be inserted into the central cavity of the structure to form metallophthalocyanines, with some metals allowing for axial ligation. Both the nature and placement of substituents on the Pc ring, as well as the nature of the metal ion, can influence and modulate the physicochemical properties of the resulting Pcs, enabling fine tuning for different advanced applications, including optoelectronics,[8–10] catalysis,[11] sensing,[12,13] liquid crystals,[14] energy conversion,[15] and medicinal chemistry.[16]

Owing to their extended π-conjugated aromatic macrocycle, phthalocyanines exhibit a strong tendency to undergo intermolecular π-π stacking interactions, which often results in aggregation phenomena in solution and in the solid state. Depending on their geometry, H-type (sandwich) and J-type (head-to-tail) aggregates can be distinguished, exhibiting significant differences in optical properties.[17] Furthermore, unsubstituted phthalocyanines suffer from poor solubility in nearly all the solvents. Both these factors can significantly affect their optical, electronic, and redox properties, ultimately influencing or even limiting their performance in practical applications.[18] In particular, limited solubility in common organic solvents not only complicates processing and purification procedures but may also hinder their effective incorporation into functional devices.[19]

Conventionally, the synthesis of phthalocyanines in solution typically involves the cyclotetramerization of suitable precursors such as phthalonitriles, 1,3-diiminoisoindolines, or phthalic acid derivatives (anhydrides, imides, amides, under the name of "Wyler method") (**Scheme 1**).[20]

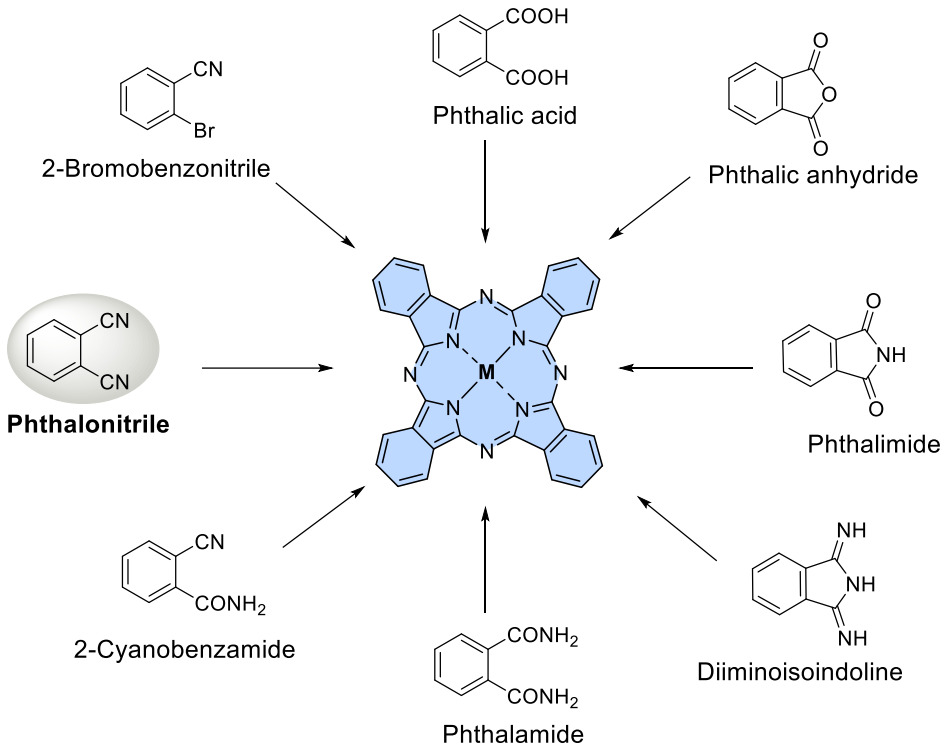

Scheme 1. Synthetic precursors for phthalocyanine macrocycle synthesis.

Pcs are traditionally synthesized in high-boiling, often toxic solvents including dimethylaminoethanol (DMAE), quinoline, and nitrobenzene typically under strongly basic conditions. When alcohols are used as solvents, particularly for the synthesis of metal-free derivatives, in situ-generated alkali metal alkoxides are frequently employed as bases. In many alternative protocols, catalytic amounts of non-nucleophilic organic bases, notably 1,8-diazabicyclo[5.4.0]undec-7-ene (DBU), are employed to promote the cyclotetramerization process, as depicted in **Scheme 2**.[21,22]

Phthalonitriles are among the most widely employed precursors utilized for the purpose,[20] and were selected as the substrates for phthalocyanine ring formation throughout this thesis. In this context, the accepted mechanism for the formation of Pcs suggests that strong bases such as DBN (1,5-Diazabicyclo[4.3.0]non-5-ene) or DBU primarily act as electron acceptors.[23,24] Under these conditions, a base-generated nucleophilic species attacks

one of the cyano groups of the phthalonitrile precursor, leading to the formation of an iminoisoindolenine-type intermediate.

The subsequent stage of the reaction involves the nucleophilic attack of the formed intermediate to the cyano group of a second phthalonitrile molecule, generating a dimer species. This species undergoes an analogous nucleophilic attack with an additional phthalonitrile unit to produce a trimer, that in turn reacts with a fourth phthalonitrile precursor to complete the ring-closure condensation, ultimately affording the phthalocyanine macrocycle. When a metal salt is present in the reaction medium, the metal cation acts as a templating agent, coordinating to the reacting intermediates and driving the macrocyclization process. Because of this effect, the synthesis of metallophthalocyanines (MPcs) generally proceeds in higher yields compared to that of the corresponding metal-free analogues (2HPcs).

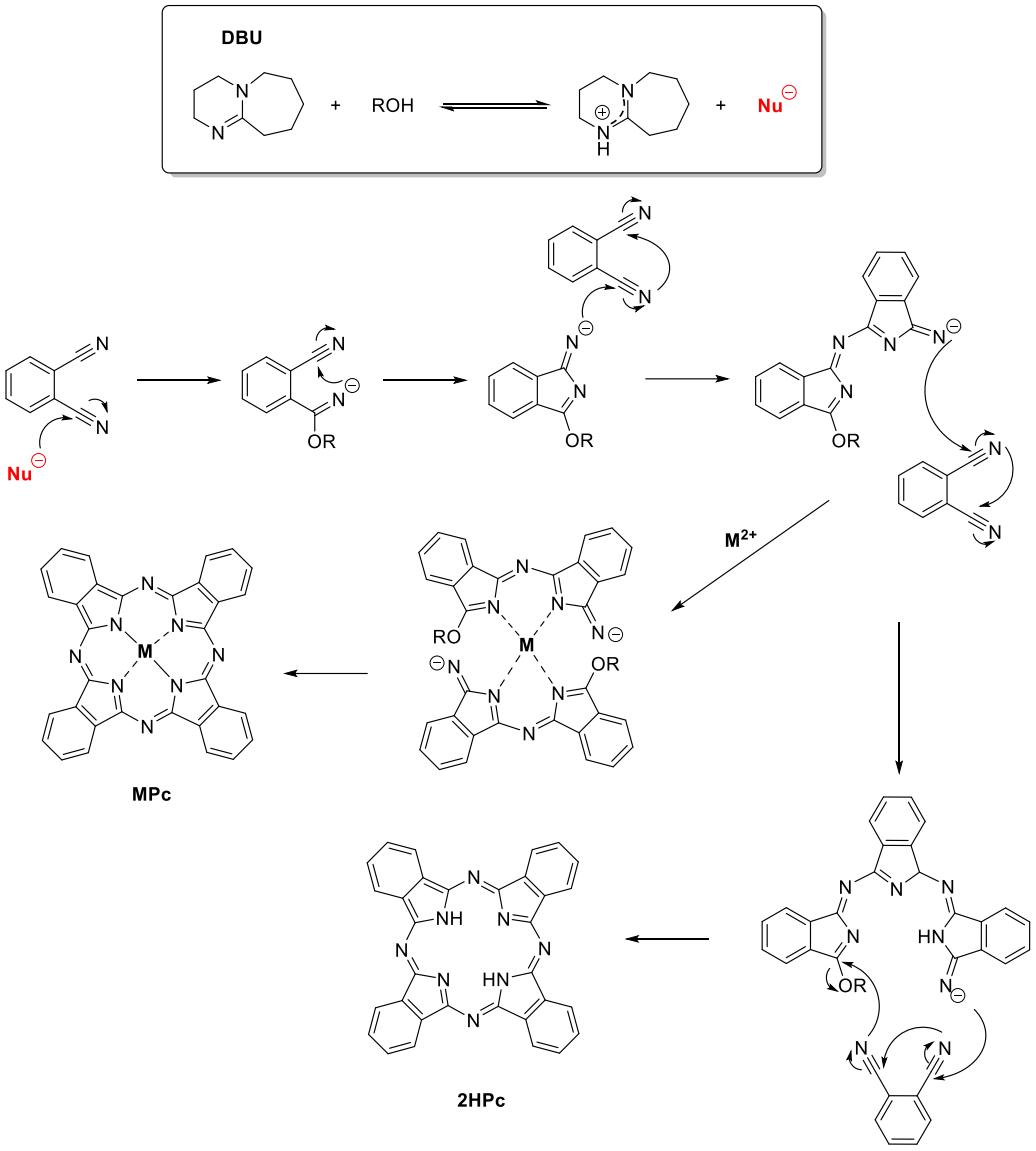

Scheme 2. Reaction mechanism of metallophthalocyanines (MPcs) and metal-free phthalocyanines (2HPcs).

Despite the highly attractive physicochemical properties of Pcs, overview of the existing literature clearly suggests that the synthesis of phthalocyanines remains notoriously challenging, especially from a sustainable perspective. Indeed, the experimental conditions for the phthalocyanine ring formation are typically harsh, including elevated temperatures (about 140-240 °C), anhydrous environment, and reaction media capable of promoting

metal-ion templation while remaining chemically inert. These demanding requirements complicate both process optimization and environmental compatibility.

In the recent years, alternative strategies, such as microwaves,[25–27] UV irradiation,[28,29] solvothermal synthesis,[30–32] and mechanochemical synthesis[5] have been explored to address these limitations. Although these approaches represent meaningful advances toward more sustainable practices, they frequently depend on specialized equipment that is not universally accessible in conventional synthetic laboratories, thereby restricting their broader implementation.

Consequently, the development of synthetic methodologies that combine both sustainability and operational simplicity remains a pressing objective for the preparation of this important class of functional molecules.

2.1.2. Pot-economical reactions

Pot-economical reactions represent an important class of synthetic strategies in modern organic chemistry, as they integrate multiple chemical transformations within a single reaction vessel. This approach directly addresses the longstanding challenge that *"[…] it would be much more efficient if one could form several bonds in one sequence without isolating the intermediates, changing the reaction conditions, or adding reagents."*[33]

Several types of pot-economical reactions can be distinguished, depending on the sequence and interconnection of the individual transformations. As showed by Prof. Dr Wei Zhang (University of Massachusetts, Boston, USA) during his talk in the webinar organized by MDPI that I attended on 30 January 2026, they can be classified into three main categories: cascade (tandem) reactions, multicomponent reactions (MCR), and one-pot stepwise synthesis (OPSS) (**Figure 3**).[34]

Cascade reactions are characterized by a single operational step in which two reactants undergo a sequence of mechanistically linked transformations under unchanged reaction conditions. Reactive intermediates are generated and consumed *in situ*, resulting in efficient construction of molecular complexity with minimal operational effort.[33]

Multicomponent reactions involve three or more starting materials reacting simultaneously in one vessel to afford a single product. These reactions are highly convergent and allow the formation of several chemical bonds in a single step. Their outstanding pot economy arises from reduced solvent usage, fewer purification steps, and excellent atom efficiency.[35]

One-pot stepwise synthesis differs from the previous approaches in that it requires multiple operational steps, such as sequential reagent addition or variation of reaction conditions, all carried out in a single reaction vessel without isolating and/or purifying the intermediates.[36] Such strategy not only improve efficiency while minimizing materials (solvent and reagent) and energy consumption, but also provide safer work conditions, by

decreasing labour and reducing chemicals handling time, offering a more practical and sustainable methodology than conventional procedures.[37,38]

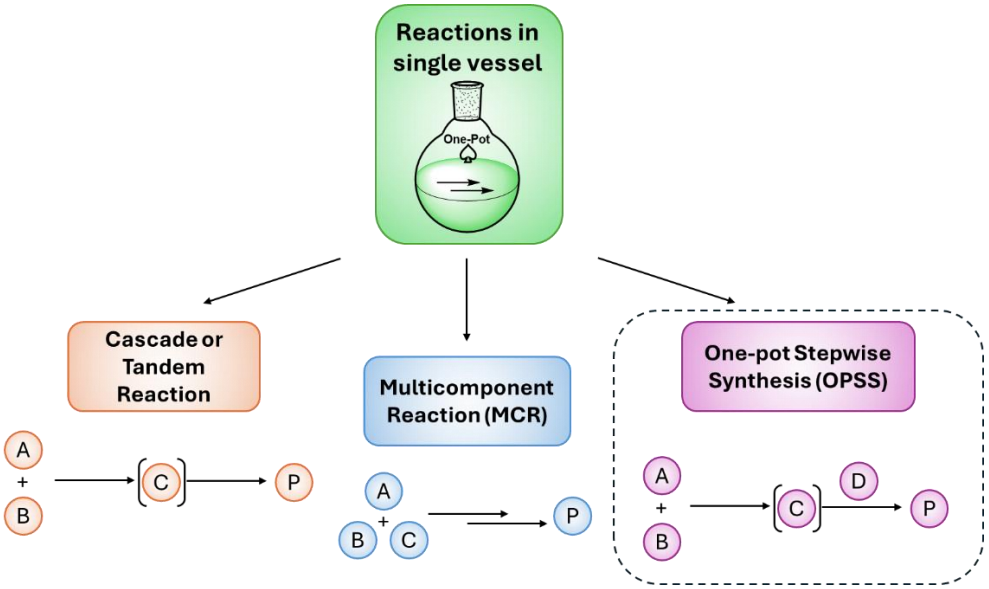

Figure 3. Schematic representation of different kinds of pot-economical reactions.

Collectively, these one-pot methodologies play a crucial role in sustainable synthesis, particularly in pharmaceutical and industrial applications, where sustainability key points, such as efficiency, scalability, and waste minimization are essential.

In light of these considerations, the first part of my PhD focused specifically on the implementation of one-pot stepwise synthesis (OPSS) for the preparation of a series of functionalised phthalocyanine derivatives.

2.2. Results and discussion

2.2.1. The one-pot approach

The results presented in this section have been reported in a recently published work.[39]

Among the various classes of functionalised phthalocyanine derivatives, aryloxy- and alkyloxy-substituted metallophthalocyanines have attracted particular attention due to their enhanced photophysical and electrochemical properties, that make them useful molecules especially in photodynamic therapy (PDT) for cancer treatment,[40,41] chemical sensors,[42] non-linear optics (NLO),[43,44] photovoltaics,[45,46] and colour filters for liquid crystal displays.[47]

As sketched in **Scheme 3**, in principle the two main synthetic routes to metallophthalocyanines bearing aryloxy- and alkyloxy-substituents at the periphery of the ring are multi-step processes and can be classified in: (Path A) metal-templated cyclization of the already chemically functionalized precursor, (Path B) metal insertion into the preformed, metal-free peripherally functionalized phthalocyanine. Both these routes involve distinct, separate synthetic steps: the insertion of the desired aryloxy group on the phthalonitrile ring via nucleophilic aromatic substitution (S_NAr) and its tetramerization in a high-boiling solvent aided by an organic base and a templating metal ion.[48–50] Consequently, several workups including purification processes are required to obtain the final product.

A third, one-pot path can condense these steps within a single reaction vessel, improving operational efficiency but also ensuring access to structurally tailored functional materials suitable for application that will be subsequently discussed throughout this doctoral thesis.[39,51]

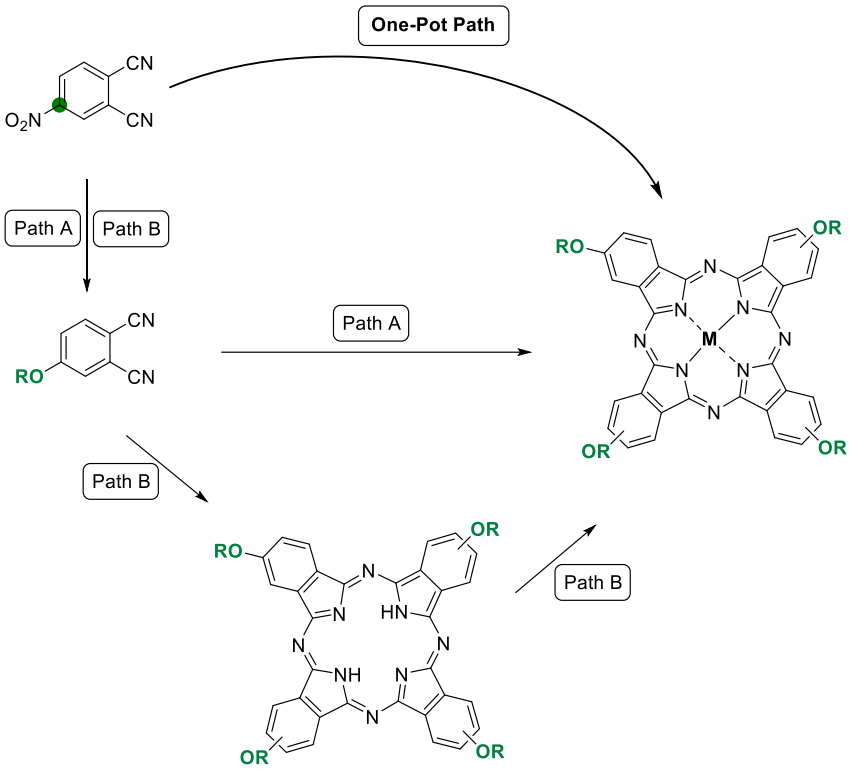

Scheme 3. Main synthetic pathways to synthesize tetra substituted phthalocyanines with a metal in the central cavity.

The literature contains only a limited number of examples of one-pot phthalocyanine syntheses.[22,52] In contrast, one-pot protocols that couple ring functionalization with macrocyclization are far less common. Nucleophilic aromatic substitution can, in principle, support such tandem processes, yet the few reported cases typically arise as unoptimized side reactions rather than deliberately designed synthetic strategies.[53] Yet, as far as can be ascertained from the literature, no general, practical, and versatile protocol for accessing a broad range of related compounds of a same sub-family has been established to date.

According to **Scheme 4**, the investigated synthetic pathway involves the initial functionalization of a phthalonitrile derivative bearing a good leaving group, such as a nitro substituent, susceptible to nucleophilic aromatic substitution. After its replacement with different phenols/alcohols, under inert atmosphere, the resulting intermediate is not isolated but instead directly used in the subsequent metal-templated cyclization step. In the

same reaction vessel, and under inert conditions, a metal salt and the base 1,8-diazabicyclo[5.4.0]undec-7-ene (DBU), commonly employed in phthalonitrile tetramerization, are thus introduced. The reaction mixture is then heated to 140-150 °C, to promote the macrocyclization process.

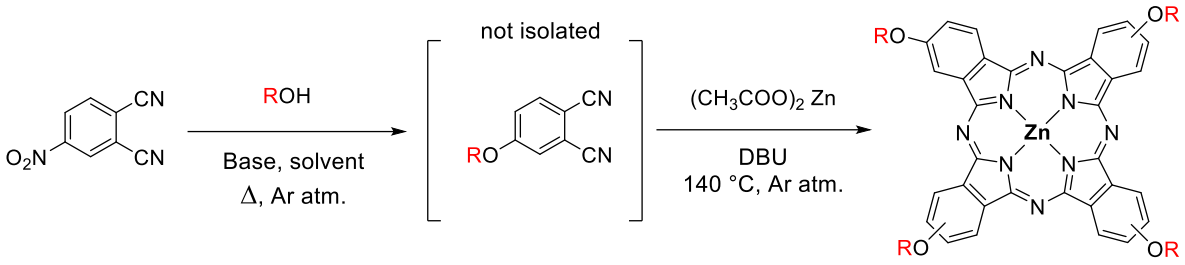

Scheme 4. Synthetic route for the one-pot synthesis of tetra aryloxy/alkyloxy metallophthalocyanines.

The study initially focused on the investigation of the synthesis of a model derivative, tetra-3,5-dimethylphenoxy zinc phthalocyanine (**Pc1**), selected to determine the optimal conditions for the procedure optimization (**Scheme 5**). The feasibility of performing two reactions sequentially in the same reaction flask has been investigated, taking advantage of the compatibility between the nucleophilic aromatic substitution (S_NAr) environment and the phthalocyanine ring formation conditions.

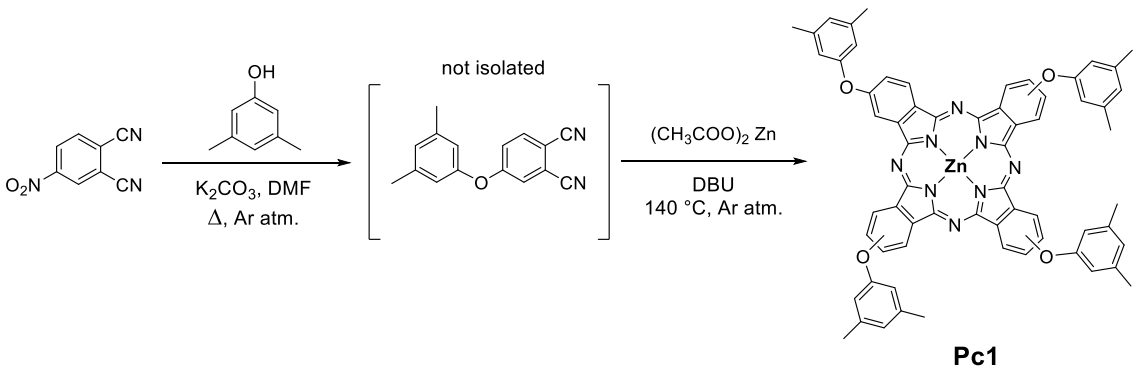

Scheme 5. Synthetic route for the synthesis of tetra-4-(3,5-dimethylphenoxy)-zinc phthalocyanine **Pc1**.

The two methyl groups on the aromatic ring of the phenol are expected to have, indeed, little influence on the reaction's progress, being weak electron-donating groups positioned in the meta position to the hydroxyl group. Their location avoids steric hindrance near the reactive site, thereby allowing us to investigate and refine the synthetic conditions while minimizing the number of variables involved. Different reaction conditions varying several parameters such as the reagents molar ratios, the base (DBU or potassium carbonate), and reaction temperature throughout the process were screened (**Table 1**).

Entry	Phthalonitrile/phenol molar ratio	Base (equivalent amount)	1° step temperature (° C)	DBU in the 2° step (° C)	Isolated yield (%)
1	1:1.1	DBU (2 eq)	60	No	29
2	1:1.1	K_2CO_3 (3 eq)	60	Yes	29
3	**1:1.1**	**DBU (2 eq)**	**60**	**Yes**	**44**
4	1:1.0	DBU (3 eq)	25	Yes	41

Table 1. Variation of the experimental conditions for the model reaction. Experimental conditions: 4-nitrophthalonitrile (500 mg, 2.89 mmol), DMF as the solvent (4 mL).

The optimal reaction conditions were achieved with a phthalonitrile/phenol ratio of 1:1.1 and DBU as the base, when the S_NAr reaction was conducted at a temperature of 60°C.

The superior performance of DBU as a base in these specific conditions can be attributed not only to its higher basicity but also to its liquid state, allowing for homogeneous dispersion in the reaction medium. The further addition of DBU in the second step was found to enhance the phthalocyanine formation. Compound **Pc1** was then straightforwardly purified by filtration on a short silica pad followed by Soxhlet extraction

of impurities in methanol, affording a 44% isolated yield calculated with respect to the limiting reagent after purification. Furthermore, since this study primarily aimed at developing a new and more sustainable synthetic procedure, no attempts were made to isolate the individual regioisomers of this compound or any of the subsequently synthesized tetra substituted phthalocyanines.

However, in an attempt to further enhance the sustainability profile of the procedure, the protocol has been investigated under a newly expanded set of experimental parameters. In this case, potassium carbonate was selected as the designated base for the nucleophilic aromatic substitution step, in which the phenol is deprotonated to generate the corresponding phenoxide, allowing displacement of the nitro group and formation of the phthalonitrile intermediate. Although other bases have been reported in related procedures,[10] potassium carbonate was chosen here for its advantageous combination of practicality, accessibility, and alignment with sustainability goals.[54–56] Its widespread use and solid performances in S_NAr chemistry therefore made it a suitable candidate for developing an efficient and more environmentally conscious one-pot synthesis.

Table 2 summarizes the reaction variables that have been scrutinized, which include the reaction medium, the molar ratio between the reagents used, the concentration of 4-nitrophthalonitrile in the reaction solvent, the amount of DBU added for the cyclotetramerization step, along with the isolated yield obtained.

Entry	Solvent	Phthalonitrile/phenol molar ratio	Phthalonitrile concentration (mmol/mL)	Amount of DBU in the 2° step (eq)	Isolated yield (%)
1	DMPU	1:1.1	0.72	0.07	19
2	DMSO	1:1.1	0.72	0.035	15
3	DMF	1:1.0	0.72	0.0	29
4	DMF	1:1.0	0.72[a]	1.0[b]	23
5	DMF	1:1.0	1.44	1.0	35
6	**DMF**	**1:1.0**	**0.72**	**1.0**	**48**

Table 2. Experimental conditions for the synthesis of **Pc1**. [a]The concentration of the aryloxyphthalonitrile intermediate (calculated assuming complete S_NAr, as indicated by TLC) decreases to 0.58 mmol/mL after DMAE addition. [b]1.0 mL of N,N-dimethylaminoethanol (DMAE) was added as a cosolvent during the cyclization step.

Solvent selection was the first parameter to be evaluated during reaction optimization. The ideal solvent needed to be chemically inert under the reaction conditions, thermally stable at reaction temperatures, and capable of supporting both reaction steps without interfering with the reaction components. Generally, N,N-dimethylformamide (DMF) stands out as the most effective for the purpose.[57]

In an effort to further align the process with principles of green chemistry, two polar aprotic and less environmentally impactful solvents, dimethyl sulfoxide (DMSO) and N,N′-dimethylpropyleneurea (DMPU), were also investigated, as they are well-suited to facilitate both nucleophilic aromatic substitution and the subsequent phthalonitrile tetramerization, while adopting a more sustainable perspective. However, under the tested conditions, neither solvent achieved satisfactory performance. DMF, on the other hand, uniquely enabled both steps to proceed efficiently in one-pot conditions. In this context, its lower intrinsic greenness is counterbalanced by higher efficacy, while the one-pot approach inherently reduces solvent use and waste generation, delivering a net process-level sustainability gain in line with current solvent-replacement guidance for S_NAr-type chemistry.[58]

Then, further optimization steps were implemented, for instance the ratio of reagents, particularly the amount of phenol relative to the phthalonitrile precursor. While many established protocols rely on a slight excess of phenol to ensure complete substitution, in this case this approach required reconsideration. Under the basic conditions employed for the macrocyclization step, any residual phenol is likely to be present as phenate anion, a nucleophilic species that might interfere with the metal-templated cyclotetramerization. Therefore, careful control of the phenol-to-phthalonitrile ratio was considered essential to

minimize potential side reactions and ensure clean progression of the one-pot process. The best result in terms of yield of the final product was achieved with 1:1.0 molar ratio, respectively, confirming the advantage of limiting phenol excess under the conditions of the subsequent macrocyclization step.

As for the second step, the addition of DBU was generally found to improve phthalocyanine yields. Catalytic amounts, which are frequently employed in the literature for phthalonitrile tetramerization, proved insufficient, with an equimolar amount required instead. This evidence suggests on one hand that potassium carbonate can promote phthalocyanine ring formation to some extent, but its basicity alone is not sufficient to achieve satisfactory yields under the selected conditions, and on the other hand that the complexity of the reaction environment, due to the presence of various by-products from the nucleophilic substitution reaction, may interfere with the catalytic activity of DBU, thus requiring higher amounts. Conversely, the addition of DMAE, as a co-solvent did not prove beneficial, likely due to unfavourable dilution effects within the reaction mixture.

In addition, increasing the concentration of 4-nitrophthalonitrile in solution did not enhance the reaction outcome; rather, a twofold increase led to a decrease in yield from 48% to 35%. In all cases, the cyclization step was carried out at 140 °C, in line with most solution-based syntheses reported in the literature using DMAE, which has a boiling point of 135-138°C.

After achieving and optimizing the best set of reaction conditions, a series of different phenols bearing both electron-withdrawing and electron-donating groups have been investigated as nucleophiles to afford various aryloxy zinc phthalocyanines (**Figure 4**).

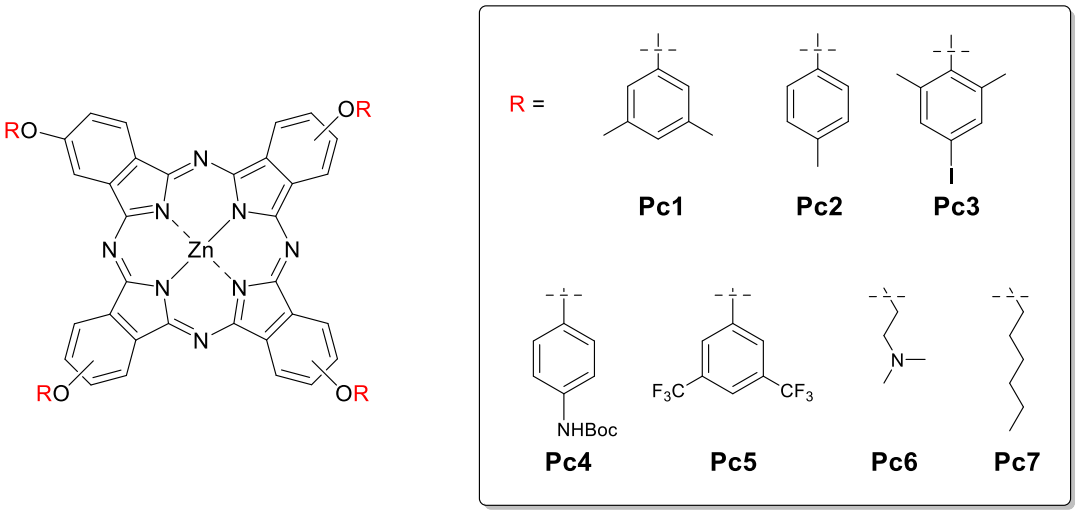

Figure 4. Chemical structure of phthalocyanine derivatives. Phthalocyanine core (black) and different modifications R (red) denote substituents at the periphery of the macrocycle ring.

The temperature variable for the SNAr required special consideration: while this synthetic step could in some cases be accomplished at room temperature, its rate and overall efficiency were strongly dependent on the substitution pattern of the phenol. Reaction conditions were therefore optimized case by case, accounting for specific electronic and steric effects. In addition to expanding the scope of this approach, efforts were made to refine the purification process in order to obtain the target phthalocyanines in a more sustainable manner.

For this purpose, solvent washings and, when applicable, Soxhlet extraction of residual by-products were explored, as both techniques allow for efficient solvent recycling. In case of more challenging purification, particularly those affected by the high solubility of the final products, a filtration on a short silica pad was employed and proved to be effective in isolating target products from reaction impurities, greatly reducing the amounts of both the stationary phase and solvents that are commonly used in the conventional column chromatography approach, while also enabling recovery and reuse of a significant fraction of the employed eluent mixtures. As a first example, the synthesis of compound **2** using 4-

nitrophthalonitrile and 4-methylphenol (*p*-cresol) as the phenolic component was carried out. In this case as well, the methyl substituent on the aromatic ring was not expected to significantly influence the course of the reaction, either by promoting or hindering the key steps.

To verify the consistency and robustness of the synthetic protocol, a small set of reaction conditions (reaction medium, reagents molar ratio, S_NAr temperature, DBU amount) was also screened for this substrate, with the results in terms of isolated yields summarized in **Table 3**.

Entry	Solvent	Phthalonitrile/phenol molar ratio	S_NAr T (° C)	Amount of DBU in the 2° step (eq)	Isolated yield (%)
1	DMPU	1:1.1	60	0.07	27
2	DMPU	1:1.1	40	0.07	30
3	DMPU	1:1.1	60	0.0[a]	18
4	DMF	1:1.1	60	0.07	28
5	**DMF**	**1:1.0**	**60**	**1.0**	**43**

Table 3. Experimental conditions for the synthesis of **Pc2**. [a]DBU (0.07 eq) was added 15 minutes after reaching the tetramerization temperature.

Also in this case, the use of a slight excess of phenol relative to 4-nitrophthalonitrile, together with equimolar amounts of DBU in the second step, was necessary to achieve the highest yields. Interestingly, adding a catalytic amount of base 15 minutes after the temperature increase required for the second step of the one-pot protocol resulted in lower yields than adding the same amount immediately when DMPU was chosen as the solvent. This may be explained by the occurrence of one or more side processes that are triggered rapidly upon heating, potentially depleting the phthalonitrile reactant through oxidation or polymerization involving the cyano groups. DMPU generally performed better as a solvent

in comparison to its performance in the synthesis of **1**, affording phthalocyanine Pc**2** up to 30% yield. However, the best results were obtained by reacting 4-nitrophthalonitrile and *p*-cresol at 60 °C in DMF, affording the target molecule in a 43% yield and confirming the efficacy of these optimized reaction conditions.

With a deeper understanding of the synthetic method, the procedure was subsequently extended to a broader set of derivatives featuring more complex substitution patterns and increased electronic and steric demands. The main results for the syntheses of compounds **Pc3-9** are reported in **Table 4**.

Compound	Phthalonitrile/phenol molar ratio	S_NAr T (° C)	Isolated yield (%)
Pc3	1:1.0	65	37
Pc4	1:1.0	75	n/d*
Pc5	1:1.0	75	27
Pc6	1:1.0	75	49
Pc7	1:1.0	60	22
Pc8	1:3.1	100	30
Pc9	1:3.1	100	31

Table 4. General conditions for the synthesis of phthalocyanines **Pc3-9**. Reactions were carried out in DMF, using 3.0 eq. of K_2CO_3 as the base for the S_NAr step, and 1.0 eq. of DBU in the cyclotetramerization step. *The results for this compound are further discussed within the text.

The synthesis of **Pc3** was explored using 2,6-dimethyl-4-iodophenol as the nucleophilic component, a substrate that combines steric congestion with electronically neutral yet synthetically valuable functionality. Indeed, the methyl substituents at the 2 and 6 positions introduce steric hindrance around the hydroxyl group, which can reduce the accessibility of the corresponding phenate anion to the electrophilic centre on the phthalonitrile during the S_NAr step. The iodine atom at the 4-position does not substantially influence the

reactivity in this context, although it provides a useful handle for potential post-functionalization. To further evaluate the behaviour of this hindered substrate under the tandem conditions, an aliquot of the crude reaction mixture was analyzed by ^{1}H NMR after completion of the first step. The phthalonitrile intermediate was identified as the major species, together with minor unidentified side products (**Figure 5**). These did not interfere with the subsequent macrocyclization, and the final zinc phthalocyanine **Pc3** was isolated in 37% yield after the standard workup and purification. This result confirms that even sterically demanding phenols can be effectively incorporated through this new one-pot protocol.

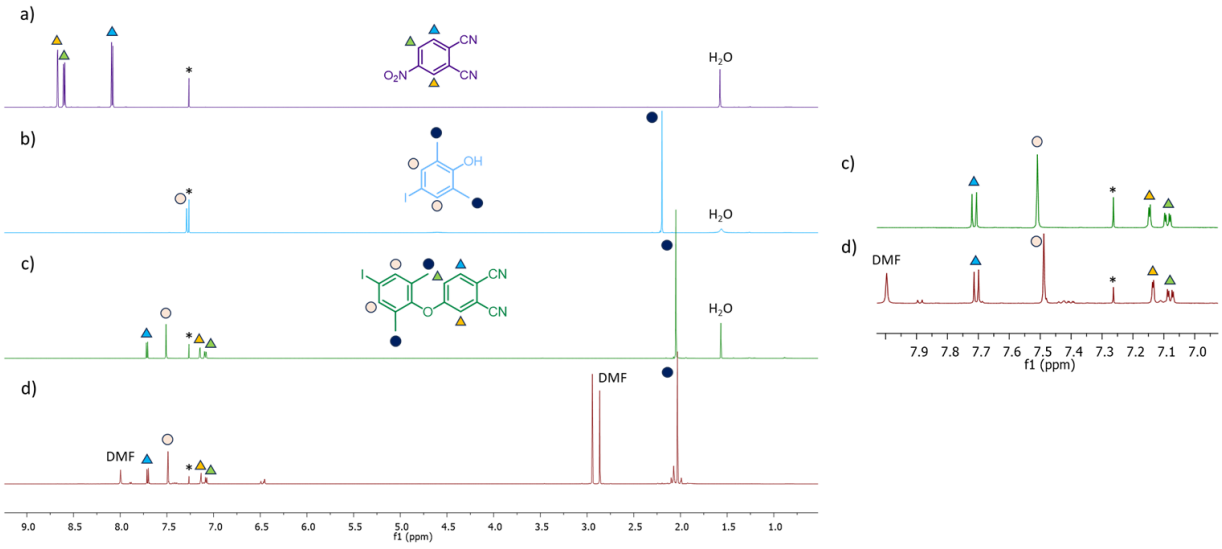

Figure 5. Left panel: Stacked ^{1}H NMR spectra showing a) 4-nitrophthalonitrile, b) 2,6-dimethyl-4-iodophenol, c) the isolated 4-(4-iodo-2,6-dimethylphenoxy)phthalonitrile intermediate and d) the crude reaction mixture after completion of the first step of the tandem sequence leading to phthalocyanine **Pc3** ($CDCl_3$, 600 MHz). Right panel: magnification of the aromatic regions of spectra c) and d). The symbol * corresponds to $CDCl_3$ residual peak.

The versatility of this approach has been also tested towards phenolic substrates bearing amino substituents. This type of functional group is well-known in organic synthesis for its

potential as a crucial derivative for further functionalization. In this case, 4-aminophenol was used as the phenolic component after primarily protecting the amino moiety with a *tert*-butyloxycarbonyl (BOC) protection group. This was important to prevent side-reactions that might occur with the amino group during phthalocyanine ring formation. The outcome of the reaction did not allow us to clearly confirm the formation of the target compound **Pc4**, as the purified product proved highly insoluble in most organic solvents, except for N-coordinating bases such as pyridine, making it impossible to obtain a clear mass spectrum to confirm its molecular weight. In some instances, interpretation was further complicated by residual solvent peaks overlapping with expected signals. IR spectroscopy shows features that could be consistent with partial thermal cleavage of the BOC group during phthalonitrile tetramerization (**Figure 6**).

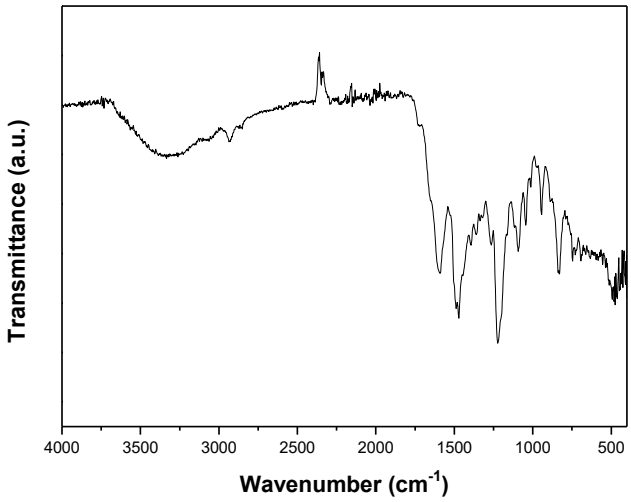

Figure 6. ATR spectrum of compound **Pc4**.

In particular, a broad absorption band around 3250 cm^{-1} may be attributable to overlapping N-H stretching modes from both carbamate and primary amine functionalities. Additionally, there is only a weak shoulder at 1721 cm^{-1}, a region typically associated with strong absorptions from BOC-derived carbonyl groups. Nevertheless, no definitive conclusion regarding the chemical structure of **Pc4** can be drawn at this stage, as the

formation of intermolecular aggregates, possibly promoted by hydrogen bonding between the phthalocyanine protecting groups, may also contribute to the reduced solubility and the poor interpretability of the spectra. However, the UV-Vis spectrum recorded in pyridine confirmed the presence of the Q and Soret bands characteristic of the phthalocyanine core. Given the potential for further derivatization or quaternization of the free amine group, additional studies are warranted to further investigate and optimize this transformation within the context of pot-economical synthetic strategies.

The synthesis of **Pc5** also required additional consideration due to the electronic nature of the substituents present on the phenolic component. In this case, the starting phenol is substituted with two trifluoromethyl groups positioned at positions 3- and 5- of the aromatic ring. These substituents are well known for their strong electron-withdrawing character, which is expected to reduce the nucleophilicity of the oxygen atom, thereby increasing the activation energy required for the S_NAr reaction with 4-nitrophthalonitrile. In practice, this prediction was confirmed by the necessity to increase the reaction temperature to 75 °C in order to achieve successful conversion of 4-nitrophthalonitrile into 4-(3,5-bis(trifluoromethyl)phenoxy)phthalonitrile. Despite the increased difficulty of the S_NAr step under these electronically demanding conditions, the subsequent cyclotetramerization proceeded smoothly, ultimately affording the desired phthalocyanine derivative **Pc5** in 27% isolated yield.

Eager to further gauge the scope of such strategy, the method has been further tested in the use of alcohols rather than phenols as nucleophiles in the aromatic nucleophilic substitution, targeting the synthesis of alkyloxy-substituted metallophthalocyanines.

Although the alkoxyde ion is a strong nucleophile, the use of aliphatic alcohols in S_NAr often requires stronger bases and more forcing conditions due to their lower acidity compared to phenols. Nevertheless, under optimized conditions, their inherent nucleophilicity may still enable the substitution to proceed efficiently, potentially even under mild conditions. To verify these hypotheses, a known compound reported in the literature, tetra-(2-dimethylaminoethoxy) zinc phthalocyanine (**Pc6**) has been synthesized,

given its relevance as a precursor to the corresponding cationic species, which have been widely investigated as telomerase inhibitors[59] and singlet oxygen generators for photodynamic therapy applications.[60] Any attempt to perform the reaction at room temperature with alkyl alcohols failed, likely due to the inability of K_2CO_3 to completely deprotonate them. This behavior mirrors prior SNAr precedents where higher basicity/temperature or longer reaction times are needed for aliphatic alcohols versus phenols.[61] As a result, the reaction time proved to be remarkably long, requiring temperatures up to 65 °C. Nonetheless, phthalocyanine **Pc6** was successfully obtained in 49% yield, a value that falls within the broad range reported in the literature and is generally considered satisfactory given the variability of the existing procedures. On the contrary, phthalocyanine **Pc7**, obtained from the reaction of 4-nitrophthalonitrile with hexan-1-ol, was isolated in moderate yield, suggesting that further optimization of the reaction and workup conditions may be required for derivatives bearing longer alkyl chains. Overall, three practical design rules emerged: limit phenol excess to avoid phenolate interference in cyclotetramerization, use ~1.0 eq DBU under one-pot conditions to offset competing side-processes and increase SNAr temperature for strongly deactivated phenols or aliphatic alcohols.

After the successful synthesis of various tetra-substituted phthalocyanine derivatives, the scope of the study was extended to include the preparation of octa-substituted analogues. For this purpose, 4,5-dichlorophthalonitrile was selected as the starting material and reacted with two different phenolic nucleophiles, as illustrated in **Scheme 6**.

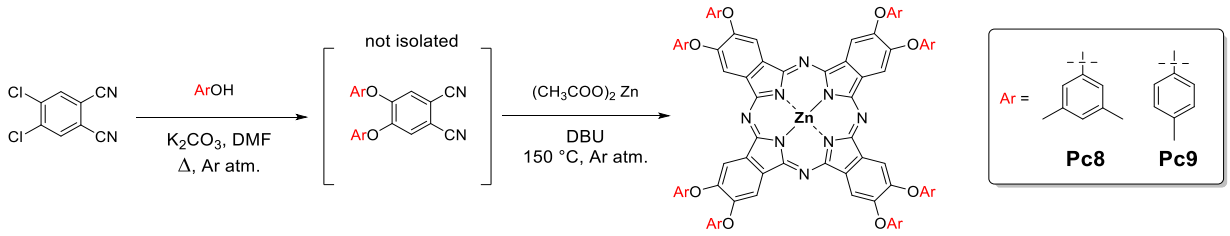

Scheme 6. Synthetic route for the synthesis of octa substituted phthalocyanines **Pc8** and **Pc9**.

A critical challenge in adapting the one-pot protocol to this system lay in the precise monitoring and control of the nucleophilic aromatic substitution step. While the initial substitution of one chlorine atom generally occurred without difficulty, the introduction of the second substituent proved considerably more challenging. This can be attributed to the combined effects of steric hindrance and electronic deactivation following the first substitution, which markedly reduce the reactivity of the second chloride leaving group. Several attempts under previously optimized conditions led to mixtures containing partially chlorinated intermediates, indicating that disubstitution was incomplete.

To address this issue, the experimental parameters were systematically adjusted by substantially increasing the reagent ratios and reaction temperature to drive the reaction to completion, as detailed in **Table 4**. The subsequent cyclotetramerization proceeded smoothly, affording the target octasubstituted zinc phthalocyanines **Pc8** and **Pc9** in 30% and 31% yield, respectively.

The structures of the target phthalocyanines were confirmed by a combination of NMR, UV-Vis, FT-IR, and mass spectrometry analysis, provided in the Experimental section.

As a matter of fact, *tetra*substituted Pcs are obtained in a mixture of four regioisomers, having point groups D_{2h}:C_s:C_{2v}:C_{4h}, according to their molecular symmetry (**Figure 7**).

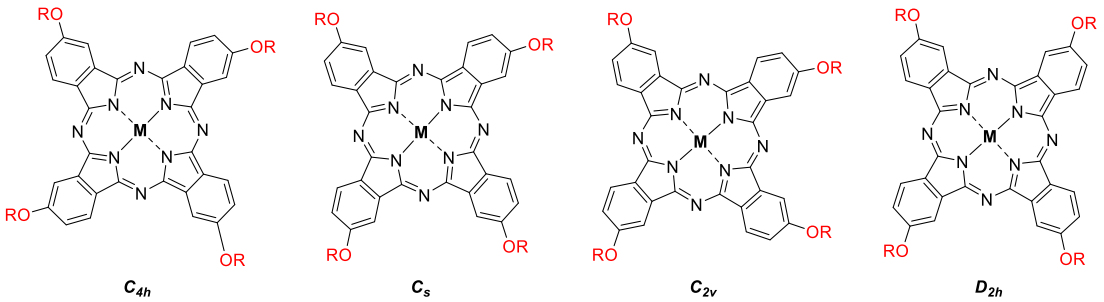

Figure 7. Regioisomers arising from tetrasubstitution of the Pc core and their symmetry point groups.

In most cases, separation of these regioisomers is not pursued, as their electronic properties are only marginally influenced by the positional isomerism of the peripheral substituents. Consequently, the mixture is often used directly in applications where these minor differences do not significantly impact performance or functionality.[62] Among the techniques used to characterize phthalocyanines, ^{1}H NMR spectroscopy proved particularly informative in highlighting this structural complexity. Indeed, the spectra of tetra substituted compounds (**Pc1**, **Pc2**, **Pc3**, **Pc5**, **Pc6**, and **Pc7**) generally display a high degree of complexity, which arises from two main factors: the lack of symmetry introduced by tetrasubstitution and the statistical formation of four possible regioisomers in variable proportions. These features result in signal broadening, splitting, and overlapping in several spectral regions.

To better illustrate this aspect, a comparative analysis of the ^{1}H NMR spectra is presented, recorded in THF-d_8, of a tetra substituted phthalocyanine (compound **Pc2**) and its octa substituted analogue (compound **Pc9**), both functionalized with 4-methylphenoxy groups (**Figure 8**).

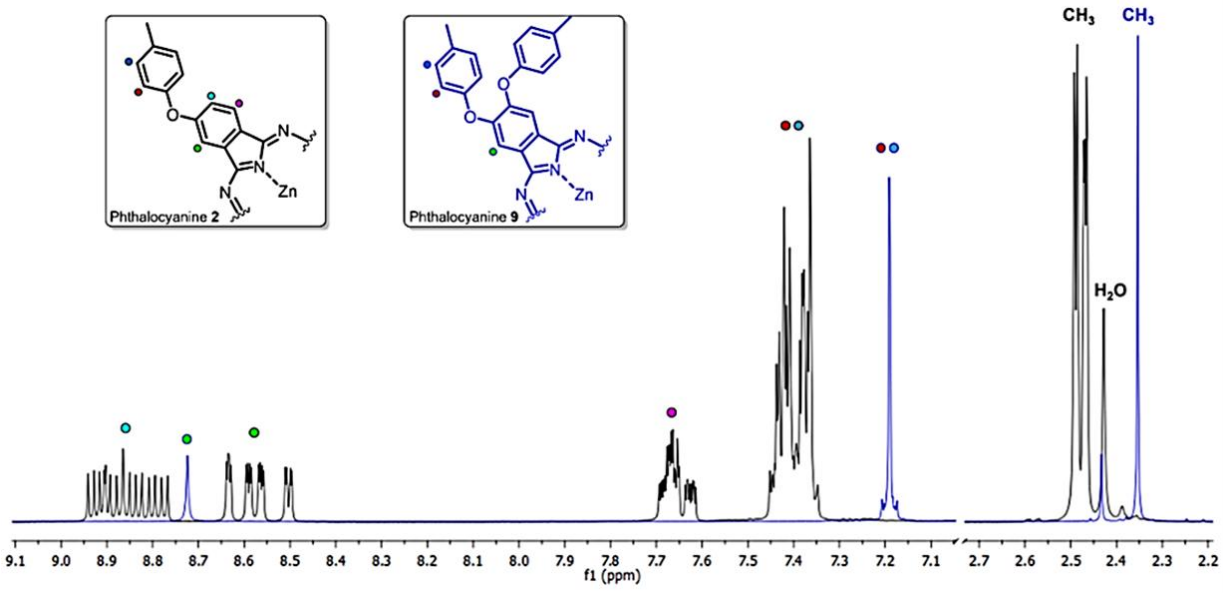

Figure 8. Comparison between ^{1}H NMR spectra of phthalocyanines **Pc2** and **Pc9** recorded in THF-d_8.

The aromatic region is particularly diagnostic: as shown in **Figure 8**, compound **Pc2** displays a dense and highly structured set of multiplets, originating from both the macrocyclic protons and the aromatic protons of the peripheral 4-methylphenoxy groups. In contrast, the octa-substituted compound **Pc9**, characterized by a higher degree of symmetry and the absence of regioisomerism, shows only two sharp signals.

Furthermore, the four aromatic protons of the 4-methylphenoxy moiety, which typically display a well-defined AA'XX' splitting characteristic of a para-substituted phenyl ring, exhibit a more complex pattern than expected. This increased complexity also extends into the aliphatic region: in compound **Pc2**, the methyl protons of the 4-methylphenoxy units appear as multiple singlets, corresponding to the different environments in the statistical mixture of regioisomers. In contrast, compound **Pc9** shows a single sharp singlet for the same methyl groups, consistent with a symmetric and chemically uniform substitution pattern. Similarly, the ^{13}C spectra of the tetra substituted compounds display a dense set of signals in the aromatic region, with each peak appearing as a cluster of closely spaced signals due to the presence of regioisomers. In contrast, the octa substituted derivatives exhibit a more defined and simplified pattern, consistent with higher molecular symmetry. This structural heterogeneity, as expected, is not reflected in the MALDI-TOF mass spectra, given that all regioisomers share the same molecular weight.

UV-Vis analysis was also used for the characterization of these molecules (**Figure 9**).

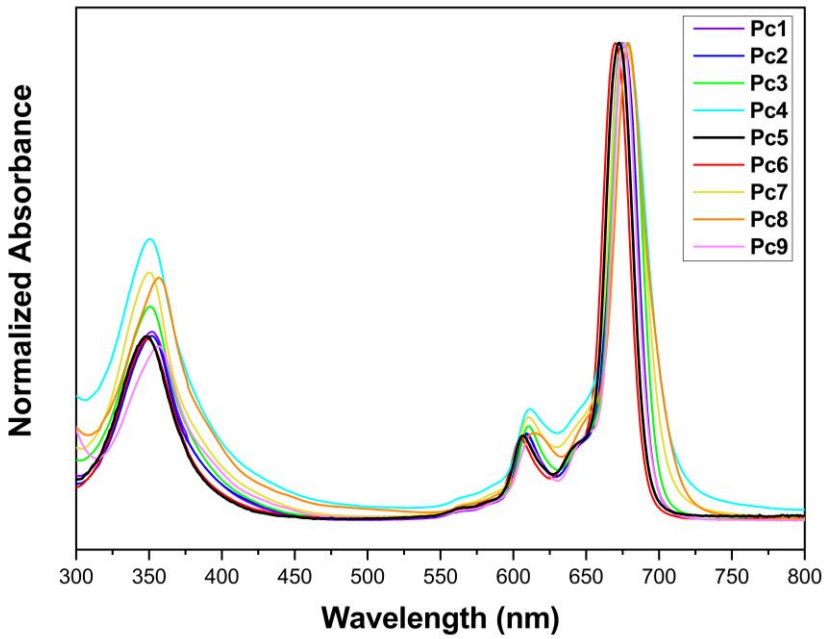

Figure 9. UV-visible spectra of the synthesized zinc phthalocyanines **Pc1-9** in THF, except for **Pc4** in pyridine.

Spectra were recorded in THF for all compounds, except for phthalocyanine **Pc4** which required pyridine to ensure adequate solubility. In all cases, the spectra displayed the characteristic features of phthalocyanine derivatives: an intense Q-band with maxima between 675 and 685 nm, typically accompanied by vibronic shoulder peaks, and a less intense Soret band centered around 350 nm. The limited variation in Q-band position across the series can be attributed to multiple factors. First, THF is a coordinating solvent capable of suppressing molecular aggregation, thereby minimizing aggregation-induced spectral shifts. Second, it is well established that substituents in the β-positions of the macrocycle exert weaker electronic effects compared to those in α-positions, resulting in a comparatively minor impact on optical absorption.

Consistently with these considerations, the variation in spectral features remained limited despite the diversity in substituent shape and electronic nature, suggesting that the

influence of the aryloxy or alkyloxy oxygen atom may dominate the overall electronic behavior.

In line with the objectives of this thesis, once the one-pot protocol had been optimized, extended to a representative series of derivatives, and the obtained compounds fully characterized, its performance was evaluated through comparison with existing literature procedures in terms of both isolated yields and environmental sustainability.

Eventually, a careful evaluation of the results obtained with the use of the new one-pot protocol in terms of yields and E-factor values has been accomplished (**Table 5**). Where possible, i.e., when the product has already been described in the literature, a comparison is made between the new synthetic procedure and the conventional two-step protocols. Notably, several derivatives reported here have no precedents in the literature, underscoring the originality and synthetic versatility of this approach.

A comprehensive evaluation of the environmental sustainability of this procedure in terms of waste generation was conducted by calculating the E-factor value for the synthesis of each phthalocyanine derivative, as summarized in **Table 5**. The E-factor (Environmental factor) is used to assess the environmental impact of a synthetic procedure, and it is defined as the ratio of the total mass of waste generated to the mass of the isolated product as the following equation:

$$E\text{-}factor = \frac{Mass\ of\ total\ waste\ (g)}{Mass\ of\ product\ (g)}.$$

It gives therefore a quantification of the mass of waste produced per unit mass of final product, thus serving as a direct indicator of the efficiency of a process with respect to waste reduction.

Water was systematically excluded from the waste count in the following calculations, in accordance with common practice in green chemistry, where it is generally not regarded as a harmful by-product. [63–65] Details about the calculation are reported in the Experimental section at the end of this Chapter.

Compound	This work			Literature			Ref.
	Yield (%)	E-factor		Total yield for two steps procedure(%)	E-factor		
		No solvent recovery	80% solvent recovery		No solvent recovery	80% solvent recovery	
Pc1	48	257.7	86.9	-	-	-	-
Pc2	43	326.2	111.3	38	1441.7	496.3	[66]
Pc3	37	556.6	176.7	-	-	-	-
Pc5	27	192.1	83.9	7	1236.7	591.6	[67]
Pc6	49	47.4	34.0	13 55	10566.8 3087.0	5320.2 1039.9	[59] [68]
Pc7	22	443.0	179.8	n/d*	n/d	-	[69]
Pc8	30	797.4	294.3	-	-	-	-
Pc9	31	751.1	289.5	-	-	-	-

Table 5. Yields and E-factor values of the aryloxy and alkyloxy zinc phthalocyanines synthesized with the new one-pot procedure compared to the two-step reported data. *Only the tetramerization yield (49%) is reported in the literature; the preceding step is not described in sufficient detail to calculate a total yield.

From a synthetic perspective, the yields obtained with the new one-pot synthesis are generally higher than those achieved for stepwise procedures. In particular, the 27% yield obtained for phthalocyanine 5 represents a substantial improvement over the previously reported value of 7% for the same compound, which holds potential for application in PDT,[67] corresponding to a 385% increase. In the few instances where the one-pot protocol led to lower yields, the method remains advantageous due to its procedural simplicity and reduced environmental impact. In the case of compound **Pc7**, although it has been previously reported, the literature provides only the yield of the tetramerization step from 4-hexyloxyphthalonitrile (49%), without sufficient detail on the preceding nucleophilic substitution. As a result, the overall two-step yield cannot be reconstructed and no meaningful comparison can be made with the new one-pot synthesis, which afforded the compound in 22% yield.

Through rigorous work-up and purification procedures, we estimate that around 80% of the organic solvents employed in the described processes are successfully recovered and reused. A notable example is the collection and repeated use of solvent mixtures from silica pad filtrations. Although slight variations in polarity may arise during recycling, the eluents remained fully suitable for comparable separations. This recovery strategy not only decreases the apparent solvent waste but also ensures a more reliable calculation of the E-factor, underscoring the sustainable character of the methodology and its efficient use of resources.

As shown, the E-factor values for the new one-pot synthesis are generally moderate, mostly below 180.0, and in some cases notably lower than those associated with the current state-of-the-art phthalocyanine syntheses.[70] It should also be emphasized that most literature E-factor values refer only to the tetramerization step, whereas the present calculation accounts for the entire one-pot process.

In cases where a direct comparison was possible, i.e. for derivatives **Pc2**, **Pc5**, and **Pc6**, E-factors obtained with the new synthesis were at least one order of magnitude lower than those calculated for the corresponding two-step protocol.

In addition, to enable a more rigorous, complete, and fair comparison between methodologies, additional E-factor values were calculated by considering an 80% solvent recovery both for this one-pot approach and the literature syntheses. The comparison clearly shows that solvent recycling exerts a large impact on reducing waste production for both traditional and one-pot methodologies. Nonetheless, even in the absence of recycling, the one-pot approach consistently displays lower E-factor values than the conventional two-step syntheses, even when the latter include solvent recovery. This demonstrates that the design of the synthetic protocol itself contributes substantially to waste reduction. When solvent recovery is applied, the superiority of the one-pot method becomes even more pronounced, reaching the lowest E-factor among all investigated scenarios.

2.2.2. Use of environmentally benign reaction media

The results presented in the following section are part of a manuscript currently in preparation for submission.

As introduced at the beginning of this chapter, a second strategy to address the ongoing challenge of synthesizing phthalocyanines through a sustainable, simple, and efficient synthetic protocol involves the use of green reaction media.

In general, solvents are extensively employed in chemical synthesis and have long been a source of concern because of the environmental and health hazards associated with their use. In particular, chlorinated hydrocarbons and aromatic solvents are characterized by toxicity and volatility, posing risks throughout their production, handling, and disposal. Despite solvent-free methodologies have been explored to mitigate these concerns, solvents remain indispensable to many organic transformations, as they ensure a homogeneous medium that promotes efficient molecular interactions and enables reactions to proceed to completion.[71,72]

Growing regulatory restrictions have led to considerable research efforts in both academia and industry toward the identification of alternative reaction media capable of combining operational efficiency with improved environmental performance.[73,74]

Water represents the most attractive solvent from an environmental perspective. However, its application is often limited by the poor solubility of organic, inherently hydrophobic substrates. The last decades have witnessed an increasing interest in searching for alternative reaction media that can serve as viable options, further beyond the new so-called "neoteric" solvents, that are emerging solvent systems such as supercritical CO_2,[75] near-critical water,[76] ionic liquids,[77] and fluorous solvents,[78] whose environmental safety remains still debatable thus limiting their broader applicability.

Within this context, it should additionally be highlighted that the identification of a solvent that can withstand the demanding reaction conditions of phthalocyanine syntheses,

such as temperatures of at least 130 °C, strongly basic and anhydrous environments, and sensitivity to oxygen that requires an inert atmosphere, while remaining environmental responsible, represents a particularly challenging task.

Solvents such as propylene glycol, anisole, glycerol, and their mixtures had been previously explored in my research group and revealed effective for more sustainable syntheses of phthalocyanines.[79,80] These solvents were able to replace conventional methods, that typically rely on high-boiling polar solvents, such as N,N-dimethylaminoethanol (DMAE), N,N-dimethylformamide (DMF), trichlorobenzene, and nitrobenzene, that are associated with significant toxicity and safety issues for both the environment and the human health, as underlined by the GSK's solvent sustainability guide, (**Figure 10**).[81]

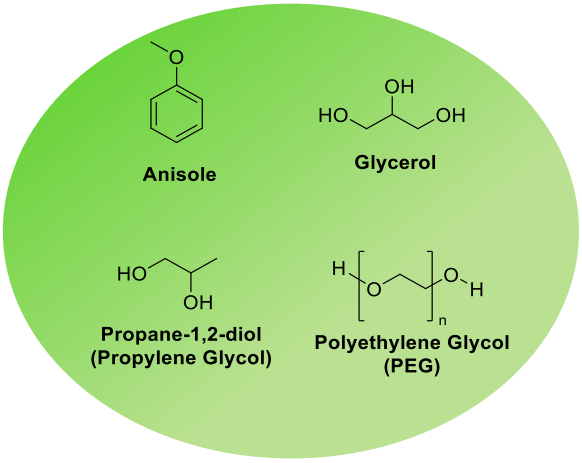

Figure 10. Examples of green solvents in organic synthesis.

Given the fact that recently liquid polymers or low melting polymers have emerged as alternative green reaction media, the investigation was extended to polyols, whose inherent versatility, distinctive polarity, thermal stability, commercial availability, nonvolatility, immiscibility with a number of organic solvents, and structural tunability, and recyclability make them a promising, yet still underexplored, class of media capable of providing a more suitable environment for robust and sustainable phthalocyanine synthesis.

Comprehensive toxicological studies support polyethylene glycol-400 (PEG-400) safe handling and disposal, further establishing its reputation as a reliable and non-hazardous

solvent.[82] PEG-400 was thus selected as a representative model polyol owing to its safety, biocompatibility, favorable physical properties, commercial availability, and cost-effectiveness, which make it a widely used and readily manageable green solvent for exploratory studies. [83,84] It is able to dissolve a wide range of substances, including both organic compounds and various inorganic salts, facilitating transformations between reactants of differing polarities. Additionally, PEG-400 can function as a phase-transfer catalyst by complexing metal cations, and promoting reactions. [85,86] Its high boiling point, thermal stability, and low vapor pressure simplify product separation by distillation or extraction, allowing reactions to be conducted at elevated temperatures with minimal solvent loss, as well as easy solvent recovery and reuse, thus minimizing waste and enhancing the sustainability of the process. [87] Moreover, PEG-400 has been documented as an efficient medium for one-pot as well as multi-component syntheses. [88]

Overall, PEG-400 emerges as a highly promising alternative to traditional organic solvents, particularly in the context of sustainable organic synthesis and its alignment with the principles of green chemistry underscores its potential to foster more sustainable practices within the chemical industry.

Firstly, the use of PEG-400 as a reaction medium for the synthesis of variously substituted phthalocyanines in solution was explored, aiming at providing a more sustainable and accessible alternative that does not require specialized equipment but rather relies on standard glassware and hot plates, basic workup and purification techniques.

Again, the synthesis of phthalocyanines under investigation were carried out using phthalonitriles as direct precursors, since this offers the advantage of high atom economy (AE), as all the phthalonitrile atoms are found in the target phthalocyanine (**Scheme 7**), limiting the atom loss to the nature of the counterion of the metal salt, if used to obtain the corresponding metal derivative.

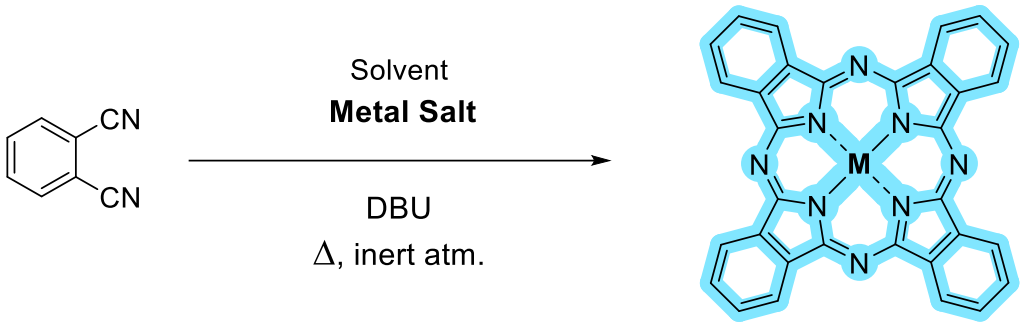

Scheme 7. Synthesis of unsubstituted metallophthalocyanine via cyclotetramerization of a phthalonitrile precursor.

As most widely established examples of the solvents traditionally employed in phthalocyanine synthesis are represented by DMAE and DMF,[65] for comparative purposes their key properties relevant to their application as reaction media are reported in **Table 6**, together with those of PEG-400. The table, developed on the basis of common Safety Data Sheets, has been designed to highlight the main differences among the three solvents, not only in terms of physical and chemical properties, but also with respect to their sustainability and safety profiles.

Category	Property	PEG-400	DMAE	DMF
Physical chemical properties	**Chemical structure**	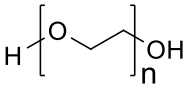 ($n \approx 8$-9)	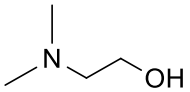	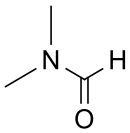
	Molecular weight (g·mol^{-1})	~380-420	89.14	73.09
	Physical state (25 °C)	Clear, viscous liquid	Clear, liquid	Clear, liquid
	Density (g·cm^{-3}, at 20 °C)	1.128	0.888	0.945
	Viscosity (mPa·s, at 20 °C)	110-125	3.8	0.8
	Polarity (dielectric constant, 25 °C)	~12[89]	~12[90]	37.6[91]

	Water solubility	Miscible	Miscible	Miscible
	Boiling point (°C)	>200	139	153
Flammability and explosion potential	**Vapor pressure (kPa, at 20 °C)**	< 0.0013	0.612	0.49
	Flash point (°C)	~235	40	58
	Autoignition temperature (°C)	-	235	445
Reactivity and stability	**Chemical stability**	Inert to bases, mild acids, incompatible with strong oxidizing agents	Incompatible with acids and strong oxidizing agents	Incompatible with reducing and strong oxidizing agents
	Physical hazards	-	H226 Flammable liquid and vapor	H226 Flammable liquid and vapor
Health	**Health hazards**	-	Severe acute and local toxicity	Reproductive toxicity
	LD_{50} oral (mg/kg, rat)	22000	1800	3000
	LD_{50} dermal (mg/kg, rabbit)	>20000	1200	1500
	LC_{50} inhalation (mg/L, 4h, rat)	-	5.97	>5.58
Environment	**LC_{50} (mg/L, 96h, freshwater fish)**	> 100	81	7.5
Composite Colour				

Table 6. Comparison of physicochemical properties of PEG-400 (Polyethylene glycol 400), DMAE (N,N-dimethylaminoethanol), and DMF (N,N-dimethylformamide) relevant to their use as reaction

media. The data are extrapolated from Safety Data Sheet by ThermoFischer Scientific, [92–94] unless otherwise stated.

Beyond the intrinsic difference between the three solvents, being PEG-400 a polyether diol and the others small polar amines or amides, and the fact that all remain liquid at ambient temperature, there are some peculiarities that deserve to be discussed. PEG-400 exhibits indeed a high boiling point (~250 °C), low volatility, and good thermal stability, making it suitable for high-temperature reactions without significant solvent loss. Its ability to dissolve a wide range of organic and inorganic compounds enables effective mixing and interaction between reagents, which is particularly beneficial for reactions involving solid substrates or poorly soluble materials.

As reported in **Table 6**, PEG-400 exhibits a relatively high viscosity, significantly greater than that of DMAE and DMF, which may pose challenges in terms of efficient substrate mixing. Nevertheless, this limitation is mitigated by the temperatures (>100 °C) at which phthalocyanine syntheses are typically conducted. At such temperatures, the viscosity of PEG-400 is substantially reduced, in line with the inverse correlation between viscosity and temperature. On the contrary, lower reaction temperatures would adversely affect the cyclotetramerization of phthalonitrile precursors into phthalocyanine products. In addition, the polar nature and hydrogen-bonding capability of PEG-400 could also stabilize reactive intermediates and improve reaction selectivity.

DMF, in contrast, has a lower viscosity and moderate boiling point (~153 °C), allowing faster diffusion and mass transport in solution. Its high polarity and excellent solvating ability for both polar and non-polar reactants make it ideal for homogeneous reactions, especially when precise control of reactant concentration is required. However, its lower boiling point necessitates careful temperature control during high-temperature reactions to prevent solvent loss. Furthermore, DMF is not fully inert although it is generally stable under many reaction conditions and may suffer from progressive decomposition triggered by strong alkali environment.

DMAE, widely used as a reference solvent for certain high-temperature syntheses, has a boiling point (~135-138 °C) compatible with the temperature used in phthalocyanine formation. Its moderate polarity and relatively low viscosity enable efficient reagent solubilization and thermal activation, while also allowing reactions to proceed under milder conditions than PEG-400. DMAE's volatility, however, require stricter temperature management during prolonged reactions.

In addition, vapor pressure PEG-400, characterized by very low vapor pressure, exhibits minimal volatility and therefore reduced atmospheric emissions, whereas DMAE and DMF, with higher vapor pressures, present a greater propensity for evaporation and potential exposure. The high flash point of PEG-400 indicates low flammability risk, while solvents with lower flash points, such as DMF, fall into more severe flammability categories according to GHS classification, reflecting increased fire hazards during handling and storage. Finally, chemical stability under normal operating conditions is very important since solvents that remain stable during storage and application, such as PEG-400, pose a lower risk of undesired side reactions compared to more reactive systems.

As far as sustainability and safety issues are concerned, **Table 6** also summarizes the main classified hazards associated with the three solvents. According to the established solvent sustainability and hazard classification criteria proposed by the GSK Solvent Sustainability Guide, and following the same methodological approach, [81] the relevant assessment categories were systematically evaluated for each solvent, leading to an overall assessment of the sustainability and safety profile, hereafter referred to as the composite score. To enable a clear and intuitive visualization of this analysis a final colour classification ("*composite colour*") was assigned, allowing each solvent to be categorised on a green, amber and red traffic light-inspired scale that reflects increasing levels of concern. Green indicates low concern, orange denotes moderate concern, and red corresponds to significant health, safety, and environmental risks.

Acute oral toxicity was evaluated using LD_{50} (median lethal dose) values and it represents the amount of a substance required to cause death in 50% of a test population following oral administration and is commonly used as a quantitative indicator of acute

toxicity. PEG-400 shows a very high LD_{50} value (22000 mg/kg) and is therefore not classified for acute oral toxicity, differently from the other solvents. Acute dermal toxicity was assessed using LD_{50} values obtained in rabbits and it represents the amount of a substance required to cause death in 50% of the test population following skin exposure and provides an estimate of acute toxicity upon dermal contact. PEG-400 exhibits a very high dermal LD_{50} value (>20000 mg/kg) and is therefore not classified for acute dermal toxicity. DMAE and DMF, with LD_{50} values of 1200 and 1500 mg/kg, respectively, fall within GHS Acute Toxicity and are classified as moderate concern. Acute inhalation toxicity was evaluated using LC_{50} (median lethal concentration) values determined in rats over a 4 h exposure period and it represents the airborne concentration of a substance expected to cause death in 50% of the exposed test population and is commonly used to assess acute toxicity via inhalation. PEG-400 is not classified for acute inhalation toxicity according to SDS information. Acute aquatic toxicity was evaluated using LC_{50} values determined for freshwater fish over 96 h. It is the median lethal concentration and represents the concentration of a substance expected to cause death in 50% of the exposed aquatic population within a defined period, serving as a standard measure of acute aquatic toxicity. PEG-400 is not classified for acute aquatic toxicity, whereas DMAE exhibits moderate toxicity, and DMF shows significant toxicity, highlighting potential environmental concerns associated with the latter.

Overall, in this scheme, PEG-400 achieves the most favourable classification (green as the composite colour) and emerges as the safest and most sustainable solvent among those evaluated, showing minimal health and ecological hazards and strong alignment with Green Chemistry Principles. On the other hand, DMAE and DMF exhibit severe human health and environmental hazards, especially DMF due to its reproductive toxicity, that require careful consideration and management. In this respect, **Table 6**, is not intended solely to compare solvents within the specific context of phthalocyanine synthesis, but also to illustrate how a systematic, category-based comparison can assist in identifying more sustainable solvent alternatives for a given reaction. This approach is consistent with the methodology adopted in the GSK Solvent Sustainability Guide and aims to provide researchers with a balanced and informative framework, thereby fostering the evaluation

and implementation of greener solvents, even when their application in specific synthetic processes is not yet fully established.

The enhanced sustainability and safety profile of PEG-400, together with its intrinsic physicochemical properties such as its low volatility, low flammability and chemical and thermal stability, that ensure good compatibility with phthalocyanine syntheses, renders it a particularly attractive candidate for further investigation in this application.

The synthesis of a representative substituted metallophthalocyanine was selected as a model reaction to preliminarily evaluate the use of PEG-400 as the sole reaction medium. Starting from 4-*tert*-butylphthalonitrile in the presence of the base and the appropriate metal salt, the reaction conditions were then optimized, including the amount of reagents and the temperature setting, to promote the cyclotetramerization and afford the resulting tetra-*tert*-butyl zinc phthalocyanine (**Scheme 8**). DBU was employed as the base and zinc acetate as the metal salt. The syntheses were generally conducted at 140 °C, a temperature selected to match the reflux point of N,N-dimethylaminoethanol (DMAE, boiling point 135-138 °C), a well-established reference solvent for this type of process, so that consistency with reported conditions was ensured while using an alternative reaction medium.

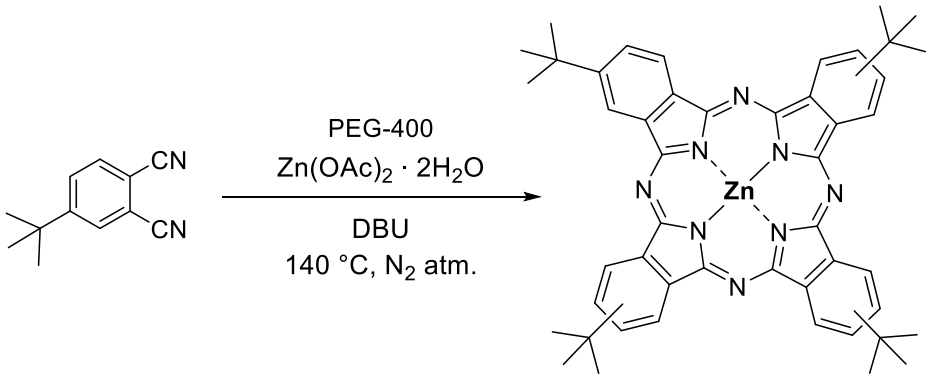

Pc10

Scheme 8. Cyclotetramerization of *tert*-butyl phthalonitrile to the target tetra-*tert*-butyl zinc phthalocyanine **Pc10** in PEG-400.

In the pursuit of enhancing the appeal of phthalocyanine synthesis in solution within the sustainable and environmentally benign framework of PEG-400, the reaction time was fixed at 6 hours, after which the mixture was cooled, quenched, and subjected to standard work-up procedures. This reaction time was established based on prior reports where metal-templated phthalocyanine syntheses were successfully conducted over comparable timescales, [31] while also representing a pragmatic compromise between environmental sustainability and temporal feasibility. Indeed, it is noteworthy that several mechanochemical syntheses of phthalocyanines have been reported to proceed within only a few minutes.[5] The present work aims therefore to evaluate whether a green solvent-based synthesis could achieve similar reliability and practicability. The outcomes in terms of isolated yields of the case study performed on the model compound are reported in **Table 7**, while varying the equivalents of solvent compared to that of the starting material and the amount of base.

Entry	PEG-400 (eq)	DBU (eq)	Isolated yield (%)
1	3.8	0.2	66
2	1.9	0.2	70
3	**1.0**	**0.2**	**77**
4	0.5	0.2	73
5	0.0	0.2	68
6*	1.0	0.00	48
7	1.0	0.1	58
8	1.0	0.3	69
9	1.0	0.4	72

Table 7. Variation of experimental parameters for the synthesis of **Pc10**, such as the equivalents of solvent compared to that of the starting material, the amount of base and the related yields. General conditions: PEG-400, 4-*tert*-butylphthalonitrile (2.71 mmol), $Zn(OAc)_2$ dihydrate (0.26 eq) treated on hot plate prior to use, T = 140 °C for 6h. * Reaction time 24h.

At first, the reaction progress was investigated as a function of the amount of solvent. Optimal results were achieved when the amount of PEG-400 was approximately equimolar to that of 4-*tert*-butylphthalonitrile (entry 3). A further reduction led to insufficient stirring and a heterogeneous reaction environment, thereby potentially undermining reproducibility under the same conditions (entry 4). By extending the concept to its extreme case, we found that the reaction could also proceed under solvent-free conditions; however, this resulted in a lower yield (entry 5).

After establishing the optimal reagent-to-solvent ratio, we investigated the effect of varying the amount of base. While the reaction could still occur with small amounts or even in the absence of DBU (entries 6, 7), the modest yield obtained under free-base conditions, even after prolonged reaction times, suggests that DBU exerts a beneficial activating effect on the nitrile groups. Interestingly, the positive influence of DBU peaked at 0.2 equivalents, beyond which the yield gradually decreased. This decline can be attributed to multiple concurrent effects. First, at high DBU concentrations, the basic additive may alter the microenvironment of PEG-400, acting as a co-solvent and increasing medium viscosity, which could hinder efficient mass transfer and diffusion of reactive intermediates. Second, unfavourable DBU-nitrile interactions may occur at elevated temperature, leading to the formation of stable adducts that compete with the coordination of zinc(II) or otherwise suppress the availability of reactive nitrile groups. Collectively, these observations indicate that DBU plays a dual role: it beneficially assists in the activation of nitrile groups at low concentrations, but in excess it perturbs the delicate balance of interactions required for efficient macrocycle formation, highlighting the importance of maintaining catalytic amounts of base to ensure high efficiency and at the same time aligning with green chemistry principles.

Subsequently, we also explored the influence of temperature on the reaction yield (**Table 8**). This investigation proceeded in parallel with the conversion of the reagent. Indeed, in all cases where the starting material was not completely consumed, 4-*tert*-butylphthalonitrile could be efficiently recovered by washing the crude product with a 2:1 methanol/water mixture, followed by evaporation of the organic phase. The resulting solid was diluted in

few millilitres of dichloromethane and extracted with a 10% w/w K_2CO_3 solution to remove any phthalimide-based byproduct. Therefore, this procedure enabled an accurate evaluation of reagent conversion, while facilitating the reuse of the recovered starting material in subsequent reactions, thereby contributing to improved resource efficiency.

Entry	T (°C)	Time (h)	Recovered phthalonitrile (mg)	Isolated yield (%)
10	125	24	33.7	75
11	115	24	95.9	66
12	100	30	156.0	48
13*	140	24	90.0	69

Table 8. Optimization study regarding the reaction temperature and time, precursor conversion and related yields for the synthesis of **Pc10**. General reaction conditions: 4-*tert*-butylphthalonitrile (2.71 mmol), PEG-400 (1 eq), DBU (0.2 eq), $Zn(OAc)_2$ dihydrate (0.26 eq) treated on hot plate prior to use. *Reaction performed in air atmosphere.

Phthalocyanine synthesis is typically carried out at high temperatures (130 - 250 °C), making protocols that allow product formation under milder conditions particularly attractive. In an attempt to further enhance the sustainability of the procedure and to explore the feasibility of the system to lower temperatures, we tried to perform the reaction at 125 °C. Interestingly, comparable yield to that of the optimized reaction was obtained, albeit at the cost of longer reaction times from 6 hours to 24 hours (entry 10). While the 15 °C temperature reduction (from 140 °C to 125 °C) is beneficial in terms of energy efficiency, the longer reaction time partially offsets this advantage. The reaction also proceeded at 115 and 100 °C, requiring 24 hours to proceed and achieving the product in modest yield (entries 11, 12), with a substantial amount of unreacted phthalonitrile remaining at 100 °C. Therefore, **Table 8** also provides insight into the recovery of unreacted 4-*tert*-butylphthalonitrile under different reaction conditions, highlighting a clear correlation between reaction temperature

and conversion. Reducing the temperature from 125 to 100 °C leads to a progressive increase in the amount of recovered starting material, accompanied by a corresponding decrease in product yield. Even upon extending the reaction time to 30 h at 100 °C, incomplete conversion was observed, indicating that temperature exerts a more significant role than reaction time in driving the formation of the phthalocyanine ring.

Finally, to evaluate whether the synthesis could be performed without the need for an inert atmosphere, the reaction was carried out in air (entry 13), yielding 69%. This indicates a non-negligible tolerance to oxygen under these conditions. Nevertheless, inert atmosphere remains preferable to maximize reproducibility and yield. This observation is consistent with the well-known reactivity of oxygen, which can promote side reactions through oxidation of the nitrile groups in phthalonitrile, thereby reducing the amount of precursor available for cyclotetramerization.

Furthermore, PEG-400 exhibits well-documented recyclability and reusability, representing a significant advantage from both environmental and practical standpoints. Indeed, its high solubility in water and several organic solvents including alcohol and acetone instead of in less polar solvents such as hexane render it easy to recover. [95]

Given that solvents typically constitute the largest contribution to process waste,[96] the possibility of recovering and reusing PEG-400, after its use as a reaction solvent, is particularly attractive for minimizing and substantially reducing the environmental footprint of a chemical process, while strongly supporting circular economy principles. PEG-400 has been shown to be readily recoverable through straightforward operations such as distillation or solvent extraction, and literature works demonstrate that the recovered solvent retains its functional efficiency and can be successfully reused in subsequent reactions without any measurable loss in yield or performance. [71] Importantly, such recovery and reuse strategies are fully compatible with standard organic chemistry laboratories and can be readily integrated into routine synthetic workflows without the need for specialized equipment or energy-intensive infrastructure, making PEG-400 a practically accessible green solvent option. By contrast, the same considerations do not apply to DMF, which presents intrinsic limitations that significantly compromise its

sustainability profile. In addition to its lower thermal stability, with decomposition occurring near its boiling point to form methylamine and carbon monoxide, DMF also forms azeotropes with water.[97] Since water is commonly employed during work-up procedures to remove solvents from crude reaction mixtures, this distinction is critical. While PEG-400 can be readily separated from the aqueous phase, DMF-water separation remains considerably more challenging, due to its azeotropic behaviour. Consequently, despite its extensive use in industry and pharmaceutics,[98] DMF recovery typically requires specialized separation methods, [99] since conventional distillation is insufficient to effectively overcome the DMF-water azeotrope limitation. These constraints limit its suitability within a circular economy framework and further underscore the clear sustainability advantage of PEG-400 in comparative solvent assessments.

On this basis, a solvent recovery test was performed using PEG-400 as the reaction medium in a representative model reaction. After completion of reaction and work-up, the precipitated target product could be separated from the reaction mixture by filtration. The aqueous filtrate was then vacuum distilled to recover PEG-400 from water, due to its limited volatility at moderate temperatures.[73]

To ascertain the applicability and limitations of this new optimised method, the syntheses of several representative derivatives were performed using the previously established reaction conditions (**Table 9**). For the purposes of this study, all the following reactions have been conducted at 140 °C, and under an inert atmosphere.

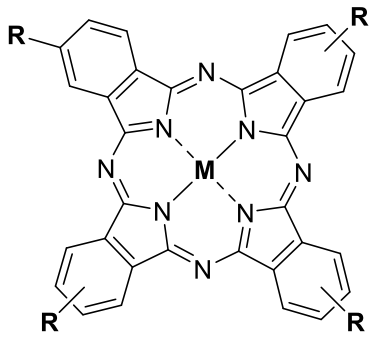

Pc 3, 10-17

Phthalocyanine	M	R	Isolated yield (%)
Pc10	Zn		77
Pc11	Co		73
Pc12	Cu		59

Pc13	Ni		64
Pc14	2H		50
Pc15	Co	H	83
Pc3*	Zn	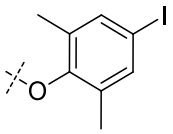	73
Pc16	Co	I	74
Pc17	Zn	I	76

Table 9. Expansion of the scope for the synthesis of **Pc 3, 10-17** using the optimized reaction conditions: phthalonitrile precursor, PEG-400 (1 eq), DBU (0.2 eq), T = 140 °C, metal salt (0.26 eq) treated on hot plate prior to use. * PEG-400 amount is 1.85 equiv.

The optimized procedure proved useful also for the synthesis of various metallophthalocyanines. For an identical phthalocyanine core, upon variation of the central metal ion, significant differences in reactivity and yield were observed, with consistently good yields for most metal salts tested, except for copper, which performed significantly less efficiently under the same reaction conditions.

The phthalocyanines thus obtained were characterized with the spectroscopic techniques for organic molecules (NMR and mass spectrometry), reported in the Experimental section at the end of this Chapter. **Figure 11** shows the UV-Visible spectra of **Pc 10-18** recorded in THF, clearly indicating the typical UV-Vis absorption profile of phthalocyanines with the characteristic Q and Soret bands.

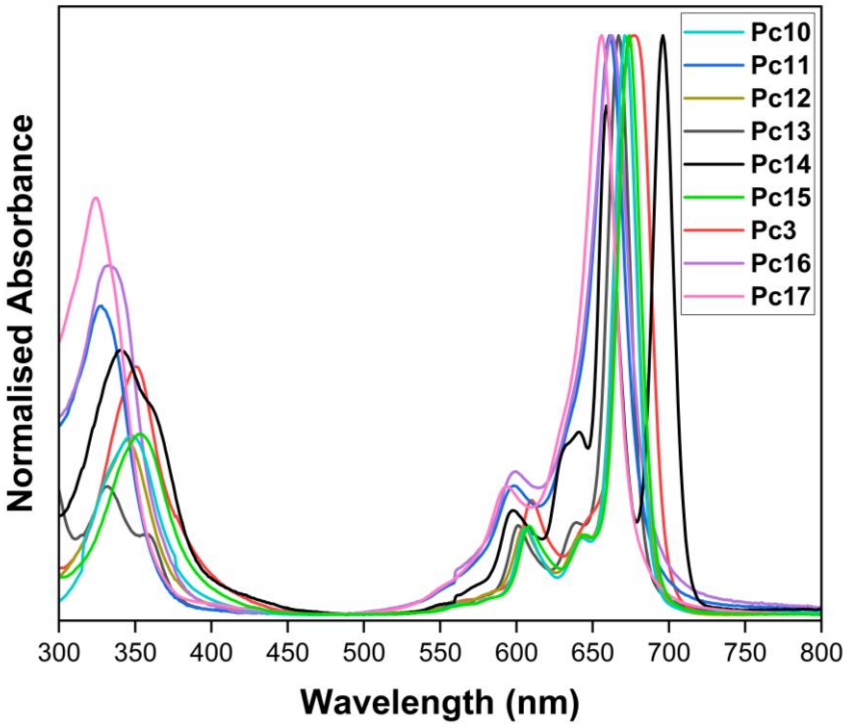

Figure 11. UV-Vis spectra of **Pc 3, 10-17** in THF.

Overall, expanding the analysis to the literature values of tetra-*tert*-butyl metallophthalocyanine synthesis, the yields obtained using PEG-400 as the reaction medium are comparable to, and in several cases significantly higher than, those reported for analogous procedures carried out in DMAE with DBU as the base. [79,100] This trend is particularly evident for metal ions such as zinc, which is generally associated with lower reactivity and reduced yields under DBU-assisted conditions. With such procedure, even this metal displays enhanced efficiency, leading to a more effective conversion of the starting phthalonitrile into the corresponding phthalocyanine. Remarkably, the metal-free derivative can likewise be obtained under these conditions, whereas literature protocols generally rely on refluxing the phthalonitrile in pentanol in the presence of lithium.[101] It is worth noting that these promising results were achieved despite the relatively high viscosity of PEG-400 that was, as expected, largely mitigated at the temperatures employed (140 °C), thereby significantly reducing its impact on reaction efficiency. Under these conditions, the combined effect of viscosity and temperature may even favour it to some extent by

stabilizing metal-coordinated intermediates and promoting macrocycle formation. The observed advantage cannot be straightforwardly ascribed to differences in solvent polarity, as the dielectric constants of PEG-400 and DMAE are comparable, as reported in **Table 6**, but it is most plausibly attributed to enhanced coordination of the solvent to the metal ion, which increases the solubility of the metal salt in the reaction medium and, in turn, promotes more effective templating during macrocycle formation.[102]

Consistently with the behaviour commonly observed for cyclotetramerizations of phthalonitriles bearing substituents at the 4-position, the resulting tetrasubstituted phthalocyanines are obtained as mixtures of regioisomers, corresponding to the different point-group symmetries D_{2h}, C_s, C_{2v}, and C_{4h}.

On the basis of these results, with regard to peripheral substitution, this procedure where PEG-400 was employed in combination with DBU proved to be highly versatile and broadly applicable to several different phthalonitrile derivatives bearing electron-donating substituents, enabling the synthesis of a wide range of metallophthalocyanines in consistently good yields. However, minor adjustments of the reaction conditions, such as operating at lower substrate concentrations to improve reagent processability, were in some cases required to achieve optimal results.

The material efficiency of the investigated synthetic procedures was evaluated using the E-factor, that has already been described in the previous paragraph. The calculations for all the synthesized molecules are summarized in **Table 10**. E-factors are reported excluding water, in accordance with literature conventions.[63] To give an insight of the actual waste generated, **Table 10** provides both the net E-factor values and the values when solvent recovery and reuse were experimentally implemented (in brackets). Details about the calculation are reported in the Experimental section at the end of this Chapter.

Phthalocyanine	Metal ion	Substituent	E-factor [solvent recycling*]
Pc10	Zn		123.0 [73.7]
Pc11	Co		76.2 [20.2]
Pc12	Cu		135.8 [103.9]
Pc13	Ni		715.6 [553.3]
Pc14	2H		190.5 [58.4]
Pc15	Co	H	68.5 [13.4]
Pc3	Zn	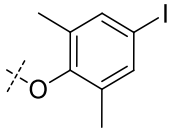	280.1 [104.1]
Pc16	Co	I	271.1 [60.6]
Pc17	Zn	I	234.7 [53.0]

Table 10. E-factor values calculated for **Pc 3, 10-17**. *Values reported in brackets refer to net E-factors calculated by accounting for solvent recovery and reuse, when experimentally implemented. Details on solvent recovery procedures and recovered amounts are provided in the Experimental section at the end of this Chapter.

For molecules synthesized from the same amount of precursor (in mmol), such as compounds Pc **10-14**, meaningful comparisons can be drawn. Compounds with comparable yields, such as **Pc10** and **Pc11** (77% and 73%, respectively), nevertheless display markedly different E-factor values, primarily due to differences in purification strategy, since the cobalt derivative did not require silica-gel filtration. Comparison of **Pc11** with the corresponding copper derivative (**Pc12**, 59% yield) further highlights that, as expected, higher yields translate into lower E-factors when comparable purification protocols, i.e. in the absence of silica gel filtration, are employed. In contrast, the calculated values for

compound **Pc13** are noticeably higher than for the other derivatives, as achieving sufficient purity in this case required full column chromatography with gradient elution, resulting in increased material consumption.

Analogous considerations regarding reaction yields apply to phthalocyanines **Pc16** and **Pc17**, which were obtained in comparable yields (74% and 76%, respectively).

The particularly low E-factor observed for compound **Pc15** upon solvent recovery can be attributed to its poor solubility, which enables purification by Soxhlet extraction of impurities using methanol; notably, this solvent was recovered at approximately 90%.

To further validate the practicality of this PEG-400-based developed protocol, since most of these reactions were carried out at small scale (500 mg of the starting material), its potential scaling-up was investigated. A multigram-scale experiment was therefore performed using phthalonitrile (5 g, 39 mmol) employing PEG-400 15.6 g, DBU 1.17 mL, cobalt acetate tetrahydrate (11 mmol, 2.534 g) and stirring for 6 hours at 140 °C under nitrogen atmosphere (**Scheme 9**). The corresponding phthalocyanine derivative **Pc15**, which can be clearly seen in the vial in **Scheme 9**, was thus isolated in 79% yield (4.4 g), after a straightforward purification, showing no significant loss in reaction efficiency nor any negative effect on the yield.

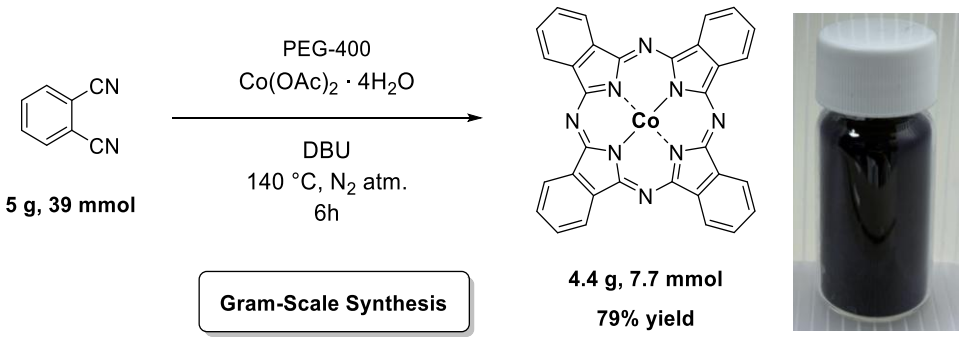

Scheme 9. Scale-up synthesis of **Pc15**.

This successful scale-up to the multigram level underscores the robustness and operational simplicity of this new PEG-based protocol, demonstrating its suitability for

preparative-scale synthesis and its potential relevance for preparative and industrial applications.

To further advance this research, and given the well-documented compatibility of this solvent with palladium-catalyzed reactions, PEG400 was explored as a reaction medium for Sonogashira and Suzuki couplings, as an exploratory step that still requires further validation. The main goal was to merge the one-pot synthetic concept with the use of a reaction medium characterized by a low environmental and toxicological impact for the preparation of more complex functionalized derivatives.[103,104]

The strategy relies on a pot-economical sequence in which a suitably functionalized phthalonitrile is first cyclotetramerized and subsequently subjected to *in situ* cross-coupling reactions without isolation of intermediates (**Scheme 10**). Furthermore, the preparation of derivatives bearing protected triple bonds is particularly attractive, as these motifs have shown promise as hole-transport materials in perovskite solar cells.[105]

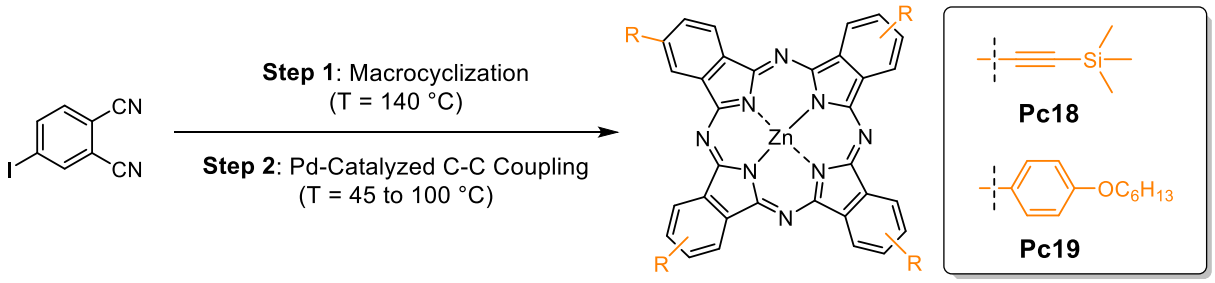

Scheme 10. One-pot approach to obtain **Pc18** and **Pc19**.

For the Sonogashira reaction, ethynyltrimethylsilane (TMSA) was employed as the alkyne partner.

The Suzuki–Miyaura reaction was investigated using commercially available 4-hexyloxyboronic acid to probe the compatibility of the system with this type of transformation. Because the use of potassium carbonate required water as a co-solvent, phase compatibility became a key factor. In this context, 2-methyltetrahydrofuran (2-

MeTHF), a sustainable solvent, proved suitable as it helped maintain solubility of the phthalocyanine while remaining partially miscible with water.

These preliminary observations support the feasibility of the coupling under the investigated conditions. These experiments were therefore mainly intended as a proof of concept to assess the compatibility of the pot-economical strategy with additional cross-coupling reactions.

A further exploratory sequence involving silyl deprotection followed by a second Sonogashira coupling was also attempted in a one-pot fashion (**Scheme 11**).[106–108]

In addition, upon deprotection of the silyl group, the resulting product could serve as a versatile intermediate for further functionalizations, including click reactions, enyne or diyne metathesis, and additional Sonogashira couplings.

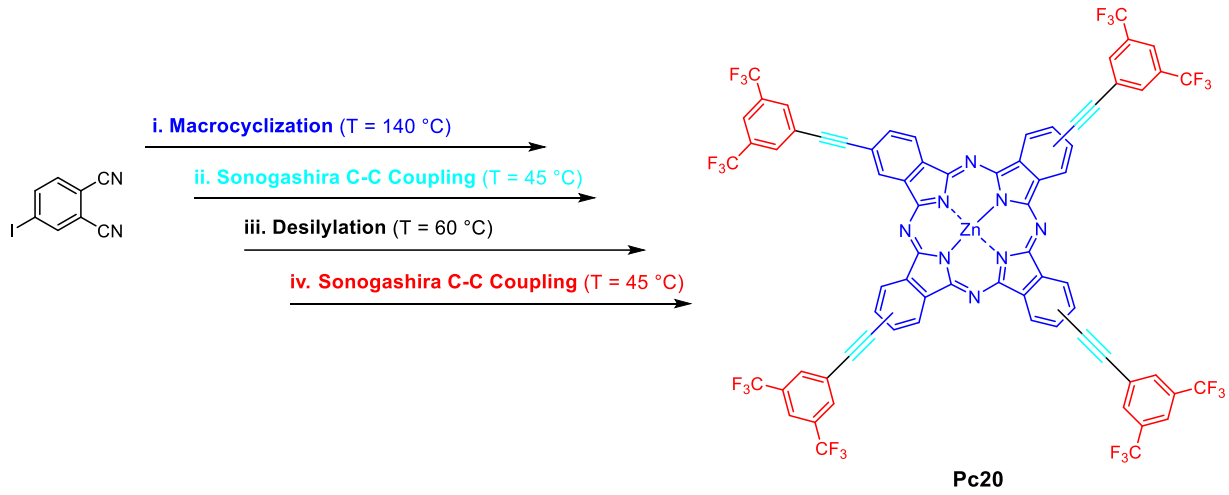

Scheme 11. One-pot approach to obtain compound **Pc20**.

Spectroscopic analyses suggested the formation of the functionalized phthalocyanine derivative, as indicated by the characteristic UV-Visible absorption of the macrocycle (**Figure 12**).

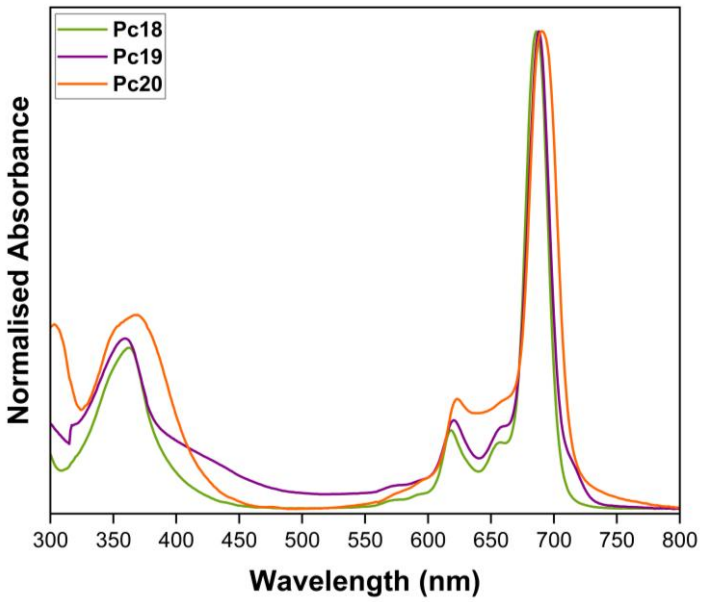

Figure 12. Normalized UV-Vis spectra of **Pc 18-20** recorded in THF.

Mass spectrometric signals consistent with the expected product are reported in the Experimental section at the end of this Chapter.

These results provide a preliminary proof of concept for the use of PEG-400 in the synthesis of more complex phthalocyanine derivatives, which require specific conditions and multiple reaction steps. While the optimization of reaction conditions and purification procedures will be addressed in future studies through a more thorough investigation, these initial experiments demonstrate that PEG-400 is generally compatible with common organic cross-coupling reactions, such as Sonogashira and Suzuki couplings. For these reasons, for these compounds only the initial spectroscopic data are reported in the Experimental section and green chemistry metrics have not been reported.

2.3. Conclusions

In conclusion, this chapter has explored two main strategies for the long-standing synthetic challenge of affording peripherally functionalised metallophthalocyanines in more sustainable ways: the one-pot approach and the use of less environmentally impactful solvents.

In the first case, a practically accessible methodology for the synthesis of tetra and octa substituted aryloxy- and alkyloxy zinc phthalocyanines has been successfully developed. The protocol demonstrated to tolerate a broad range of nucleophiles, affords nine compounds in moderate yields (22-49%), and in most cases avoids intermediate isolation and column chromatography, highlighting its operational simplicity and practicality. Comparative analysis with conventional two-step procedures demonstrates improved or comparable synthetic performance alongside a marked reduction in waste generation, as confirmed by significantly lower E-factor values.

The enhanced environmental profile of this method, assessed through the quantitative calculation of green chemistry metrics, is accounted for the synergistic contribution of the one-pot design together with the streamlined purification steps and the possibility of solvent recovery, underscoring not only the environmental but also the economic advantage of this approach, and offering a practical alternative implementable in routine laboratory settings, relying solely on conventional heating and standard laboratory glassware.

Regarding the second strategy, glycerol, anisole, and PEG-400 have been explored as sustainable and versatile alternative to conventional high-boiling polar solvents in the synthesis of variously substituted and unsubstituted metallophthalocyanines. In particular, PEG-400 has emerged as an operationally robust, versatile, recyclable, and scalable reaction medium, offering a practical and more sustainable platform for the synthesis of variously metallophthalocyanines bearing different substituents at the periphery of the ring.

Furthermore, it has been demonstrated as a proof of concept the likely successful use of this reaction medium in the multi-step cross-coupling transformations for the synthesis of highly functionalized phthalocyanine derivatives and related advanced materials.

Importantly, the sustainability gains achieved at the level of material synthesis extend beyond the laboratory scale, positively impacting the environmental footprint of the devices in which these materials are implemented, a perspective that will be addressed in the next chapter.

2.4. Experimental section

2.4.1. Materials

All the glassware used was oven-dried at 110 °C for at least 24 hours prior to use. All reagents and solvents were purchased from Merck Life Science, TCI Chemicals, and Carlo Erba Reagents and used without further purification. 4-Iodophthalonitrile was purchased and purified by column chromatography using DCM as the eluent, whereas 4-(4-iodo-2,6-dimethylphenoxy)phthalonitrile was synthesized according to a previously reported green procedure, for which sustainability and cost assessments have already been described.[109] N,N-Dimethylformamide was used freshly distilled. PEG-400 was stored on 3Å molecular sieves. Reactions were monitored by thin-layer chromatography (TLC) employing a polyester layer coated with 250 mm F254 silica gel. Chromatographic filtrations, when needed, were performed using silica gel 60A 35–70.

2.4.2. Instrumentation

NMR spectra were recorded on a Bruker AVANCE 600 NMR spectrometer operating at a proton frequency of 600.13 MHz; chemical shifts (δ) are given in ppm relative to the residual solvent peak of the deuterated solvent. Infrared spectra were recorded on a Shimadzu FT-IR prestige-21 spectrometer (Kyoto, Japan) using an attenuated total reflectance (ATR) unit. UV-Vis spectra were recorded on a Perkin-Elmer Lambda 950 UV-vis/NIR spectrophotometer. MALDI-TOF spectra were recorded at Toscana Life Science facility in a MALDI-TOF/TOF Ultraflex III (Bruker). High-resolution mass spectroscopy (HRMS) measurements were performed using an Orbitrap Exploris 120 mass spectrometer (ThermoFisher Scientific) coupled to an atmospheric pressure matrix-assisted laser desorption/ionization (AP-MALDI (ng)) ultra-high resolution (UHR) ion source (MassTech Inc.). Instrumental setup and sample preparation are described elsewhere.[110]

2.4.3. General procedure for solvent recovery

For each reaction, to minimize the amount of DMF and DBU in the recoverable mixture, we removed it separately during the filtration of the quenched reaction (with 1 N HCl), followed by washings with water. Then, the mixed water-methanol waste generated from crude and product washings in several reactions was collected into a single flask to reach a working volume of approximately 150–200 mL, suitable for distillation. Methanol does not form binary azeotropes with water and was therefore recovered using a standard distillation setup (atmospheric pressure) equipped with a Vigreux column to improve separation efficiency.

Individual solvents employed for washings were recovered by simple atmospheric distillation according to their boiling points, discarding the initial and final fractions of the distillate.

For each filtration, the solvent mixtures were recovered individually for the filtration on silica pad of each reaction by collecting the packing solvent, deposition solvent, and eluted fractions. Eluted fractions corresponding to the desired product were collected together and concentrated to dryness using a rotary evaporator, discarding only a small initial fraction. The recovered solvent mixtures were reused in subsequent filtrations, adjusting the volume when necessary, with freshly prepared solvent mixtures of the same nominal composition. Since the separation is relatively simple, phthalocyanines being the only macrocyclic products and polar impurities remaining at the baseline (Rf ~ 0), the choice of eluent does not require a narrow polarity window, provided that it is not so polar as to co-elute the polar impurities with the target compound.

2.4.4. Green Chemistry metrics calculation

The E-factor (Environmental factor) is used to assess the environmental impact of a chemical process and is defined as the ratio of the total mass of waste generated to the mass of the isolated product.

General equation for the calculation of E-factor:

$$E\text{-}factor = \frac{Mass\ of\ total\ waste\ (g)}{Mass\ of\ product\ (g)}$$

In all calculations, water is excluded from the waste count. This exclusion is consistent with standard practices in green chemistry, where water is typically not considered a harmful by-product.[63]

An estimated 80% of the organic solvents used in the processes described in our paper are recovered and reused, thanks to careful work-up and purification procedures. In particular, solvent mixtures employed in silica pad filtrations are collected and reused multiple times. Although slight variations in polarity may occur upon reuse, the recycled eluents remained suitable for similar separations. This solvent recovery significantly reduces the amount of waste attributed to the process, leading to a more accurate and representative E-factor. The approach reflects an emphasis on sustainability through the minimization of solvent waste and the efficient use of resources.

For literature-reported procedures in which complete experimental details were not available, reasonable approximations were employed to estimate the E-factor, most of which were derived from established sources:[64,70]

- It was assumed that crude products obtained from 1.0 g of starting material would require two washes with 20 mL of water or aqueous solvent mixtures, as well as two washes with 15 mL of organic solvents.
- In cases involving solvent extraction, it was estimated that three separate extractions with 50 mL of organic solvent (totaling 150 mL), along with 1 g of a drying agent such

as Na_2SO_4 or $MgSO_4$, would be necessary to isolate 1 g of crude product from the reaction mixture.

- For crystallization steps, it is assumed that 100 mL of solvent are required to isolate 1 g of product, with the procedure performed only once.
- For purifications involving column chromatography, the processing of 1 g of product was assumed to require 400 mL of eluent and a silica gel column packed with 263 g of 60 μm silica gel, as previously reported under ideal conditions (i.e., efficient separation with Rf > 0.3 and optimal sample loading).[111]
- The density of all aqueous solutions (e.g. HCl 1N or aqueous salt solutions) was approximated to 1.0 g/mL.

These standardized approximations were consistently applied across all procedures to facilitate direct comparison while preserving realistic estimates of material consumption and waste production.

2.4.5. General one-pot procedure for the synthesis of tetra-substituted-zinc phthalocyanines Pc 1-7

Phenol/alcohol (1.0 eq) and anhydrous K_2CO_3 (3 eq) were stirred in 4 mL of DMF at room temperature for 30 minutes. Then, 4-nitrophthalonitrile (1 eq, 0.5 g) was added in one portion and the reaction mixture was stirred at the chosen temperature until the complete disappearance of 4-nitrophthalonitrile was confirmed by TLC. Zinc acetate dihydrate (0.27 eq), pre-dried in an oven at 110°C for at least 6 hours, and DBU (1 eq) were then added and the reaction mixture was stirred at 140°C under argon atmosphere until completion of the reaction. After quenching with HCl 1M, the resulting precipitate was filtered, washed with water and methanol, and dried under vacuum.

2.4.6. General one-pot procedure for the synthesis of octa-substituted-zinc-phthalocyanines Pc8 and Pc9

Phenol (3.1 eq) K_2CO_3 (3 eq) were stirred in 4 mL of DMF at room temperature for 30 minutes. Then, 4,5-dichlorophthalonitrile (1 eq, 0.2 g) was added and the reaction mixture was stirred at 100 °C until its complete disappearance was observed by TLC. Zinc acetate dihydrate (0.27 eq), pre-dried in an oven at 110°C for at least 6 hours, and DBU (1 eq) were then added and the reaction mixture was stirred at 150 °C under argon atmosphere until completion of the reaction. After quenching with HCl 1M, the resulting precipitate was filtered, washed with water and methanol, and dried under vacuum.

2.4.7. General procedure for the optimized cyclotetramerization of phthalonitriles in PEG-400

The desired phthalonitrile (1.0 eq), PEG-400 (1.0 eq), DBU (0.2 eq), and the appropriate metal salt (0.26 eq) were charged into a 10 mL one-necked round-bottom flask equipped with a magnetic stirrer under a nitrogen atmosphere. The reaction mixture was heated at 140 °C for 6 h, during which it changed color from a clear, colorless solution to dark blue. After cooling to room temperature, the mixture was treated with 1 N HCl, diluted with methanol, and the resulting solid was collected by filtration. The solid was subsequently washed with methanol or methanol/water mixtures. When required, further purification was achieved by repeated washings with suitable solvents or by filtration through a short pad of silica gel using an appropriate solvent mixture. In the latter case, the isolated phthalocyanine was finally washed with methanol and dried under vacuum to constant weight.

2.4.8. Synthesis, Green Chemistry metric calculation and characterization of tetra-(3,5-dimethylphenoxy)-zinc-phthalocyanine Pc1

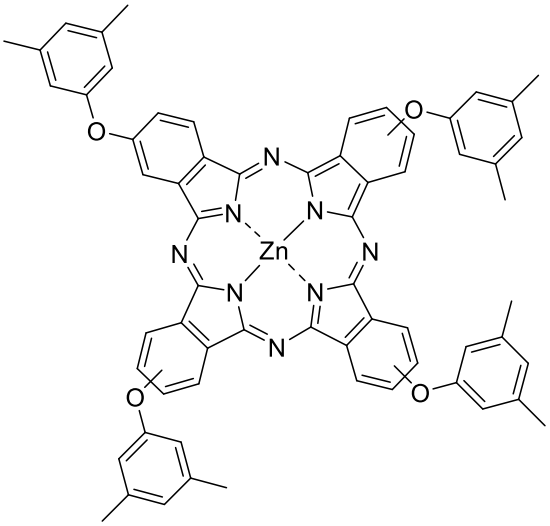

Purification of the crude was carried out by short pad filtration on silica gel, using THF for sample loading and a 3:1 hexane:THF mixture as the eluent. The target compound was obtained as a blue solid in 48% yield. ^{1}H NMR (600 MHz, THF-d_8): δ = 9.01 – 8.91 (m, 4H), 8.65 – 8.60 (m, 4H), 7.72 – 7.70 (m, 4H), 7.12 – 6.93 (m, 12H), 2.44 – 2.41 (m, 24H, CH_3) ppm; ^{13}C NMR (150 MHz, THF-d_8): δ = 160.62, 160.58, 160.54, 160.48, 160.40, 160.37, 158.99, 158.93, 158.89, 158.84, 158.81, 141.28, 141.24, 141.23, 141.19, 140.88, 140.86, 140.82, 140.80, 134.43, 134.33, 134.27, 126.59, 126.57, 126.53, 126.51, 126.49, 126.42, 126.41, 124.89, 124.74, 124.71, 121.38, 121.34, 118.49, 118.47, 118.39, 118.37, 118.36, 118.26, 118.23, 112.92, 112.87, 112.83, 21.75 ppm. FT-IR: ν = 2918, 2849, 2828, 1611, 1584, 1456, 1393, 1335, 1292, 1256, 1217, 1173, 1134, 1084, 1043, 1022, 951, 999, 820, 559, 534 cm^{-1}. UV-vis (THF): λ_{max} = 675, 352 nm. MALDI-TOF $[M]^{\bullet+}$: m/z = 1056.41, (Calcd: 1056.31).

E-factor calculation for compound **Pc1**

Chemical	**Volume (mL)**	**Density (g/mL)**	**Mass (g)**	**Mass of solvents considered toward E-factor (after 80% solvent recovery) (g)**
3,5-dimethylphenol			0.36	
DMF	4.0	0.948	3.792	
K_2CO_3			1.2	
4-nitrophthalonitrile			0.5	
Zinc acetate dihydrate			0.172	
DBU	0.4	1.018	0.407	
Water	30.0		30.0	
HCl 1N			2.0	
Silica gel			8.0	
THF	19.5	0.888	17.32	3.463
Hexane	37.5	0.661	24.79	4.958
Methanol	45.0	0.792	35.64	7.128

Amount of product = 0.364 g (48% yield)

Total E-Factor = 257.7

E-factor 80% solvent recovery = 86.9

^{1}H NMR spectrum of tetra-(3,5-dimethylphenoxy)-zinc-phthalocyanine **Pc1** in THF-d_8

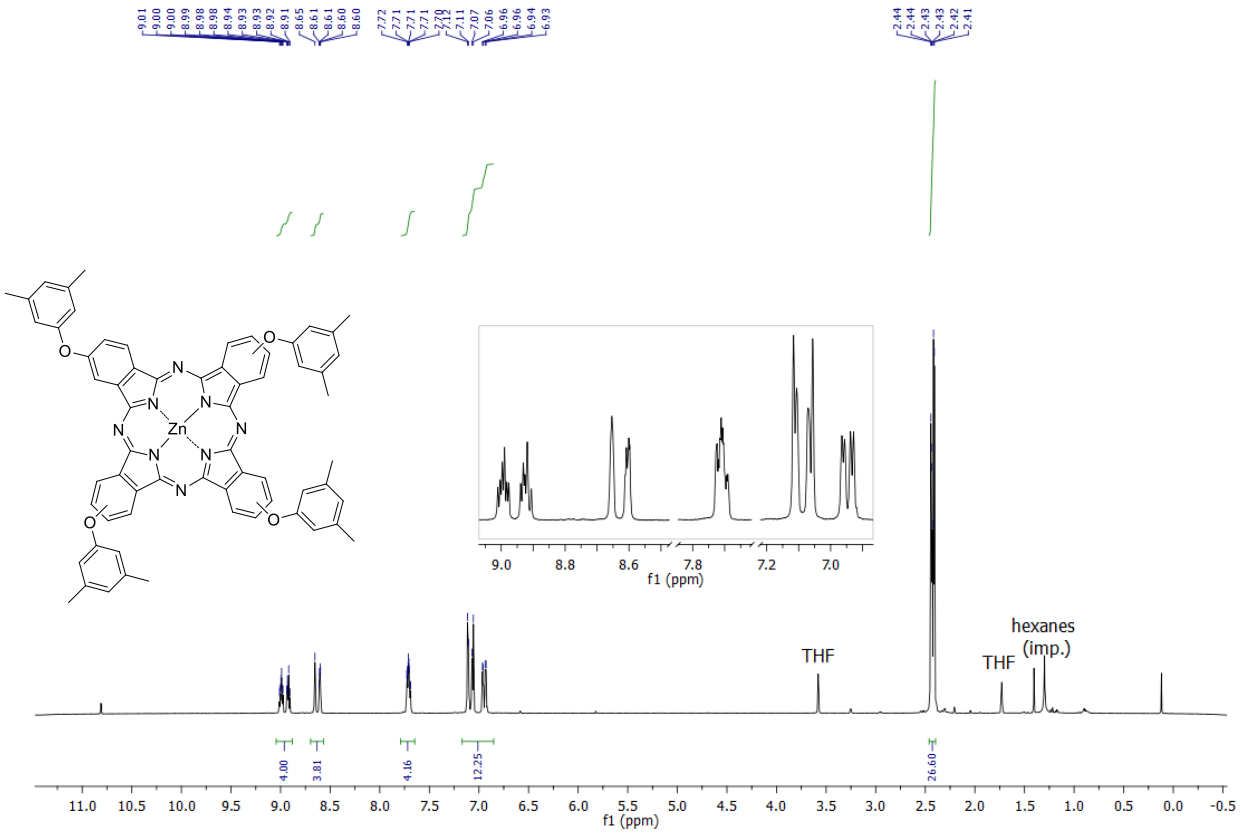

^{13}C NMR spectrum of tetra- (3,5-dimethylphenoxy)-zinc-phthalocyanine **Pc1** in THF-d_8

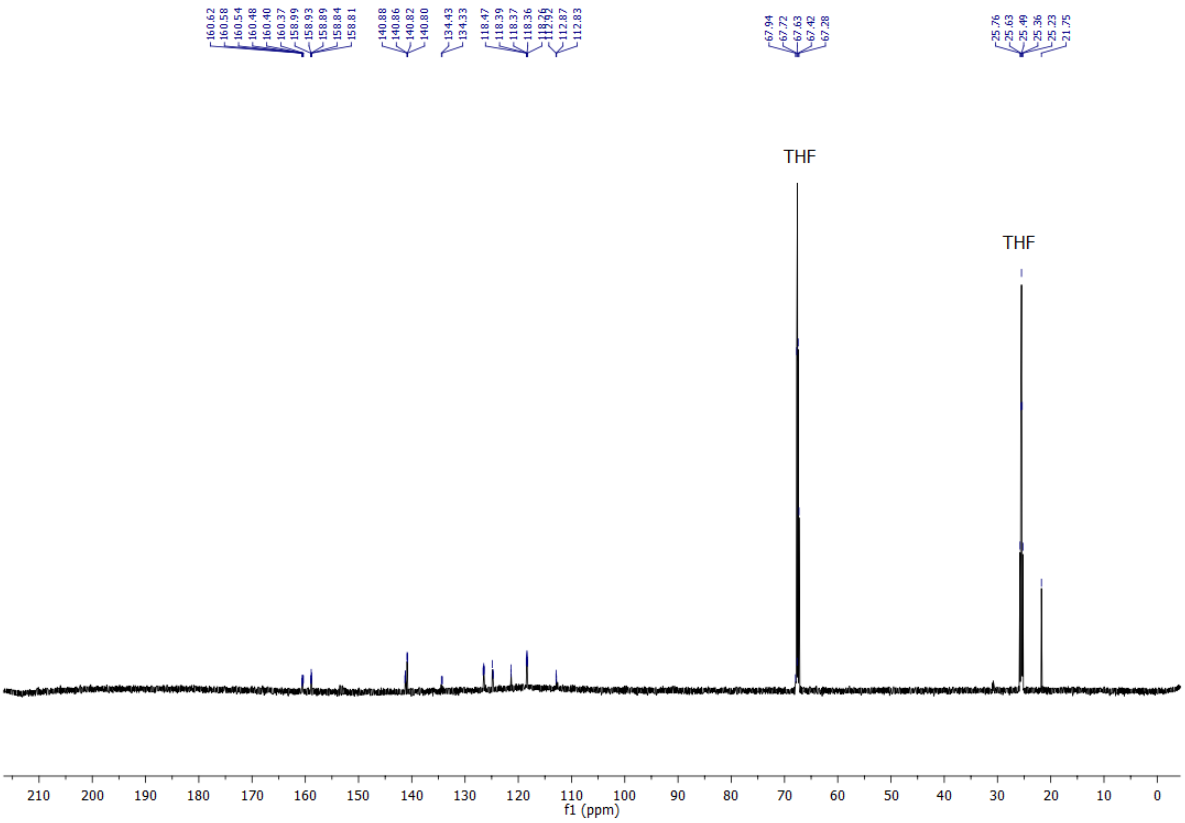

ATR spectrum of tetra-(3,5-dimethylphenoxy)-zinc-phthalocyanine **Pc1**

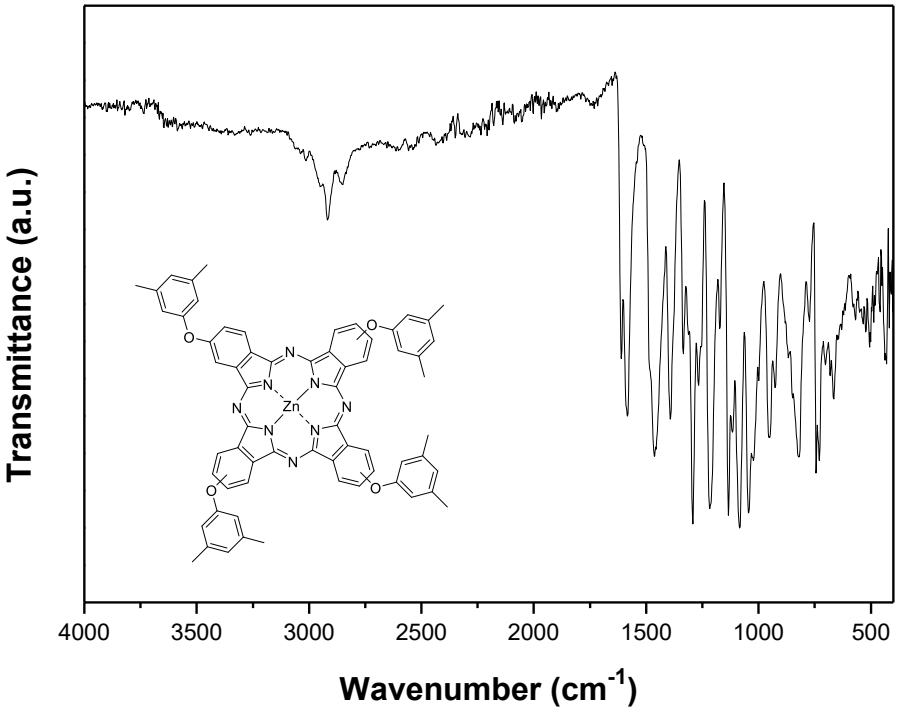

MALDI-TOF spectrum of tetra-(3,5-dimethylphenoxy)-zinc-phthalocyanine **Pc1**

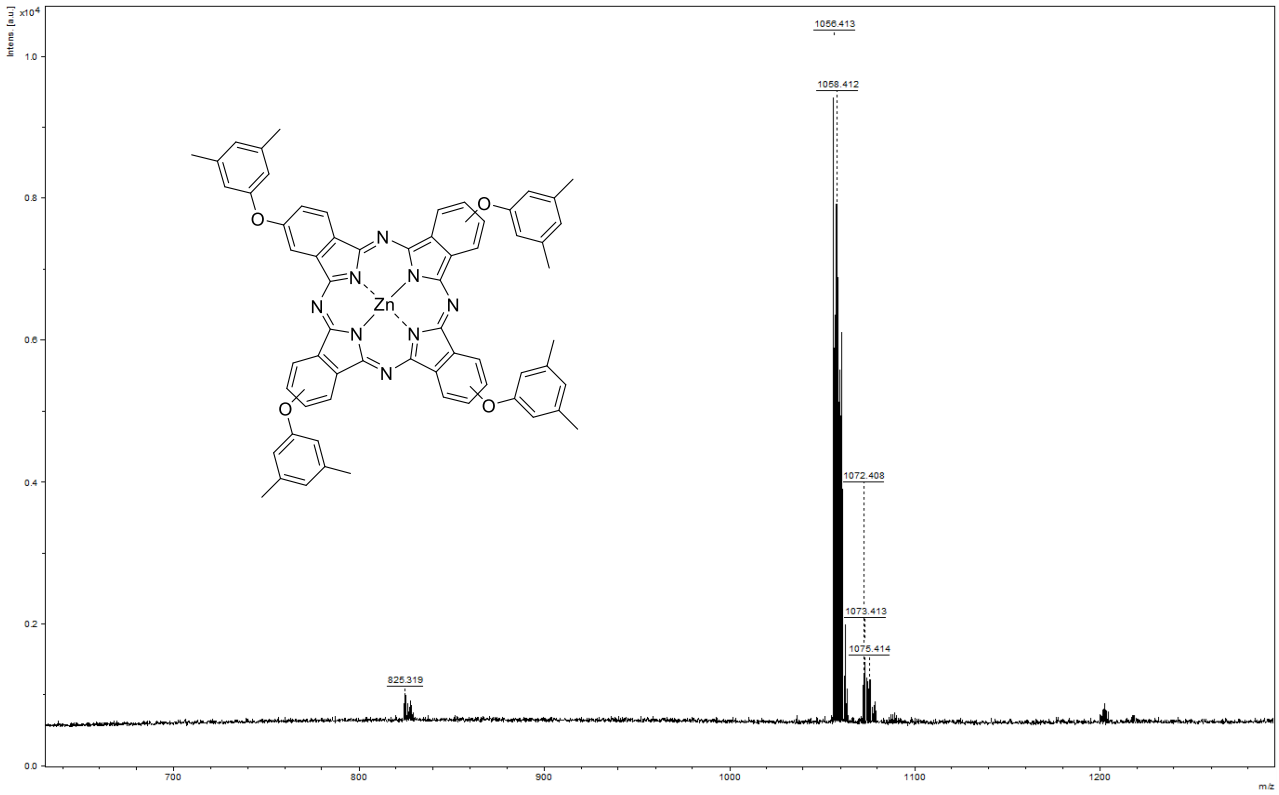

2.4.9. Synthesis, Green Chemistry metric calculation and characterization of tetra-(*p*-tolyloxy)-zinc-phthalocyanine Pc2

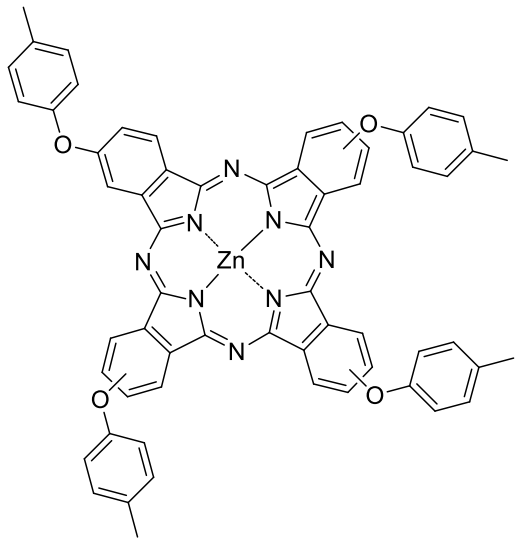

Purification of the crude was carried out by short pad filtration on silica gel, using THF for sample loading and a 3:1 hexane:THF mixture as the eluent. The target compound was obtained as a blue solid in 43% yield. ^{1}H NMR (600 MHz, THF-d_8): δ = 8.94 – 8.77 (m, 4H), 8.64 – 8.50 (m, 4H) 7.69 – 7.61 (m, 4H), 7.45 – 7.35 (m, 16H), 2.49 – 2.47 (m, 12H) ppm; ^{13}C NMR (150 MHz, THF-d_8): δ = 160.70, 160.66, 160.62, 160.54, 156.60, 156.58, 156.51, 156.44, 156.38, 156.34, 153.49, 152.46, 141.14, 141.08, 141.06, 134.47, 134.45, 134.31, 134.30, 134.24, 134.22, 134.08, 134.03, 134.00, 131.61, 131.54, 124.87, 124.84, 124.64, 124.59, 120.92, 120.88, 120.81, 120.77, 120.71, 120.68, 120.60, 120.57, 112.47, 112.38, 112.32, 111.95, 111.87, 111.78, 21.17 ppm. FT-IR: ν = 3024, 2922, 2860, 1602, 1504, 1472, 1393, 1335, 1259, 1227, 1205, 1161, 1115, 1086, 1043, 1016, 945, 889, 868, 816, 743, 668, 498 cm^{-1}. UV-vis (THF): λ_{max} = 675, 352 nm. MALDI-TOF $[M]^{\bullet+}$: m/z = 1000.37, (Calcd: 1000.25).

E-factor calculation for compound **Pc2**

Chemical	**Volume (mL)**	**Density (g/mL)**	**Mass (g)**	**Mass of solvents considered toward E-factor (after 80% solvent recovery) (g)**
4-methylphenol			0.319	
DMF	4.0	0.948	3.792	
K_2CO_3			1.2	
4-nitrophthalonitrile			0.5	
Zinc acetate dihydrate			0.172	
DBU	0.4	1.018	0.407	
Water	28.0		28.0	
HCl 1N			2.0	
Silica gel			10.0	
THF	28.75	0.888	25.53	5.106
Hexane	76.25	0.661	50.40	10.08
Methanol	10.0	0.792	7.92	1.584

Amount of product = 0.313 g (43% yield)

Total E-factor = 326.2

E-factor 80% solvent recovery = 111.3

E-factor calculation for compound **Pc2** synthesized according to the literature method[66]

Chemical	**Volume (mL)**	**Density (g/mL)**	**Mass (g)**	**Mass of solvents considering an 80% recovery (g)**
4-methylphenol			6.92	
4-nitrophthalonitrile			5.41	
DMSO	60.0	1.100	66.0	
K_2CO_3			10.35	
Dichloromethane	200.0	1.327	265.4	53.08
Na_2CO_3 5% solution in water	200.0		200.0	
Sodium sulfate			7.0	
Hexane	680.0	0.661	449.48	89.90

Amount of product = 6.83 g (73% yield)

E-factor = 147.0

E-factor assuming 80% solvent recovery = 63.2

Chemical	**Volume (mL)**	**Density (g/mL)**	**Mass (g)**	**Mass of solvents considering an 80% recovery (g)**
4-(*p*-methylphenoxy)phthalonitrile			2.34	
Zinc powder			1.308	

Ammonium molibdate			0.2	
Neutral alumina			263.0	
Toluene	3.0	0.862	2.586	0.52
THF	1025.0	0.888	910.2	182.04
Chloroform	30.0	1.489	44.67	8.93
Methanol	450.0	0.792	356.4	71.28

Amount of product = 1.22 g (52% yield)

E-factor =1294.7

E-factor assuming 80% solvent recovery = 433.1

Total yield: 38%, total E-factor: 1441.7, total E-factor assuming 80% solvent recovery = 496.3

^{1}H NMR spectrum of tetra-(*p*-tolyloxy)-zinc-phthalocyanine **Pc2** in THF-d_8

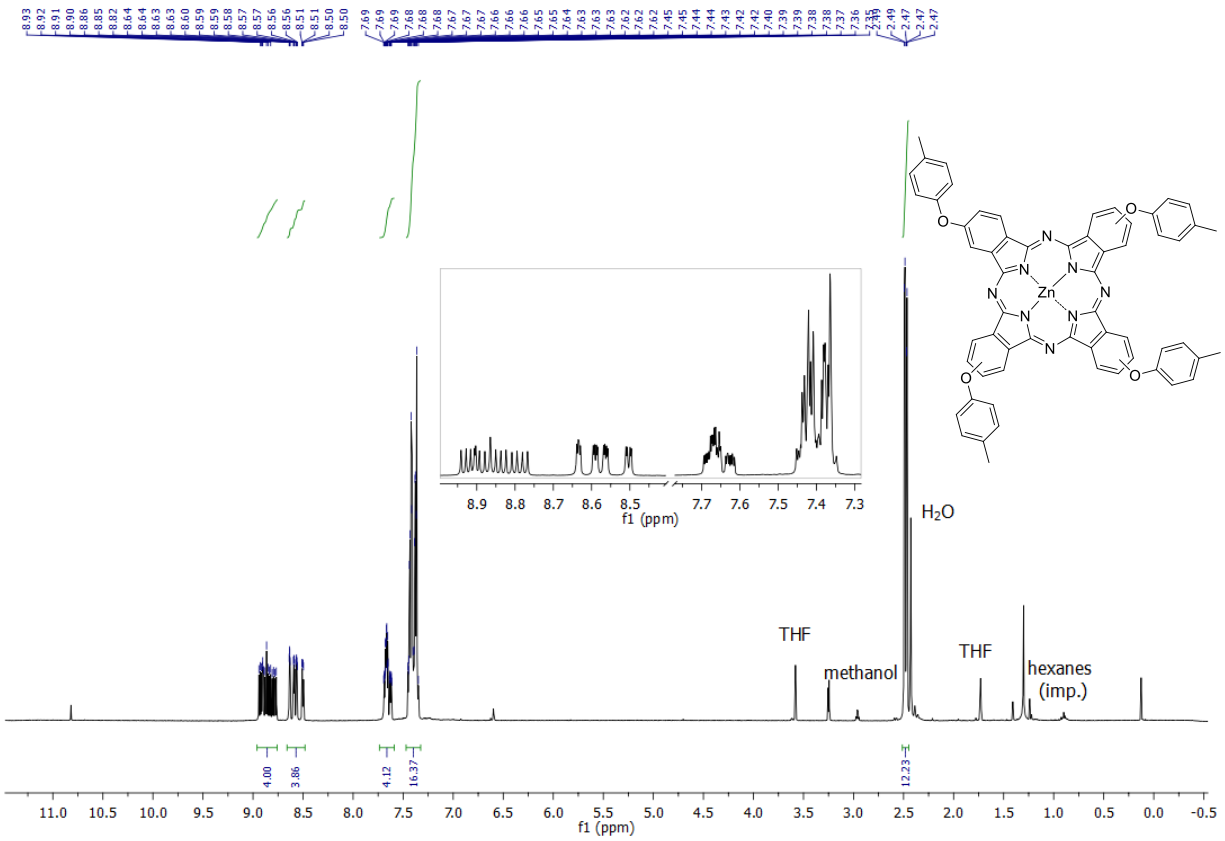

^{13}C NMR spectrum of tetra-(*p*-tolyloxy)-zinc-phthalocyanine **Pc2** in THF-d_8

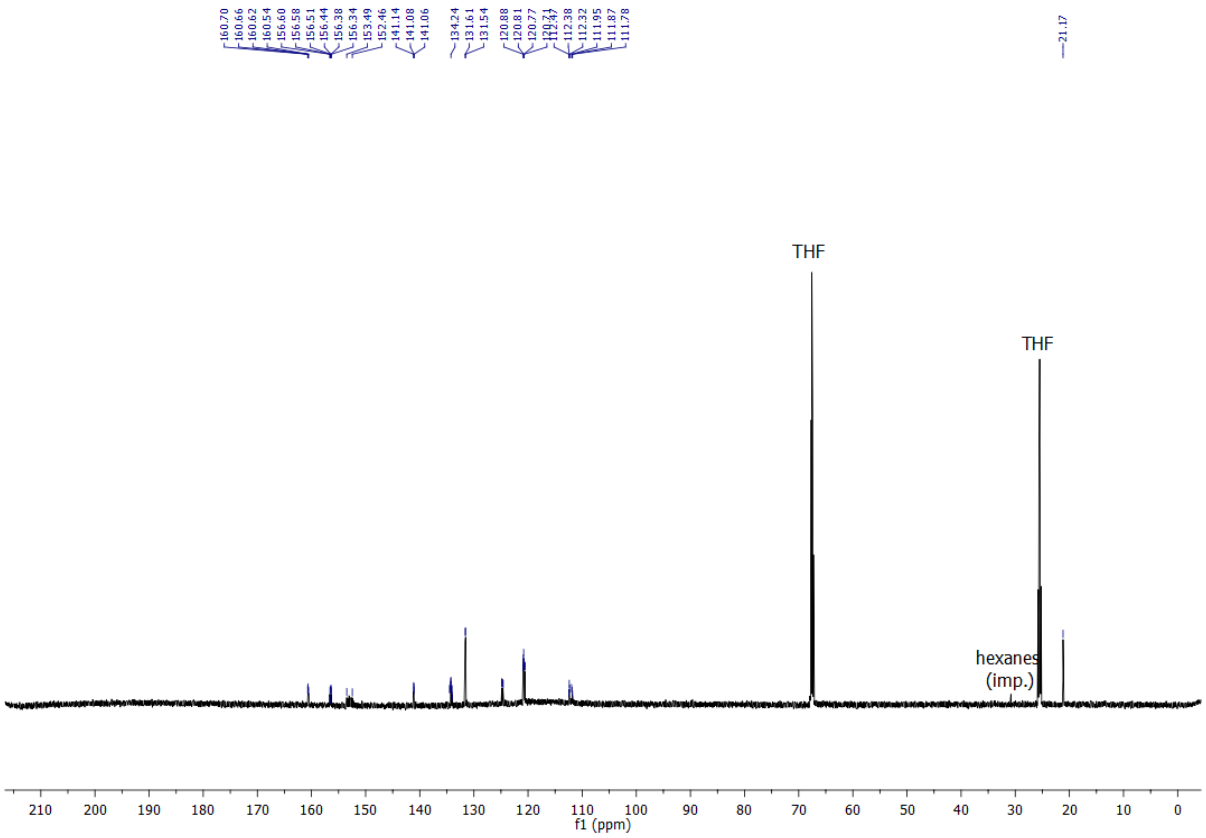

ATR spectrum of tetra-(*p*-tolyloxy)-zinc-phthalocyanine **Pc2**

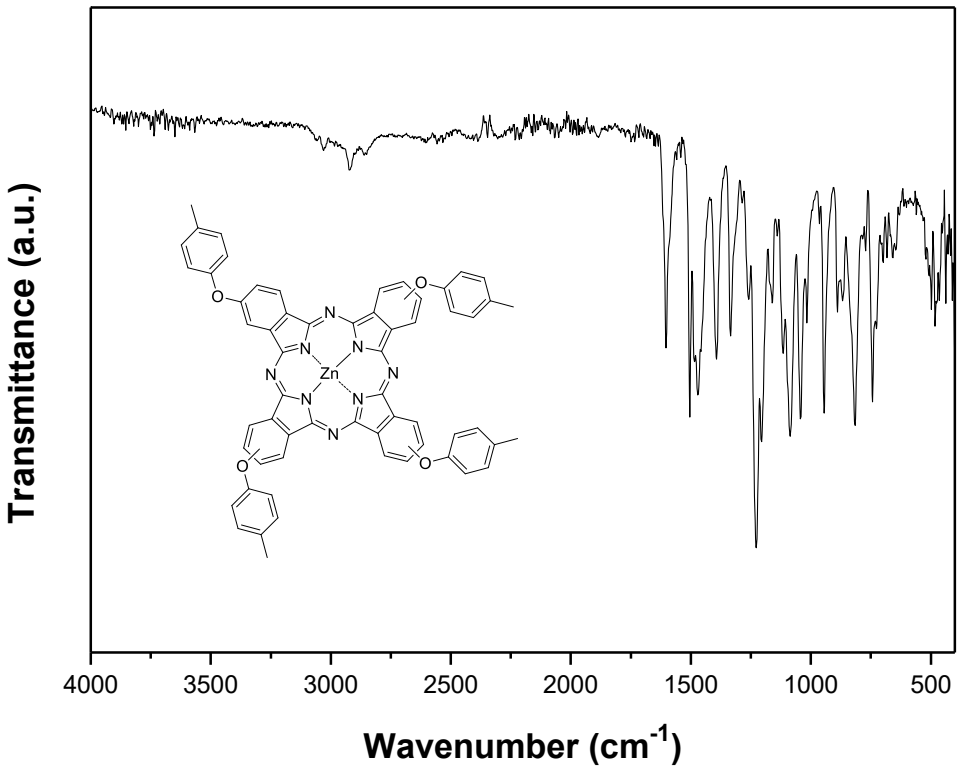

MALDI-TOF spectrum of tetra-(*p*-tolyloxy)-zinc-phthalocyanine **Pc2**

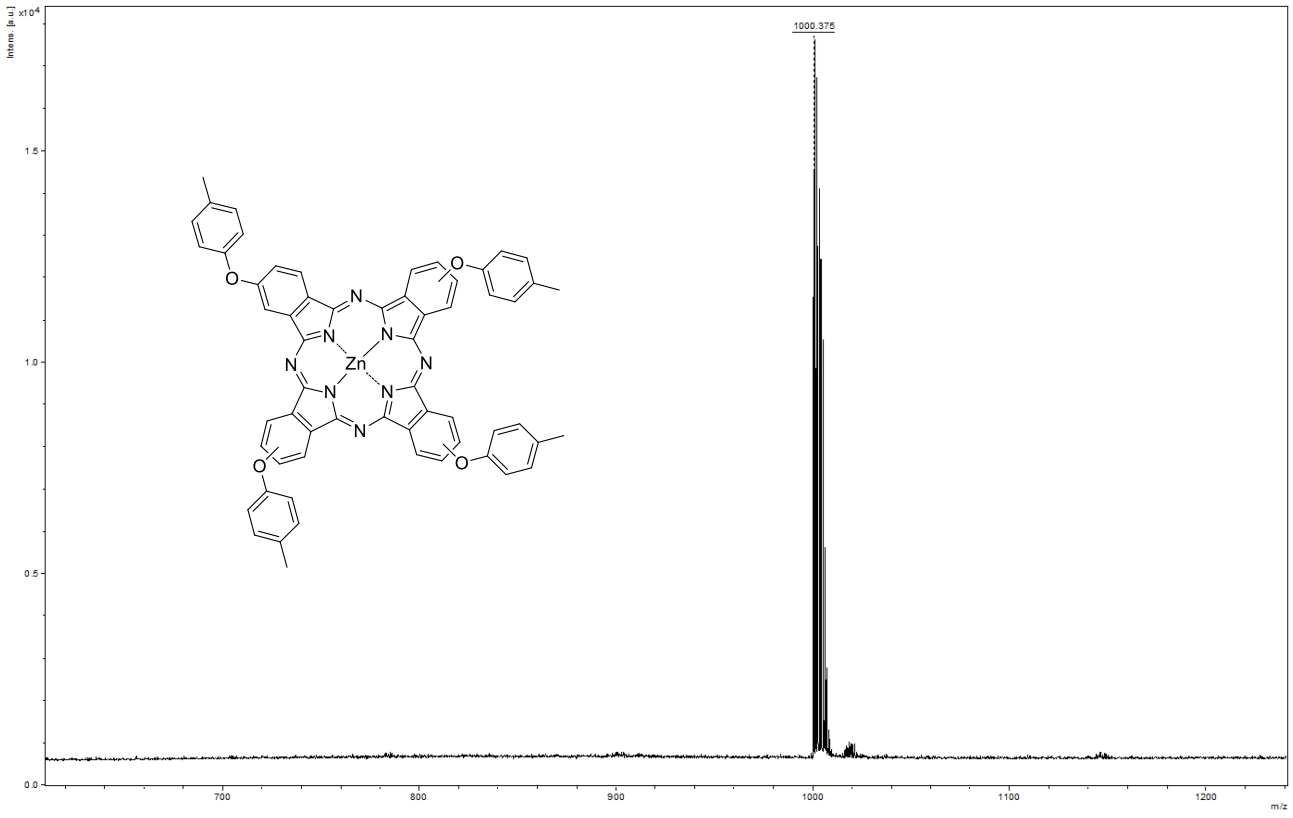

2.4.10. Synthesis, Green Chemistry metric calculation and characterization of tetra-(4-iodo-2,6-dimethylphenoxy)-zinc-phthalocyanine Pc3

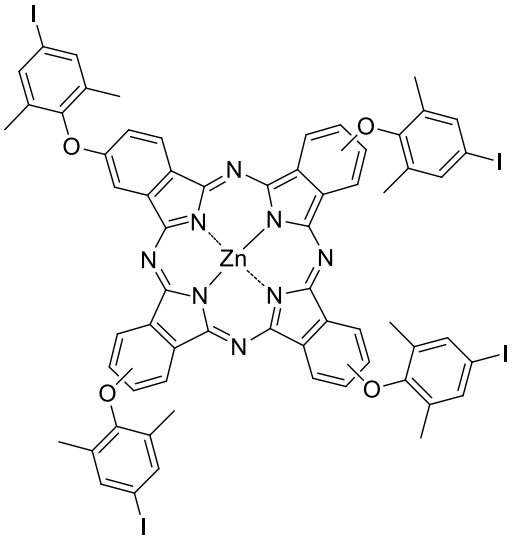

Purification of the crude was performed by short pad filtration on silica gel, using THF for sample loading and a gradient elution with increasing polarity (from 4:1 to 1:1 petroleum ether:THF). The target compound was obtained as a blue solid in 37% yield. ^{1}H NMR (600 MHz, Pyr-*d*$_5$) δ = 9.36 – 9.68 (m, 4H), 8.87 – 9.19 (m, 4H), 7.74 (m, 4H), 7.60 – 7.67 (m, 8H), 2.19 (m, 24H) ppm; ^{13}C NMR (150 MHz, Pyr-*d*$_5$): δ = 159.92, 159.75, 159.60, 151.66, 151.64, 151.54, 151.54, 151.50, 142.92, 142.92, 138.41, 138.39, 138.35, 134.18, 134.18, 125.68, 125.68, 117.55, 117.49, 117.02, 116.88, 114.87, 114.86, 90.73, 90.71, 90.70, 90.64, 90.61, 79.53, 79.09, 34.77, 34.71, 30.55, 30.24, 29.34, 24.15, 24.15, 21.15, 16.53, 16.50, 15.99, 15.96, 15.96 ppm. FT-IR: ν = 2926, 2850, 1607, 1460, 1392, 1337, 1268, 1213, 1179, 1115, 1084, 1038, 944, 852, 813, 764, 743 cm^{-1}. UV-vis (THF): λ_{max} = 677, 351 nm. MALDI-TOF $[M]^{\bullet+}$: m/z = 1559.83, (Calcd: 1559.90).

E-factor calculation for compound **Pc3**

Chemical	**Volume (mL)**	**Density (g/mL)**	**Mass (g)**	**Mass of solvents considered toward E-factor (after 80% solvent recovery) (g)**
4-iodo-2,6-dimethylphenol			0.365	
DMF	2.5	0.948	2.37	
K_2CO_3			0.6	
4-nitrophthalonitrile			0.25	
Zinc acetate dihydrate			0.086	
DBU	0.2	1.018	0.204	
Water	4.5		4.5	
HCl 1N			0.5	
Silica gel			13.0	
THF	40.5	0.888	35.96	7.193
Petroleum ether	66.0	0.666	43.96	8.791
Methanol	25.0	0.792	19.8	3.96

Amount of product = 0.210 g (37% yield)

Total E-factor = 556.6

E-factor 80% solvent recovery = 176.7

^{1}H NMR spectrum of tetra-(4-iodo-2,6-dimethylphenoxy)-zinc-phthalocyanine **Pc3** in Pyr-d_5

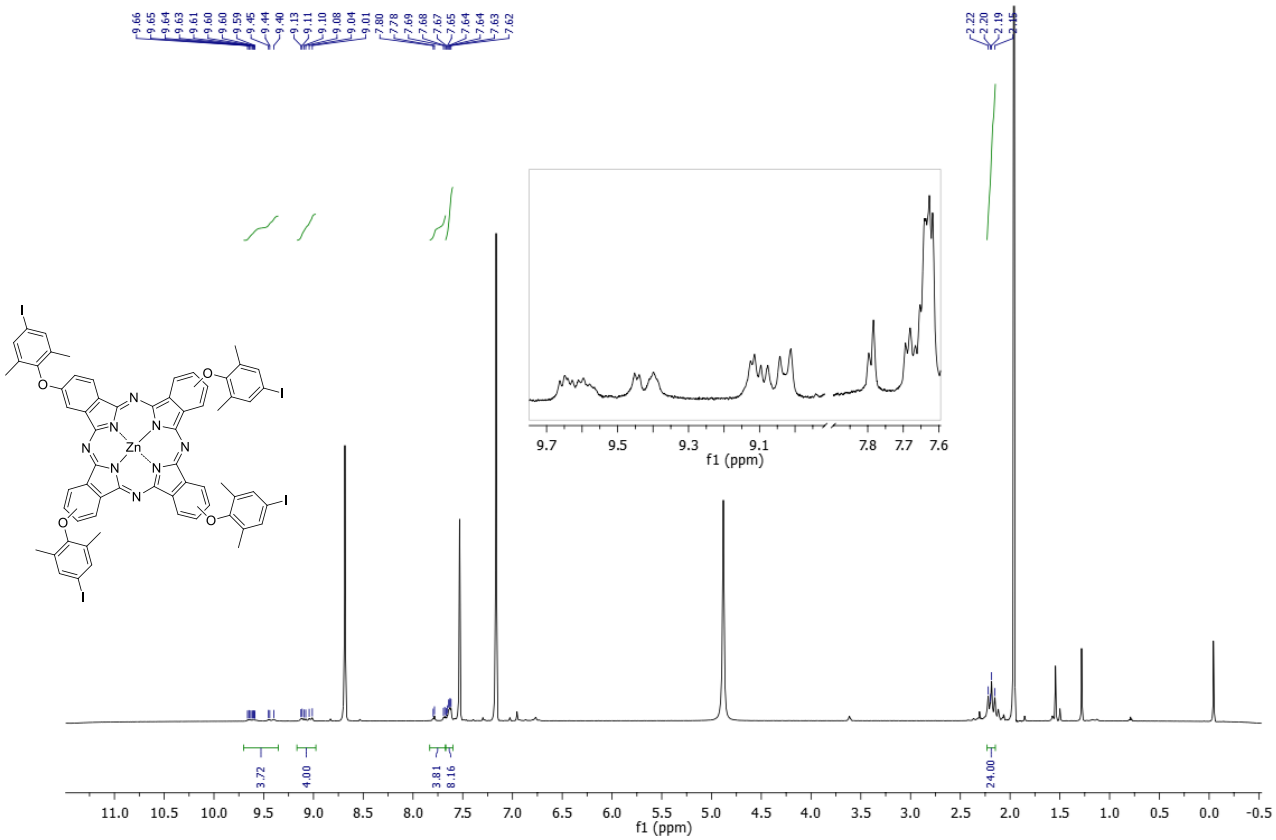

^{13}C NMR spectrum of tetra-(4-iodo-2,6-dimethylphenoxy)-zinc-phthalocyanine **Pc3** in Pyr-d_5

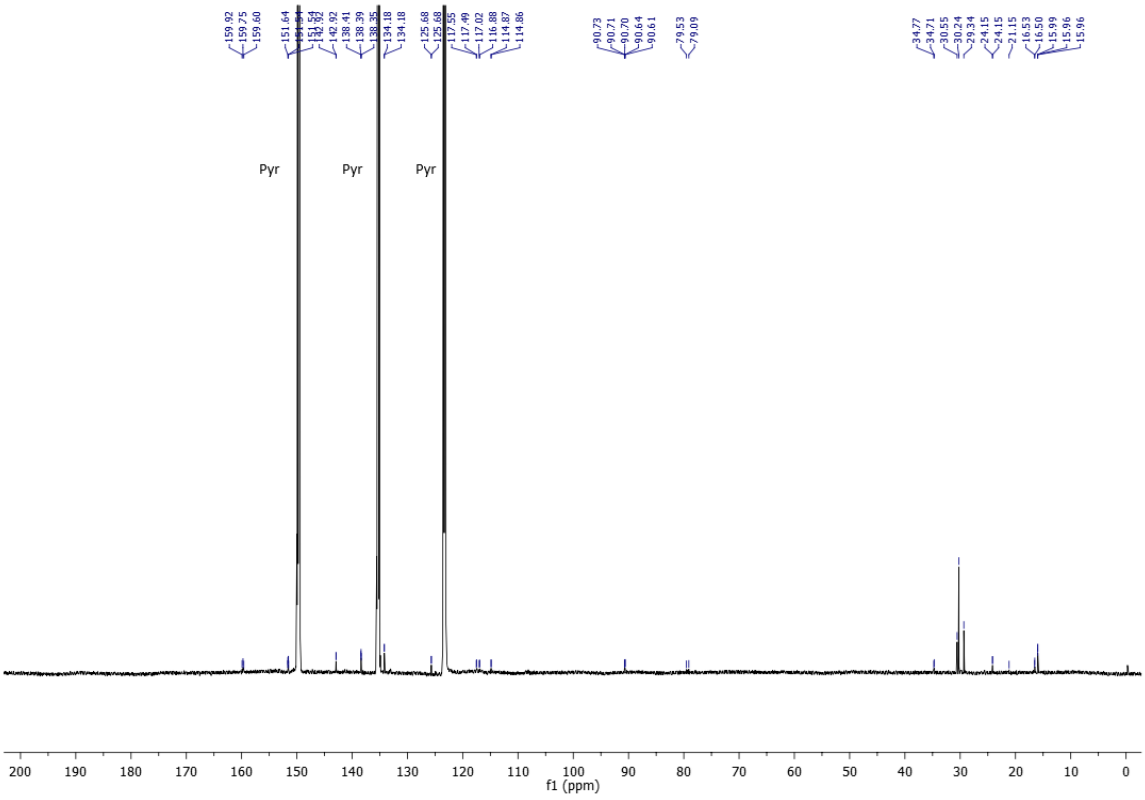

ATR spectrum of tetra-(4-iodo-2,6-dimethylphenoxy)-zinc-phthalocyanine **Pc3**

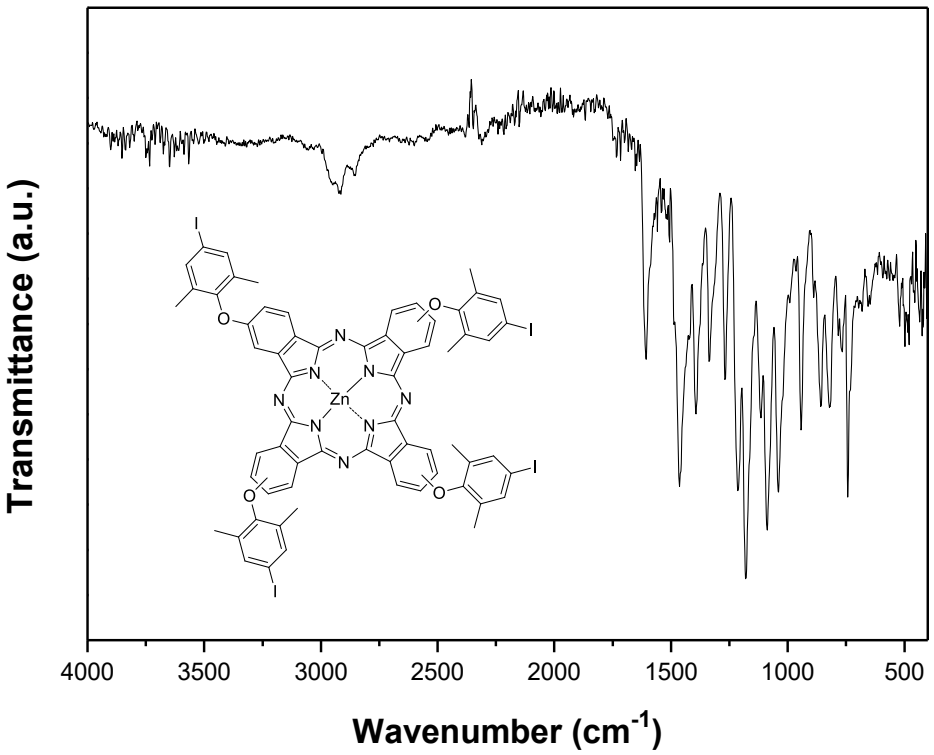

MALDI-TOF spectrum of tetra-(4-iodo-2,6-dimethylphenoxy)-zinc-phthalocyanine **Pc3**

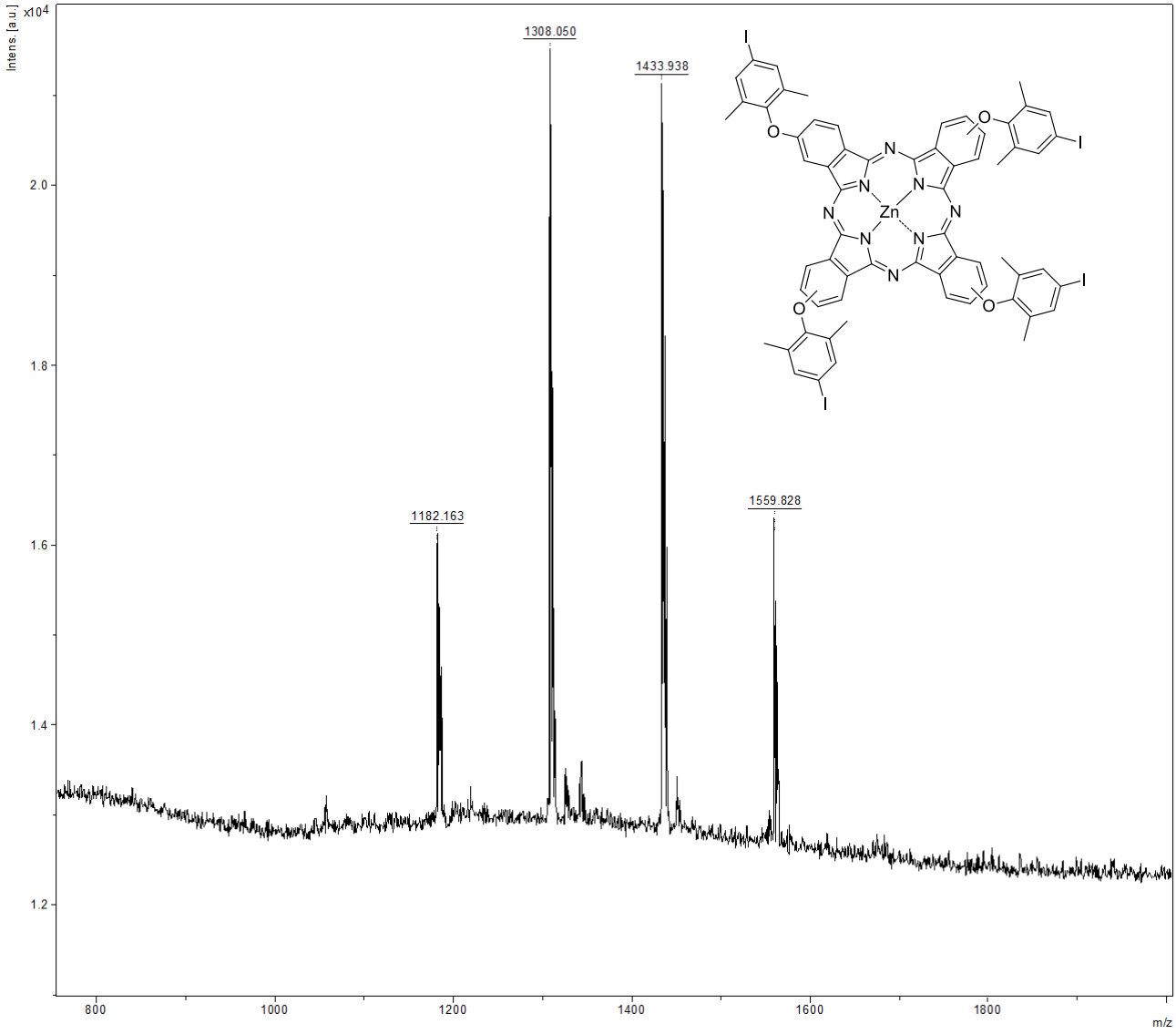

2.4.11. Synthesis and characterization of *tert*-butyl(4-hydroxyphenyl)carbamate 4a

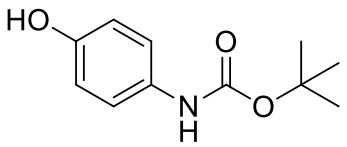

The synthesis was carried out according to the procedure reported in the literature.[112] Briefly, in a one-neck round-bottom flask 4-aminophenol (0.5 g, 1 eq) was stirred in 8 mL of glycerol, then Boc_2O (1 eq) was added. The reaction mixture was stirred at room temperature until complete disappearance of 4-aminophenol was observed in the TLC monitoring. The resulting reaction mixture was extracted with a mixture of petroleum ether/ethyl acetate (9:1), the combined organic layer was dried over anhydrous magnesium sulphate and concentrated under reduced pressure. Purification of the raw product by crystallization with hexane gave the target product in 86% yield as a white solid. ^{1}H NMR (600 MHz, $CDCl_3$): δ = 7.17 – 7.16 (m, 2H), 6.74 – 6.73 (m, 2H), 6.35 (bs , 1H), 5.33 (bs, 1H), 1.51 (s, 9H) ppm; ^{13}C NMR (150 MHz, $CDCl_3$): δ = 153.56, 152.04, 130.99, 121.4, 115.74, 80.46, 28.38.

^{1}H NMR spectrum of *tert*-butyl(4-hydroxyphenyl)carbamate **4a** in $CDCl_3$

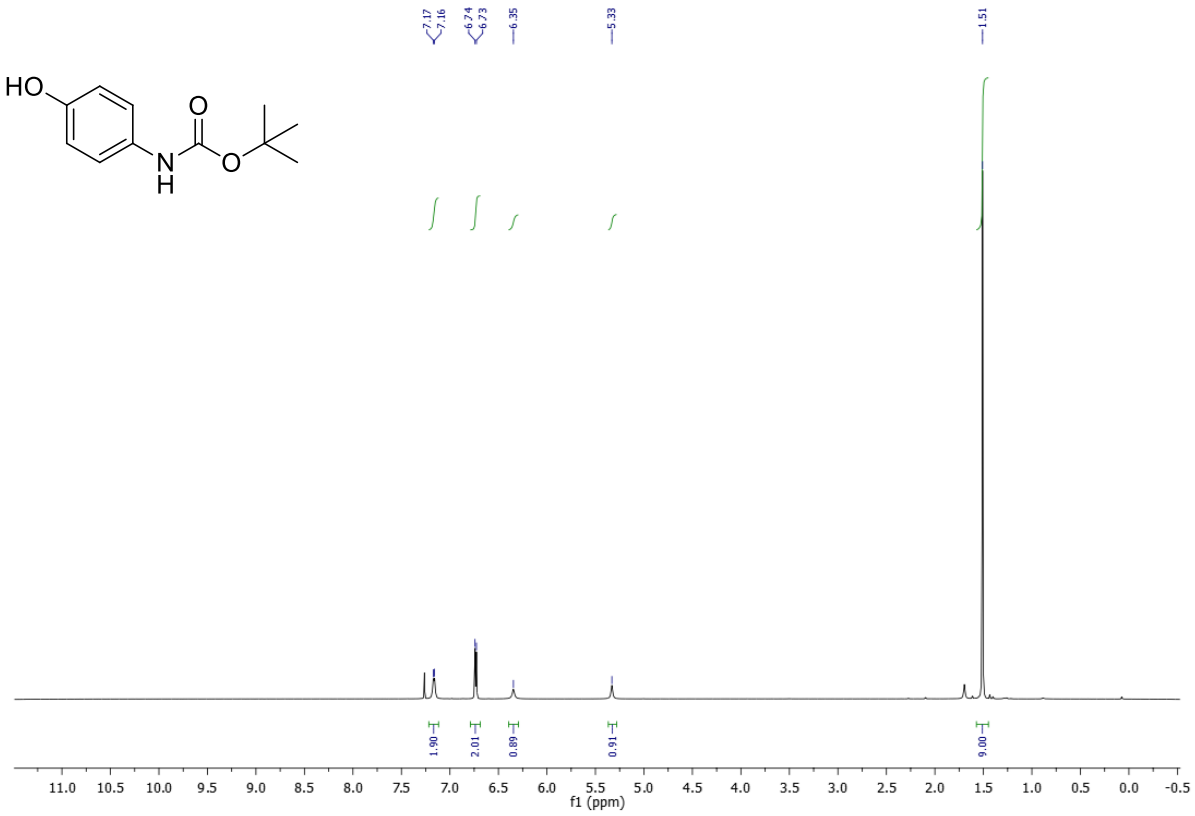

^{13}C NMR spectrum of *tert*-butyl(4-hydroxyphenyl)carbamate **4a** in $CDCl_3$

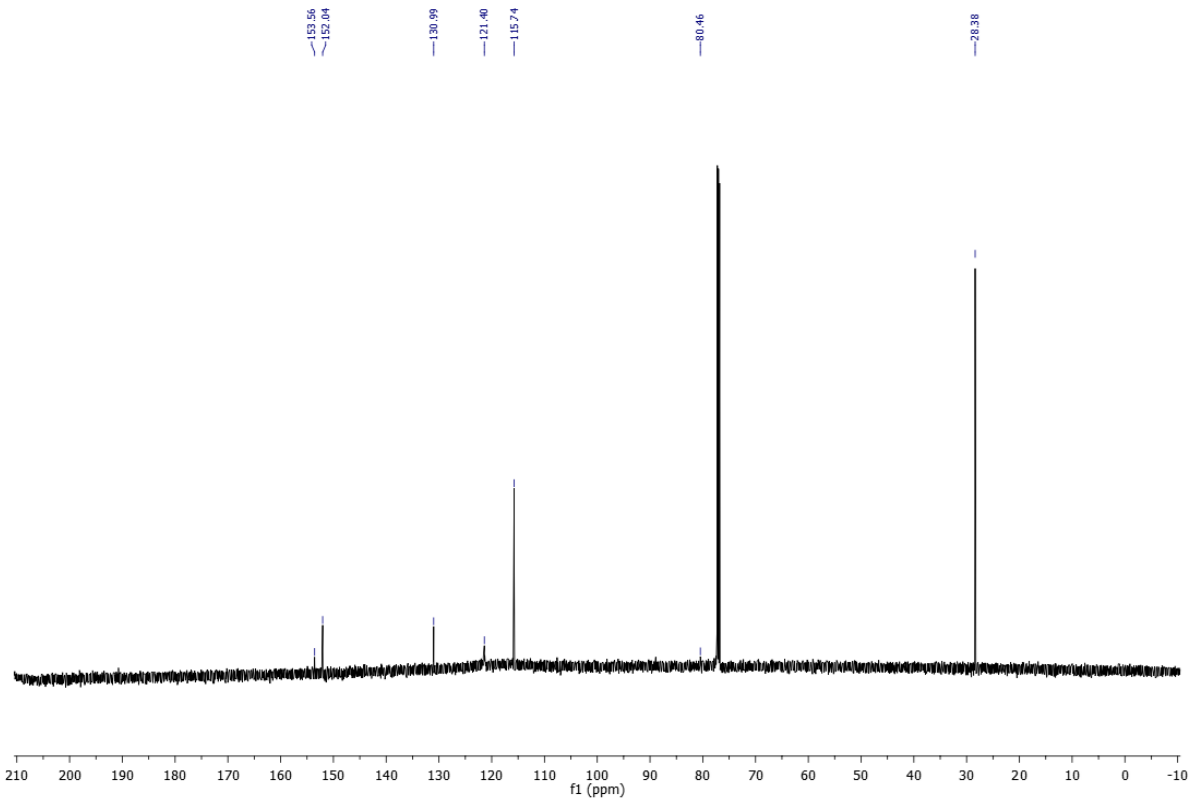

2.4.12. Synthesis and characterization of phthalocyanine Pc4

Purification of the crude by Soxhlet extraction with methanol gave a phthalocyanine-based product as a green solid. FT-IR: ν = 3309, 2930, 2860, 1721, 1593, 1484, 1466, 1395, 1362, 1333, 1314, 1267, 1220, 1112, 1092, 1041, 1007, 946, 885, 832, 743, 724, 696 cm^{-1}. UV-vis (Pyridine): λ_{max} = 685, 355 nm.

2.4.13. Synthesis, Green Chemistry metric calculation and characterization of tetra-(3,5-bis(trifluoromethyl)phenoxy)-zinc-phthalocyanine Pc5

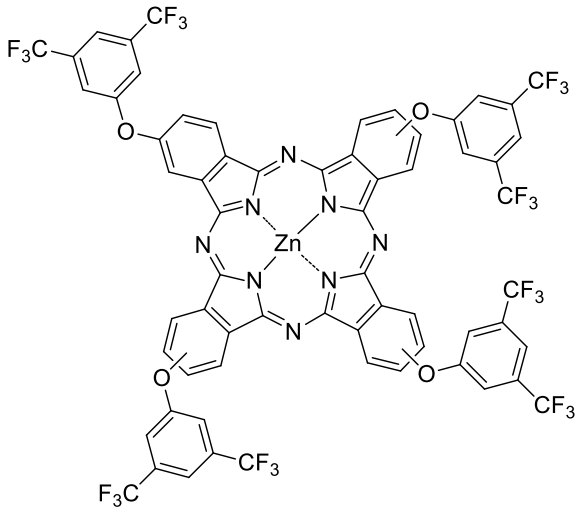

Purification of the crude was performed by short pad filtration on silica gel, using a 5:3 hexane:ethyl acetate mixture for both sample loading and elution. The target compound was obtained as a blue solid in 27% yield. ^{1}H NMR (600 MHz, THF-d_8): δ = 9.17 – 9.06 (m, 4H), 8.80-8.75 (m, 4H), 8.05-7.84 (m, 16H) ppm; ^{13}C NMR (150 MHz, THF-d_8): δ = 160.59, 160.57, 160.54, 157.96, 157.94, 157.86, 157.78, 157.76, 141.32, 141.29, 141.25, 141.20, 141.18, 141.13, 135.94, 135.92, 135.86, 135.84, 134.67, 134.65, 134.63, 134.61, 134.45, 134.43, 134.41, 134.39, 134.32, 125.52, 125.49, 125.46, 124.44 (q, CF3, J = 272 Hz), 122.21, 122.17, 119.88, 119.84, 119.81, 118.07, 118.02, 117.96, 117.93, 117.91, 117.85, 114.43, 114.40, 114.37, 114.33 ppm. FT-IR: ν = 1607, 1487, 1460, 1337, 1275, 1231, 1171, 1125, 1105, 1084, 1045, 961, 945, 914, 885, 847, 735, 700, 681, 617, 449, 436 cm^{-1}. UV-vis (THF): λ_{max} = 672, 350 nm. MALDI-TOF [M]$^{\bullet+}$: m/z = 1488.20, (Calcd: 1488.08).

E-factor calculation for compound **Pc5**

Chemical	**Volume (mL)**	**Density (g/mL)**	**Mass (g)**	**Mass of solvents considered toward E-factor (after 80% solvent recovery) (g)**
3,5-bis(trifluoromethyl)phenol			0.678	
DMF	4.0	0.948	3.792	
K_2CO_3			1.2	
4-nitrophthalonitrile			0.5	
Zinc acetate dihydrate			0.172	
DBU	0.4	1.018	0.407	
Water	29.0		29.0	
Silica gel			10.0	
Hexane	31.4	0.661	20.755	4.151
Ethyl acetate	20.6	0.902	18.501	3.716

Amount of product = 0.290 g (27% yield)

Total E-factor = 192.1

E-factor 80% solvent recovery = 83.9

E-factor calculation for compound **Pc5** synthesized according to the literature method[67]

Chemical	**Volume (mL)**	**Density (g/mL)**	**Mass (g)**	**Mass of solvents considering an 80% recovery (g)**
4-nitrophthalonitrile			1.0	
3,5-bis(trifluoromethyl)phenol			1.66	
DMF	40.0	0.948	37.92	
K_2CO_3			7.98	
Ethanol	130.0	0.789	102.57	20.514

Amount of product = 1.3 g (63% yield)

E-factor = 115.2

E-factor assuming 80% solvent recovery = 52.1

Chemical	**Volume (mL)**	**Density (g/mL)**	**Mass (g)**	**Mass of solvents considering an 80% recovery (g)**
3,5-bis(trifluoromethyl)phenoxy]phthalonitrile			0.06	
Zinc acetate			0.01	
Dimethylaminoethanol	2.0		1.78	
Hexane	4.5	0.661	2.97	0.594
Silica gel			2.89	
Dichloromethane	4.26	1.327	5.65	1.13
Methanol	0.14	0.792	0.11	0.022

Amount of product = 0.012 g (11% yield)

E-factor = 1121.5

E-factor assuming 80% solvent recovery = 539.5

Total yield: 7%, total E-factor: 1236.7, total E-factor assuming 80% solvent recovery = 591.6

^{1}H NMR spectrum of tetra-(3,5-bis(trifluoromethyl)phenoxy)-zinc-phthalocyanine **Pc5** in THF-d_8.

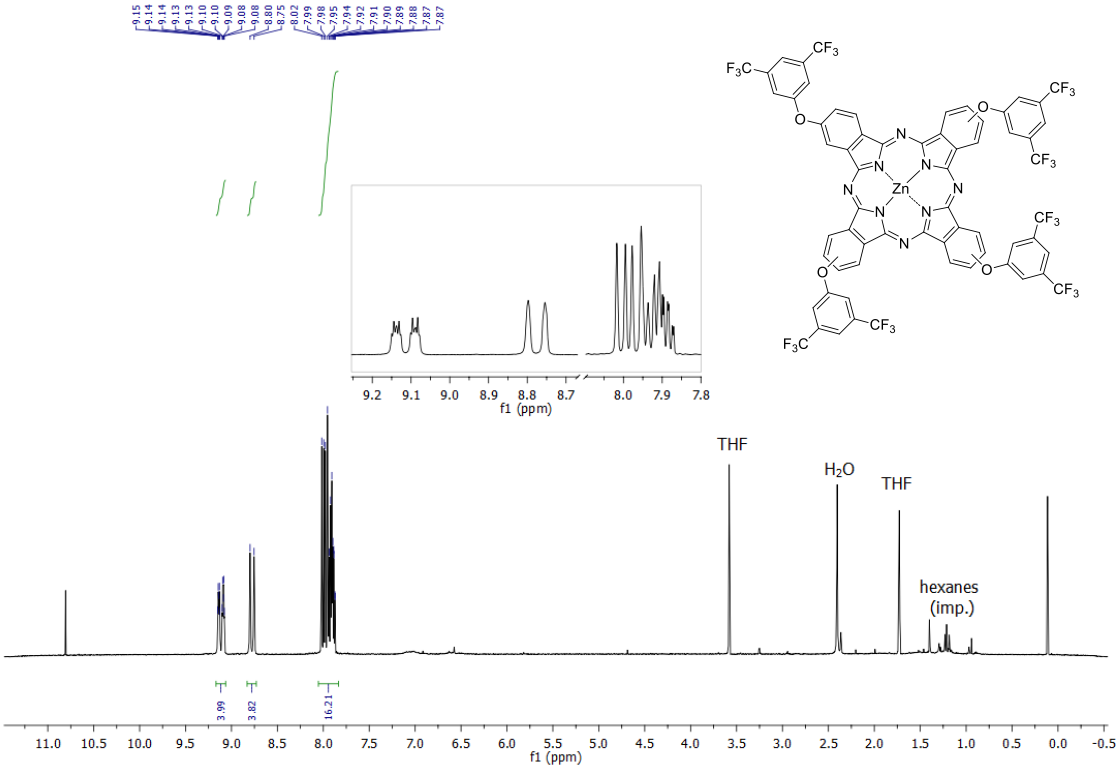

^{13}C NMR spectrum of tetra-(3,5-bis(trifluoromethyl)phenoxy)-zinc-phthalocyanine **Pc5** in THF-d_8

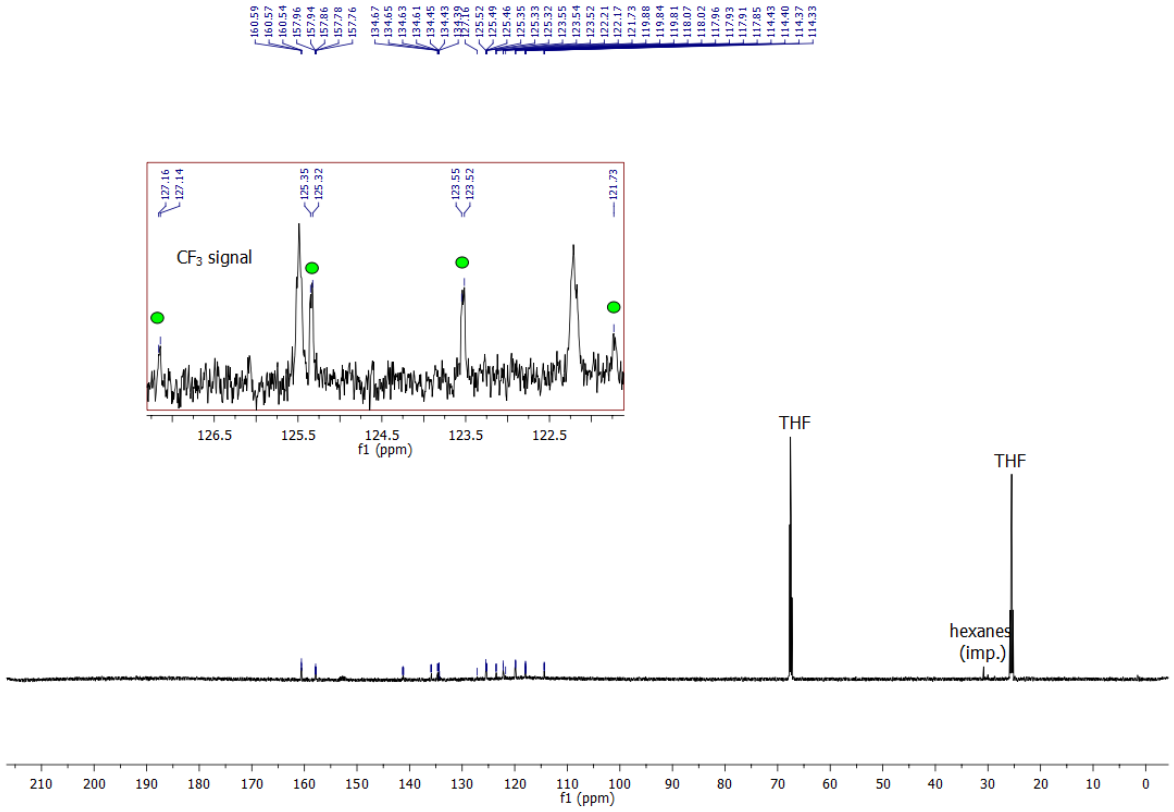

ATR spectrum of tetra-(3,5-bis(trifluoromethyl)phenoxy)-zinc-phthalocyanine **Pc5**

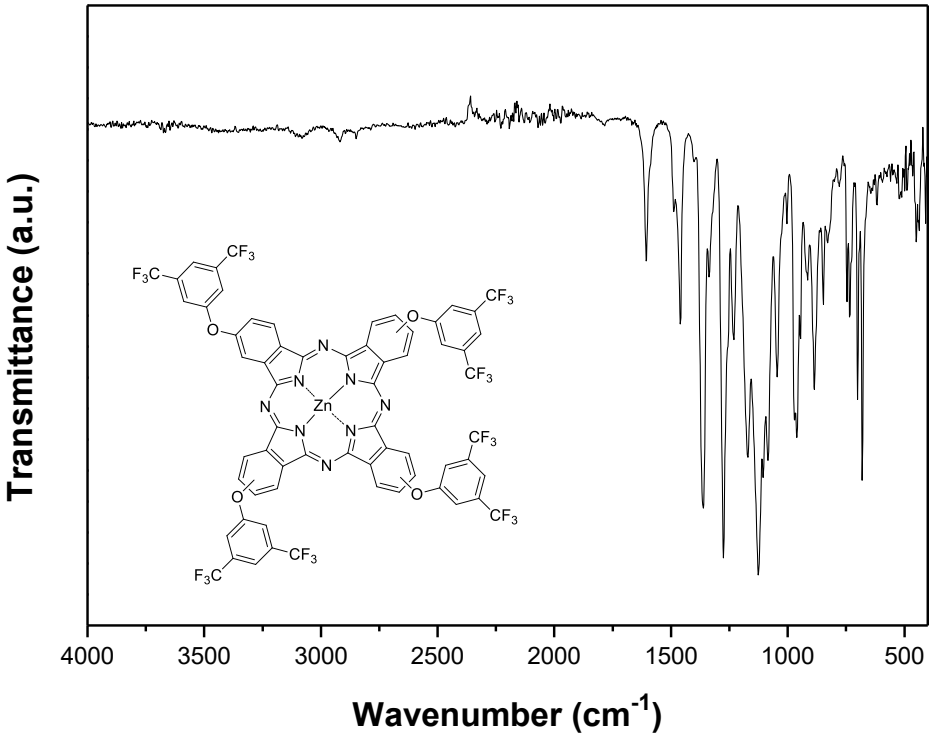

MALDI-TOF spectrum of tetra-(3,5-bis(trifluoromethyl)phenoxy)-zinc-phthalocyanine **Pc5**

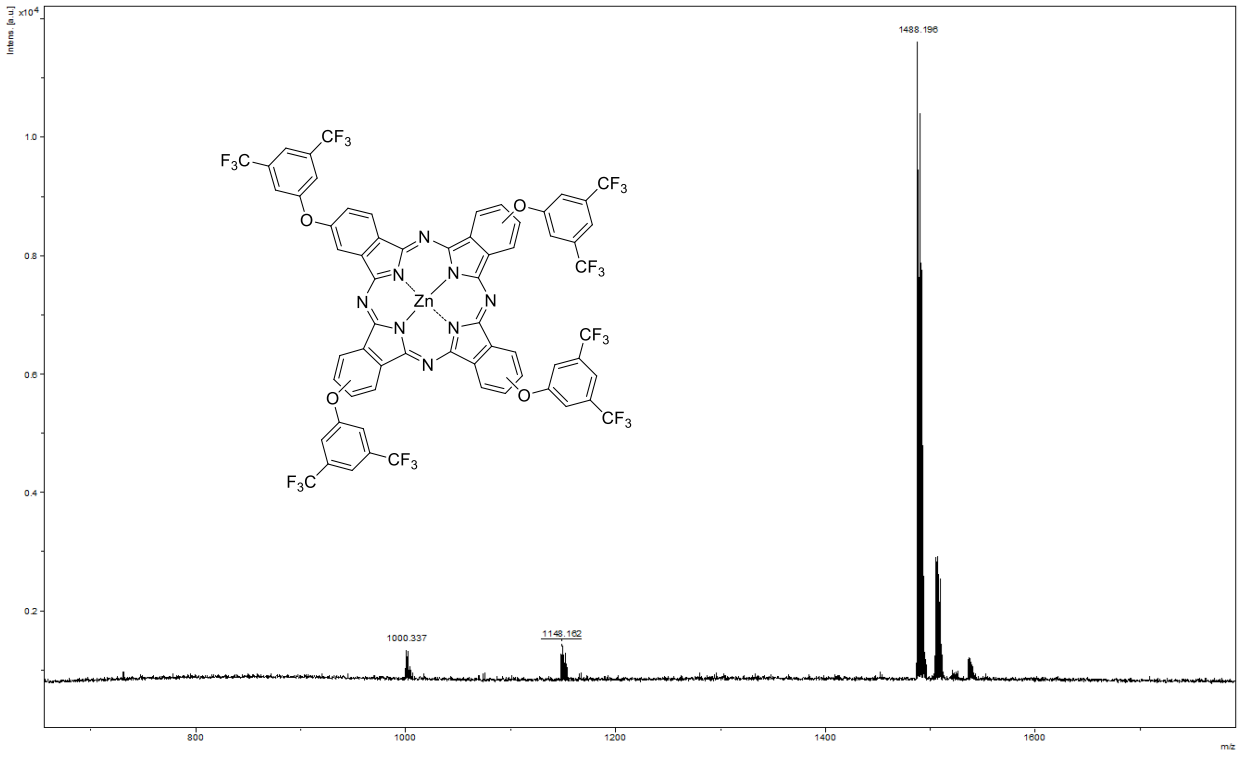

2.4.14. Synthesis, Green Chemistry metric calculation and characterization of tetra-(2-dimethylaminoethoxy)-zinc-phthalocyanine Pc6

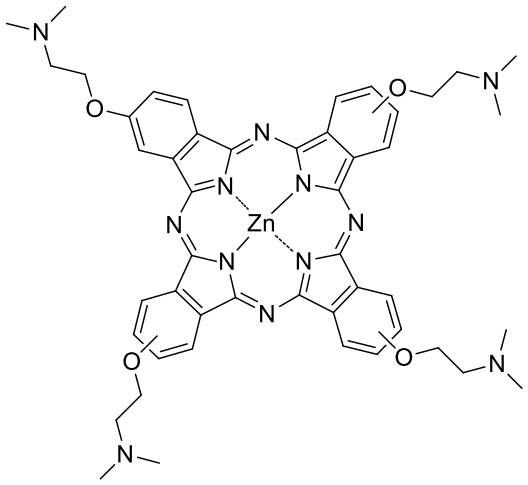

Purification of the crude by several washings with a 3:1 water:methanol mixture gave the target product in 49% yield as a green solid. ^{1}H NMR (600 MHz, Pyr-d_5) δ = 9.56 (m, 4H), 9.30 (d, J = 8.1 Hz, 4H), 7.84 – 7.92 (m, 4H), 4.56 (m, 8H), 2.92 (m, 8H), 2.40 (s, 12H), 2.35 (s, 12H) ppm; ^{13}C NMR (150 MHz, Pyr-d_5): δ = 161.49, 161.27, 153.54, 141.12, 132.08, 132.06, 118.67, 118.63, 115.87, 113.99, 112.54, 108.54, 106.59, 106.52, 67.47, 67.45, 67.37, 67.35, 58.56, 58.52, 57.95, 57.88, 45.90, 45.84, 45.63, 45.50, 37.20, 29.79, 29.75, 23.49, 23.45 ppm. FT-IR: ν = 2935, 2859, 2830, 2781, 2370, 2322, 2212, 1606, 1508, 1488, 1456, 1436, 1388, 1337, 1278, 1229, 1112, 1089, 1040, 952, 836, 827, 770, 746, 727 cm^{-1}. UV-vis (THF): λ_{max} = 677, 351 nm. MALDI-TOF $[M]^{\bullet+}$: m/z = 924.32, (Calcd: 924.35).

E-factor calculation for compound **Pc6**

Chemical	**Volume (mL)**	**Density (g/mL)**	**Mass (g)**	**Mass of solvents considered toward E-factor (after 80% solvent recovery) (g)**
2-(dimethylamino)ethanol	0.4	0.89	0.356	
DMF	4.0	0.948	3.792	
K_2CO_3			1.2	
4-nitrophthalonitrile			0.5	
Zinc acetate dihydrate			0.172	
DBU	0.4	1.018	0.407	
Water	34.0		4.5	
HCl 1N	4.0		4.0	
Methanol	7.0	0.792	5.544	1.109

Amount of product = 0.330 g (49% yield)

Total E-factor: 47.4

E-factor 80% solvent recovery = 34.0

E-factor calculation for compound **Pc6** synthesized according to the literature

Synthetic procedure with 13% total yield.[59]

- The amount of DMF was estimated to be 4 mL. To calculate the quantity of solvent required for extraction, a crude product mass of 0.75 g was assumed.

Chemical	**Volume (mL)**	**Density (g/mL)**	**Mass (g)**	**Mass of solvents considering an 80% recovery (g)**
4-nitrophthalonitrile			0.5	
1,2-(dimethylamino)-ethanol			0.356	
K_2CO_3			4.0	
DMF	4.0	0.948	3.792	
Chloroform (extraction)	398.2	1.489	592.92	118.584
Na_2SO_4			0.75	
Silica gel			197.25	
Methanol	14.3	0.792	11.326	2.265

Amount of product = 0.565 g (91% yield)

E-factor = 1434.2

E-factor assuming 80% solvent recovery = 579.0

- A crude product mass of 250 mg was assumed.

Chemical	**Volume (mL)**	**Density (g/mL)**	**Mass (g)**	**Mass of solvents considering an 80% recovery (g)**
4-(2-(dimethylamino)ethoxy)phthalonitrile			0.215	

DBU			0.152	
Pentanol	8.0		6.488	
Zinc acetate			0.064	
Aqueous acetic acid	6.45	1.0	6.45	
Diethyl ether	6.45	0.713	4.599	0.92
Ethyl acetate	6.45	0.902	5.818	1.164
Dichloromethane	6.45	1.327	8.559	1.712
Chloroform	83.95	1.489	125.001	25.00
K_2CO_3	37.5		37.5	
Silica gel			65.75	
Methanol	40.0		31.68	6.336

Amount of product = 0.032 g (14% yield)

E-factor = 9132.6

E-factor assuming 80% solvent recovery = 4741.2

Total yield: 13%, total E-factor: 10566.8, Total E-factor assuming 80% solvent recovery = 5320.2

Synthetic procedure with 55% total yield:[68]

The corresponding phthalonitrile precursor for this synthesis was prepared according to the literature.[59]

- For the calculation of extraction solvent volumes, it was assumed that 0.6 g of crude product was obtained.

Chemical	**Volume (mL)**	**Density (g/mL)**	**Mass (g)**	**Mass of solvents considering an 80% recovery (g)**
4-(2-(dimethylamino)ethoxy)phthalonitrile			0.5	
DMAE	0.7	0.890	0.623	
Butan-1-ol	0.7	0.810	0.567	
Zinc acetate			0.15	
Dichloromethane	90.0	1.327	119.43	23.886
Na_2SO_4			0.6	
Al_2O_3			50.0	
Chloroform	240.0	1.489	357.36	71.472

Amount of product = 0.32 g (60% yield)

E-factor = 1652.8

E-factor assuming 80% solvent recovery = 460.9

Total yield: 55%, total E-factor: 3087.0, total E-factor assuming 80% solvent recovery: 1039.9

^{1}H NMR spectrum of tetra-(2-dimethylaminoethoxy)-zinc-phthalocyanine **Pc6** in Pyr-d_5

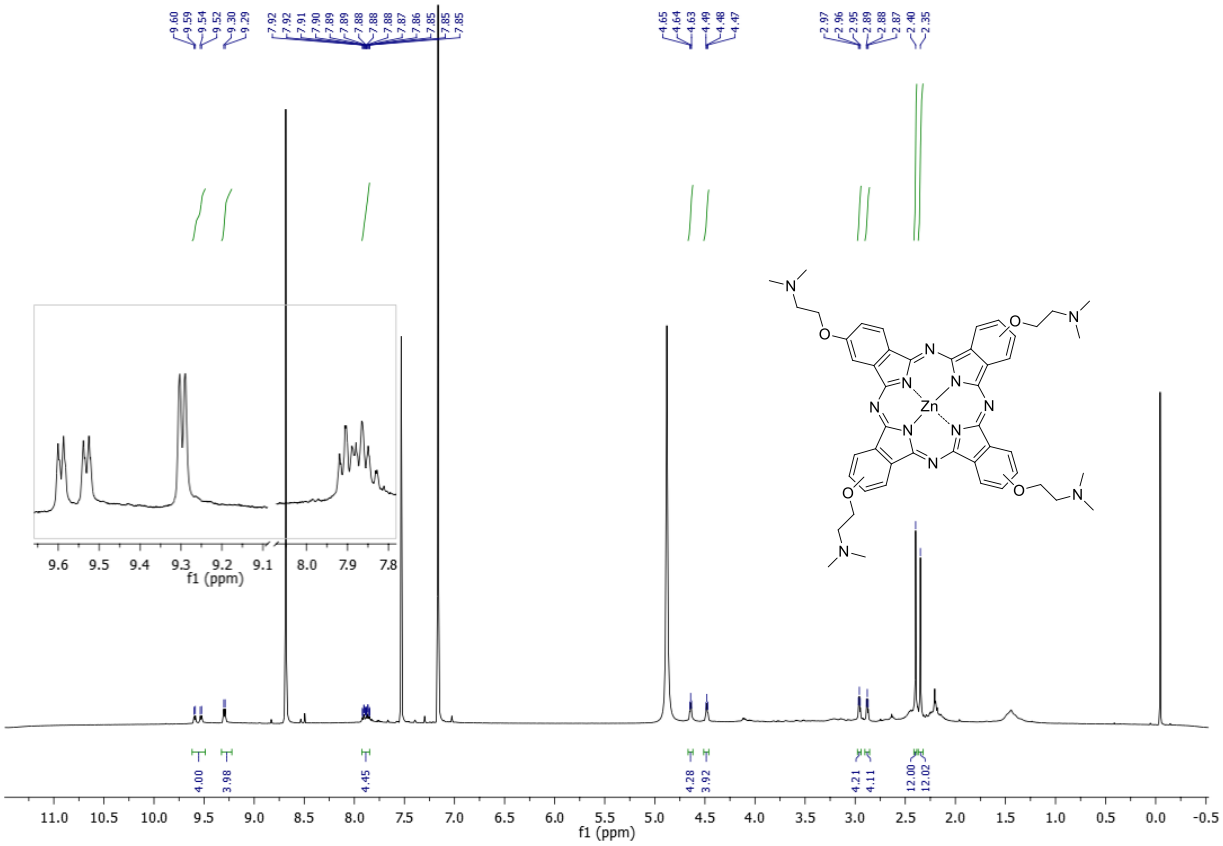

^{13}C NMR spectrum of tetra-(2-dimethylaminoethoxy)-zinc-phthalocyanine **Pc6** in Pyr-d_5

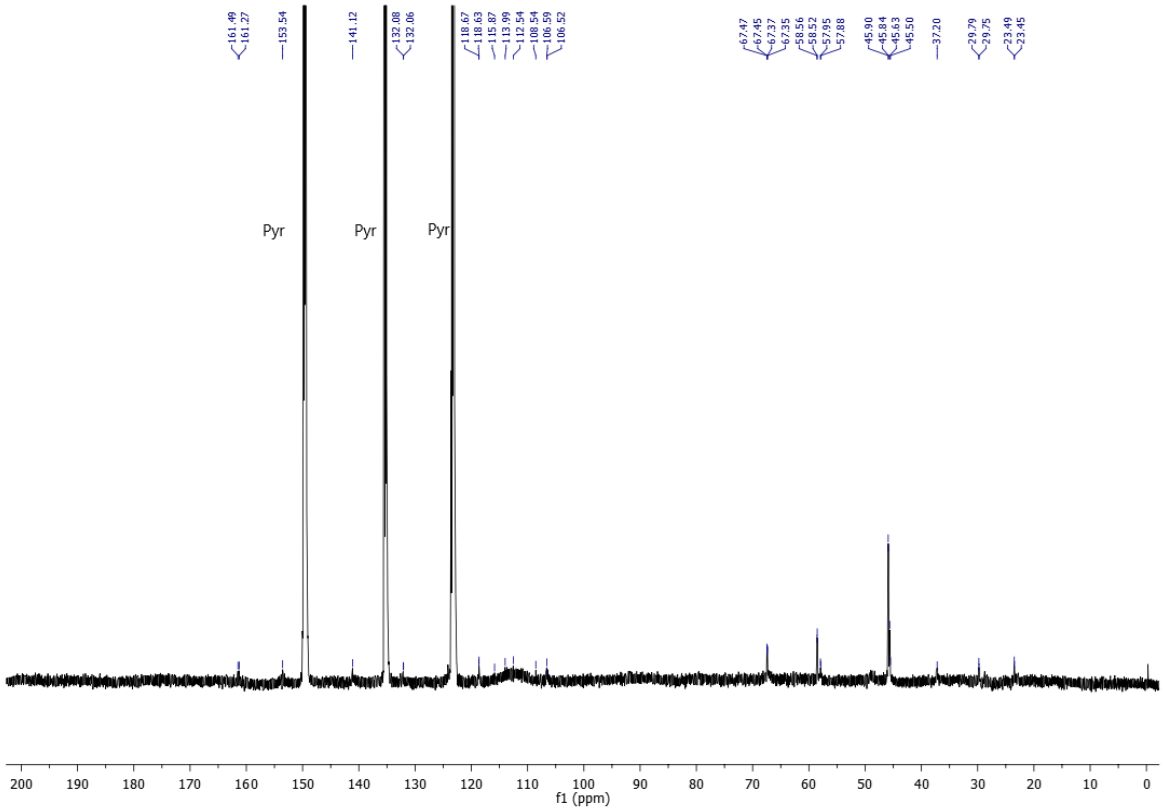

ATR spectrum of tetra-(2-dimethylaminoethoxy)-zinc-phthalocyanine **Pc6**

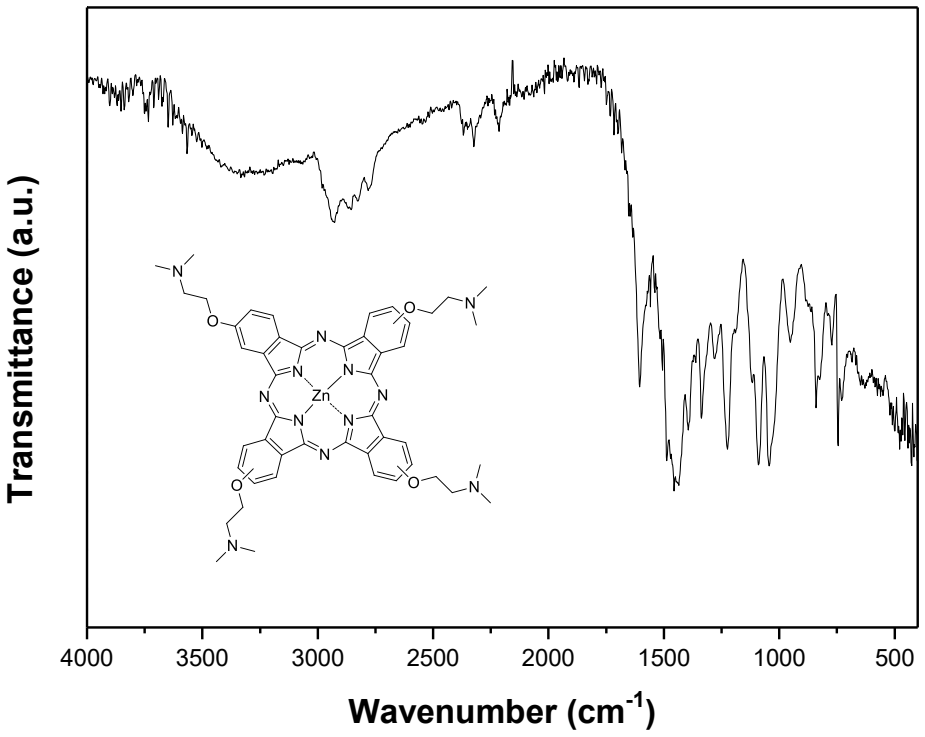

MALDI-TOF spectrum of tetra-(2-dimethylaminoethoxy)-zinc-phthalocyanine **Pc6**

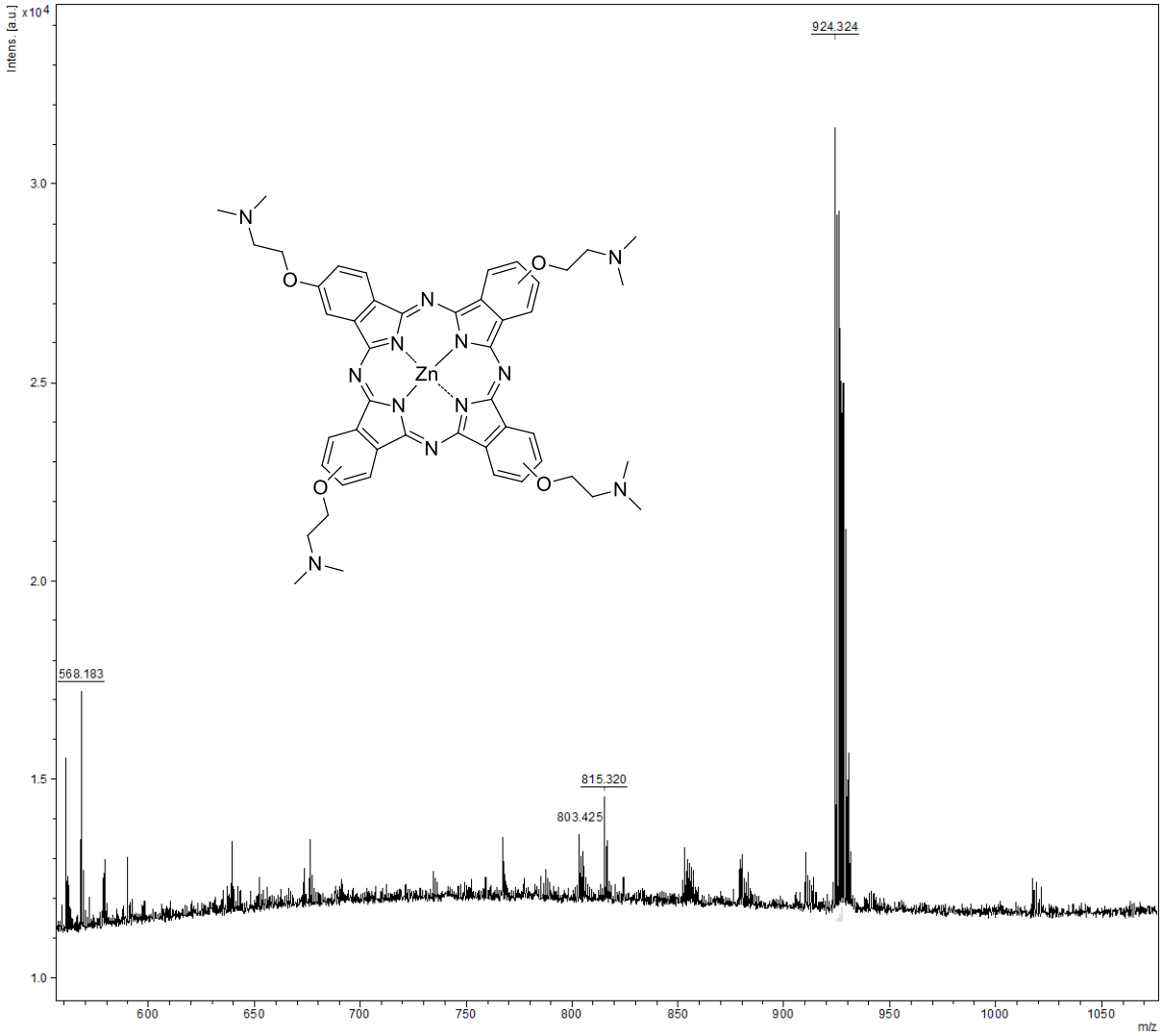

2.4.15. Synthesis, Green Chemistry metric calculation and characterization of tetra-(hexyloxy)-zinc-phthalocyanine Pc7

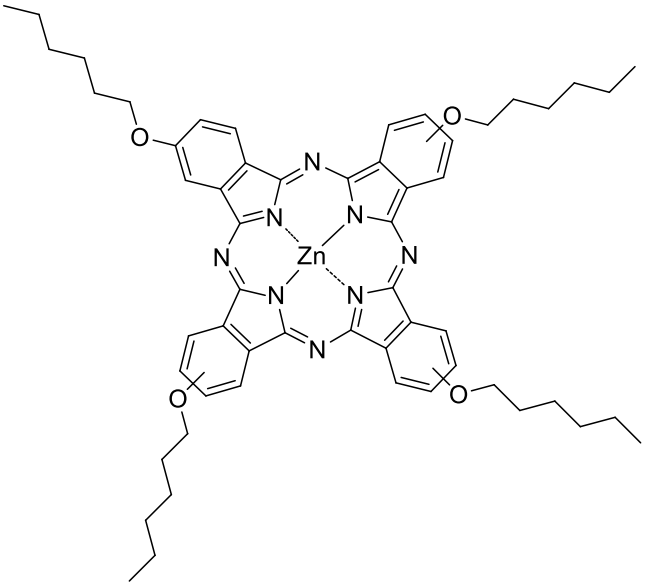

Purification of the crude was carried out by short pad filtration on silica gel, using THF for sample loading and a 2:1 hexane:THF mixture as the eluent. The target compound was obtained as a blue solid in 22% yield. ^{1}H NMR (600 MHz, THF-d_8): δ = 8.98 – 8.88 (m, 4H), 8.55 – 8.51 (m, 4H), 7.57 – 7.49 (m, 4H), 4.49 (bs, 8H), 2.14 – 2.09 (m, 8H), 1.82 – 1.78 (m, 8H), 1.61 – 1.53 (m, 16H), 1.08 – 1.04 (m, 12H) ppm; ^{13}C NMR (150 MHz, THF-d_8): δ = 161.94, 132.52, 125.90, 124.03, 69.41, 32.87, 30.74, 27.05, 23.73, 14.55 ppm. FT-IR: ν = 2954, 2925, 2859, 2361, 2341, 2321, 1603, 1495, 1460, 1384, 1335, 1277, 1228, 1112, 1083, 1046, 946, 874, 846, 818, 770, 746, 726, 658 cm^{-1}. UV-vis (THF): λ_{max} = 676, 349 nm. MALDI-TOF [M+H]$^{+}$: m/z = 977.522, (Calcd: 976.43).

E-factor calculation for compound **Pc7**

Chemical	**Volume (mL)**	**Density (g/mL)**	**Mass (g)**	**Mass of solvents considered toward E-factor (after 80% solvent recovery) (g)**
Hexan-1-ol	0.4	0.814	0.326	
DMF	4.0	0.948	3.792	
K_2CO_3			1.2	
4-nitrophthalonitrile			0.5	
Zinc acetate dihydrate			0.172	
DBU	0.4	1.018	0.407	
HCl 1N	2.0		2.0	
Water	22.0		22.0	
Silica gel			10.0	
THF	20.0	0.888	17.76	3.552
Hexane	30.0	0.661	19.83	3.966
Methanol	19.0	0.792	15.048	3.010

Amount of product = 0.16 g (22% yield)

Total E-factor = 443.0

E-factor 80% solvent recovery = 179.8

^{1}H NMR spectrum of tetra-(hexyloxy)-zinc-phthalocyanine **Pc7** in THF-d_8.

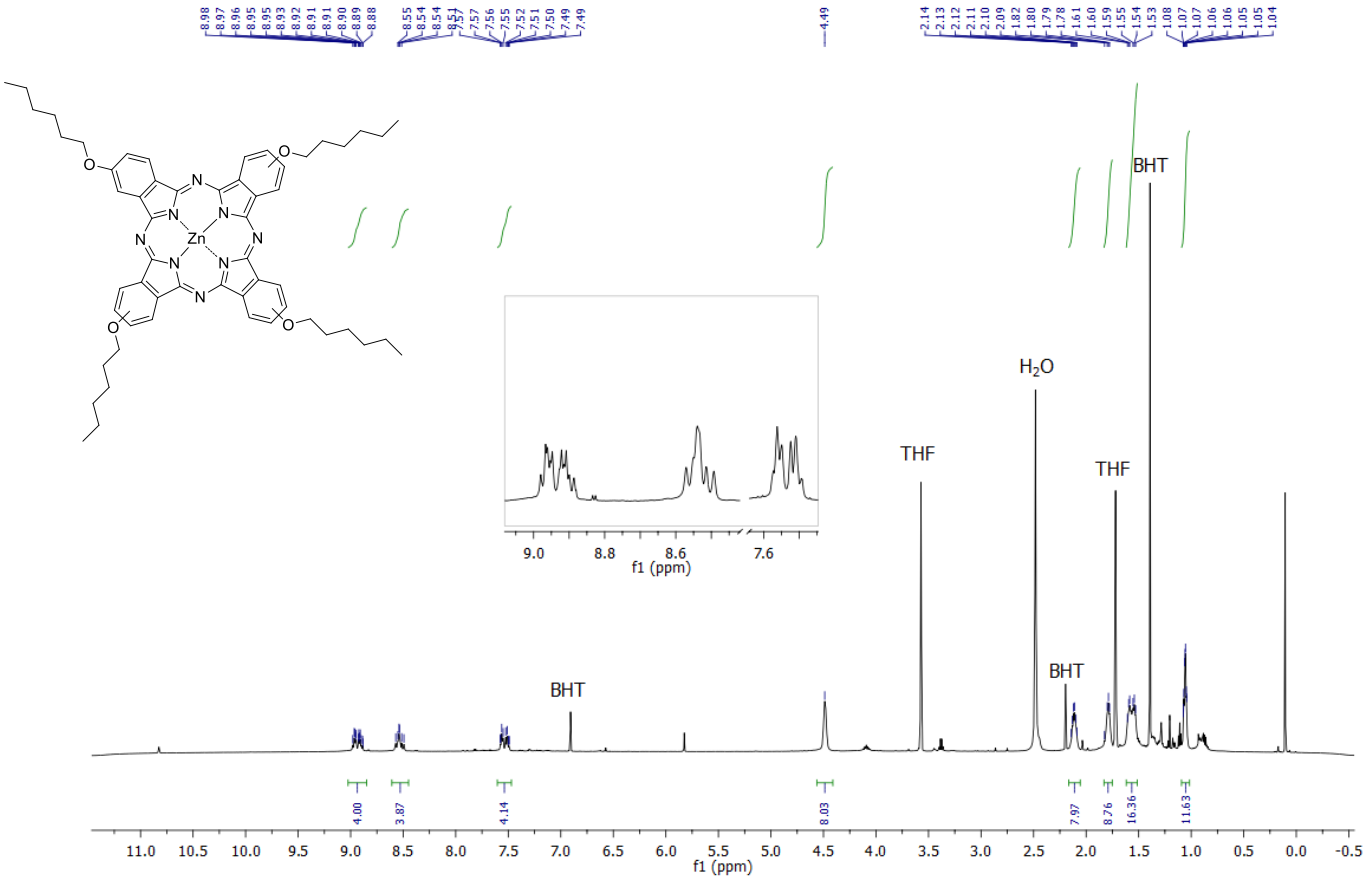

^{13}C NMR spectrum of tetra-(hexyloxy)-zinc-phthalocyanine **Pc7** in THF-d_8

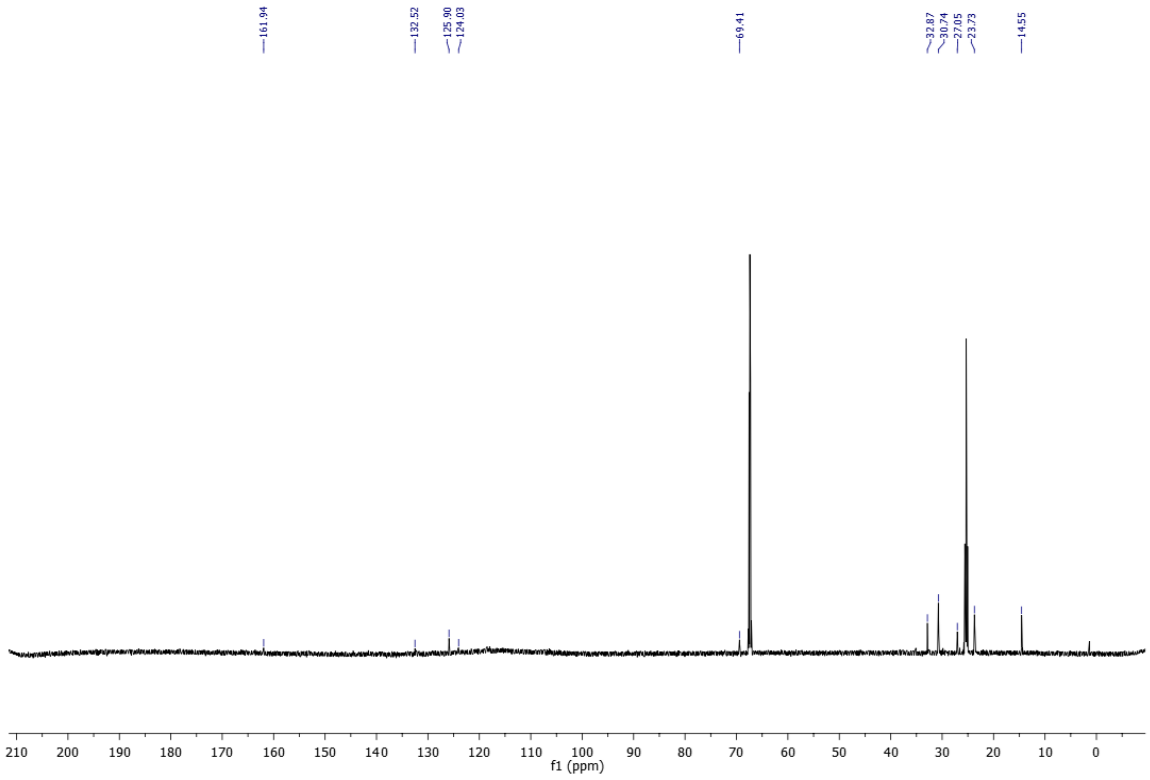

ATR spectrum of tetra-(hexyloxy)-zinc-phthalocyanine **Pc7**

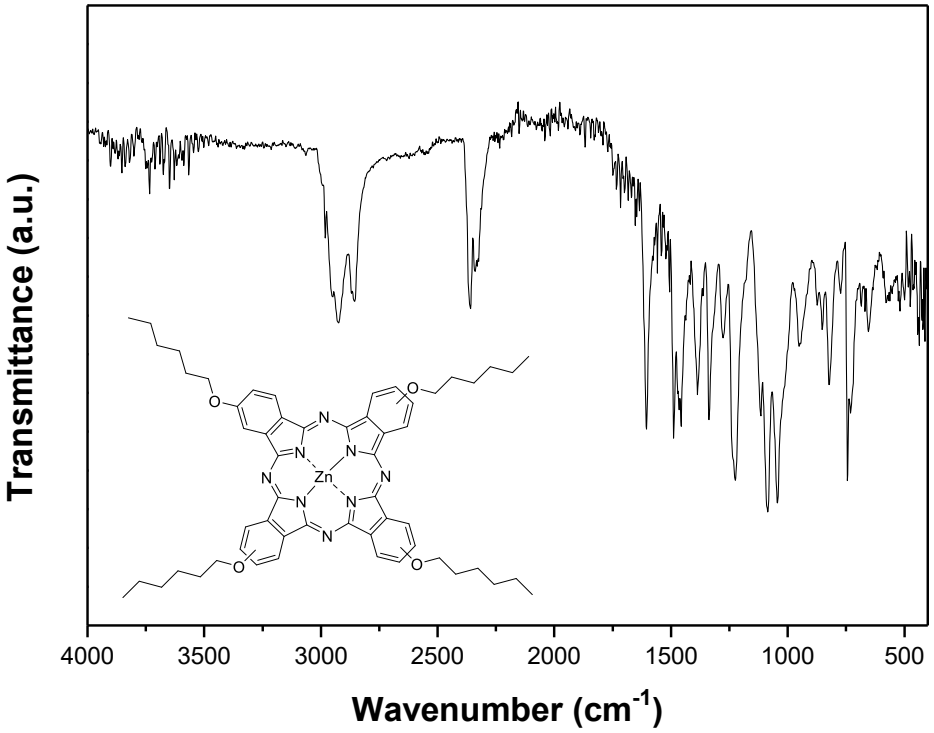

MALDI-TOF spectrum of tetra-(hexyloxy)-zinc-phthalocyanine **Pc7**

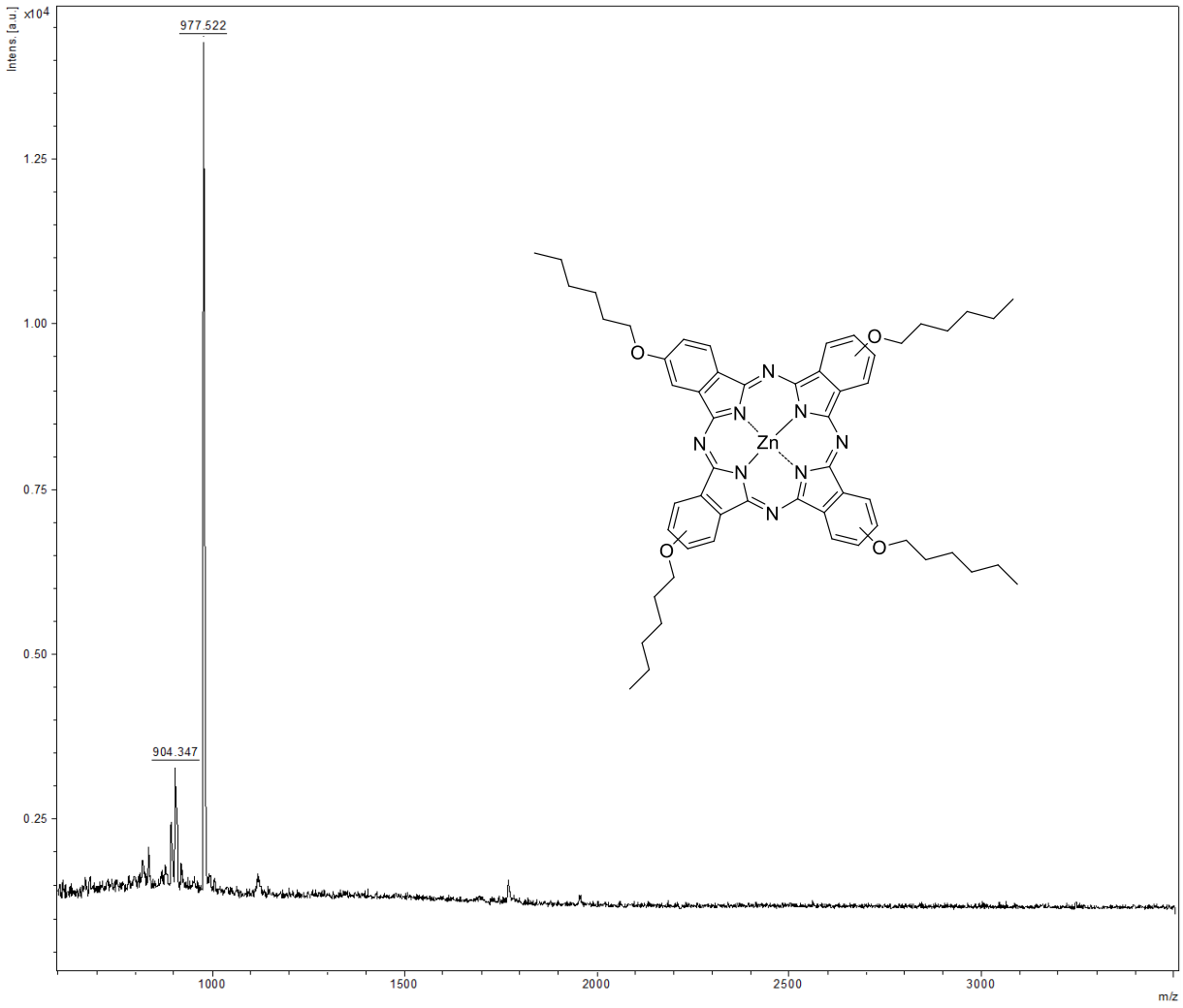

2.4.16. Synthesis, Green Chemistry metric calculation and characterization of octakis(3,5-dimethylphenoxy)-zinc-phthalocyanine Pc8

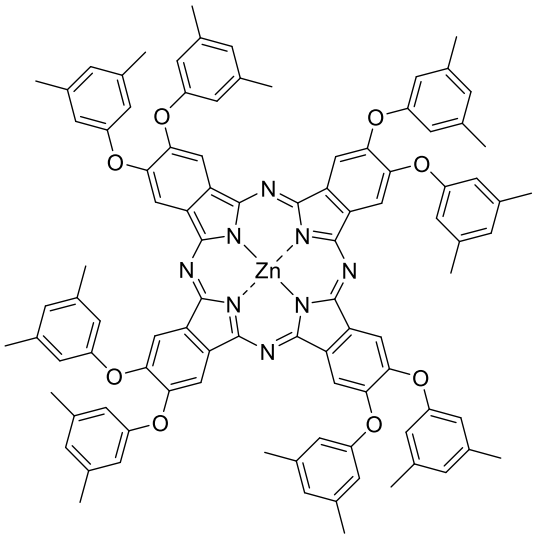

Purification of the crude was carried out by short pad filtration on silica gel, using THF for sample loading and a 2:1 petroleum ether:THF mixture as the eluent. The target compound was obtained as a green solid in 30% yield. ^{1}H NMR (600 MHz, THF-d_8): 8.75 (s, 8H), 6.89 (s, 16H), 6.79 (m, 8H), 2.31 (s, 48H) ppm; ^{13}C NMR (150 MHz, THF-d_8): 159.03, 151.29, 140.23, 135.58, 125.80, 116.82, 115.53, 21.58 ppm. FT-IR: ν = 3011, 2918, 2853, 1614, 1587, 1445, 1396, 1389, 1261, 1177, 1132, 1086, 1038, 1022, 947, 868, 833, 744, 723, 683 cm^{-1}. UV-vis (THF): λ_{max} = 679, 357 nm. MALDI-TOF [M+H]$^{+}$: m/z =1536.639, (Calcd: 1539.124).

E-factor calculation for compound **Pc8**

Chemical	**Volume (mL)**	**Density (g/mL)**	**Mass (g)**	**Mass of solvents considered toward E-factor (after 80% solvent recovery) (g)**
3,5-dimethylphenol			0.368	
DMF	4.0	0.948	3.792	
K_2CO_3			0.423	
4,5-dichlorophthalonitrile			0.2	
Zinc acetate dihydrate			0.06	
DBU	0.152	1.018	0.155	
HCl 1N	5.0		5.0	
Water	10.0		10.0	
Silica gel			10.0	
THF	30.0	0.888	26.64	5.328
Hexane	60.0	0.661	39.66	7.932
Methanol	10.0	0.792	7.92	1.584

Amount of product = 0.118 g (30% yield)

Total E-factor = 797.4

E-factor 80% solvent recovery = 294.3

^{1}H NMR spectrum of octakis(3,5-dimethylphenoxy)-zinc-phthalocyanine **Pc8** in THF-d_8

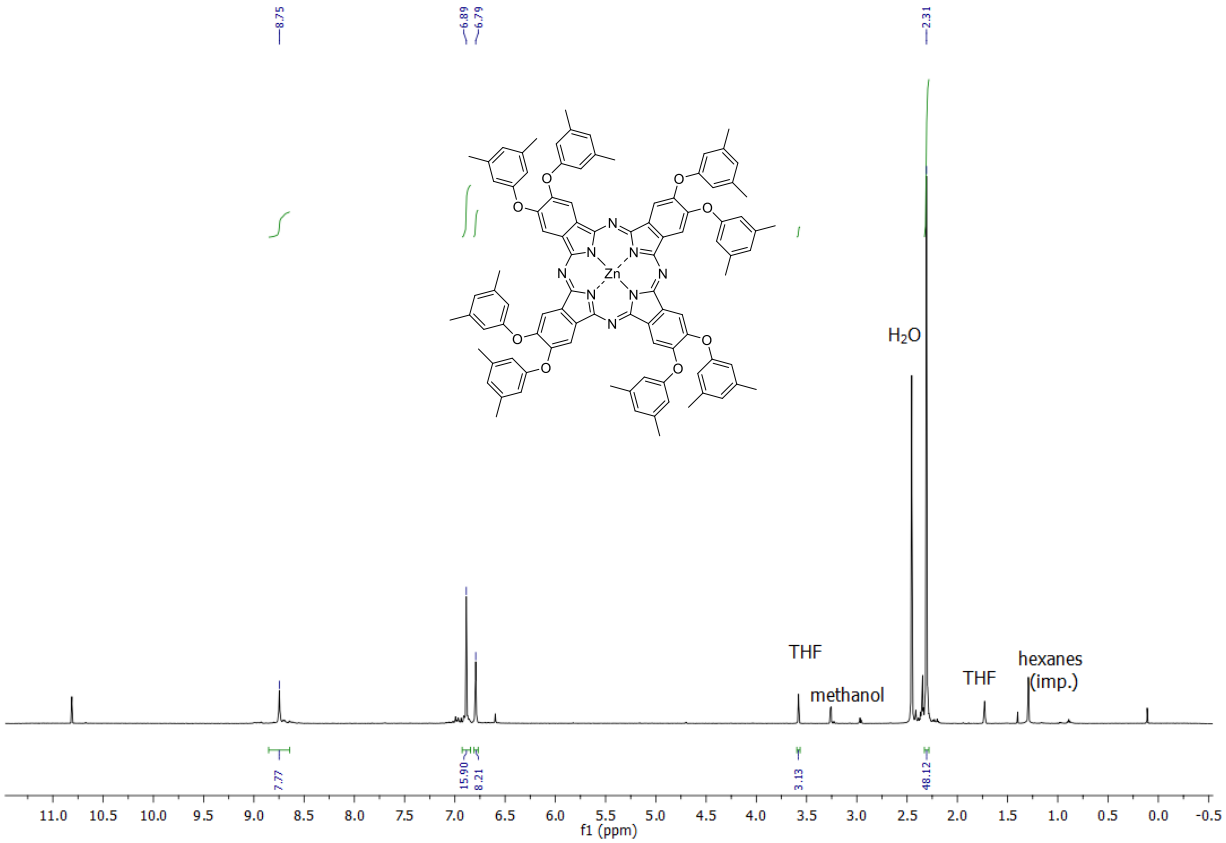

^{13}C NMR spectrum of octakis(3,5-dimethylphenoxy)-zinc-phthalocyanine **Pc8** in THF-d_8

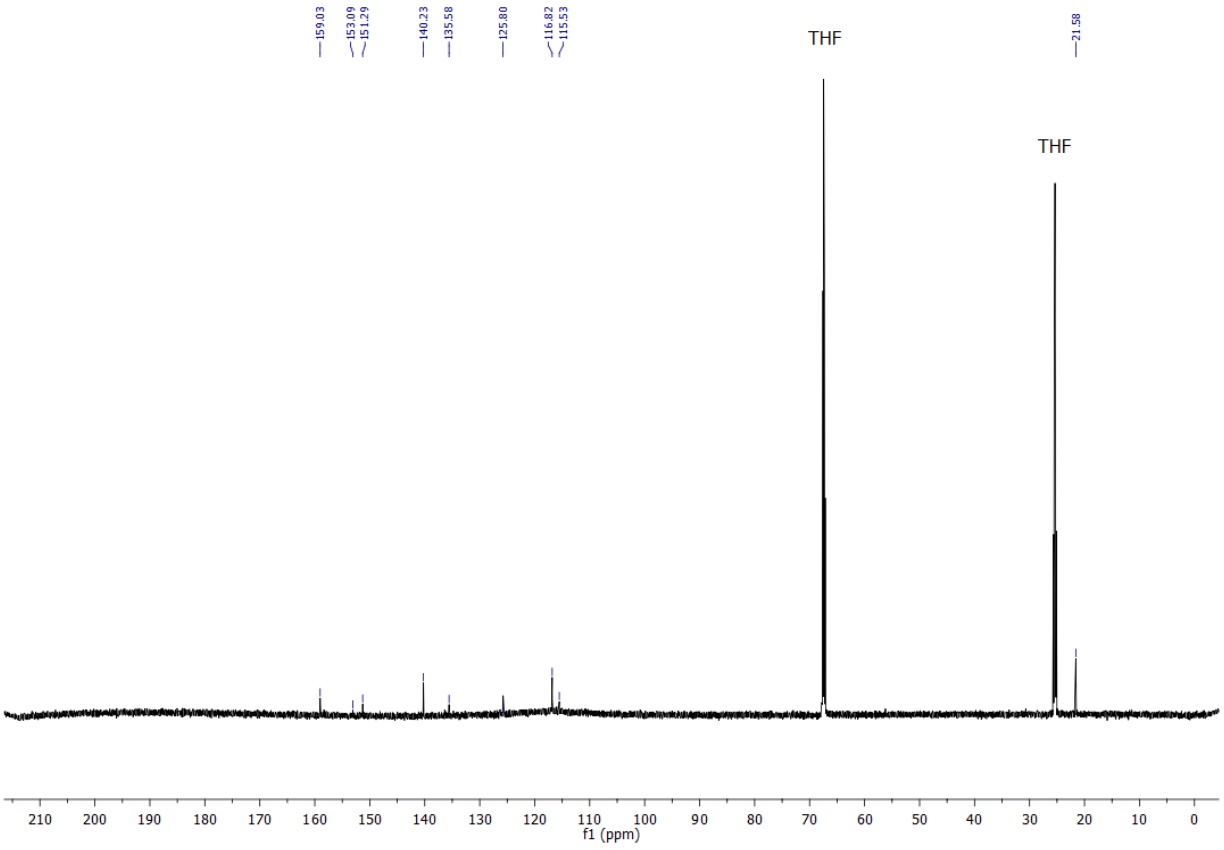

ATR spectrum of octakis(3,5-dimethylphenoxy)-zinc-phthalocyanine **Pc8**

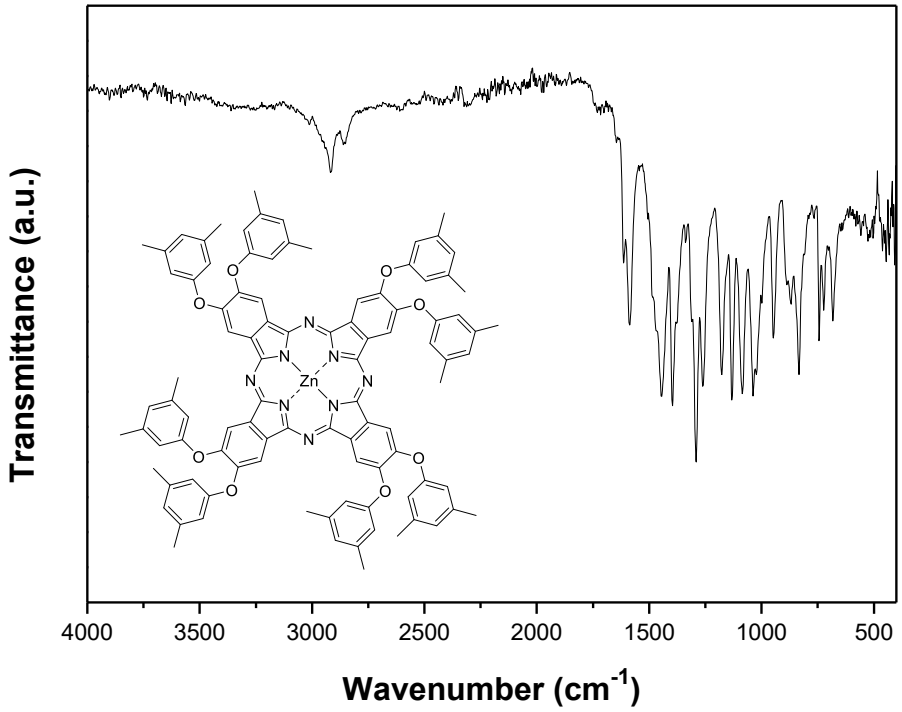

MALDI-TOF spectrum of octakis(3,5-dimethylphenoxy)-zinc-phthalocyanine **Pc8**

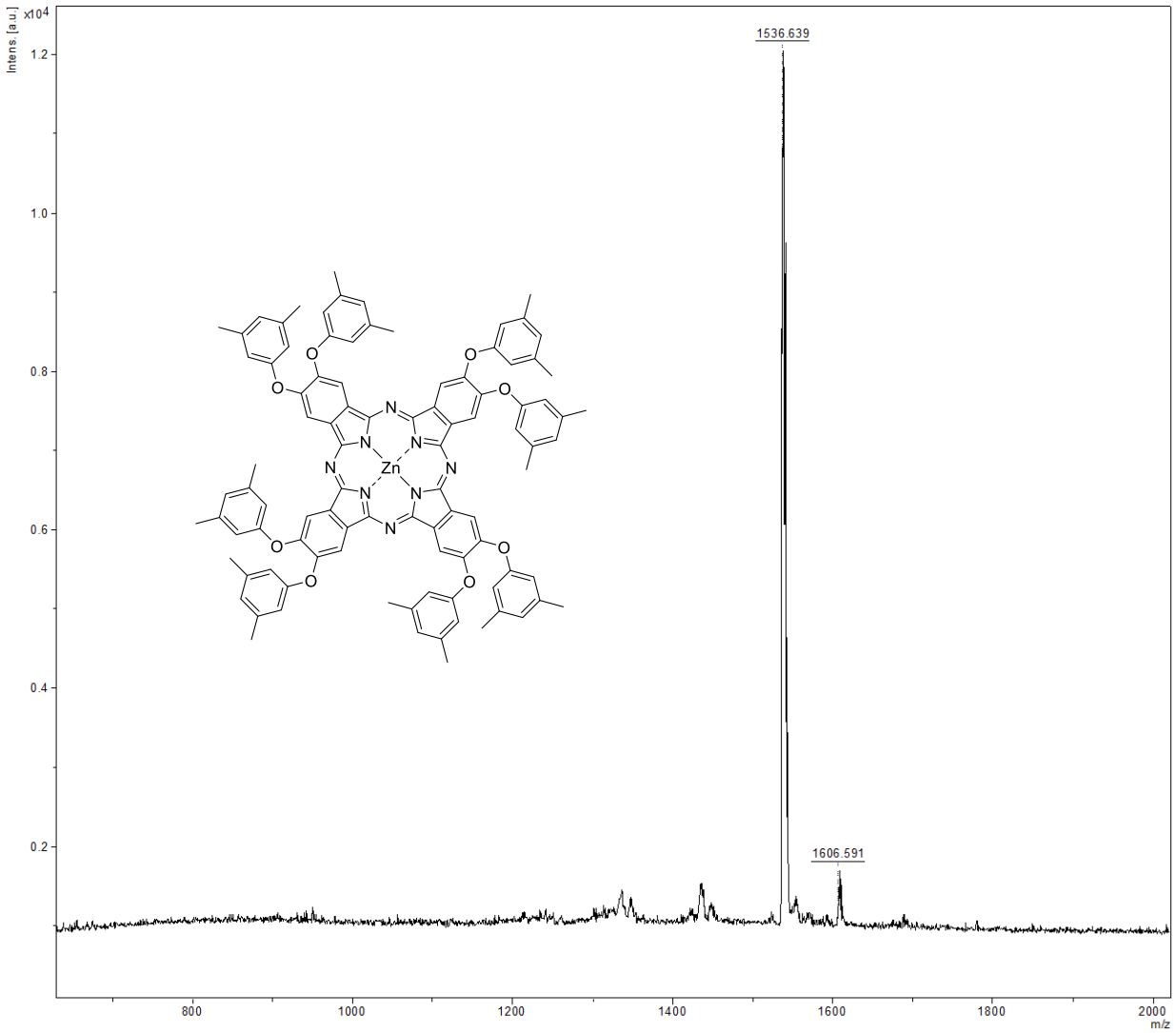

2.4.17. Synthesis, Green Chemistry metric calculation and characterization of octakis(*p*-tolyloxy)-zinc-phthalocyanine Pc9

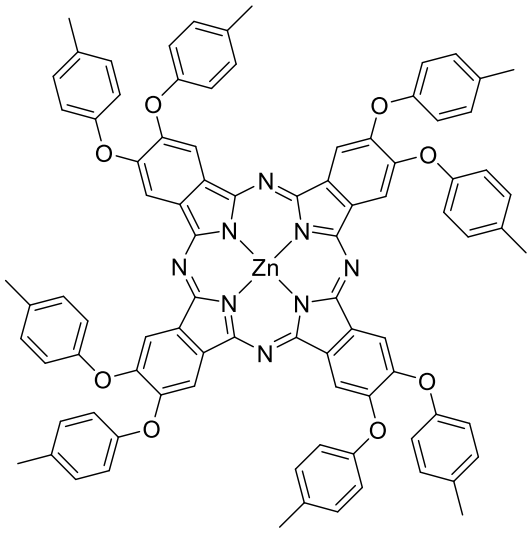

Purification of the crude was performed by short pad filtration on silica gel, using THF for sample loading and gradient elution with increasing polarity, from 7:1 to 3:1 to 2:1 petroleum ether:THF. The target compound was obtained as a green solid in 31% yield. ^{1}H NMR (600 MHz, THF-d_8): 8.72 (s, 8H), 7.20 – 7.17 (m, 32H), 2.35 (s, 24H) ppm; ^{13}C NMR (150 MHz, THF-d_8): 156.95, 152.86, 151.27, 135.53, 133.41, 131.15, 119.06, 115.28, 21.05. FT-IR: ν = 3028, 2918, 2855, 1605, 1504, 1485, 1447, 1398, 1337, 1265, 1202, 1173, 1138, 1090, 1028, 953, 890, 860, 810, 725, 698, 486, 473 cm^{-1}. UV-vis (THF): λ_{max} = 676, 356 nm. MALDI-TOF $[M+H]^+$: m/z =1425.052, (Calcd: 1426.908).

E-factor calculation for compound **Pc9**

Chemical	**Volume (mL)**	**Density (g/mL)**	**Mass (g)**	**Mass of solvents considered toward E-factor (after 80% solvent recovery) (g)**
4-methylphenol			0.34	
DMF	4.0	0.948	3.792	
K_2CO_3			0.423	
4,5-dichlorophthalonitrile			0.2	
Zinc acetate dihydrate			0.061	
DBU	0.152	1.018	0.155	
HCl 1N	5.0		5.0	
Water	10.0		10.0	
Silica gel			10.0	
THF	17.7	0.888	15.73	3.146
Hexane	57.3	0.661	38.16	7.630
Methanol	15.0	0.792	11.88	2.376

Amount of product = 0.114 g (31% yield)

Total E-factor = 751.1

E-factor 80% solvent recovery = 289.5

^{1}H NMR spectrum of octakis(*p*-tolyloxy)-zinc-phthalocyanine **Pc9** in THF-d_8

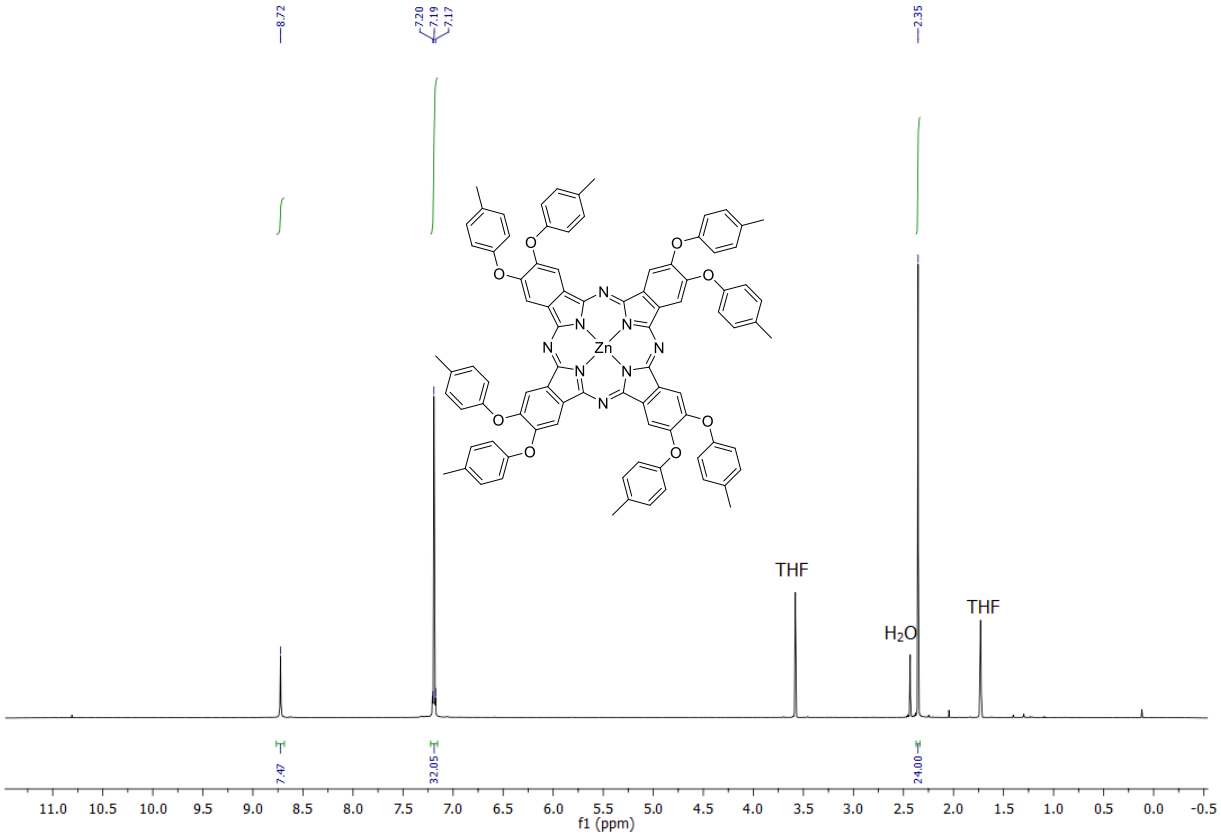

^{13}C NMR spectrum of octakis(*p*-tolyloxy)-zinc-phthalocyanine **Pc9** in THF-d_8

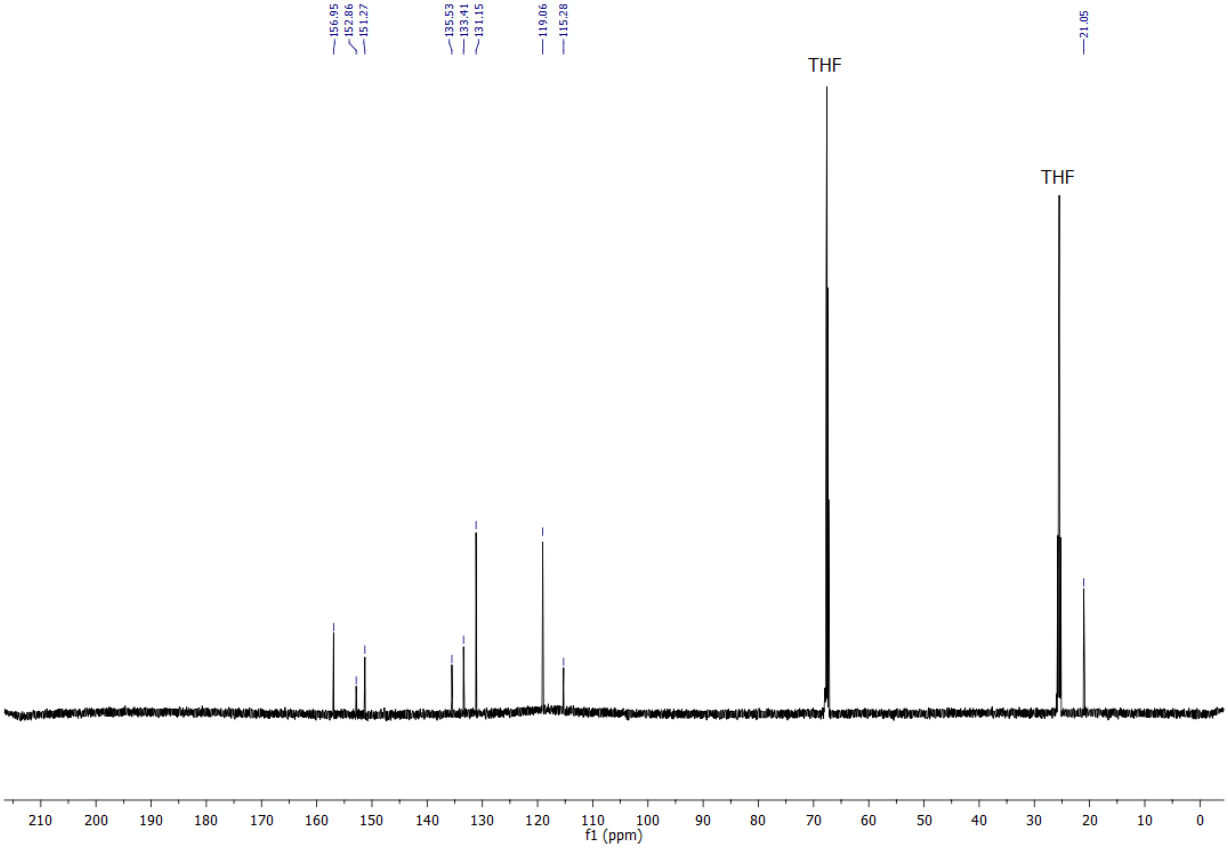

ATR spectrum of octakis(*p*-tolyloxy)-zinc-phthalocyanine **Pc9**

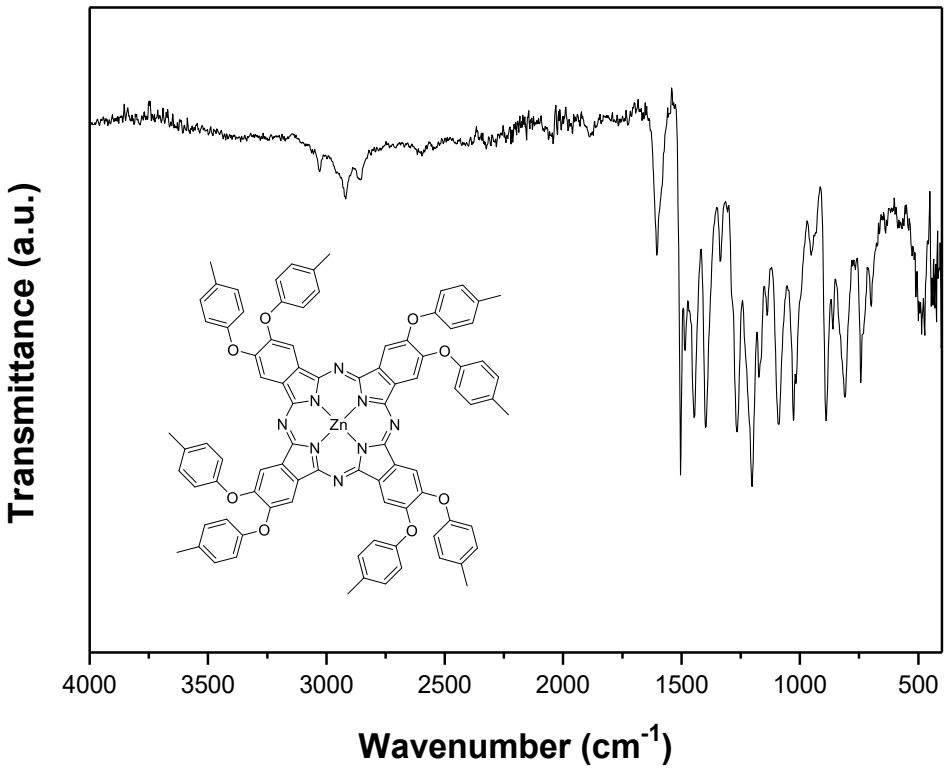

MALDI-TOF spectrum of octakis(*p*-tolyloxy)-zinc-phthalocyanine **Pc9**

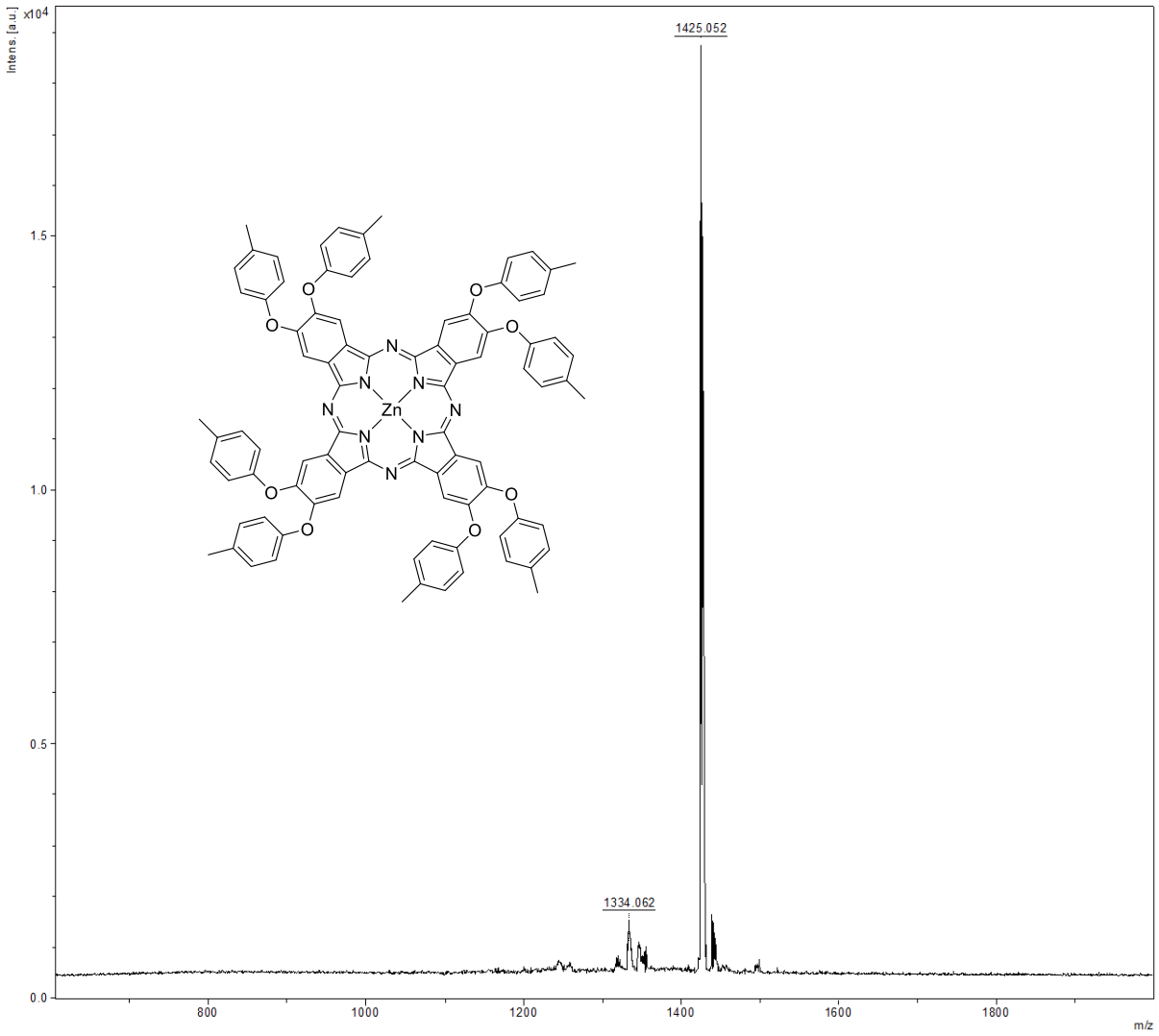

2.4.18. Synthesis, Green Chemistry metric calculation and characterization of tetra-*tert*-butyl-zinc-phthalocyanine Pc10

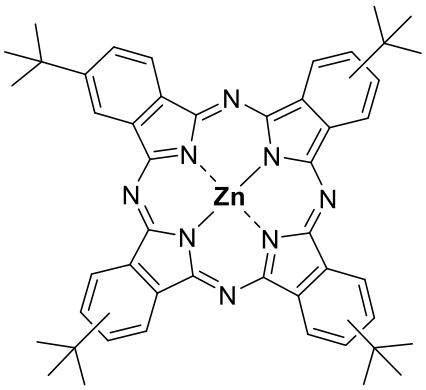

The reaction was carried out following the general procedure for the optimized cyclotetramerization of phthalonitriles in PEG-400. 4-*tert*-Butylphthalonitrile (500.6 mg, 2.7 mmol), PEG-400 (1.08 g, 2.7 mmol), DBU (83.3 mg, 0.5 mmol), and zinc acetate dihydrate (157.6 mg, 0.7 mmol) were employed. After completion of the reaction and cooling to room temperature, the mixture was diluted with methanol (2.0 mL) and 1 N HCl (1.0 mL). The resulting precipitate was collected by filtration. Additional methanol/water (1:1, 10.0 mL) was used for washing.

The crude product was purified by filtration through a short pad of silica gel (8.43 g). The crude solid was loaded onto the silica using THF (3.0 mL). Packing and elution were performed using hexane/THF (40.0 mL). The collected solid was further washed with methanol/water (1:1, 10.0 mL) and dried under vacuum to constant weight to afford compound **1** as a purple crystalline solid (418 mg, 77% yield). UV-vis (THF): λ_{max} = 671, 347 nm. ^{1}H NMR (600 MHz, DMSO) 9.41 – 9.20 (m, 8H), 8.34 – 8.28 (m, 4H), 1.79 – 1.77 (m, 36H). AP-MALDI-(-) $[M]^{\bullet-}$: m/z = 800.3298, (Calcd: 800.33).

E-factor calculation for compound **Pc10**

Chemical	**Volume (mL)**	**Density (g/mL)**	**Mass (g)**	**Mass of solvents considered toward E-factor (after 80% solvent recovery) (g)**
4-*tert*-butylphthalonitrile			0.5006	
PEG-400			1.08	
DBU			0.0833	
Zinc acetate dihydrate			0.1576	
HCl 1N	1.0		1.0	
Water	15		15	
Methanol	15	0.792	11.88	2.38
Silica gel			8.43	
Hexane	30	0.661	19.83	3.97
THF	10	0.888	8.88	1.78

Amount of product = 0.418 g (77% yield)

E-Factor = 123.0

E-factor 80% solvent recovery = 73.7

^{1}H NMR spectrum of tetra-*tert*-butyl-zinc-phthalocyanine **Pc10** in DMSO-d_6

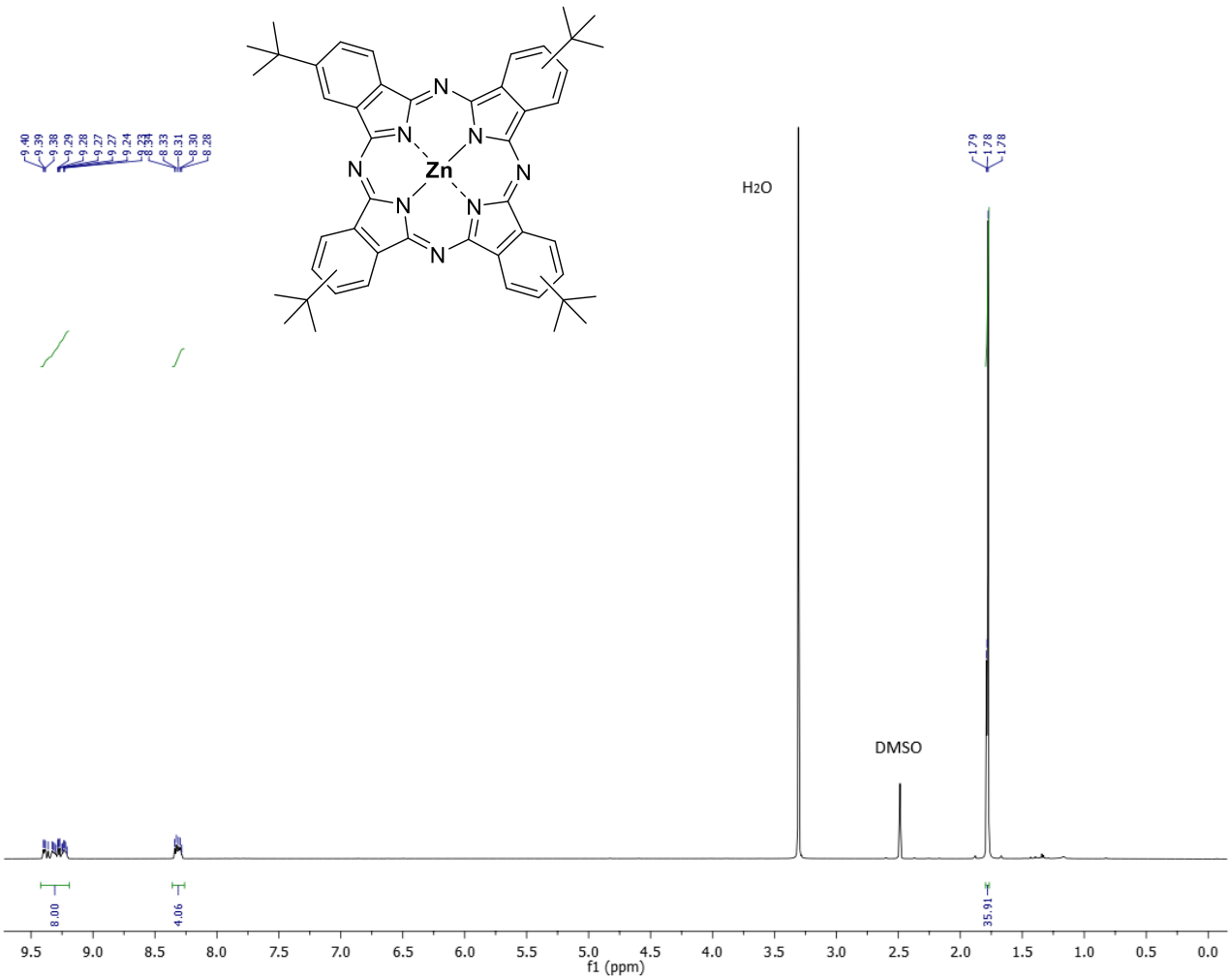

AP-MALDI-(-) spectrum of tetra-*tert*-butyl-zinc-phthalocyanine **Pc10**

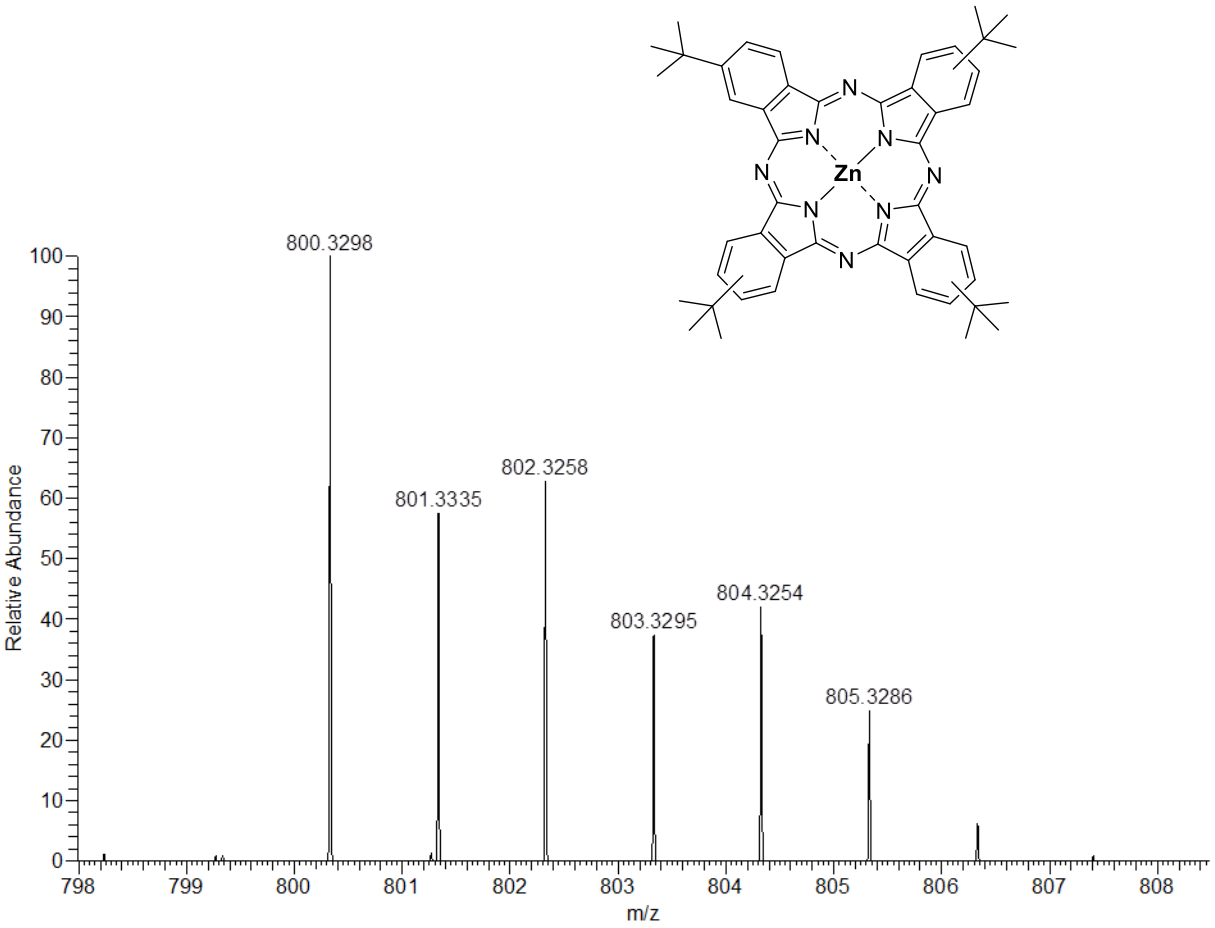

2.4.19. Synthesis, Green Chemistry metric calculation and characterization of tetra-*tert*-butyl-cobalt-phthalocyanine Pc11

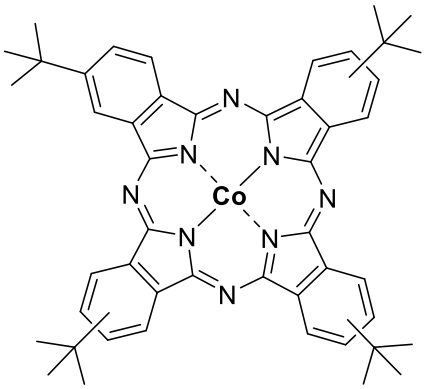

The reaction was carried out following the general procedure for the optimized cyclotetramerization of phthalonitriles in PEG-400. 4-*tert*-Butylphthalonitrile (499.7 mg, 2.7 mmol), PEG-400 (1.07 g, 2.7 mmol), DBU (85.0 mg, 0.6 mmol), and cobalt acetate tetrahydrate (178.2 mg, 0.7 mmol) were employed. After completion of the reaction and cooling to room temperature, the mixture was diluted with methanol (2.0 mL), 1 N HCl (1.0 mL) and water (1.0 mL). The resulting precipitate was collected by filtration and washed with water/methanol mixture (2:1, 10.0 mL).

The product was then purified by thorough washings with 30 mL of acetonitrile in 5 portions to obtain compound **Pc11** as a purple crystalline solid solid in 73% yield (396.7 mg). UV-vis (THF): λ_{max} = 661, 327 nm. AP-MALDI-(-) $[M]^{\bullet-}$: m/z = 795.3337, (Calcd: 795.33).

E-factor calculation for compound **Pc11**

Chemical	**Volume (mL)**	**Density (g/mL)**	**Mass (g)**	**Mass of solvents considered toward E-factor (after 80% solvent recovery) (g)**
4-*tert*-butylphthalonitrile			0.4997	
PEG-400			1.07	
DBU			0.085	
Cobalt acetate tetrahydrate			0.1782	
HCl 1N	1		1	
Water	7.66		7.66	
Methanol	5.33	0.792	4.22	0.84
Acetonitrile	30.0	0.786	23.58	4.72

Amount of product = 0.3967 g (73% yield)

E-factor = 76.2

E-factor 80% solvent recovery = 20.2

AP-MALDI-(-) mass spectrum of tetra-*tert*-butyl-cobalt-phthalocyanine **Pc11**

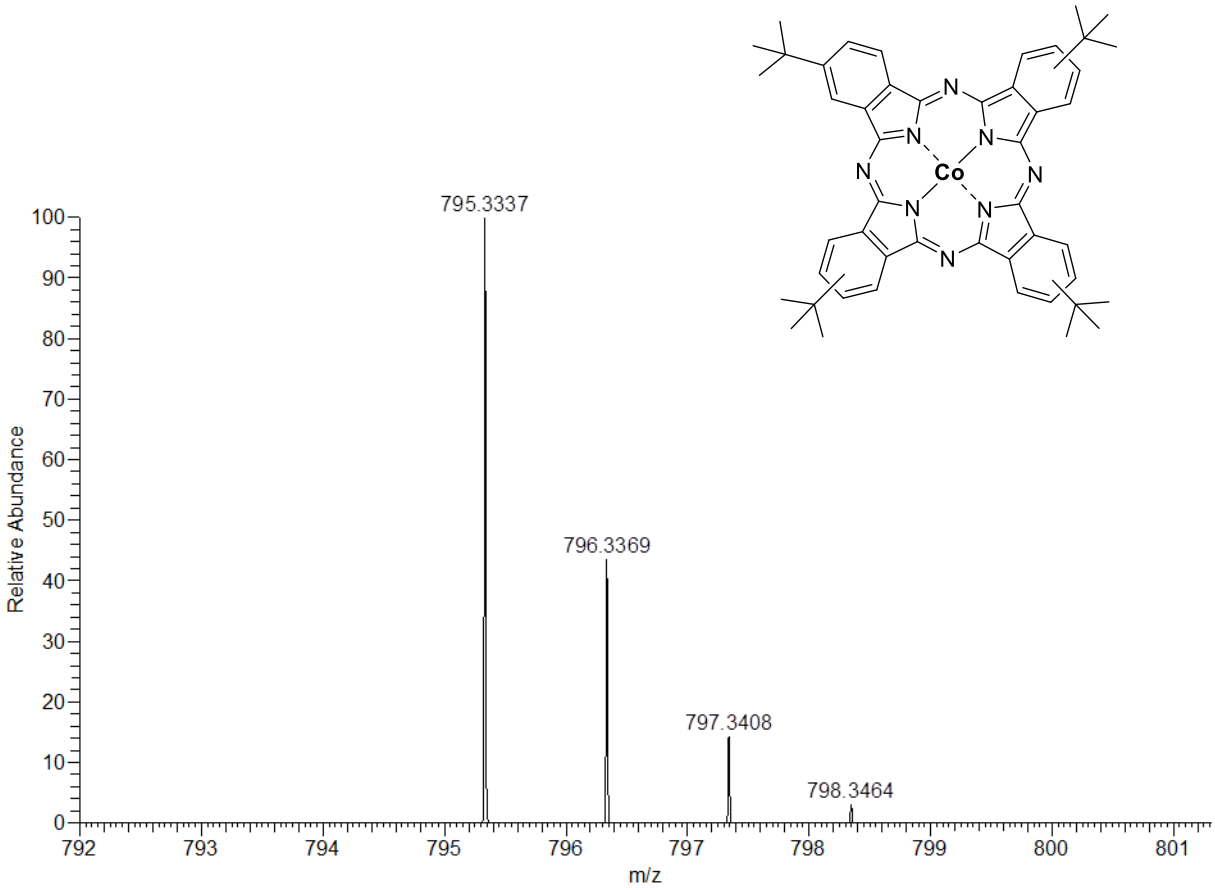

2.4.20. Synthesis, Green Chemistry metric calculation and characterization of tetra-*tert*-butyl-copper-phthalocyanine Pc12

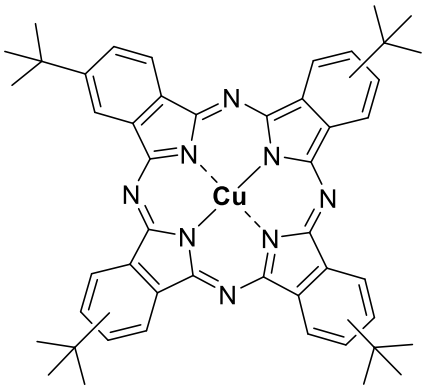

The reaction was carried out following the general procedure for the optimized cyclotetramerization of phthalonitriles in PEG-400. 4-*tert*-Butylphthalonitrile (500.1 mg, 2.7 mmol), PEG-400 (1.06 g, 2.7 mmol), DBU (94.1 mg, 0.6 mmol), and copper acetate monohydrate (141.7 mg, 0.7 mmol) were employed. After completion of the reaction and cooling to room temperature, the mixture was diluted with methanol (2.0 mL) and 1 N HCl (1.0 mL). The resulting precipitate was collected by filtration and washed with methanol/water mixture (2:1, 21.0 mL) and an ethanolic KOH solution (0.045 M, prepared from KOH (90.0 mg) in ethanol (28.0 g). After drying under vacuum to constant weight, compound **Pc12** was obtained as a purple crystalline solid (318.5 mg, 59% yield). UV-vis (THF): λ_{max} = 671, 344 nm. AP-MALDI-(-) $[M]^{\bullet-}$: m/z = 799.3308, (Calcd: 799.33).

E-factor calculation for compound **Pc12**

Chemical	**Volume (mL)**	**Density (g/mL)**	**Mass (g)**	**Mass of solvents considered toward E-factor (after 80% solvent recovery) (g)**
4-*tert*-butylphthalonitrile			0.5001	
PEG-400			1.06	
DBU			0.0941	
Copper acetate monohydrate			0.1417	
HCl 1N	1		1	
Water	7		7	
Methanol	16	0.792	12.672	2.53
KOH			0.090	
Ethanol			28	

Amount of product = 0.3185 g (59% yield)

E-factor = 135.8

E-factor 80% solvent recovery = 103.9

AP-MALDI-(-) mass spectrum of tetra-*tert*-butyl-copper-phthalocyanine **Pc12**

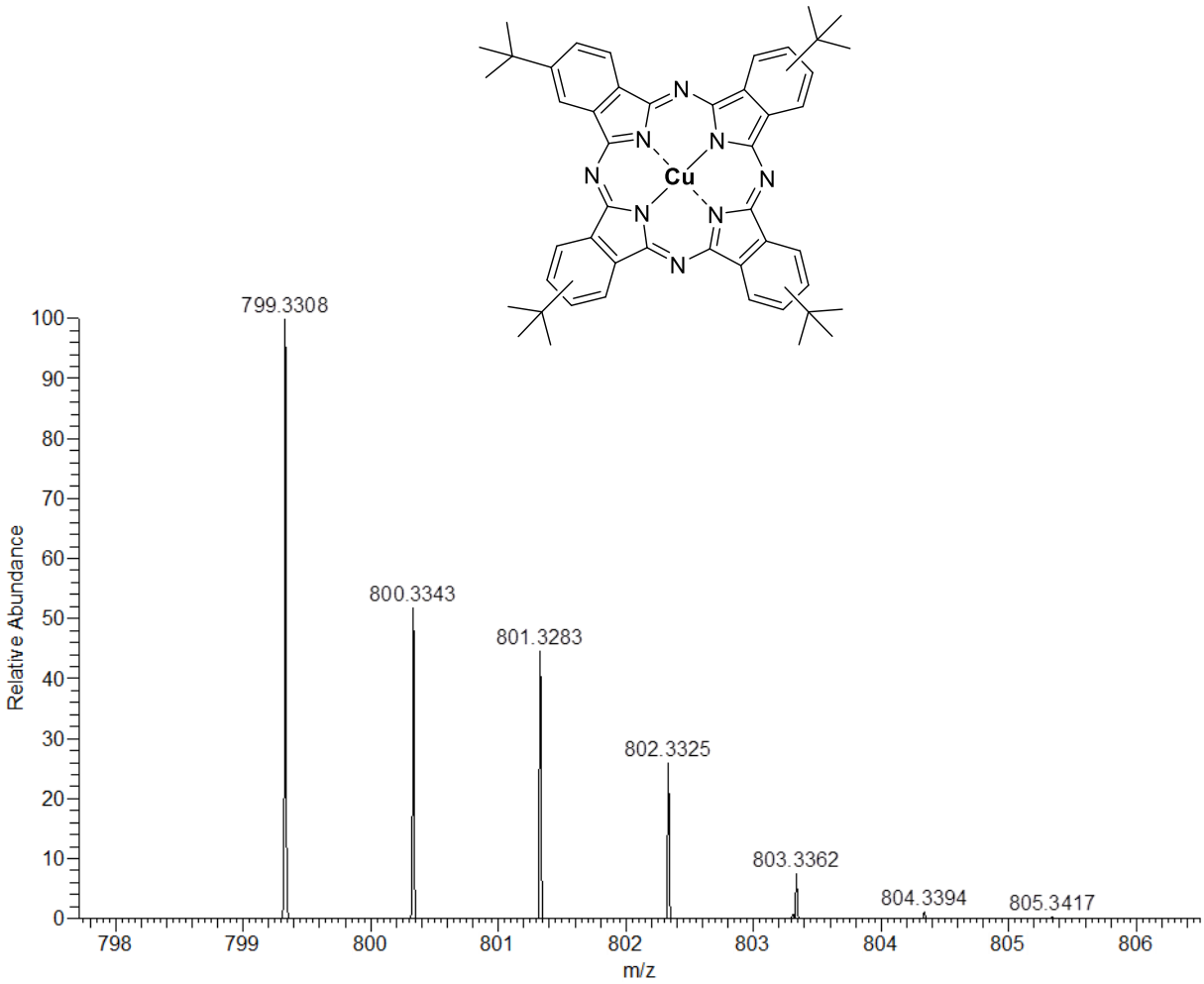

2.4.21. Synthesis, Green Chemistry metric calculation and characterization of tetra-*tert*-butyl-nickel-phthalocyanine Pc13

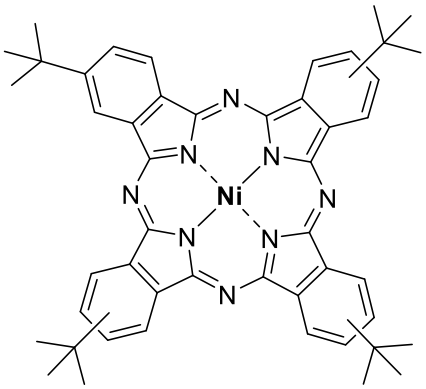

The reaction was carried out following the general procedure for the optimized cyclotetramerization of phthalonitriles in PEG-400. 4-*tert*-Butylphthalonitrile (500.4 mg, 2.7 mmol), PEG-400 (1.06 g, 2.7 mmol), DBU (85.0 mg, 0.6 mmol), and nickel acetate tetrahydrate (179.0 mg, 0.7 mmol) were employed. After completion of the reaction and cooling to room temperature, the mixture was diluted with methanol (2.0 mL) and 1 N HCl (1.0 mL). The resulting precipitate was collected by filtration and washed with water/methanol mixture (2:1, 10.0 mL). The crude product was purified by column chromatography on silica gel (25 g). The column was packed with hexane (100 mL). The sample was loaded onto the column using THF (2 mL). Elution was carried out with hexane/THF mixtures as follows: 10:1 (22 mL), 9:1 (50 mL), 4:1 (4 × 20 mL), and 3:1 (3 × 20 mL). The desired product was obtained as a blue solid (347.2 mg, 64% yield). ^{1}H NMR (600 MHz, THF) δ 8.66 – 7.68 (m, 12H), 1.90 – 1.75 (m, 36H). UV-vis (THF): λ_{max} = 667, 332 nm. AP-MALDI-(-) $[M]^{\bullet-}$: m/z = 794.3363, (Calcd: 794.34).

E-factor calculation for compound **Pc13**

Chemical	**Volume (mL)**	**Density (g/mL)**	**Mass (g)**	**Mass of solvents considered toward E-factor (after 80% solvent recovery) (g)**
4-*tert*-butylphthalonitrile			0.5004	
PEG-400			1.06	
DBU			0.085	
Nickel acetate tetrahydrate			0.179	
HCl 1N	1.0		1.0	
Water	6.6		6.6	
Methanol	5.5	0.792	4.36	0.87
Silica gel			25	
Hexane 100%	100	0.661	66.1	13.22
Hexane (solvent mixtures)	174	0.661	115.014	
THF	40	0.888	35.52	

Amount of product = 0.3472 g (64% yield)

E-factor = 715.6

E-factor 80% solvent recovery = 553.3

^{1}H NMR spectrum of tetra-*tert*-butyl-nickel-phthalocyanine **Pc13** in THF-d_8

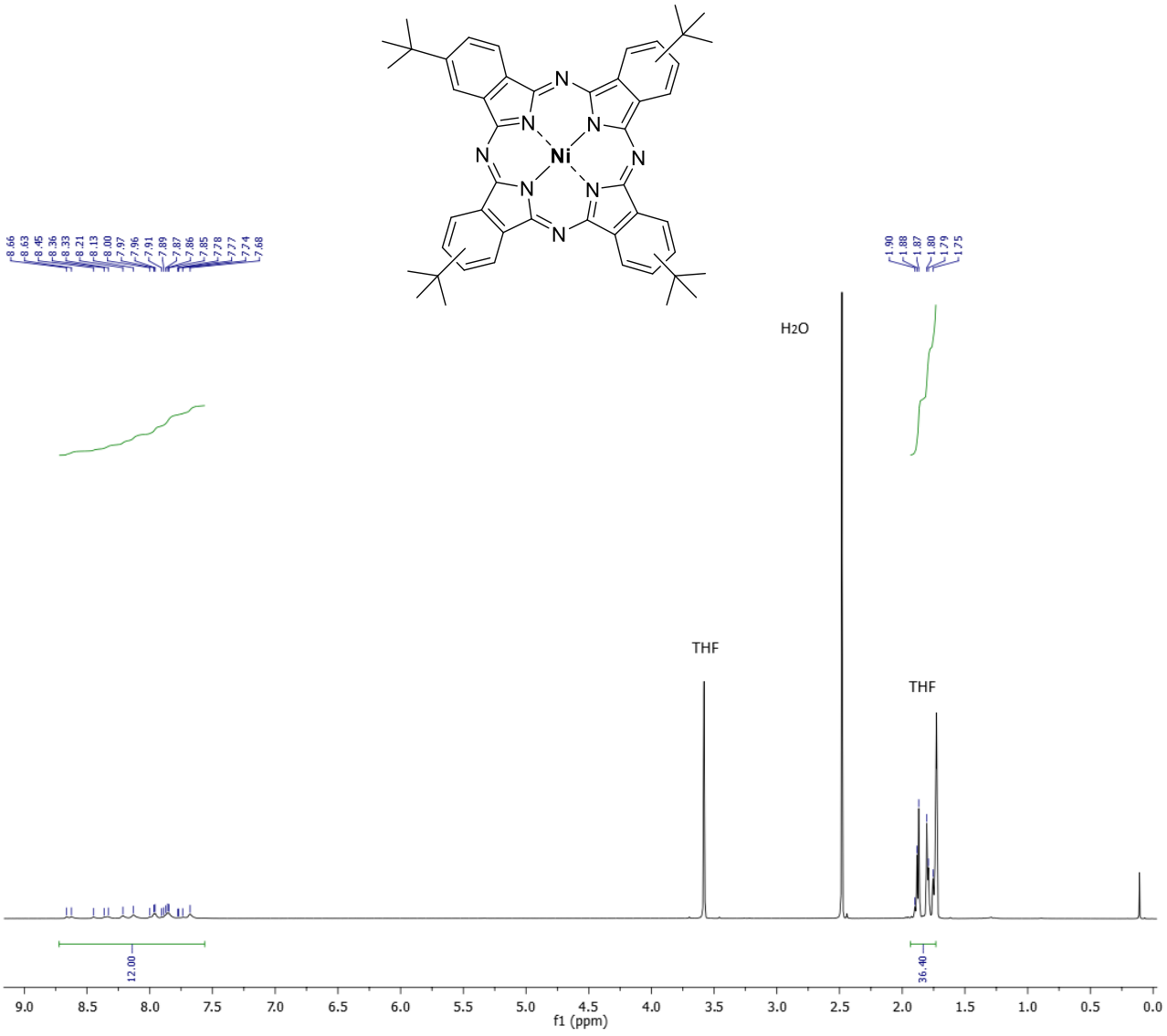

AP-MALDI-(-) mass spectrum of tetra-*tert*-butyl-nickel-phthalocyanine **Pc13**

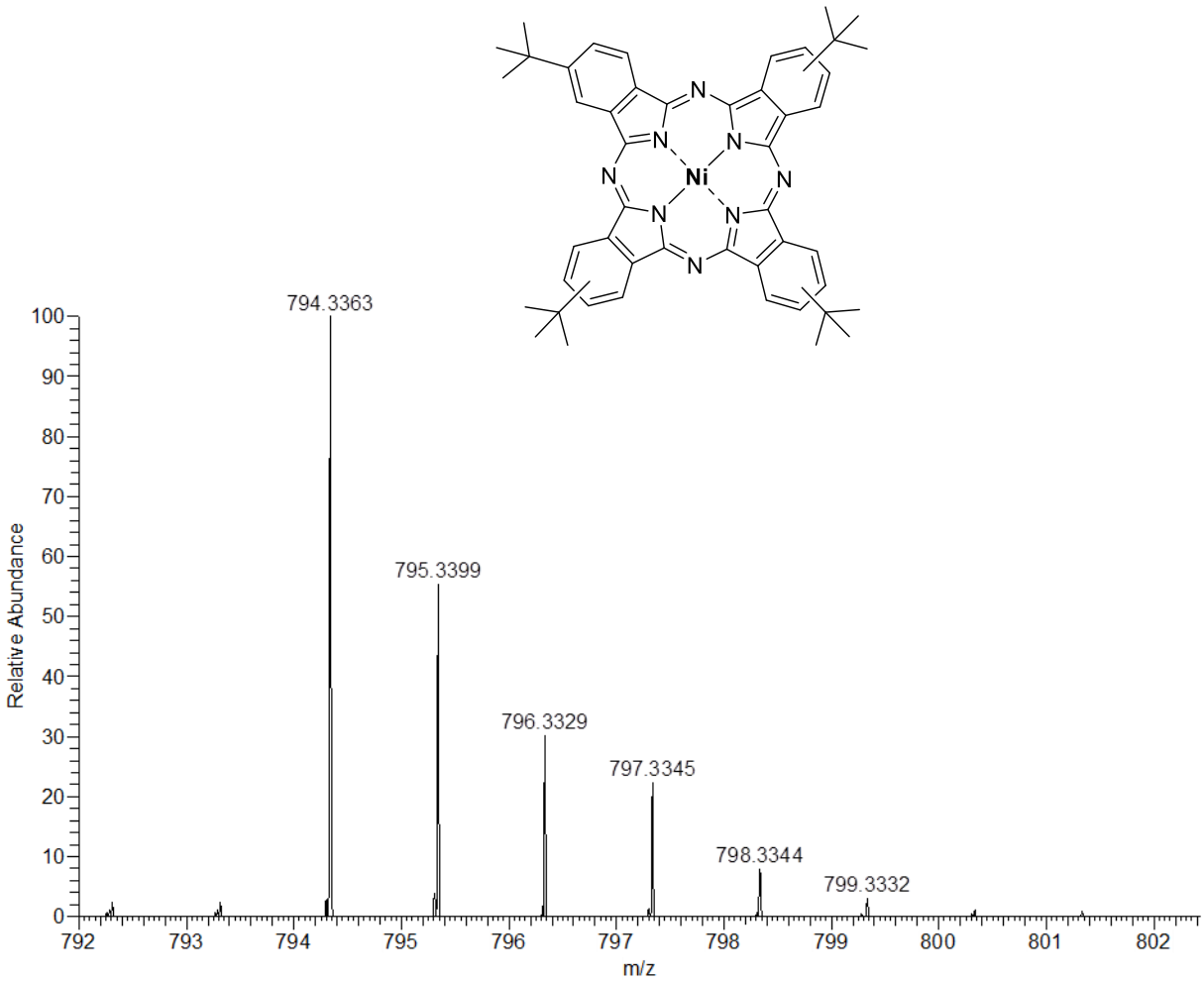

2.4.22. Synthesis, Green Chemistry metric calculation and characterization of tetra-*tert*-butyl-phthalocyanine Pc14

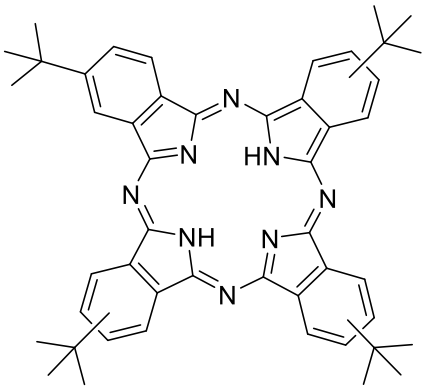

The reaction was carried out following the general procedure for the optimized cyclotetramerization of phthalonitriles in PEG-400. 4-*tert*-Butylphthalonitrile (500.1 mg, 2.7 mmol), PEG-400 (1.06 g, 2.7 mmol), and DBU (84.2 mg, 0.5 mmol) were employed. After completion of the reaction and cooling to room temperature, the reaction mixture was diluted with 1 M HCl (1.0 mL), water (1.0 mL), and methanol (3.0 mL). The mixture was transferred, filtered, and washed with additional methanol (20 mL). The crude product was purified by filtration through a short pad of silica gel (4 g) using hexane/THF (2:1, 21 mL; 14 mL hexane and 7 mL THF) as eluent. The collected fractions were combined and washed with water/methanol (1:1, 20 mL total, in portions). Drying under vacuum afforded phthalocyanine **Pc14** as a purple crystalline solid (252.0 mg, 50% yield). ^{1}H NMR (600 MHz, Pyr) δ 9.34 – 9.23 (m, 2H), 9.15 – 9.04 (m, 4H), 8.98 – 8.93 (m, 2H), 8.39 – 8.22 (m, 4H), 1.91 – 1.81 (m, 36H), -2.55 – -2.62 (m, 2H). UV-vis (THF): λ_{max} = 696, 342 nm. AP-MALDI-(-) $[M]^{\bullet-}$: m/z = 738.4164, (Calcd: 738.42).

E-factor calculation for compound **Pc14**

Chemical	**Volume (mL)**	**Density (g/mL)**	**Mass (g)**	**Mass of solvents considered toward E-factor (after 80% solvent recovery) (g)**
4-*tert*-butylphthalonitrile			0.5001	
PEG-400			1.06	
DBU			0.0842	
HCl 1N	1.0		1.0	
Water	11		11	
Methanol	33	0.792	26.14	5.23
Silica gel			4	
Hexane	14	0.661	9.254	1.85
THF	7	0.888	6.22	1.24

Amount of product = 0.252 g (50% yield)

E-factor = 190.5

E-factor 80% solvent recovery = 58.4

^{1}H NMR spectrum of tetra-*tert*-butyl-phthalocyanine **Pc14** in Pyr-d_5

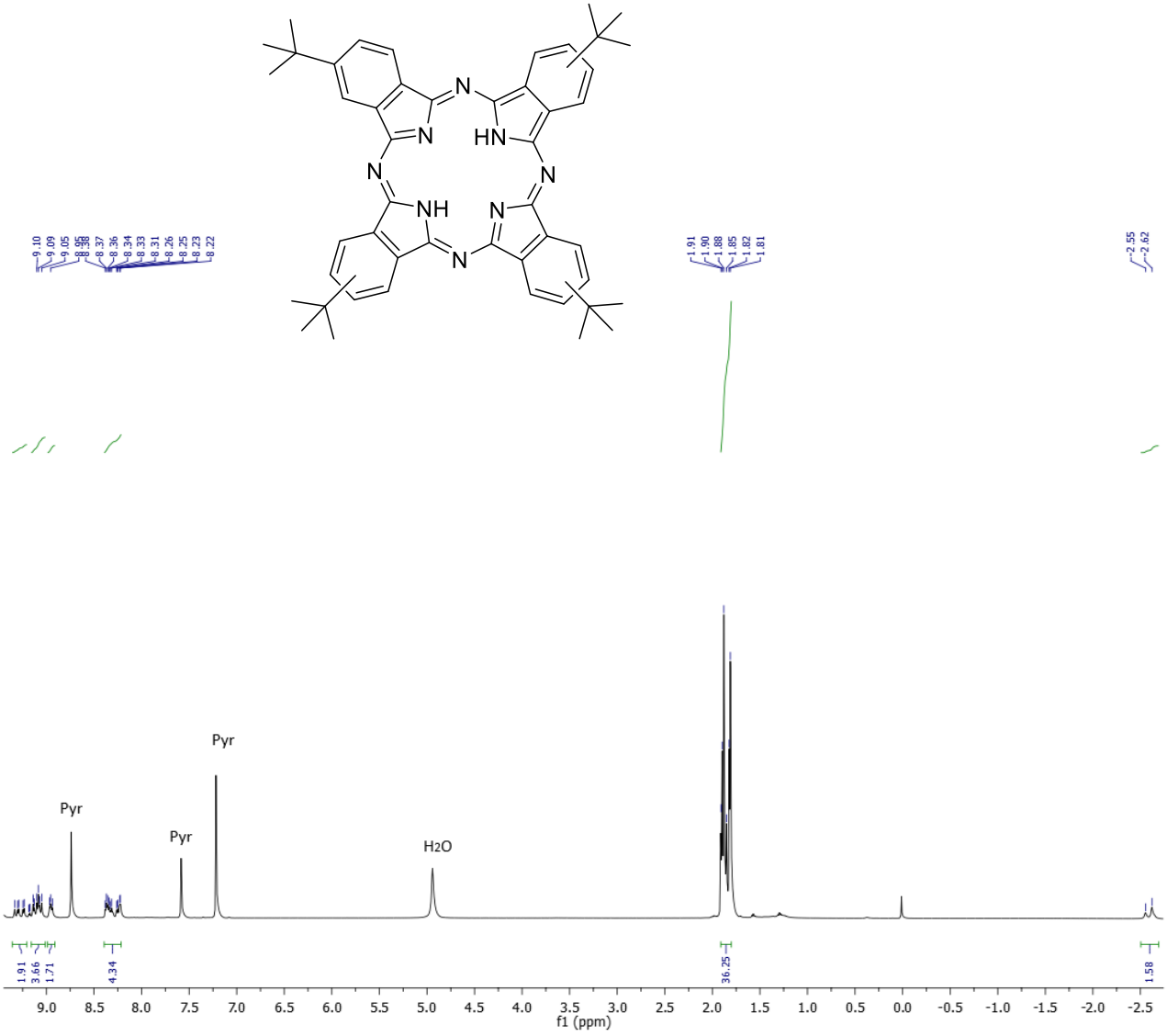

AP-MALDI-(-) mass spectrum of tetra-*tert*-butyl-phthalocyanine **Pc14**

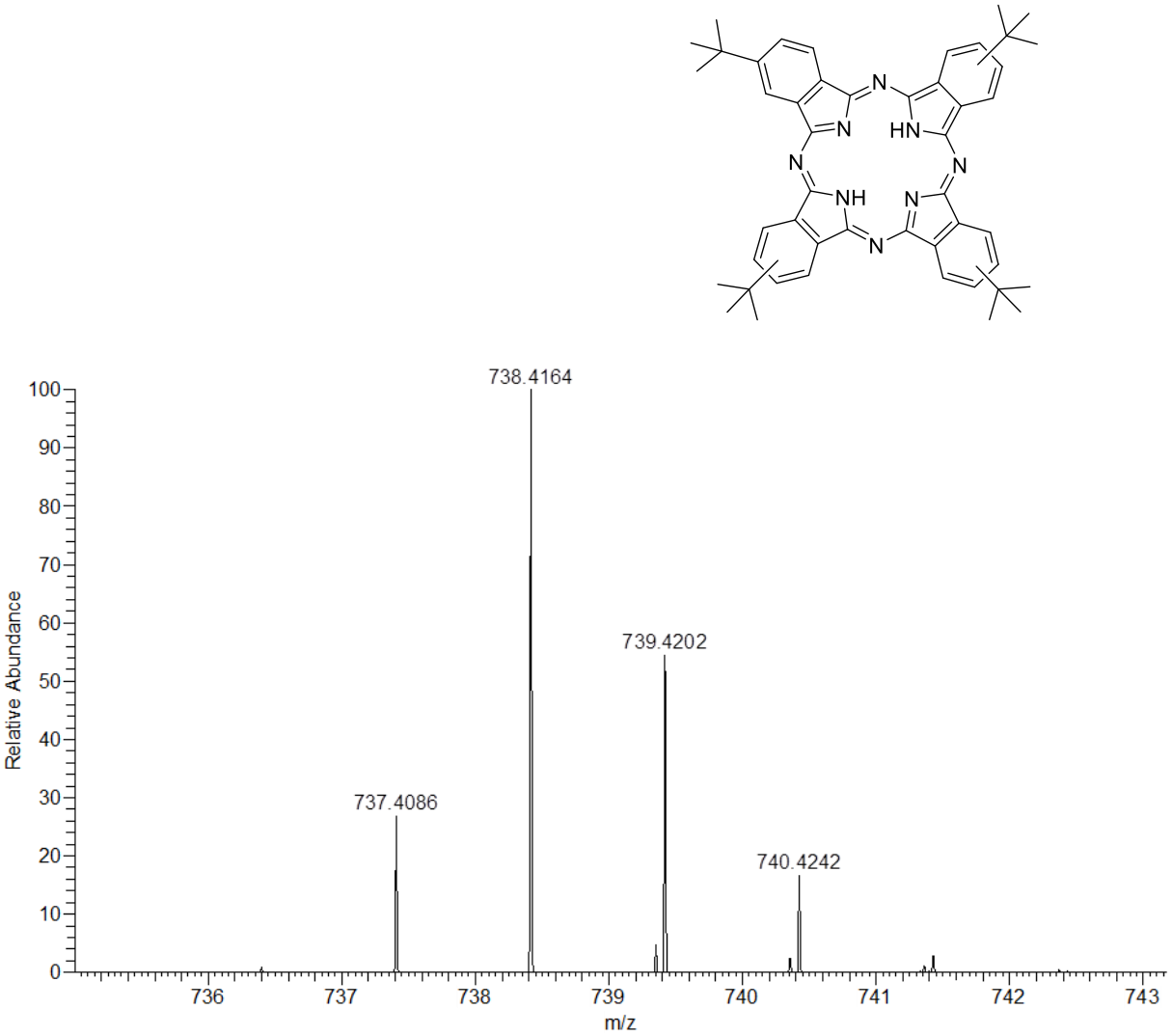

2.4.23. Synthesis and characterization of cobalt-phthalocyanine Pc15

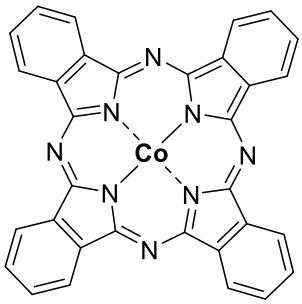

The reaction was carried out following the general procedure for the optimized cyclotetramerization of phthalonitriles in PEG-400. Phthalonitrile (694.2 mg, 5.4 mmol), PEG-400 (2.12 g, 5.3 mmol), DBU (153.1 mg, 1.0 mmol), and cobalt acetate tetrahydrate (351.8 mg, 1.4 mmol) were employed.

After completion of the reaction and cooling to room temperature, the reaction mixture was diluted with 1 N HCl (2 mL) and methanol (10 mL), stirred for 5 min, and filtered. The collected solid was washed with hot methanol (40 mL total, in portions) until the washings became nearly colorless. The product was dried under vacuum to constant weight to afford the desired phthalocyanine (646.3 mg, 83% yield). UV-vis (THF): λ_{max} = 656, 324 nm. AP-MALDI-(+) $[M]^{\bullet+}$: m/z = 571.08, (Calcd: 571.0825).

E-factor calculation for compound **Pc15**

Chemical	**Volume (mL)**	**Density (g/mL)**	**Mass (g)**	**Mass of solvents considered toward E-factor (after 90% solvent recovery) (g)**
Phthalonitrile			0.6942	
PEG-400			2.12	
DBU			0.1531	
Cobalt acetate tetrahydrate			0.3518	
HCl 1N	2		2	
Methanol	50	0.792	39.6	3.96

Amount of product = 0.6463 g (83% yield)

E-factor = 68.5

E-factor 90% solvent recovery = 13.4

AP-MALDI-(+) mass spectrum of cobalt phthalocyanine **Pc15**

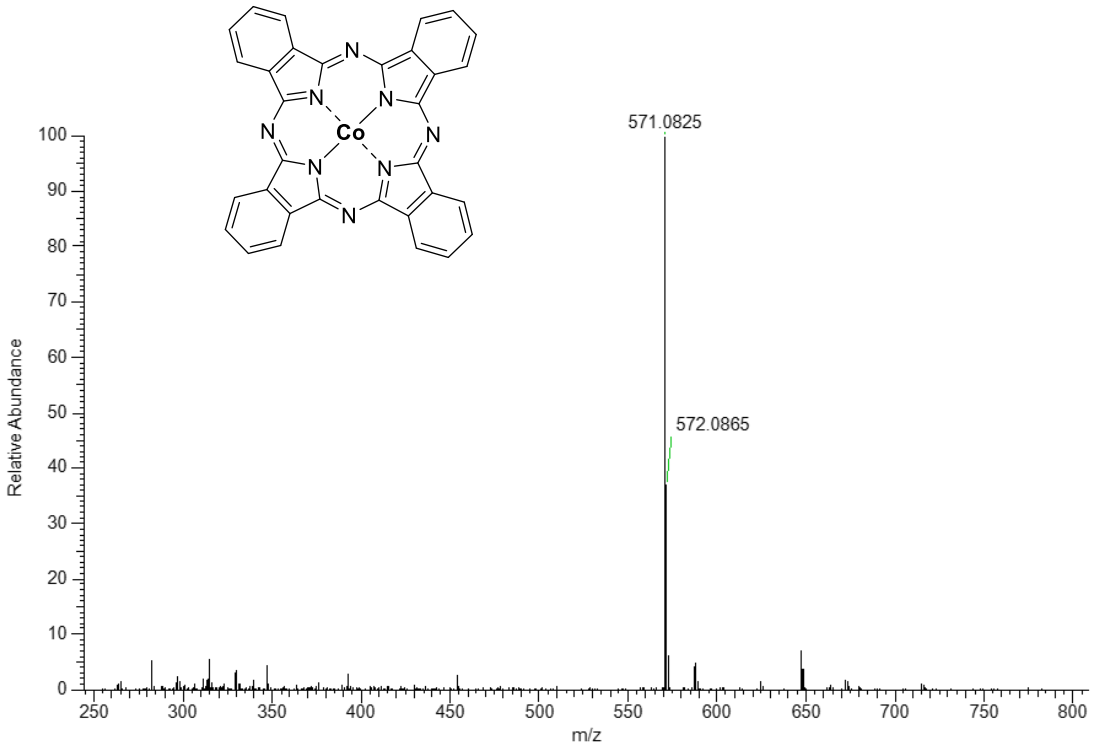

2.4.24. Synthesis, Green Chemistry metric calculation and characterization of tetra-(4-iodo-2,6-dimethylphenoxy)-zinc-phthalocyanine Pc3

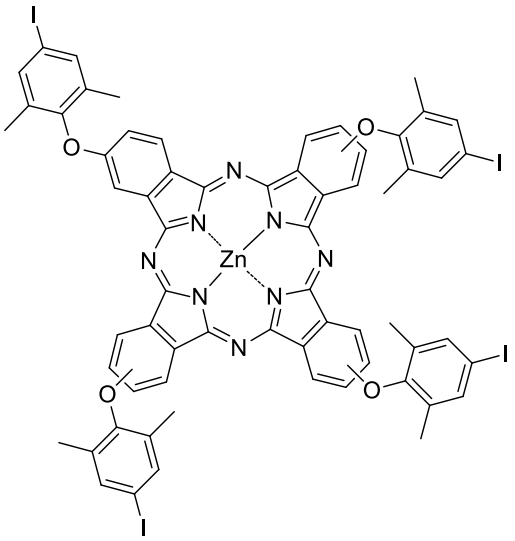

The reaction was carried out following the general procedure for the optimized cyclotetramerization of phthalonitriles in PEG-400. 4-(4-iodo-2,6-dimethylphenoxy)phthalonitrile (500 mg, 1.35 mmol), PEG-400 (1 g, 2.5 mmol), DBU (80 mg, 0.5 mmol), and zinc acetate dihydrate (75 mg, 0.35 mmol) were employed.

After completion of the reaction and cooling to room temperature, the reaction mixture was treated with 1 N HCl (2 mL), and water (3 mL) and stirred thoroughly. The solid was collected by filtration and further washed with further water (1.5 mL). The crude product was purified by column chromatography on silica gel (10 g). The column was packed with hexane (30 mL). The sample was loaded onto the column using THF (10 mL). Elution was carried out with hexane/THF 4:1 (4 × 25 mL). The collected fractions were combined and washed with water/methanol (1:3, 12 mL total, in portions). Drying under vacuum afforded phthalocyanine **Pc3** as a blue solid. ^{1}H NMR (600 MHz, Pyr-d_5) δ = 9.36 – 9.68 (m, 4H), 8.87 – 9.19 (m, 4H), 7.74 (m, 4H), 7.60 – 7.67 (m, 8H), 2.19 (m, 24H) ppm; ^{13}C NMR (150 MHz, Pyr-d_5): δ = 159.92, 159.75, 159.60, 151.66, 151.64, 151.54, 151.54, 151.50, 142.92, 142.92, 138.41,

138.39, 138.35, 134.18, 134.18, 125.68, 125.68, 117.55, 117.49, 117.02, 116.88, 114.87, 114.86, 90.73, 90.71, 90.70, 90.64, 90.61, 79.53, 79.09, 34.77, 34.71, 30.55, 30.24, 29.34, 24.15, 24.15, 21.15, 16.53, 16.50, 15.99, 15.96, 15.96 ppm. FT-IR: ν = 2926, 2850, 1607, 1460, 1392, 1337, 1268, 1213, 1179, 1115, 1084, 1038, 944, 852, 813, 764, 743 cm^{-1}. UV-vis (THF): λ_{max} = 677, 351 nm. MALDI-TOF $[M]^{\bullet+}$: m/z = 1559.83, (Calcd: 1559.90).

E-factor calculation for compound **Pc3**

Chemical	**Volume (mL)**	**Density (g/mL)**	**Mass (g)**	**Mass of solvents considered toward E-factor (after 80% solvent recovery) (g)**
2,6-dimethyl-4-iodo-phthalonitrile			0.5	
PEG-400			1	
DBU			0.08	
Zinc acetate dihydrate			0.075	
HCl 1N	2		2	
Water	7.5		7.5	
Methanol	9	0.792	7.128	
Silica gel			10	5.328
Hexane	95	0.661	62.795	12.559
THF	30	0.888	26.64	1.4256

Amount of product = 0.385 g (73% yield)

E-factor = 280.1

E-factor 80% solvent recovery = 104.1

2.4.25. Synthesis, Green Chemistry metric calculation and characterization of tetra-iodo-cobalt-phthalocyanine Pc16

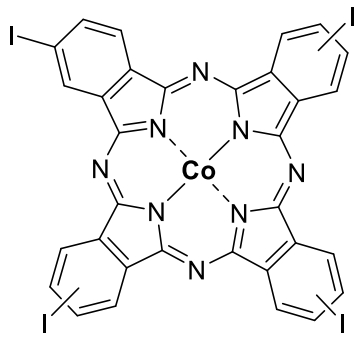

The reaction was carried out following the general procedure for the optimized cyclotetramerization of phthalonitriles in PEG-400. 4-iodophthalonitrile (259.3 mg, 1.0 mmol), PEG-400 (425 mg, 1.1 mmol), DBU (33.4 mg, 0.2 mmol), and cobalt acetate tetrahydrate (67.2 mg, 0.27 mmol) were employed.

After completion of the reaction and cooling to room temperature, the reaction mixture was treated with 1 N HCl (1 mL), methanol (7 mL), and water (1 mL), and the resulting suspension was stirred thoroughly. The solid was collected by filtration and further washed with methanol (10 mL). Washing with hot acetone (50 mL in 5 portions) was performed, until the washings became colorless. Drying under vacuum afforded the desired product (200.1 mg, 74% yield). UV-vis (THF): λ_{max} = 662, 333 nm. AP-MALDI-(-) $[M]^{\bullet-}$: m/z = 1074.6713, (Calcd: 1074.67).

.

E-factor calculation for compound **Pc16**

Chemical	**Volume (mL)**	**Density (g/mL)**	**Mass (g)**	**Mass of solvents considered toward E-factor (after 80% solvent recovery) (g)**
4-iodophthalonitrile			0.2593	
PEG-400			0.425	
DBU			0.0334	
Cobalt acetate tetrahydrate			0.0672	
HCl 1N	1		1	
Water	1		1	
Methanol	17	0.792	13.464	2.693
Acetone	50	0.784	39.2	7.84

Amount of product = 0.2001 g (74% yield)

E-factor = 271.1

E-factor 80% solvent recovery = 60.6

AP-MALDI-(-) mass spectrum of tetra-iodo cobalt phthalocyanine **Pc16**

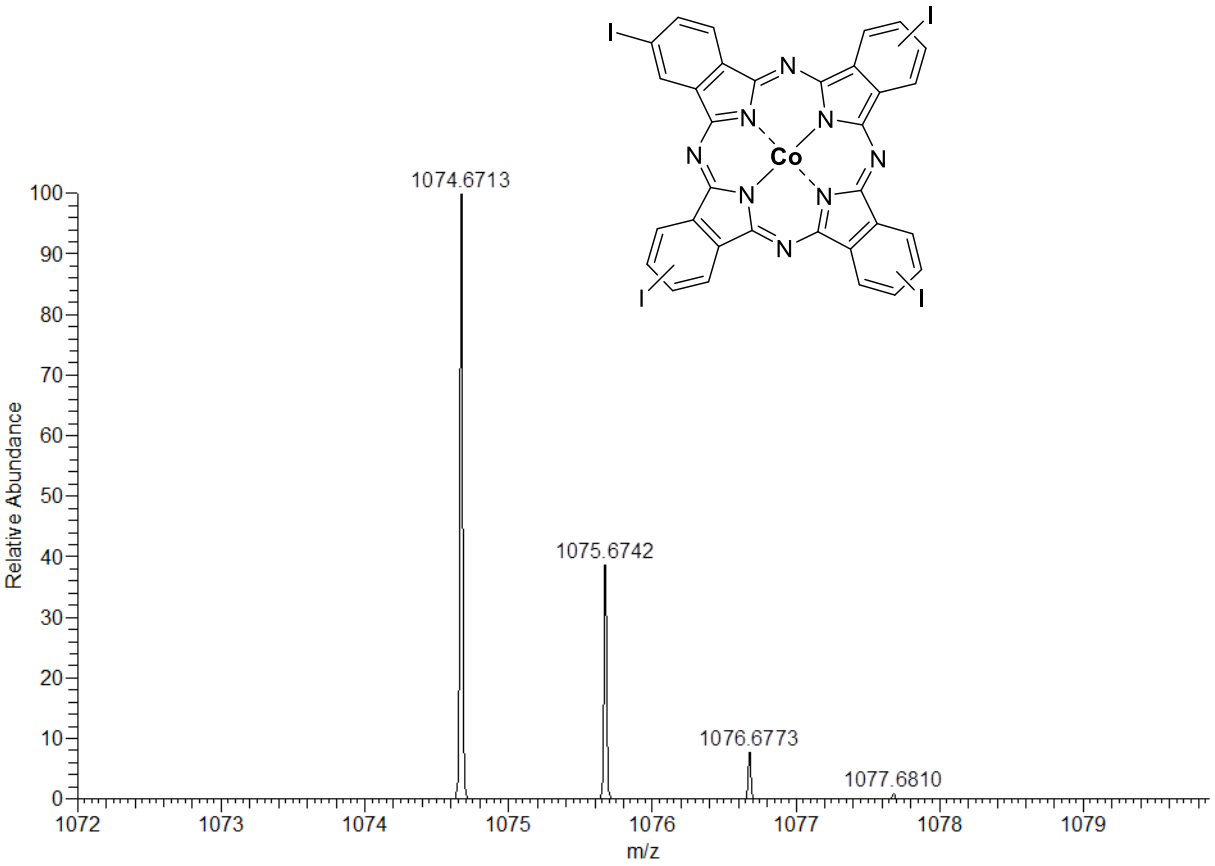

2.4.26. Synthesis, Green Chemistry metric calculation and characterization of tetra-iodo-zinc-phthalocyanine Pc17

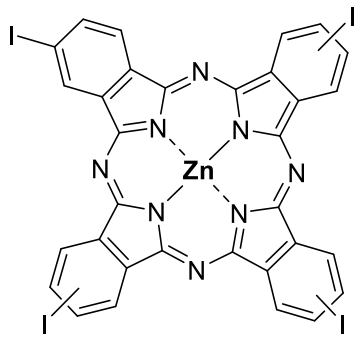

The reaction was carried out following the general procedure for the optimized cyclotetramerization of phthalonitriles in PEG-400. 4-iodophthalonitrile (254.5 mg, 1.0 mmol), PEG-400 (413 mg, 1.0 mmol), DBU (31.1 mg, 0.2 mmol), and zinc acetate dihydrate (57.1 mg, 0.26 mmol) were employed. After completion of the reaction and cooling to room temperature, the reaction mixture was treated with 1 N HCl (1 mL) and methanol (4 mL) and filtered. The collected solid was then washed with methanol (55 mL total, in portions of 10 mL, with a final 5 mL portion) until the washings became nearly colorless. Drying under vacuum afforded the desired product as a blue solid (205.7 mg, 76% yield). ^{1}H NMR (600 MHz, THF) δ 9.28 – 9.24 (m, 4H), 8.71 – 8.65 (m, 4H), 8.41 – 8.40 (m, 4H). UV-vis (THF): λ_{max} = 674, 353 nm. AP-MALDI-(-) $[M]^{\bullet-}$: m/z = 1079.6660, (Calcd: 1079.67).

E-factor calculation for compound **Pc17**

Chemical	**Volume (mL)**	**Density (g/mL)**	**Mass (g)**	**Mass of solvents considered toward E-factor (after 80% solvent recovery) (g)**
4-iodophthalonitrile			0.2545	
PEG-400			0.413	
DBU			0.0311	
Zinc acetate dihydrate			0.0572	
HCl 1N	1		1	
Methanol	59	0.792	46.728	9.3456

Amount of product = 0.2057 g (76% yield)

E-factor = 234.7

E-factor 80% solvent recovery = 53.0

^{1}H NMR spectrum of tetra-iodo-zinc-phthalocyanine **Pc17** in THF-d_8

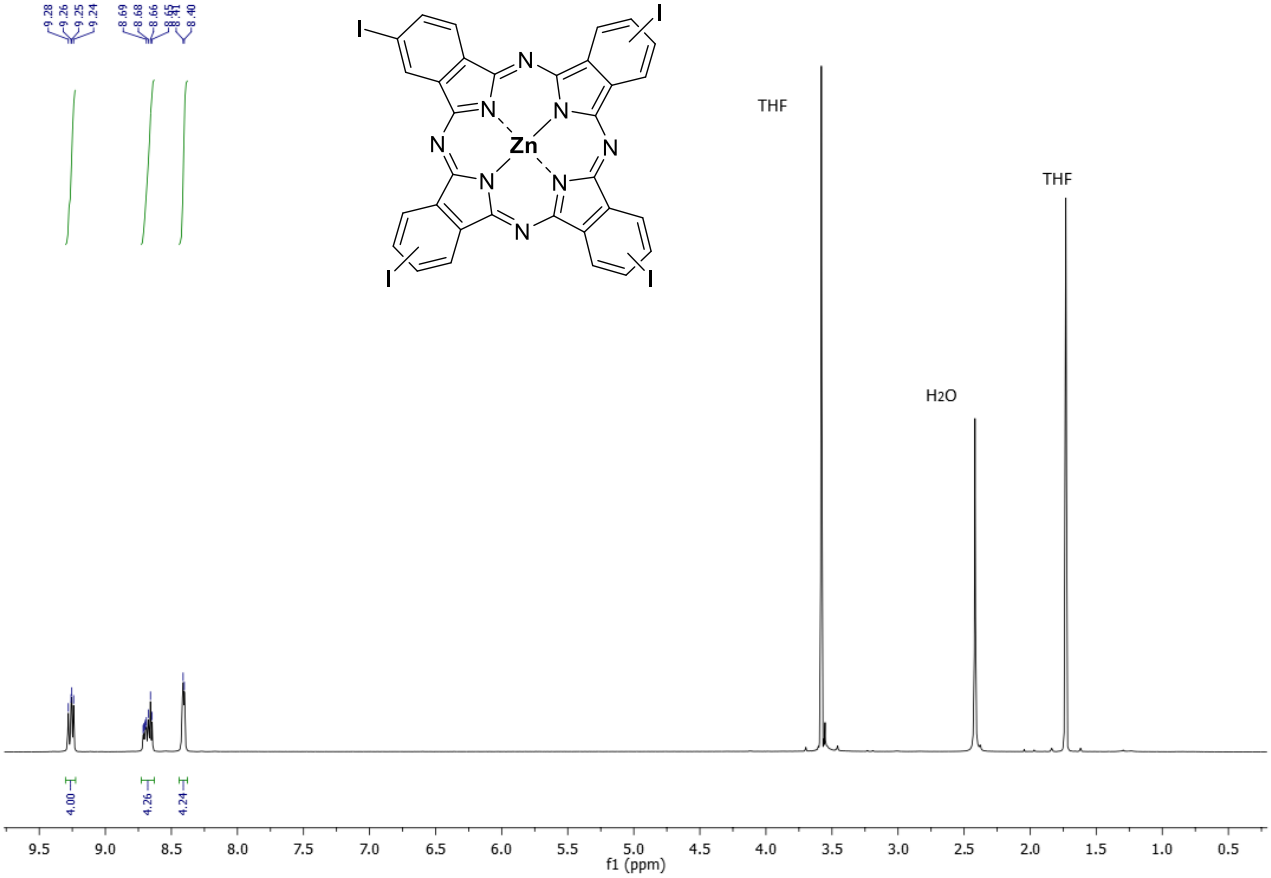

AP-MALDI-(-) mass spectrum of tetra-iodo zinc phthalocyanine **Pc17**

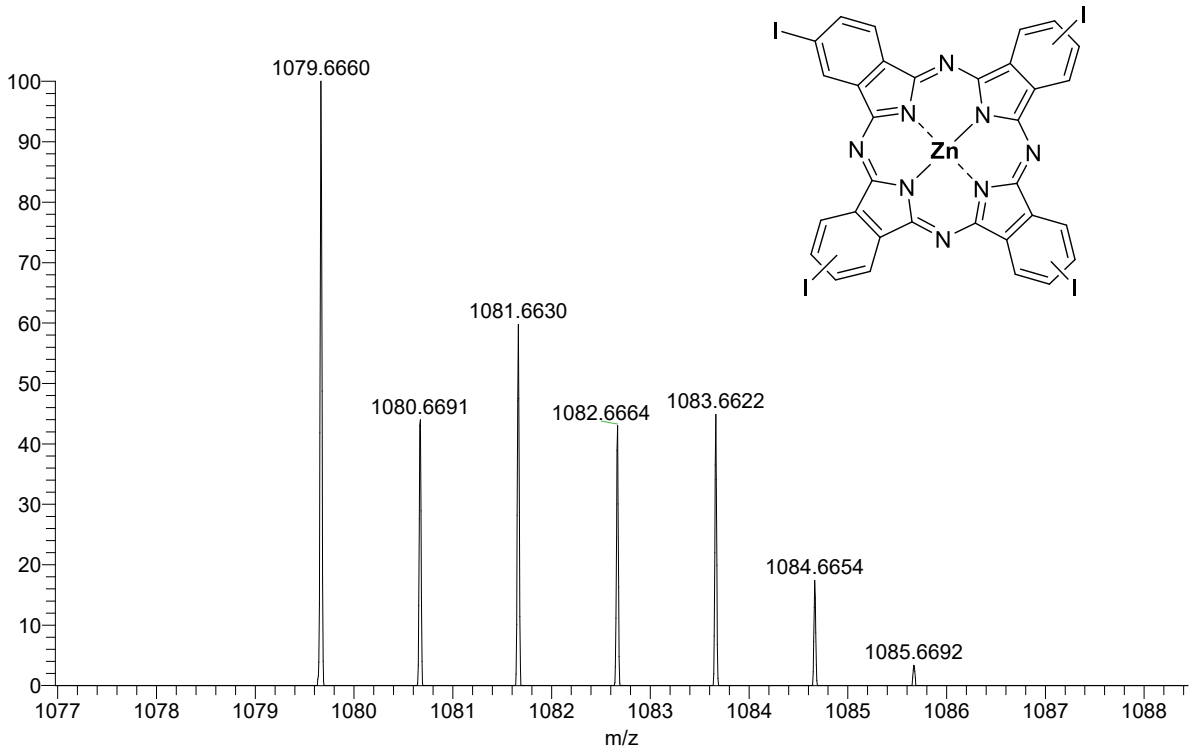

2.4.27. Synthesis and preliminary characterization of phthalocyanine Pc18

4-Iodophthalonitrile (338 mg, 1.33 mmol), PEG-400 (514 mg, 1.30 mmol), DBU (38.5 mg, 0.25 mmol), and zinc acetate dihydrate (76 mg, 0.35 mmol) were charged into a 10 mL one-necked round-bottom flask equipped with a magnetic stirrer under a nitrogen atmosphere. The reaction mixture was heated at 140 °C until complete consumption of the starting material was confirmed by TLC. The temperature was then lowered to 45 °C, and triethylamine (0.556 mL, 403.7 mg, 3.99 mmol), $Pd(PPh_3)_2Cl_2$ (18.7 mg, 0.027 mmol), copper(I) iodide (3.5 mg, 0.025 mmol), and ethynyltrimethylsilane (0.28 mL, 195.9 mg, 1.99 mmol) were added. The reaction mixture changed color from dark blue to dark blue-green. Reaction progress was monitored by TLC, and after 4 h complete consumption of the zinc tetraiodophthalocyanine intermediate was observed, with only a single spot detected. The reaction was then quenched by addition of 1 N HCl (2 mL) and methanol (2 mL). The resulting precipitate was collected by filtration, washed with water/methanol (1:2, 10 mL), and dried. The crude product was further purified by filtration through a short pad of silica gel (3.52 g) using hexane/THF (3:1, 30 mL) as the eluent. The isolated solid was finally washed with water/methanol (1:2, 10 mL) and dried under vacuum to constant weight to afford 272.6 mg of a blue solid.

AP-MALDI-(-) mass spectrum of **Pc18**

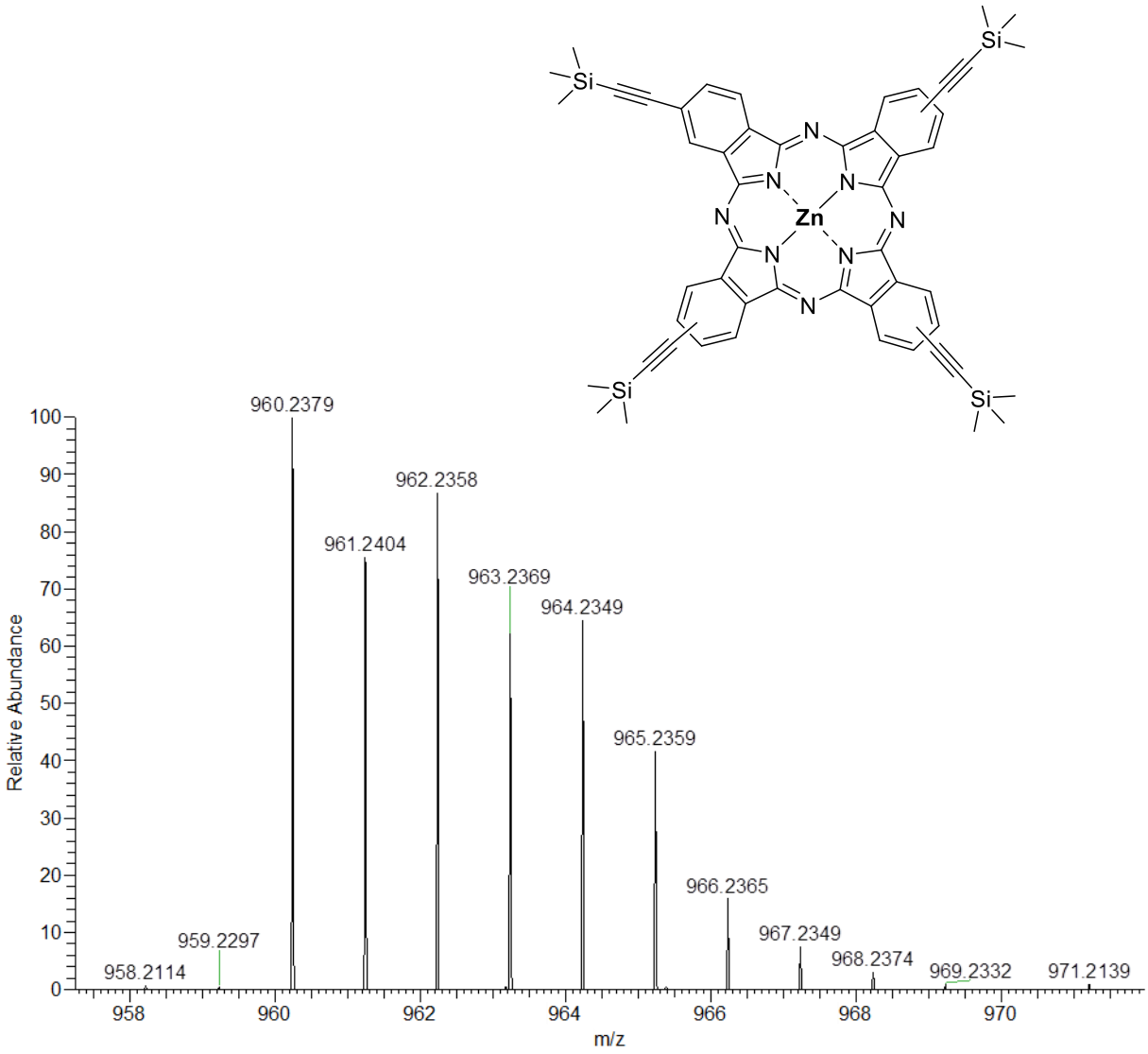

[M]$^{\bullet-}$: m/z = 960.2379, (Calcd: 960.24).

2.4.28. Synthesis and preliminary characterization of phthalocyanine Pc19

The reaction was carried out following the same procedure described for phthalocyanine **Pc18** up to the completion of the first Sonogashira coupling, monitoring reaction progress by TLC, with the following amounts: phthalonitrile tetramerization: 4-iodophthalonitrile (342.8 mg, 1.35 mmol), PEG-400 (520.1 mg, 1.30 mmol), DBU (49.1 mg, 0.30 mmol), zinc acetate dihydrate (77.9 mg, 0.35 mmol). Upon complete consumption of 4-iodophthalonitrile, monitored by TLC, the temperature was lowered to 120 °C. K_2CO_3 (373.1 mg, 2.7 mmol), $Pd(PPh_3)_2Cl_2$ (28.4 mg, 0.04 mmol), and 4-hexyloxyboronic acid (389.8 mg, 1.75 mmol) were added, together with water (0.5 mL) and 2-methylTHF (0.3 mL) to enhance solubility and ensure efficient stirring of the reaction mixture. When TLC monitoring showed no further evolution of the reaction, the mixture was quenched with 1 N HCl (1 mL) and diluted with water/methanol (1:1, 4 mL). The resulting precipitate was filtered and washed with methanol (30 mL). The obtained crude solid (425 mg) was further washed with hot methanol (30 mL). The crude product was purified by column chromatography on silica gel (50 g). The column was packed and initially eluted with hexane (100 mL in total). Elution was initially performed with hexane:THF 75:1 (100 mL), followed by hexane:THF 9:1 (100 mL), which allowed the separation of a bright yellow byproduct. The eluent was then changed to hexane:THF 4:1 (200 mL). Two fractions compatible with the expected phthalocyanine, possibly contaminated with partially substituted phthalocyanine derivatives, were collected.

AP-MALDI-(-) mass spectrum of **Pc19**

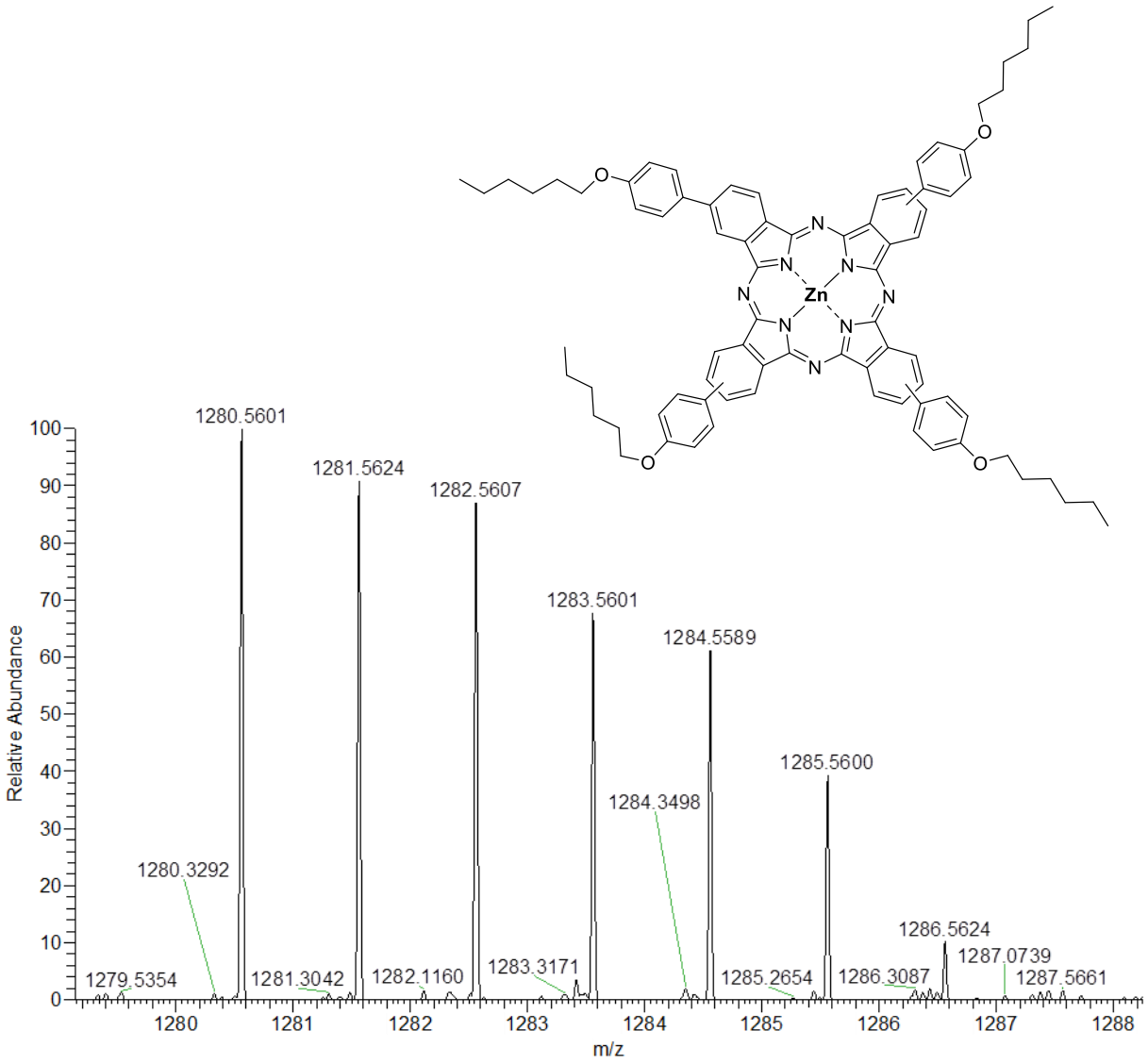

[M]$^{\bullet-}$: m/z = 1280.5601, (Calcd: 1280.56).

2.4.29. Synthesis and preliminary characterization of phthalocyanine Pc20

The reaction was carried out following the same procedure described for phthalocyanine **Pc18** to the completion of the first Sonogashira coupling, monitoring reaction progress by TLC, with the following amounts. For phthalonitrile tetramerization: 4-iodophthalonitrile (254.4 mg, 1.00 mmol), PEG-400 (416 mg, 1.04 mmol), DBU (31.5 mg, 0.25 mmol), zinc acetate dihydrate (60.1 mg, 0.27 mmol); for Sonogashira coupling with TMSA: triethylamine (0.45 mL, 326.7 mg, 3.2 mmol), $Pd(PPh_3)_2Cl_2$ (17.2 mg, 0.024 mmol), copper(I) iodide (3.9 mg, 0.028 mmol), and ethynyltrimethylsilane (0.25 mL, 173.5 mg, 1.77 mmol) were added. Upon complete consumption of the zinc tetraiodophthalocyanine and its partially substituted intermediates, tetrabutylammonium fluoride trihydrate (2.5 g, 8.0 mmol) was added, and the reaction mixture was stirred briefly, together with THF (0.5 mL) to enhance solubility and ensure efficient stirring of the reaction mixture. The second Sonogashira coupling was then carried out by addition of triethylamine (0.45 mL, 326.7 mg, 3.20 mmol), $Pd(PPh_3)_2Cl_2$ (14.5 mg, 0.021 mmol), copper(I) iodide (4.1 mg, 0.030 mmol), and 3,5-bis(trifluoromethyl)-4-iodobenzene (0.266 mL, 510.4 mg, 1.50 mmol). The reaction mixture was stirred overnight at 40 °C. After completion, the reaction mixture was poured into water (50 mL), followed by addition of 1 N HCl (1 mL). The resulting precipitate was collected by filtration, washed with methanol (5 mL), and dried to afford a crude product (270 mg). Purification was performed by filtration through a short pad of silica gel (4.0 g). Elution with hexane/THF (1:1, 40 mL) resulted in partial retention of the phthalocyanine on the stationary phase; complete elution was achieved using THF alone (20 mL). Removal of the solvent under reduced pressure, followed by washing of the residue with methanol (10 mL), afforded 160.5 mg of a blue solid.

AP-MALDI-(-) mass spectrum of **Pc20**

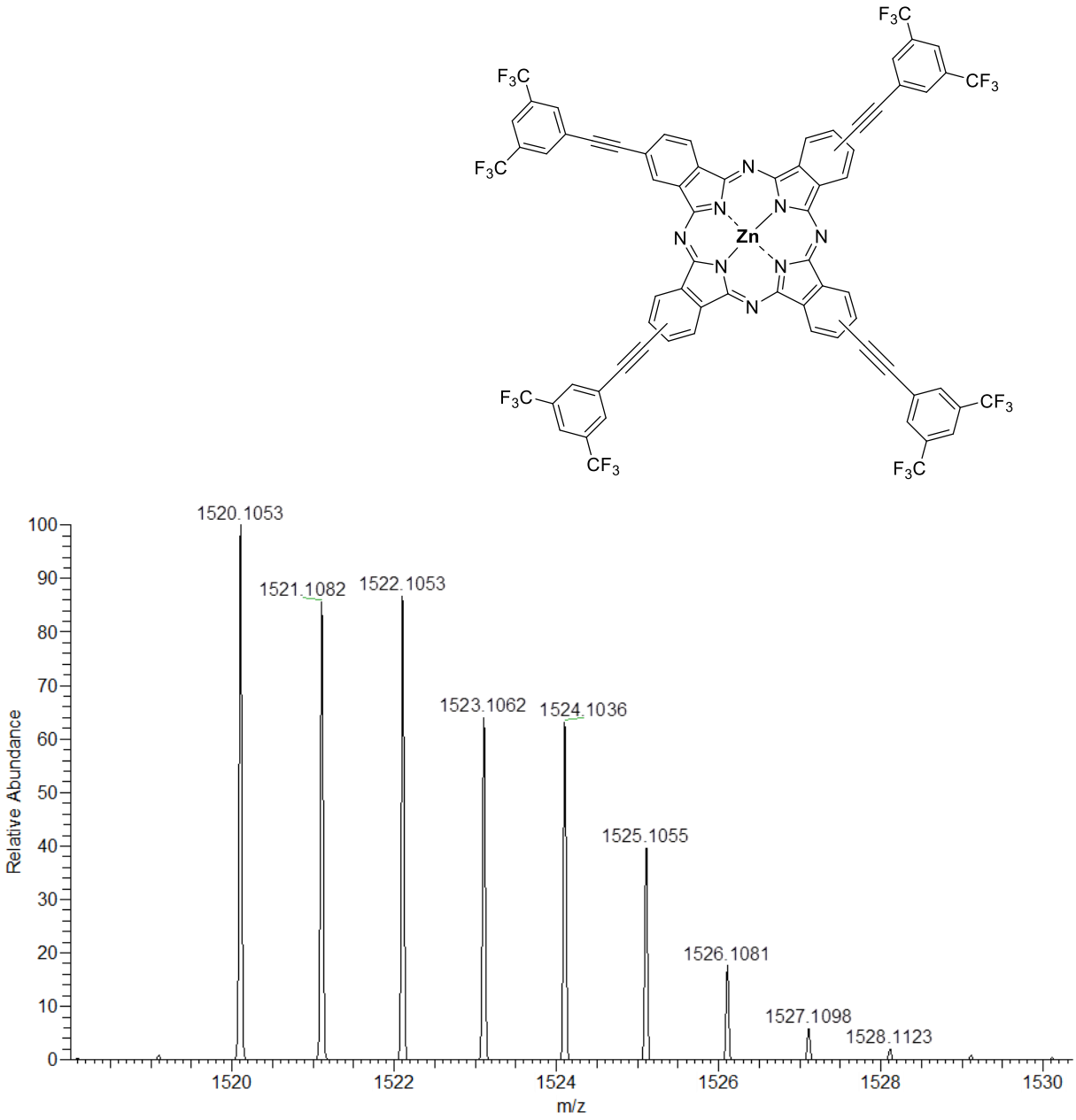

[M]$^{\bullet-}$: m/z = 1520.1053, (Calcd: 1520.10).

2.5. Bibliography

1. Chandrasekhar, S., Prakash, S. J. & Rao, C. L. Poly (ethylene Glycol) (400) as Superior Solvent Medium against Ionic Liquids for Catalytic Hydrogenations with PtO_2. *J. Org. Chem.* **71**, 2196–2199 (2006).
2. Braun, A. & Tcherniac, J. A. Braun und J. Tcherniac: tfber die Produkte der Einwirkung von Acetanhydrid auf Phthalamid. *Ber. Dtsch. Chem. Ges.* **40**, 2709–2714 (1907).
3. Linstead, R. P. *J. Chem. Soc.* 1016–1017 (1934).
4. De La Torre, G., Claessens, C. G. & Torres, T. Phthalocyanines: Old dyes, new materials. Putting color in nanotechnology. *Chem. Commun.* 2000–2015 (2007).
5. Langerreiter, D., Kostiainen, M. A., Kaabel, S. & Anaya-Plaza, E. A Greener Route to Blue: Solid-State Synthesis of Phthalocyanines. *Angew. Chemie - Int. Ed.* **61**, (2022).
6. Senge, M. O., Sergeeva, N. N. & Hale, Karl, J. Classic highlights in porphyrin and porphyrinoid total synthesis and biosynthesis. *Chem Soc Rev* **50**, 4730–4789 (2021).
7. Tang, F. *et al.* Phthalocyanine J-aggregate nanoparticles with enormous-redshifted and intense absorption : Potential structure-J-aggregation relationships and application in tumor-associated macrophages-targeted phototheranostics. *Chem. Eng. J.* **496**, 154272–154283 (2024).
8. Urbani, M., de la Torre, G., Nazeeruddin, M. K. & Torres, T. Phthalocyanines and porphyrinoid analogues as hole- and electron-transporting materials for perovskite solar cells. *Chem Soc Rev* **48**, 2738–2766 (2019).
9. Grant, T. M. *et al.* Boron Subphthalocyanines and Silicon Phthalocyanines for Use as Active Materials in Organic Photovoltaics. *Chem. Rec.* **19**, 1093–1112 (2019).
10. Podapangi, S. K., Mancini, L., Takhellambam, D., Xu, J. & Angelo, L. Improved Perovskite Solar Cells with Environmentally Friendly Phthalocyanine Hole Extracting Interlayer. *ACS Appl. Energy Mater.* **9**, 5, 2541–2554 (2026).
11. Sorokin, A. B. Phthalocyanine metal complexes in catalysis. *Chem. Rev.* **113**, 10, 8152–8191 (2013).
12. Ziya, Z., Kılınç, N., Atilla, D. & Gül, A. Recent studies chemical sensors based on phthalocyanines. *J. Porphyr. Phthalocyanines* **13**, 11, 1179–1187 (2009).
13. Nieuwenhuizen, M. S., Nederlof, A. J., Barendsz, A. W. (Metallo)phthalocyanines as chemical interfaces on a surface acoustic wave gas sensor for nitrogen dioxide. *Anal. Chem.* **60**, 3, 230–235 (1988).
14. Basova, T., Hassan, A., Durmus, M., Gurek, A. G. & Ahsen, V. Liquid crystalline

metal phthalocyanines: Structural organization on the substrate surface. *Coord. Chem. Rev.* **310**, 131–153 (2016).

15. Song, Y. *et al.* Ultrathin , Cationic Covalent Organic Nanosheets for Enhanced CO_2 Electroreduction to Methanol. *Adv. Mater.* **36**, 2310037–2310046 (2024).

16. Ogura, S. I., Tabata, K., Fukushima, K., Kamachi, T. & Okura, I. Development of phthalocyanines for photodynamic therapy. *J. Porphyr. Phthalocyanines* **10**, 1116–1124 (2006).

17. Ayari, S., Arnoux, P., Ouzari, H. I. & Frochot, C. Photophysical studies of Zn(II) tetra, *tert*-butyl phthalocyanine. *Comptes Rendus. Chim.* **27**, 473–480 (2024).

18. Valiente-Gabioud, A. A. *et al.* Phthalocyanines as Molecular Scaffolds to Block Disease-Associated Protein Aggregation. *Acc. Chem. Res.* **49**, 801–808 (2016).

19. Gounden, D., Nombona, N. & van Zyl, W. E. Recent advances in phthalocyanines for chemical sensor, non-linear optics (NLO) and energy storage applications. *Coord. Chem. Rev.* **420**, 213359 (2020).

20. Sharman, W. M. & Van Lier, J. E. Synthesis of Phthalocyanine: Precursors in *The Porphyrin Handbook: Phthalocyanines: Synthesis* vol. 15 (Elsevier Inc., 2012).

21. Merey, S. & Bekaroglu, Ö. Synthesis and characterization of novel phthalocyanines with four tridentate NNS substituents and four chloro groups. *Dalt. Trans.* 4503–4510 (1999).

22. Yamamoto, S., Dudkin, S. V., Kimura, M. & Kobayashi, N. Phthalocyanine Synthesis in *Handbook of Porphyrin Science* 1–168 (2019).

23. Tomoda, H., Saito, S., Ogawa, S. & Shiraishi, S. Synthesis of phthalocyanines from phthalonitrile with organic strong bases. *Chem. Lett.* **9**, 1277–1280 (1980).

24. Wöhrle, D., Schnurpfeil, G. & Knothe, G. Efficient synthesis of phthalocyanines and related macrocyclic compounds in the presence of organic bases. *Dye. Pigment.* **18**, 91–102 (1992).

25. Villemin, D., Hammadi, M., Hachemi, M. & Bar, N. Applications of Microwave in Organic Synthesis: An Improved One-step Synthesis of Metallophthalocyanines and a New Modified Microwave Oven for Dry Reactions. *Molecules* **6**, 831–844 (2001).

26. Duruk, E. G., Yenilmez, H. Y., Altindal, A. & Bayir, Z. A. Microwave-assisted synthesis of novel nonperipherally substituted metallophthalocyanines and their sensing behaviour for a broad range of Lewis bases. *Dalt. Trans.* **44**, 10060–10068 (2015).

27. Moiseeva, E. O. *et al.* Tetraiodophthalocyanines : Simple and convenient synthetic protocol and structural modification via Sonogashira cross-coupling reaction. *Inorganica Chim. Acta* **535**, 120855 (2022).

28. Youssef, T. E. Efficient green procedures for the preparation of novel tetraalkynyl-substituted phthalocyanines. *Polyhedron* **29**, 1776–1783 (2010).

29. Saito, Y., Higuchi, T., Sugimori, H. & Yabu, H. One-Pot UV-Assisted Synthesis of Metal Phthalocyanine Nanocrystals. *ChemNanoMat* **1**, 92–95 (2015).

30. Li, D. *et al.* A novel and green route for solvothermal synthesis of manganese phthalocyanine crystals. *Dye. Pigment.* **113**, 200–204 (2015).

31. Li, D. *et al.* Green synthesis and characterization of crystalline zinc phthalocyanine and cobalt phthalocyanine prisms by a simple solvothermal route. *CrystEngComm* **20**, 2749–2758 (2018).

32. Li, D. *et al.* A green route to prepare metal-free phthalocyanine crystals with controllable structures by a simple solvothermal method. *RSC Adv.* **11**, 31226–31234 (2021).

33. Tietze, L. F. Domino Reactions in Organic Synthesis. *Chem. Rev.* **96**, 115–136 (1996).

34. Ma, X. & Zhang, W. Recent developments in one-pot stepwise synthesis (OPSS) of small molecules. *ISCIENCE* **25**, 105005 (2022).

35. Zhu, J. & Bienayme, H. Multicomponent Reactions. Wiley VCH (2005).

36. Hayashi, Y. Pot economy and one-pot synthesis. *Chem. Sci.* **7**, 866–880 (2016).

37. Mandal, K., Ghose, S., Mandal, M., Majumder, D., Talukdar, S., Chakraborty, I., Panda, S. K. Notes on useful materials and synthesis through various chemical solution techniques in Chemical Solution Synthesis for Materials Design and Thin Film Device Applications. Elsevier (2021).

38. Mekky, A. E. M. & Sanad, S. M. H. New Bis(pyrazolo[5,1-b]quinazolines) and Bis(9H-xanthenediones) Linked to Alkane Cores: One-Pot Synthesis, Antibacterial Screening, and SAR Study. *Chem. Biodivers.* **202401700**, 1–13 (2024).

39. Palmeri, F., Raglione, V., Mancini, L. & Zanotti, G. A versatile and practical one-pot strategy for a greener, waste-minimized synthesis of aryloxyand alkyloxy-substituted metallophthalocyanines via tandem SNAr-cyclotetramerization. *Org. Chem. Front.* **13**, 1199–1210 (2026).

40. Tuhl, A. *et al.* Tetra and octa(2,6-di-iso-propylphenoxy)-substituted phthalocyanines: *J. Porphyr. Phthalocyanines* **16**, 163–174 (2012).

41. Lo, P. C. *et al.* The unique features and promises of phthalocyanines as advanced photosensitisers for photodynamic therapy of cancer. *Chem. Soc. Rev.* **49**, 1041–1056 (2020).

42. Sun, Q., Feng, W., Yang, P., You, G. & Chen, Y. Highly selective room-temperature NO_2 sensors based on a fluoroalkoxy-substituted phthalocyanine. *New J. Chem.* **42**, 6713–6718 (2018).

43. Wang, Z. *et al.* The effect of peripheral substituents attached to phthalocyanines on the third order nonlinear optical properties of graphene oxide-zinc(II)phthalocyanine hybrids. *RSC Adv.* **5**, 94144–94154 (2015).

44. Giribabu, L. *et al.* Sterically demanded unsymmetrical zinc phthalocyanines for dye-sensitized solar cells. *Dye. Pigment.* **98**, 518–529 (2013).

45. Guo, J. *et al.* Boosting the performance and stability of perovskite solar cells with phthalocyanine-based dopant-free hole transporting materials through core metal and peripheral groups engineering. *Org. Electron.* **64**, 71–78 (2019).

46. Jiang, X. *et al.* Molecular Engineering of Copper Phthalocyanines : A Strategy in Developing Dopant-Free Hole-Transporting Materials for Efficient and Ambient-Stable Perovskite Solar Cells. **1803287**, 1–9 (2019).

47. Namgoong, J. W. *et al.* Aryloxy- and chloro-substituted zinc(II) phthalocyanine dyes: Synthesis, characterization, and application for reducing the thickness of color filters. *Dye. Pigment.* **154**, 128–136 (2018).

48. Furuyama, T., Maeda, K., Maeda, H. & Segi, M. Chemoselective Synthesis of Aryloxy-Substituted Phthalocyanines. *J. Org. Chem.* **84**, 14306–14312 (2019).

49. Paris, J. *et al.* Phthalocyanine–titanate nanotubes: a promising nanocarrier detectable by optical imaging in the so-called imaging window. *RSC Adv.* **5**, 6315–6322 (2015).

50. Brewis, M., Clarkson, G. J., Humberstone, P., Makhseed, S. & Mckeown, N. B. The Synthesis of Some Phthalocyanines and Napthalocyanines Derived from Sterically Hindered Phenols. *Chem. - A Eur. J.* **4**, 1633–1640 (1998).

51. McKeown, N. B. Phthalocyanines: Synthesis in *The Porphyrin Handbook* vol. 15 (Elsevier Inc., 2003).

52. Feng, Z. *et al.* One-pot synthesis of copper phthalocyanine polymer : An efficient CO_2 fixation catalyst. *Mater. Today Commun.* **41**, 110875–110884 (2024).

53. Lo, P., Cheng, D. Y. Y. & Ng, D. K. P. Phthalocyanine Synthesis in Ionic Liquids: Preparation of Differently Substituted Phthalocyanines in Tetrabutylammonium Bromide. New York 41–180 (2005).

54. Brewis, M., Clarkson, G. J., Helliwell, M., Holder, A. M. & Mckeown, N. B. The Synthesis and Glass-Forming Properties of Phthalocyanine-Containing Poly (arylether) Dendrimers. *Chem. - A Eur. J.* **6**, 4630–4636 (2000).

55. Bhattacharya, A., Suarez, V., Tamez, V. & Wu, J. Eco-friendly reductive acetamidation of arylnitro compounds by thioacetate anion through in situ catalytic regeneration : application in the synthesis of Acetaminophen TM. *Tetrahedron Lett.* **47**, 3221–3223 (2006).

56. Lin, T.-M. *et al.* Potassium Carbonate as a Low-Cost and Highly Active Solid Base Catalyst for Low-Temperature Methanolysis of Polycarbonate. *ChemSusChem* **18**, 1–

11 (2025).

57. Durmus, M. & Nyokong, T. Synthesis , photophysical and photochemical studies of new water-soluble indium (III) phthalocyanines. *Photochem. Photobiol. Sci.* **6**, 659–668 (2007).

58. Jordan, A., Hall, C. G. J., Thorp, L. R. & Sneddon, H. F. Replacement of Less-Preferred Dipolar Aprotic and Ethereal Solvents in Synthetic Organic Chemistry with More Sustainable Alternatives. *Chem. Rev.* **122**, 6749–6794 (2022).

59. Zhang, L. *et al.* Synthesis and evaluation of cationic phthalocyanine derivatives as potential inhibitors of telomerase. *Bioorganic Med. Chem.* **16**, 303–312 (2008).

60. Ruiz-González, R. *et al.* Cationic phthalocyanine dendrimers as potential antimicrobial photosensitisers. *Org. Biomol. Chem.* **15**, 9008–9017 (2017).

61. Bıyıklıo, Z., Durmus, M. & Kantekin, H. Tetra-2- [2- (dimethylamino) ethoxy] ethoxy substituted zinc phthalocyanines and their quaternized analoques : Synthesis , characterization , photophysical and photochemical properties. *J. Photochem. Photobiol. A Chem.* **222**, 87–96 (2011).

62. McKeown, N. B. *Phthalocyanine Materials : Synthesis , Structure and Function* Cambridge University Press , 1998 ; ISBN Book Review. (Cambridge University Press, 1998).

63. Sheldon, R. A. The E factor at 30: a passion for pollution prevention. *Green Chem.* **25**, 1704–1728 (2023).

64. Osedach, T. P., Andrew, T. L. & Bulović, V. Effect of synthetic accessibility on the commercial viability of organic photovoltaics. *Energy Environ. Sci.* **6**, 711–718 (2013).

65. Zanotti, G., Palmeri, F. & Raglione, V. Phthalocyanines Synthesis: A State-of-The-Art Review of Sustainable Approaches Through Green Chemistry Metrics. *Chem. – A Eur. J.* **30**, e202400908 (2024).

66. Shankar, R., Vasudevan, P. & Narendra, K. Synthesis , Characterisation , Association in Solution and Electrical Conductivity in Solid State of a Few Aryloxy Substituted Soluble Phthalocyanines. *Synth. React. Inorg. Met. Chem.* **27**, 1277–1297 (1997).

67. Korkmaz, E. *et al.* Investigation of photophysical and photochemical properties of phthalocyanines bearing fluorinated groups. *Monatshefte fur Chemie* **151**, 181–190 (2020).

68. Pinto, S. M. A. *et al.* The quest for biocompatible phthalocyanines for molecular imaging : Photophysics , relaxometry and cytotoxicity studies. *J. Inorg. Biochem.* **154**, 50–59 (2016).

69. Gören, H. Y., Çelik, G. G. & Gürek, A. G. Heat gun-assisted rapid and efficient synthesis of tetra-substituted Zinc (II) phthalocyanines functionalized with alkylthio or alkoxy chains. *Org. Commun.* **17**, 265–271 (2024).

70. Zanotti, G., Palmeri, F. & Raglione, V. Phthalocyanines Synthesis: A State-of-The-Art Review of Sustainable Approaches Through Green Chemistry Metrics. *Chem. - A Eur. J.* **30**, (2024).

71. Zhang, Z., Yin, L., Wang, Y., Liu, J. & Li, Y. Indium tribromide in poly (ethylene glycol) (PEG): a novel and efficient recycle system for chemoselective deprotection of. *Green Chem.* **6**, 563–565 (2004).

72. Tanaka, K. & Toda, F. Solvent-Free Organic Synthesis. *Chem. Rew.* **100**, 1025–1074 (2000).

73. Kidwai, M., Bhatnagar, D. & Mishra, N. K. Polyethylene glycol (PEG) mediated green synthesis of 2,5-disubstituted 1,3,4-oxadiazoles catalyzed by ceric ammonium nitrate (CAN). *Green Chem. Lett. Rev.* **3**, 55–59 (2010).

74. Poliakoff, M., Fitzpatrick, J. M., Farren, T. R. & Anastas, P. T. Green Chemistry : Science and Politics of Change. *Science* **297**, 807–811 (2002).

75. Behles, J. A. & Desimone, J. M. Developments in CO_2 research. *Pure Appl. Chem.* **73**, 1281–1285 (2001).

76. Brunner, G. Near critical and supercritical water . Part I . Hydrolytic and hydrothermal processes. *J. Supercrit. Fluids* **47**, 373–381 (2009).

77. Wasserscheid, P. & Keim, W. Ionic Liquids- New 'solutions' for Transition Metal Catalysis. *Angew. Chemie - Int. Ed.* **39**, 3772–3789 (2000).

78. Studer, A. *et al.* Fluorous Synthesis : A Fluorous-Phase Strategy for Improving Separation Efficiency in Organic Synthesis. *Science* **275**, 823–827 (1997).

79. Zanotti, G., Imperatori, P., Paoletti, A. M. & Pennesi, G. Sustainable Approaches to the Synthesis of Metallophthalocyanines in Solution. *Mol.* **26**, 1760 (2021).

80. Podapangi, S. K. *et al.* Green Anisole Solvent-Based Synthesis and Deposition of Phthalocyanine Dopant-Free Hole-Transport Materials for Perovskite Solar Cells. *Energies* **16**, 3643–3660 (2023).

81. Alder, C. M. *et al.* Updating and further expanding GSK's solvent sustainability guide. *Green Chem.* **18**, 3879–3890 (2016).

82. Chen, J., Spear, S. K., Huddleston, J. G. & Rogers, R. D. Polyethylene glycol and solutions of polyethylene glycol as green reaction media. *Green Chem.* **7**, 64–82 (2005).

83. Reddy, B. S., Naidu, A. & Dubey, P. K. PEG-600-mediated, green and efficient, tandem syntheses ofN-subtituted-2-styrylquinazolin-4- ones. *Green Chem. Lett. Rev.* **6**, 254–261 (2013).

84. Zalipsky, S. & Harris, J. M. *Introduction to Chemistry and Biological Applications of Poly (Ethylene Glycol)*. (American Chemical Society, 1997).

85. Hoffmann, M. M. Polyethylene glycol as a green chemical solvent. *Curr. Opin. Colloid Interface Sci.* **57**, 101537 (2022).

86. Chen, J., Spear, S. K., Huddleston, J. G. & Rogers, R. D. Polyethylene glycol and solutions of polyethylene glycol as green reaction media. *Green Chem.* **7**, 64–82 (2005).

87. Sharma, U., Kumar, N., Verma, P. K., Kumar, V. & Singh, B. Zinc phthalocyanine with PEG-400 as a recyclable catalytic system for selective reduction of aromatic nitro compounds. *Green Chem.* **14**, 2289–2293 (2012).

88. Hasaninejad, A. & Beyrati, M. Eco-friendly polyethylene glycol (PEG-400): A green reaction medium for one-pot, four-component synthesis of novel asymmetrical bis-spirooxindole derivatives at room temperature. *RSC Adv.* **8**, 1934–1939 (2018).

89. Sengwa, R. J., Kaur, K. & Chaudhary, R. Dielectric properties of low molecular weight poly (ethylene glycol) **608**, 599–608 (2000).

90. Journal, A. I., Jadhavpatil, V. L., Undre, P. B. & Helambe, S. N. Dielectric relaxation in water- dimethylaminoethanol mixtures as a function of composition and temperature. *Integr. Ferroelectr.* **185**, 1–10 (2017).

91. Corradini, F. *et al.* solvent system at various temperatures. 0–4 (1992).

92. ThermoFischer Scientific. Polyethylene glycol 400 Safety Data Sheet. *Safety data Sheet* 1–11 (2023).

93. ThermoFischer Scientific. N,N-Dimethylethanolamine Safety Data Sheet. 1–10 (2025).

94. ThermoFischer Scientific. N,N-Dimethylformamide (DMF) Safety Data Sheet. 1–15 (2023).

95. Kidwai, M., Jahan, A. & Bhatnagar, D. Polyethylene glycol as an efficient and reusable solvent medium for the synthesis of thiohydantoins using K_2CO_3 as catalyst. *J. Sulfur Chem.* **31**, 161–167 (2010).

96. Chandrasekhar, S., Prakash, S. J. & December, R. V. Poly (ethylene Glycol) (400) as Superior Solvent Medium against Ionic Liquids for Catalytic Hydrogenations with PtO_2. *J. Org. Chem.* **71**, 2196–2199 (2006).

97. Drive, C. *Purification of Laboratory Chemicals*. (2009).

98. Heravi, M. M., Ghavidel, M. & Mohammadkhani, L. Beyond a solvent : triple roles of dimethylformamide in organic chemistry. *RSC Adv.* **8**, 27832–27862 (2018).

99. Zhang, Z., Xu, S. & Wu, Y. Recent Advances of Pervaporation Separation in DMF / H 2 O Solutions : A Review. *Membranes (Basel).* **11**, 455 (2021).

100. Silva, C. B. *et al.* Concentration and solvent effects , photochemical and photophysical properties of methyl and *tert*-butyl zinc (II) and aluminum (III)

phthalocyanines. *J. Mol. Struct.* **1246**, 131103–131116 (2021).

101. Li, R. *et al.* Electron-Donating or -Withdrawing Nature of Substituents Revealed by the Electrochemistry of Metal-Free Phthalocyanines. *Inorg. Chem.* **45**, 2327–2334 (2006).

102. Chen, J., Spear, S. K., Huddleston, J. G. & Rogers, R. D. Polyethylene glycol and solutions of polyethylene glycol as green reaction media. *Green Chem.* **7**, 64–82 (2005).

103. Li, J., Liu, W. & Xie, Y. Recyclable and Reusable $Pd(OAc)_2$ / DABCO / PEG-400 System for Suzuki - Miyaura Cross-Coupling Reaction. *J. Org. Chem.* **70**, 5409–5412 (2005).

104. Wei, T., Zhang, T., Huang, B., Tuo, Y. & Cai, M. Recyclable and reusable $NiCl_2(PPh_3)_2$/CuI/PEG400/H_2O system for the sonogashira coupling reaction of aryl iodides with alkynes. *Appl. Organometal. Chem.* **29**, 846–849 (2015).

105. Jiang, X. *et al.* A solution-processable copper(II) phthalocyanine derivative as a dopant-free hole-transporting material for efficient and stable carbon counter electrode-based perovskite solar cells. *J. Mater. Chem. A* **5**, 17862–17866 (2017).

106. Sevim, A. M., Yenilmez, H. Y. & Bayir, Z. A. Synthesis and photophysical properties of novel (trifluoromethyl) phenylethynyl-substituted metallophthalocyanines. *Polyhedron* **62**, 120–125 (2013).

107. Mujkic, M. & Lentz, D. Syntheses of highly unsaturated isocyanides via organometallic pathways. *Dalt. Trans.* **41**, 839–849 (2012).

108. Maya, E. M., Haisch, P., Vazquez, P. & Torres, T. Synthesis and Characterization of Tetraethynylphthalocyanines. *Tetrahedron* **54**, 4397–4404 (1998).

109. Raglione, V., Palmeri, F., Mattioli, G. & Porcelli, F. Glycerol as Reaction Medium for Sonogashira Couplings : A Green Approach for the Synthesis of New Triarylamine-Based Materials with Potential Application in Optoelectronics. *Chem. - A Eur. J.* **30**, 1–10 (2024).

110. Di Noi, A. *et al.* AP-MALDI-MS reveals adulteration of dried oregano leaves. *J. Food Compos. Anal.* **139**, 107121–107131 (2025).

111. Ghiglietti, E., Incarbone, A., Mattiello, S. & Beverina, L. Efficient Copper-Free Sonogashira Coupling in Water and under Ambient Atmosphere. *European J. Org. Chem.* **27**, e202400223 (2024).

112. Ingale, A. P., More, V. K., Gangarde, U. S. & Shinde, S. V. Chemoselective N-*tert*-butyloxycarbonylation of amines in glycerol. *New J. Chem.* **42**, 10142–10147 (2018).

Chapter 3. Development of a sustainable and cost-effective phthalocyanine-based electrochemical device

3.1 Introduction

3.1.1. Overview of sensing platforms

As outlined in Chapter 1, over recent decades Green Chemistry has emerged as a guiding paradigm to address the urgent need to reduce the release of hazardous pollutants into natural ecosystems while advancing effective strategies for their monitoring and remediation.[1,2]

Owing to their versatility, selectivity, and reliability in the real-time detection of chemical species, sensing devices have become increasingly important in recent years in the modern analytical science and are now widely employed in several application fields, such as environmental monitoring, healthcare sector, and telemedicine.[3]

A sensor is defined as a device capable of detecting and measuring a physical, chemical, or biological stimulus and converting it into a quantifiable, analytically useful signal that can be interpreted by an observer or processed by an electronic system.[4] It is therefore a complex system integrating material science, transduction physics, electronics, and signal processing, thus playing a foundational role in contemporary technological ecosystems, ranging from industrial automation and biomedical diagnostics to environmental monitoring and smart infrastructures.[5]

The defining characteristic of a sensor lies in its ability to respond selectively and reproducibly to a specific stimulus, such as temperature, pressure, displacement, light intensity, or chemical concentration, while minimizing interference from other

environmental variables. The principle underlying their operation consists of capturing a molecular interaction or binding event and converting it into a measurable output.

From a structural perspective, a sensor typically consists of three core components connected in series (**Figure 1**). The first is the receptor, that is the sensing or recognition element, which directly interacts with the analyte or the physical quantity that must be detected. This element undergoes a measurable change in one of its intrinsic properties (e.g., electrical resistance, capacitance, inductance, optical absorption, mechanical deformation) in response to external stimuli. The second is the transducer, that converts the physical or chemical variation into an electrical signal, as electrical outputs are generally more suitable for amplification, transmission, and processing. Depending on the operating principle, this conversion may be electrical, optical, thermal, electrochemical, resistive, capacitive, or piezoelectric in nature. The third is the electronic system. It is a signal-processing unit that performs amplification, filtering, linearization, impedance matching, and analog-to-digital conversion, thereby enhancing signal integrity and ensuring compatibility with downstream processing units (display), where the results are showed in an understandable and user-friendly manner. The output signal on the display can be numeric, graphic, or figural, depending on the requirements of the end user.[6]

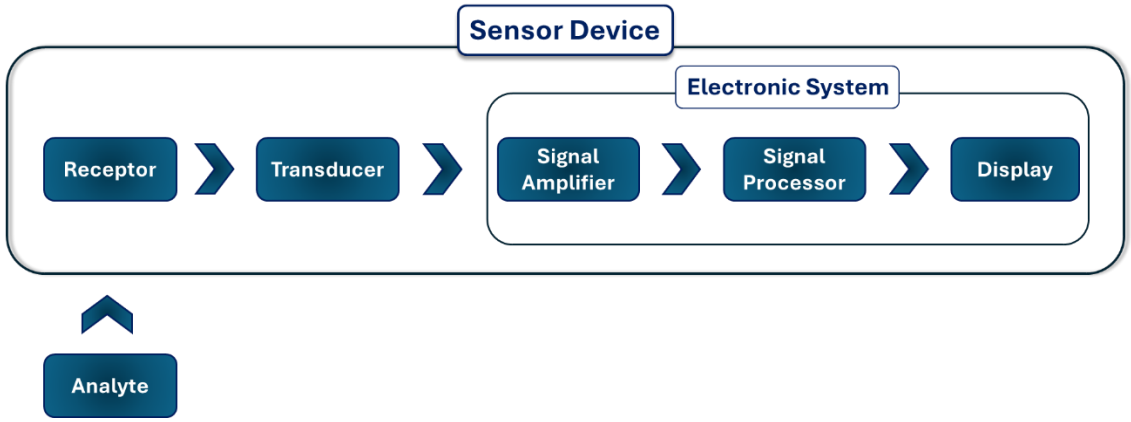

Figure 1. Illustration scheme of the main elements of a sensor device.

The performance of a sensor is evaluated according to several parameters, including sensitivity, resolution, accuracy, precision, repeatability, linearity, response time, and stability. These characteristics determine the reliability and suitability of a sensor for specific applications.

Sensors may be classified according to the kind of receptor (e.g. when it is a biological component such as an enzyme, aptamer, nucleic acid, or antibody the sensor is called biosensor) or to their mode of signal transduction (i.e. electrochemical, optical, or thermal sensors) or, alternatively, a combination of the two.

Electrochemical sensors have gained wide attention as a promising alternative to conventional laboratory-based analytical measurements (atomic spectroscopy, or mass spectrometry) for applications in environmental monitoring, medical diagnostics, and chemical analysis, especially for *in situ* analyses, due to their inherent advantages, namely high sensitivity, fast real-time response, user-friendliness, cost-effectiveness, and adaptability to portable formats.[7–11] In these devices, an electrode functions as a transducer within an electrolyte environment and constitutes a fundamental component of the sensor. An electrochemical sensor typically comprises a set of electrodes, such as working, counter, and reference electrodes fabricated on a supporting surface.[12]

Some approaches frequently rely on biosensors which, though highly selective, are hindered by the high cost and low stability of their biological components, as well as by laborious extraction and preparation procedures. Due to the intrinsic fragility of many natural enzymes, immobilized enzyme-based systems still face significant limitations, including immature immobilization technologies, reduced catalytic activity, and elevated production costs.[13] In particular, the stabilization and long-term storage of the enzymatic component often require immobilization onto inert matrices, a step that, while indispensable, further increases the complexity and cost of biosensor fabrication. Additionally, even though recent efforts have explored the use of electrolytes, polyelectrolytes, and polyols as stabilizers, showing that both the storage and operational

stability of biosensors can be improved, these approaches do not fully overcome the intrinsic fragility of enzymatic components. [14–16]

This kind of devices have been progressively adopted for the detection of analytes of clinical and environmental significance, owing to their portability, cost-effectiveness, high sensitivity, and capability to function reliably within complex sample matrices [17–19] and their analytical performance is frequently improved through the integration of nanomaterials, which enhance electron transfer kinetics, increase signal amplification, and introduce selective recognition sites.[20–22] Nevertheless, conventional fabrication strategies for nanomaterials used in electrode modification often rely on hazardous substances, including hydrazine,[23] sulfuric acid,[24] and volatile organic solvents such as toluene and benzene, thereby raising considerable concerns regarding human health and environmental safety.[25,26]

In addition, many of these devices are designed for single use, with the electrodes being discarded immediately after operation. Given the increasing market demand, this practice contributes to rising waste generation and poses environmental concerns. Moreover, since these devices are frequently manufactured on a large scale at the industrial level, their production can, to some extent, constitute a non-negligible source of environmental pollution, partially counteracting their positive impact, particularly in environmental applications.

Consequently, the sustainability of each stage of sensor development represents a critical consideration as it significantly influences the overall ecological footprint of electrochemical sensors.

This has led to the urgent need to rethink electrochemical sensor fabrication strategies, taking into account both analytical performance (including sensitivity, stability, reproducibility, and scalability) and environmental impact in the detection of toxic contaminants, in accordance with the principles of green chemistry and sustainable engineering.[27]

Considering this, various aspects that are involved in the fabrication of electrochemical sensors need to be reconsidered from a sustainability perspective.

Figure 2 shows a representation of the lifecycle of a sensor device, most plausibly based on a screen-printed electrode (SPE) platform, encompassing its fabrication, functionalization, storage and transport, practical use, and final disposal.[28] Rather than depicting isolated technical steps, the scheme conveys an integrated manufacturing and application strategy aligned with scalable production and sustainable analytical practices. These can be broadly summarized in three main stages and constitute the critical points that warrant deeper investigation to achieve a fully sustainable sensor manufacturing and application workflow.

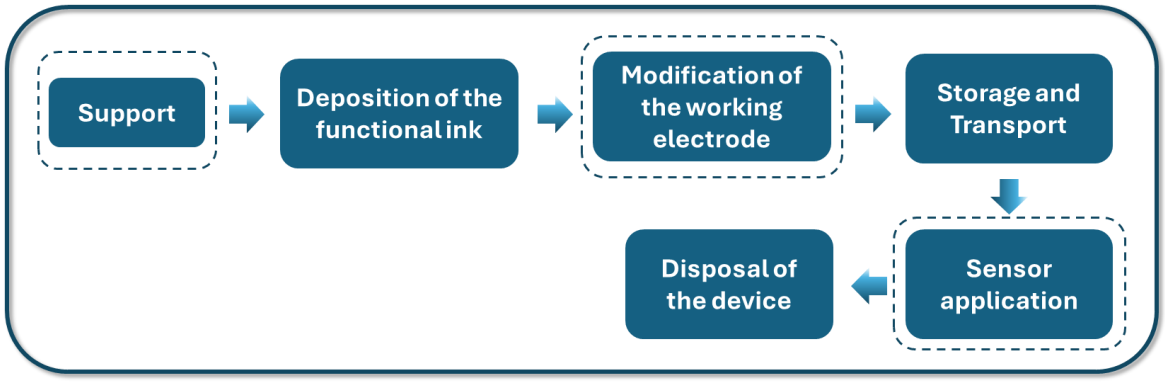

Figure 2. Generic process flow diagram of electrochemical sensors fabrication.

First, the selection of electrode materials (surface support) should focus on low-impact alternatives, such as biodegradable composites, bismuth, tin, or zinc oxide, which reduce environmental and health risks while maintaining analytical performance. Second, the reagents used to modify the sensor surface should be replaced with greener, less hazardous options, including plant extracts, natural acids, and other biocompatible agents, while the physical processes itself that is employed for surface modification should also be sustainable, energy-efficient, and environmentally benign, ensuring overall safe and eco-

friendly electrode functionalization. Third, the choice of solvents should prioritize environmentally friendly alternatives, such as water and water-based solutions, which offer biocompatibility, non-toxicity, and high cost-effectiveness.

Materials such as ceramics, paper, textiles, glass, and biodegradable polymers like polyethylene glycol, and poly(butylene adipate-co-terephthalate), cellulose acetate, polylactic acid are commonly employed as surface support for electrochemical sensors. The choice of surface support material is particularly significant not only for ensuring the mechanical stability and functional performance of the device, but also for its end-of-life management. Indeed, the nature of the surface support directly influences the environmental impact associated with disposal after use. Selecting materials that are recyclable, biodegradable, or derived from renewable resources can substantially reduce the ecological footprint of the sensor. Conversely, supports composed of non-degradable or hazardous components may complicate waste treatment and increase environmental burden.

In recent years, disposable test strips, called screen-printed electrodes (SPEs), have increasingly emerged as versatile and effective electrochemical sensors, offering a practical alternative to conventional laboratory-based analytical procedures for several environmental applications, such as water quality, organic compounds analysis, bacteria and radioelements, gas pollutants, and heavy metal detection.[29] These devices typically incorporate planar working electrodes, commonly composed of carbon (C-SPE), gold, or similar conductive materials, together with a silver reference electrode, all printed onto an inexpensive plastic or ceramic support (**Figure 3**).[30]

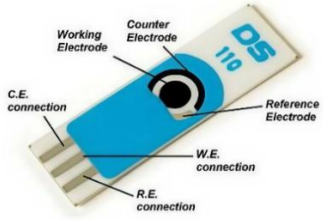

Figure 3. DropSens C-SPE.[31]

In this configuration, each strip functions as a miniaturized self-contained, single-use, and easy-portable electrochemical cell, onto which a small sample droplet can be applied, enabling rapid, non-invasive, and on-site sample analysis with minimal operational complexity.[29]

Since the 1990s, screen-printing technology, adapted from the microelectronics industry, has facilitated the large-scale production of these low-cost, single-use small sensors with high reproducibility and reliability. This manufacturing approach has contributed significantly to their growing adoption, particularly for decentralized monitoring and real-time analytical applications.

SPEs are fabricated by depositing different functional inks onto ceramic or plastic supports using patterned polyester screens designed according to specific analytical needs. Different types of inks are deposited using a mask to form the working electrodes and establish the electrical pathways necessary for signal transduction. The masking is essential to precisely delimit the active sensing area, ensuring controlled exposure of the electrode surface and improving analytical reproducibility.[32] Printing inks can be carbon, silver, gold-based and they can be tailored through the modification with or incorporation of metals, enzymes, polymers, or complexing agents to enhance analytical specificity and signal response. Graphite-based inks are especially preferred due to their low cost, ease of processing, and technological simplicity, making them highly suitable for scalable and economically sustainable sensor development.

A major advantage of SPEs lies in their exceptional versatility and flexibility in machine-controlled manufacturing, particularly in relation to electrode modification, which is a critical factor can effectively influence the overall sensor performance, including sensitivity and selectivity of the measurements.

Indeed, the physical modification of the electrode surface plays a pivotal role in defining the physicochemical properties of the sensing interface, directly influencing the selectivity, sensitivity, and reliability of the analytical response. Such modifications are typically achieved through a process known as immobilization, in which chemical or biological

components are immobilized onto the electrode surface. Once immobilized, these elements are responsible for generating a chemical, electrochemical, or otherwise detectable signal upon interaction with specific target analytes, effectively translating molecular recognition events into measurable outputs.

Through this immobilization process, layers of functional material are formed on the electrode surface, providing a tailored environment that enhances electron transfer, stabilizes the recognition elements, and introduces additional catalytic or binding functionalities. The substances used in this process may include diverse (bio)recognition elements such as enzymes, but also metal complexes, polymeric and nanostructured materials, or other functional molecular materials, each selected according to the specific analytical purpose. The careful design and implementation of these surface modifications are essential for optimizing the performance of the sensor, as even subtle variations in layer composition, thickness, or uniformity can significantly impact signal quality and reproducibility.

This post-fabrication functionalization is therefore of paramount importance, not only because it allows the customization of the sensor for a particular target or application, but also because it fundamentally determines the practical applicability and reliability of disposable SPE-based devices. By enabling precise control over the interfacial properties of the electrode, surface engineering transforms a simple printed electrode into a high-performance, application-specific sensor capable of meeting the rigorous demands of modern analytical and on-site monitoring contexts.

The adoption of environmentally responsible materials and deposition strategies further enhances the sustainability of SPE-based devices. By carefully selecting inks and modifiers that are non-toxic, water-soluble, or derived from renewable sources, and by applying immobilization methods that minimize hazardous reagents and energy consumption, it becomes possible to produce high-performance sensors that comply with green chemistry principles without compromising analytical capabilities.[33]

The adoption of green deposition methodologies that minimize the use of hazardous reagents and energy-intensive processes, together with an environmental responsible choice of the materials used in the entire manufacturing process of a sensor device, stand out as crucial factors for the development of new green electrochemical sensors, fully embodying the principles of eco-engineering and sustainable design while preserving, or even enhancing, the analytical capabilities.[27,34]

Building on these advantages, the final aim of this doctoral thesis is the development of new electrochemical sensors that are more sustainable than current state-of-the-art devices. This approach illustrates how the combination of SPE technology and the sustainable modification of the working electrode, that includes sustainable material selection and synthesis, and environmentally friendly deposition methods, can lead to high-performance, eco-compatible electrochemical devices suitable for environmental monitoring application (**Figure 4**).

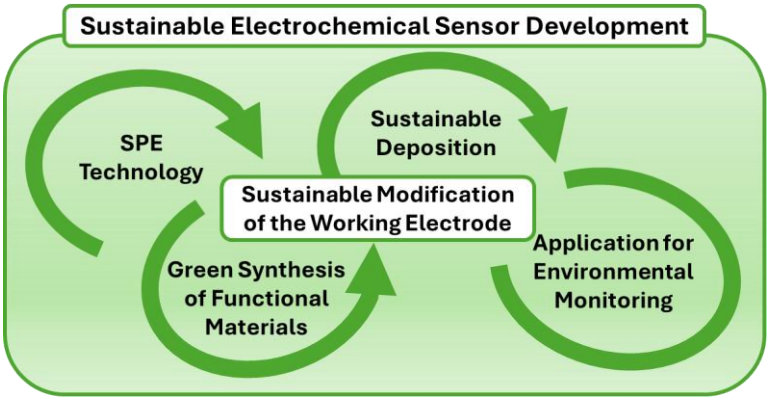

Figure 4. Schematic representation of the synergistic framework of sustainable electrochemical sensor development, that underpins this doctoral thesis.

The following paragraphs are therefore structured on multiple, interconnected levels: first, achieving the green synthesis of molecular materials capable of providing interactions with the target analyte; second, employing environmentally friendly deposition methods

for electrode surface modification; and third, implementing the resulting device for the practical detection of a target pollutant: catechol. These three levels are closely interrelated, forming a synergistic framework in which advances in material design, deposition methodology, and device applications mutually reinforce one another, collectively driving the development of sustainable, high-performance electrochemical sensors.

3.1.2. Phthalocyanine-based sensors

The present study focuses on the implementation of sustainable strategies, that have thoroughly been discussed and validated for the preparation of a series of peripherally functionalized phthalocyanines, aiming at the synthesis of functional derivatives suitable for sensing applications.

Along with the increasing awareness of environmental challenges and responding to the urgent need to develop effective strategies for the monitoring of hazardous pollutants into natural ecosystems, after the optimization of the manufacturing of the novel green electrochemical device, the study explored its practical use in the detection of a toxic pollutant, catechol.

Catechol (1,2-dihydroxybenzene, $C_6H_6O_2$) is an aromatic phenolic compound and represents a prominent example of environmentally concerning pollutants. As a versatile chemical raw material, catechol finds extensive application in diverse industrial sectors, including cosmetics, pharmaceuticals, pulp and paper production, dye and textile processing, and the food industry.[35] Its massive use inevitably leads to the generation of large volumes of waste containing catechol and related phenols, that if improperly disposed of could pose serious risks to both human health and the environment, due to their well-established toxicity, persistence, and carcinogenic potential. [36] In fact, catechol and other phenolic derivatives are characterized by low biodegradability in natural ecosystems, which allows their accumulation and increases their negative impact on aquatic and terrestrial life.[37]

Although catechol may originate from natural processes, such as the decomposition of plant material, industrial sources including the pharmaceutical sector, dye and textile manufacturing, pesticide formulation, and the pulp and paper industry are by far the most significant contributors to its presence into aquatic systems. [38,39] As a result, strategies to manage this pollutant must address both its removal from contaminated effluents and its reliable detection at trace levels in the environment.[40]

Considerable progress has been made in the development of sustainable methods for the removal of catechol from wastewater, often based on adsorption, photocatalysis, or biological treatments.[41] Nevertheless, while remediation is crucial, it is equally important to devise rapid, reliable, and cost-effective methods for catechol detection, which would allow both real-time monitoring and prevention of excessive accumulation. [42,43]

Within sensing applications, phthalocyanines are particularly interesting for their dual role as molecular receptors and electrocatalysts, with tunable electronic and optical properties that allow selective interactions with target analytes. [44,45] Moreover, when employed for electrode surface modification, they enhance electron-transfer kinetics, and improve the overall analytical response of electrochemical sensors.[46] In addition, electrode modification with metallophthalocyanines provides the additional benefit of preventing surface fouling, thereby enhancing stability, sensitivity, and selectivity, as well as contributing to improved durability and reproducibility.[47,48]

Collectively, their tunable electronic structure, redox versatility, resistance to deactivation, and strong analyte affinity make phthalocyanines highly promising platforms for the development of advanced chemical sensors, capable of complementing or, in some cases, offering robust alternatives to enzyme-based systems.[49]

In the context of phthalocyanine applications, both in device fabrication and under defined experimental conditions, solubility represents a crucial physicochemical parameter that must be carefully considered. Given their general poor solubility, their processing often requires the use of solvents, such as DMF, that are toxic or hazardous, raising in this way concerns regarding the sustainability of their use.

In the rational design of soluble phthalocyanines, the key parameters under synthetic control that can enhance solubility and modulate aggregation behavior include the substitution pattern, either at the macrocyclic periphery and/or at the axial positions, and the selection of the central metal ion.[50]

The former is a common strategy to mitigate the aggregation of phthalocyanines. Indeed, the steric and electronic (donating or withdrawing) nature of the substituents plays a decisive role in disrupting π-π interactions, by disrupting planarity, thereby decreasing aggregation and improving molecular dispersion and processability.[51–53] This substitution alters their absorbance characteristics, leading to tailored new and intriguing photophysical properties of the macrocycle.[54]

Another widely employed strategy to mitigate the aggregation of phthalocyanines involves the incorporation of metal ions into the central cavity of the macrocycle. Metal coordination can modulate the planarity of the phthalocyanine framework, thereby reducing intermolecular π–π stacking interactions within the chromophoric system.[55] For instance, the introduction of metal centers such as titanium or magnesium has been reported to alter the molecular geometry through coordination bonds, leading to a decreased degree of planarity and, consequently, a diminished tendency toward π-π stacking in solution.[56,57]

Therefore, careful molecular design aimed at balancing solubility, aggregation tendency, and functional performance is essential for the successful implementation of phthalocyanines in advanced technological and catalytic applications.

Water is widely regarded as the most sustainable solvent available in chemical and materials science, owing to its abundance, low cost, non-toxicity, and minimal environmental impact. From the perspective of green chemistry, water satisfies several of the fundamental principles aimed at reducing hazardous substances, preventing waste generation, and minimizing risks to human health and ecosystems. Unlike many conventional organic solvents, often volatile, flammable, and toxic, water is non-flammable, readily available, and inherently safer to handle, store, and dispose of.

Its high polarity and unique hydrogen-bonding capability enable the dissolution or dispersion of a broad range of ionic and polar compounds, making it particularly suitable for environmentally benign synthetic and processing routes. In addition, water exhibits a high heat capacity, which allows efficient thermal control during chemical reactions and reduces the likelihood of uncontrolled exothermic processes. From an industrial standpoint, the use of water can significantly lower solvent-related emissions, reduce the need for complex ventilation systems, and minimize hazardous waste treatment requirements.

In the context of electrochemical sensor fabrication, water represents an ideal medium for deposition processes, particularly when combined with water-soluble functional materials. Its compatibility with biological or biological-like components further enhances its suitability for sensor development.

Overall, when employed judiciously and within optimized process conditions, water embodies the core objectives of sustainable chemistry: safety, renewability, reduced environmental burden, and alignment with eco-efficient technological innovation. The peculiar solubility properties of phthalocyanines can present significant challenges when processing them in aqueous environments. Achieving water solubility is therefore a major objective, particularly for applications that require environmental compatibility or are biologically oriented (such as for the Photodynamic Therapy, PDT). Adequate solubility in water over a range of concentrations and pH values is crucial not only to facilitate practical handling and processing, but also to ensure reliable performance in devices and functional systems.[50]

3.1.3. Water-soluble phthalocyanines

In the present study, water solubility constitutes an important requirement for the development of sustainable phthalocyanines that can be readily handled and processed in aqueous media. Such a feature is essential to enable their effective implementation in

sensing applications, where compatibility with aqueous environments and operational stability are critical parameters. Therefore, molecular design strategies were specifically oriented toward enhancing hydrophilicity while preserving the intrinsic photophysical properties of the macrocyclic core.

Since phthalocyanines are intrinsically hydrophobic, the achievement of inherent water solubility typically relies on two principal approaches: the introduction of ionic substituents or strongly hydrophilic groups, such as carbohydrates or polyethylene glycol chains.

Depending on the nature of these substituents, water-soluble phthalocyanines can thus be classified into three main categories: anionic, cationic, and non-ionic (**Figure 5**). Each class exhibits distinct physicochemical properties that influence solubility, aggregation behaviour, and suitability for specific applications.

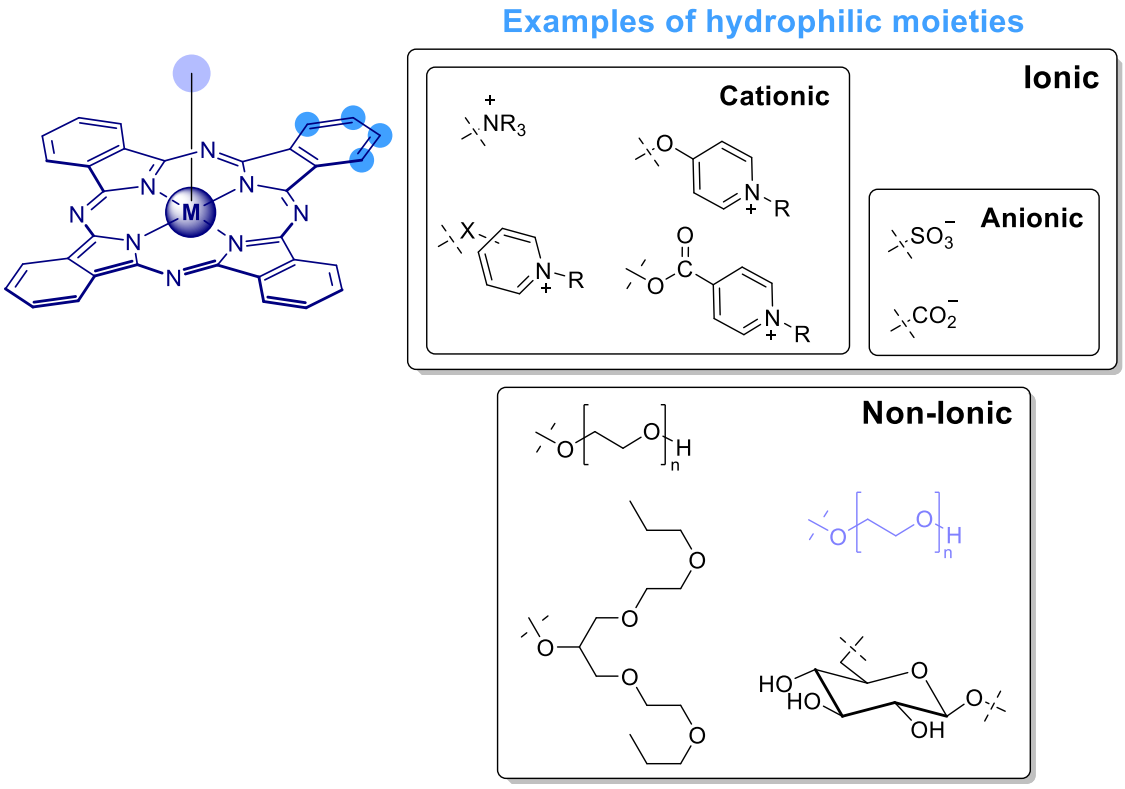

Figure 5. Three main categories of water-soluble phthalocyanines with the corresponding examples of hydrophilic moieties.

Anionic phthalocyanines are commonly functionalized with sulfonyl or carboxyl groups. Sulfonated phthalocyanines typically require harsh and hazardous reagents, such as nitrobenzene and oleum (fuming sulfuric acid containing approximately 30% free SO_3), making their synthesis both environmentally and operationally challenging.[58] Carboxylated metallophthalocyanines, including tetra-carboxylated, are also widely used as anionic water-soluble derivatives and are often prepared from trimellitic acid or trimellitic anhydride via a two-step sequence involving cyclotetramerization to tetra-amides followed by hydrolysis under strong acidic or alkaline conditions.[59] These compounds generally exhibit good solubility in alkaline aqueous media, where the carboxyl groups are deprotonated. However, their synthesis commonly involves toxic starting materials, harsh conditions, and multistep procedures, which negatively affect their environmental footprint.[60]

Cationic phthalocyanines are typically obtained by functionalization with quaternary amines or pyridine units. The usual synthetic strategy involves constructing a phthalocyanine core bearing amine groups, followed by quaternization through multi-methylation using strong methylating agents such as methyl bromide, methyl iodide, or dimethyl sulfate which are highly toxic, posing significant safety and environmental risks.[61] Pyridine-substituted phthalocyanines can be prepared either from pyridine-substituted phthalonitriles or by introducing pyridine into the phthalocyanine structure via aromatic substitution, esterification, or palladium-catalyzed coupling reactions.[50,62,63] However, pyridine itself is hazardous, which raises additional concerns regarding the safety and sustainability of these synthetic routes.

Non-ionic water-soluble phthalocyanines are typically functionalized either by direct addition to the phthalocyanine ring or by linker atoms such as oxygen, sulfur, or nitrogen, with highly hydrophilic moieties such as carbohydrates and polyethylene glycol chains, with different chain lengths and architectures.[64,65] In general, increasing the number or branching of hydrophilic chains enhances solubility in aqueous and polar media and reduces aggregation by sterically hindering interactions between phthalocyanine cores.[66] In

particular, PEGylation is attracting significant interest as it enhances chemical inertness, biocompatibility, serum half-life, and tumor cell accumulation, desirable properties for biomedical applications including PDT. Similarly, glycosylated phthalocyanines, being highly biocompatible and water-soluble, have been shown to provide the potential for selective recognition of targeted cancer cells.[67]

Despite their relative safety and improved environmental profile compared to ionic derivatives, the synthesis of non-ionic water-soluble phthalocyanines is often long and involves multiple synthetic steps, especially for branched PEG substituted Pcs, thus generating significant amounts of chemical waste and raising important considerations in the environmental assessment of their production.

3.2. Results and discussion

3.2.1. Preparation of tetra-4-PEG-400-substituted phthalocyanine derivatives

The one-pot synthetic procedure was adopted to access water-soluble PEGylated phthalocyanine derivatives intended for green electrochemical sensing applications.

As depicted in **Scheme 1**, the first step involves the replacement of the nitro group of the starting material through a nucleophilic aromatic substitution using K_2CO_3 as a sustainable base for the generation of alcoholate ion. The resulting intermediate has not been isolated but directly used as the reagent of the subsequent cyclotetramerization. After increasing properly the temperature, metal salt and DBU were added in the same reaction vessel, leading to the appearance of the green nuance, characteristic of the macrocycle formation.

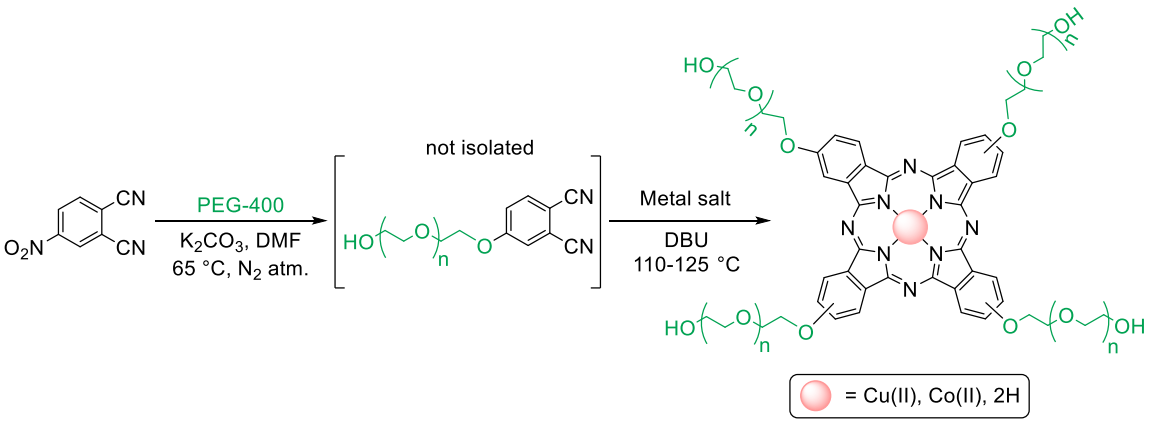

Scheme 1. Synthetic pathway for the preparation of tetra-4-PEG-400-substituted metallo and metal-free phthalocyanines (4-PEGMPc and 4-PEG2HPc).

The new functional materials, 4-PEGCuPc, 4-PEGCoPc and 4-PEG2HPc, have been afforded in satisfactory yields (62%, 50%, and 40%, respectively) demonstrating the versatility of the one-pot strategy, previously validated only for zinc phthalocyanines. The environmental impact of the syntheses was assessed using the E-factor metric, that were all below 100 for the three derivatives, and details of the calculation of E-factors are reported in the Experimental section at the end of this Chapter.

A direct comparison of the absorption spectra of the three water-soluble phthalocyanines in the same solvent, DMSO, is provided in **Figure 6**.

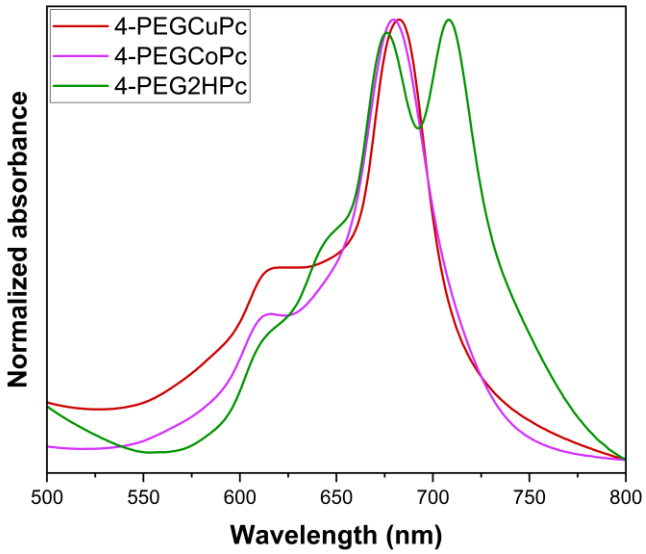

Figure 6. Normalized UV-vis spectra of the water-soluble pegylated phthalocyanines in DMSO.

The functionalization with four PEG-400 substituents enhances the solubility in polar media, as clearly displays the characteristic absorption bands of phthalocyanines in the visible region (600-800 nm). The main absorption band of 4-PEGCuPc and 4-PEGCoPc, known as Q band, is peaked at 682 and 679 nm, respectively, that according to the reported literature is due to the π-π^* transitions from the highest occupied molecular orbital (HOMO) to the lowest unoccupied molecular orbital (LUMO).[69–71] This feature is particularly well resolved in dimethyl sulfoxide (DMSO), indicating the prevalence of monomeric species in this solvent. At the same time, some degree of aggregation is observed in aqueous media, where a secondary band appears at lower wavelengths, that can be attributed to H-type aggregation of the phthalocyanine macrocycles. UV-visible absorption spectra of the new water-soluble metallophthalocyanines recorded in DMSO and water at a fixed concentration of 1×10^{-5} M are reported in the Experimental section at the end of this Chapter.

The spectrum of 4-PEG2HPc (the metal-free derivative) displays in DMSO a splitting of the Q band into two components of comparable intensity, a phenomenon typically attributed to changes in molecular symmetry resulting from the absence of a central metal ion.[68]

3.2.2. Drop-casting immobilization of tetra-4-PEG-400-substituted copper phthalocyanine on C-SPE

With the aim of developing a sustainable electrochemical sensor, the functional water-soluble metallophthalocyanines thus obtained were subsequently deposited onto the carbon working electrode surface, to achieve a new water-soluble metallophthalocyanine-based electrochemical sensor.

Various deposition techniques are available to immobilize material onto the electrode surfaces, thus modifying the sensor and offering distinct advantages depending on the intended application.

Drop-casting is the simplest, cost-effective, and environmentally benign method. The minimal energy requirements of drop-casting combined with the intrinsic water solubility of the functionalized phthalocyanines, that enabled their direct processing in aqueous media, further reinforced the overall sustainability of the sensor fabrication.

The selection of phthalocyanines as functional molecules for electrode modification was mainly motivated by their well-known properties. In addition, considering the carbon-based nature of the working electrode, it can be hypothesized that the extended π-electron system of phthalocyanines may promote π–π interactions with the sp^2-hybridized carbon surface, potentially facilitating stable immobilization on the interface. Furthermore, metallophthalocyanine complexes have been chosen as suitable electrocatalysts thanks to their ability to change their oxidation states while preserving their stability during the electrocatalytic process.[69]

The working solution of phthalocyanine was prepared by dissolving the synthesized water-soluble 4-PEG-CuPc in MilliQ water (2 μg/μL). This solution was deposited onto the working electrode surface by drop-casting, applying 15 portions of 2 μL each, for a total of 30 μL, corresponding to 60 μg of deposited molecular layer. After each 2 μL deposition, the layer was allowed to dry for one minute under irradiation from an IR lamp.

3.2.3. Electrochemical detection of catechol with the new phthalocyanine-based sensor (SPE@PEGCuPc)

Electrochemical interactions between the modified SPE surface and the target analyte (catechol) were examined with cyclic voltammetry (CV) to evaluate the changes in electron transfer at the surface of the modified electrode, considering that the mechanism for catechol detection is a two-electron process based on the electrocatalysis of catechol oxidation to its corresponding 1,2-benzoquinone (**Scheme 2**).

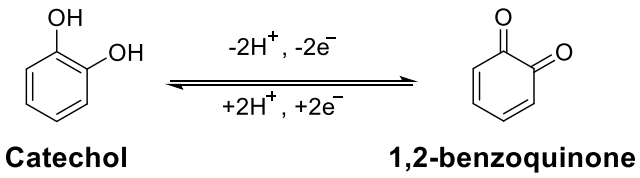

Scheme 2. The electrochemical oxidation of catechol.

The measurements were performed placing 100 μL droplet of 50 mM PBS buffer solution at pH 7 on the electrode surface. Then, 5 μL of catechol solution 1 mM were added to the 100 μL droplet of the buffer solution, resulting in a 50 μM final concentration of catechol in the droplet. All measurements were repeated three times, and therefore the values reported represent the mean ± standard deviation of three independent measurements.

Figure 7, that shows only one of these three measurements and is provided solely as a visual example, presents the cyclic voltammograms recorded for four different systems: the bare SPE with only buffer solution (black curve), the bare SPE in the presence of catechol 50 μM in buffer solution (orange curve), the SPE modified with 4-PEGCuPc with only buffer (blue curve), and the modified SPE in the presence of 5 μL of catechol 1 mM in buffer (pink curve). This comparative representation allows a direct evaluation of the electrochemical behavior of the two electrodes, both in their intrinsic state and upon interaction with the target analyte.

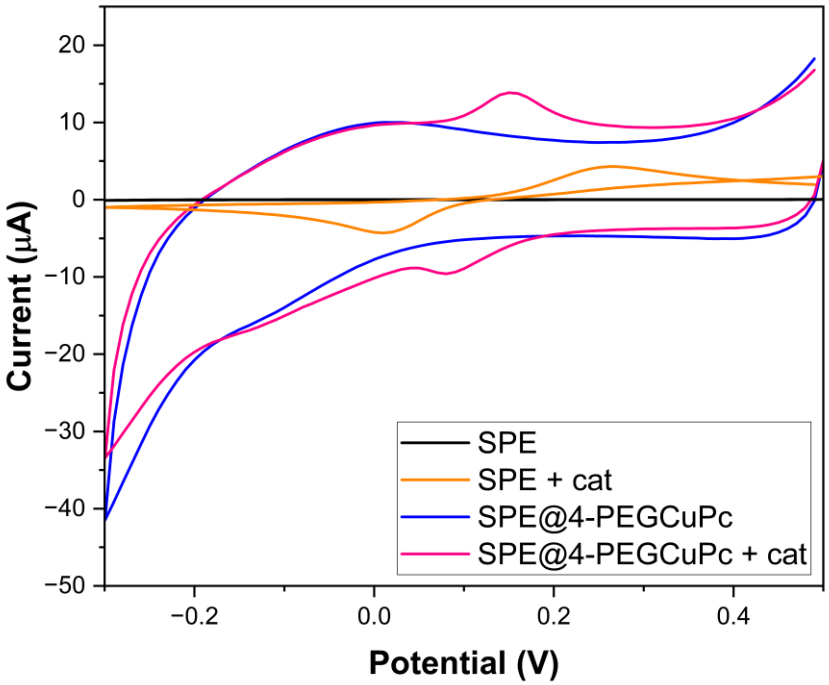

Figure 7. CV recorded for the bare SPE (black curve), the bare SPE in the presence of catechol (orange curve), the SPE modified with 4-PEGCuPc (blue curve), and the modified SPE in the presence of catechol (pink curve).

As expected, the bare SPE exhibits its characteristic background response, while the addition of catechol leads to the appearance of oxidation and reduction peaks associated

with its redox activity, based on established investigations already reported.[69,72] Similarly, the modified SPE displays a distinct voltammetric profile attributable to the presence of the 4-PEGCuPc layer. Upon exposure to catechol, the modified electrode also generates a clear electrochemical response, confirming its ability to recognize and detect the analyte.

Although both the bare and the modified SPE can detect catechol, substantial differences can be observed in their electrochemical responses. The most evident improvement observed with the 4-PEGCuPc-modified electrode is the shift of the catechol oxidation peak toward lower potentials, from 0.27 V for the bare SPE to 0.15 V for the modified electrode. This decrease in oxidation potential suggests a facilitated electron-transfer process, highlighting the electrocatalytic role of the functional layer deposited on the electrode surface. In practical terms, the modified interface reduces the energy required for catechol oxidation, thereby enhancing the overall efficiency of the sensing process.

In addition to this favorable shift in potential, an increase in peak current is observed, rising from 2.04 ± 0.02 μA at the bare SPE to 3.12 ± 0.05 μA at the modified electrode. This enhancement in current response reflects an improved sensitivity of the system, likely due to stronger interfacial interactions and more efficient charge transfer promoted by the 4-PEGCuPc layer. The combined effect of lower oxidation potential and higher peak current ultimately translates into superior analytical performance, enabling the detection of lower concentrations of catechol in solution.

Overall, the modification of the SPE with 4-PEGCuPc not only improves the electrochemical response toward the target pollutant but also enhances the global performance of the sensor, confirming the contribution of the functional material to the analytical characteristics of the sensor and so the effectiveness of the surface engineering strategy adopted in this work.

The study revealed that the modified electrode with water-soluble 4-PEGCuPc was a successful electrocatalyst for catechol oxidation, providing an efficient detection of the pollutants in aqueous environment.

To build the calibration plot, chronoamperometry analyses were performed, applying a potential equal to 0.2 V and an interval time of 0.1 s. This potential value was chosen to ensure the complete oxidation of catechol. The oxidation of catechol to benzoquinone was specifically monitored, providing a direct assessment of the sensor's response (**Figure 8**). The sensor response is expressed as the difference between the analyte and the background current signals.

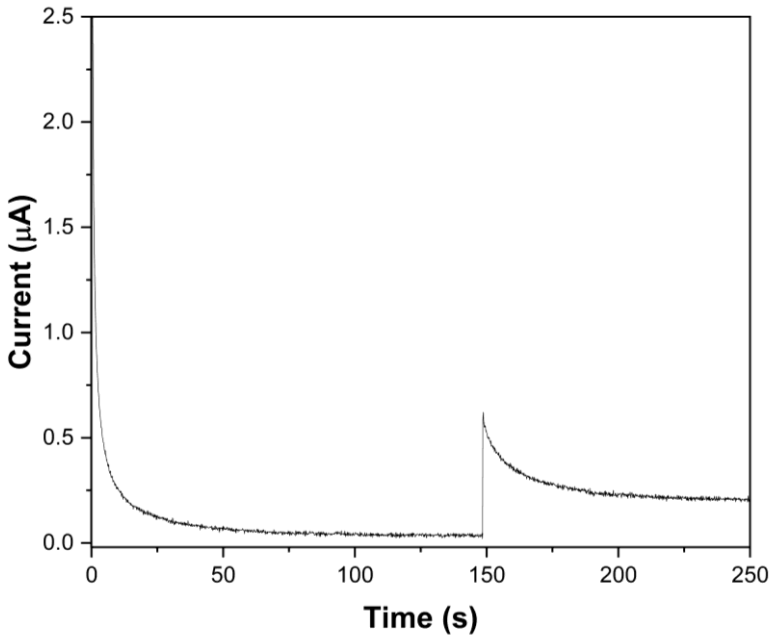

Figure 8. Example of chronoamperometric measurement for 100 μL of catechol solution 20 μM in 50 mM PBS buffer at pH 7.

The current response as a function of catechol concentration follows the trend described by the following equation.:

$$\Delta\mu A = a + b * C, \text{ with } \Delta\mu A = I_p - I_b$$

where I_p is the plateau current (μA), I_b is the base-line current (μA), a is the intercept, b is the slope, and C is the concentration of catechol (**Figure 9**).

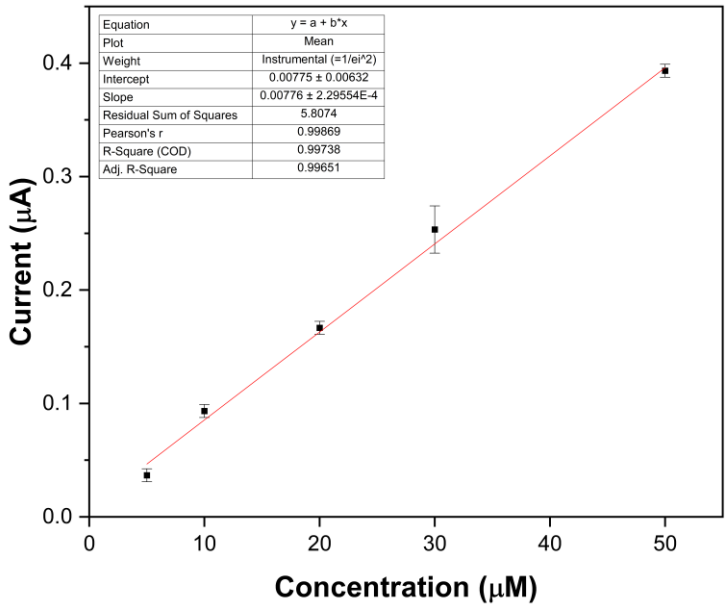

Figure 9. Calibration plot for different catechol concentrations (5, 10, 20, 30, 50 μM). Number of repetitions is n = 3. Measurement volume: 100 μL, 50 mM PBS buffer at pH 7.

The calibration curve is given by $\Delta\mu A = 0.00775 + 0.00776 * C$, with an $R^2 = 0.997$. The limit of detection (LOD) for the newly developed electrochemical sensor is 2.45 μM, and was statistically calculated as follows:

$$k * \frac{\sigma}{b}$$

where k is a statistical constant equal to 3.3, and σ is the standard deviation of chronoamperometric signals for three different measurements at the same concentration, and b is the sensitivity of the method (determined as the slope of the previously described calibration curve).[73,74]

To evaluate the reusability of the newly developed electrochemical sensor, a series of washing procedures was performed on the same electrode surface using distilled water. Following each washing step, CV measurements were carried out under identical

experimental conditions to those previously applied, exposing the washed sensor to the same concentration of catechol of 50 μM.

The results obtained are highly promising. As shown in **Figure 10** (left panel), the oxidation peak current in subsequent CV measurements recorded after every ten washing cycles remains essentially unchanged, even up to 100 washing steps, a limit arbitrarily established for practical reasons. This finding clearly demonstrates that the sensor can be effectively reused after its initial application, maintaining consistent analytical performance in catechol detection even after repeated measurements and washing procedures (up to 100 cycles), without any observable loss of efficiency.

From a sustainability perspective, this aspect is of particular significance. The ability to reuse the sensor multiple times reduces reliance on single-use operation, thereby minimizing material consumption and preventing the excessive generation of electronic waste. Consequently, the demonstrated reusability of the device represents a substantial contribution toward the development of more sustainable electrochemical sensing platforms.

Furthermore, as shown in **Figure 10** (right panel), the peak potential associated with catechol oxidation remains unchanged after every ten washing cycles. This observation is particularly significant, as it indicates that the interfacial properties of the modified electrode surface are preserved throughout repeated use. The stability of the oxidation peak potential suggests that no substantial alteration of the electroactive layer occurs during the washing procedures, and that the molecular recognition and electron-transfer processes remain unaffected.

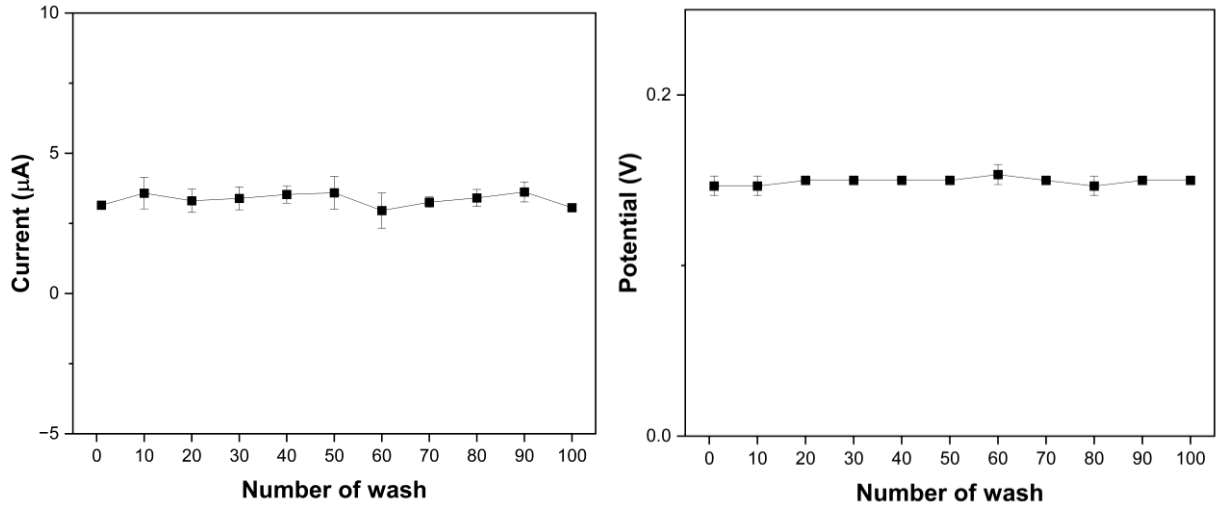

Figure 10. Plot peak current signal (left panel) and peak potential (right panel) of the CV measurements *versus* number of washes (up to 100) for the electrochemical sensor fabricated through modification of SPE with drop-casting of 4-PEGCuPc. Number of repetitions is $n = 3$. Measurement: 100 μL, 50 μM catechol concentration, 50 mM PBS buffer pH 7.

Such electrochemical stability confirms the robustness of the deposited functional layer and excludes possible degradation, or restructuring of the sensing interface. From an analytical standpoint, the constancy of the peak potential ensures reproducibility and reliability of the measurements, which are essential parameters for practical sensing applications. Moreover, from a sustainability perspective, the preservation of both peak current and peak potential further supports the feasibility of reusing the sensor without compromising performance, reinforcing its suitability as a durable and environmentally responsible analytical device.

The main advantage of the proposed system is the remarkably simple eco-friendly fabrication procedure, consisting of the straightforward drop-casting of a fully aqueous phthalocyanine solution onto the electrode surface with the possibility of recycling.

This approach is highly accessible and easily reproducible, as it does not require specialized instrumentation, toxic organic solvents, nor additional matrixes. In contrast,

examples reported in the literature, and summarized in **Table 1**, rely on the use of hazardous solvents, for example DMF (entry 2), incorporation of additional materials to assist deposition and enhance performance such as polymers (e. g. chitosan, CHI, or poly 2,3-dihydrothieno-1,4-dioxin-polystyrenesulfonate, PEDOT:PSS) (entry 3 and 4), nanoparticles (e. g. gold nanoparticles, AuNPs, carbon nanotubes paste, CNTP, or graphene oxide, GO) (entry 4), ionic liquids (IL^+) (entry 2), or even surfactants (e. g. stearic acid) (entry 6). Hybrid configurations in which efficiency in catechol detection arises from the synergistic contribution of enzymatic components (e. g. laccase, Lac, or tyrosinase, Tyr) (entry 3,4,6) that are co-immobilized with the phthalocyanine complexes are also employed.[75,76] Other devices fabrication are reported to employ a more complex immobilization strategy composed by multiple techniques, such as dipping and Langmuir-Blodgett (LB), as well as complex molecular materials, such as triple-decker architectures (e. g. $Eu_2Pc(Pc(OPh)_8)_2$) (entry 6).

Entry	Bio/Sensor	Immobilization technique	Solvents used	R^2	LOD (μM)	Ref.
1	**4-PEGCuPc**	**Drop-casting**	**H_2O**	**0.997**	**2.45**	**This work**
2	4(4-(3-formylphenoxy)) CuPc	Drop-casting	DMF	0.988	0.48	[69]
3	[CHI/IL^+ / sulphonatedCuPc]$_2$ /Lac	Multiple immersion steps	PBS buffer	0.981	$9.98 \cdot 10^{-3}$	[75]
4	[CHI/ sulphonatedCuPc /CHI/AuNPs]/ Lac	Multiple immersion steps	H_2O and acetic acid aqueous solution	0.991	$5.89 \cdot 10^{-2}$	[76]
5	PEDOT:PSS/ CuPc	Spin-coating	H_2O	0.992	2.99	[77]
6	Tyr/stearic acid/Eu_2Pc	Immersion-LB	$CHCl_3$ and H_2O	0.997	$6.3 \cdot 10^{-2}$	[78]

	$[Pc(OPh)_8]_2$					
7	Tyr/CoPc-CNTP	Drop-casting, immersion	H_2O and PBS buffer	0.985	1.66	[79]
8	Me_4(N,N-diethylaminoethoxy)CoPc/GO	Multiple immersion steps	H_2O	0.986	0.53	[80]

Table 1. Parameters of different (bio)chemical sensors reported in the literature compared to those of the chemical sensor developed in this study.

Another main advantage of the sensing platform developed in this work is the remarkable operational stability upon repeated washing cycles of the electrode surface. The stability of the sensor was evaluated by performing one scan every ten washing cycles, up to 100 washes. The results show that the peak potential remains unchanged even after 100 washing cycles, while the current decreases by only 2%.

Although further investigations are ongoing to fully elucidate the molecular-level mechanism, the enhanced electrochemical response observed for the phthalocyanine-modified SPE toward catechol can reasonably be attributed to a synergistic combination of interfacial and electrocatalytic effects.

First, the planar and highly π-conjugated structure of the metallophthalocyanine is expected to promote π-π stacking interactions with the aromatic ring of catechol. Moreover, the presence of the central copper(II) ion likely plays a crucial electrocatalytic role. The redox-active metal center could mediate the oxidation of catechol to 1,2-benzoquinone, and enhancing the peak current.

In addition, the immobilized phthalocyanine layer may improve the interfacial electron-transfer kinetics by providing a conductive and chemically compatible pathway between the analyte and the carbon electrode surface. The extended π-system of the macrocycle,

combined with its affinity for the sp^2 carbon framework of the electrode, likely facilitates efficient electronic communication as well as anchoring to the surface.

Overall, the sensing mechanism is therefore proposed to arise from the synergistic interplay of π-π interactions, metal-centered electrocatalysis, improved charge-transfer kinetics, and anti-fouling effects at the modified electrode interface.

3.2.4. Preliminary study of electrospray deposition (ESD) for an alternative green immobilization of tetra-4-PEG-400-substituted phthalocyanines on C-SPE

To explore another kind of green deposition method for the immobilization of water-soluble metallophthalocyanines onto the electrode surface, the Electrospray Deposition (ESD) technique was investigated.

The ESD technique has attracted considerable attention due to its capability to produce sprays of charged nanoaggregates, (bio)macromolecules, proteins, natural and synthetic polymers that can in this way be gently deposited onto surfaces at very low kinetic energies (soft landing). Indeed, due to their substantial size and mass, these materials cannot be thermally evaporated. Consequently, their deposition is typically achieved via drop-casting.[81] ESD represents a valuable alternative, beyond drop casting, to facilitating the incorporation of sizable molecular architectures into electronic devices and circuits, thus allowing their deposition from liquid to any conductive support. [82–84]

Both home-made and commercially available ESD systems have been developed, encompassing a wide range of configurations and levels of technical complexity. In general, the technology employs a low-concentration solution of the target molecule delivered through a capillary held at high voltage relative to a grounded counter electrode. The applied electric field overcomes surface tension at the emitter tip, generating a "Taylor cone" and producing a spray of charged droplets. As the solvent evaporates, the total electric charge within the droplets is no longer balanced by surface tension, so they

progressively fragment through Coulombic explosions into smaller droplets until complete solvent evaporation occurs and gaseous molecular ions are ultimately generated and deposited onto the surface.[85]

In this way, this technique enables, at ambient or controlled atmospheres, the formation of thin films composed of finely dispersed particles, significantly reducing cost and processing time compared to vacuum-based techniques. Moreover, ESD is easily automated and requires only minimal amounts of material, allowing safe and compact implementation.[86]

In particular, such soft-landing approach, carried out under mild conditions (room temperature and atmospheric pressure), has been previously employed to successfully immobilize biological components on sensor surfaces in a sustainable and cost-effective manner, and has therefore proven to be an efficient green alternative to other common immobilization methods.[87] Indeed, the ESD led to the development of enzyme-based biosensors, enabling the immobilization of laccase onto the electrode surface, while preserving its catalytic activity and at the same time ensuring the reliable detection of catechol in real aqueous samples, without the use of additional matrixes.[88]

On the basis of the encouraging results in terms of performance in catechol detection and long-term stability of the obtained biosensors, the ESD technique has been investigated for the fabrication of water-soluble metallophthalocyanines-based electrochemical sensors for catechol detection.

With the goal of reducing costs and overall remaining attentive to sustainability principles, this new sensing platform is designed to achieve comparable catalytic activity and selectivity to enzymatic systems, while being entirely free of biological components. By removing the biological element, such chemical sensor could thus overcome limitations related to enzyme fragility and operational constraints, while preserving the key advantages demonstrated by the earlier biosensors, offering high selectivity and reliability in catechol detection. This strategy illustrates how insights from biocatalytic systems can inspire the

design of chemical sensors that maintain high performance while addressing practical and economic considerations.

Water-based solution of 4-PEGCuPc was prepared and sprayed using a customized ESD setup that is described hereafter and depicted in **Figure 11**.

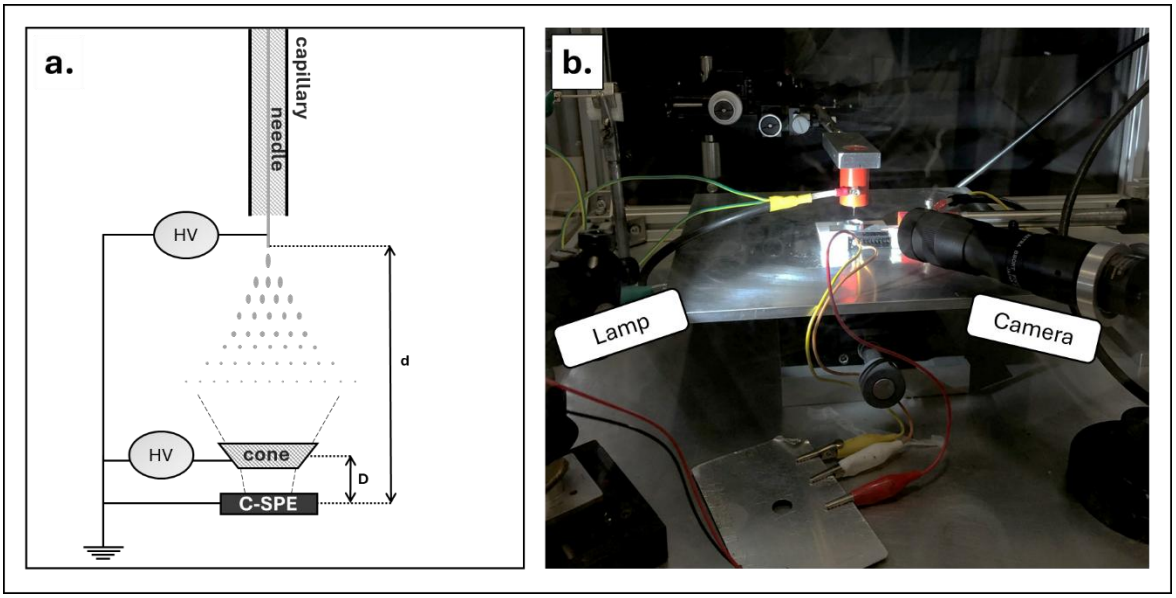

Figure 11. (a) Scheme of the ESD setup with the relevant parameters: the needle and the cone voltages (HV), the distances between the needle and the electrode (d), and between the cone and the electrode (D); (b) Photographic image of the real setup including also the lamp and the camera used during the deposition experiments.

The entire setup is inside a protected environment (deposition chamber) at ambient pressure and temperature to avoid jet fluctuations. The stability of the jet, illuminated by a lamp, was monitored in real time during the entire deposition by means of a digital camera. The relative position of both the lamp and the camera was adjested in order to achieve the best contrast of the image of the cone.

The setup comprises a Pump 11 Elite infusion system (Harvard Apparatus) coupled to a 250 µL Hamilton syringe, which is linked to a silica capillary with a 300 µm internal

diameter. The pump drives the solution from the syringe through the capillary for spraying. At the end of the capillary a steel needle (100 μm inner diameter) is polarized at 3.90 kV. Between the needle and the electrode, a focusing conical shape electrode (cone) has been added, set at 1.70 kV, to improve the control of the deposition area in the process, and has an upper diameter of 12 mm and a lower diameter of 6 mm.[89] The distance between the electrode and the needle (d) is 15 mm while the distance between the cone and the electrode (D) is 4 mm. The alignment between the spray needle, the focusing cone electrode, and the electrode is a crucial parameter for spray deposition, as well as the composition of the sprayed solution.[90]

To improve the efficiency of the deposition process, with the aim of achieving spray definition and ensuring that the characteristic shape of the Taylor cone is visible and stable within the entire deposition time, an optimization study was carried out by screening different solvent mixtures for the solution of the synthesized water-soluble phthalocyanine (4-PEGCuPc). A water/alcohol mixture was used because, at the applied potentials, it is required to promote droplet explosion during deposition, enabling the formation of a dry deposit.[91]

All the depositions have been carried out using a solution of 4-PEGCuPc (2 μg/μL) and setting a deposition time of 30 minutes with a pump flow rate of 1 μL/min, at room temperature and exposed to atmospheric pressure. The results are summarized in **Table 2**.

Entry	Solvent mixture (v/v)	Spray definition	Coating centered
1	H_2O / EtOH (9:1)	Poor	-
2	H_2O / EtOH (8:2)	Poor	-
3	H_2O / EtOH (6:4)	Poor	-
4	H_2O / EtOH (2:8)	Good	-
5	**H_2O / *i*-PrOH (2:8)**	**Excellent**	**Highly centered**

Table 2. Optimization study of deposition parameters: solvent mixture, quality of the spray and of the centered coating.

For water/ethanol mixtures (Entries 1-3), the spray is unstable and poorly defined, producing irregular droplets that are reflected in the low quality of the resulting film. A slight adjustment to the ethanol content (Entry 4) improves the spray definition. Notably, switching to a water/isopropanol mixture (Entry 5) produces excellent spray behavior which results in good focusing (**Figure 12a**), leading to deposition centered on the working electrode (**Figure 12 b,c**).

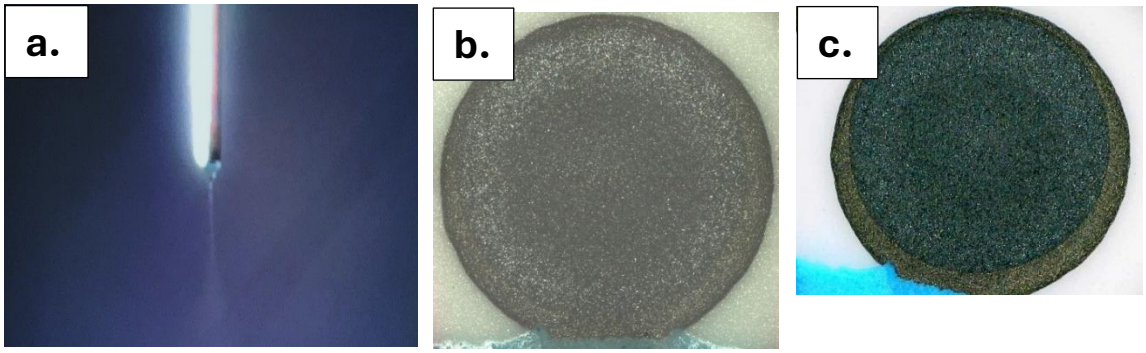

Figure 12. (a) Photographic image of the Taylor cone generated during ESD deposition of the 4-PEGCuPc solution; (b) Optical microscope image and (c) microscope image of the ESD-deposited 4-PEGCuPc on the surface electrode.

Overall, these results highlight the critical role of solvent choice in achieving controlled ESD.

3.2.5. Electrochemical detection of catechol with the phthalocyanine-based sensor fabricated through ESD (SPE@PEGCuPc)

After obtaining the optimized deposition conditions, the working solution was prepared by dissolving 4-PEGCuPc in a mixture 20% of water in isopropanol (2 μg/μL) and the ESD process was thus performed by spraying this solution at a flow rate of 1 μL/min for 30 minutes. All the deposition tests were performed using a fresh solution.

From an electrochemical perspective, the oxidation peak potential of catechol recorded at the ESD-fabricated sensor, light pink curve, (0.15 ± 0.02 V) was lower than the peak potential of the bare, non-modified electrode, orange curve, in the presence of catechol (0.27 ± 0.01 V) indicating that the fundamental redox mechanism and thermodynamic aspects of the oxidation process remain unchanged regardless of the immobilization strategy (**Figure 13**).

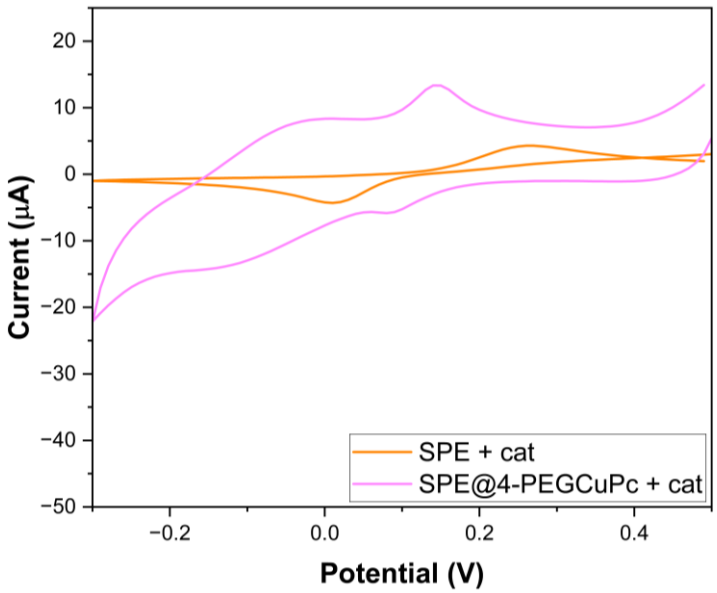

Figure 13. CV recorded for the bare SPE in the presence of catechol (orange curve) and the SPE modified with 4-PEGCuPc through ESD (light pink) in the presence of catechol.

Furthermore, in terms of current intensity, the ESD-modified sensor exhibited increase in peak current (3.8 ± 0.5 μA) compared to that of the bare SPE in the presence of catechol (2.04 ± 0.02 μA), suggesting enhanced interfacial electron-transfer efficiency due to the phthalocyanine layer.

Reusability tests performed to this sensor revealed that its performance progressively decreased upon repeated washing cycles (**Figure 14**, left panel).

A similar behavior was observed in terms of peak potential. As shown in **Figure 14**, right panel, the oxidation potential of catechol at the ESD-modified electrode exhibited more pronounced fluctuations and progressively shifted toward more positive values with increasing washing cycles.

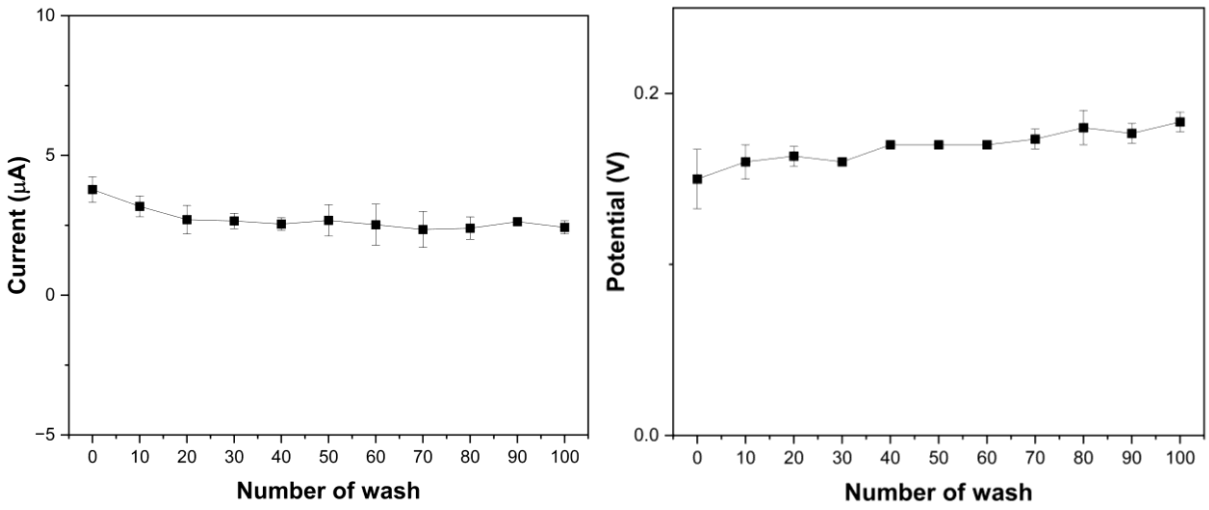

Figure 14. Plot current signal (left panel) and peak potential (right panel) *versus* number of washes (up to 100) for the electrochemical sensor fabricated via modification of SPE with 4-PEGCuPc through ESD. Number of repetitions is n = 3. Measurement volume: 100 μL, 50 μM catechol concentration, 50 mM PBS buffer pH 7.

A direct comparison between the DC- and ESD-modified electrodes with 4-PEGCuPc was not possible, as during the electrospray deposition process, part of the sprayed solution

accumulated on the surface of the focusing cone rather than reaching the electrode surface. Therefore, the effective amount of phthalocyanine deposited on the electrode could not be accurately determined. This prevented a reliable quantitative comparison with the drop-casting sensor at the same molecular loading. For this reason, the ESD experiments were considered only for qualitative evaluation of the sensing behavior.

3.2.6. Exploration of different tetra-4-PEG-400-substituted phthalocyanines deposited through ESD on C-SPE

To further investigate in a qualitative way the influence of the metal center on the electrocatalytic behavior, additional sensors were fabricated using two other phthalocyanines structurally identical to the previously used 4-PEGCuPc, differing only in the central metal atom. One of these contains cobalt as the metal center (4-PEGCoPc), while the other is metal-free (4-PEG2HPc).

The objectives of this study were twofold: first, to determine whether the cobalt derivative could achieve similar electrochemical performance to the drop-cast sensor prepared with 4-PEGCuPc; and second, to evaluate whether the metal-free derivative exhibits any intrinsic electrocatalytic activity, despite the absence of a central metal atom.

The two phthalocyanines were also successfully processed in the isopropanol/water (8:2 v/v) solvent mixture and deposited by electrospray under the same conditions and solution concentration used for the corresponding copper phthalocyanine derivative.

The CV measurements were performed as previously described, repeating the analyses three times and reporting the obtained values as the mean ± standard deviation of three independent measurements. **Figure 15** shows the CV measurements of the bare SPE and ESD-modified SPE with tetra-4-PEG-400-substituted metal and metal-free phthalocyanines, before the addition of catechol.

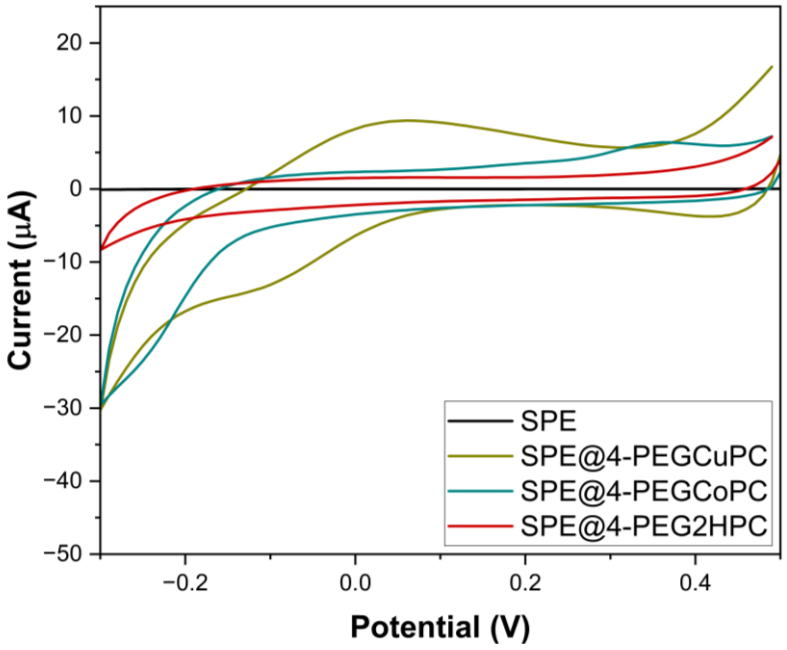

Figure 15. CV recorded for the bare SPE (black curve), the SPE modified through ESD with 4-PEGCuPc (green curve), 4-PEGCoPc (cyan curve), and 4-PEG2HPc (red curve). Measurement: 100 μL of 50 mM PBS buffer pH 7.

Interestingly, the trend observed in catechol detection revealed distinct performances among the different phthalocyanines, as can be easily visible in **Figure 16** and can be summarized as follows.

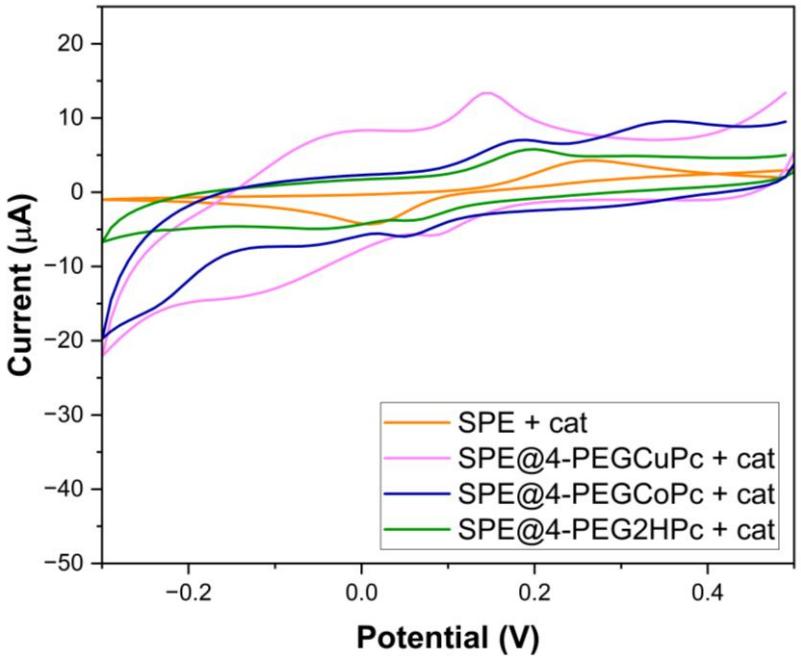

Figure 16. CV recorded for the bare SPE in the presence of catechol (orange curve), the SPE modified through ESD with 4-PEGCuPc (light pink curve), 4-PEGCoPc (blue curve), and 4-PEG2HPc (green curve) in the presence of catechol.

Regarding the electrochemical response to catechol in terms of current, 4-PEGCuPc exhibited the highest response, reaching 3.8 ± 0.5 μA, whereas the corresponding cobalt phthalocyanine (4-PEGCoPc) showed a lower value of 1.53 ± 0.07 μA. An interesting observation came from the investigation on the sensor fabricated by depositing through ESD the 4-PEG2HPc. Despite lacking a metal center in its macrocycle, it still exhibited a measurable response to catechol, albeit smaller, with a current of 1.9 ± 0.4 μA and a decrease in the potential of the oxidation peak (0.20 ± 0.01 V) with respect to the bare SPE (0.27 ± 0.01 V), suggesting that the extended π-conjugated macrocycle itself could contribute to electron transfer. Therefore, the catalytic effect cannot be attributed solely to the central metal ion. The further improvement observed upon metal incorporation could support a synergistic mechanism in which both the macrocycle and the coordinated metal promote the oxidation of catechol, with the metal center acting as a catalytic enhancer rather than the sole active site.

3.3. Conclusions

Overall, these results suggest that high-performance electrochemical sensors can be designed and fabricated in accordance with green chemistry and sustainable engineering principles.

The adoption of a one-pot synthetic strategy minimized solvent use, purification steps, material input, and energy consumption, while the functional material was sustainably immobilized onto the electrode surface via the simplest coating method, drop-casting, from a 100% aqueous solution. The resulting device was successfully validated for environmental monitoring, enabling efficient and reliable detection of catechol.

Notably, the results demonstrated also the remarkable operational stability of the sensor upon repeated washing cycles. Both the oxidation peak current and peak potential associated with catechol detection remained essentially unchanged even after up to 100 washing cycles of the electrode surface, indicating that the interfacial properties of the modified electrode surface are preserved and that no significant alteration of the electroactive layer occurs during reuse. This high reusability represents an important advantage, contributing to the development of more sustainable electrochemical sensing platforms by reducing material consumption and electronic waste.

The environmental impact of both the synthetic route and the fabrication process was evaluated within a lifecycle perspective, integrating analytical performance with sustainability criteria. This comprehensive approach led to the development of a new eco-compatible sensor in which sustainability is embedded at every stage, from molecular synthesis and aqueous deposition to the final device, whose demonstrated reusability further reduces waste generation.

Further investigations could focus on the long-term storage stability of the system, with the goal of enabling storage at room temperature for several months without affecting its performance, while also pursuing cost-effective regeneration of the developed sensor. By

using low-cost ultrasound treatments and green solvent cleaning, optimized to restore performance without damaging the electrode, could enable its reuse across different applications and promoting circular, sustainable sensing technologies.

In addition, since DMF is currently used in the synthesis of the deposited material, future efforts could also be directed toward developing even greener synthetic strategies that avoid the use of this solvent.

Eventually, future work, especially computational investigations, could be diverted to elucidate the molecular-level mechanism underlying catechol detection, providing deeper insight into the interfacial processes governing analyte recognition and electrocatalysis and guiding further optimization of sensor performance, such as the improvement of the limit of detection.

3.4. Experimental section

3.4.1. Materials

All reagents and solvents were purchased from Merck Life Science, TCI Chemicals, and Carlo Erba Reagents and used without further purification. In particular, ethanol (99.8%), isopropanol (99.8%), and catechol (99%) were purchased from Sigma Aldrich (Merck Group) and used as provided by the company. N,N-Dimethylformamide (DMF) was used freshly distilled. All the reactions were performed in a two-necked round-bottom flask equipped with a reflux condenser and a magnetic stirrer. All the glassware used was kept at least 24 hours in an oven at 110 °C. Reactions were monitored by thin-layer chromatography (TLC) employing a polyester layer coated with 250 mm F254 silica gel. Chromatographic filtrations, when needed, were performed using silica gel 60A 35–70. Buffer and all the aqueous solutions were prepared using double-distilled water (Milli-Q system, Millipore). Catechol was used in 1 mM solution with PBS buffer at pH 7, that was obtained by diluting a solution of catechol 50 mM in milliQ water. Working stability studies of sensors were performed through Cyclic Voltammetry using a 50 μM final concentration of catechol and 50 mM PBS buffer at pH 7, in a total volume of 100 μL of test solution, that was placed on the surface electrode of the SPE. The screen-printed electrodes used for the tests were the Metrohm DropSens screen-printed carbon electrodes DRP-110 with carbon working and counter electrodes, and an Ag reference electrode. After a conditioning potential of 0.5 V applied for 5 s, a potential of 0.5 V vs Ag reference electrode was applied, and at -0.3 V the scan direction was reversed, and eventually at 0.5 V the scan direction was reversed another time. The scan rate was 0.05 V/s, with a step potential of 0.01 V. In the chronoamperometric measurements performed for the sensor calibration curve, the sensor response was expressed as the difference between the analyte and the background current signals. The measurements were conducted placing 100 μL of catechol solution at the desired concentration on the electrode surface. Catechol solutions were prepared by diluting a solution of catechol 1 mM in 50 mM PBS buffer solution at pH 7. The electrode

surface of the SPE, functionalized with 4-PEGCuPC via drop-casting, was conditioned with three washes using 100 μL of PBS buffer pH 7 before the chronoamperometric measurements.

3.4.2. Instrumentation

^{1}H NMR spectra were recorded on a Bruker AVANCE 600 NMR spectrometer operating at a proton frequency of 600.13 MHz; chemical shifts (δ) are given in ppm relative to TMS. UV-Vis spectra were recorded on a PerkinElmer Lambda 950 UV-Vis/NIR spectrophotometer. High-resolution mass spectrometry (HRRMS) was performed using a Q Exactive UHMR Hybrid Quadrupole-Orbitrap mass spectrometer (Thermo Fisher) in positive polarity. The samples were dissoved in LC-MS-grade MeOH (c = 50 μM) and directly introduced into the mass spectrometer using gold-coated capillary needles prepared in-house. The instrument parameters used for MS spectra collection were the following: capillary voltage of 1.5 kV, scan range of 350 to 2000 m/z, HCD collision voltage of 0 V, source fragmentation of 0 V, and in-source trapping of 0 V. The ion transfer optics were set as follows: injection flatapole of 5 V, inner-flatapole lens of 4 V, bent flatapole of 2 V, and transfer multipole of 0 V. The resolution of the instrument was 200,000 at m/z = 400, the nitrogen pressure in the HCD cell was maintained at approximately 2.1×10^{-10} mbar, and the source temperature was kept at 100 °C. Calibration of the instrument was performed using a 2 mg/mL solution of cesium iodide in water. Data were analyzed using the Xcalibur 3.0 (Thermo Scientific) software package. The image of the deposit on the C-SPE was acquired using the Malvern Panalytical Morphology G3ID and the Ninyoon 4K WiFi Microscope. The electrochemical experiments were carried out at room temperature by cyclic voltammetry (CV) conducted using a portable, handheld, PalmSens4 battery operated potentiostat/galvanostat (Palm Instrument, The Netherlands). It was connected to a computer via USB and Bluetooth and controlled by PSTrace software version 5.12 for Windows11.

3.4.3. Green Chemistry metrics calculation

As previously described, the general equation for the calculation of E-factor is:

$$E\text{-}factor = \frac{Mass\ of\ total\ waste\ (g)}{Mass\ of\ product\ (g)}$$

In all calculations, water is excluded from the waste count. An estimated 80% of the organic solvents used in the processes are recovered and reused, as described in the Experimental section at the end of Chapter 2.

3.4.4. General procedure for the synthesis of tetra-4-PEG-400-substituted metallophthalocyanines

The phthalocyanines were synthesized similarly as described previously.[92] Briefly, PEG-400 (1.02 eq, 0.588 g) and anhydrous potassium carbonate (3 eq) were stirred in 2 mL of DMF at room temperature for 20 minutes under a nitrogen atmosphere. Then, 4-nitrophthalonitrile (1 eq, 0.25 g) was added and the reaction mixture was stirred at 65 °C until complete disappearance of 4-nitrophthalonitrile was observed in the TLC monitoring. Copper acetate monohydrate or cobalt acetate tetrahydrate (0.27 eq), pretreated on hot plate for 5 minutes, and DBU (0.2 mL) were then added and the reaction mixture was stirred at 110 °C under a nitrogen atmosphere until completion of the reaction. After cooling to room temperature, the reaction mixture was extracted with dichloromethane/water, to remove unreacted PEG-400, and the organic phase was collected. The solvent was evaporated under reduced pressure (recovering the dichloromethane), and the dark green waxy crude was dried under vacuum and then purified as follows.

3.4.5. Synthesis, Green Chemistry metric calculation and characterization of tetra-4-PEG-400-substituted copper phthalocyanine

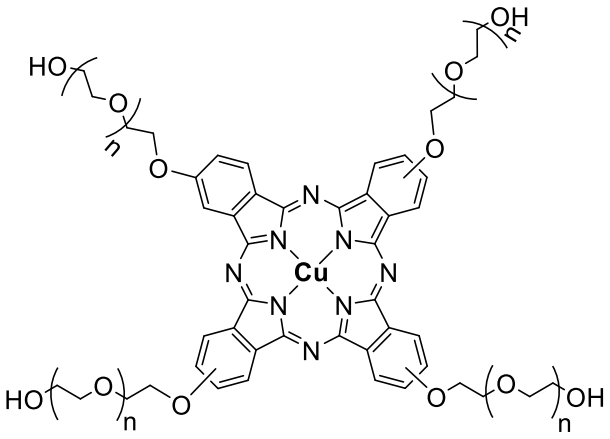

Purification of the crude by filtration on silica gel pad using isopropanol, water, acetone to remove impurities and eventually pyridine gave the target product in 62% yield as a green waxy solid. UV-vis: $\lambda_{Q\ band}$ (DMSO) = 682 nm. HRMS-ESI (polydisperse distribution) calcd for n=8.1 m/z = 2003.33, found m/z = 2004.87.

E-factor calculation

Chemical	**Volume (mL)**	**Density (g/mL)**	**Mass (g)**	**Mass actually considered in the E-factor calculation with 80% of solvent recovery (g)**
PEG-400			0.588	
DMF	2.0	0.95	1.9	
K_2CO_3			0.6	

4-nitrophthalonitrile			0.25	
Copper acetate monohydrate			0.078	
DBU	0.2	1.02	0.204	
Water	10.0	1.0	10	
DCM	24	1.33	31.92	6.384
Silica gel			10	
Isopropanol	30.0	0.786	23.58	4.716
Water	10.0	1.0	10	
Acetone	10.0	0.784	7.84	1.568
Pyridine	10.0	0.982	9.82	1.964

Amount of product = 0.485 g (62% yield)

E-factor = 178.0

E-factor (including 80% solvent recovery) = 57.3

UV-vis spectra of tetra-4-PEG-400-substituted copper phthalocyanine at a concentration of 1×10^{-5} M in DMSO and water

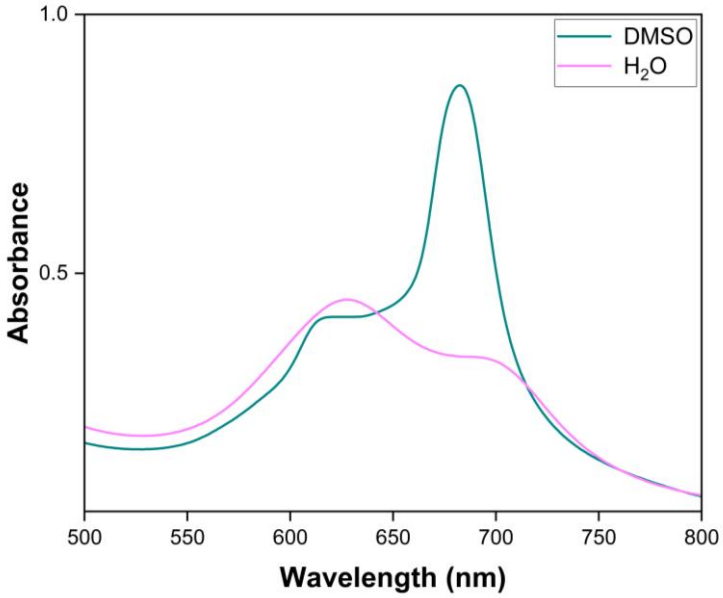

HRMS-ESI of tetra-4-PEG-400-substituted copper phthalocyanine

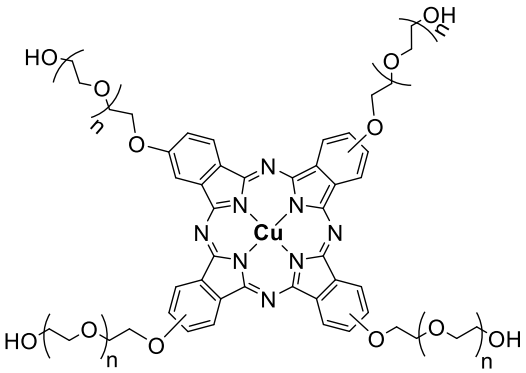

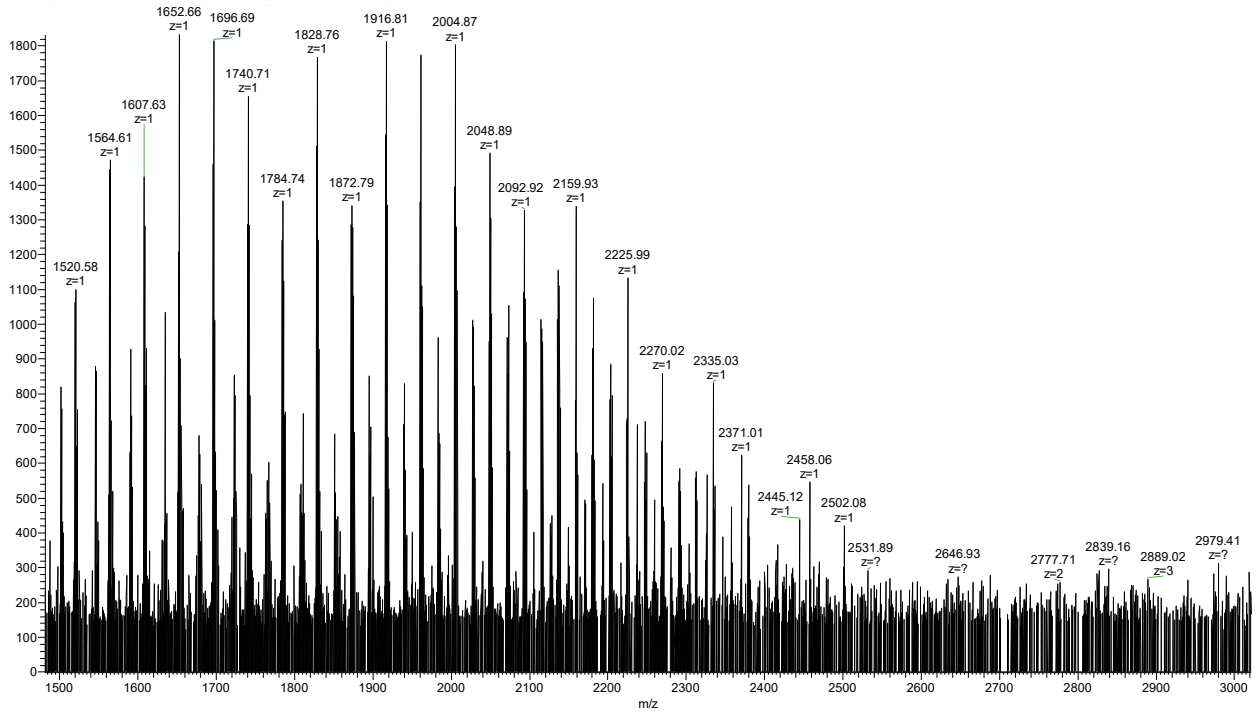

3.4.6. Synthesis, Green Chemistry metric calculation and characterization of tetra-4-PEG-400-substituted cobalt phthalocyanine

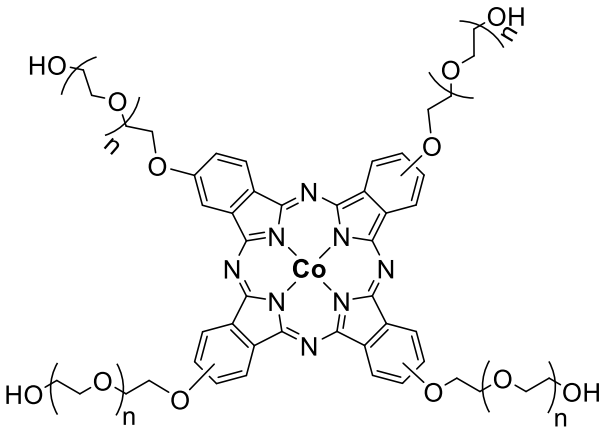

Purification of the crude by filtration on silica gel pad using a mixture of dichloromethane/ethanol (9:1) as eluent, gave the target product in 50% yield as a blue waxy solid. UV-vis: $\lambda_{Q\ band}$ (DMSO) = 679 nm. HRMS-ESI (polydisperse distribution) calcd for n=9.6 m/z = 2261.45, found m/z = 2258.97.

E-factor calculation

Chemical	**Volume (mL)**	**Density (g/mL)**	**Mass (g)**	**Mass actually considered in the E-factor calculation with 80% of solvent recovery (g)**
PEG-400			0.588	
DMF	2.0	0.95	1.9	
K_2CO_3			0.6	

4-nitrophthalonitrile			0.25	
Cobalt acetate tetrahydrate			0.097	
DBU	0.2	1.02	0.204	
Water	8.0	1.0	8.0	
DCM	54.0	1.33	71.82	14.364
Silica gel			7	
Ethanol	4.0	0.792	8.17	1.634

Amount of product = 0.389 g (50% yield)

E-factor = 232.0

E-factor (including 80% solvent recovery) = 67.5

UV-vis spectra of tetra-4-PEG-400-substituted cobalt phthalocyanine at a concentration of 1×10^{-5} M in DMSO and water

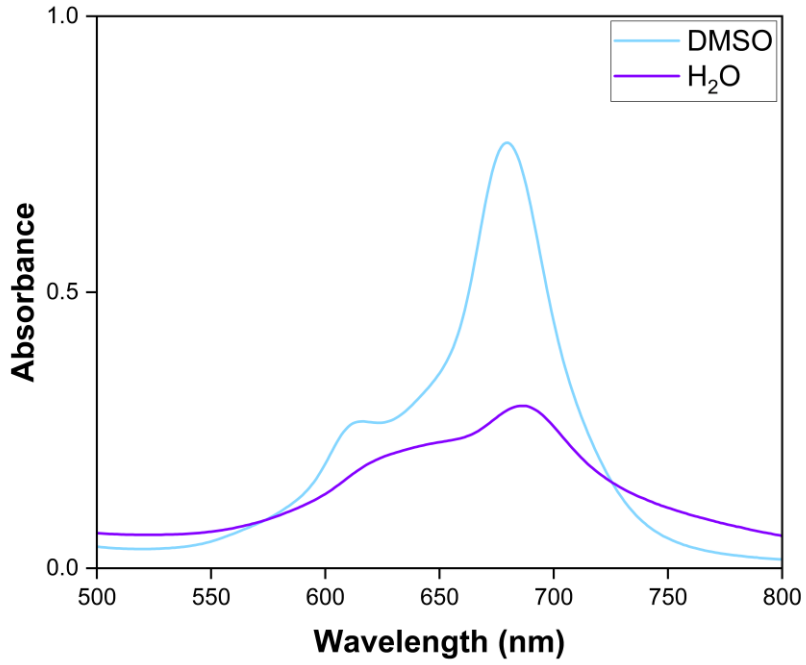

HRMS-ESI of tetra-4-PEG-400-substituted cobalt phthalocyanine

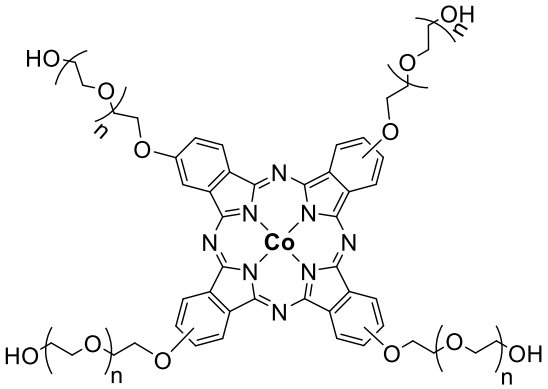

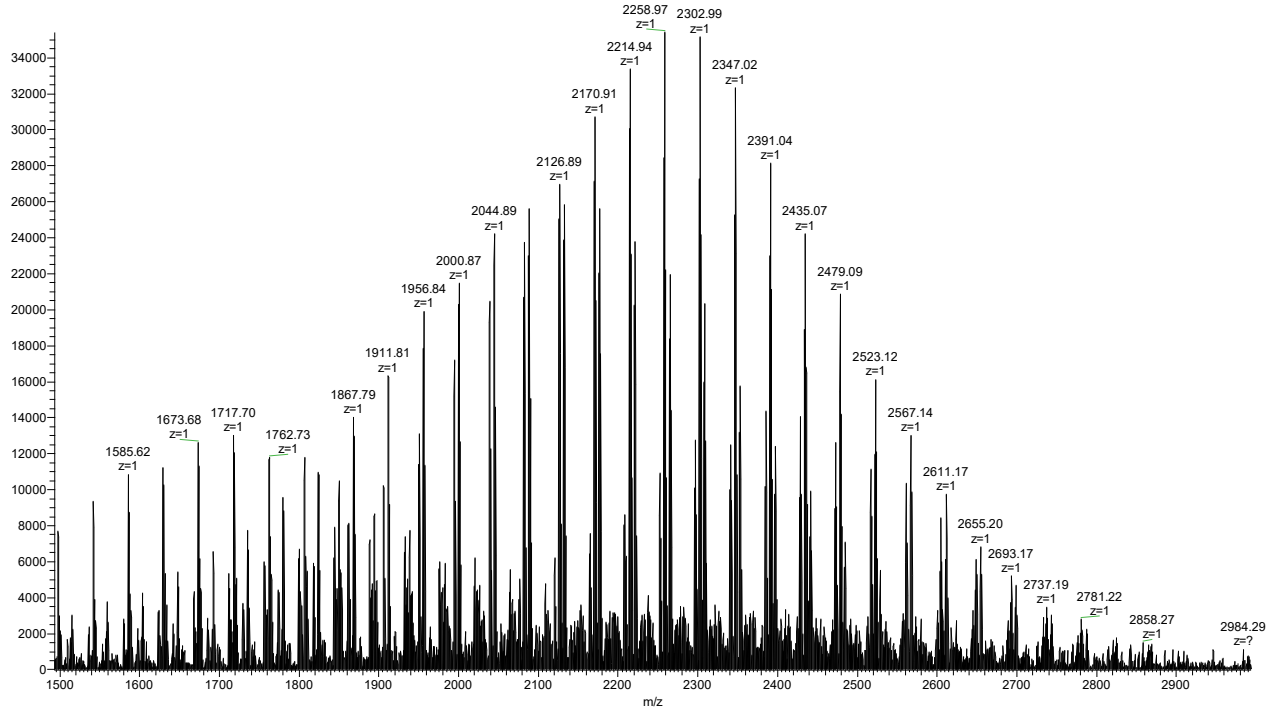

3.4.7. Synthesis, Green Chemistry metric calculation and characterization of tetra-4-PEG-400-substituted metal-free phthalocyanine

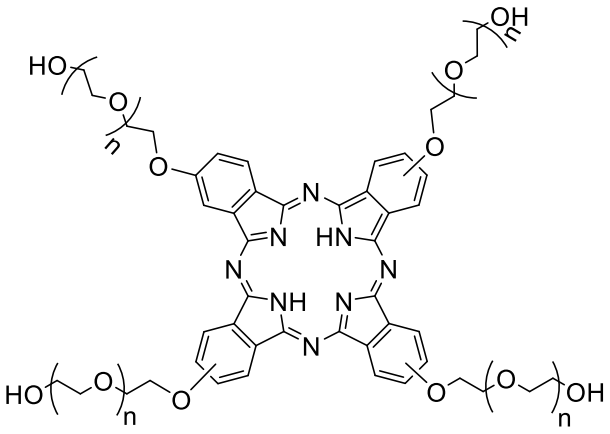

The synthesis was carried out according to the general procedure, with the main difference of the cyclization step. Therefore, after complete disappearance of 4-nitrophthalonitrile on TLC monitoring, DBU (0.2 mL) was added and the reaction mixture was stirred at 125 °C under a nitrogen atmosphere until completion of the reaction. After cooling to room temperature, the reaction mixture was extracted with dichloromethane/water and the organic phase was collected. The solvent was then evaporated under reduced pressure (recovering the dichloromethane) and the crude dried under vacuum. Purification of the crude by filtration on silica gel pad using isopropanol, water, acetone to remove impurities and eventually pyridine gave the target product in 40% yield as a green waxy solid. ^{1}H NMR (600 MHz, $CDCl_3$) δ 7.73 (dd, *J* = 13.9, 8.3 Hz, 4H, Ar-H), 7.35 – 7.30 (m, 4H, Ar-H), 7.22 (dd, *J* = 8.3, 2.3 Hz, 2H, Ar-H), 7.17 (dd, *J* = 8.3, 2.2 Hz, 2H, Ar-H), 4.27 – 4.20 (m, CH_2-PEG), 3.91 – 3.86 (m, CH_2-PEG), 3.73 – 3.71 (m, CH_2-PEG), 3.69 – 3.59 (m, CH_2-PEG) ppm. UV-vis: $\lambda_{Q\ band}$ (DMSO) = 708, 677 nm. HRMS-ESI (polydisperse distribution) calcd for n=8.7 m/z = 2046.07, found m/z = 2054.99.

E-factor calculation

Chemical	Volume (mL)	Density (g/mL)	Mass (g)	Mass actually considered in the E-factor calculation with 80% of solvent recovery (g)
PEG-400			0.588	
DMF	2.0	0.95	1.9	
K_2CO_3			0.6	
4-nitrophthalonitrile			0.25	
DBU	0.2	1.02	0.204	
Water	5.0	1.0	5	
DCM	18	1.33	23.94	4.788
Silica gel			10	
Isopropanol	30.0	0.786	23.58	4.716
Water	10.0	1.0	10	
Acetone	10.0	0.784	7.84	1.568
Pyridine	10.0	0.982	9.82	1.964

Amount of product = 0.301 g (40% yield)

E-factor = 260.5

E-factor (including 80% solvent recovery) = 87.3

^{1}H NMR of tetra-4-PEG-400-substituted metal-free phthalocyanine in $CDCl_3$

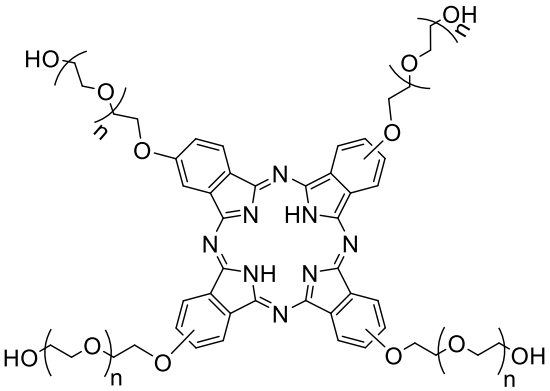

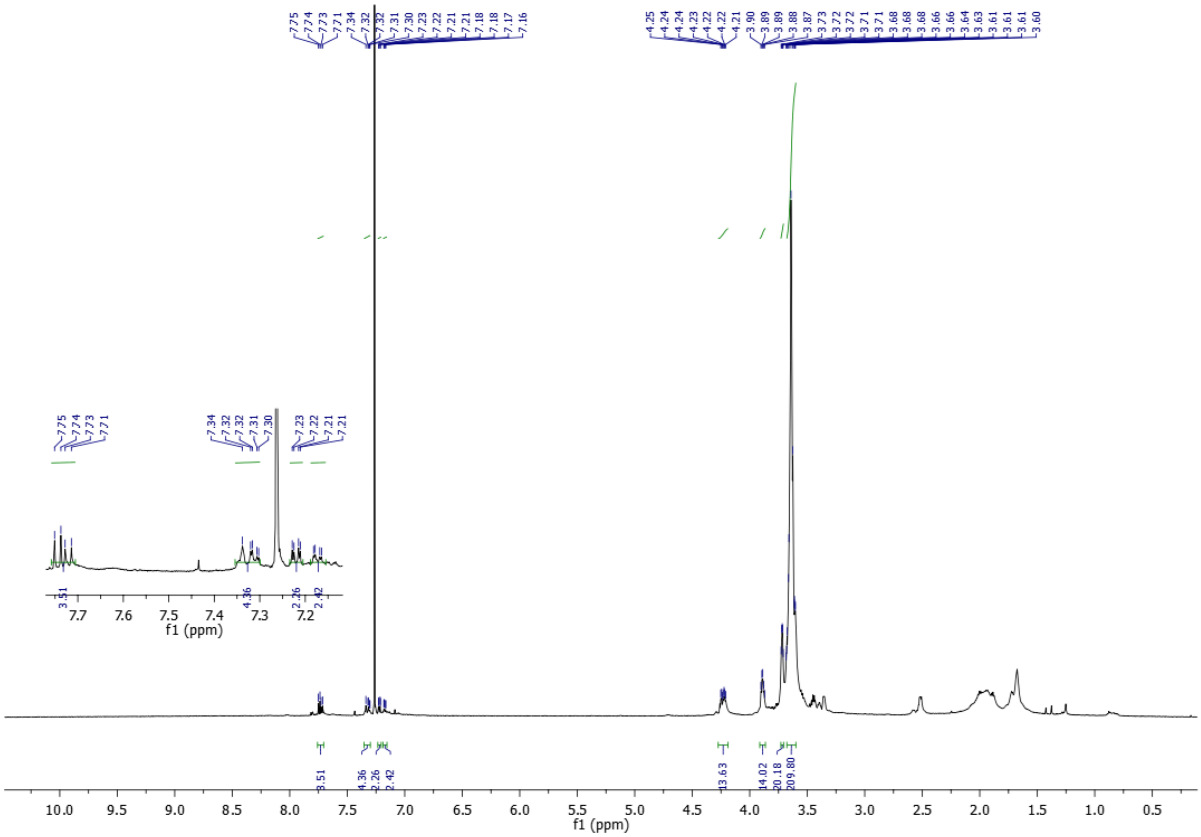

HRMS-ESI of tetra-4-PEG-400-substituted metal-free phthalocyanine

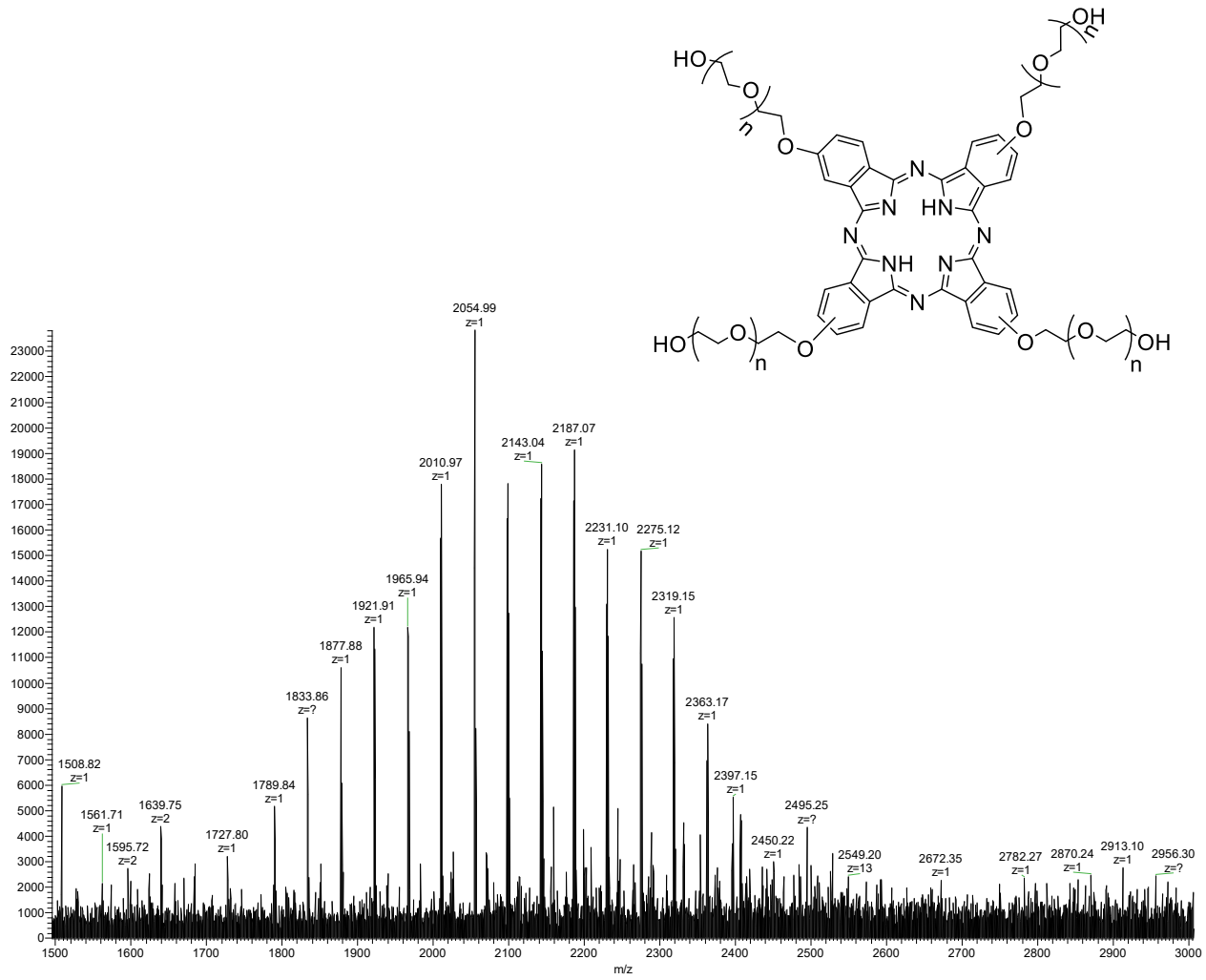

UV-vis spectra of tetra-4-PEG-400-substituted metal-free phthalocyanine at a concentration of 1×10^{-5} M in DMSO and water

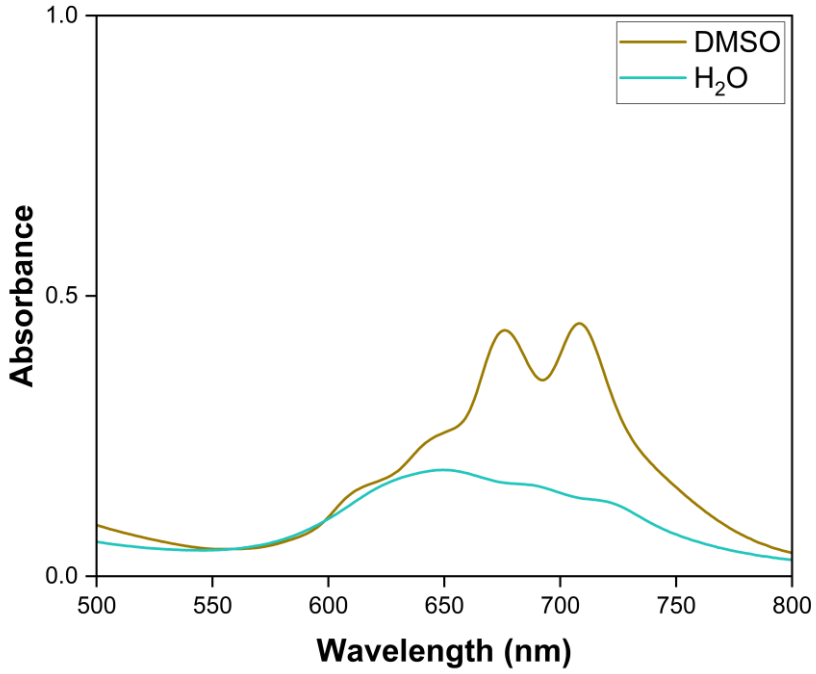

3.5. Bibliography

1. Anastas, P. T. & Warner, J. C. Green Chemistry: Theory and Practice. Oxford (1998).
2. Ahmad, Y., Kumar, R. & Kumar, A. Environmental waste management strategies and vermi transformation for sustainable development. *Environ. Challenges* **13**, 100747 (2023).
3. Javaid, M., Haleem, A., Rab, S., Pratap, R. & Suman, R. Sensors for daily life : A review. *Sensors Int.* **2**, 100121–100131 (2021).
4. Nagabooshanam, S. Emerging Sensors for Environmental Monitoring. Elsevier (2025).
5. Abdulhussain, S. H. *et al.* A Comprehensive Review of Sensor Technologies in IoT : Technical Aspects , Challenges , and Future Directions. *Computers* **14**, 342–396 (2025).
6. Lamkin-kennard, K. A. & Popovic, M. B. Chapter 4 in Sensors: Natural and Synthetic Sensors. Biomechatronics. Elsevier Inc. (2019).
7. Hanrahan, G., Patil, G., Wang, J. & Hanrahan, G. Electrochemical sensors for environmental monitoring : design , development and applications. *J. Environ. Monit.* **6**, 657–664 (2004).
8. Jalalvand, A. R. & Karami, M. M. Sensing and Bio-Sensing Research Roles of nanotechnology in electrochemical sensors for medical diagnostic purposes : A review. *Sens. Bio-Sensing Res.* **47**, 100733 (2025).
9. Baranwal, J., Barse, B., Gatto, G. & Broncova, G. Electrochemical Sensors and Their Applications : A Review *Chemosensors.* **10**, 363 (2022).
10. Diaconu, I. *et al.* Electrochemical immunosensors in breast and ovarian cancer. *Clin. Chim. Acta* **425**, 128–138 (2013).
11. Pusta, A., Tertiș, M., Cristea, C. & Mirel, S. Wearable sensors for the detection of biomarkers for wound infection. *Biosensors* **12**, 1–20 (2022).
12. Costa, J. N. Y. *et al.* Single-Response Duplexing of Electrochemical Label-Free Biosensor from the Same Tag. *Adv. Healthc. Mater.* **13**, 2303509–2302523 (2024).
13. Tang, Q., Li, Y., Liu, W., Li, B. & Jin, Y. One-step synthesis of biomimetic copper – cysteine nanoparticle with excellent laccase-like activity. *J. Mater. Sci.* **57**, 10072–10083 (2022).
14. Yang, J., Li, D., Fu, J., Huang, F. & Wei, Q. TiO_2 -CuCNFs based laccase biosensor for enhanced electrocatalysis in hydroquinone detection. *JEAC* **766**, 16–23 (2016).
15. Roy, J. J., Abraham, T. E., Abhijith, K. S., Kumar, P. V. S. & Thakur, M. S. Biosensor for the determination of phenols based on Cross-Linked Enzyme Crystals (CLEC) of

laccase. **21**, 206–211 (2005).

16. Chaniotakis, N. A. Enzyme stabilization strategies based on electrolytes and polyelectrolytes for biosensor applications. *Anal Bioanal Chem.* **378**, 89–95 (2004).

17. Bounegru, A. V., Iacob, A. D., Iticescu, C. & Georgescu, P. L. Electrochemical Sensors and Biosensors for the Detection of Pharmaceutical Contaminants in Natural Waters — A Comprehensive Review. *Chemosensors* **13**, 65–99 (2025).

18. Kalambate, P. K. *et al.* Electrochemical (bio) sensors go green. *Biosens. Bioelectron.* **163**, 112270–112286 (2020).

19. Zabitler, D., Ülker, E., Turan, K., Erdoğan, N. Ö. & Tığ, A. G. Electrochemical Sensor for Biological Samples Monitoring. *Top. Catal.* **69**, 95–125 (2026).

20. Hemdan, M. *et al.* Recent advances in nano-enhanced biosensors : Innovations in design , applications in healthcare , environmental monitoring , and food safety , and emerging research challenges. *Sens. Bio-Sensing Res.* **48**, 100783–100794 (2025).

21. Jalalvand, A. R. & Karami, M. M. Roles of nanotechnology in electrochemical sensors for medical diagnostic purposes : A review. *Sens. Bio-Sensing Res.* **47**, 100733–100758 (2025).

22. Machín, A. & Màrquez, F. Next-Generation Chemical Sensors : The Convergence of Nanomaterials , Advanced Characterization , and Real-World Applications. *Chemosensors* **13**, 345–389 (2025).

23. Pei, Y. *et al.* Electrochemical preparation of Pt nanoparticles modi fi ed nanoporous gold electrode with highly rough surface for e ffi cient determination of hydrazine. *Sensors Actuators B. Chem.* **304**, 127416–127424 (2020).

24. Saleh, H. M. & Hassan, A. I. Synthesis and Characterization of Nanomaterials for Application in Cost-Effective Electrochemical Devices. *Sustainability* **15**, 10891–10943 (2023).

25. Unterlass, M. M. Green Synthesis of Inorganic – Organic Hybrid Materials : State of the Art and Future Perspectives. *Eur. J. Inorg. Chem.* 1135–1156 (2016).

26. Giannakoudakis, D. A. *et al.* Carbon-Based Nanocatalysts (CnCs) for Biomass Valorization and Hazardous Organics Remediation. *Nanomaterials* **12**, 1679–1719 (2022).

27. Meher, A. K. & Zarouri, A. Green Analytical Chemistry — Recent Innovations. *Analytica* **6**, 1–32 (2025).

28. Gokhale, N. A., Rao Vusa, C. S. & Panda, S. A natural fibre based sustainable and high- performance platform for electrochemical sensors. *RSC Sustain.* **2**, 1849–1858 (2024).

29. Hayat, A. & Marty, J. L. Disposable Screen Printed Electrochemical Sensors: Tools

for Environmental Monitoring. *Sensors* **14**, 10432–10453 (2014).

30. Ferrari García-Miranda, A., J. Rowley-Neale, S. & Banks, C. E. Screen-printed electrodes : Transitioning the laboratory in-to-the field. *Talanta Open* **3**, 100032–100042 (2021).

31. DropSens Screen-Printed electrode (2012).

32. Pérez-Fernández, B., Costa-García, A. & de la Escosura- Muñiz, A. Electrochemical (Bio) Sensors for Pesticides Detection Using Screen-Printed Electrodes. *Biosensors* **10**, 1–26 (2020).

33. Piro, B., Tran, H. V. & Thu, V. T. Sensors Made of Natural Renewable Materials: Efficiency, Recyclability or Biodegradability—The Green Electronics. *Sensors* **20**, 5898–5951 (2020).

34. Yáñez-Sedeño, P., Campuzano, S. & Pingarrón, J. M. Electrochemical (bio) sensors : promising tools for green analytical chemistry. *Curr. Opin. Green Sustain. Chem.* **19**, 1–7 (2019).

35. Donar, Y. O. *et al.* Recent developments and modification strategies in electrochemical sensors based on green nanomaterials for catechol detection. *Trends Environ. Anal. Chem.* **41**, e00223 (2024).

36. Schweigert, N., Zehnder, A. J. B. & Eggen, R. I. L. Minireview Chemical properties of catechols and their molecular modes of toxic action in cells , from microorganisms to mammals. **3**, 81– 91 (2001).

37. Fakhruddin, F. K. A. N. M. Recent advances in the development of biosensor for phenol : a review. *Rev Environ Sci Biotechnol* **11**, 261–274 (2012).

38. Wei, X. *et al.* Deciphering the Changes of Sludge Toxicity and the Succession of Dominant Bacteria During the Process of Catechol Degradation by Acclimated Sludge. *Waste and Biomass Valorization* **13**, 4285–4296 (2022).

39. Zheng, Y. *et al.* Laccase biosensor fabricated on fl ower – shaped yolk – shell SiO 2 nanospheres for catechol detection. *Colloids Surfaces A* **538**, 202–209 (2018).

40. El, N. *et al.* Future Trends and Innovations in the Treatment of Industrial Effluent. Advances in Insect Physiology vol. 12, Elsevier (2025).

41. Benjelloun, M. *et al.* Recent advances and environmentally friendly methods for catechol removal from wastewater. *J. Water Process Eng.* **76**, 108115–108132 (2025).

42. Saleem, Q. *et al.* A highly explicit electrochemical biosensor for catechol detection in real samples based on copper-polypyrrole. *RSC Adv.* **13**, 13443–13455 (2023).

43. Jiang, D. *et al.* Simultaneous biosensing of catechol and hydroquinone via a truncated cube- shaped Au/PBA nanocomposite. *Biosens. Bioelectron.* **124–125**, 260–267 (2019).

44. Bohrer, F. I. *et al.* Comparative Gas Sensing in Cobalt , Nickel , Copper , Zinc , and Metal-Free Phthalocyanine Chemiresistors. *J. Am Chem. Soc.* **131,** 848–855 (2009).

45. Dunbar, A. D. F. *et al.* Detection of Volatile Organic Compounds Using Porphyrin Derivatives. *J. Phys. Chem. B* **114**, 36, 211697–11702 (2010).

46. Gounden, D., Nombona, N. & van Zyl, W. E. Recent advances in phthalocyanines for chemical sensor , non-linear optics (NLO) and energy storage applications. *Coord. Chem. Rev.* **420**, 213359–213370 (2020).

47. Reddy, S. M. Materials for Chemical Sensing., Springer (2017).

48. Akinyemi, A. A., Mashazi, P. N. Efficacious Detection of Epinephrine in the Midst of an Interference (ASCORBIC ACID) Employing Designed Gold Electrode with Cobalt Octacarboxyphenoxy Phthalocyanines. **02**, 42–54 (2025).

49. Demir, E., Silah, H. & Uslu, B. Phthalocyanine Modified Electrodes in Electrochemical Analysis. *Crit. Rev. Anal. Chem.* **52**, 425–461 (2022).

50. Dumoulin, F., Durmuş, M., Ahsen, V. & Nyokong, T. Synthetic pathways to water-soluble phthalocyanines and close analogs. *Coord. Chem. Rev.* **254**, 2792–2847 (2010).

51. Gorduk, S. Highly soluble HOPEMP-functionalized phthalocyanines for photodynamic activity : Photophysical , photochemical and aggregation properties. *J. Mol. Struct.* **1217**, 128478–128488 (2020).

52. Li, R. *et al.* Electron-Donating or -Withdrawing Nature of Substituents Revealed by the Electrochemistry of Metal-Free Phthalocyanines. *Inorg. Chem.* **45**, 2327–2334 (2006).

53. Li, S. *et al.* " Alkyl-Substituted Phenoxy " Spacer Strategy : Antiaggregated and Highly Soluble Zinc Phthalocyanines for Color Films. *ACS Omega* **9**, 50774–50785 (2024).

54. Namgoong, J. W. *et al.* Aryloxy- and chloro-substituted zinc(II) phthalocyanine dyes: Synthesis, characterization, and application for reducing the thickness of color filters. *Dye. Pigment.* **154**, 128–136 (2018).

55. Kumar, A., Brunet, J., Varenne, C., Ndiaye, A. & Pauly, A. Phthalocyanines based QCM sensors for aromatic hydrocarbons monitoring : Role of metal atoms and substituents on response to toluene. *Sensors Actuators B. Chem.* **230**, 320–329 (2016).

56. Thiruppathiraja, T., Arokiyanathan, A. L., Aazaad, B., Silviya, R. & Lakshmipathi, S. H , OH and COOH functionalized magnesium phthalocyanine as a catalyst for oxygen reduction reaction (ORR) - A DFT study. *Int. J. Hydrogen Energy* **45**, 8540–8548 (2020).

57. Zafer, S., Tarakci, D. K., Gurol, I., Ahsen, V. & Harbeck, M. Governing the sorption and sensing properties of titanium phthalocyanines by means of axial ligands. *Sensors Actuators B Chem.* **229**, 581–586 (2016).

58. Paquette, B., Ali, H., Langlois, R. & van Lier, J. E. Biological activities of phthalocyanines -VIII. Cellular distribution in V-79 Chinese hamster cells and phototoxicity of selectively sulfonated aluminum phthalocyanines. *Photochem. Photobiol.* **47**, 215–220 (1988).

59. Bai, M. *et al.* Trimellitic anhydride- and pyromellitic dianhydride-originated tetrakis/octakis(octyloxycarbonyl)phthalocyaninato metal complexes. *Inorg. Chem. Commun.* **28**, 99–103 (2013).

60. Shaposhnikov, G. P., Maizlish, V. E. & Kulinich, V. P. Carboxy-substituted Phthalocyanine Metal Complexes. *Russ. J. Gen. Chem.* **75**, 1480–1488 (2005).

61. Fujishiro, R. *et al.* Synthesis , photodynamic activities , and cytotoxicity of new water-soluble cationic gallium (III) and zinc (II) phthalocyanines. *J. Inorg. Biochem.* **192**, 7–16 (2019).

62. Tolbin, A. Y. & Tomilova, L. G. Synthesis and spectroscopic properties of new water soluble phthalocyanines containing pyridinium hydrochloride fragments. *Russ. Chem. Bull. Int. Ed.* **56**, 2433–2437 (2007).

63. Sharman, W. M. & Lier, J. E. Van. A new procedure for the synthesis of water-soluble tri- cationic and -anionic phthalocyanines. *J. Porphyr. Phthalocyanines* **9**, 651–658 (2005).

64. Bächle, F., Hanack, M. & Ziegler, T. Synthesis and Spectroscopic Evaluation of Two Novel Glycosylated Zinc(II)-Phthalocyanines. *Molecules* **20**, 18367–18386 (2015).

65. Li, H., Fronczek, F. R. & Vicente, M. G. H. Pegylated phthalocyanines : synthesis and spectroscopic properties. *Tetrahedron Lett.* **52**, 6675–6678 (2011).

66. Ayhan, M. M., Özpınar, G. A., Durmuş, M. & Gürek, A. G. Effects of position (α or β) and linker heteroatom (O or S) of substituent on the photophysicochemical behavior of poly(oxyethylene) substituted ZnPcs and assessment of J-aggregation or protonation using TD-DFT computations. *Dalt. Trans.* **42**, 14892–14904 (2013).

67. Ömeroğlu, İ. & Durmuş, M. Water-soluble phthalocyanine photosensitizers for photodynamic therapy. *Turkish J. Chem.* **47**, 837–863 (2023).

68. Isago, H. Optical Spectra of Phthalocyanines and Related Compounds, Springer (2015).

69. Ndebele, N., Sen, P. & Nyokong, T. Electrocatalytic activity of Schiff base containing copper phthalocyanines towards the detection of catechol : Effect of heteroatoms and asymmetry. *Polyhedron* **210**, 115518–115528 (2021).

70. Mack, J. & Stillman, M. J. Assignment of the optical spectra of metal phthalocyanines through spectral band deconvolution analysis and ZINDO calculations. *Coord. Chem. Rev.* **219–221**, 993–1032 (2001).

71. Mack, J. & Kobayashi, N. Low Symmetry Phthalocyanines and Their Analogues.

Chem. Rev. **111**, 281–321 (2011).

72. Alessio, P. *et al.* Detection of catechol using mixed Langmuir – Blodgett films of a phospholipid and phthalocyanines as voltammetric sensors. *Analyst* **135**, 2591–2599 (2010).

73. Pavinatto, A. *et al.* Ultrasensitive biosensor based on polyvinylpyrrolidone / chitosan / reduced graphene oxide electrospun nano fi bers for 17 α – Ethinylestradiol electrochemical detection. *Appl. Surf. Sci.* **458**, 431–437 (2018).

74. Alghamdi, A. F., Hefnawy, M. & Al-Rashood, S. Development and Validation of Electrochemical Method for Quantification of Palbociclib (Anticancer Agent) in Biological Matrices Using Square Wave- Adsorptive Stripping Voltammetry. *Int. J. Electrochem. Sci.* **15**, 3517–3533 (2020).

75. Salvo-Comino, C., Garcia-Hernandez, C., Garcia-Cabezon, C. & Rodriguez-Mendez, M. L. Promoting laccase sensing activity for catechol detection using LBL assemblies of chitosan / ionic liquid / phthalocyanine as immobilization surfaces. *Bioelectrochemistry* **132**, 107407–107415 (2020).

76. Salvo-Comino, C. *et al.* Biosensors Platform Based on Chitosan / AuNPs / Phthalocyanine Composite Films for the Electrochemical Detection of Catechol . The Role of the Surface Structure. *Sensors* **20**, 2152–2162 (2020).

77. García-Hernández, C., García-Cabezón, C., Martín-Pedrosa, F., José Antonio, D. S. & Rodríguez-Méndez, M. L. Layered composites of PEDOT / PSS / nanoparticles and PEDOT / PSS / phthalocyanines as electron mediators for sensors and biosensors. *Beilstein J. Nanotechnol.* **7**, 1948–1959 (2016).

78. Liu, Q., Zou, L., Sun, Q., Li, X. & Chen, Y. A voltammetry biosensor based on self-assembled layers of a heteroleptic tris(phthalocyaninato) europium triple-decker complex and tyrosinase for catechol detection. *Enzyme Microb. Technol.* **139**, 109578 (2020).

79. Apetrei, I. M., Rodriguez-Mendez, M. L., Apetrei, C. & de Saja, J. A. Enzyme sensor based on carbon nanotubes / cobalt (II) phthalocyanine and tyrosinase used in pharmaceutical analysis. *Sensors Actuators B. Chem.* **177**, 138–144 (2013).

80. Wu, H. *et al.* Direct Coupling of Phthalocyanine Cobalt(II) and Graphene via Self-Driven Layer-by-Layer Assembly for Efficient Electrochemical Detection of Catechol. *J. Electrochem. Soc.* **167**, 027533 (2020).

81. Konnerth, R. *et al.* Tuning the deposition of molecular graphene nanoribbons by surface functionalization. *Nanoscale* **7**, 12807–12811 (2015).

82. de Jonge, L., van den Beucken, J., Leeuwenburgh, S., Wolke, J. & Jansen, J. Electrospray Deposition of Bioactive Alkaline Phosphatase Coatings. *Key Eng. Mater.* **361–363**, 589–592 (2008).

83. Buchko, C. J., Chen, L. C., Shen, Y. & Martin, D. C. Processing and microstructural characterization of porous biocompatible protein polymer thin films. *Polymer* **40**, 7397–7407 (1999).

84. Hoyer, B., Sørensen, G., Jensen, N., Nielsen, D. B. & Larsen, B. Electrostatic Spraying : A Novel Technique for Preparation of Polymer Coatings on Electrodes. *Anal. chem.* **68**, 3840–3844 (1996).

85. Fantuzzi, P. *et al.* Fabrication of three terminal devices by ElectroSpray deposition of graphene nanoribbons. *Carbon N. Y.* **104**, 112–118 (2016).

86. Castrovilli, M. C. *et al.* Electrospray deposition of starch-containing laccase : A green technique for low-cost and eco-friendly biosensors. *Biosens. Bioelectron.* **267**, 116758 (2025).

87. Castrovilli, M. C. *et al.* Fabrication of a New, Low-Cost, and Environment-Friendly Laccase- Based Biosensor by Electrospray Immobilization with Unprecedented Reuse and Storage Performances. *ACS Sustain. Chem. Eng.* **10**, 1888–1898 (2022).

88. Castrovilli, M. C. *et al.* Improved reuse and storage performances at room temperature of a new environmentally friendly lactate oxidase biosensor prepared by ambient electrospray immobilization. *Green Chem.* **25**, 5257–5266 (2023).

89. Kuwahata, Y., Takehara, H. & Ichiki, T. Comprehensive study on electrospray deposition in the single Taylor cone–jet mode by changing the spatial electric potential using a ring-shaped ternary electrode. *AIP Adv.* **10**, 045107–045114 (2020).

90. Morais, A. Í. S. *et al.* Fabrication of Polymeric Microparticles by Electrospray : The Impact of Experimental Parameters. *J. Funct. Biomater.* **11**, 4–26 (2020).

91. Sánchez-vicente, C., Santos, J. P., Sayago, I., Mazzola, V. & Sacco, L. Room-Temperature Environmental Gas Detection : Performance Comparison of Nanoparticle-Based Sensors Fabricated by Electrospray , Drop-Casting , and Dry Printing Based on Spark Ablation. *Chemosensors* **13**, 219–238 (2025).

92. Palmeri, F., Raglione, V., Mancini, L. & Zanotti, G. A versatile and practical one-pot strategy for a greener, waste-minimized synthesis of aryloxyand alkyloxy-substituted metallophthalocyanines via tandem S_NAr-cyclotetramerization. *Org. Chem. Front.* **13**, 1199–1210 (2026).

Chapter 4. Sustainable and cost-effective colorimetric sensor devices: the salophen case study

4.1. Introduction

4.1.1. Colorimetric sensor devices for metal detection

This Chapter will provide a description of part of the work conducted during my visiting PhD period at the University of Edinburgh.

The detection of metal ions constitutes a cornerstone of modern analytical chemistry, owing to its broad relevance in environmental monitoring, industrial processes, catalysis, and chemical research.[1] From an environmental perspective, metal ion detection is essential for the assessment and control of pollutants in nature such as surface waters, groundwater, soils, and sediments. Industrial activities, mining operations, corrosion of metallic infrastructures, and the extensive use of metal-containing agrochemicals are among the primary sources of metal contamination.[2] Unlike many organic pollutants, metal ions are intrinsically non-degradable and tend to persist in the environment, where they may accumulate and exert long-term toxic effects on ecosystems and human health.[3] Consequently, sensitive and accessible analytical tools capable of detecting metal ions at low concentrations are indispensable for environmental surveillance and risk assessment. The development of efficient, selective, and reliable sensing strategies for metal ions has therefore become an increasingly important scientific challenge, particularly in light of growing environmental concerns and the urgent need for sustainable technological solutions.[4]

At the same time, metal ion detection plays a crucial role in chemical research and industrial chemistry, particularly in the context of reaction monitoring and catalysis. Trace amounts of metal can profoundly influence reaction mechanisms, kinetics, and selectivity,

even when they are not intentionally introduced into the system. This phenomenon has gained increasing attention in recent years under the concept of hidden catalysis, whereby trace metal impurities originating from reagents, solvents, or glassware, unexpectedly catalyse chemical transformations.[5,6] In such cases, the ability to detect metal ions directly within reaction mixtures becomes essential for ensuring reproducibility, understanding reaction pathways, and validating claims of metal-free catalysis.[7,8] The relevance of this issue is effectively captured by the evocative title of the review by Luque *et al. "To be or not to be metal-free"*, underscoring the ongoing debate surrounding the true nature of ostensibly metal-free transformations.[9]

Metal ion sensing systems therefore represent valuable tools allowing for detection at concentrations below regulatory thresholds, not only for environmental applications but also for fundamental and applied chemical research.[10]

Optical and colorimetric sensors are especially attractive in this regard, as they offer simplicity of operation, low cost, rapid response times, and the possibility of visual detection by naked-eye without the need for sophisticated instrumentation.

Colorimetric sensors rely on observable changes in colour resulting from specific interactions between a sensing molecule and a target analyte. These changes are typically associated with modifications of the electronic structure of the sensor, often induced by metal coordination, charge transfer processes, or conformational rearrangements. The direct relationship between colour variation and analyte concentration makes colorimetric sensing particularly suitable for on-site analysis, environmental screening, and real-time monitoring. Nevertheless, many colorimetric sensors suffer from limitations related to selectivity, stability, toxicity of materials, solvent requirements, and lack of reusability.[11,12] Furthermore, in order to enhance performance, these devices often rely on nanomaterials, frequently based on metallic components, which further compromises the overall sustainability of their production.[13]

These challenges further emphasize the importance of reconsidering sensor design from a broader and more sustainable viewpoint. It is within this context that the aim of the

present study is situated. The work described in this Chapter was conceived to contribute to this shift in paradigm, while remaining fully aligned with the sustainability objectives of the Rome Technopole Project, within the context of which my doctoral research is developed.

4.1.2. Copper ions: environmental impact and detection

Among the transition metal ions, copper is an essential trace element and occupies a particularly prominent position in biological and microbial sciences, as it is involved in numerous key processes. Indeed, due to its redox properties, copper-containing enzymes play critical roles in electron transfer processes, oxygen binding, and oxidation catalysis.[14] However, despite these important physiological functions, excessive amounts of copper can be potentially toxic, posing significant risks to both the environment and the human health. It is widely known that elevated concentrations of copper in aquatic environment and soil, that can result from industrial effluents and agricultural waste, respectively, can cause severe contamination, leading to oxidative stress, disruption of metabolic processes, and impaired growth and reproduction of aquatic organisms.[15,16] In humans, excessive copper intake has been associated with gastrointestinal disorders, liver and kidney damage, and neurological effects.[17]

Given this context and considering the steadily increasing significance of this metal in recent years both for scientific interest and technological applications, as highlighted by the growing number of publications indexed in the Web of Science (**Figure 1**), the development of effective strategies for the detection as well as for the recovery of copper ions, are of paramount importance.

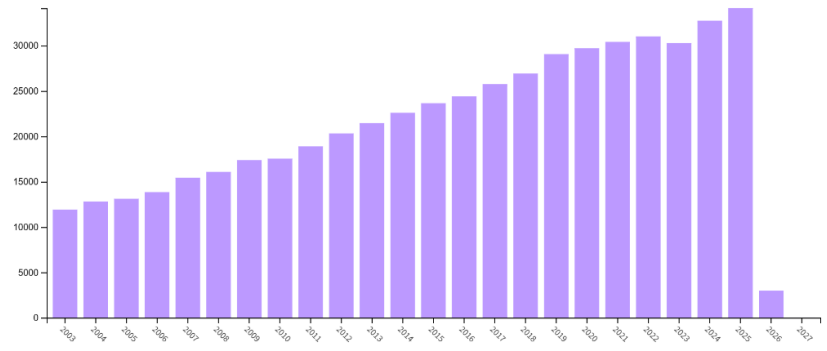

Figure 1. Number of publications per year on copper, obtained from the Web of Science database (search topic: "Copper", results sorted by year), assessed February 13, 2026.

Although the Twelve Principles of Green Chemistry provide a framework for sustainable chemical design, their application in sensor development remains limited, highlighting the need for sensing platforms conceived according to life-cycle sustainability principles.[18]

An additional and often overlooked aspect of sustainability in metal ion sensing is the potential for metal sequestration and recovery. In environmental applications, detection alone does not fully address the problem and represents only the first step, as the ultimate goal involves the removal or immobilization of toxic species to mitigate their ecological impact. Sensors capable of binding metal ions strongly and selectively can therefore serve a dual function, acting not only as analytical tools but also as active agents for environmental remediation and waste valorisation.[19]

In the specific case of copper, the recovery approach is particularly relevant. Copper is a strategically important material widely used in electrical, electronic, and catalytic applications. The possibility of capturing copper(II) ions from contaminated environments or industrial residues and reintroducing them into productive cycles represents an attractive strategy for reducing environmental impact while enhancing resource efficiency, in a circular economy.

4.2. Results and discussion

4.2.1. Sustainable synthesis of salophen

Within this conceptual framework, the present study adopts a deliberately simple case study to explore and demonstrate a sustainable approach to sensor design and fabrication. The system investigated is based on a salophen structure, a Schiff-base ligand that has been extensively used in the coordination chemistry. Schiff-bases are an exceptionally versatile class of ligands, with widespread applicability that is attributed to straightforward synthetic protocols, extensive structural tunability, strong metal-chelating capabilities, and pronounced photophysical responses upon coordination with metal ions.[20] Formed through the condensation of amines with carbonyl compounds, Schiff bases generate imine functionalities that provide effective coordination sites for a broad spectrum of metal ions, supporting their use in catalysis, biomimetic studies, molecular electronics, and chemical sensing.[21,22]

The copper(II)-salophen complex is a well-known and thoroughly characterized coordination compound, whose structural, electronic, and spectroscopic properties have been widely reported.[23] As such, the novelty of this work lies in the methodological and conceptual approach adopted for the development of an optical colorimetric sensor, exploiting the simple and well-established salophen-copper(II) system as a model platform to demonstrate how a sensor can be rationally designed, fabricated, and tested while explicitly integrating sustainability considerations at every stage of its realization.

In particular, this study addresses sustainability in the synthesis of the sensing molecule, prioritizing greener and highly efficient synthetic routes, guiding the choice of materials and reagents by considerations based on safety and environmental impact. The analytical evaluation of the sensor is carried out using green methodologies, with special emphasis on the use of aqueous or environmentally benign solvents in spectroscopic techniques such as UV-visible absorption spectroscopy. Furthermore, the sensor reversible interaction with

copper(II) ions is explored, enabling regeneration and reuse after detection, as well as the potential sequestration and recovery of the metal ion.

The study began with the synthesis of the salophen ligand, a molecule selected for the investigation of its selective interactions with target metal ions. In line with a strategic and sustainable sensor design, a green synthesis of the molecule was explored. A new synthetic strategy has been evaluated, employing glycerol as the solvent.

In recent years, glycerol has gained significant interest as a sustainable solvent for organic synthesis due to its non-toxic, biodegradable, and environmentally benign nature. It is abundantly available as a by-product of triglyceride transesterification in the production of natural fatty acid derivatives, [24] which makes it and its mixtures an inexpensive and renewable resource with reduced environmental burden.[25]

Its distinctive physicochemical properties, such as high polarity, strong hydrogen-bonding capacity, and negligible vapor pressure, have enabled its effective and sustainable use in a wide variety of organic reactions, including cross-couplings and multicomponent transformations.[26,27]

In addition, its potential for recovery and reuse further enhances its sustainability credentials by contributing to waste minimization and improved process mass efficiency.

For the first time, this solvent was used as the reaction medium for the synthesis of this class of molecules. Although some sustainable synthetic routes for salophen-like structures have already been reported,[28,29] the goal of this work was to validate an environmentally friendly synthesis, given the well-documented sustainability profile of this reaction medium, that did not require specialized equipment, such as mechanochemical setups. This approach aligns with the principles of green chemistry while maintaining accessibility and reproducibility in the laboratory. In **Scheme 1** a practical route for the successful synthesis of the target ligand in 93% yield by the condensation of 1,2-diamine with 2-hydroxy-4-parabenzaldehyde in glycerol at 80 °C is reported.

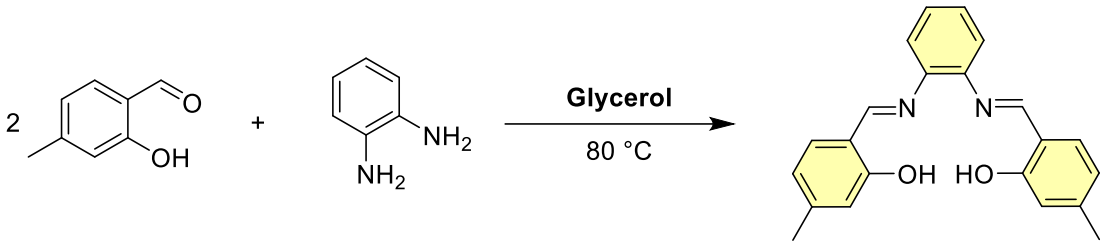

Scheme 1. Synthetic route for the salophen-ligand under investigation.

To benchmark the efficiency of this new glycerol-based procedure against a conventional method in solution, the same reaction was also performed in ethanol and the results in terms of yields are reported in **Table 1**.

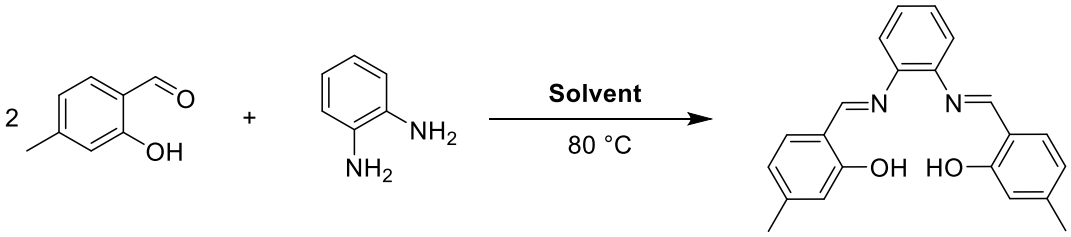

Solvent	Isolated yield (%)
Ethanol	60
Glycerol	**93**

Table 1. Results in terms of isolated yields for the salophen ligand synthesis when different solvents were used.

Notably, the use of glycerol led to a significant increase in yield, reaching 93%, and enhanced the sustainability profile of the reaction. This improvement is evident not only from the huge previously discussed advantages of glycerol as a green solvent but also from a quantitative green chemistry assessment discussed later.

Furthermore, to test glycerol recyclability, after the first synthesis of the salophen ligand, the product was easily separated from the reaction mixture due to precipitation, using washings with water. After removing water through vacuum distillation, the recovered glycerol was reused in subsequent reactions. Glycerol could indeed be recycled, with yields remaining consistent for up to three cycles (**Figure 2**).

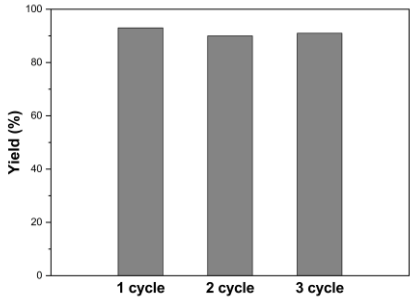

Figure 2. Results in terms of isolated yields of the salophen ligand synthesis using the recycled glycerol.

To quantitatively assess the sustainability of the reaction, beyond the extensively discussed E-factor, other two Green Chemistry metrics were calculated, that are Process Mass Intensity (PMI), and Reaction Mass Efficiency (RME). They are materials-based metrics, and their values take into account the material efficiency of the investigated process. Details on the calculations are reported in the Experimental section at the end of this Chapter.

Results and comparisons, in terms of yields and green metrics, are summarized in **Table 2**. The green metrics for the subsequent reactions when recovered glycerol was used are also calculated and reported in **Table 2**, showing that the E-factor values further decrease upon solvent reuse and highlighting the environmental benefits of recycling the solvent without loss of efficiency.

Procedure	Isolated yield (%)	E-factor	PMI	RME (%)
Ethanol	60	5.8	6.8	54.7
Glycerol (1° cycle)	**93**	**5.4**	**6.7**	**84.5**
Glycerol (2° cycle)	90	1.5	2.8	81.3
Glycerol (3° cycle)	91	1.5	2.8	82.1

Table 2. Results in terms of isolated yields and green chemistry metrics for the salophen ligand synthesis in different experimental conditions.

To further quantitatively evaluate the sustainability profile of the glycerol-based reaction, a multidimensional approach was conducted. A radar plot assessment tool was constructed to visually represent and benchmark the greenness of the reactions performed in different experimental conditions across key Green Chemistry metrics. Each axis of the radar chart corresponds to a recognized sustainability parameter, including the E-factor, PMI, and RME. Yield is also present to give an assessment of the efficiency conversion of the reaction.

Taking inspiration from the literature,[30] integrating these complementary metrics within a single graphical representation allows for a comprehensive and intuitive evaluation of the reaction performance from a green chemistry perspective. This approach not only highlights the strengths and areas for improvement of the synthetic protocol under investigation but also provides a rationale and practical framework for guiding further optimization toward more sustainable chemical processes.

From a practical standpoint, and to allow meaningful comparison among inherently different green metrics, a normalization procedure was applied to account for their distinct scales and directional interpretations. Yield and RME, both expressed as percentages, were maintained and directly reported on a 0-100 scale, where values approaching 100% indicate a greener and more efficient process. In contrast, since lower values of E-factor and PMI correspond to improved sustainability, these parameters were converted using an inverse transformation, defined as:

$$Score = \left(\frac{1}{1+X}\right) * 100, Score = \left(\frac{2}{1+Y}\right) * 100,$$

Where X and Y are the calculated E-factor and PMI values, respectively. As a result, under ideal conditions, where an E-factor approaching 0 and a PMI approaching 1, the corresponding normalized scores converge toward 100%, thus aligning all metrics within a common and consistent interpretative framework, where higher values, on a scale from 0 to 100, reflect better environmental performance. The green-shaded region represents the performance of the most sustainable organic reaction with an ideal situation in which all the green metrics values reach 100%. Consequently, the closer an experimental reaction profile approaches with this green area, the more sustainable and environmentally favourable the process can be considered.

Procedure	**Isolated yield (%)**	**E-factor (%)**	**PMI (%)**	**RME (%)**
Ethanol	60	14.7	25.6	54.7
Glycerol (1° cycle)	93	15.6	26.0	84.5
Glycerol (2° cycle)	90	40.0	52.6	81.3
Glycerol (3° cycle)	91	40.0	52.6	82.1

Table 3. Scores used in the radar plot, obtained by the inverse conversion.

Based on the obtained scores for E-factor and PMI (**Table 3**), the radar plot was thus constructed, making evident that the procedures involving glycerol as the solvent are much closer to the maximum of greenness (green-shaded area) than the procedure using ethanol (**Figure 3**).

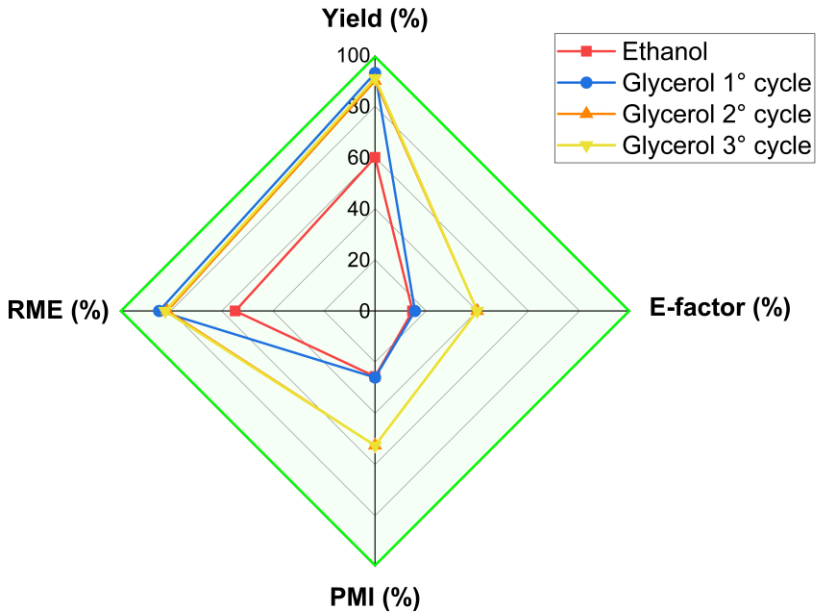

Figure 3. Graphical representation of the overall sustainability profile evaluated for different salophen synthetic protocols.

This radar plot can serve as a useful tool having the potential to be widely adopted as a practical guide for green sensor but also for green synthesis development, advancing the field towards responsible innovation aligned with global sustainability objectives.

4.2.2. Fabrication of the colorimetric salophen sensor

After the preparation of the sensing molecule, the optimization of UV-Vis analytical conditions was then conducted within a sustainable framework, prioritizing the use of green solvents with minimal environmental impact (**Table 4**). In particular, the selection process required a careful balance among multiple factors: solvent sustainability, fulfilment of solubility criteria, and optimal spectroscopic properties.

The chosen solvents had to exhibit an appropriate UV cut-off, preventing interference in the wavelength range of interest and allowing accurate measurement of the ligand-metal interactions. Moreover, the solvents had to efficiently dissolve the synthesized ligand, salophen, ensuring homogeneous solutions suitable for spectroscopic analysis. Then, miscibility with the ligand solution was required to allow for accurate dilution without precipitation or phase separation. Eventually, the solvents needed to solubilize the tested metal salts under equivalent counterion conditions, thereby enabling consistent comparison across different metal-ligand complexes.

An additional layer of optimization was introduced by evaluating the influence of the counterions associated with the metal salts. Both acetates and chlorides were investigated to identify potential differences in solubility, complex formation, and spectral behaviour.

Given that pH is a critical parameter that can strongly influence ligand-metal complexation and UV-Vis absorbance, aqueous solutions were prepared using pH-controlled buffers, maintaining a neutral environment to minimize potential interference in the measurements.

Through systematic testing, the optimal conditions were identified. The ligand stock solution was prepared in dimethyl sulfoxide (DMSO) and subsequently diluted with a 1:2 mixture of DMSO and bis-tris (bis-(2-hydroxyethyl)-imino-tris-(hydroxymethyl)-methan) buffer (pH 7.2). Metal salts with chloride counterions were dissolved in DMSO prior to measurements. These conditions effectively balanced sustainability, good spectral absorption and solubility both of the ligand and of the metal salts for the study of salophen-metal complexes.

Solvent of the ligand solution	**Solvent for the dilution of the ligand solution**	**Solvent of the metal ions solutions**	**Anions**
DMSO	DMSO	DMSO	Acetates
2-MeTHF	Water	Water	Chlorides

DMSO	Bis-Tris Buffer (pH 7.2)	Bis-Tris Buffer (pH 7.2)	Chlorides
DMSO	Bis-Tris Buffer (pH 7.2)	Bis-Tris Buffer (pH 7.2)	Acetates
DMSO	Phosphate Buffer (pH 7.5)	DMSO	Chlorides
DMSO	DMSO/Phosphate Buffer 1:1 (pH 7.5)	DMSO	Chlorides
DMSO	DMSO/Phosphate Buffer 1:2 (pH 7.5)	DMSO	Chlorides
DMSO	**DMSO/Bis-Tris Buffer 1:2 (pH 7.2)**	**DMSO**	**Chlorides**

Table 4. Solvents and solvent mixtures screening for UV-Vis analytical measurements.

Following the optimization of the analytical conditions, the metal-binding selectivity of the salophen ligand was systematically investigated through UV-visible absorption spectroscopy. The absorption spectral changes of the ligand (10 μM) were recorded upon addition of one equivalent of different metal ions, introduced as their chloride salt solutions (Fe(II), Fe(III), Zn(II), Mn(II), Cu(II), Ni(II), Cr(II), Sn(II), Co(II), Pd(II), Ru(III), Pt(II), Rh(III), Pb(II), Cd(II)) in DMSO/bis-tris buffer (1:2 v/v, pH 7.2).

As shown in **Figure 4a**, which also shows the absorption spectrum of the free ligand for comparison, the uncoordinated salophen displays two dominant absorption bands peaked at 265 and 327 nm, and a shoulder at 377 nm, attributable to π-π* transitions of the conjugated aromatic system and to n-π* transitions, respectively. Upon addition of copper(II), while the band at 265 nm remains observable, two additional absorption bands clearly emerge at 317 nm and 403 nm. The appearance of these new bands is accompanied by a redistribution of spectral intensity, indicating a substantial modification of the ligand's electronic structure upon coordination. In particular, the band at 317 nm can be reasonably assigned to the ligand π-π* transitions perturbed by metal coordination, whereas the higher-wavelength absorption at 403 nm is consistent with the formation of the copper(II)-salophen complex and may be attributed to ligand-to-metal charge transfer (LMCT)

transitions.[23] The formation of this lower-energy band, absent in the spectrum of the free ligand, is particularly significant, as it reflects the extension of conjugation and altered electronic distribution resulting from chelation of the copper(II) ion within the tetradentate Schiff-base framework. Such spectral changes unequivocally support the formation of a new coordination species under the selected experimental conditions.[31]

In contrast, the addition of Fe(II), Fe(III), Zn(II), Mn(II), Ni(II), Cr(II), Sn(II), Co(II), Pd(II), Ru(III), Pt(II), Rh(III), Pb(II), Cd(II) produced absorption spectra largely overlapping with that of the free ligand, with no comparable emergence of new bands. In fact, despite minor variations in intensity were observed in some cases, no distinct spectral signatures indicative of stable complex formation were detected, suggesting any metal-ligand binding. These findings demonstrate that, under the adopted solvent composition and pH conditions, the salophen ligand exhibits a pronounced preference for copper(II) over the other tested metal ions. Notably, the coordination process is accompanied by a distinct and visually perceptible colour change. As illustrated in **Figure 4b**, the solution of the free ligand (10 μM) exhibits a pale yellow appearance, whereas the addition of one equivalent of $CuCl_2$ produces an immediate transition to a more intense light yellow, consistent with the emergence of the 403 nm absorption band. Moreover, no visible colour change is observed to the naked eye for the ligand solution in the presence of 1 equivalent of different metal ions (chlorides) in DMSO/bis-tris buffer 1:2 (pH 7.2), further supporting the selectivity toward copper(II) (**Figure 4c**).

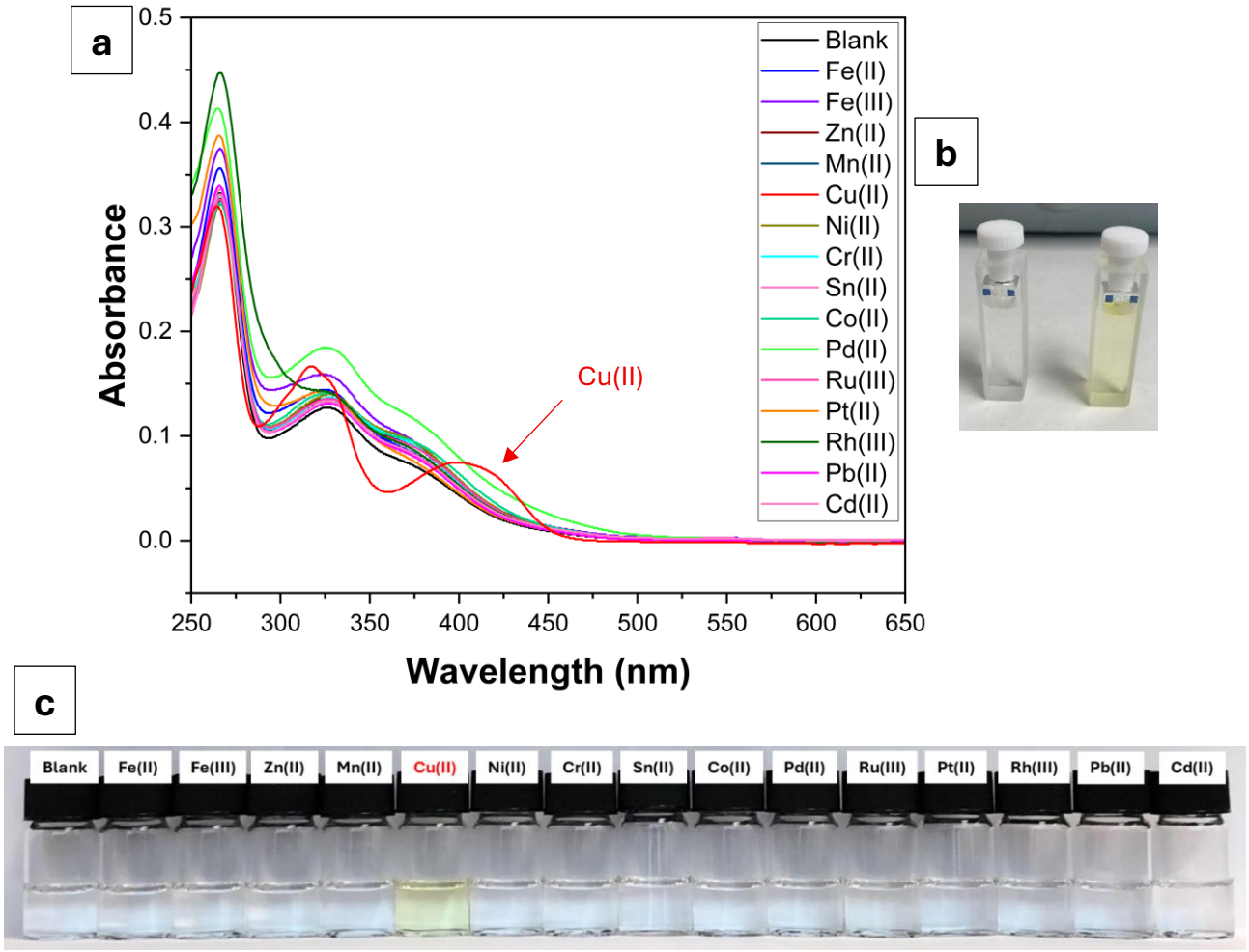

Figure 4. (a) Absorption spectral changes of ligand (10 μM) in the presence of 1 equivalent of different metal ions in DMSO/bis-tris buffer 1:2 (pH 7.2); (b) Colour change of ligand solution (10 μM) in the presence of 1eq. of copper(II) (right), compared to the blank withouth the metal (left); (c) Photographs of ligand solutions (10 μM) in the presence of 1 equivalent of different metal ions.

On the basis of these results, a quantitative investigation of the sensing response toward Cu(II) was subsequently undertaken. A calibration curve was constructed by monitoring the absorption changes of a 10 μM solution of the ligand upon incremental addition of $CuCl_2$ (from 0.5 to 2 equiv.) in DMSO/bis-tris buffer 1:2, pH 7.2 at room temperature (**Figure 5a**). Progressive addition of copper(II) resulted in systematic and concentration-dependent growth of the absorption band at 403 nm, enabling the establishment of a linear relationship between absorbance and copper(II) concentration within the investigated range. The

interaction between the ligand and Cu(II) was further investigated by UV-vis titration experiments. Upon progressive addition of copper(II) (up to 3.2 equiv., corresponding to approximately 2 ppm of copper(II)), the absorption band at 403 nm did not show a further increase in intensity but instead approached a plateau, indicating saturation behavior (**Figure 5b**). Notably, this concentration lies in the low ppm range, comparable to the levels of copper reported to influence iron-catalyzed reactions in studies by Bolm and Buchwald, highlighting the potential relevance of strong ligand-copper(II) interactions even at trace metal concentrations.[32]

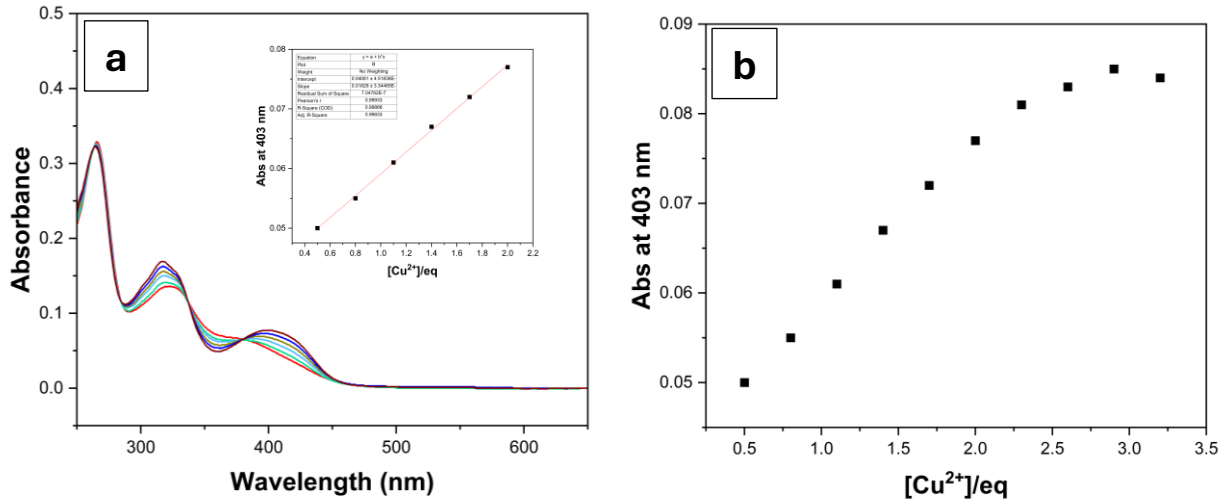

Figure 5. (a) Absorption spectral changes of the ligand (10 μM) upon addition of copper(II) (up to 2 equiv.) in DMSO/bis-tris buffer 1:2 pH 7.2 at room temperature. Inset: linear fitting of the absorbance at 403 nm *versus* the number of equivalents of copper(II) added (calibration curve); (b) Absorbance at 403 nm *versus* the number of equivalents of copper(II) added (up to 3.2 equiv.).

4.2.3. Paper-based test-strips fabrication and analysis

The naked-eye response further substantiates the suitability of the system as a colorimetric sensor, combining spectroscopic sensitivity with operational simplicity. The

study was therefore extended toward the fabrication of paper-based colorimetric test strips for metal ion detection.

This transition is part of a broader project aimed at developing an integrated sensing device capable of simultaneously detecting multiple metal ions in solution, not only for environmental monitoring but also for identifying trace metal species potentially responsible for hidden catalysis. The resulting device, conceived to be portable, user-friendly, and suitable for on-site analysis, is commonly described in the literature as a "sensor array".[33] When integrated with pattern recognition techniques, such systems exhibit an enhanced ability to discriminate subtle variations generated by structurally similar targets, thereby enabling the simultaneous detection of multiple analytes within complex matrices.

The fabrication of the test strips positively impacts several key sustainability dimensions, as well. First, material efficiency is improved, as only minute quantities of ligand are required to functionalize each strip. Second, energy consumption is reduced, since detection occurs at room temperature without the need for continuous spectroscopic instrumentation. Third, safety and environmental compatibility are enhanced, owing to the use of cellulose, a renewable, biodegradable, and low-cost substrate, as the supporting matrix. Finally, the portability and disposability of the strips reduce infrastructural requirements, aligning the device with decentralized and on-site environmental monitoring strategies.[34]

Compared to solution-based UV-Vis measurements, which require cuvettes, solvents, and powered instrumentation, the paper-based format represents a substantial reduction in operational resource demand and enhances practical applicability, thereby demonstrating how device miniaturization and substrate selection contribute directly to green performance metrics. In this context, integration with smartphone-based image acquisition and processing systems is envisaged, enabling detection and quantification of even subtle colour variations through digital analysis.[35] Smartphones have indeed become increasingly integrated with diverse sensing platforms, including test-strips, microchips, and portable detectors, owing to their global accessibility and inherent portability. In such systems,

smartphones often function as the controller, data analyser, and display interface for fast, real-time, and *in situ* monitoring, while simplifying device architecture, reducing fabrication costs, and advancing green sensor electronics.[35]

Numerous colorimetric paper sensors for Cu(II) have been reported in the literature, often relying on synthetic dyes, nanoparticles (e.g., gold or silver nanostructures), polymeric matrices, or multi-step surface functionalization procedures. While many of these systems achieve high sensitivity, they may involve complex fabrication protocols, non-renewable materials, or limited reusability.[36–38]

In contrast, the sensor developed in this study is based on a well-known Schiff-base ligand, immobilized through a simple soaking-and-drying procedure on commercially available filter paper, without the need for additional crosslinking agents, nanomaterials, or elaborate surface treatments. In this sense, the proposed salophen-based paper sensor embodies a complementary paradigm within the field of colorimetric metal detection: rather than pursuing maximum sensitivity through increasing structural and material complexity, it demonstrates that established coordination chemistry can be strategically reinterpreted to produce accessible, low-impact, and reliable sensing platforms aligned with green chemistry and circular economy principles.

Moreover, the sustainability-oriented design of the present device, encompassing green synthesis of the ligand, aqueous-compatible detection conditions, and minimal material consumption, distinguishes it from conventional approaches primarily optimized for analytical performance alone. Although the sensitivity of highly engineered nanomaterial-based systems may in some cases be superior, the balance achieved here between selectivity, simplicity, cost-effectiveness, and environmental responsibility represents a significant advantage for practical environmental monitoring applications.

The test strips were prepared by immersing ordinary filter paper into the ligand solution (20 mM in DMSO), ensuring complete impregnation of the substrate. The soaked paper was subsequently dried at room temperature, and the cycle was repeated another time, to obtain the functionalized test strips ready for use. The dried strips were then immersed in different

metal ion chloride solutions (10 μM in DMSO/bis-tris buffer mixture 1:2, pH 7.2), allowing coordination between the immobilized ligand and the metal ions, and then dried at room temperature. Under standard lighting conditions, the copper-treated strip exhibited a slightly more intense yellow coloration compared to the blank and to strips exposed to other metal ions (**Figure 6**).

Figure 6. Photographic images of the strips upon immersion in different metal ion solutions (10 μM in DMSO/bis-tris buffer mixture 1:2, pH 7.2).

However, the difference was not sufficiently pronounced to allow immediate and unequivocal discrimination by the naked eye. Therefore, to further strengthen the analytical robustness of the colorimetric evaluation as well as to ensure an objective and reproducible evaluation of the colorimetric response, digital image analysis was performed using Trigit, a freely accessible online software specifically developed for quantitative colour discrimination.[39] Unlike purely visual inspection, which is inherently subjective and dependent on observer perception, Trigit enables numerical extraction of chromatic information from digital images, thereby transforming qualitative colour variations into quantifiable analytical parameters.

The software operates by analysing selected Regions Of Interest (ROI) within an image and extracting the corresponding RGB (Red-Green-Blue) coordinates. Each measured colour is thus described as a three-component vector in RGB space, where the intensity of each channel ranges from 0 to 255. Instead of relying on a single pixel, the colour value is a

mean derived by the software by averaging all pixels contained within the selected area, thereby reducing local variability and improving measurement reliability. Consequently, the output provided by Trigit represents the spatially averaged colour of the defined ROI, ensuring reproducible and objective colorimetric analysis. In addition to mean RGB values (denoted as μR, μG, μB), the associated standard deviations are provided (σR, σG, σB), allowing evaluation of colour homogeneity and reproducibility across the analysed area, an important aspect for paper-based devices, where slight surface heterogeneities may influence the chromatic response. Photographic images of the strips were thus acquired using a smartphone camera. To ensure reproducibility across all samples, the device was positioned at a fixed distance of 15 cm from the test strip during image acquisition. Controlled and uniform lighting conditions were maintained throughout the imaging process to reduce potential interference from shadows or uneven illumination. **Table 5** shows the results obtained by Trigit analysis of the so-collected pictures.

With regard to the strip immersed in the copper solution, while the mean R value remains relatively consistent with those of the other strips and the blank. the mean G and B values show a marked deviation from those measured for the other metal-treated strips and for the control (blank) strip, which was not immersed in any metal solution. This quantitatively demonstrates the actual chromatic difference between the strip immersed in the copper solution and the others (including the blank), a distinction that was previously only slightly perceptible to the naked eye.

	μR	**μG**	**μB**	**σR**	**σG**	**σB**
Blank	240.38	230.24	145.44	1.09	1.06	1.14
Fe(II)	240.17	229.43	146.31	1.21	1.38	1.51
Fe(III)	241.69	231.61	146.57	1.16	1.25	1.24
Zn(II)	240.29	229.36	147.00	1.29	1.24	1.71
Mn(II)	241.51	230.51	148.51	0.87	0.87	0.87

Cu(II)	**239.41**	**207.92**	**84.83**	**1.29**	**1.78**	**4.76**
Ni(II)	241.05	230.05	148.13	1.26	1.26	1.21
Cr(II)	239.87	228.87	146.87	0.99	0.99	0.99
Sn(II)	239.68	231.03	150.71	1.25	1.36	1.60
Co(II)	239.38	230.48	147.78	2.07	1.71	1.73
Pd(II)	239.00	228.80	144.12	0.90	0.97	1.17
Ru(III)	240.46	230.07	145.98	1.79	1.54	2.79
Pt(II)	239.75	230.87	145.35	1.81	1.41	1.69
Rh(III)	241.52	230.81	147.63	1.21	1.13	1.76
Pb(II)	241.12	230.40	148.30	0.98	1.12	1.02
Cd(II)	240.55	229.55	147.58	0.89	0.89	0.88

Table 5. Results in terms of mean RGB values and the corresponding standard deviations of the paper-based test-strips by Trigit analysis.

The RGB data were further conceptualized within a three-dimensional colour space representation, an approach specifically introduced in this study to facilitate intuitive visualization of chromatic variations (**Figure 7**). By plotting each sample as a point in a three-dimensional coordinate system defined by the R, G, and B axes, as provided by Trigit analysis, it becomes possible to directly observe the spatial distribution and relative positioning of colours. This graphical representation allows immediate visual assessment of how far a given sample deviates from the reference region corresponding to the reference (blank).

Moreover, the use of digital image processing tools such as Trigit aligns with the sustainability-driven philosophy of this study, as it requires only standard imaging devices

(e.g., smartphone cameras) and eliminates the need for dedicated colorimetric instrumentation, thereby supporting the development of accessible and portable sensing platforms.

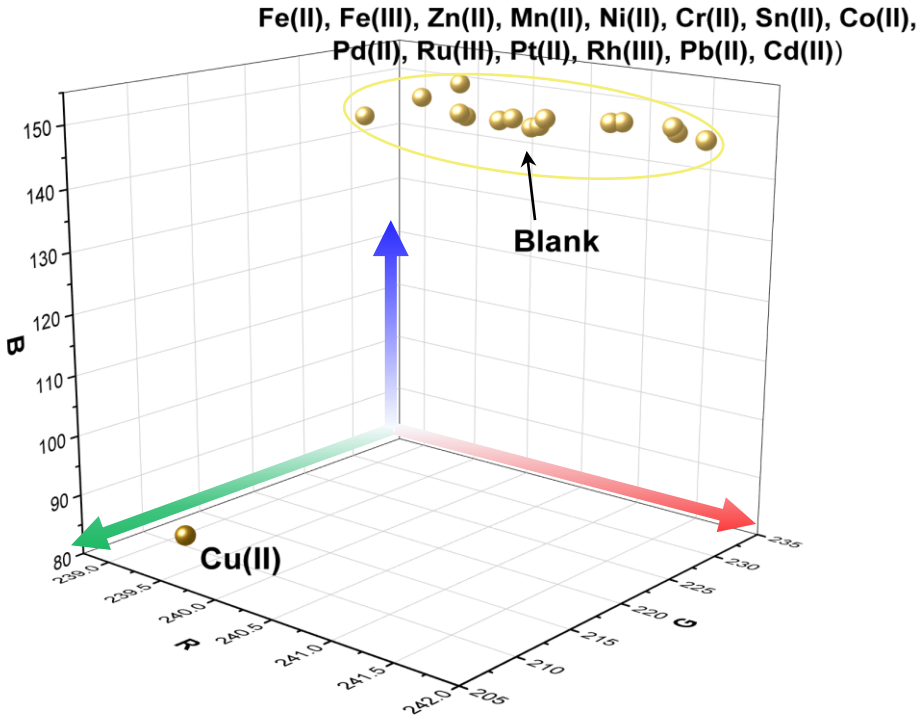

Figure 7. 3D Scatter colour space representation of the paper-based test-strips immersed in different metal solutions (10 μM) in DMSO/bis-tris buffer mixture 1:2, pH 7.2 by Trigit analysis.

The three-dimensional colour space representation enables a rapid and clear visualization of the different chromatic response of the copper(II)-treated strip compared to those exposed to the other metal ions. In particular, the data point corresponding to Cu(II) is clearly separated from the others, while the strips treated with Fe(II), Fe(III), Zn(II), Mn(II), Ni(II), Cr(II), Sn(II), Co(II), Pd(II), Ru(III), Pt(II), Rh(III), Pb(II), Cd(II) cluster in a region close to the blank, that corresponds to the reference, where the ligand was immobilized but not subsequently exposed to any metal ion solution. This graphical approach provides an immediate and intuitive confirmation of the distinct colour variation induced by copper(II). The combination of paper-based sensing and digital image analysis

thus provides a simple yet analytically rigorous platform, bridging qualitative naked-eye detection with quantitative assessment and at the same time confirming solution-based UV-vis analysis.

Overall, the combined spectroscopic validation, and solid-state implementation converge to demonstrate a coherent and sustainability-driven sensor development strategy. The salophen-Cu(II) system thus serves not merely as a proof-of-concept for copper detection, but as a model illustrating how classical coordination chemistry can be strategically redesigned into an environmentally responsible analytical platform.

To further investigate the effect of metal ion concentration on the colorimetric response, an additional experiment was performed by increasing the concentration of the copper(II) solution used for strip immersion by three orders of magnitude, from 10 μM to 10 mM, while keeping all other experimental conditions unchanged. The resulting color variation observed on the paper-based test strips and analyzed by Trigit gave the results displayed in **Figure 8**.

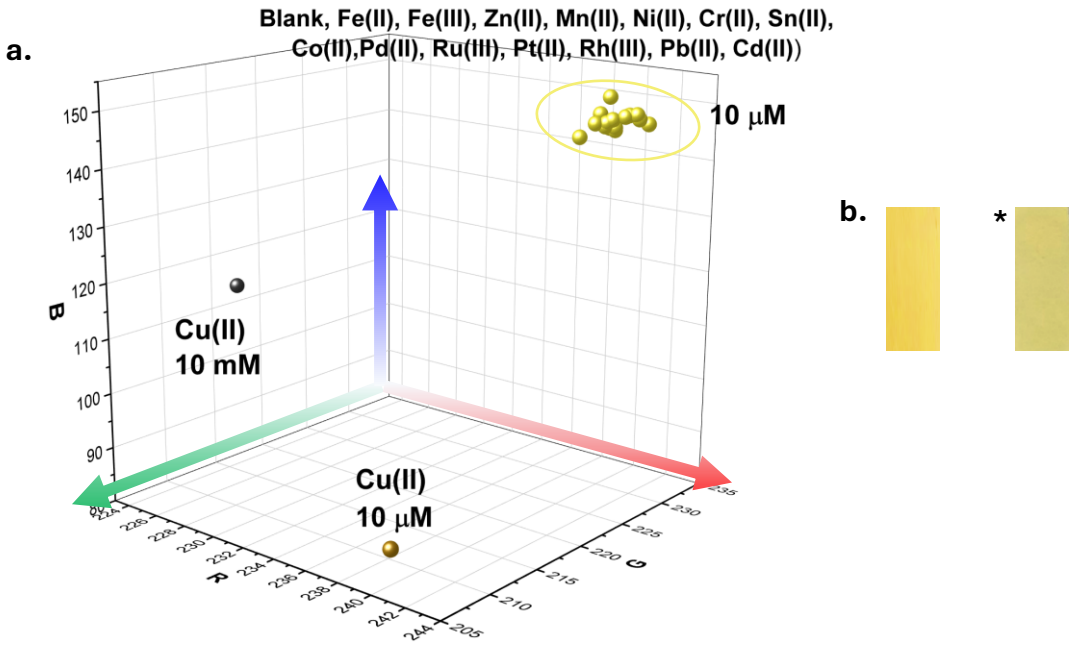

Figure 8. (a) 3D Scatter colour space representation of the paper-based test-strips immersed in different metal solutions (10 μM) compared to that immersed in copper(II) solution (10 mM) in

DMSO/bis-tris buffer mixture 1:2, pH 7.2 by Trigit analysis; **(b)** Photographic images of the strips upon immersion in copper(II) solutions (10 μM, left, and 10 mM, right) in DMSO/bis-tris buffer mixture 1:2, pH 7.2. *The results in terms of mean RGB values and the corresponding standard deviations of the strip immersed in copper(II) solution (10 mM) by Trigit analysis are 224.90, 214.97, 115.62, 0.40, 0.39, 0.21, respectively.

This enhancement of the colorimetric response in the paper-based format, visually detected by the position in the 3D colour space of the strip immersed in a more concentrated copper(II) solution that is even further from the cluster of the blank particularly along the R (Red) axis, can be rationalized by considering mass transport and binding phenomena within the porous cellulose matrix.

Unlike homogeneous solution systems, where ligand and metal ions are uniformly distributed at the molecular level, the solid-state configuration introduces diffusional constraints and spatial heterogeneity. The coordination process is governed not only by thermodynamic affinity but also by the rate and extent of copper(II) diffusion through the fibrous network of the paper substrate. At low copper concentrations (10 μM), the number of copper(II) ions available for interaction with the immobilized ligand may be insufficient to fully occupy accessible coordination sites across the paper surface. Moreover, diffusion limitations within the microporous structure of cellulose can reduce the effective contact between metal ions and ligand-functionalized regions. As a result, only partial complexation occurs, leading to a moderate chromatic response that, although analytically detectable, remains visually subtle.

At increased copper(II) concentration to 10 mM, the higher driving force for mass transfer enhances metal ion penetration into the paper matrix and promotes more extensive coordination with the immobilized salophen units, thereby intensifying the overall colour signal. Under this regime, the visual response becomes dominated by the cumulative optical contribution of a larger number of coordinated sites, producing the markedly deeper coloration observed experimentally.

These considerations highlight an important distinction between solution-phase and solid-state sensing: while the intrinsic affinity of salophen for copper(II) governs selectivity, the perceptibility of the colorimetric response in the paper device is modulated by mass transport phenomena, surface loading, and site accessibility. Understanding these factors is essential for future optimization of the device, for instance through controlled ligand loading or paper pre-treatment to enhance analyte-ligand interaction efficiency.[40] It is important to emphasize that this requirement does not contradict the higher intrinsic sensitivity observed in the UV-Vis solution-phase measurements; rather, it reflects the inherent differences between homogeneous spectroscopic detection and solid-state colorimetric sensing, where mass transport limitations, surface coverage, and light scattering within the cellulose matrix can attenuate the perceived intensity of the optical signal.

From an application-oriented perspective, this behaviour suggests a dual-mode functionality of the sensor: semi-quantitative detection at low concentrations via digital colour processing, and immediate visual screening at higher contamination levels. Such flexibility may prove advantageous in environmental monitoring scenarios, where preliminary on-site assessment can be followed by more refined quantitative analysis when necessary.

4.2.4. Evaluation of the recovery of the metal after extraction

At this stage, while UV-Vis spectroscopy had already demonstrated higher sensitivity compared to the paper-based test strips, the study naturally progressed to the consideration of complex recovery. In particular, the possibility of retrieving the copper(II)-salophen complex following the solution-phase UV experiments was evaluated, in line with the sustainability-oriented approach adopted throughout this work.

2-Methyltetrahydrofuran was selected as an extraction solvent guided by both environmental and chemical criteria: 2-MeTHF is recognized as a green solvent due to its low toxicity, biodegradability, and derivation from renewable resources, while its immiscibility with aqueous media and suitable solubilizing properties for the copper(II)-salophen complex made it ideal for the intended extraction procedure. Upon addition of 2-MeTHF to the analysed solution containing the ligand and copper chloride, the Cu(II)-salophen complex preferentially partitioned into the organic phase, demonstrating enhanced solubility in this medium (**Figure 9**).

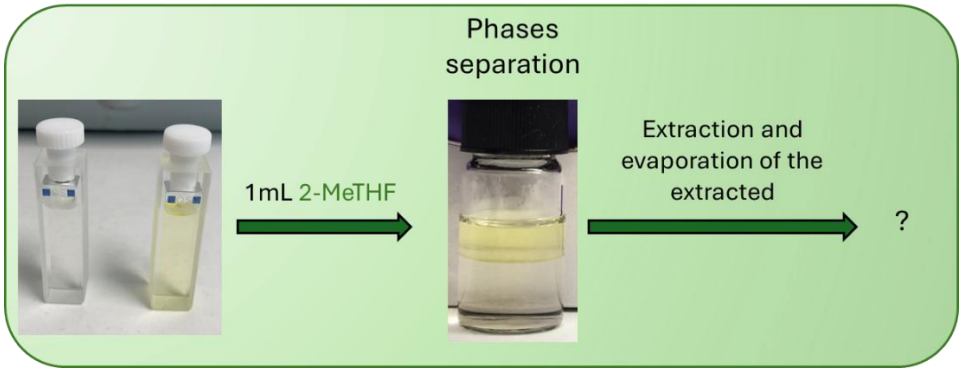

Figure 9. Schematic representation of the recovery strategy.

The initial strategy envisioned the separation of the organic layer, solvent removal, and subsequent characterization by infrared spectroscopy. The resulting spectrum was to be compared with that of a reference Cu(II)-salophen complex synthesized independently, in order to confirm structural integrity and successful extraction. However, the extremely limited quantity of recovered complex from the analysed solution rendered IR analysis impractical, as the sample mass was insufficient to generate a reliable spectrum.

Consequently, an alternative analytical approach was adopted, capable of confirming the presence of the copper(II)-salophen complex with minimal sample requirements. The organic phase was evaporated and subsequently analysed using electrospray ionization

mass spectrometry (ESI-MS). The resulting spectrum is reported in the Experimental section of this chapter.

This method unequivocally verified the presence of the target complex, providing direct evidence of its successful extraction into the 2-MeTHF phase and confirming the feasibility of recovering the complex from the post-UV reaction mixture.

This recovery experiment not only demonstrated the potential for reusing the complex, thus contributing to waste minimization, but also exemplifies the integration of green chemistry principles in both analytical methodology and solvent selection. By combining sustainable solvent use with sensitive mass spectrometric detection, it is possible to achieve both environmental responsibility and rigorous chemical validation, even when working with limited quantities of analyte.

The recovered complex, obtained through extraction into 2-MeTHF and confirmed by ESI-MS, presents opportunities for further utilization beyond analytical purposes, in the perspective of circular economy. In particular, such complexes are widely reported in the literature for catalytic applications,[41] highlighting the potential to valorise metal species recovered from aqueous media rather than discarding them as waste. This approach exemplifies a practical implementation of circular economy principles within chemical sensing and environmental remediation contexts.

4.2.5. Preparation of other ligands for future work

Future work could focus on the investigation of additional ligands, that has been already synthesized (**Table 6**), evaluating their potential use for metal detection, particularly in the context of environmental monitoring and hidden catalysis.

	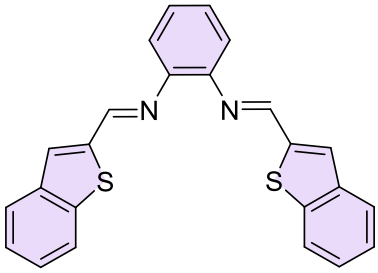	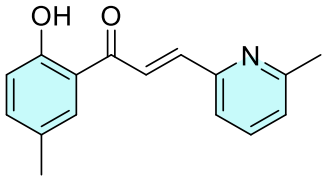
Isolated yield (%)	64	17
E-factor	1.5	26.8
PMI	2.5	96.0
RME (%)	58.8	16.2

Table 6. Chemical structure and results in terms of green chemistry metrics of ligands that can be further explored for green metal detection.

4.3. Conclusions

In conclusion, by demonstrating the effective colorimetric detection of copper ions using a sustainably designed sensor based on a well-known coordination system, this work proposes a paradigm in which sensor development is not driven solely by performance metrics such as sensitivity and selectivity, but also by environmental responsibility and long-term applicability. Such a tool can become instrumental for researchers in the field, offering a standardized method to assess and compare the sustainability of different sensor designs, by evaluating green attributes of the sensor system across several critical dimensions, including synthetic efficiency, use of non-toxic materials, solvent greenness in analytical procedures, energy consumption, and sensor reusability/regeneration. By quantifying and visualizing key environmental and practical parameters, it facilitates informed decision-making throughout the sensor development process, promoting the adoption of more sustainable practices.

In this sense, the study aims to serve as a model for the sustainable development of optical sensors, showing that established chemical systems can be reinterpreted and repurposed within a green chemistry framework to address contemporary challenges in environmental monitoring, analytical chemistry, and resource management.

The study could be subsequently further advanced through the investigation of the repeatability of the so-prepared system, especially the paper-based platform, that can be easily affected by environmental changes.

4.4 Experimental section

4.4.1. Materials

All glassware was cleaned using base (KOH, *i*-PrOH) and aqueous acid (HNO_3) baths. All reported reaction temperatures correspond to external bath temperatures. Substrates were purified using hexane and ethyl acetate on a gradient of 100:0 to 0:100 with flow rates of 10-110 mL min^{-1} depending on the size of column and ΔR_f. Reaction solvent ethanol (absolute, VWR) was used as received. Solvents for filtration, transfers, chromatography, and recrystallisation were dichloromethane (CH_2Cl_2) (ACS grade, amylene stabilised), ether (Et_2O) (Fisher, BHT stabilised ACS grade), ethyl acetate (EtOAc) (Fisher, ACS grade), hexane (Optima), methanol (MeOH) (ACS grade), 2-methyltetrahydrofuran (2-MeTHF), pentane (ACS grade), and hexane (40–60°C, ACS grade). Paper filter paper was purchased from Sigma Aldrich (Whatman). All reagents were purchased from Sigma Aldrich, Alfa Aesar, Acros Organics, Tokyo Chemical Industries UK, Fluorochem and Apollo Scientific, or synthesised within the laboratory. The precaution of wearing gloves was exercised when preparing heavy metal stock solutions to prevent exposure. All heavy metal waste was disposed of appropriately.

4.4.2. Instrumentation

^{1}H and ^{13}C NMR spectra were recorded on Bruker Avance III 400 and 500 MHz spectrometers. Chemical shifts are reported in parts per million (ppm). ^{1}H NMR spectra were referenced to the residual protonated solvent peak ($CHCl_3$: 7.26 ppm). ^{13}C NMR spectra were referenced to the solvent peak ($CDCl_3$: 77.00 ppm). Multiplicities are indicated by app. (apparent), br. (broad), s (singlet), d (doublet), t (triplet), q (quartet), quin. (quintet), sext. (sextet), hept. (heptet), oct. (octet), non. (nonet). Coupling constants, J, are reported in Hertz and rounded to the nearest 0.1 Hz. Integration is provided and assignments are indicated.

UV analysis was performed using Shimadzu UV-1900 UV Spectrophotometer. Mass spectrometry (MS) was performed by the University of Edinburgh, School of Chemistry. High resolution mass spectra were recorded on a VG autospec, or Thermo/Finnigan MAT 900, mass spectrometer. Electrospray Ionization (ESI^+) spectra were performed using a time-offlight (TOF) mass analyzer. Data are reported in the form of m/z (intensity relative to the base peak = 100). Analytical thin-layer chromatography was performed on aluminium-backed silica plates (Merck 60 F254). Product spots were visualised by UV light at 254 nm or staining with $KMnO_4$. Flash column chromatography was performed on silica gel (Merck Kielselgel 60, 40-63 μm) or if specified, carried out on a Teledyne ISCO CombiFlash NextGen 300+ using RediSep Rf normal phase silica flash columns (12, 25, 40, or 80 g; 20-40 microns).

4.4.3. Green Chemistry metrics calculation

The E-factor calculation had been extensively described in the Experimental section at the end of Chapter 2.

The process mass intensity (PMI) is defined as the ratio of the total mass of all input materials employed in a process to the mass of isolated product. It provides a comprehensive measure of material efficiency, as it accounts for reagents, solvents, and auxiliary substances used throughout the reaction and purification steps. In this work, PMI values were calculated including water, thereby offering a gross descriptor of the overall material consumption at laboratory scale.

General equation for the calculation of PMI:

$$PMI = \frac{Mass\ of\ all\ input\ materials\ (g)}{Mass\ of\ product\ (g)}$$

The Reaction Mass Efficiency (RME) assesses how efficiently the reactants are incorporated into the final product, thereby indicating the intrinsic material efficiency of the reaction.

General equation for the calculation of RME:

$$RME = \frac{Mass\ of\ the\ product\ (g)}{Mass\ of\ reagents\ (g)} * 100$$

The organic solvents used in the processes are recovered and reused as described in the Experimental section at the end of Chapter 2.

4.4.4. Synthesis, Green Chemistry metrics calculation and characterization of 6,6'-((1E,1'E)-(1,2-phenylenebis(azaneylylidene))bis(methaneylylidene))bis(3-methylphenol)

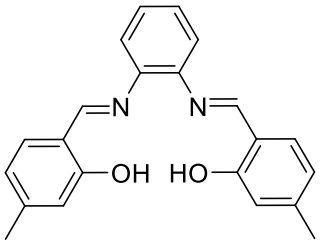

Ethanol procedure: according to a reported procedure,[31] a solution of 2-hydroxy-4-methylbenzaldehyde (2 mmol, 0.272 g) in 5 mL of absolute ethanol was added dropwise to a solution of *o*-phenylenediamine (1 mmol, 0.108 g) in 5 mL of absolute ethanol. The reaction mixture was heated under reflux for 5 hours. The mixture was cooled at room temperature to form a precipitate that was filtered, washed with ethanol (1 mL) and dried. The resulting compound was recrystallized from ethanol (2 mL) to yield the target product as a bright orange solid (0.208 g, 0.6 mmol, 60%).

Glycerol procedure, first cycle: 2-hydroxy-4-methylbenzaldehyde (2 mmol, 0.272 g) and *o*-phenylenediamine (1 mmol, 0.108 g) were added in a vial. Glycerol (1 mL) was then added. The reaction mixture was heated at 85 °C for 5 hours. The mixture was cooled at room temperature to form a precipitate that was filtered, washed with water (1 mL) and dried. The resulting compound was recrystallized from ethanol (5 mL) to yield the target product as a bright orange solid (first cycle: 0.321 g, 0.93 mmol). For the second and third cycle, after removing water through vacuum distillation, the recovered glycerol was reused in subsequent reactions giving the target product as a bright orange solid (second cycle: 0.309 g, 0.9 mmol, 90%; third cycle: 0.312 g, 0.91 mmol, 91%). ^{1}H NMR (500 MHz, $CDCl_3$)13.03 (s, 2H, OH), 8.60 (s, 2H, -CH=N), 7.35 – 7.31 (m, 2H, arom. CH), 7.28 (bs, 2H, arom. CH), 7.25 – 7.21 (m, 2H, arom. CH), 6.87 (bs, 2H, arom. CH), 6.75 (d, J = 7.8 Hz, 2H, arom. CH), 2.37 (s, 6H, CH_3) ppm. ^{13}C NMR (126 MHz, $CDCl_3$) 163.5, 161.51, 144.65, 142.82,

132.31, 127.52, 120.31, 119.93, 118.0, 117.16, 22.08 ppm. HRMS (ESI^+) Calcd for $C_{22}H_{20}N_2O_2$ = 344.15; Found 345.15975.

E-factor calculation

Ethanol procedure

Chemical	**Volume (mL)**	**Density (g/mL)**	**Mass (g)**	**Mass considered in the E-factor calculation with 90% solvent recovery (g)**
2-hydroxy-4-methylbenzaldehyde			0.272	
o-phenylenediamine			0.108	
EtOH	13	0.789	10.257	1.0257

Amount of product = 0.208 g (60% yield)

E-factor = 50.14

E-factor (including 90% solvent recovery by vacuum distillation) = 5.8

PMI = 6.8

RME = 54.7%

Glycerol procedure

	Chemical	**Volume (mL)**	**Density (g/mL)**	**Mass (g)**	**Mass considered in the E-factor calculation with**

					90% solvent recovery (g)
First cycle	2-hydroxy-4-methylbenzaldehyde			0.272	
	o-phenylenediamine			0.108	
	Glycerol	1	1.26	1.26	
	Water	1	1.0	1.0	0.1
	EtOH	5	0.789	3.945	0.3945
Second cycle	2-hydroxy-4-methylbenzaldehyde			0.272	
	o-phenylenediamine			0.108	
	Water	1	1.0	1.0	0.1
	EtOH	5	0.789	3.945	0.3945
Third cycle	2-hydroxy-4-methylbenzaldehyde			0.272	
	o-phenylenediamine			0.108	
	Water	1	1.0	1.0	0.1
	EtOH	5	0.789	3.945	0.3945

First cycle:

Amount of product = 0.321 g (93% yield)

E-factor (including 90% solvent recovery by vacuum distillation) = 5.3

PMI = 6.7

RME = 84.5%

Second cycle:

Amount of product = 0.309 g (90% yield)

E-factor (including 90% solvent recovery by vacuum distillation) = 1.5

PMI = 2.8

RME = 81.3%

Third cycle:

Amount of product = 0.312 g (91% yield)

E-factor (including 90% solvent recovery by vacuum distillation) = 1.5

PMI = 2.8

RME = 82.1%

^{1}H NMR (500 MHz, $CDCl_3$) Spectrum of 6,6'-((1E,1'E)-(1,2-phenylenebis(azaneylylidene))bis(methaneylylidene))bis(3-methylphenol)

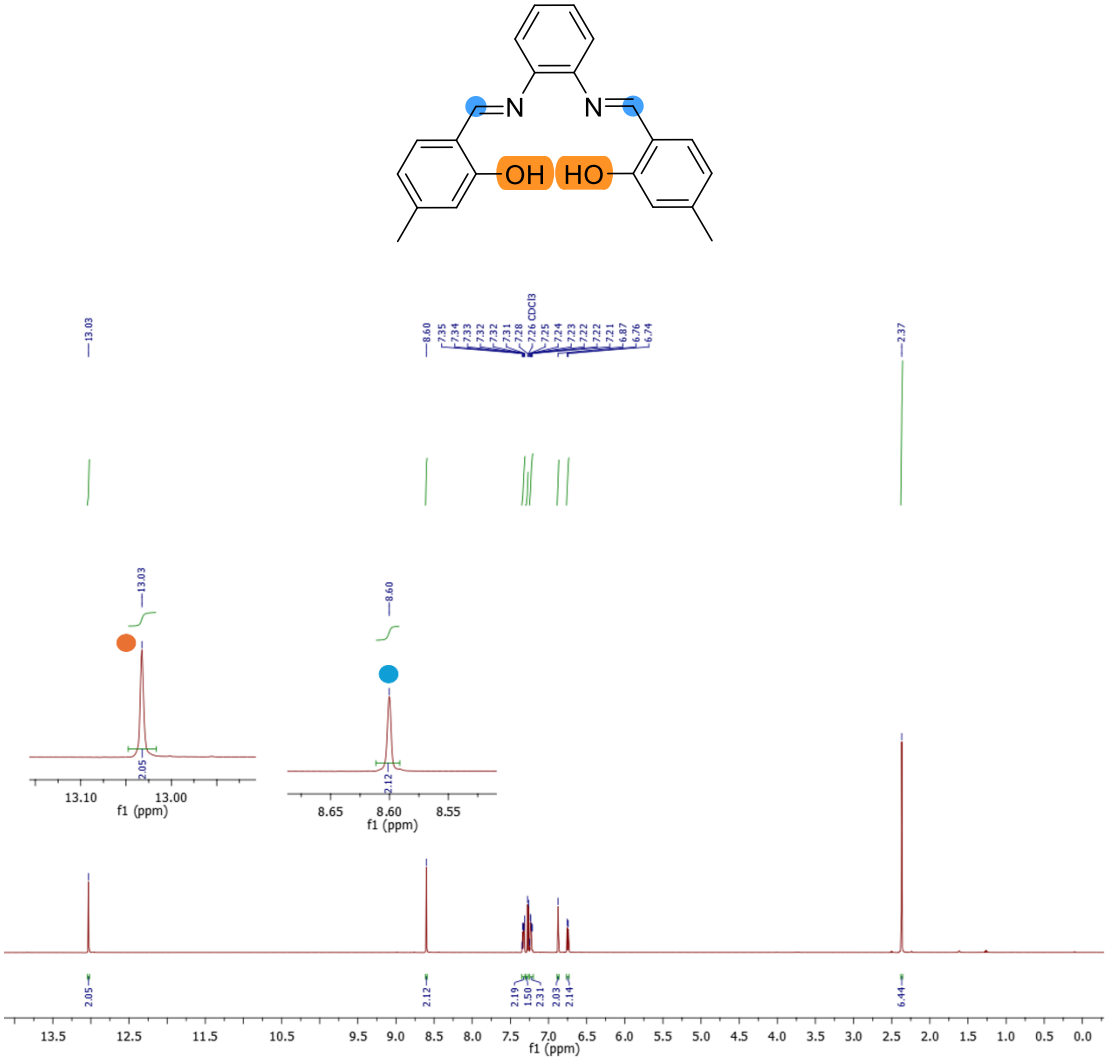

^{13}C NMR (126 MHz, $CDCl_3$) Spectrum of 6,6'-((1E,1'E)-(1,2-phenylenebis(azaneylylidene))bis(methaneylylidene))bis(3-methylphenol)

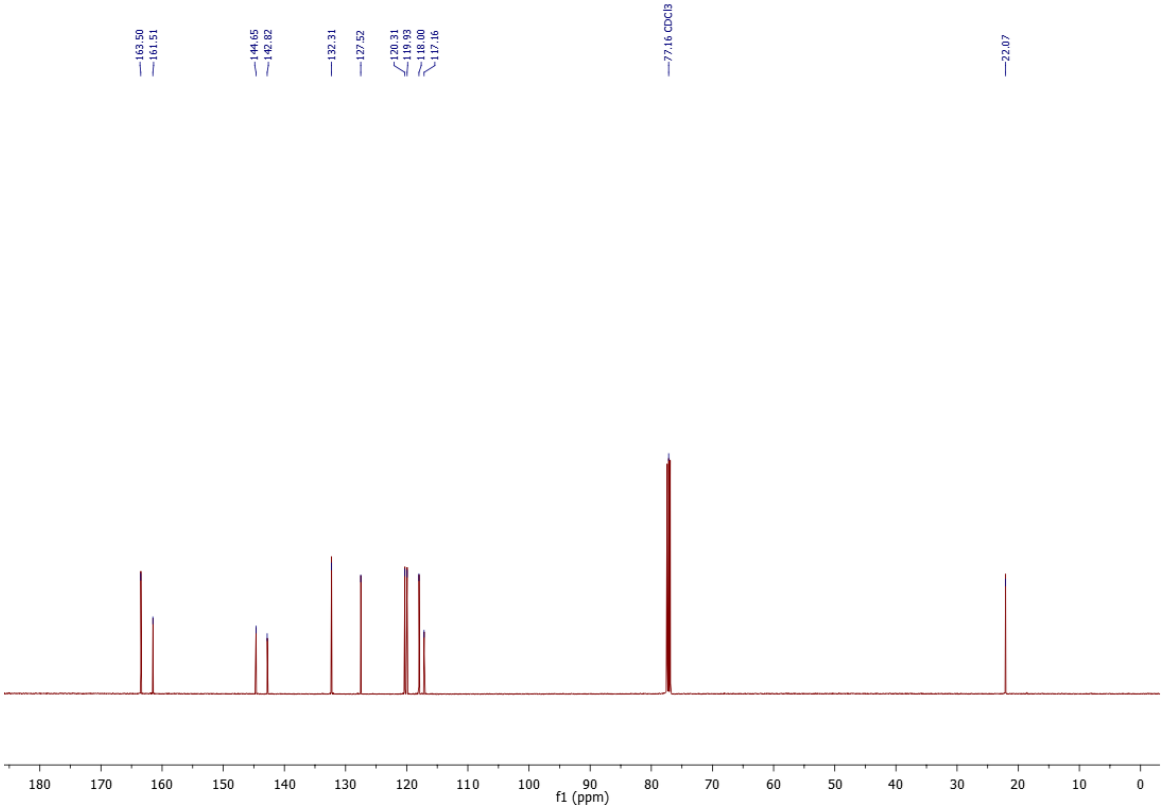

Mass spectra of (1E,1'E)-N,N'-(1,2-phenylene)bis(1-(benzo[b]thiophen-2-yl)methanimine)

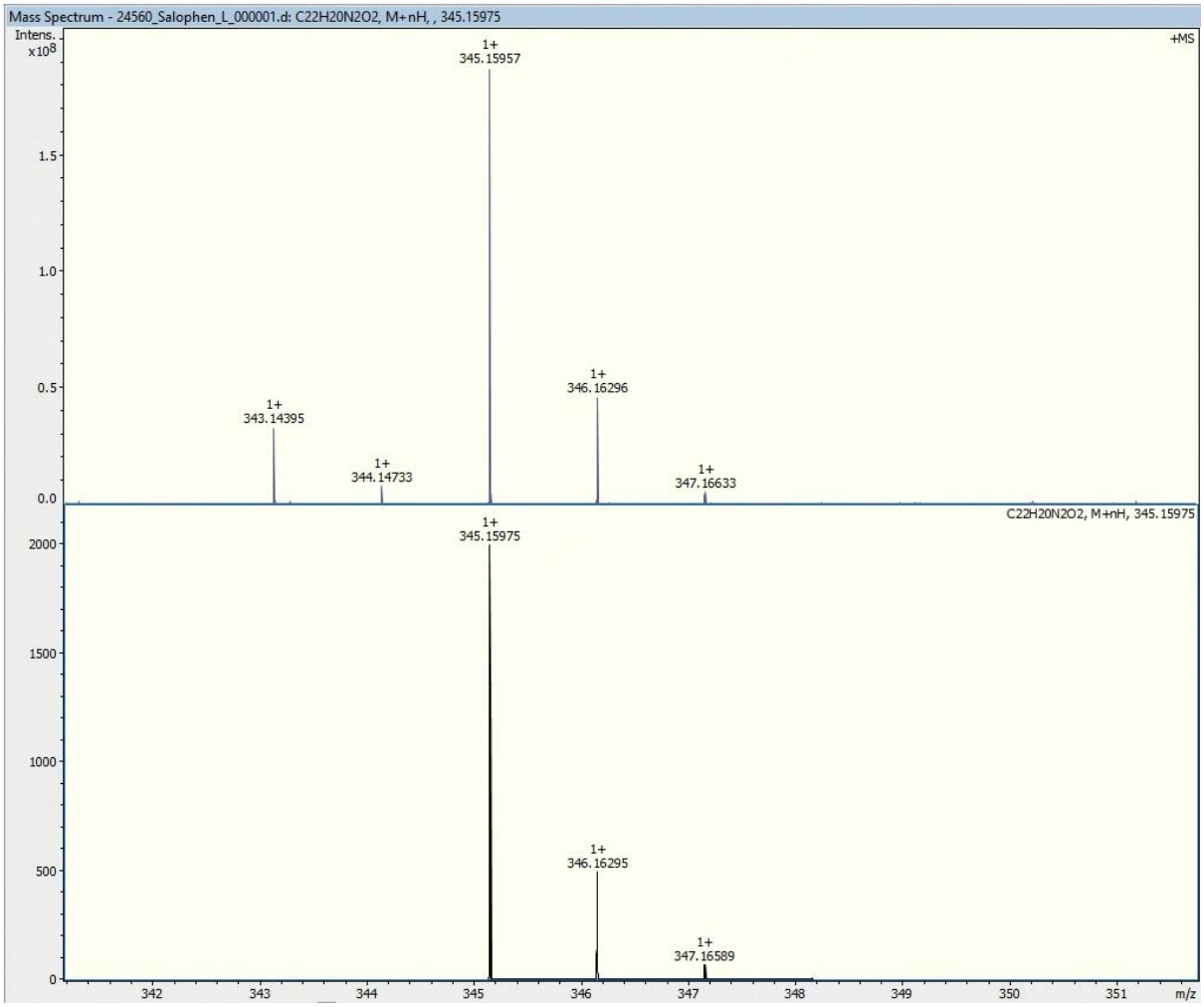

Mass spectra of the complex (1E,1'E)-N,N'-(1,2-phenylene)bis(1-(benzo[b]thiophen-2-yl)methanimine) - Copper(II)

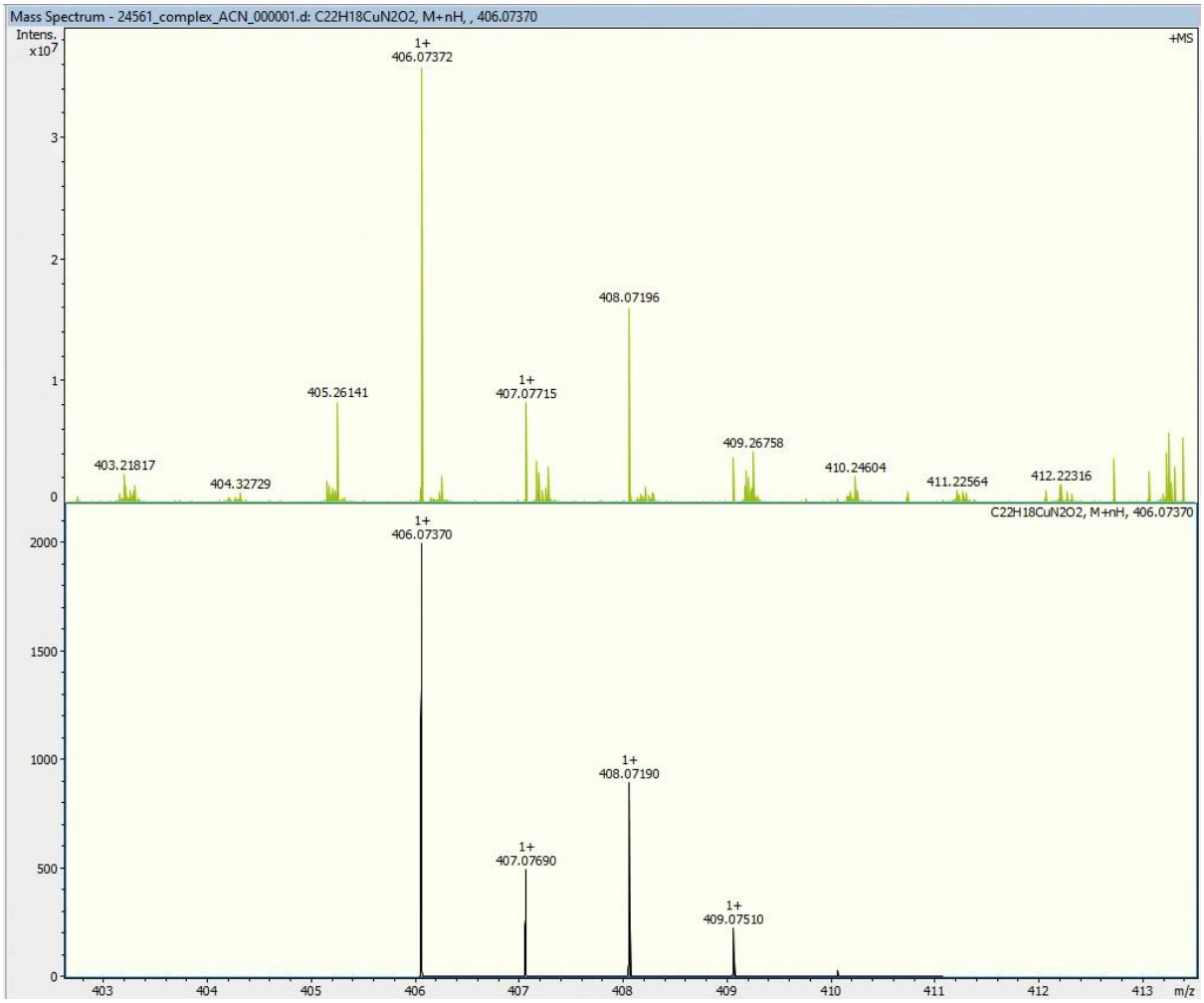

4.4.5. Synthesis, Green Chemistry metrics calculation and characterization of (1E,1'E)-N,N'-(1,2-phenylene)bis(1-(benzo[b]thiophen-2-yl)methanimine)

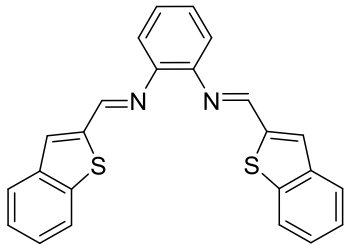

Benzo[b]thiophene-2-carbaldehyde (4 mmol, 0.648 g) and *o*-phenylenediamine (2 mmol, 0.216 g) were combined in a vial and stirred at 35 °C for 3 h. The resulting solid was then dried under reduced pressure and subsequently recrystallized from methanol (5 mL) giving the target product as a yellow solid (0.508 g, 1.28 mmol, 64%). ^{1}H NMR (500 MHz, $CDCl_3$) 8.75 (s, 2H), 7.85 (dd, J = 7.8, 0.8 Hz, 2H), 7.81 (dd, J = 6.9, 1.3 Hz, 2H), 7.69 (s, 2H), 7.41 – 7.35 (m, 4H), 7.27 (s, 4H) ppm. ^{13}C NMR (126 MHz, $CDCl_3$) 155.40, 143.83, 143.43, 141.50, 139.63, 129.38, 126.93, 126.43, 124.90, 124.75, 123.03, 121.91 ppm.

E-factor calculation

Chemical	**Volume (mL)**	**Density (g/mL)**	**Mass (g)**	**Mass considered in the E-factor calculation with 90% solvent recovery (g)**
benzo[b]thiophene-2-carbaldehyde			0.648	
o-phenylenediamine			0.216	
MeOH	5	0.792	3.96	0.396

Amount of product = 0.508 g (64% yield)

E-factor (including 90% solvent recovery by vacuum distillation) = 1.5

PMI = 2.5

RME = 58.8%

^{1}H NMR (500 MHz, $CDCl_3$) Spectrum of (1E,1'E)-N,N'-(1,2-phenylene)bis(1-(benzo[b]thiophen-2-yl)methanimine)

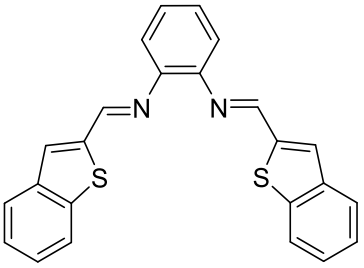

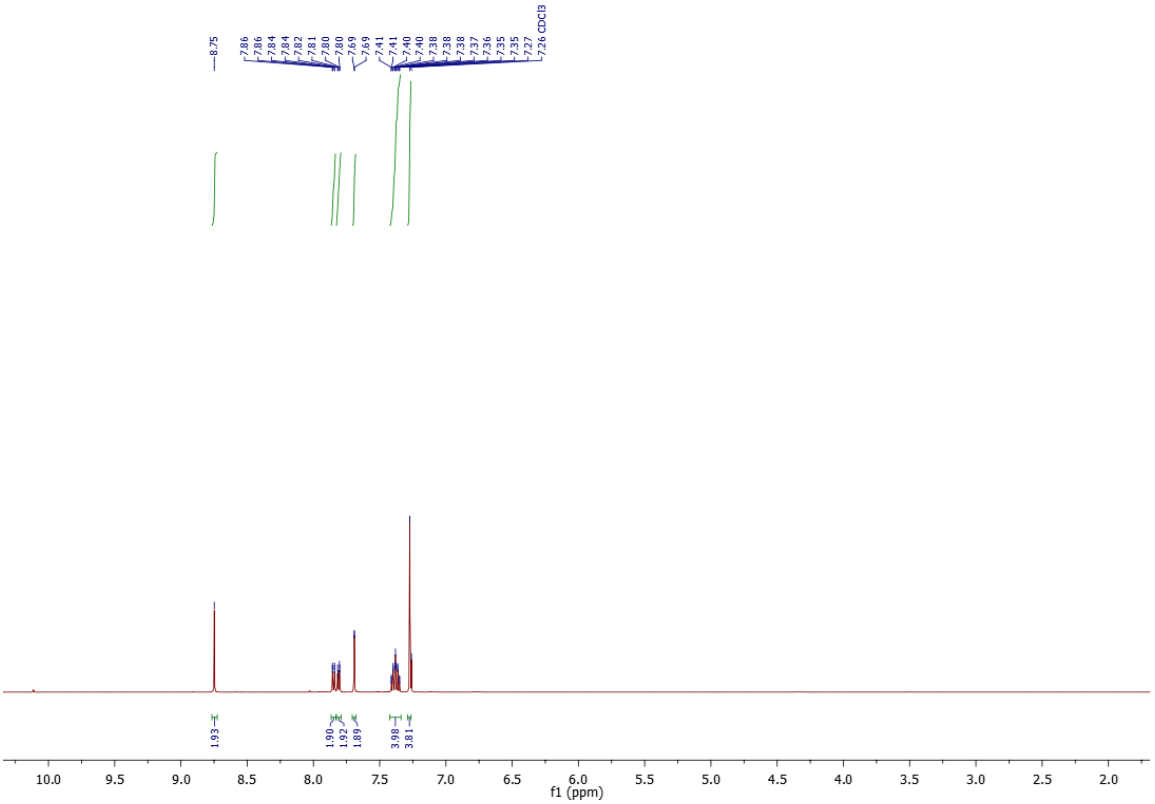

^{13}C NMR (126 MHz, $CDCl_3$) Spectrum of (1E,1'E)-N,N'-(1,2-phenylene)bis(1-(benzo[b]thiophen-2-yl)methanimine)

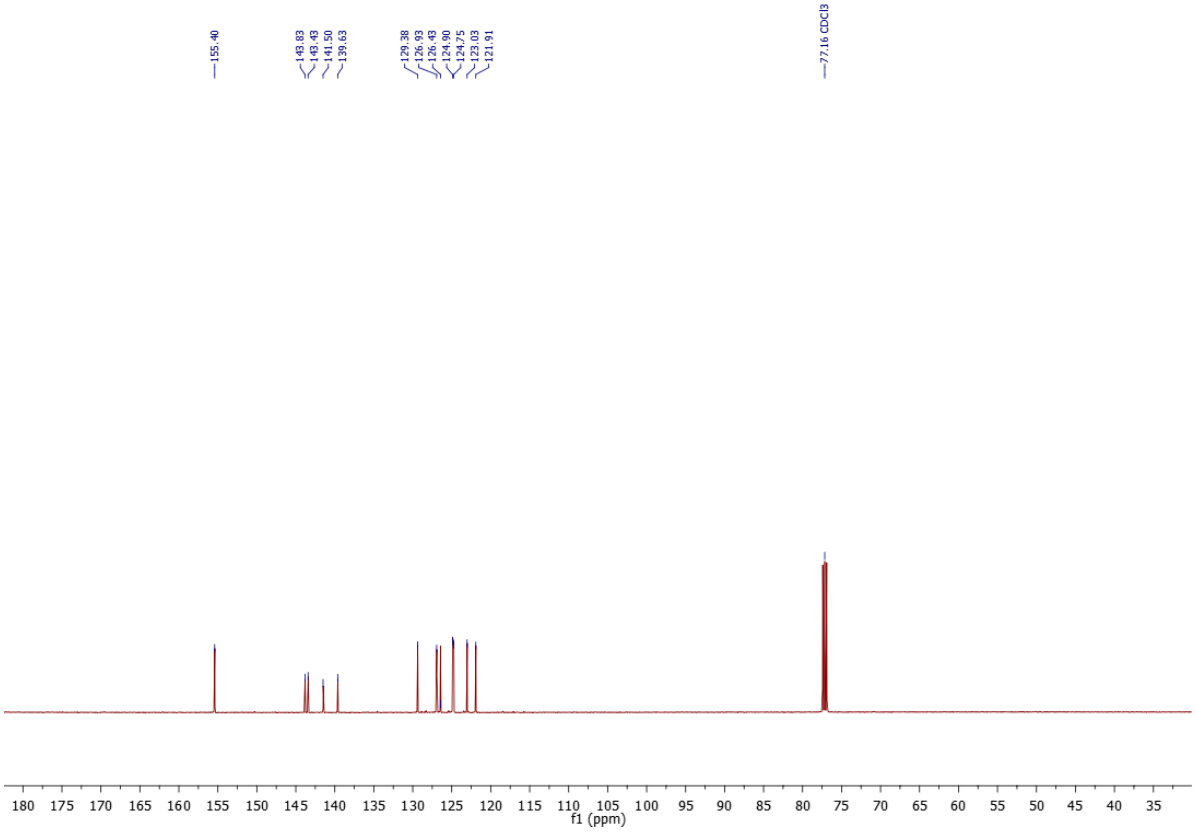

4.4.6. Synthesis, Green Chemistry metrics calculation and characterization of (E)-1-(2-hydroxy-5-methylphenyl)-3-(6-methylpyridin-2-yl)prop-2-en-1-one

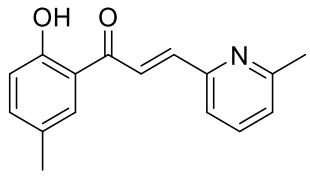

6-methylpicolinaldehyde (1 mmol, 0.121 g) and 1-(2-hydroxy-5-methylphenyl)ethan-1-one (1 mmol, 0.150 g) were ground together with sodium hydroxide (0.85 mmol, 0.034 g) in a mortar for 15 minutes. The reaction mixture was then treated with EtOAc and washed with HCl 3M, and dried over Na_2SO_4. The product was obtained as an orange solid (0.044 g, 0.17 mmol, 17%). ^{1}H NMR (500 MHz, $CDCl_3$) 12.61 (s, 1H), 8.21 (d, J = 15.1 Hz, CH=CH), 7.83 (d, J = 15.1 Hz, 2H), 7.64 (t, J = 7.7 Hz, 1H), 7.33 – 7.30 (m, 2H), 7.18 (dd, J = 7.8, 1.1 Hz, 1H), 6.93 (d, J = 8.4 Hz, 1H), 2.65 (s, 3H), 2.36 (s, 3H) ppm. ^{13}C NMR (126 MHz, $CDCl_3$) 194.27, 161.74, 159.37, 152.39, 143.73, 137.84, 137.15, 130.10, 128.13, 124.68, 123.94, 123.17, 119.91, 118.38, 24.86, 20.72 ppm.

E-factor calculation

Chemical	**Volume (mL)**	**Density (g/mL)**	**Mass (g)**	**Mass considered in the E-factor calculation with 90% solvent recovery (g)**
6-methylpicolinaldehyde			0.121	
1-(2-hydroxy-5-methylphenyl)ethan-1-one			0.150	

NaOH			0.034	
HCl 3M	3	1.0	3.0	
Ethyl acetate	10	0.902	9.02	0.902
Na_2SO_4			0.015	

Amount of product = 0.044 g (17% yield)

E-factor (including 90% solvent recovery by vacuum distillation) = 26.8

PMI = 96.0

RME = 16.2%

^{1}H NMR (500 MHz, $CDCl_3$) Spectrum of (E)-1-(2-hydroxy-5-methylphenyl)-3-(6-methylpyridin-2-yl)prop-2-en-1-one

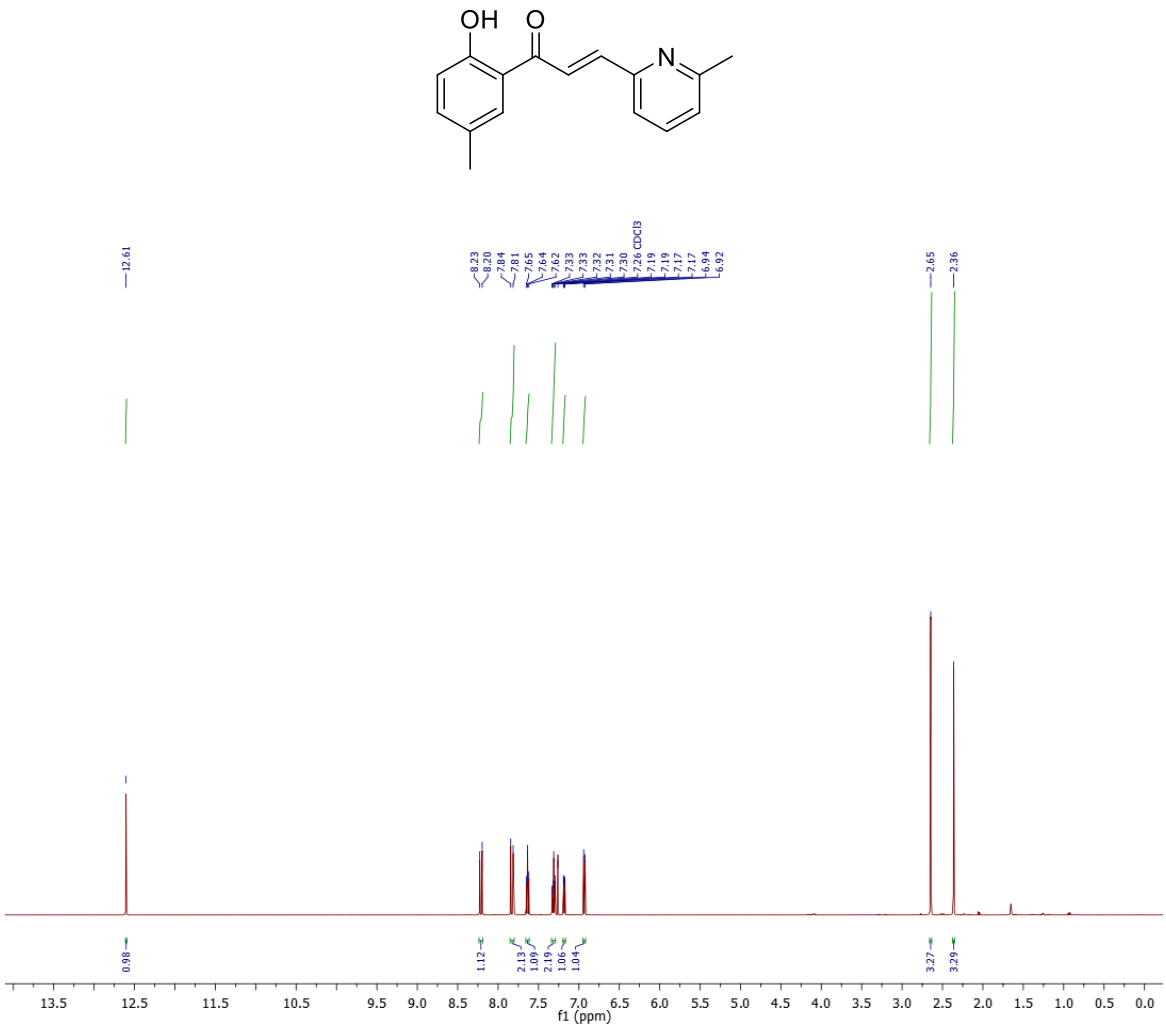

^{13}C NMR (126 MHz, $CDCl_3$) Spectrum of (E)-1-(2-hydroxy-5-methylphenyl)-3-(6-methylpyridin-2-yl)prop-2-en-1-one

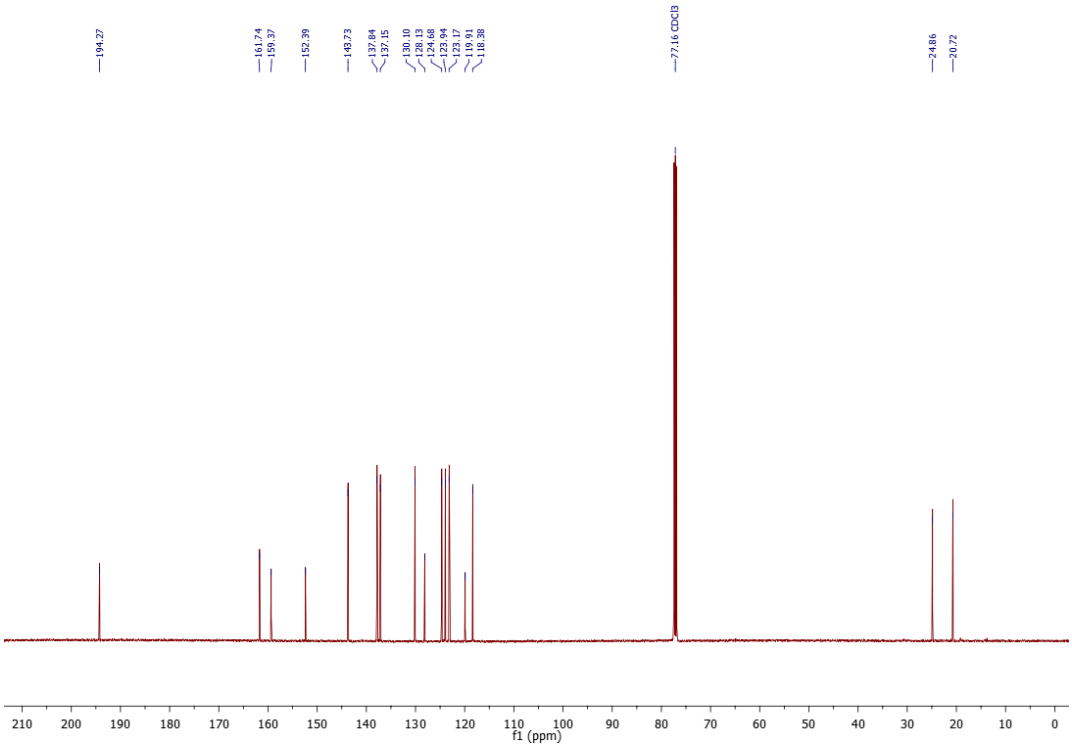

4.5. Bibliography

1. Machín, A. & Màrquez, F. Next-Generation Chemical Sensors : The Convergence of Nanomaterials , Advanced Characterization , and Real-World Applications. *Chemosensors* **13**, 345–389 (2025).
2. Ondrasek, G., Shepherd, J., Rathod, S. & Dharavath, R. Metal contamination - a global environmental issue: sources, implications and advances in mitigation. *RSC Adv.* **15**, 3904–3927 (2025).
3. Ali, H., Khan, E. & Ilahi, I. Environmental Chemistry and Ecotoxicology of Hazardous Heavy Metals : Environmental Persistence,Toxicity, and Bioaccumulation. *J. Chem.* 6730305 (2019).
4. Langari, M. M., Lvova, L., Paolesse, R. & Labidi, J. The Development of Optical Sensors for Heavy Metal Ions detection on Nanocellulose substrate. *EuroSensors* 356–357.
5. Bedford, R. B. *et al.* Iron-catalysed Suzuki coupling ? A cautionary tale. *Tetrahedron Lett.* **50**, 6110–6111 (2009).
6. Macleod, J. & Thomas, S. P. Colorimetric indication of hidden catalysis. *Nat. Chem.* **18**, 173–180 (2026).
7. Arvela, R. K. *et al.* A Reassessment of the Transition-Metal Free Suzuki-Type Coupling Methodology. *J. Org. Chem.* **70**, 161–168 (2005).
8. Buchwald, S. L. & Bolm, C. On the Role of Metal Contaminants in Catalyses with Fe_3Cl_3. *Angew. Chemie - Int. Ed.* **48**, 5586–5587 (2009).
9. Arancon, R. A. D., Ki, S. & Luque, R. To be or not to be metal-free : trends and advances in coupling chemistries. *Org. Biomol. Chem.* **12**, 10–35 (2014).
10. Rasheed, T. *et al.* Fluorescent sensor based models for the detection of environmentally-related toxic heavy metals. *Sci. Total Environ.* **615**, 476–485 (2018).
11. Polvani, A. *et al.* Colourimetric membrane sensor technologies for heavy metal monitoring in freshwater. *Sens. Diagn.* **5**, 326–336 (2026).
12. Carneiro, M. C. C. G., Rodrigues, L. R., Moreira, F. T. C. & Sales, M. G. F. Colorimetric Paper-Based Sensors against Cancer Biomarkers. *Sensors* **22**, 3221–3257 (2022).
13. Bastami, T. R., Bayat, M. & Paolesse, R. Naked-EyeDetection of Morphine by Au@AgNanoparticles-Based Colorimetric Chemosensors. *Sensors* **22**, 2072–2091 (2022).
14. Festa, R. A. & Thiele, D. J. Copper : An essential metal in biology. *Curr. Biol.* **21**,

R877–R883 (2011).

15. Poggere, G. *et al.* Soil contamination by copper : Sources , ecological risks , and mitigation strategies in Brazil. *J. Trace Elem. Miner.* **4**, 100059–100073 (2023).

16. Clearwater, S. J., Farag, A. M. & Meyer, J. S. Bioavailability and toxicity of dietborne copper and zinc to fish. *Comp. Biochem. Physiol. Part C* **132**, 269–313 (2002).

17. Binesh, A. & Venkatachalam, K. Copper in Human Health and Disease : A Comprehensive Review. *J. Biochem. Mol. Toxicol.* **38**, e70052 (2024).

18. Kumar, A. & Maiti, P. Paper-based sustainable biosensors. *Mater. Adv.* **5**, 3563–3586 (2024).

19. Tian, Y. & Olivetti, E. A. Strategies for industrial residue valorization through metal recovery , use in construction , or CO_2 mineralization. *Waste Manag.* **203**, 114824 (2025).

20. Reena, V. N., Kumar, K. S. & Nithyaja, B. Design and development of a Schiff base – based sensor aiding different spectroscopic techniques for metal ion detection via optical and Raman methods. *J. Photochem. Photobiol.* **31**, 100275 (2026).

21. Barreras-contreras, L. A. *et al.* Schiff Bases and Metal Complexes as Multifunctional Platforms : Bridging Bioinorganic Chemistry , Catalysis , Sensing , and Energy Applications. *Bioinorg. Chem. Appl.* **2025**, 8829417 (2025).

22. You, G. R., Park, G. J., Lee, J. J. & Kim, C. A colorimetric sensor for the sequential detection of Cu^{2+} and CN^- in fully aqueous media: practical performance of Cu^{2+}. *Dalt. Trans.* **44**, 9120–9129 (2015).

23. Shaghaghi, Z., Kheyrollahpoor, M. & Haeili, M. Optical , electrochemical , thermal , biological and theoretical studies of some chloro and bromo based metal-salophen complexes. *J. Mol. Struct.* **1200**, 127107–127121 (2020).

24. Gu, Y. & Jérome, F. Glycerol as a sustainable solvent for green chemistry. *Green Chem.* **12**, 1127–1138 (2010).

25. Wolfson, A., Snezhko, A., Meyouhas, T. & Tavor, D. Glycerol derivatives as green reaction mediums. *Green Chem. Lett. Rev.* **5**, 7–12 (2012).

26. Raglione, V., Palmeri, F., Mattioli, G. & Porcelli, F. Glycerol as Reaction Medium for Sonogashira Couplings : A Green Approach for the Synthesis of New Triarylamine-Based Materials with Potential Application in Optoelectronics. *Chem. - A Eur. J.* **30**, 1–10 (2024).

27. Gu, Y., Barrault, J. & Jérome, F. Trapping of Active Methylene Intermediates with Alkenes , Indoles or Thiols : Towards Highly Selective Multicomponent. *Adv. Synth. Catal.* **351**, 3269–3278 (2009).

28. Hum, G. *et al.* Multigram Mechanochemical synthesis of a Salophen Complex: A

Comparative Analysis. *ACS Sustain. Chem. Eng.* **9**, 1152–1160 (2021).

29. Leon, F. *et al.* Mechanosynthesis and photophysics of colour-tunable photoluminescent group 13 metal complexes with sterically demanding salen and salophen ligands. *Faraday Discuss.* **241**, 63–78 (2023).

30. Hessel, V. *et al.* Quantitative Sustainability Assessment of Flow Chemistry − From Simple Metrics to Holistic Assessment `. *ACS Sustain. Chem. Eng.* **9**, 9508–9540 (2021).

31. Jiang, N. *et al.* Design , synthesis and evaluation of multifunctional salphen derivatives for the treatment of Alzheimer ' s disease. *Eur. J. Med. Chem.* **87**, 540–551 (2014).

32. Buchwald, S. L. & Bolm, C. On the Role of Metal Contaminants in Catalyses with FeCl3. *Angew. Chemie - Int. Ed.* **48**, 5586–5587 (2009).

33. Li, T., Zhu, X., Hai, X., Bi, S. & Zhang, X. Recent Progress in Sensor Arrays: From Construction Principles of Sensing Elements to Applications. *ACS Sensors* **8**, 994–1016 (2023).

34. Korotcenkov, G. Paper-Based Sensors : Fantasy or Reality? *Nanomaterials* **15**, 89–126 (2025).

35. Meza Lòpez, F. de L. *et al.* Smartphone-Based Rapid Quantitative Detection Platform with Imprinted Polymer for Pb (II) Detection in Real Samples. *Polymers* **16**, 1523–1541 (2024).

36. Ratnarathorn, N., Chailapakul, O., Henry, C. S. & Dungchai, W. Simple silver nanoparticle colorimetric sensing for copper by paper-based devices. *Talanta* **99**, 552–557 (2012).

37. Ye, Y., Lv, M., Zhang, X. & Zhang, Y. Colorimetric determination of copper(II) ions using gold nanoparticles as a probe. *RSC Adv.* **5**, 102311–102317 (2015).

38. Chai, W. *et al.* Gold Nanoparticle-Based Probe for Colorimetric Detection of Copper Ions. *J. Nanosci. Nanotechnol.* **17**, 502–506 (2017).

39. Tjandra, A. D., Heywood, T. & Chandrawati, R. Trigit : A free web application for rapid colorimetric analysis of images. *Biosens. Bioelectron. X* **14**, 100361–100375 (2023).

40. López-Marzo, A. M. & Merkoçi, A. Paper-based sensors and assays: a success of the engineering design and the convergence of knowledge areas. *Lab Chip* **16**, 3150–3176 (2016).

41. Abbaspour, S., Keivanloo, A., Bakherad, M. & Sepehri, S. Salophen Copper (II) Complex-Assisted Click Reactions for Fast Synthesis of 1 , 2 , 3-Triazoles Based on Naphthalene-1 , 4-dione Scaffold , Antibacterial Evaluation , and Molecular Docking Studies. *Chem. Biodivers.* **16**, e1800410 (2019).

Chapter 5. Sustainable organometallic catalysis

5.1. Introduction

5.1.1. Earth-Abundant metals in green organic synthesis

This chapter will focus on the second part of the work conducted during my visiting PhD period at the University of Edinburgh.

The increasing global awareness of environmental challenges and resource limitations has profoundly reshaped the priorities of modern chemical research. Within this evolving scenario, organic synthesis faces the urgent task of combining efficiency and molecular complexity with environmental responsibility and human health protection. Traditional synthetic methodologies often rely on stoichiometric reagents, hazardous solvents, and precious transition metals; all of which are increasingly incompatible with the principles of sustainable development. As a result, the search for alternative strategies that minimize waste generation, reduce toxicity, and improve resource efficiency has become a central objective in contemporary synthetic chemistry.

In this context, catalysis represents one of the most powerful tools for green chemistry. By replacing classical stoichiometric processes with catalytic methodologies, it becomes possible to dramatically enhance atom economy, decrease energy consumption, and limit the production of undesired by-products.[1] Catalytic systems enable the selective activation and transformation of substrates under more mild conditions, thereby reducing both environmental impact and operational costs. The development of innovative catalytic strategies is therefore not merely an academic pursuit, but a necessary step towards a more sustainable chemical industry.

A key challenge in advancing sustainable catalysis lies in the choice of the metal(s) used. Historically, many highly efficient catalytic transformations have relied on Platinum Group

Metals (PGMs), such as palladium, rhodium, iridium, and platinum. While these metals offer remarkable reactivity and selectivity, their scarcity, high cost, and potential toxicity pose significant environmental and economic concerns. Furthermore, the extraction and disposal of PGMs are associated with substantial ecological and geopolitical burdens, rendering their large-scale application increasingly problematic in the long term.[2]

In light of this, in recent years impressive efforts have been devoted to developing new catalytic systems based on Earth-abundant elements, particularly first-row transition metals such as iron, manganese, titanium, and aluminium. These metals are characterized by natural abundance, lower toxicity, reduced environmental footprint in sourcing and disposal, and significantly lower costs compared to PGMs. Beyond these sustainability advantages, first-row transition metals exhibit unique electronic structures and reactivity profiles that open new opportunities for catalytic innovation.[3] In this context, the identification and implementation of catalytic platforms based on Earth-abundant elements offer a tangible strategy to address the sustainability concerns associated with precious metals. Moreover, the transition away from PGM catalysts not only mitigates environmental and economic limitations, but also unlocks complementary reactivity patterns, enabling bond disconnections that are inefficient or, in some cases, unattainable with current systems.[3] Direct C–H functionalisation reactions have emerged as a particularly attractive target for investigation in sustainable synthesis. By allowing the selective transformation of inert C–H bonds into C–C or C–X bonds, these reactions provide a powerful means to efficiently increase molecular complexity and with minimal waste and effort.[4]

Recent research has focused on the development of methods using Earth-abundant metals in place of precious-metals as catalysts. Manganese-based systems, in particular, have demonstrated promising reactivity in the activation and functionalisation of arene C–H bonds. Nevertheless, and despite the remarkable results, these systems still present significant challenges in modern organometallic chemistry, as they often require the presence of a directing group to achieve regioselectivity, limiting their generality and practical applicability. [5]

Such selectivity could be obtained by carefully tuning the metal centre, ligand environment, and reaction conditions to exploit the subtle electronic and steric differences between C−H bonds, and success in this area would not only enhance the efficiency of molecular synthesis but also align directly with green chemistry principles by minimizing waste, avoiding excess reagents, and reducing the number of synthetic steps.

Aryl boronic acids (Ar–$B(OH)_2$) and aryl boronic esters (Ar–$B(OR)_2$) are bench-stable and highly versatile intermediates that have become key building blocks in modern organic synthesis.[6] Their utility was first demonstrated in the Suzuki–Miyaura cross-coupling reaction, enabling the efficient formation of $C(sp^2)$–$C(sp^2)$ bonds. Over time, their applications have expanded since organoboron compounds are widely used as synthetic intermediates and C–H bond functionalization offers numerous potential applications in the preparation of fine chemicals. C–H bond functionalization provides a versatile platform for modifying aromatic C–H bonds in numerous ways (**Figure 1**). In particular, the products obtained from aromatic C–H borylation can serve not only as key intermediates for cross-coupling reactions, but also as a platform for a series of different functionalization, enabling the conversion of arenes into phenols, amines, when followed by additional steps or work-ups, as well as to regioselective halogenation, among the others.[7] This unique versatility, combined with stability, and ease of handling, has made the development of efficient synthetic routes to aryl boronic esters a topic of continuous interest.

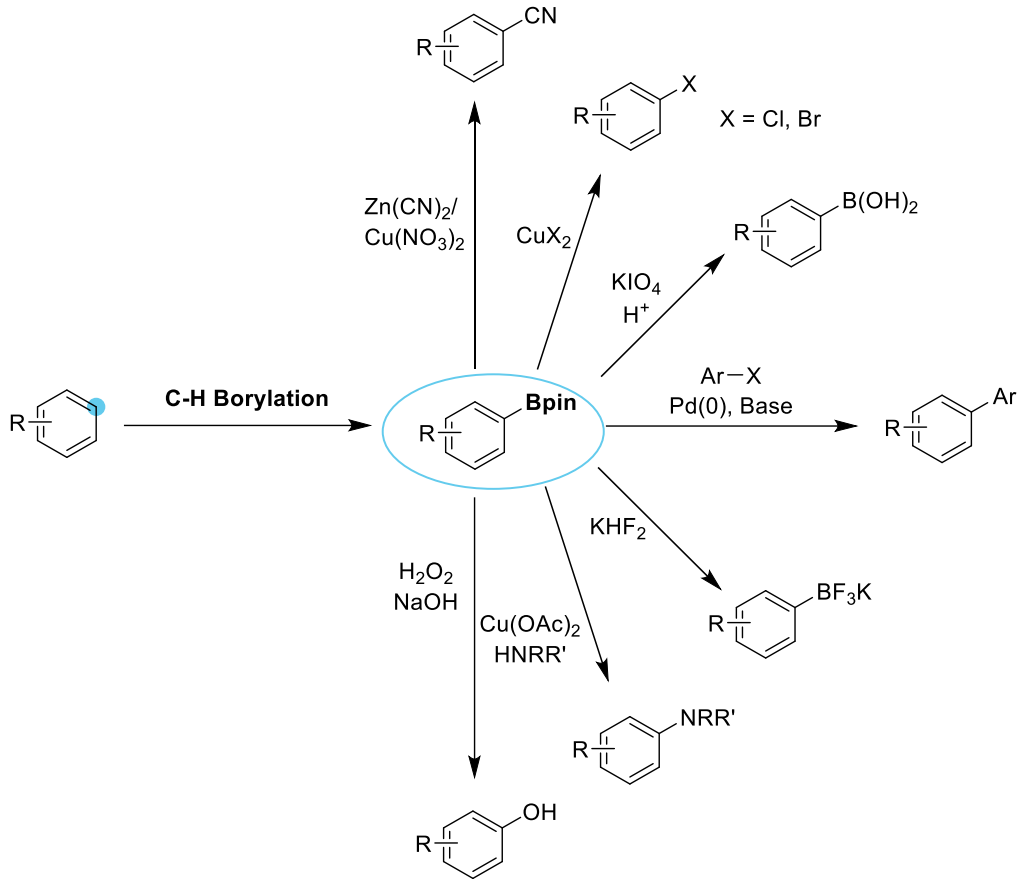

Figure 1. Key examples of the versatility of aryl boronic esters in organic synthesis.

Traditionally, aryl boronic esters were synthesized by the reaction of organometallic reagents, such as Grignard or organolithium species, with boron electrophiles including trialkyl borates ($B(OR)_3$). Despite high regioselectivity, these procedures require stoichiometric amounts of air- and moisture-sensitive reagents, which limit functional group tolerance and pose operational hazards. Later, Miyaura introduced the palladium-catalyzed borylation of (pseudo)halides using bis(pinacolato)diboron (B_2pin_2), providing milder reaction conditions and improved practicality. Nonetheless, this approach remains constrained by the need for prefunctionalized halide substrates, as the site of borylation is predetermined by the halide position.

As far as alkenes are concerned, a viable way to achieve the corresponding borylated products is hydroboration, but this limits the applicability of the method to unsaturated substrates (**Scheme 1**).

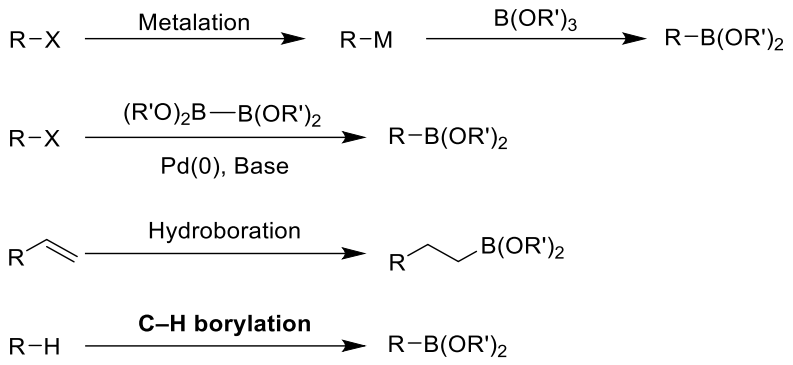

Scheme 1. Main synthetic routes to achieve aryl boronic esters from unsaturated substrates.

Besides these synthetic routes, direct C–H borylation has emerged as a more sustainable and atom-economical strategy, enabling the functionalization of C–H bonds without prior functionalization. This one-step process increases molecular complexity by activating typically inert and readily available hydrocarbons, that are thus used as direct feedstocks and converted into valuable functionalized compounds.[8]

As a result, during my visiting PhD period at the University of Edinburgh, I had the opportunity to be involved in the research project focused on the development and exploration of innovative strategies to advance catalytic systems based on Earth-abundant metals. In particular, the work aimed at enabling efficient and selective C–H activation of carbo- and heteroarenes in the absence of directing groups, while maintaining alignment with the principles of sustainable synthesis, remaining fully consistent with the objectives of this thesis and, more broadly, with those of the Rome Technopole Project. The results presented in the following section are part of a manuscript currently in preparation for submission.

5.1.2. Manganese-catalysed C–H borylation of arenes

The current state-of-the-art methods for direct C–H borylation typically use second- and third-row transition metal catalysts, most commonly ruthenium, rhodium, and iridium, with well-defined catalysts including [RuH_2(3-phenylindenyl)($SiEt_3$)], [Rh(PMe_3)$_2$(CO)Cl], and [Ir(Cl)(COD)]$_2$/Phenantroline, that present challenges related to cost, toxicity, and environmental impact, as well as concerns regarding long-term availability. Given the growing demand for more sustainable synthetic methodologies, it is imperative to identify viable alternatives to existing approaches. Although notable advances have been achieved in the development of cobalt-,[9] iron-,[10] and nickel-[11] based catalysts for C–H borylation, (**Figure 2**), manganese catalysts remain under explored in this field.

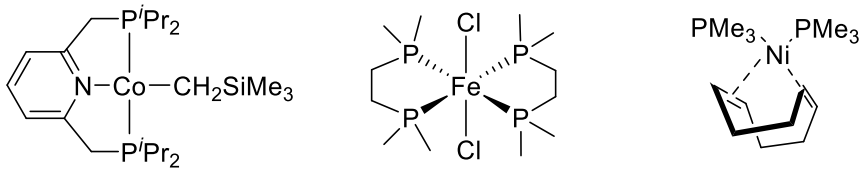

Chirik *et al.* **(2014)** Thomas *et al.* **(2020)** Li *et al.* **(2024)**

Figure 2. Examples of first-row transition metal catalysts used for C–H borylation.

Manganese is the third most abundant transition metal in the Earth's crust, so offers potential as a sustainable C–H borylation catalyst. This body of work highlights both the potential and the limitations of a new manganese-based system for C–H borylation, particularly regarding substrate scope, functional group tolerance, and the requirement for light activation.

Manganese-catalyzed systems for the C–H borylation of arenes remain scarce, with only few examples reported in the literature. Based on what has already been reported, it is well-

known that manganese complexes can mediate C–H borylation of carboarenes under stoichiometric or catalytic conditions with UV irradiation.[12] Recently, the application of a manganese-based catalyst was extended and validated for the borylation of heteroarenes such as furans and thiophenes under blue light irradiation.[13] Notwithstanding, such approaches required a large excess of the arene to achieve satisfactory reactivity and longer reaction times.[14] Furthermore, most notably, N-heteroarenes or substituted carboarenes were largely unreactive, and functional groups susceptible to reduction or halides were not tolerated.

5.2. Results and discussion

5.2.1. Investigation and optimization of reaction conditions

Taking advantage of the extensive experience of the Thomas group in the field,[13] the challenge was to design a practical and operationally simple manganese-based catalyst using bench-stable, commercially available reagents, with the carboarene as the limiting reagent, while assessing regioselectivity as well as functional group tolerance.

Preliminary studies conducted by Adrián Moreno González, a former PhD student in the Thomas group, had been carried out to establish a crossover between Mn-catalysed hydrogen isotope exchange (HIE) and C–H borylation before I joined the project. Based on their successful application in the catalytic HIE of arenes, several manganese hydride complexes [LMn(CO)$_3$H] were chosen for investigation as potential manganese-based catalysts for efficient C–H borylation. Starting from the initial reaction conditions reported by Thomas and co-workers for the borylation of furan and thiophene derivatives, employing blue light (460 nm) and a manganese-based catalyst, a model reaction was selected (**Scheme 2**).[13]

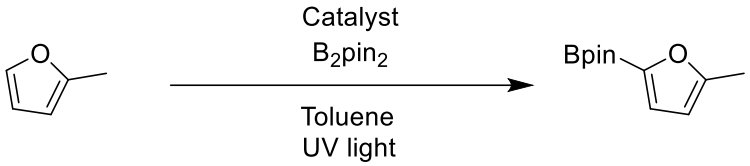

Scheme 2. Representative reaction under investigation. Conditions: 2-Methylfuran (0.2 mmol), B_2pin_2 (1.2 eq.), catalyst (10 mol%), toluene (0.5 mL), 32 °C, 24 h, UV light (365 nm).

Conducting the model reaction in toluene, under UV light irradiation (365 nm), [dmpeMn(CO)$_3$H] was identified as the most suitable manganese-based catalyst for the C–H borylation under investigation. However, it has been realized that the use of the pre-formed manganese hydride posed a barrier to operational simplicity so was questioned if this was strictly necessary. Indeed, enhanced reactivity was achieved when the bromide precursor [dmpeMn(CO)$_3$Br] was used together with an activator; KO^{t}Bu. The role played by alkoxides as *in situ* activators of B_2pin_2 is well documented.[15,16] However, after screening several alkoxide species (such as methoxide and ethoxide salts), KO^{t}Bu provided higher yields of the representative reaction and revealed to be the most efficient activator in such reaction conditions. The most successful result was achieved when [dmpeMn(CO)$_3$Br] and potassium *tert*-butoxide (KO^{t}Bu) were used as the precatalyst and the activator, respectively. Hence, after also having optimized both the starting material amount and the precatalyst loading, a subsequent optimization was carried out, aiming at finding the final best conditions for the model reaction (**Scheme 3**).

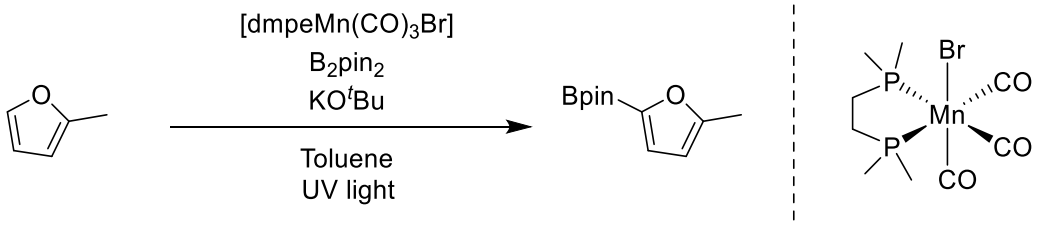

Scheme 3. Representative reaction examined. Conditions: 2-Methylfuran (0.2 mmol), B_2pin_2 (1.2 eq.), KO^{t}Bu (1.2 eq.), [dmpeMn(CO)$_3$Br] (10 mol%), toluene (0.5 mL), 32 °C, 24 h, UV light (365 nm). Yields were determined by ^{1}H NMR spectroscopy using 1,3,5-trimethoxybenzene as an internal standard.

After a thorough study of the topic and careful evaluation of the synthetic challenge, and making use of the previous optimization, my first contribution focused on control experiments (**Table 1**, entries 1 and 2). The use of UV light proved essential, as no reactivity was observed when the reaction was simply heated under reflux. Furthermore, the use of two lamps did not lead to any improvement of the reaction efficiency (entry 3), thus demonstrating the need for just one UV lamp. The presence of the activator also proved to be an important factor for the reaction efficiency, while, as far as the choice of the borylation reagent is concerning, B_2pin_2 was found to be better than HBpin (entry 5), a bonus given the higher stability and easier handling of the former compared to the latter. Attempts to increase the yield by using an increased amount of activator (entry 6) as well as by using a stoichiometric amount of the precatalyst failed (entry 7).

Entry	Deviation From Standard Conditions	Yield (%)
1	**None**	**44**
2	No light	0
3	Two lamps	37
4	No KO^{t}Bu	14
5	Boron source = HBpin	20
6	KO^{t}Bu 2.2 eq	37
7	Stoichiometric precatalyst loading	34

Table 1. Control experiments for the representative reaction.

A screening of several reaction media was thus conducted, aiming at identifying conditions that could minimize the formation of side products and maximize the reaction efficiency (**Table 2**). The solvents evaluated included hexane, tetrahydrofuran (THF), cyclopentyl methyl ether (CPME), and methyl *tert*-butyl ether (MTBE). Given the sensitivity of the reaction to oxygen and moisture, all solvents were dried, degassed and distilled prior to use. Beyond achieving improved reaction efficiency, particular attention was devoted to the identification of a more sustainable alternative to toluene as the reaction medium, in light of its well-established hazardous safety profile. The solvent screening demonstrated that MTBE afforded the highest yield (entry 5), thereby establishing it as the solvent of choice for subsequent optimization studies, while also supporting the adoption of potentially more sustainable reaction conditions owing to its comparatively improved environmental profile to that of toluene.[17] Extending the reaction time from 24 hours to 48 hours did not lead to a significant improvement in the product formation (yield 60%, compared to that in standard conditions, 55%).

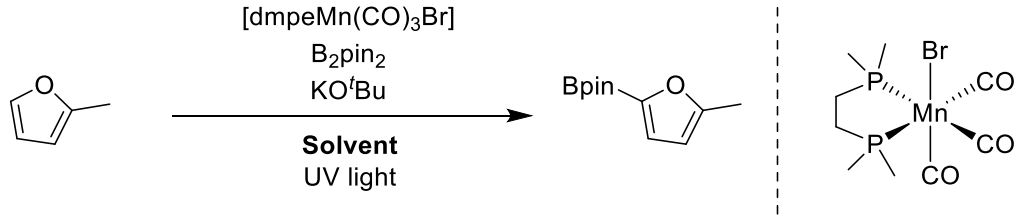

Entry	Solvent	Yield (%)
1	Toluene	44
2	Hexane	44
3	THF	7
4	CPME	30
5	**MTBE**	**55**

Table 2. Optimization of the reaction medium. Conditions: 2-Methylfuran (0.2 mmol), B_2pin_2 (1.2 eq.), KO^{t}Bu (1.2 eq.), [dmpeMn(CO)$_3$Br] (10 mol%), solvent (0.5 mL), 32 °C, 24 h, UV light (365 nm). Yields were determined by ^{1}H NMR spectroscopy using 1,3,5-trimethoxybenzene as an internal standard.

5.2.2. Substrate scope

Once the reaction conditions were optimized, the scope of this reaction was assessed across several substrates (**Scheme 4**).

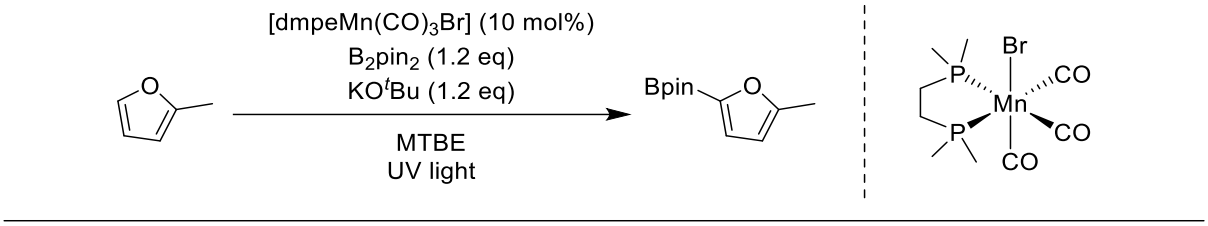

Furans and Thiophenes

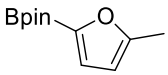

51%

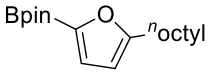

69%

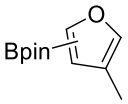

35%
2-:5-
43:57

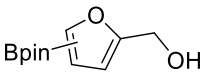

40%
4-:5-
20:80*

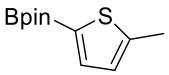

70%

Pyrroles and Indoles

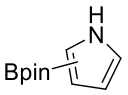

25%
2-:2,5-bis
57:43*

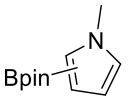

35%
2-:3-:2,5-bis
43:43:14

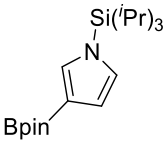

57%

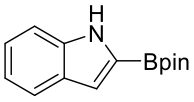

43%

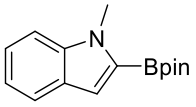

57%

N-Heteroarenes and Carboarenes

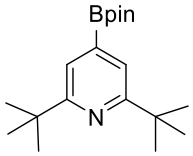

79%

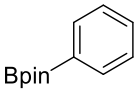

13%**

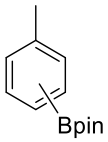

8%
m:*p*
66:34**

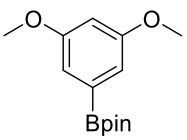

28%

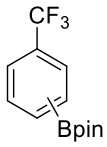

55%
m:*p*:di-*m*
45:45:10**

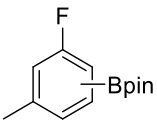

35%
5-:6-
27:73

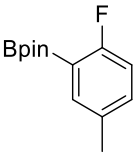

27%

Unsuccessful substrates

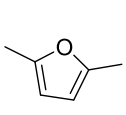

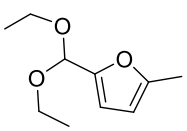

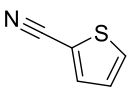

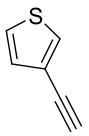

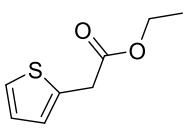

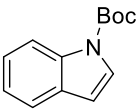

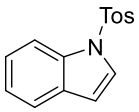

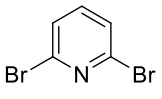

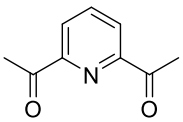

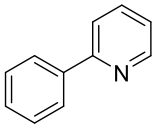

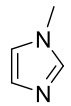

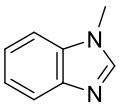

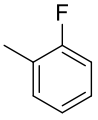

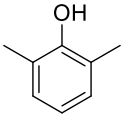

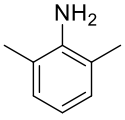

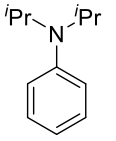

Scheme 4. Substrate scope for the manganese-catalysed C–H borylation of carboarenes and heteroarenes. Conditions: Arene substrate (0.2 mmol), B_2pin_2 (0.24 mmol), KO^tBu (0.24 mmol), [dmpeMn(CO)$_3$Br] (10 mol%), MTBE (0.5 mL), 32 °C, 24 h, UV light (365 nm). Isolated yields are reported. Product ratios were determined by ^{1}H NMR spectroscopy. *Starting material pre-mixed with 1 equivalent of HBpin. **Yields were determined by ^{1}H NMR spectroscopy using 1,3,5-trimethoxybenzene as internal standard.

For furan derivatives, C–H borylation occurred preferentially at the C2 or C5 positions. Changing the C2 substituent from methyl to *n*-octyl led to an increased yield. In the case of 3-methylfuran, the reaction produced a mixture of 5- and 2- borylated products, with no exclusive C2 position borylation. The system also tolerated a free alcohol group when pre-mixed with an equivalent of HBpin. Overall, 2-methylthiophene displayed high reactivity, yielding the borylated product at the C5 position in 70%.

For the first time, a manganese-based catalytic system was successfully applied to the C–H borylation of N-containing heteroarenes. Unprotected pyrrole underwent direct borylation under these reaction conditions, giving a mixture of 2- and 2,5-bis-borylated products. When pyrrole was pre-mixed with HBpin, acting as a 'traceless' protecting group, the yield increased from 10 to 25% without affecting the regioselectivity. N-Substituted pyrroles bearing electron-donating groups showed borylation at the C3 position, in particular N-methyl pyrrole gave a mixture of 2-, 3-, and 2,5-bis-borylated products, whereas the bulkier N-Si(^{i}Pr)$_3$ derivative exclusive gave C3 borylation. Indoles were efficiently borylated with regioselectivity for the C2 position, although no reactivity was observed when unprotected indole was pre-mixed with HBpin. The sterically hindered 2,6-di-*tert*-butylpyridine was also compatible with the system, providing exclusive *para*-selective C–H borylation.

The methodology was also applied to carboarenes. Benzene underwent mono-borylation, albeit in low yield. Toluene afforded a statistical mixture of *meta*- and *para*-borylated products, with no *ortho*-substitution, likely due to steric hindrance. This steric effect was

further highlighted by the exclusive C5 position borylation of 1,3-dimethoxybenzene. Substrates bearing electron-withdrawing groups showed enhanced reactivity, in particular trifluorotoluene gave higher yields than toluene, as a mixture of *para*-, *meta*-, and di-*meta*-borylated products. Fluorotoluene derivatives underwent selective *ortho*-borylation relative to the fluorine atom, although partial defluorination was observed under the standard conditions, similar to what has been reported for iron-based catalysts.[18]

Substrates with terminal alkynes did not react, with ^{1}H NMR showing recovery of starting material. Reducible functional groups, such as nitriles and esters, were incompatible, and attempts to protect carbonyls as acetals failed. N-substituted indoles with bulky, electron-withdrawing groups (e.g., Boc, tosyl) were unreactive, likely due to steric hinderance of the C2 position. Less hindered pyridine derivatives also showed no reactivity, and other N-heteroarenes, including oxazole, imidazole, and benzimidazole, were unreactive. For carboarenes, alcohols were not tolerated even when pre-mixed with HBpin, and anilines, including N,N-disubstituted derivatives, did not undergo C–H borylation.

5.3. Conclusions

In conclusion, a new manganese-catalysed C–H borylation protocol has been successfully developed and applied to a range of furan derivatives, providing moderate yields as well as high regioselectivity for the C2 and C5 positions, further demonstrating the trend of the functionalization of the C–H bond α to the heteroatom that is common also in the conventional systems.[19] The procedure was applied even to hetero- and carboarenes, giving lower yields than those obtained with iron- and cobalt-based catalysts, especially for the simplest arenes, benzene and toluene.[9,18] By contrast, the potential of this procedure lies in the successful application to N-containing heteroarenes, especially to the regioselectivity borylation of indoles, that typically show lower yields and complex mixtures, compared to other already reported iron-based catalysts.[18]

By relying solely on bench-stable and commercially available reagent (potassium *tert*-butoxyde), in combination with the use of UV light irradiation (365 nm), and an *in situ* activation of a readily synthesised and bench-stable precatalyst, this procedure represents the first manganese-based system in which the arene can be used as the limiting reagent. Furthermore, the protocol has the advantage of using bis(pinacolato)diboron (B_2pin_2) that is readily available and a higher stable and easier to handle boron source compared to pinacolborane (HBpin).

Scope and limitation studies showed an expansion on the current reactivity of manganese catalysts and that, for the first time, a manganese-catalysed approach could be extended to direct C–H borylation of the challenging N-containing heteroarenes, such as pyrrole, indole, and pyridine. In these cases, steric effects governed regioselectivity, with bulky substituents hindering reaction at the C2 position of both pyrrole and indole derivatives. Ongoing studies aim to clarify the reaction mechanism, the influence of the ligand, and the requirement for light irradiation.

By being both chemically robust and environmentally responsible, this method contributes to advance the field of sustainable organometallic catalysis and offers a practical and viable way for affording valuable and highly versatile functionalised organic molecules, such as aryl boronic esters, paving also the way to further investigation on Earth-abundant metals in promoting key organic transformations in increasingly sustainable ways.

5.4 Experimental section

5.4.1. Materials

All reactions were performed in oven (120 °C) dried glassware under an atmosphere of anhydrous argon or nitrogen, unless otherwise indicated. All air- and moisture-sensitive reactions were carried out using standard vacuum line and Schlenk techniques, or in a glovebox with a purified argon atmosphere. All glassware was cleaned using base (KOH, *i*-PrOH) and aqueous acid (HNO_3) baths. All reported reaction temperatures correspond to external bath temperatures. Analytical thin-layer chromatography was performed on aluminium-backed silica plates (Merck 60 F254). Product spots were visualised by UV light at 254 nm or staining with $KMnO_4$. Flash column chromatography was performed on silica gel (Merck Kielselgel 60, 40-63 μm) or if specified, carried out on a Teledyne ISCO CombiFlash NextGen 300+ using RediSep Rf normal phase silica flash columns (12, 25, 40, or 80 g; 20-40 microns). Substrates were purified using hexane and ethyl acetate on a gradient of 100:0 to 0:100 with flow rates of 10-110 mL min^{-1} depending on the size of column and ΔR_f. All solvents for air- and moisture sensitive techniques were obtained from an anhydrous solvent system (Innovative Technology). Reaction solvents tetrahydrofuran (THF) (Fisher, HPLC grade), ether (Et_2O) (Fisher, BHT stabilised ACS grade), and dichloromethane (CH_2Cl_2) (Fisher, unstabilised HPLC grade) were dried by percolation through two columns packed with neutral alumina under a positive pressure of argon. Reaction solvent toluene (ACS grade) was dried by percolation through a column packed with neutral alumina and a column packed with Q5 reactant (supported copper catalyst for scavenging oxygen) under a positive pressure of argon. Reaction solvent ethanol (absolute, VWR) was used as received. Solvents for filtration, transfers, chromatography, and recrystallisation were dichloromethane (CH_2Cl_2) (ACS grade, amylene stabilised), ether (Et_2O) (Fisher, BHT stabilised ACS grade), ethyl acetate (EtOAc) (Fisher, ACS grade), hexane (Optima), methanol (MeOH) (ACS grade), pentane (ACS grade), and hexane (40–60°C, ACS grade). All reagents were purchased from Sigma Aldrich, Alfa Aesar, Acros Organics,

Tokyo Chemical Industries UK, Fluorochem and Apollo Scientific, or synthesised within the laboratory.

5.4.2. Instrumentation

^{1}H, ^{11}B, ^{13}C, ^{19}F, ^{31}P NMR spectra were recorded on Bruker Avance III 400 and 500 MHz spectrometers. Chemical shifts are reported in parts per million (ppm). ^{1}H NMR spectra were referenced to the residual protonated solvent peak ($CHCl_3$: 7.26 ppm). ^{13}C NMR spectra were referenced to the solvent peak ($CDCl_3$: 77.00 ppm). Multiplicities are indicated by app. (apparent), br. (broad), s (singlet), d (doublet), t (triplet), q (quartet), quin. (quintet), sext. (sextet), hept. (heptet), oct. (octet), non. (nonet). Coupling constants, J, are reported in Hertz and rounded to the nearest 0.1 Hz. Integration is provided and assignments are indicated. Lamp: HepatoChem P301-30-1 365 nm.

5.4.3. General procedure and characterization of the borylation of arenes

In a glove box with a purified argon atmosphere, potassium *tert*-butoxide (23 mg, 0.24 mmol), bis(pinacolato)diboron (58 mg, 0.24 mmol), [dmpeMn(CO)$_3$Br] (7.4 mg, 0.01 mmol), the corresponding heteroarene (0.2 mmol) and anhydrous MTBE (0.7 mL) were added to an NMR tube. The tube was sealed and shaken, then removed from the glove box and irradiated with UV light (365 nm) for 24 hours. The reaction mixture was exposed to air and filtered directly through a silica plug (ca. 3 g SiO_2 15 mm Ø) with ethyl acetate. The analytical data were in accordance with those previously reported.[20–27] C-B ^{13}C resonance was not observed, unless otherwise stated.

5.4.4. Synthesis and characterization of the manganese precatalyst [dmpeMn(CO)$_3$Br]

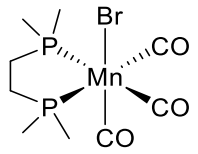

Dmpe [bis(dimethylphosphino)ethane] (1.1 mmol, 1.1 equiv., 0.17 g) was added dropwise to a suspension of [Mn(CO)$_5$Br] (0.28 g, 1.0 mmol) in anhydrous toluene (5 mL) under an argon atmosphere. The reaction mixture was heated under reflux under nitrogen for one hour. Anhydrous hexane (15 mL) was added to form a precipitate that was filtered, washed with hexane (3 x 5 mL) and dried to give [dmpeMn(CO)$_3$Br] as a yellow solid (0.28 g, 0.76 mmol, 76%). ^{1}H NMR: (500 MHz, $CDCl_3$) 2.18 – 2.10 (m, 2H), 1.85 – 1.77 (m, 2H), 1.77 – 1.73 (m, 6H), 1.60– 1.58 (m, 6H). ^{13}C NMR: (126 MHz, $CDCl_3$) 222.1, 218.0, 28.5 (app. t, J = 21.3 Hz), 16.3 (dd, J = 15.5, 13.1 Hz), 14.1 (dd, J = 15.5, 13.1 Hz). ^{31}P NMR: (202 MHz, $CDCl_3$) 56.7 (s).

^{1}H NMR (500 MHz, $CDCl_3$) Spectrum of [dmpeMn(CO)$_3$Br]

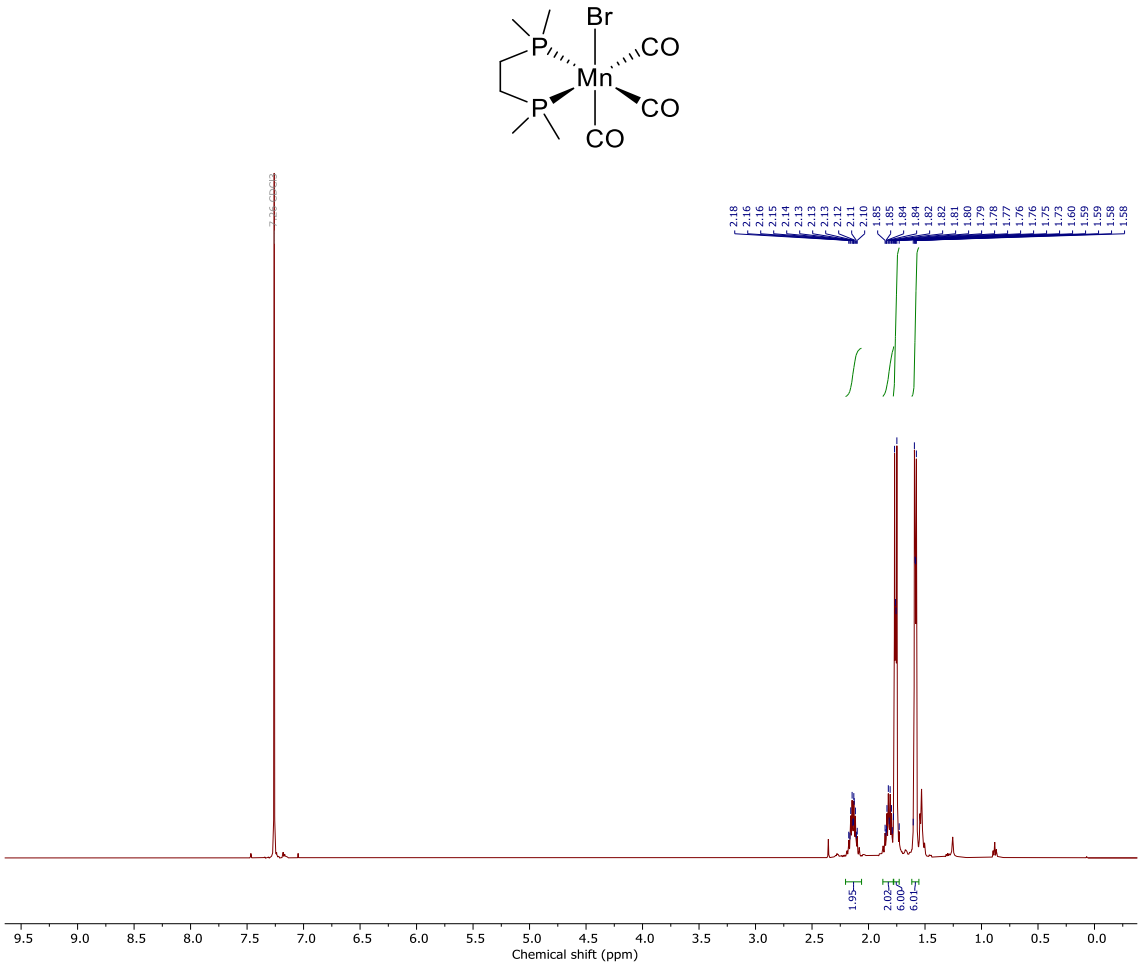

^{13}C NMR (126 MHz, $CDCl_3$) Spectrum of [dmpeMn(CO)$_3$Br]

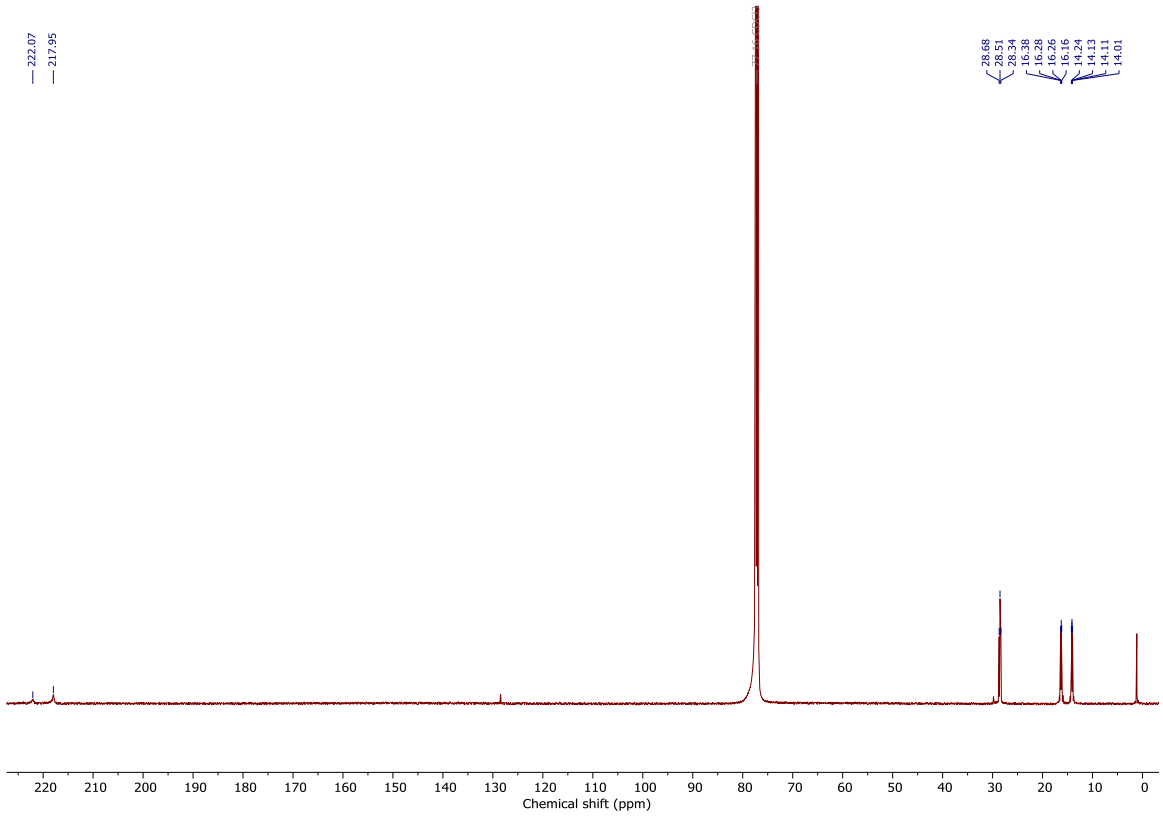

^{31}P NMR (202 MHz, $CDCl_3$) Spectrum of [dmpeMn(CO)$_3$Br]

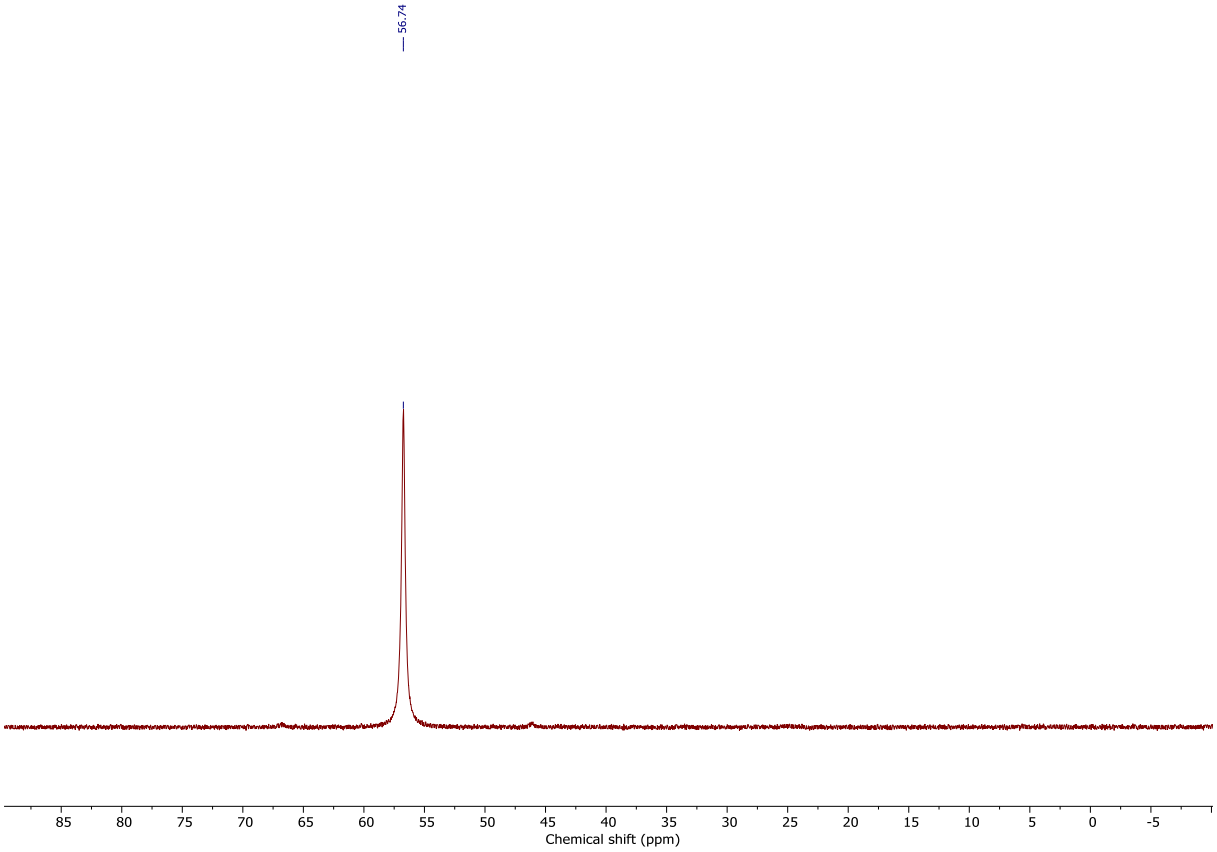

5.4.5. Synthesis and characterization of 5-(4,4,5,5-Tetramethyl-1,3,2-dioxaborole)-2-methylfuran

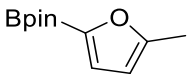

According to the general procedure, potassium *tert*-butoxide (23 mg, 0.24 mmol), bis(pinacolato)diboron (58 mg, 0.24 mmol), [dmpeMn(CO)$_3$Br] (7.4 mg, 0.02 mmol), and 2-methylfuran (18 mL, 0.2 mmol) in anhydrous MTBE (0.5 mL) were reacted. The crude product was purified by flash column chromatography (Teledyne ISCO CombiFlash NextGen 300+, 12 g, 40 mL min^{-1}, hexane/ethyl acetate 10:1) to give 5-(4,4,5,5-tetramethyl-1,3,2-dioxaborole)-2-methylfuran as a colourless oil (21 mg, 0.10 mmol, 51%). ^{1}H NMR: (500 MHz, $CDCl_3$) 6.99 (d, J = 3.2 Hz, 1H), 6.05–6.02 (m, 1H), 2.36 (s, 3H), 1.34 (s, 12H); ^{11}B NMR: (160 MHz, $CDCl_3$) 27.0. ^{13}C NMR: (126 MHz, $CDCl_3$) 157.9, 125.0, 107.0, 84.2, 24.9, 14.1.

^{1}H NMR (500 MHz, $CDCl_3$) Spectrum of 5-(4,4,5,5-tetramethyl-1,3,2-dioxaborole)-2-methylfuran

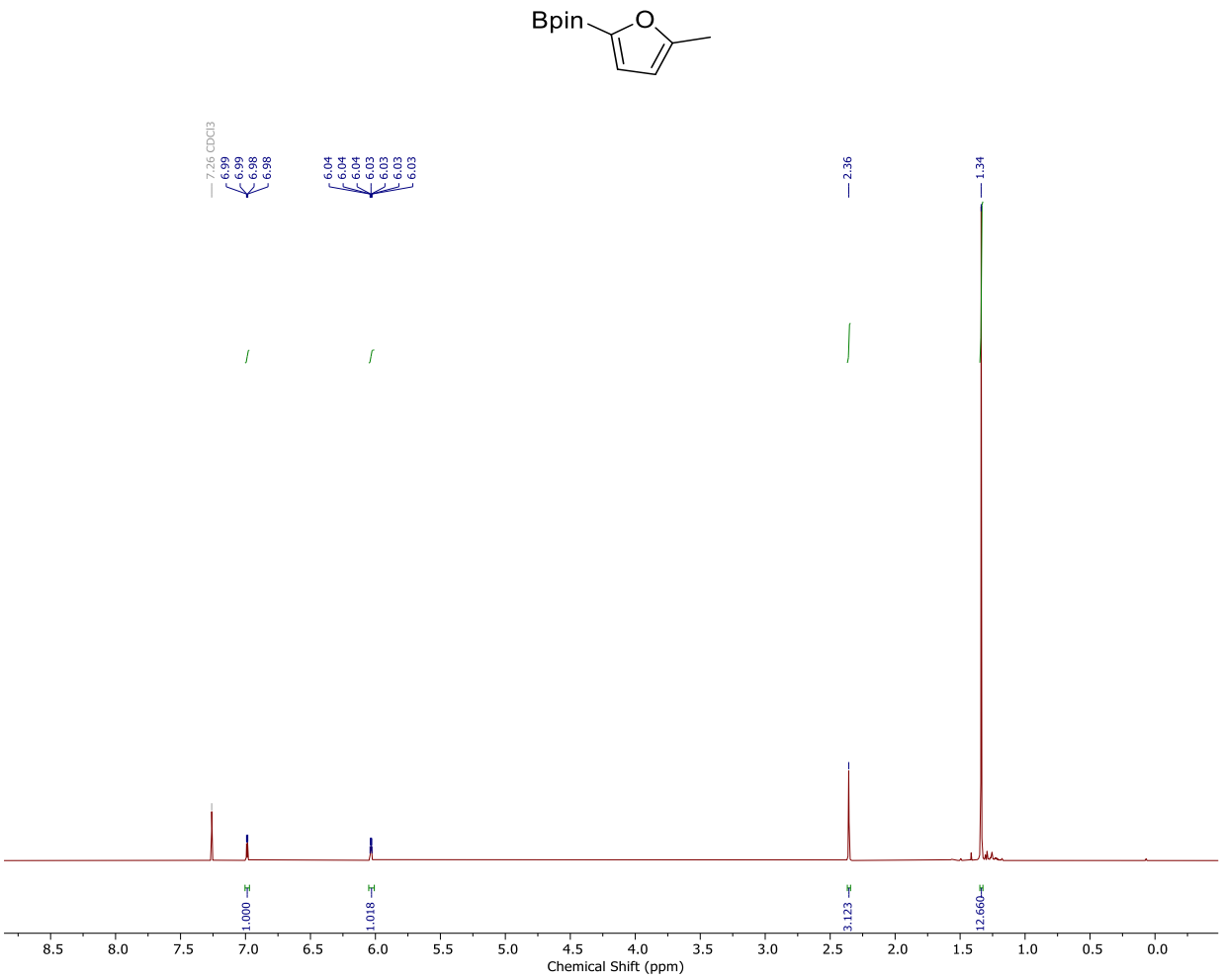

^{11}B NMR (160 MHz, $CDCl_3$) Spectrum of 5-(4,4,5,5-tetramethyl-1,3,2-dioxaborole)-2-methylfuran

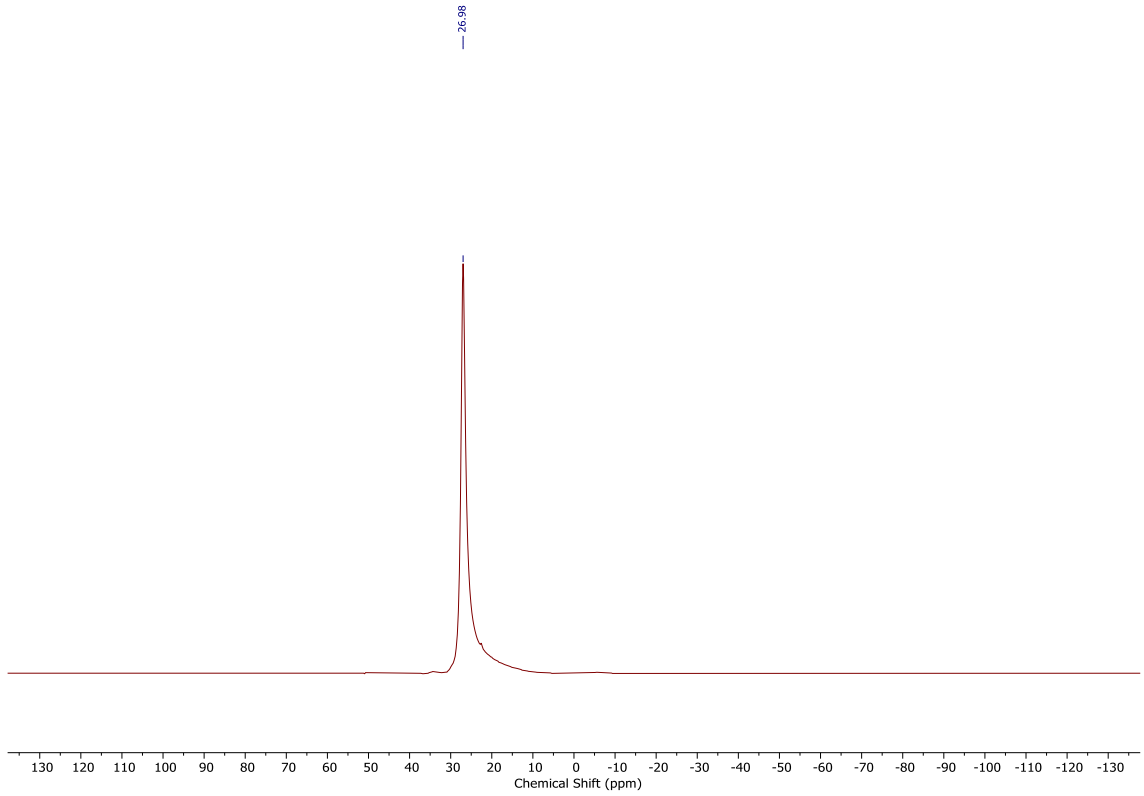

^{13}C NMR (126 MHz, $CDCl_3$) Spectrum of 5-(4,4,5,5-tetramethyl-1,3,2-dioxaborole)-2-methylfuran

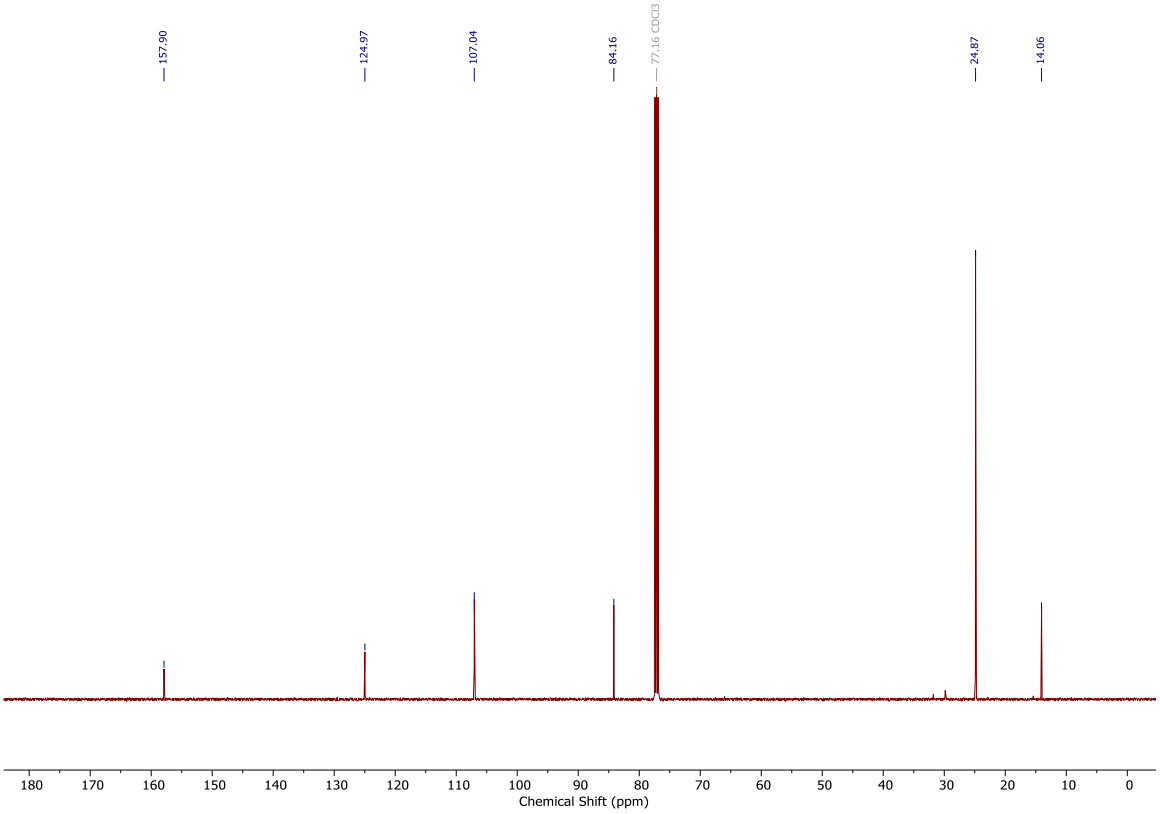

5.4.6. Synthesis and characterization of 5-(4,4,5,5-Tetramethyl-1,3,2-dioxaborole)-2-octylfuran

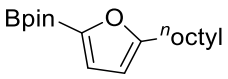

According to the general procedure, potassium *tert*-butoxide (23 mg, 0.24 mmol), bis(pinacolato)diboron (58 mg, 0.24 mmol), [dmpeMn(CO)$_3$Br] (7.4 mg, 0.02 mmol), and 2-octylfuran (40 mL, 0.2 mmol) in anhydrous MTBE (0.5 mL) were reacted. The crude product was purified by flash column chromatography (Teledyne ISCO CombiFlash NextGen 300+, 12 g, 40 mL min^{-1}, hexane/ethyl acetate 10:1) to give 5-(4,4,5,5-tetramethyl-1,3,2-dioxaborole)-2-octylfuran as a colourless oil (43 mg, 0.14 mmol, 69%). ^{1}H NMR: (500 MHz, $CDCl_3$) 6.99 (app. d, J = 3.2 Hz, 1H), 6.03 (d, J = 3.2 Hz, 1H), 2.67 (t, J = 7.7 Hz, 1H), 1.70–1.55 (m, 2H), 1.40–1.18 (m, 24H), 0.87 (t, J = 6.9 Hz, 3H). ^{11}B NMR: (160 MHz, $CDCl_3$) 27.0. ^{13}C NMR: (126 MHz, $CDCl_3$) 162.5, 124.8, 106.0, 84.1, 32.0, 29.4, 29.4, 29.3, 28.5, 28.2, 24.9, 22.8, 14.2.

^{1}H NMR (500 MHz, $CDCl_3$) Spectrum of 5-(4,4,5,5-tetramethyl-1,3,2-dioxaborole)-2-octyllfuran

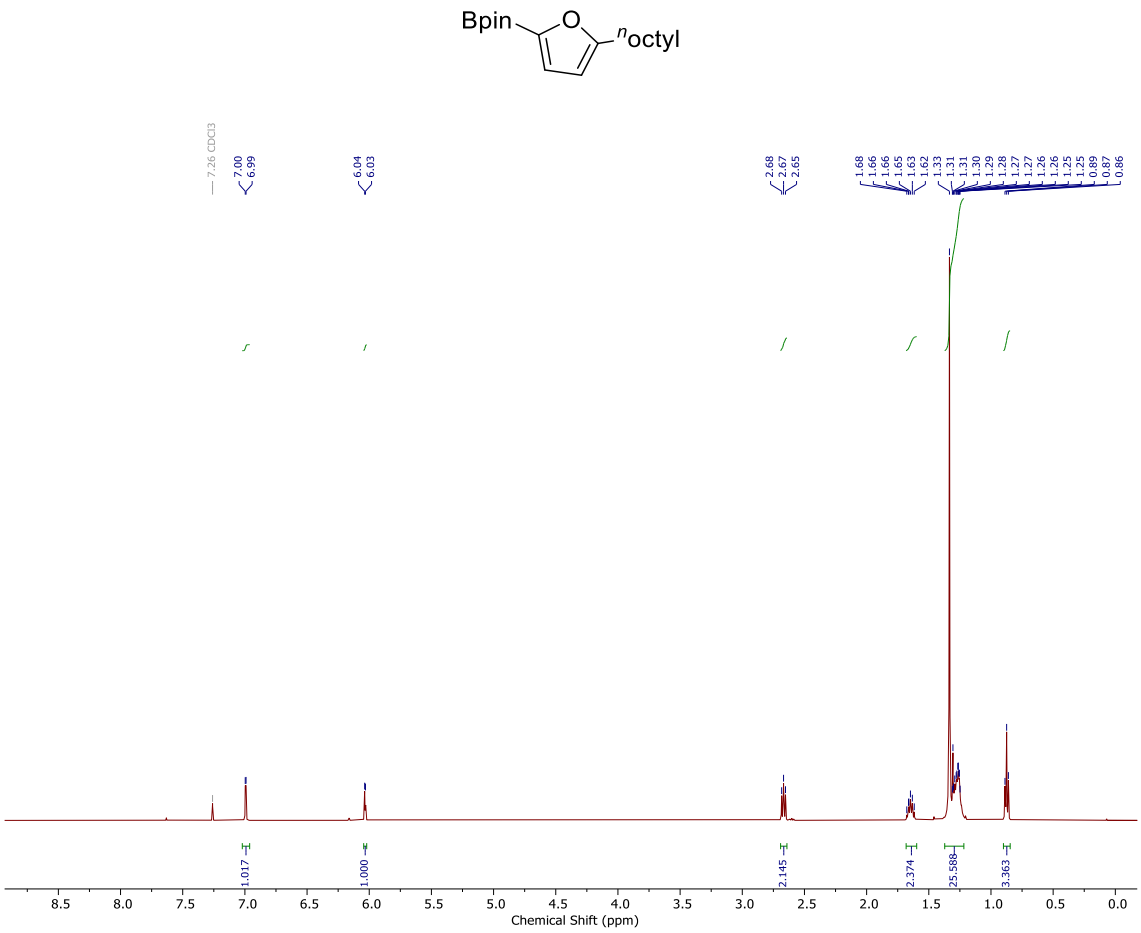

^{11}B NMR (160 MHz, $CDCl_3$) Spectrum of 5-(4,4,5,5-tetramethyl-1,3,2-dioxaborole)-2-octylfuran

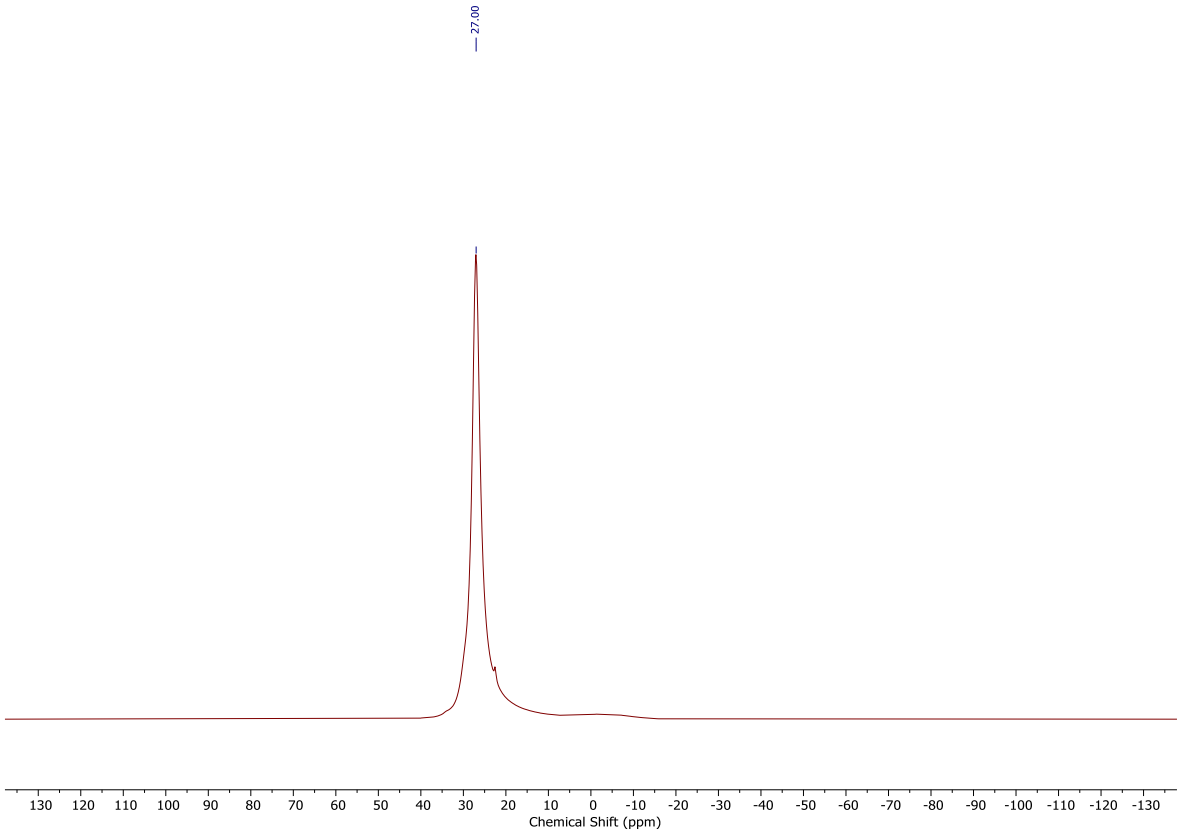

^{13}C NMR (126 MHz, $CDCl_3$) Spectrum of 5-(4,4,5,5-tetramethyl-1,3,2-dioxaborole)-2-octylfuran

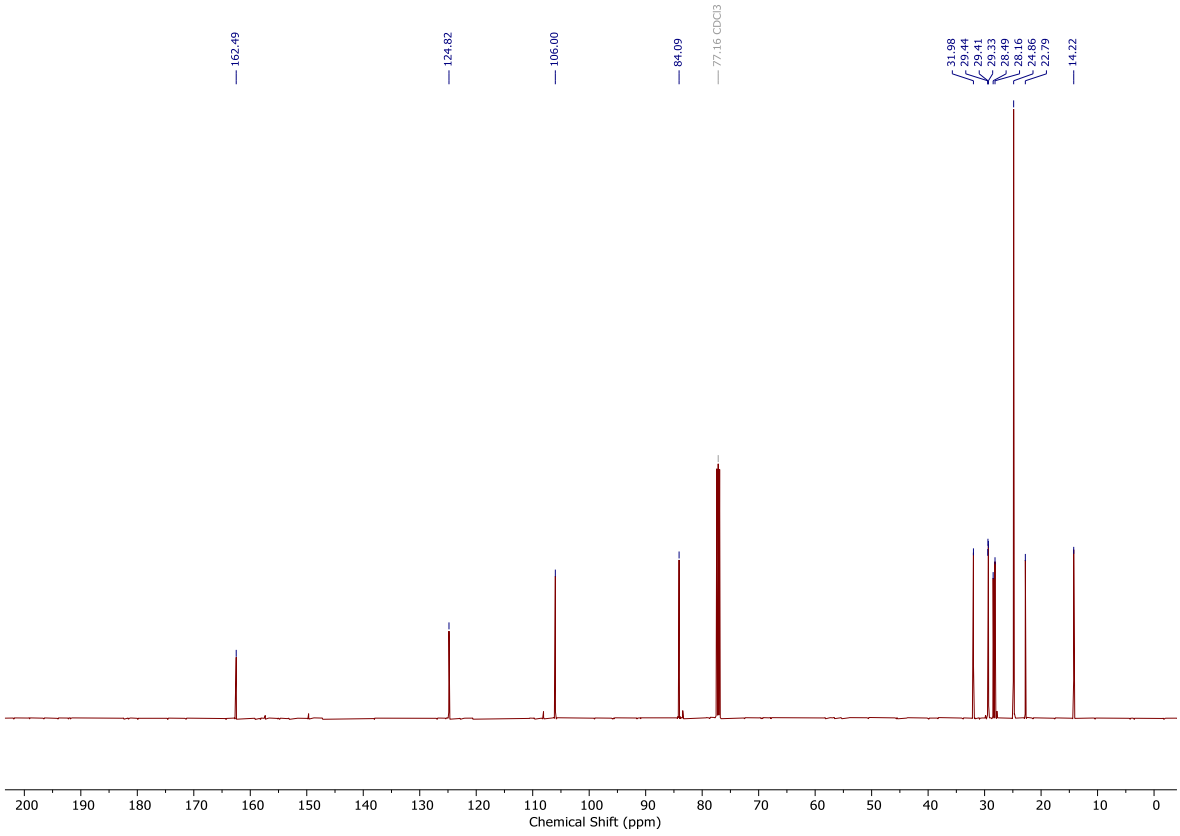

5.4.7. Synthesis and characterization of 2-(4,4,5,5-Tetramethyl-1,3,2-dioxaborole)-4-methylfuran and 2,5-bis(4,4,5,5-tetramethyl-1,3,2-dioxaborole)-3-methylfuran

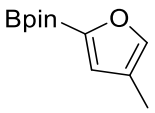

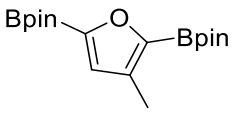

According to the general procedure, potassium *tert*-butoxide (23 mg, 0.24 mmol), bis(pinacolato)diboron (58 mg, 0.24 mmol), [dmpeMn(CO)$_3$Br] (7.4 mg, 0.02 mmol), and 3-methylfuran (18 mL, 0.2 mmol) in anhydrous MTBE (0.5 mL) were reacted. The crude product was purified by flash column chromatography (Teledyne ISCO CombiFlash NextGen 300+, 12 g, 40 mL min^{-1}, hexane/ethyl acetate 10:1) to give 2-(4,4,5,5-tetramethyl-1,3,2-dioxaborole)-4-methylfuran as a colourless oil (8 mg, 0.04 mmol, 20%) and 2-(4,4,5,5-tetramethyl-1,3,2-dioxaborole)-3-methylfuran as a colourless solid (10 mg, 0.03 mmol, 15%). Product distribution 2-:2,5-bis = 57:43

2-(4,4,5,5-tetramethyl-1,3,2-dioxaborole)-4-methylfuran: ^{1}H NMR: (500 MHz, $CDCl_3$) 7.41–7.39 (m, 1H), 6.91 (s, 1H), 2.04 (d, J = 1.2 Hz, 3H), 1.33 (s, 12H). ^{11}B NMR: (160 MHz, $CDCl_3$) 27.0. ^{13}C NMR: (126 MHz, $CDCl_3$) 144.5, 126.0, 120.8, 84.3, 24.9, 9.5.

2,5-bis(4,4,5,5-tetramethyl-1,3,2-dioxaborole)-3-methylfuran: ^{1}H NMR: (500 MHz, $CDCl_3$) 6.90 (s, 1H), 2.23 (s, J = 1.2 Hz, 3H), 1.31 (m, 24H). ^{11}B NMR: (160 MHz, CDCl3) 27.1. ^{13}C NMR: (126 MHz, $CDCl_3$) 135.4, 126.2, 84.1, 83.7, 24.8, 24.7, 10.6.

^{1}H NMR (500 MHz, $CDCl_3$) Spectrum of 2-(4,4,5,5-tetramethyl-1,3,2-dioxaborole)-4-methylfuran

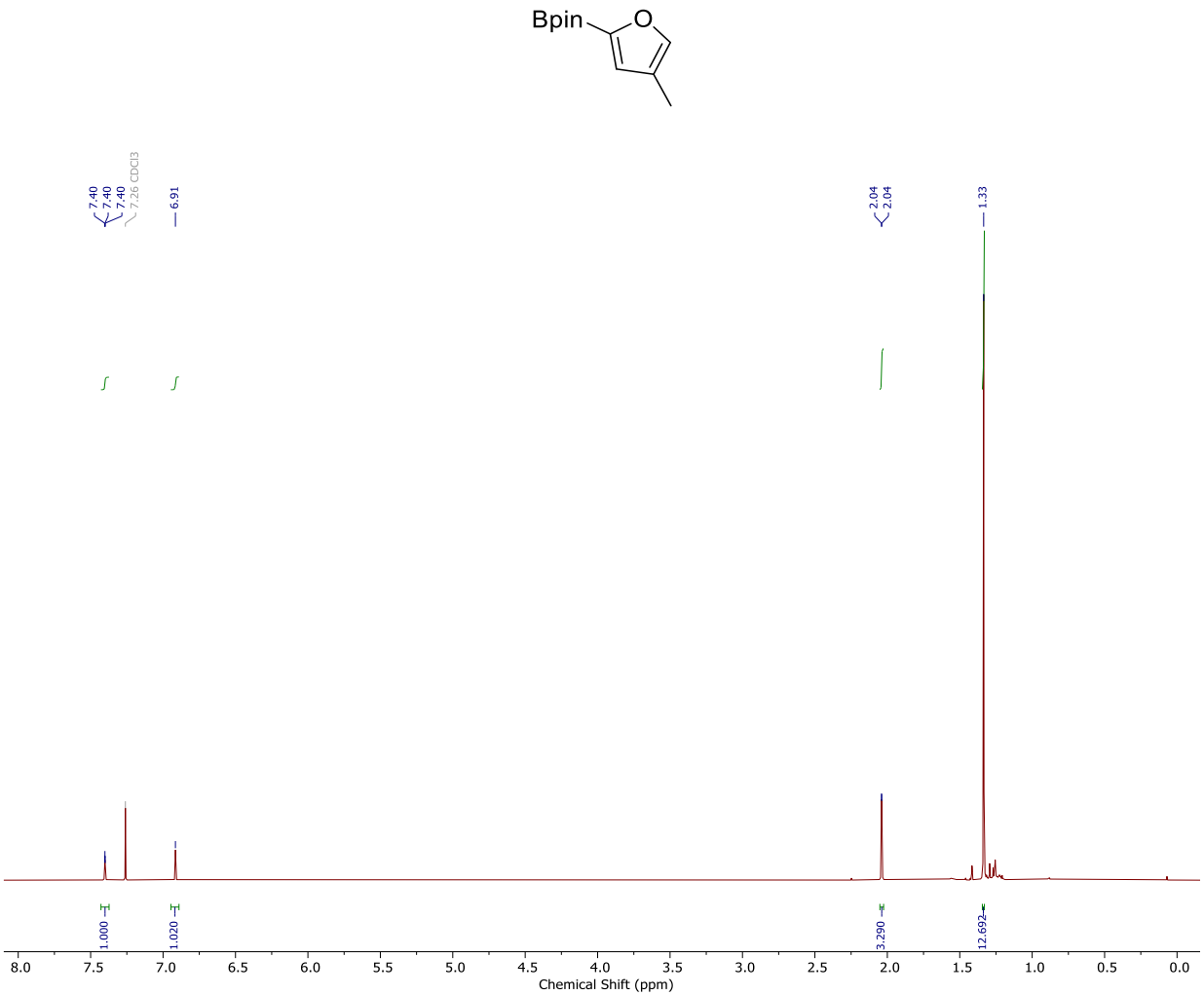

^{11}B NMR (160 MHz, $CDCl_3$) Spectrum of 2-(4,4,5,5-tetramethyl-1,3,2-dioxaborole)-4-methylfuran

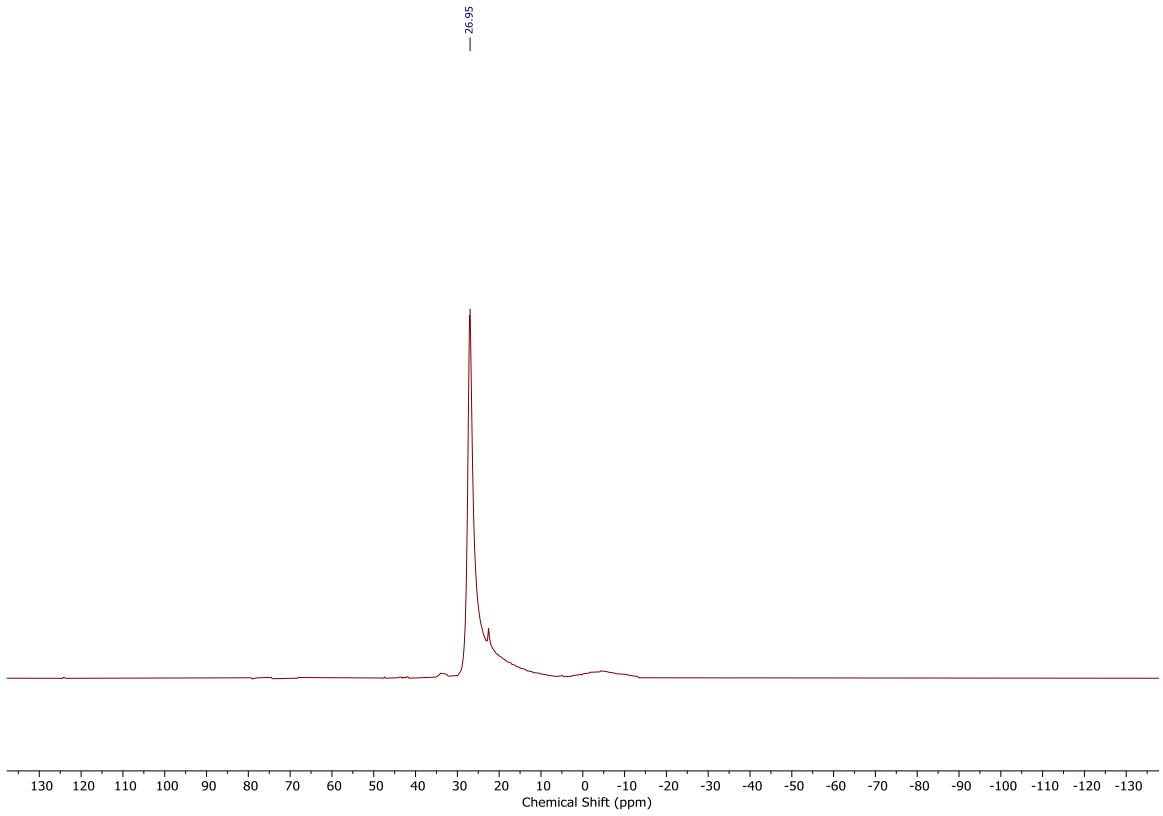

^{13}C NMR (126 MHz, $CDCl_3$) Spectrum of 2-(4,4,5,5-tetramethyl-1,3,2-dioxaborole)-4-methylfuran

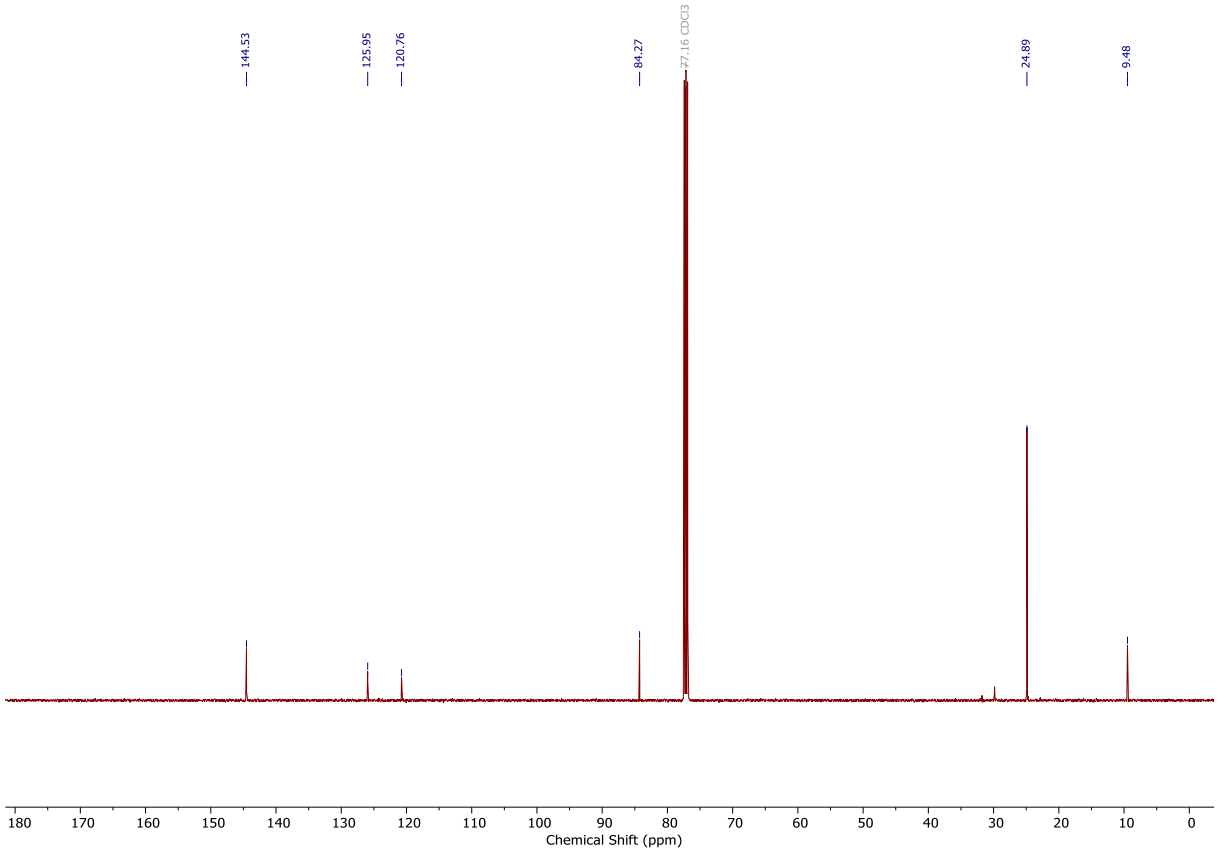

^{1}H NMR (500 MHz, $CDCl_3$) Spectrum of 2,5-bis(4,4,5,5-tetramethyl-1,3,2-dioxaborole)-2-methylfuran

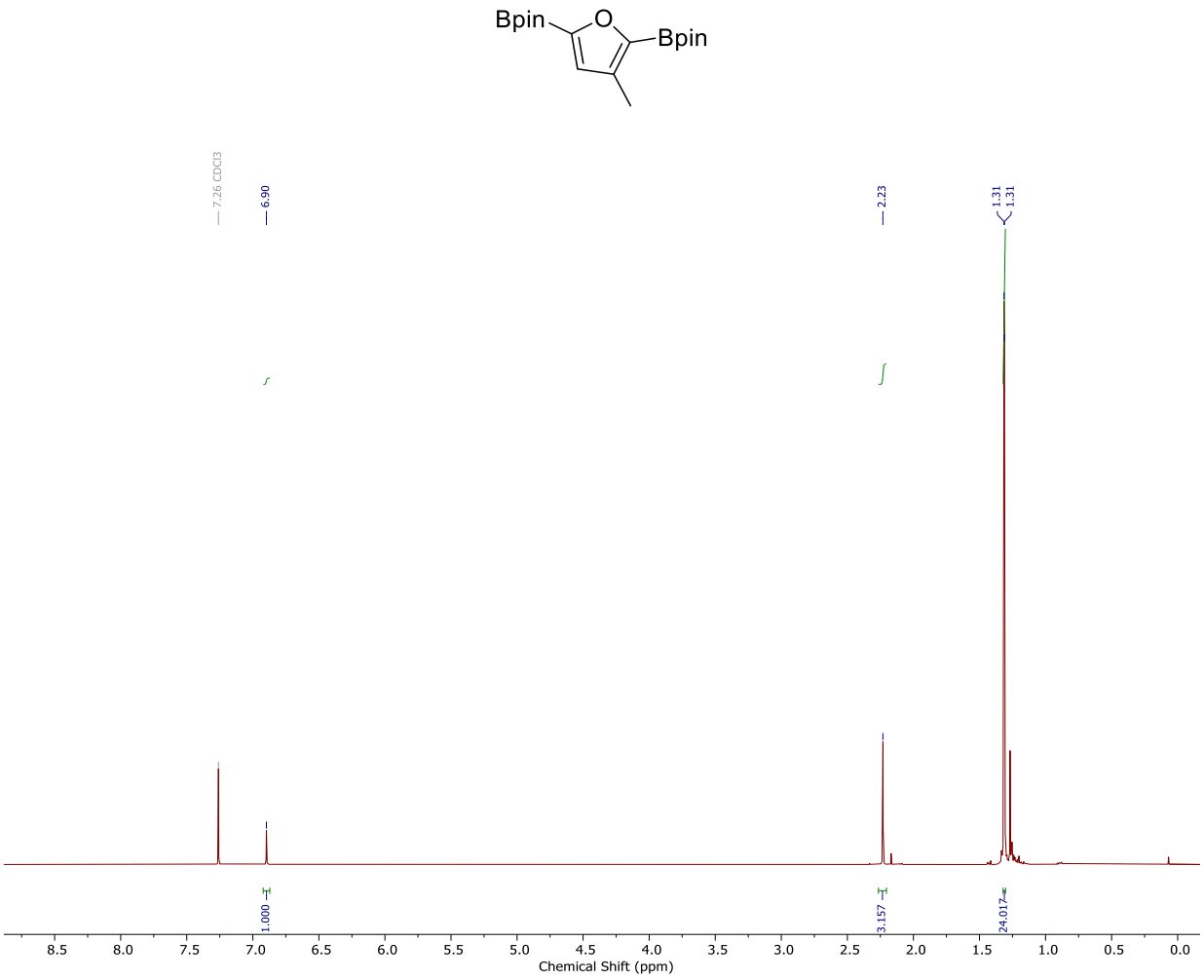

^{11}B NMR (160 MHz, $CDCl_3$) Spectrum of 2,5-bis(4,4,5,5-tetramethyl-1,3,2-dioxaborole)-2-methylfuran

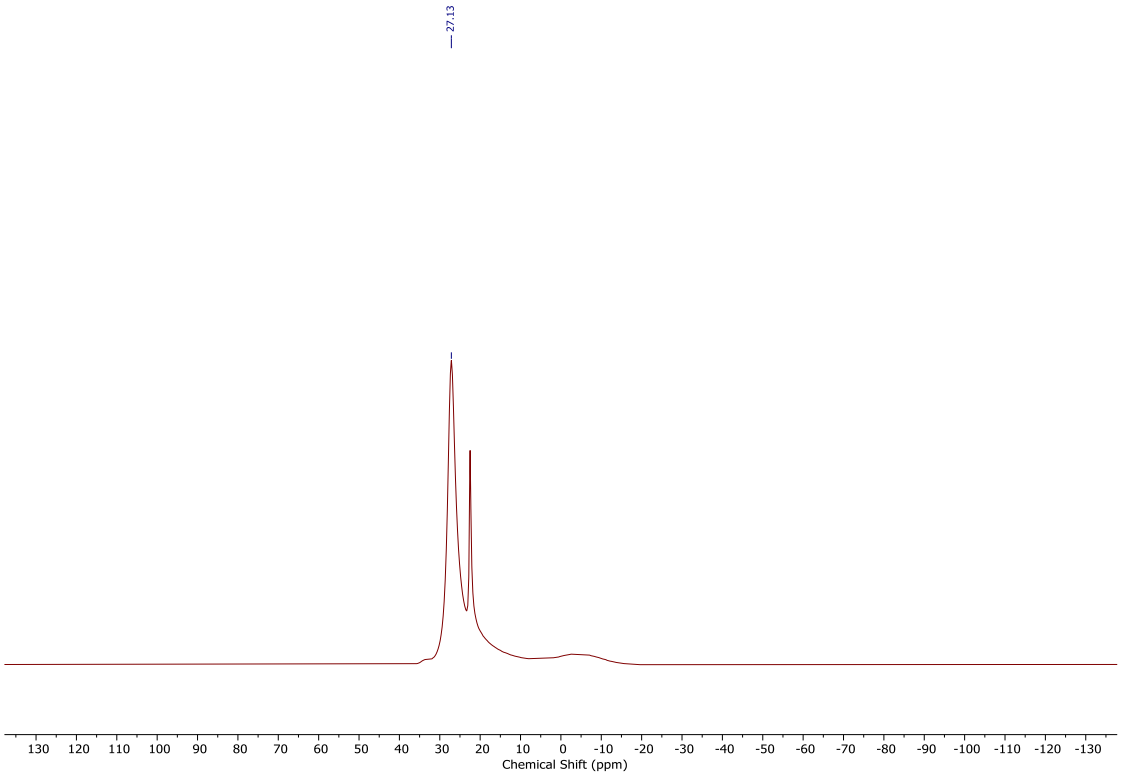

^{13}C NMR (126 MHz, $CDCl_3$) Spectrum of 2,5-bis(4,4,5,5-tetramethyl-1,3,2-dioxaborole)-2-methylfuran

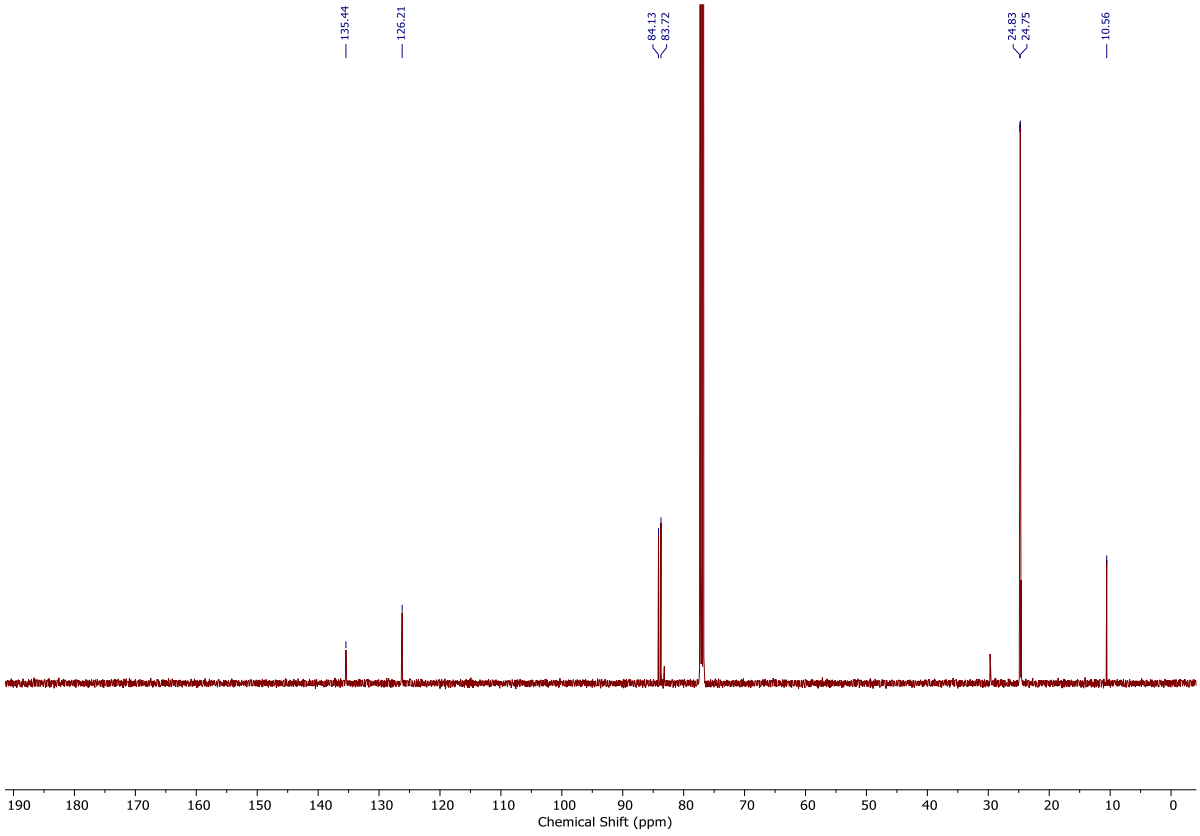

5.4.8. Synthesis and characterization of 5-(4,4,5,5-Tetramethyl-1,3,2-dioxaborole)furfuryl alcohol and 4-(4,4,5,5-Tetramethyl-1,3,2-dioxaborole)furfuryl alcohol

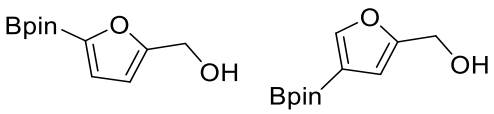

According to the general procedure, potassium *tert*-butoxide (23 mg, 0.24 mmol), bis(pinacolato)diboron (58 mg, 0.24 mmol), [dmpeMn(CO)$_3$Br] (7.4 mg, 0.02 mmol), furfuryl alcohol (17 mL, 0.2 mmol), and HBpin (29 mL, 0.2 mmol) in anhydrous MTBE (0.5 mL) were reacted. The crude product was purified by flash column chromatography (Teledyne ISCO CombiFlash NextGen 300+, 12 g, 40 mL min^{-1}, hexane/ethyl acetate 10:1) to give an inseparable mixture of 5-(4,4,5,5-tetramethyl-1,3,2-dioxaborole)furfuryl alcohol and 4-(4,4,5,5-tetramethyl-1,3,2-dioxaborole)furfuryl alcohol in a 80:20 5-:4- ratio as a colourless oil (18 mg, 0.08 mmol, 40%)

5-(4,4,5,5-tetramethyl-1,3,2-dioxaborole)furfuryl alcohol: ^{1}H NMR: (500 MHz, $CDCl_3$) 7.03 (d, *J* = 3.3 Hz, 1H), 6.34 (d, *J* = 3.3 Hz, 1H), 4.66 (s, 2H), 1.35 (s, 12H). ^{11}B NMR: (160 MHz, $CDCl_3$) 27.0. ^{13}C NMR: (126 MHz, $CDCl_3$) 159.3, 124.5, 108.5, 84.4, 57.8, 24.9.

4-(4,4,5,5-tetramethyl-1,3,2-dioxaborole)furfuryl alcohol: ^{1}H NMR: (500 MHz, $CDCl_3$) 7.73 (s, 1H), 6.48 (s, 1H), 4.61 (s, 2H), 1.31 (s, 12H). ^{11}B NMR: (160 MHz, $CDCl_3$) 29.6. ^{13}C NMR: (126 MHz, $CDCl_3$) 154.7, 151.4, 111.5, 83.7, 57.5, 24.9.

^{1}H NMR (500 MHz, $CDCl_3$) Spectrum of 5-(4,4,5,5-tetramethyl-1,3,2-dioxaborole)furfuryl alcohol and 4-(4,4,5,5-tetramethyl-1,3,2-dioxaborole)furfuryl alcohol

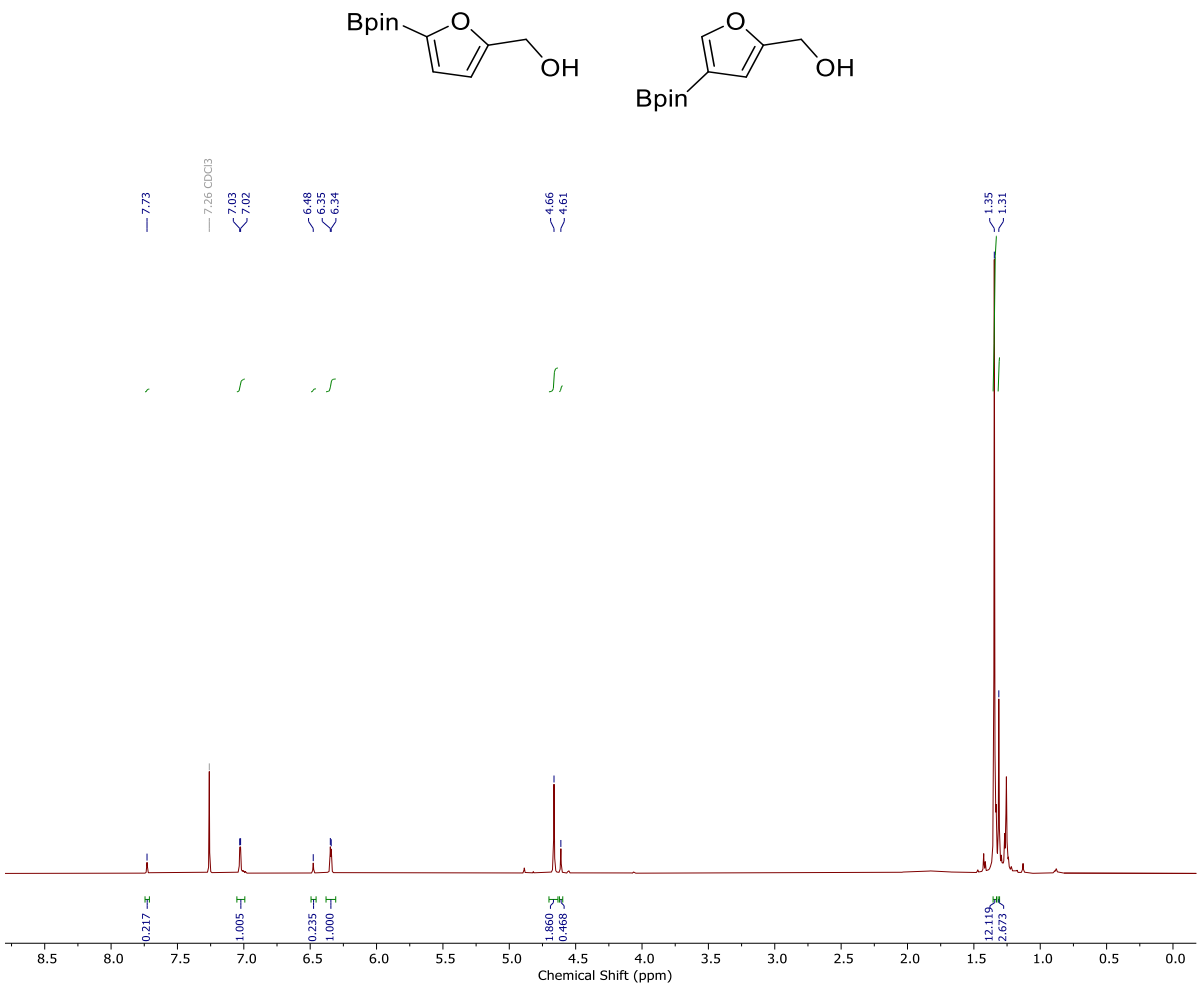

^{11}B NMR (160 MHz, $CDCl_3$) Spectrum of 5-(4,4,5,5-tetramethyl-1,3,2-dioxaborole)furfuryl alcohol and 4-(4,4,5,5-tetramethyl-1,3,2-dioxaborole)furfuryl alcohol

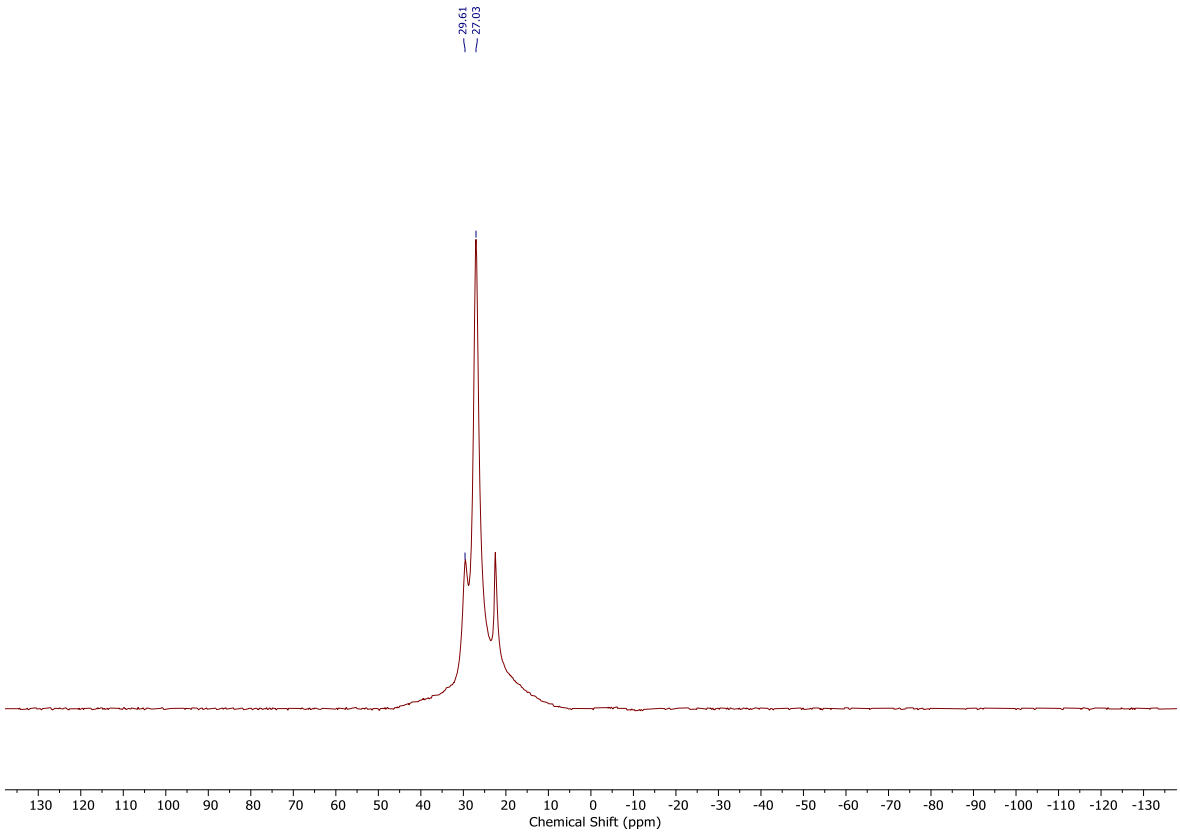

^{13}C NMR (126 MHz, $CDCl_3$) Spectrum of 5-(4,4,5,5-tetramethyl-1,3,2-dioxaborole)furfuryl alcohol and 4-(4,4,5,5-tetramethyl-1,3,2-dioxaborole)furfuryl alcohol

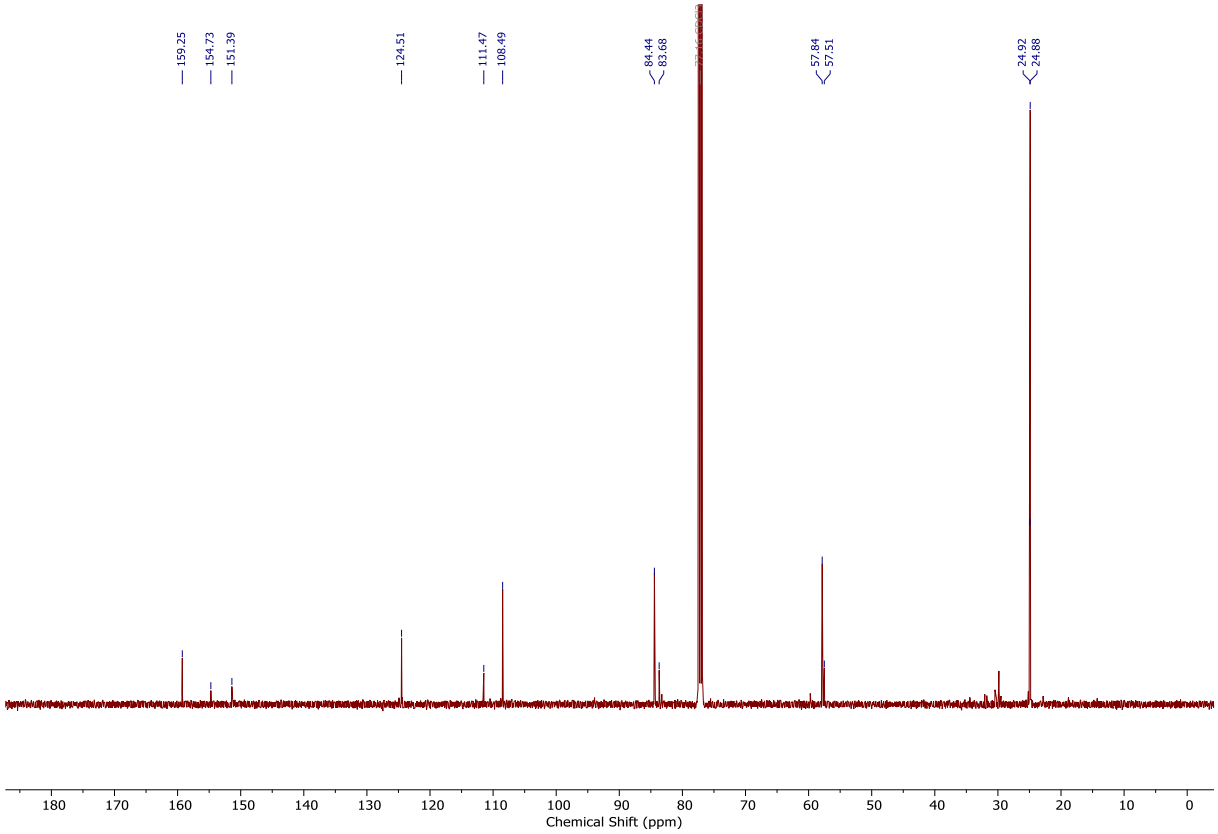

5.4.9. Synthesis and characterization of 5-(4,4,5,5-Tetramethyl-1,3,2-dioxaborole)-2-methylthiophene

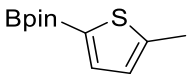

According to the general procedure, potassium *tert*-butoxide (23 mg, 0.24 mmol), bis(pinacolato)diboron (58 mg, 0.24 mmol), [dmpeMn(CO)$_3$Br] (7.4 mg, 0.02 mmol), and 2-methylthiophene (19 mL, 0.2 mmol) in anhydrous MTBE (0.5 mL) were reacted. The crude product was purified by flash column chromatography (Teledyne ISCO CombiFlash NextGen 300+, 12 g, 40 mL min^{-1}, hexane/ethyl acetate 10:1) to give 5-(4,4,5,5-tetramethyl-1,3,2-dioxaborole)-2-methylthiophene as a colourless oil (31 mg, 0.14 mmol, 70%). ^{1}H NMR: (500 MHz, $CDCl_3$) 7.45 (d, J = 3.4 Hz, 1H), 6.86–6.82 (m, 1H), 2.53 (d, J = 1.0 Hz, 3H), 1.33 (m, 12H). ^{11}B NMR: (160 MHz, $CDCl_3$) 28.8. ^{13}C NMR: (126 MHz, $CDCl_3$) 147.7, 137.8, 127.1, 84.0, 24.9, 15.5.

^{1}H NMR (500 MHz, $CDCl_3$) Spectrum of 5-(4,4,5,5-tetramethyl-1,3,2-dioxaborole)-2-methylthiophene

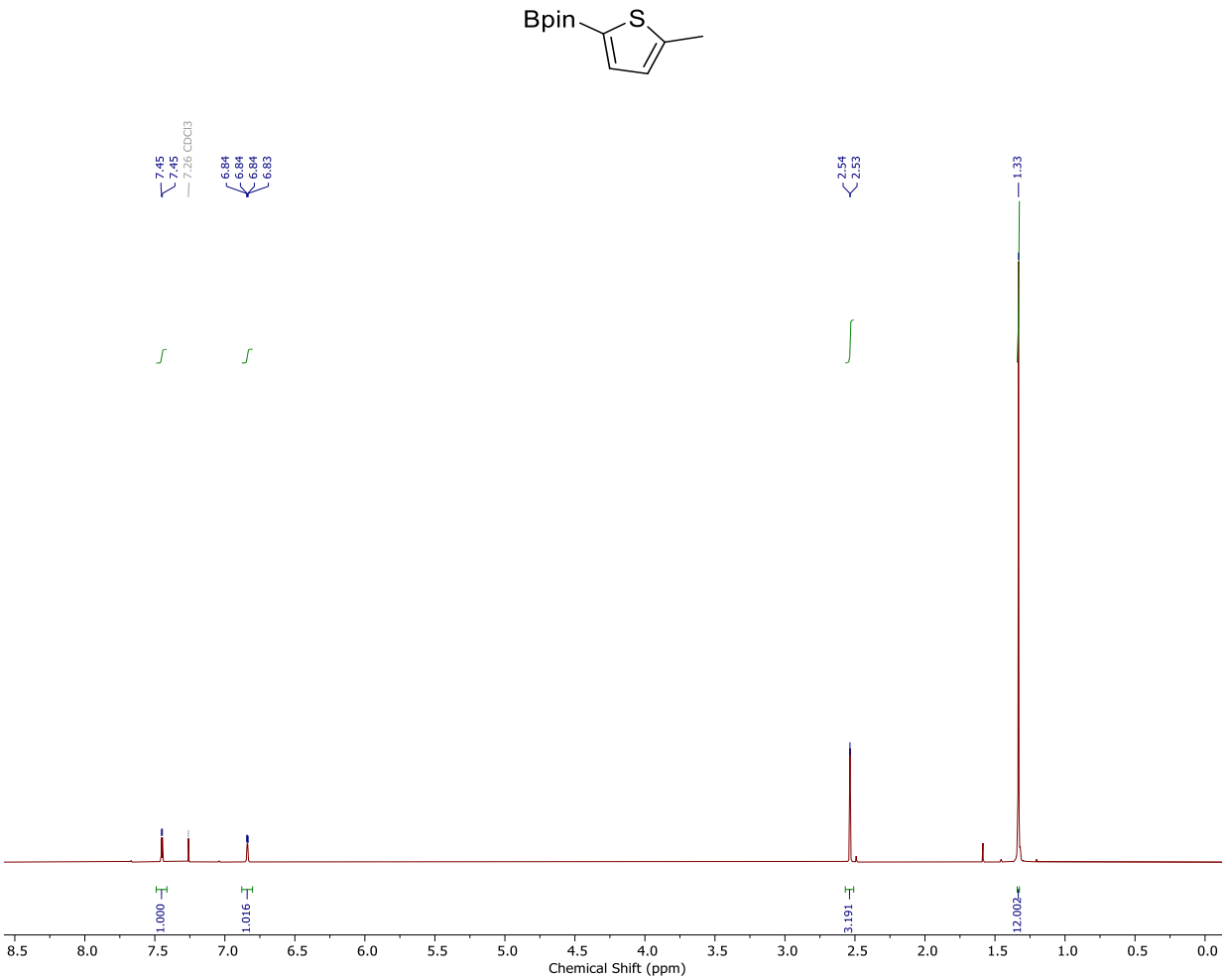

^{11}B NMR (160 MHz, $CDCl_3$) Spectrum of 5-(4,4,5,5-tetramethyl-1,3,2-dioxaborole)-2-methylthiophene

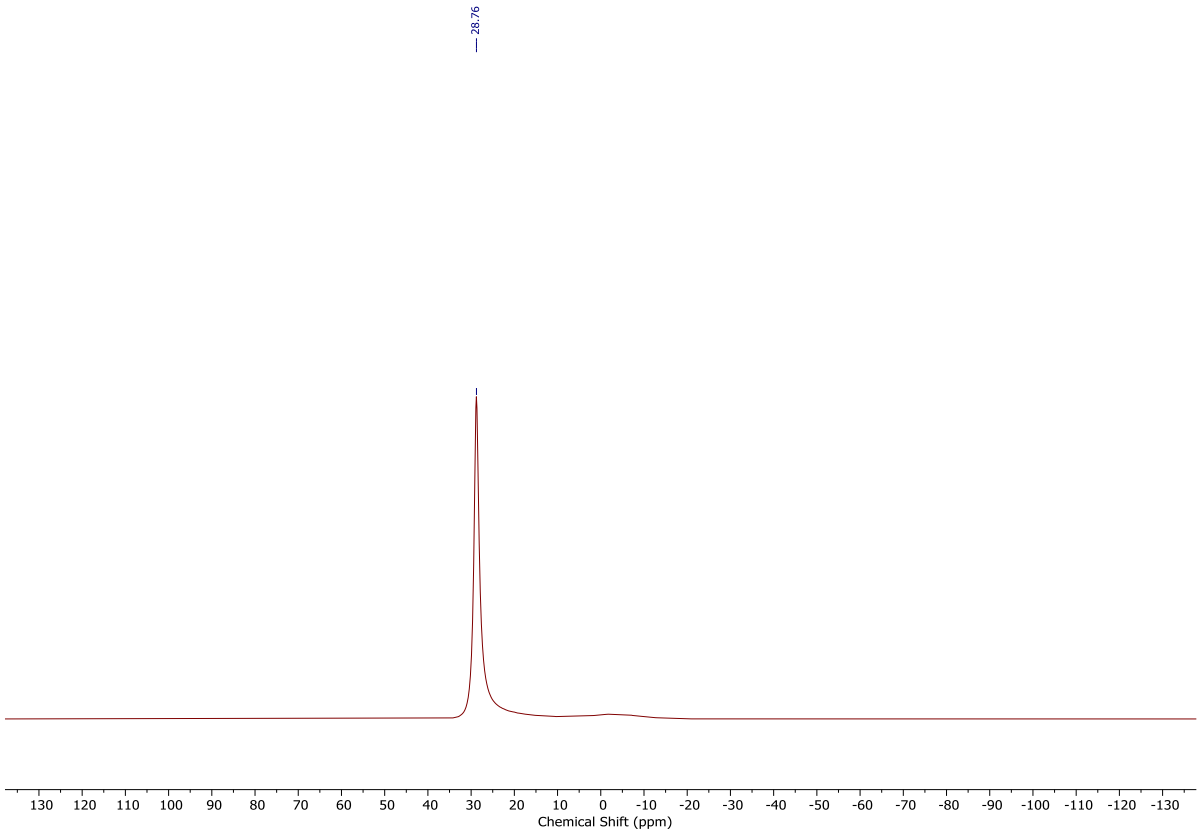

^{13}C NMR (126 MHz, $CDCl_3$) Spectrum of 5-(4,4,5,5-tetramethyl-1,3,2-dioxaborole)-2-methylthiophene

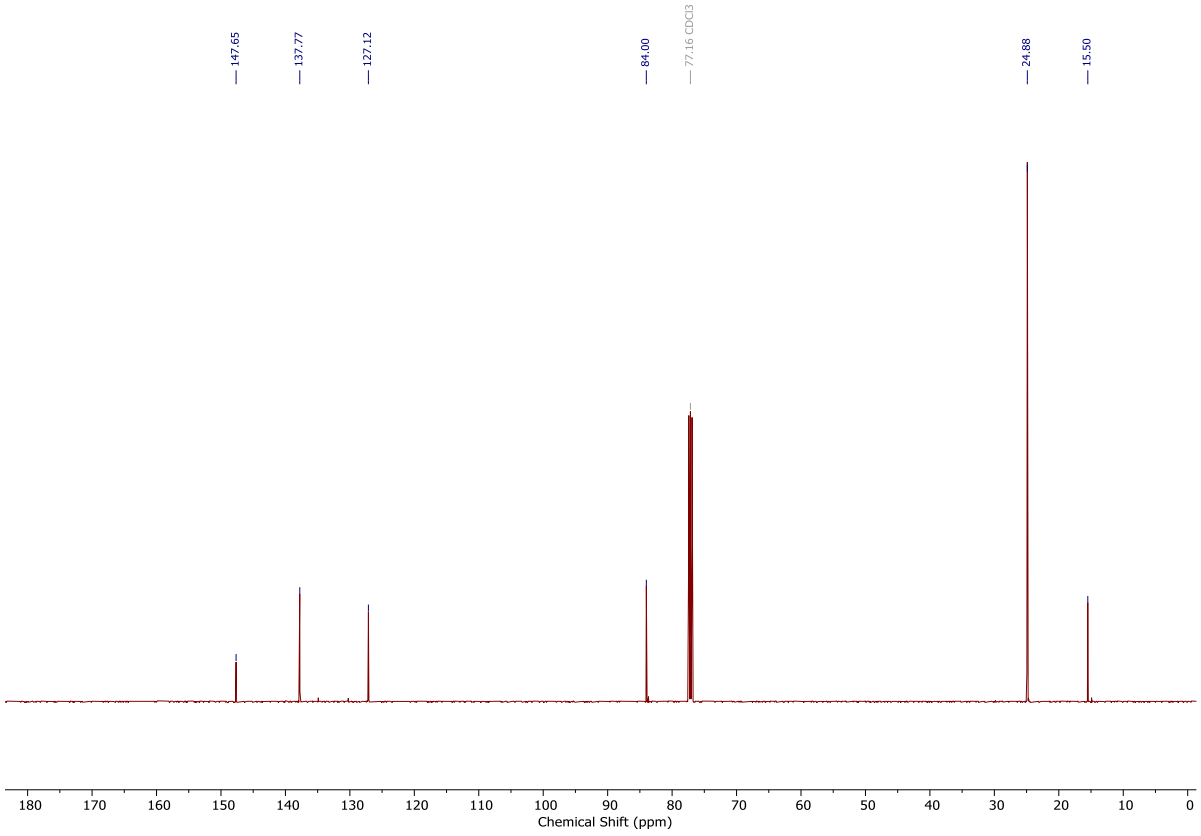

5.4.10. Synthesis and characterization of 2-(4,4,5,5-Tetramethyl-1,3,2-dioxaborole)pyrrole and 2,5-bis(4,4,5,5-tetramethyl-1,3,2-dioxaborole)pyrrole

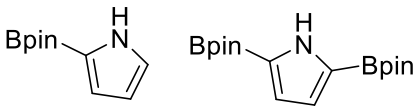

According to the general procedure, potassium *tert*-butoxide (23 mg, 0.24 mmol), bis(pinacolato)diboron (58 mg, 0.24 mmol), [dmpeMn(CO)$_3$Br] (7.4 mg, 0.02 mmol), and pyrrole (14 mL, 0.2 mmol) in anhydrous MTBE (0.5 mL) were reacted. The crude product was purified by flash column chromatography (Teledyne ISCO CombiFlash NextGen 300+, 12 g, 40 mL min^{-1}, hexane/ethyl acetate 10:1) to give an inseparable mixture of 2-(4,4,5,5-tetramethyl-1,3,2-dioxaborole)pyrrole and 2,5-bis(4,4,5,5-tetramethyl-1,3,2-dioxaborole)pyrrole as a colourless oil (12 mg, 0.05 mmol, 25%). Product distribution 2-:2,5- = 57:43.

2-(4,4,5,5-tetramethyl-1,3,2-dioxaborole)pyrrole: ^{1}H NMR: (500 MHz, $CDCl_3$) 8.82 (br. s, 1H), 7.02 – 6.95 (m, 1H), 6.90 – 6.84 (m, 2H), 6.30 (d, J = 3.0 Hz), 1.32 (s, 12H). ^{11}B NMR: (160 MHz, $CDCl_3$) 27.8. ^{13}C NMR: (126 MHz, $CDCl_3$) 122.8, 120.2, 109.9, 83.7, 24.9.

2,5-bis(4,4,5,5-tetramethyl-1,3,2-dioxaborole)pyrrole: ^{1}H NMR: (500 MHz, $CDCl_3$) 9.27 (br. s, 1H), 6.83 (d, J = 2.3 Hz, 2H), 1.31 (s, 24H). ^{11}B NMR: (160 MHz, $CDCl_3$) 27.8. ^{13}C NMR: (126 MHz, $CDCl_3$) 120.6, 83.9, 24.9.

^{1}H NMR (500 MHz, $CDCl_3$) Spectrum of 2-(4,4,5,5-tetramethyl-1,3,2-dioxaborole)pyrrole and 2,5-bis(4,4,5,5-tetramethyl-1,3,2-dioxaborole)pyrrole

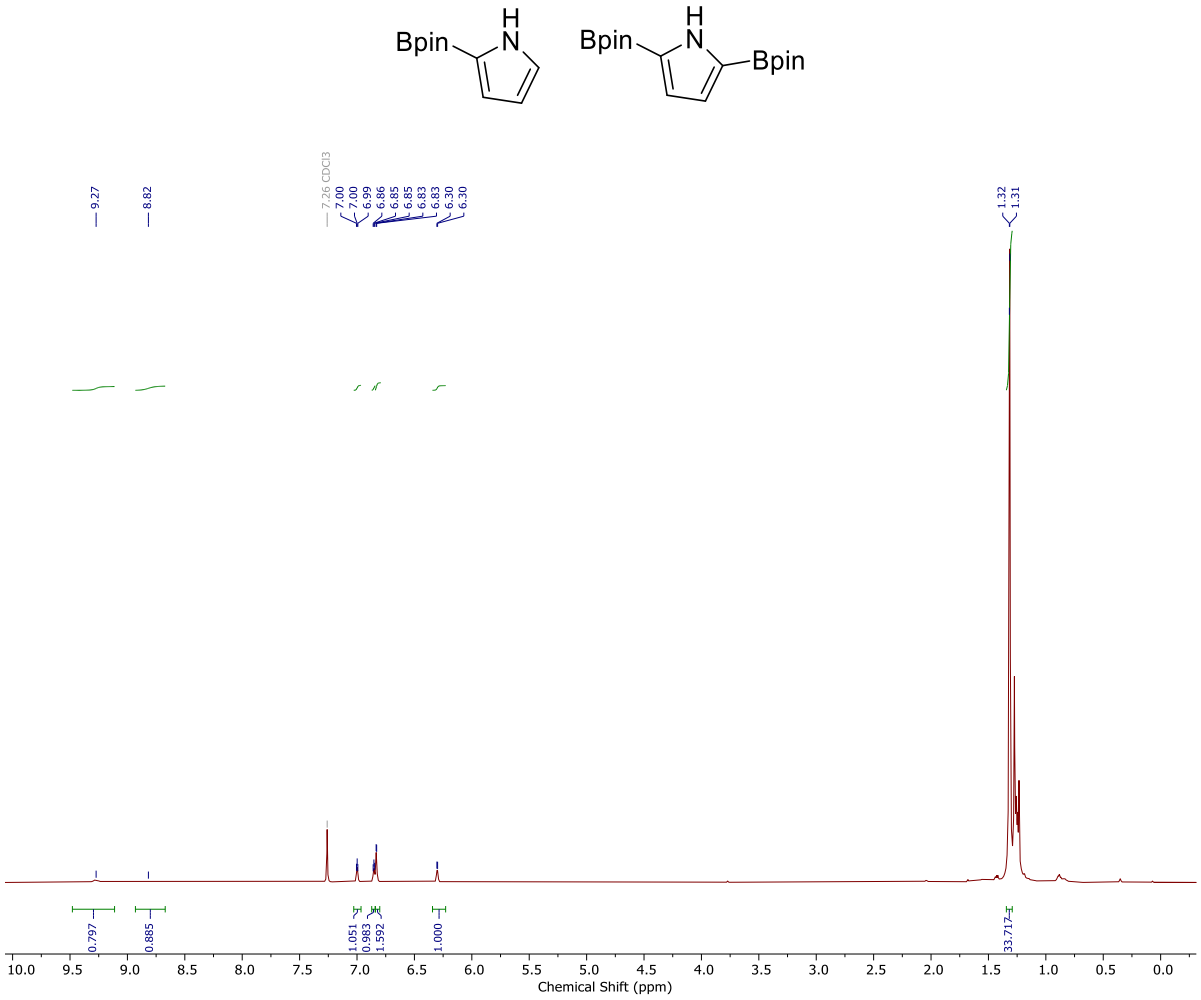

^{11}B NMR (160 MHz, $CDCl_3$) Spectrum of 2-(4,4,5,5-tetramethyl-1,3,2-dioxaborole)pyrrole and 2,5-bis(4,4,5,5-tetramethyl-1,3,2-dioxaborole)pyrrole

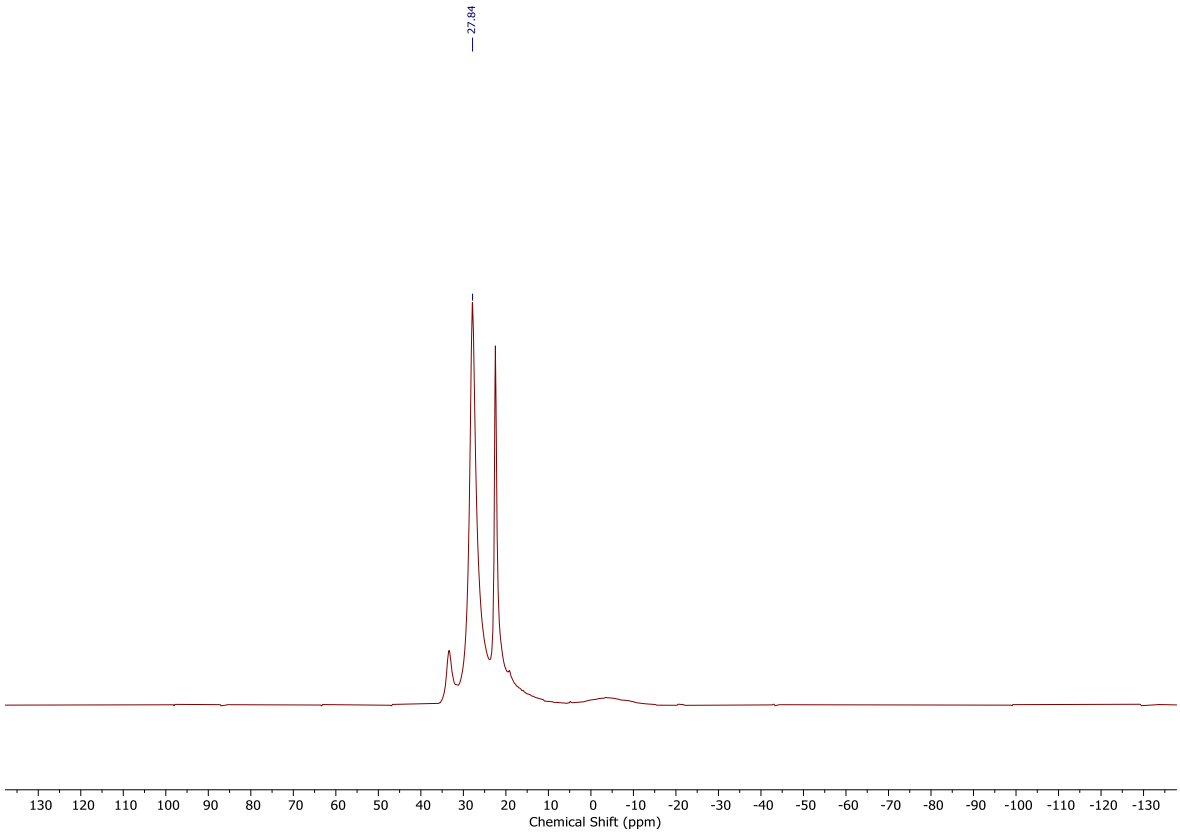

^{13}C NMR (126 MHz, $CDCl_3$) Spectrum of 2-(4,4,5,5-tetramethyl-1,3,2-dioxaborole)pyrrole and 2,5-bis(4,4,5,5-tetramethyl-1,3,2-dioxaborole)pyrrole

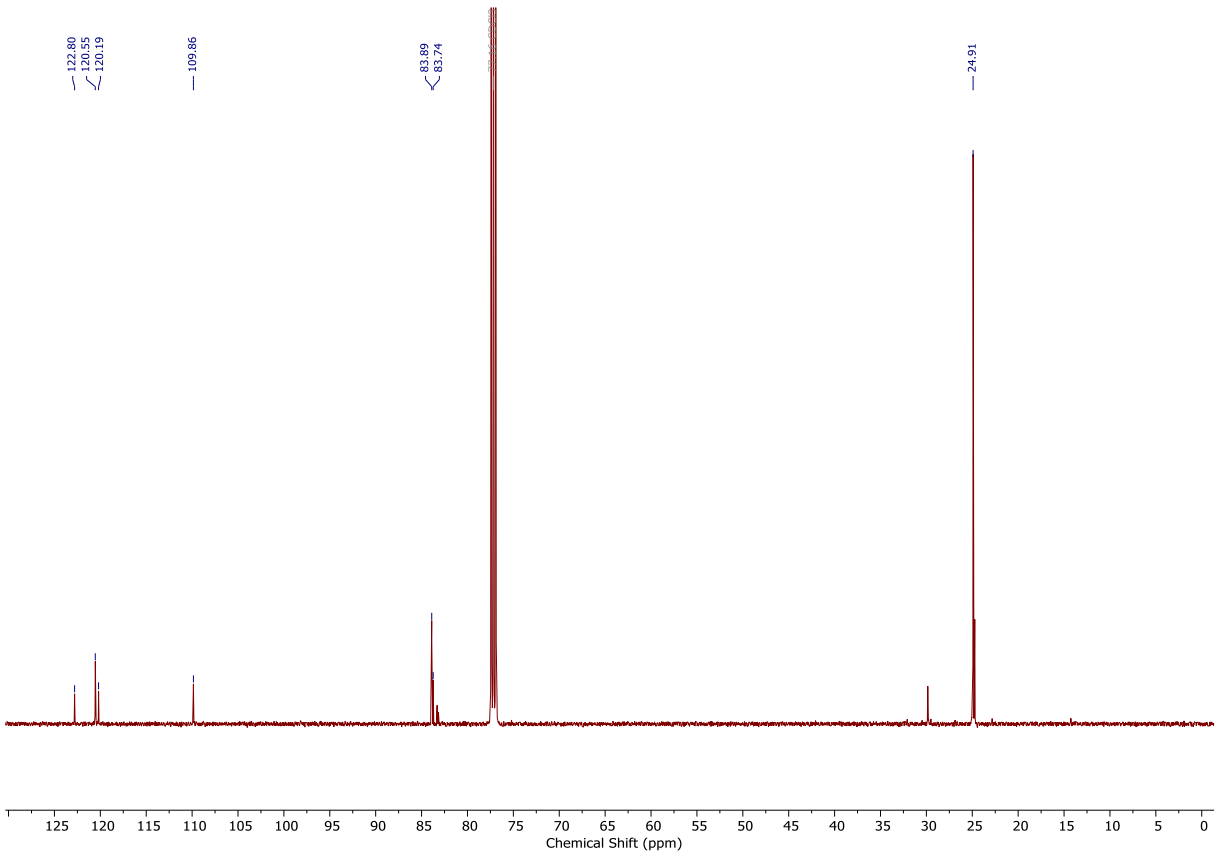

5.4.11. Synthesis and characterization of 2-(4,4,5,5-Tetramethyl-1,3,2-dioxaborole)-N-methylpyrrole, 3-(4,4,5,5-tetramethyl-1,3,2-dioxaborole)-N-methylpyrrole and 2,5-bis(4,4,5,5-tetramethyl-1,3,2-dioxaborole)-N-methylpyrrole

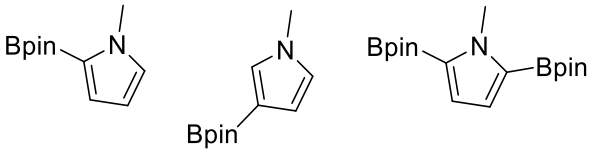

According to the general procedure, potassium *tert*-butoxide (23 mg, 0.24 mmol), bis(pinacolato)diboron (58 mg, 0.24 mmol), [dmpeMn(CO)$_3$Br] (7.4 mg, 0.02 mmol), and N-methylpyrrole (18 mL, 0.2 mmol) in anhydrous MTBE (0.5 mL) were reacted. The crude product was purified by flash column chromatography (Teledyne ISCO CombiFlash NextGen 300+, 12 g, 40 mL min^{-1}, hexane/ethyl acetate 10:1) to give 2-(4,4,5,5-tetramethyl-1,3,2-dioxaborole)-N-methylpyrrole as a colourless oil (6 mg, 0.03 mmol, 15%), and an inseparable mixture of 3-(4,4,5,5-tetramethyl-1,3,2-dioxaborole)-N-methylpyrrole and 2,5-bis(4,4,5,5-tetramethyl-1,3,2-dioxaborole)-N-methylpyrrole as a colourless oil (7 mg, 0.04 mmol, 20%). Total isolated product yield (2-:3-:2,5-) = 35% (43:43:14).

2-(4,4,5,5-tetramethyl-1,3,2-dioxaborole)-N-pyrrole: ^{1}H NMR: (500 MHz, $CDCl_3$) 6.84 – 6.78 (m, 2H), 6.15 (dd, J = 3.6, 2.4 Hz, 1H), 3.84 (s, 3H), 1.31 (s, 12H). ^{11}B NMR: (160 MHz, $CDCl_3$) 30.0. ^{13}C NMR: (126 MHz, $CDCl_3$) 128.3, 122.1, 108.5, 83.2, 36.7, 24.9.

3-(4,4,5,5-tetramethyl-1,3,2-dioxaborole)-N-pyrrole: ^{1}H NMR: (500 MHz, $CDCl_3$) 8.82 (br. s, 1H), 7.02 – 6.95 (m, 1H), 6.90 – 6.84 (m, 2H), 6.30 (d, *J* = 3.0 Hz), 1.32 (s, 12H). ^{11}B NMR: (160 MHz, $CDCl_3$) 27.8. ^{13}C NMR: (126 MHz, $CDCl_3$) 122.8, 120.2, 109.9, 83.7, 24.9.

2,5-bis(4,4,5,5-tetramethyl-1,3,2-dioxaborole)-N-pyrrole: ^{1}H NMR: (500 MHz, $CDCl_3$) 9.27 (br. s, 1H), 6.83 (d, *J* = 2.3 Hz, 2H), 1.31 (s, 24H). ^{11}B NMR: (160 MHz, $CDCl_3$) 27.8. ^{13}C NMR: (126 MHz, $CDCl_3$) 120.6, 83.9, 24.9.

^{1}H NMR (500 MHz, $CDCl_3$) Spectrum of 2-(4,4,5,5-tetramethyl-1,3,2-dioxaborole)-N-methylpyrrole

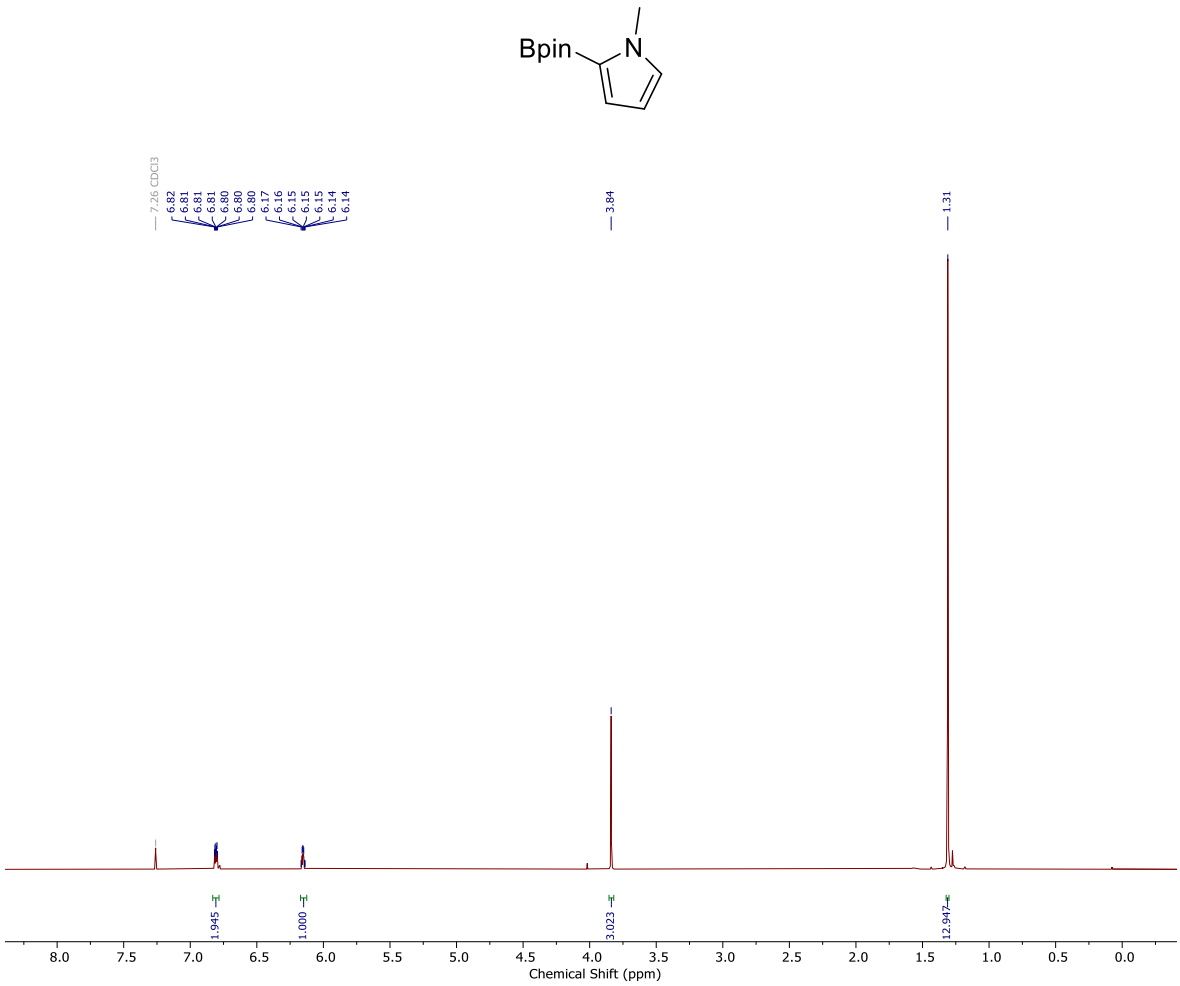

^{11}B NMR (160 MHz, $CDCl_3$) Spectrum of 2-(4,4,5,5-tetramethyl-1,3,2-dioxaborole)-N-methylpyrrole

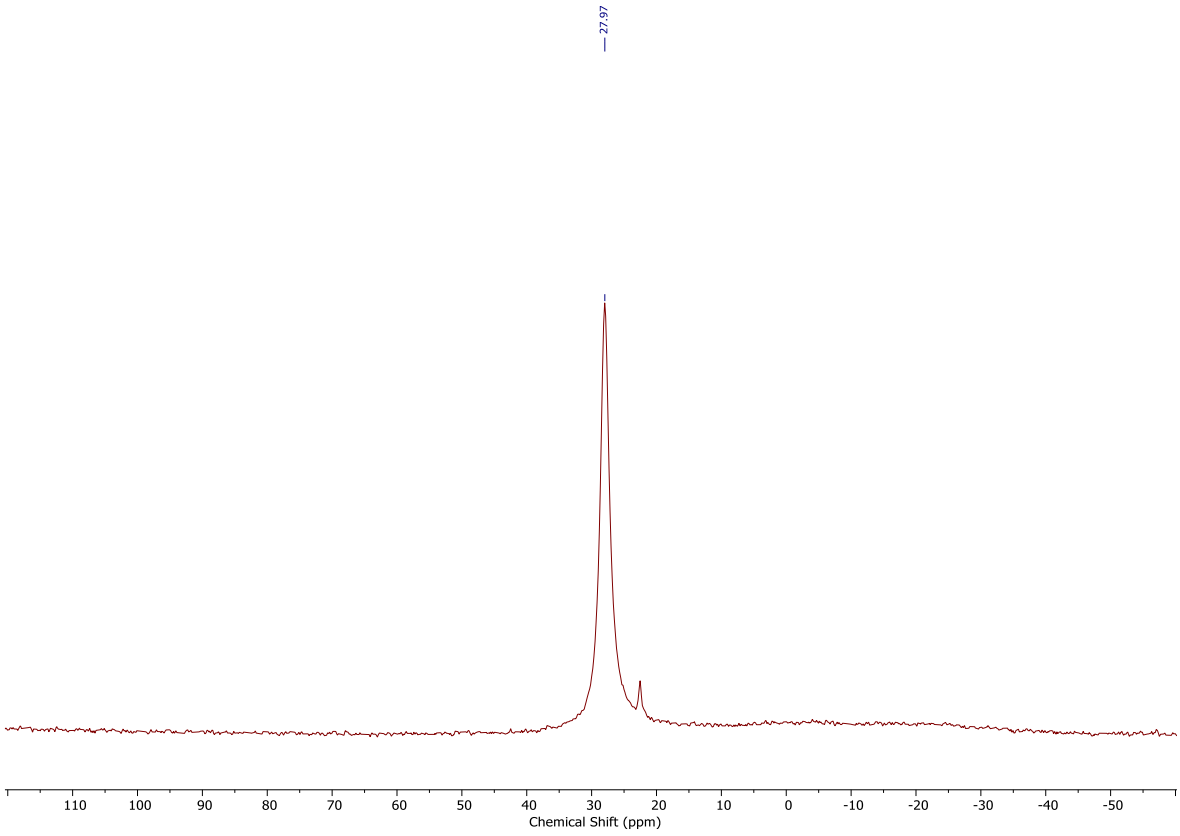

^{13}C NMR (126 MHz, $CDCl_3$) Spectrum of 2-(4,4,5,5-tetramethyl-1,3,2-dioxaborole)-N-methylpyrrole

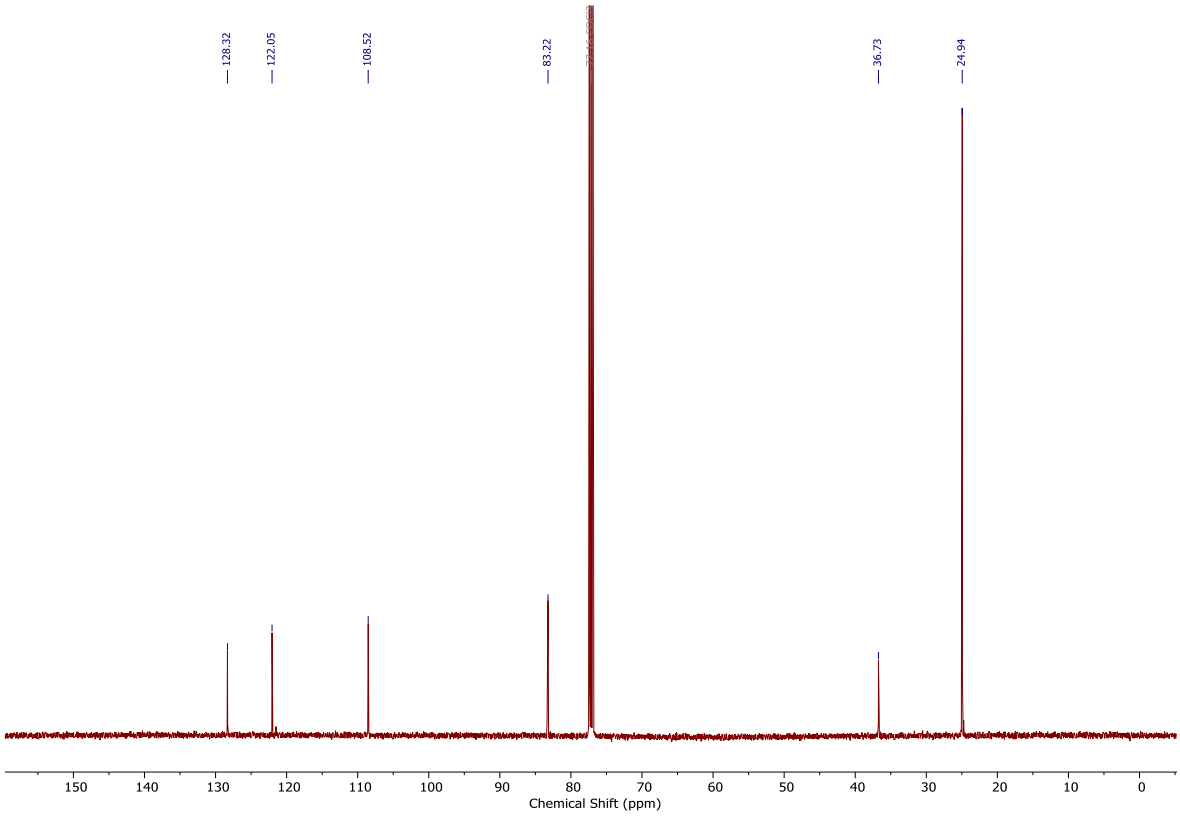

^{1}H NMR (500 MHz, $CDCl_3$) Spectrum of 3-(4,4,5,5-tetramethyl-1,3,2-dioxaborole)-N-methylpyrrole and 2,5-bis(4,4,5,5-tetramethyl-1,3,2-dioxaborole)-N-methylpyrrole

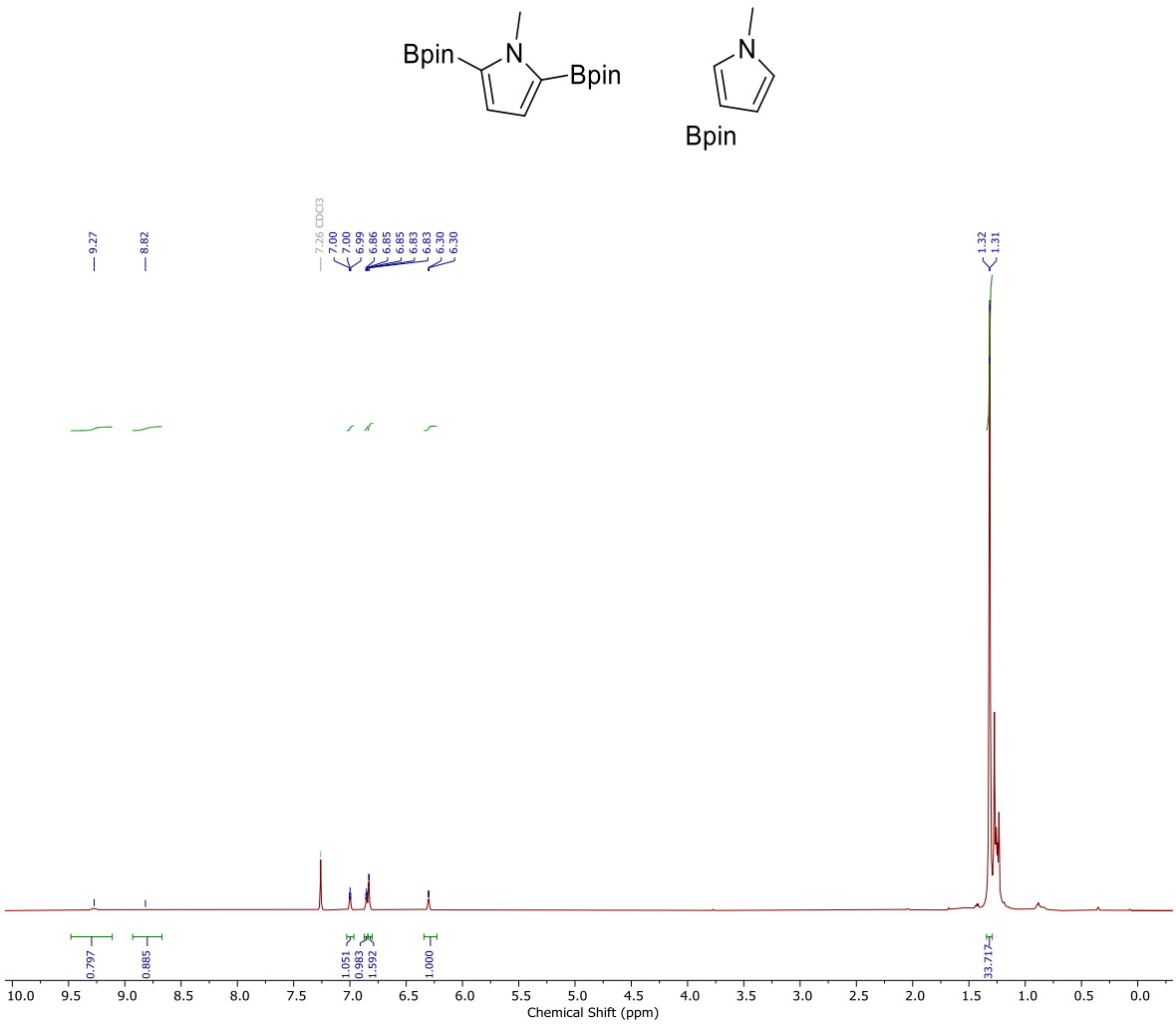

^{11}B NMR (160 MHz, $CDCl_3$) Spectrum of 3-(4,4,5,5-tetramethyl-1,3,2-dioxaborole)-N-methylpyrrole and 2,5-bis(4,4,5,5-tetramethyl-1,3,2-dioxaborole)-N-methylpyrrole

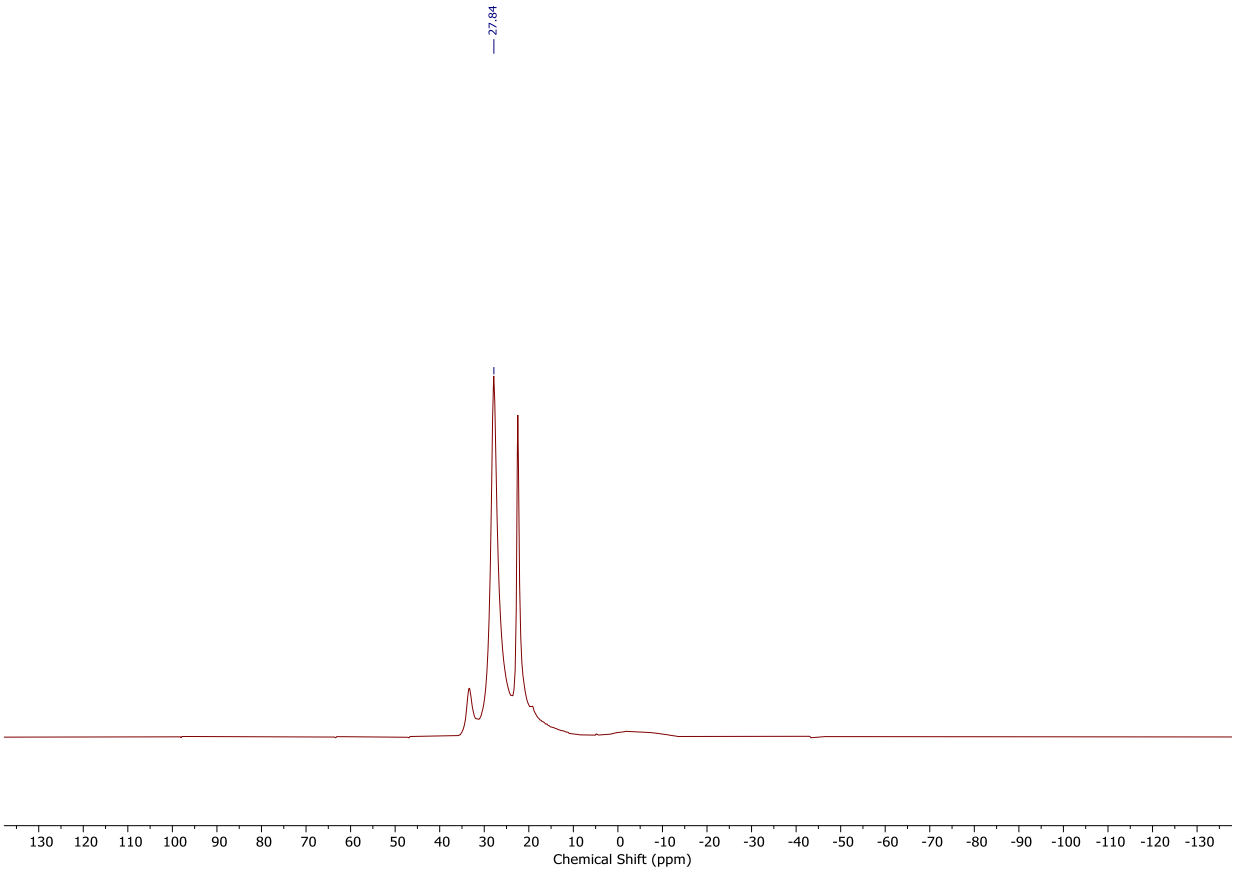

^{13}C NMR (126 MHz, $CDCl_3$) Spectrum of 3-(4,4,5,5-tetramethyl-1,3,2-dioxaborole)-N-methylpyrrole and 2,5-bis(4,4,5,5-tetramethyl-1,3,2-dioxaborole)-N-methylpyrrole

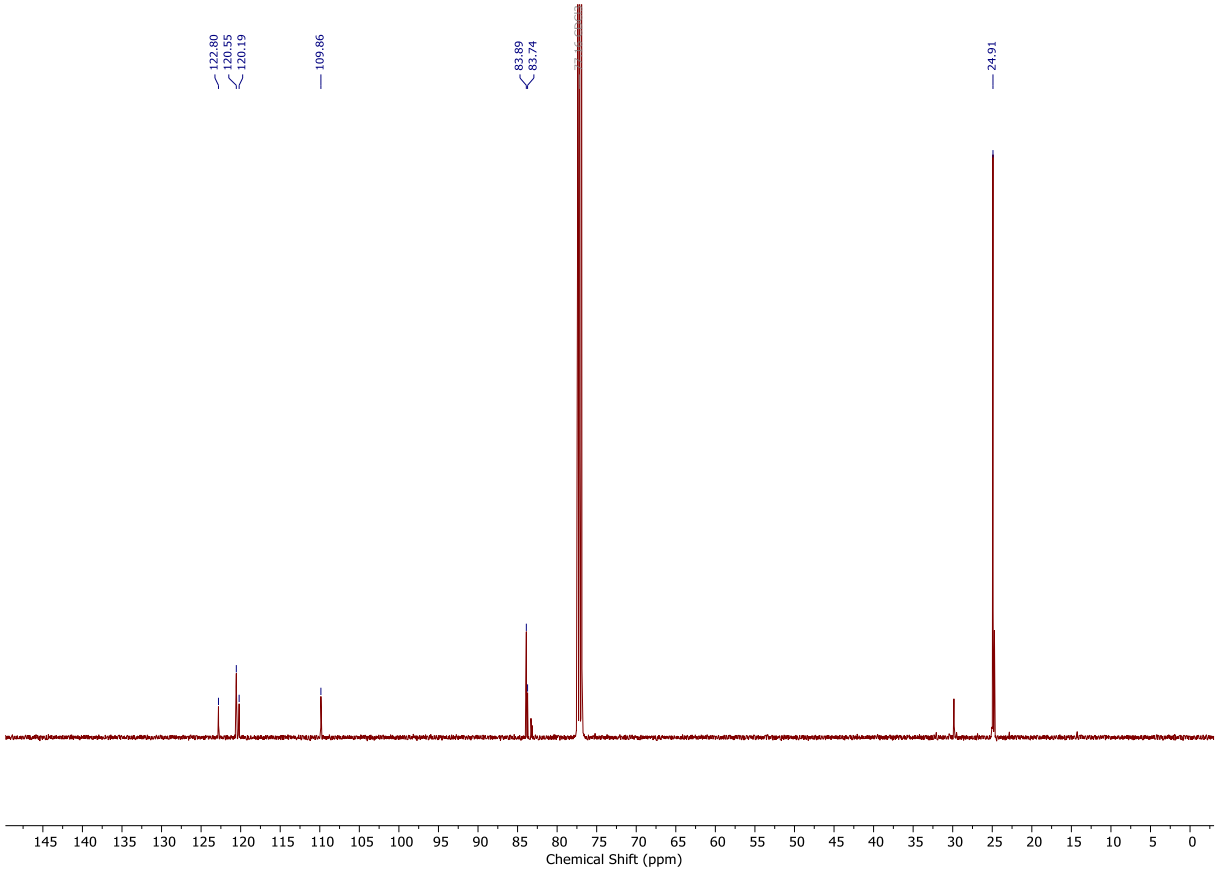

5.4.12. 3-(4,4,5,5-Tetramethyl-1,3,2-dioxaborole)-N-triisopropylpyrrole

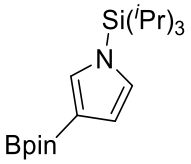

According to the general procedure, potassium *tert*-butoxide (23 mg, 0.24 mmol), bis(pinacolato)diboron (58 mg, 0.24 mmol), [dmpeMn(CO)$_3$Br] (7.4 mg, 0.02 mmol), and N-N-triisopropylpyrrole (49 mL, 0.2 mmol) in anhydrous MTBE (0.5 mL) were reacted. The crude product was purified by flash column chromatography (Teledyne ISCO CombiFlash NextGen 300+, 12 g, 40 mL min^{-1}, hexane/ethyl acetate 10:1) to give 3-(4,4,5,5-Tetramethyl-1,3,2-dioxaborole)-N-triisopropylpyrrole as a colourless oil (38 mg, 0.11 mmol, 57%). ^{1}H NMR: (500 MHz, $CDCl_3$) 7.23 (app. t, J = 1.6 Hz, 1H), 6.81 (dd, J = 2.7, 1.9 Hz, 1H), 6.62 (dd, J = 2.7, 1.3 Hz, 1H), 1.46 (hept, J = 7.5 Hz, 3H), 1.32 (s, 12H), 1.09 (d, J = 7.5 Hz, 18H). ^{11}B NMR: (160 MHz, $CDCl_3$) 30.2. ^{13}C NMR: (126 MHz, $CDCl_3$) 133.8, 125.1, 115.8, 82.9, 25.0, 18.0, 11.8.

^{1}H NMR (500 MHz, $CDCl_3$) Spectrum of 3-(4,4,5,5-Tetramethyl-1,3,2-dioxaborole)-N-triisopropylpyrrole

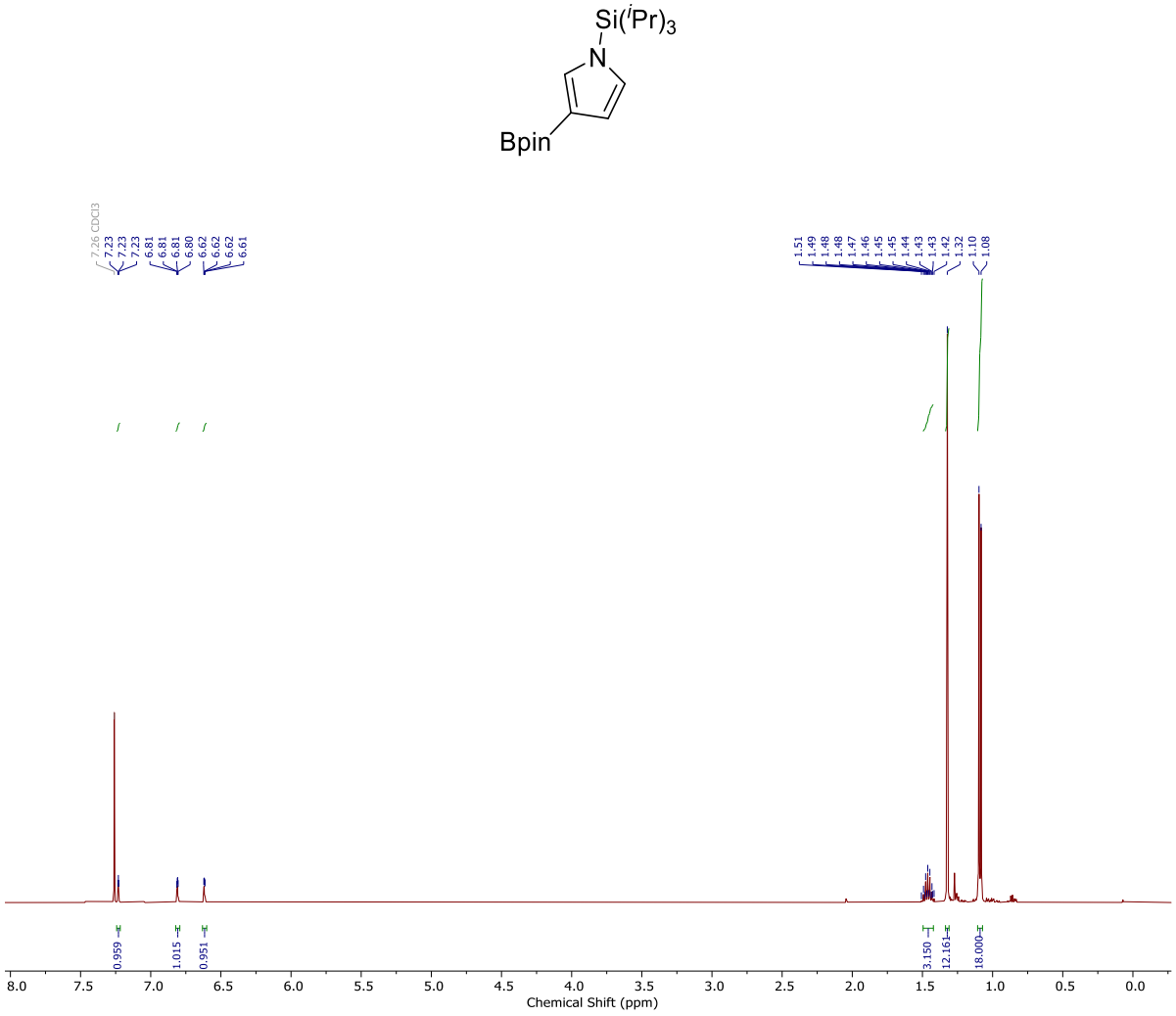

^{11}B NMR (160 MHz, $CDCl_3$) Spectrum of 3-(4,4,5,5-Tetramethyl-1,3,2-dioxaborole)-N-triisopropylpyrrole

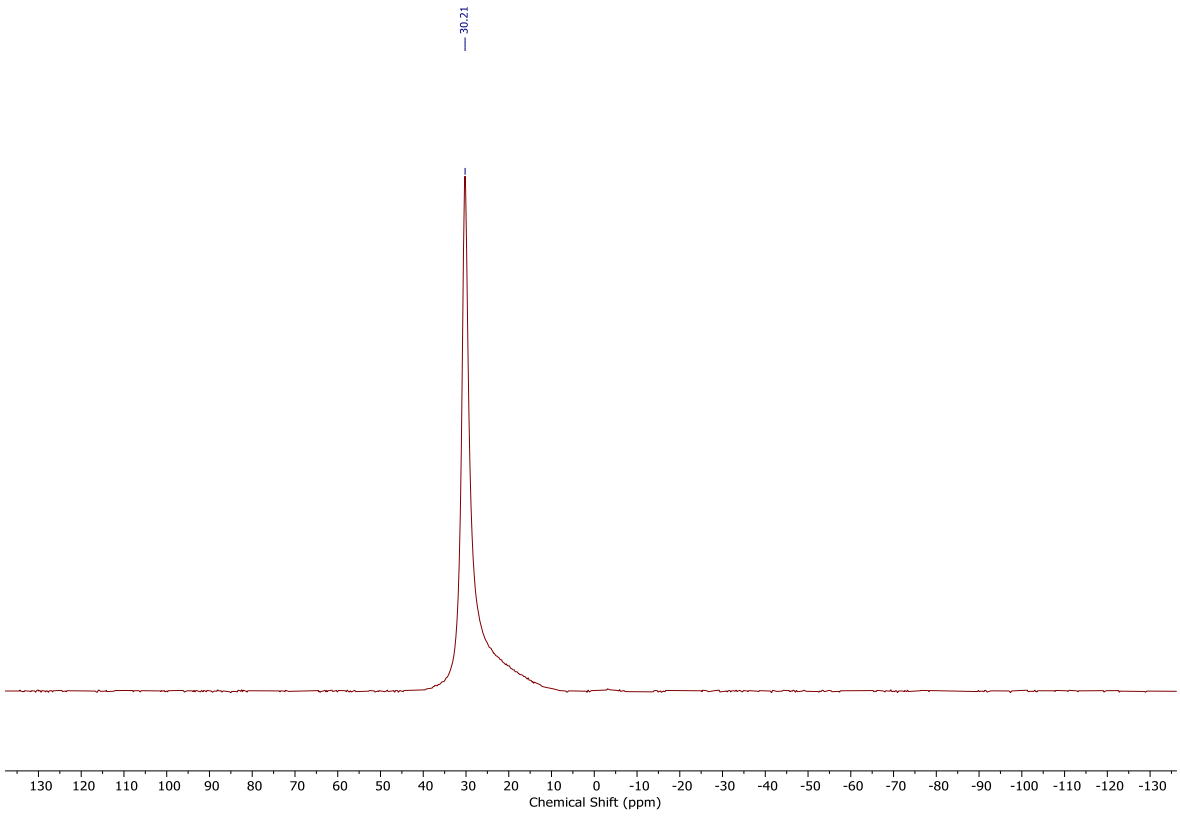

^{13}C NMR (126 MHz, $CDCl_3$) Spectrum of 3-(4,4,5,5-Tetramethyl-1,3,2-dioxaborole)-N-triisopropylpyrrole

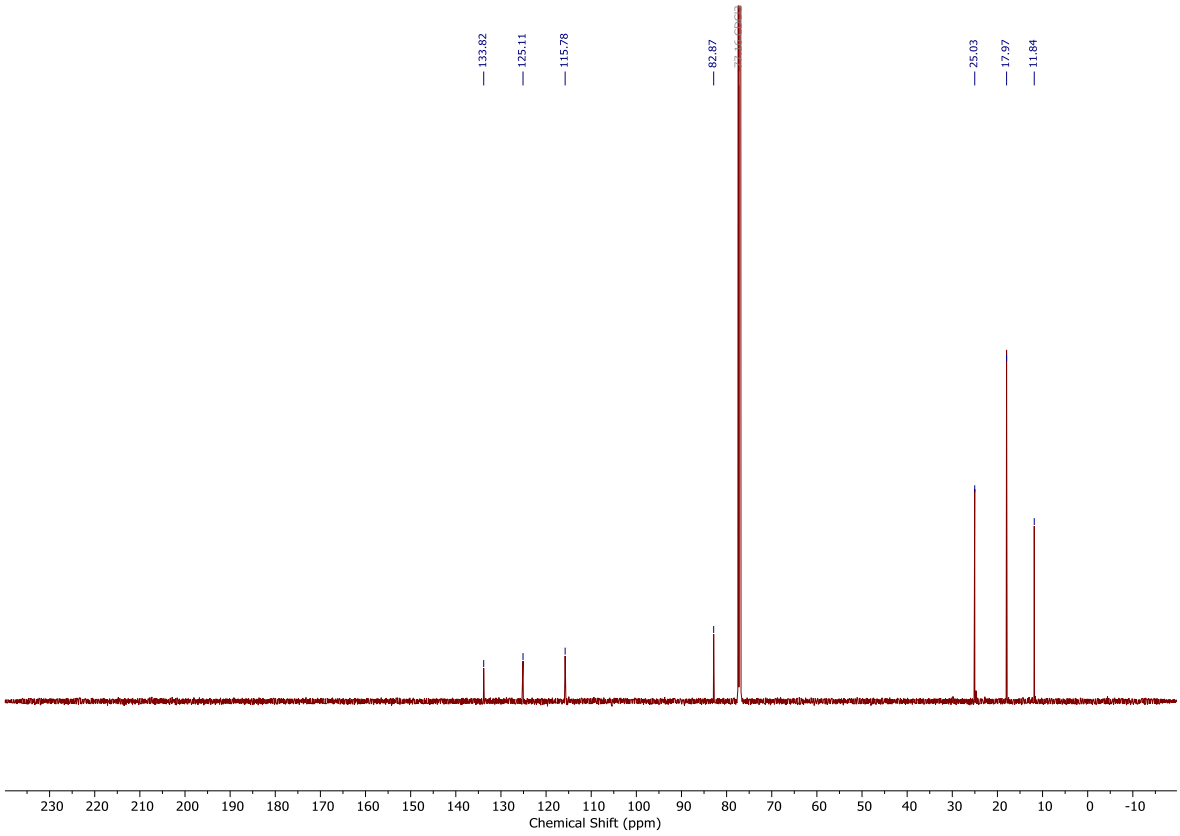

5.4.13. Synthesis and characterization of 2-(4,4,5,5-Tetramethyl-1,3,2-dioxaborole)indole

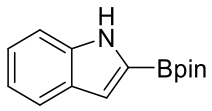

According to the general procedure, potassium *tert*-butoxide (23 mg, 0.24 mmol), bis(pinacolato)diboron (58 mg, 0.24 mmol), [dmpeMn(CO)$_3$Br] (7.4 mg, 0.02 mmol), and indole (23 mg, 0.2 mmol) in anhydrous MTBE (0.5 mL) were reacted. The crude product was purified by flash column chromatography (Teledyne ISCO CombiFlash NextGen 300+, 12 g, 40 mL min^{-1}, hexane/ethyl acetate 10:1) to give 2-(4,4,5,5-tetramethyl-1,3,2-dioxaborole)indole as a colourless oil (22 mg, 0.09 mmol, 43%). ^{1}H NMR: (500 MHz, $CDCl_3$) 8.54 (br. s, 1H), 7.6 (dd, *J* = 8.0, 1.0 Hz, 1H), 7.39 (d, *J* = 8.2, 1.0 Hz, 1H), 7.25 – 7.20 (m, 1H), 7.12 (dd, J = 2.1, 1.0 Hz, 1H), 7.11 – 7.08 (m, 1H), 1.37 (s, 12H). ^{11}B NMR: (160 MHz, $CDCl_3$) 28.6. ^{13}C NMR: (126 MHz, $CDCl_3$) 138.4, 128.5, 123.8, 121.8, 120.0, 114.0, 111.4, 84.3, 25.0.

^{1}H NMR (500 MHz, $CDCl_3$) Spectrum of 2-(4,4,5,5-tetramethyl-1,3,2-dioxaborole)indole

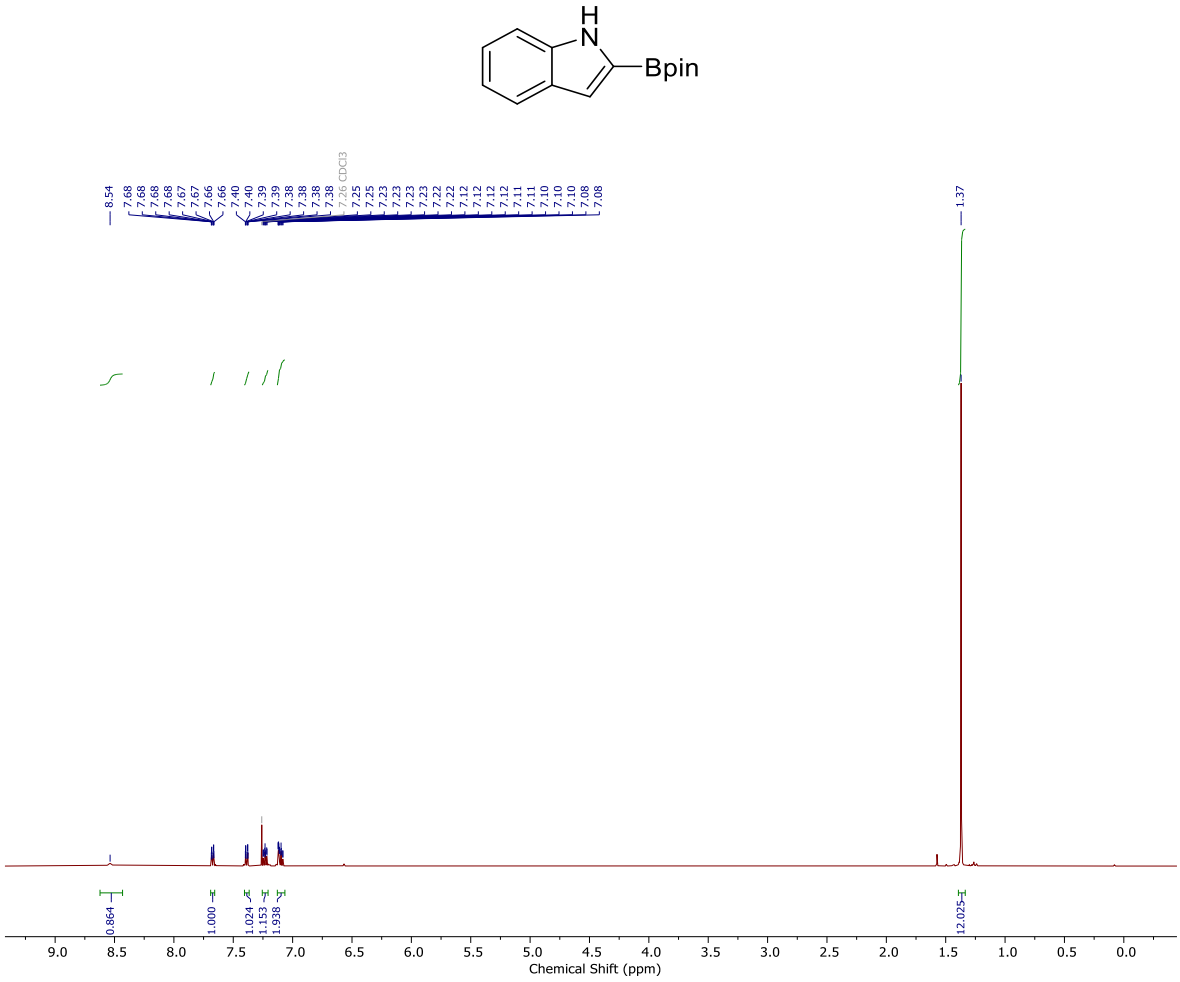

^{11}B NMR (160 MHz, $CDCl_3$) Spectrum of 2-(4,4,5,5-tetramethyl-1,3,2-dioxaborole)indole

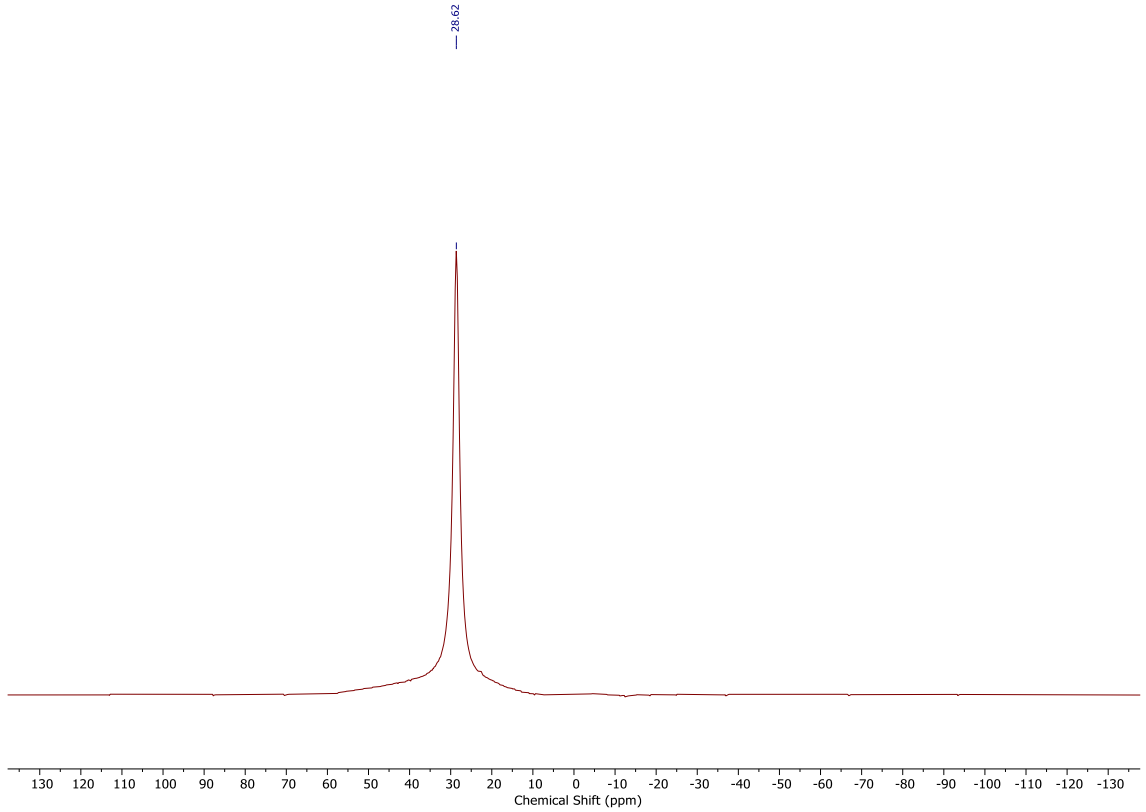

^{13}C NMR (126 MHz, $CDCl_3$) Spectrum of 2-(4,4,5,5-tetramethyl-1,3,2-dioxaborole)indole

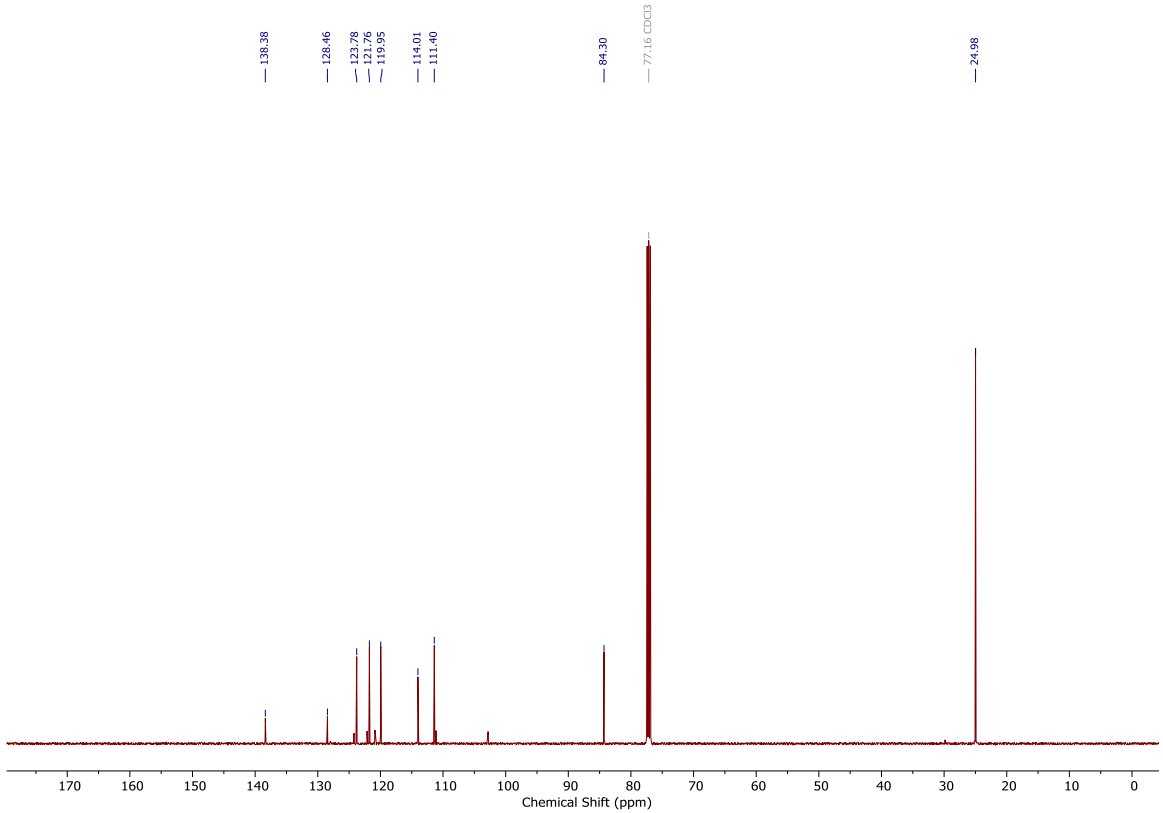

5.4.14. Synthesis and characterization of 2-(4,4,5,5-Tetramethyl-1,3,2-dioxaborole)-N-methylindole

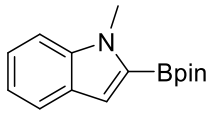

According to the general procedure, potassium *tert*-butoxide (23 mg, 0.24 mmol), bis(pinacolato)diboron (58 mg, 0.24 mmol), [dmpeMn(CO)$_3$Br] (7.4 mg, 0.02 mmol), and N-methylindole (25 mL, 0.2 mmol) in anhydrous MTBE (0.5 mL) were reacted. The crude product was purified by flash column chromatography (Teledyne ISCO CombiFlash NextGen 300+, 12 g, 40 mL min^{-1}, hexane/ethyl acetate 10:1) to give 2-(4,4,5,5-tetramethyl-1,3,2-dioxaborole)-N-methlyindole as a colourless oil (28 mg, 0.11 mmol, 57%). ^{1}H NMR: (500 MHz, $CDCl_3$) 7.64 (dt, *J* = 8.0, 1.0 Hz, 1H), 7.36 – 7.33 (m, 1H), 7.28 – 7.24 (m, 1H), 7.13 (d, J = 0.9 Hz, 1H), 7.10 – 7.06 (m, 1H), 3.97 (s, 3H), 1.37 (s, 12H). ^{11}B NMR: (160 MHz, $CDCl_3$) 28.6. ^{13}C NMR: (126 MHz, $CDCl_3$) 140.3, 128.0, 123.3, 121.7, 119.4, 114.4, 109.8, 83.8, 32.4, 25.0.

^{1}H NMR (500 MHz, $CDCl_3$) Spectrum of 2-(4,4,5,5-tetramethyl-1,3,2-dioxaborole)-N-methlyindole

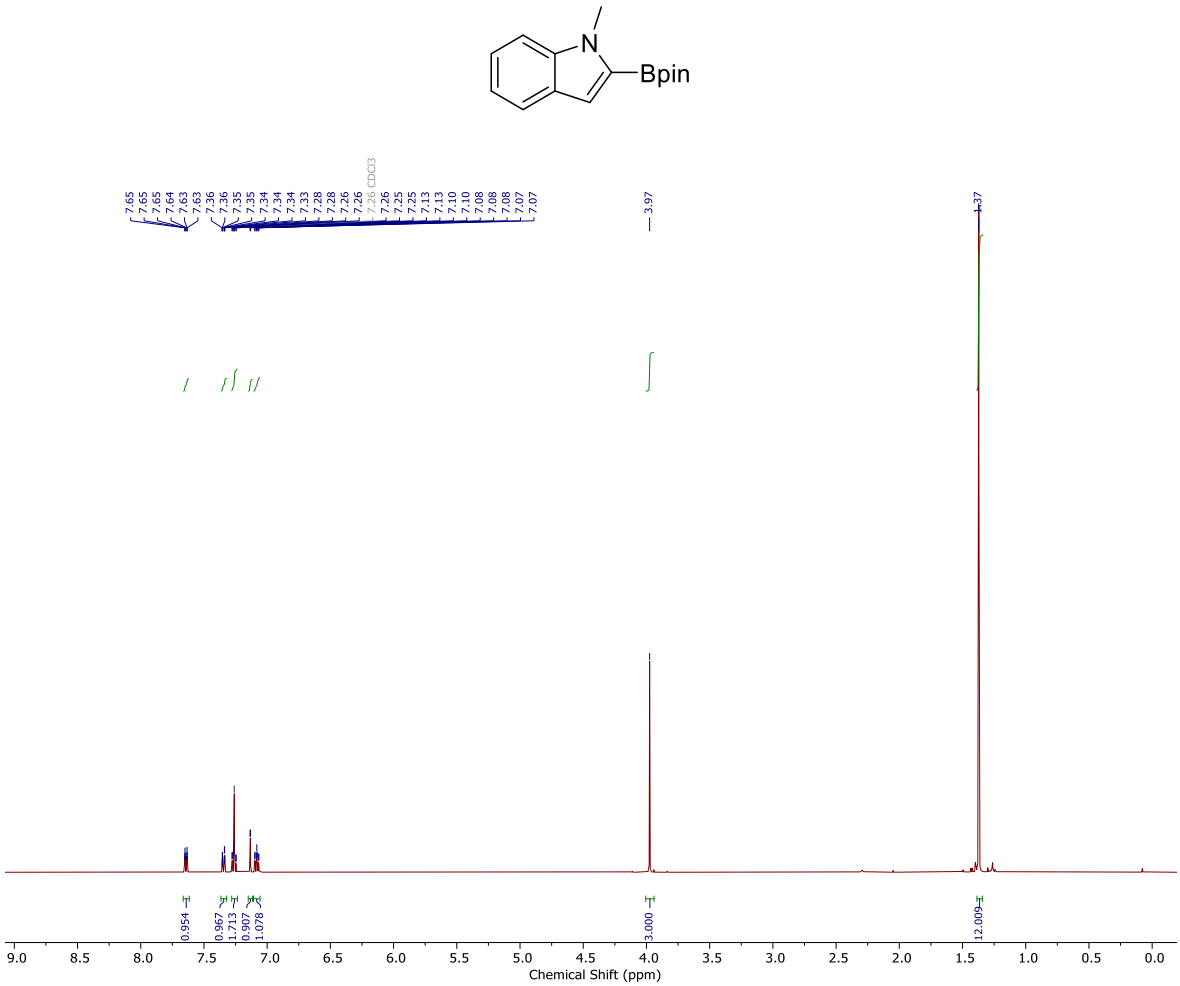

^{11}B NMR (160 MHz, $CDCl_3$) Spectrum of 2-(4,4,5,5-tetramethyl-1,3,2-dioxaborole)-N-methlyindole

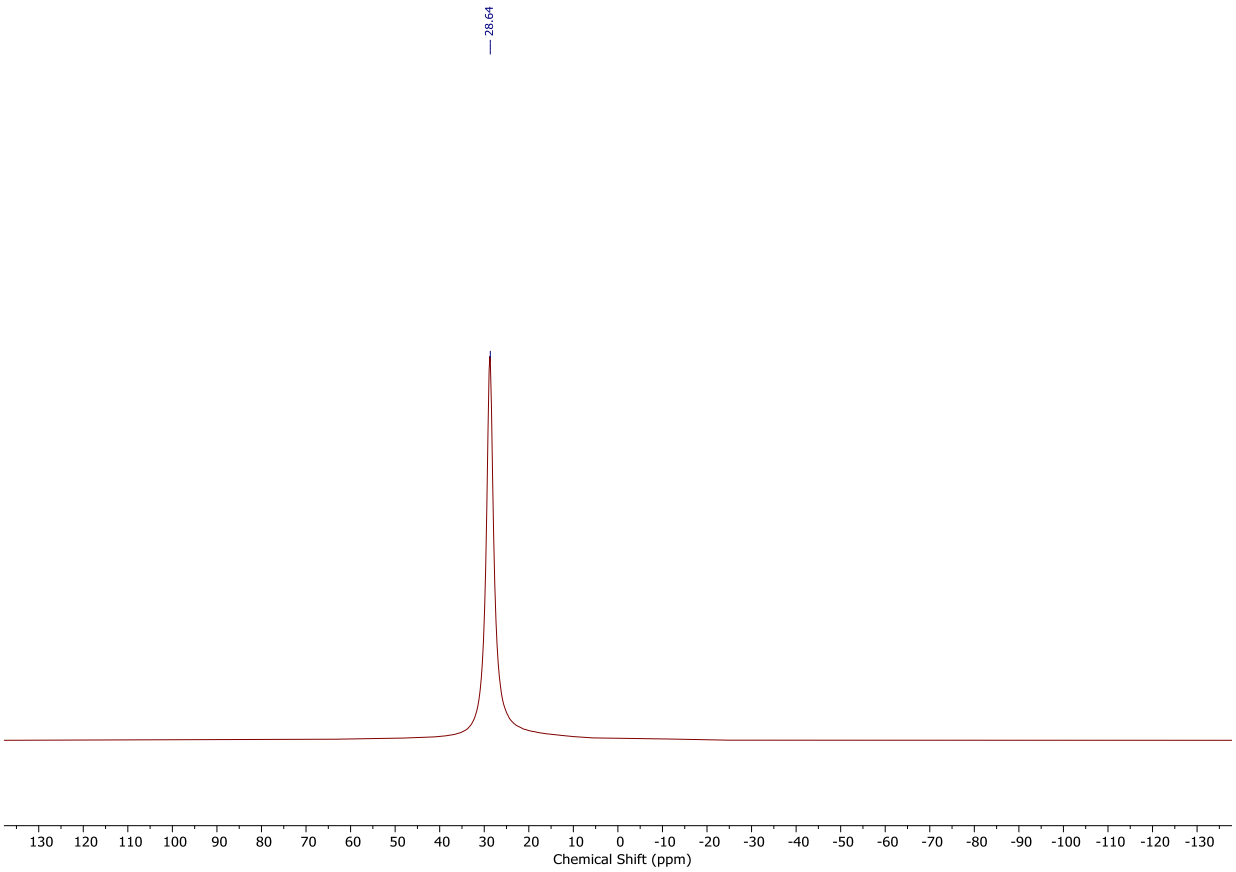

^{13}C NMR (126 MHz, $CDCl_3$) Spectrum of 2-(4,4,5,5-tetramethyl-1,3,2-dioxaborole)-N-methlyindole

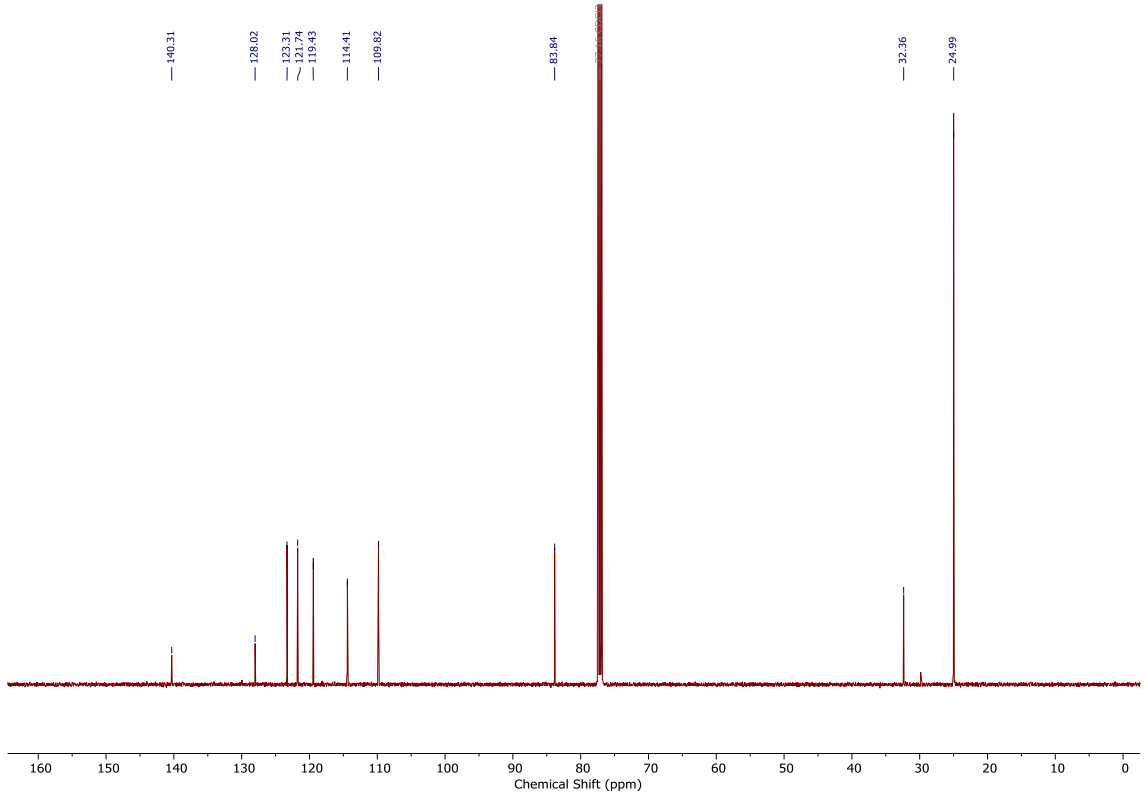

5.4.15. Synthesis and characterization of 2,6-di-*tert*-butyl-4-(4,4,5,5-tetramethyl-1,3,2-dioxaborole)pyridine

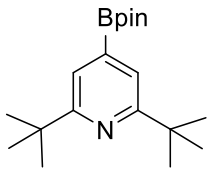

According to the general procedure, potassium *tert*-butoxide (23 mg, 0.24 mmol), bis(pinacolato)diboron (58 mg, 0.24 mmol), [dmpeMn(CO)$_3$Br] (7.4 mg, 0.02 mmol), and N-methylindole (45 mL, 0.2 mmol) in anhydrous MTBE (0.5 mL) were reacted. The crude product was purified by flash column chromatography (Teledyne ISCO CombiFlash NextGen 300+, 12 g, 40 mL min^{-1}, hexane/ethyl acetate 10:1) to give 2,6-di-*tert*-butyl-4-(4,4,5,5-tetramethyl-1,3,2-dioxaborole)pyridine as an amorphous colourless solid (51 mg, 0.16 mmol, 79%). ^{1}H NMR: (500 MHz, $CDCl_3$) 7.44 (s, 2H), 1.36 (s, 18H), 1.35 (s, 12H). ^{11}B NMR: (160 MHz, $CDCl_3$) 30.8. ^{13}C NMR: (126 MHz, $CDCl_3$) 167.0, 120.5, 84.3, 37.8, 30.4, 25.0.

^{1}H NMR (500 MHz, $CDCl_3$) Spectrum of 2,6-di-*tert*-butyl-4-(4,4,5,5-tetramethyl-1,3,2-dioxaborole)pyridine

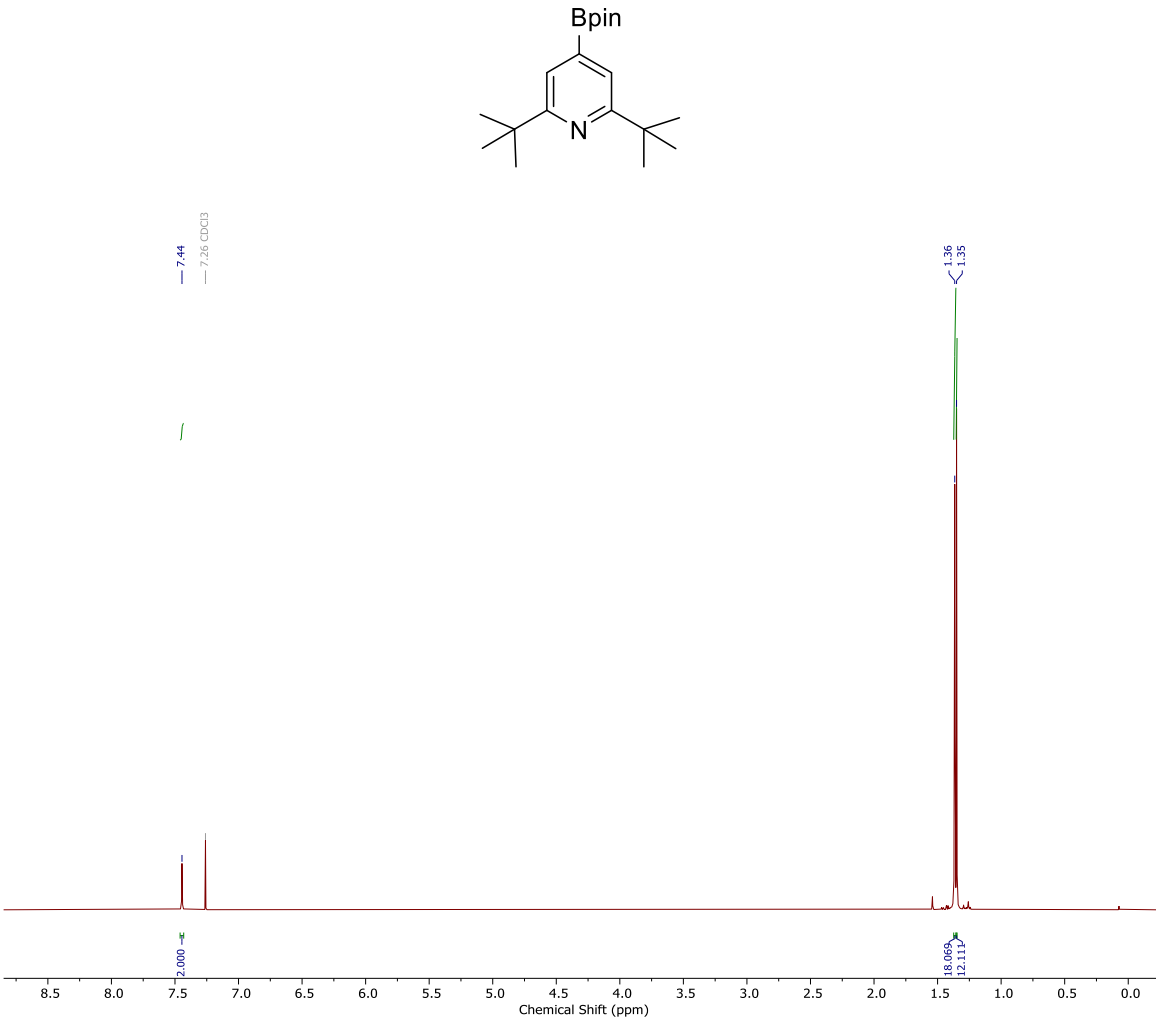

^{11}B NMR (160 MHz, $CDCl_3$) Spectrum of 2,6-di-*tert*-butyl-4-(4,4,5,5-tetramethyl-1,3,2-dioxaborole)pyridine

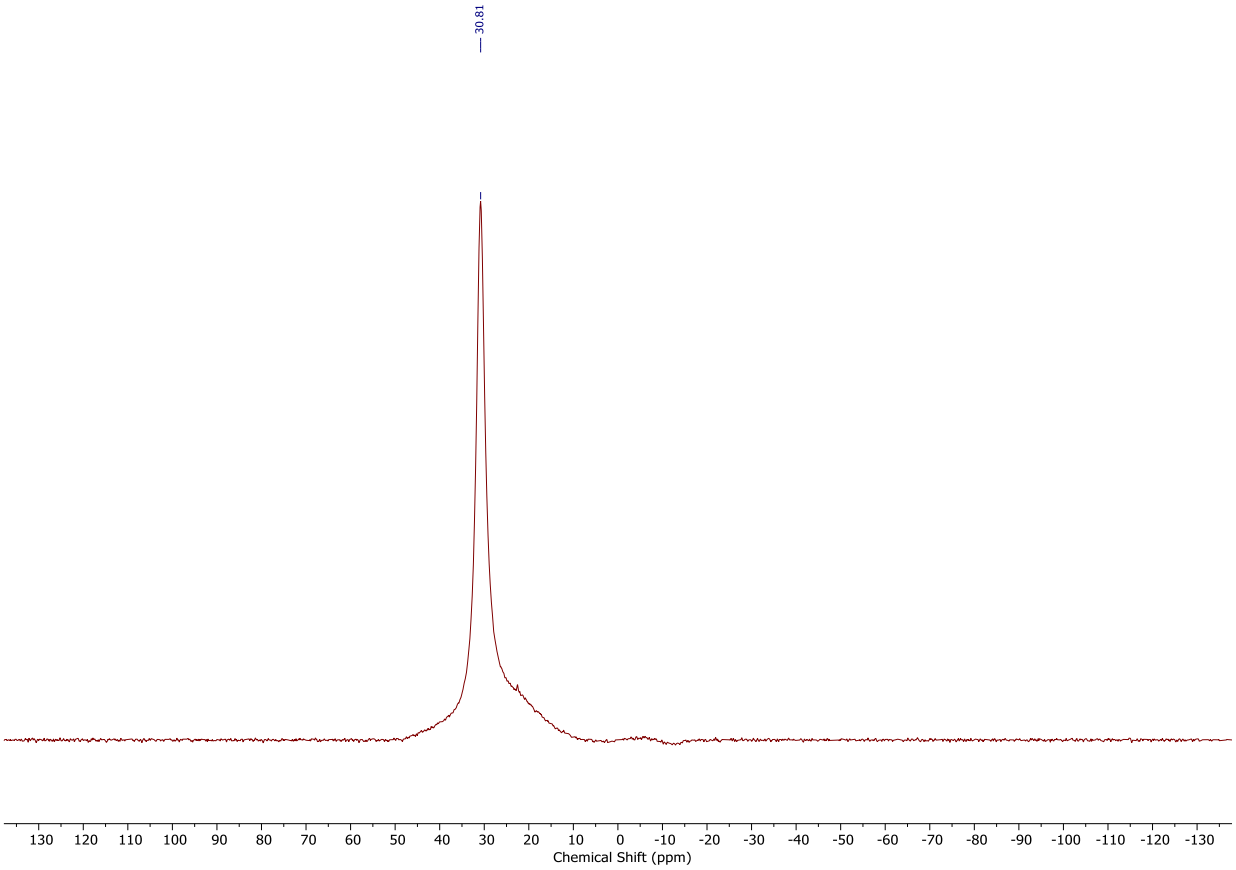

^{13}C NMR (126 MHz, $CDCl_3$) Spectrum of 2,6-di-*tert*-butyl-4-(4,4,5,5-tetramethyl-1,3,2-dioxaborole)pyridine

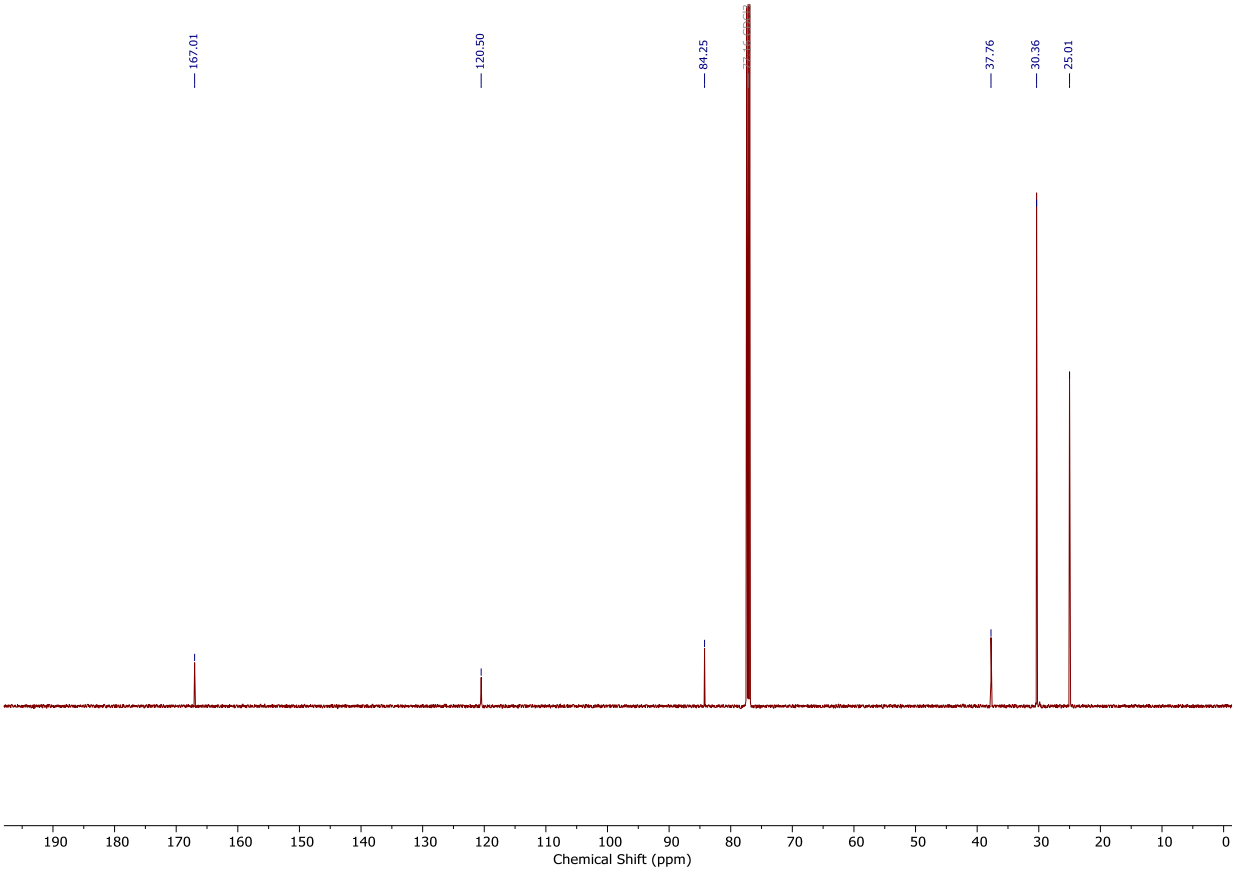

5.4.16. Synthesis and characterization of (4,4,5,5-Tetramethyl-1,3,2-dioxaborole)benzene

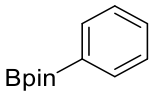

According to the general procedure, potassium *tert*-butoxide (23 mg, 0.24 mmol), bis(pinacolato)diboron (58 mg, 0.24 mmol), [dmpeMn(CO)$_3$Br] (7.4 mg, 0.02 mmol), and benzene (18 mL, 0.2 mmol) in anhydrous MTBE (0.5 mL) were reacted to give (4,4,5,5-tetramethyl-1,3,2-dioxaborole)benzene (13%) as determined by ^{1}H NMR spectroscopy of the crude reaction mixture. ^{1}H NMR: (500 MHz, $CDCl_3$) 7.81 – 7.78 (m, 2H), 7.47 – 7.41 (m, 1H), 7.39 – 7.34 (m, 2H), 1.34 (s, 12H). ^{13}C NMR: (126 MHz, $CDCl_3$) 134.9, 131.4, 127.8, 83.6, 25.0.

^{1}H NMR (500 MHz, $CDCl_3$) Spectrum of the crude reaction mixture of (4,4,5,5-tetramethyl-1,3,2-dioxaborole)benzene

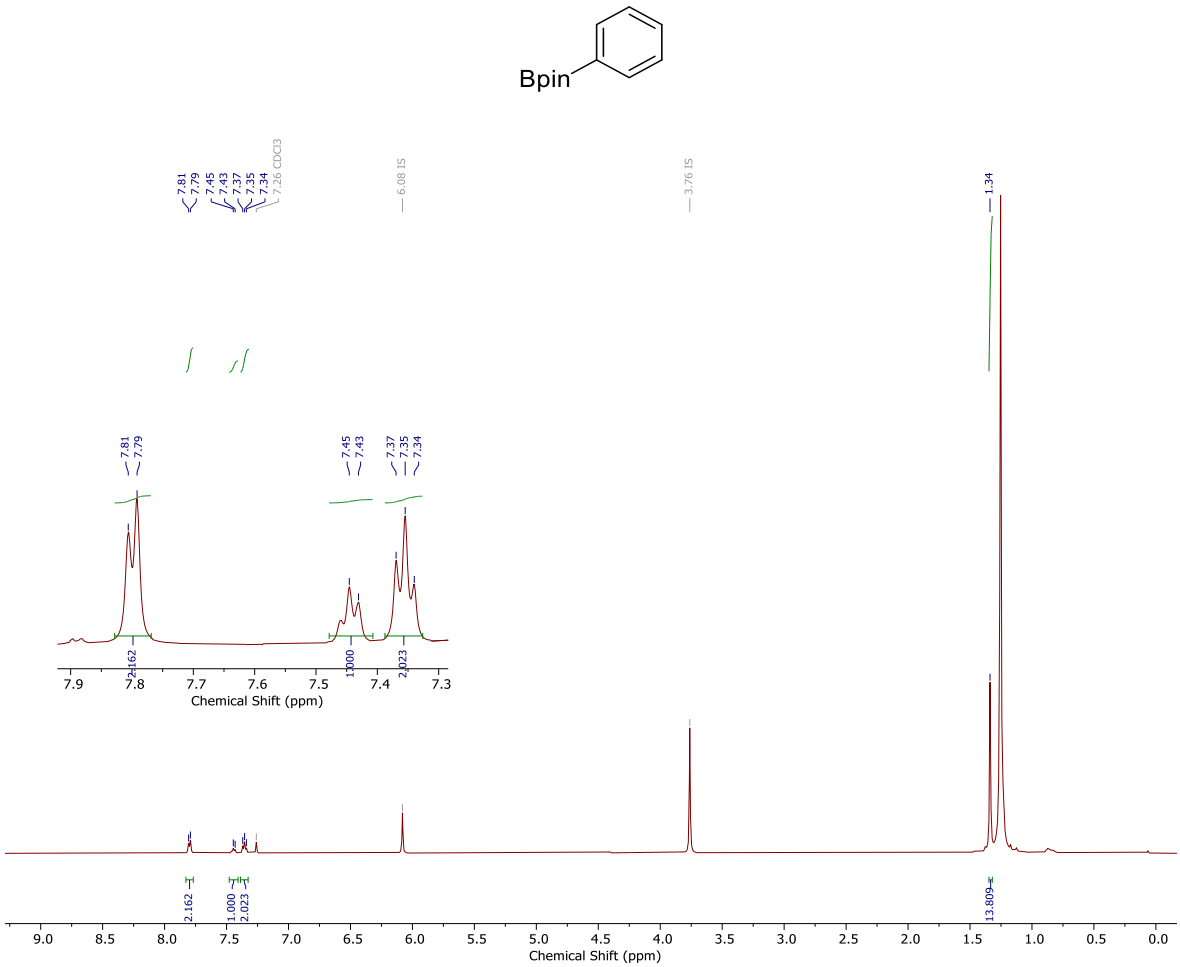

^{13}C NMR (126 MHz, $CDCl_3$) Spectrum of the crude reaction mixture of (4,4,5,5-tetramethyl-1,3,2-dioxaborole)benzene

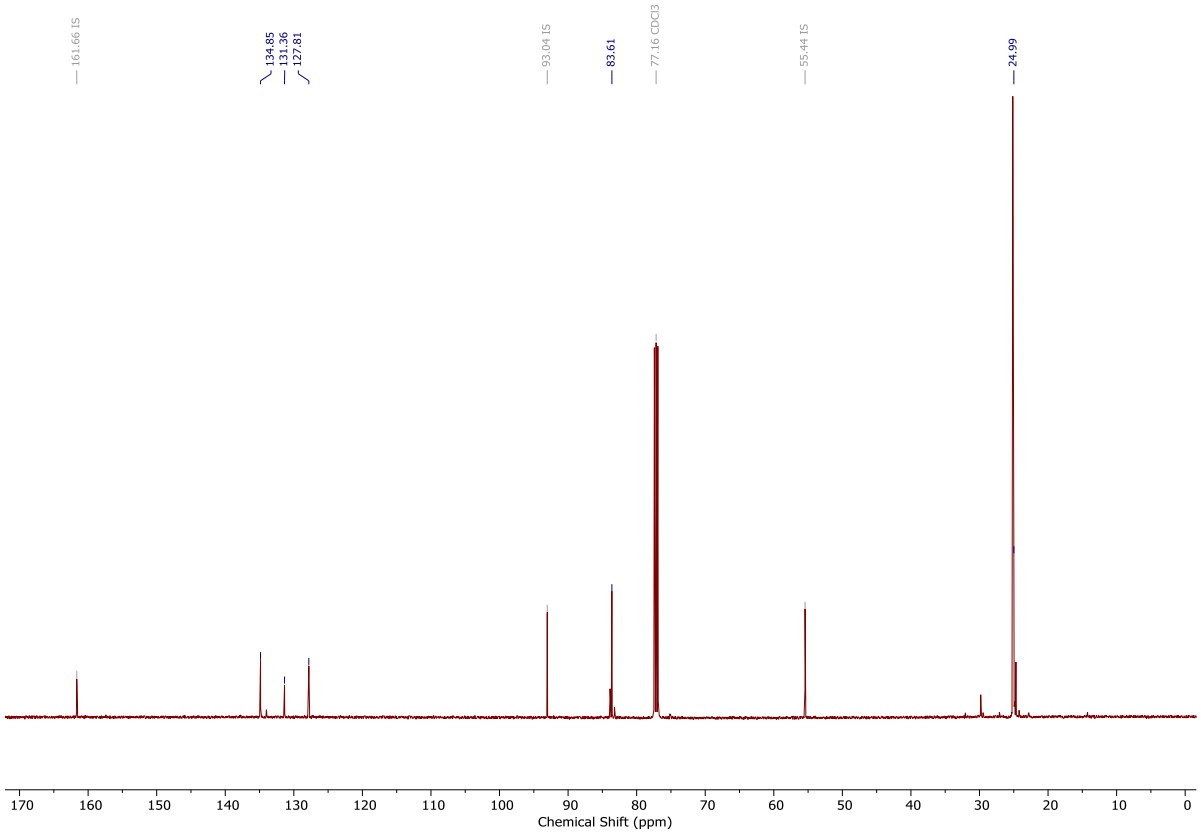

5.4.17. Synthesis and characterization of 3-(4,4,5,5-Tetramethyl-1,3,2-dioxaborole)toluene and 4-(4,4,5,5-tetramethyl-1,3,2-dioxaborole)toluene

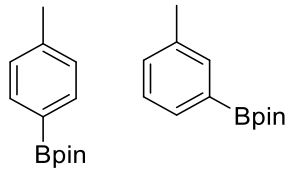

According to the general procedure, potassium *tert*-butoxide (23 mg, 0.24 mmol), bis(pinacolato)diboron (58 mg, 0.24 mmol), [dmpeMn(CO)$_3$Br] (7.4 mg, 0.02 mmol), and toluene (21 mL, 0.2 mmol) in anhydrous MTBE (0.5 mL) were reacted to give 3-(4,4,5,5-tetramethyl-1,3,2-dioxaborole)toluene and 4-(4,4,5,5-tetramethyl-1,3,2-dioxaborole)toluene in a 66:33 3-:4- ratio (8%) as determined by ^{1}H NMR spectroscopy of the crude reaction mixture.

3-(4,4,5,5-Tetramethyl-1,3,2-dioxaborole)toluene: ^{1}H NMR: (500 MHz, $CDCl_3$) 7.63 (br. s, 1H), 7.61 – 7.59 (m, 1H), 7.27 (d, *J* = 1.3 Hz, 2H), 2.35 (s, 3H), 1.34 (s, 12H). ^{13}C NMR: (126 MHz, $CDCl_3$) 137.3, 135.5, 132.2, 131.9, 127.8, 83.9, 25.0, 21.4.

4-(4,4,5,5-Tetramethyl-1,3,2-dioxaborole)toluene: ^{1}H NMR: (500 MHz, $CDCl_3$) 7.70 (d, *J* = 7.9 Hz, 2H), 7.18 (d, *J* = 7.9 Hz, 2H), 2.36 (s, 3H), 1.33 (s, 12H). ^{13}C NMR: (126 MHz, $CDCl_3$) 141.5, 135.0, 128.6, 83.7, 25.0, 21.9.

^{1}H NMR (500 MHz, $CDCl_3$) Spectrum of the crude reaction mixture of (4,4,5,5-tetramethyl-1,3,2-dioxaborole)toluene

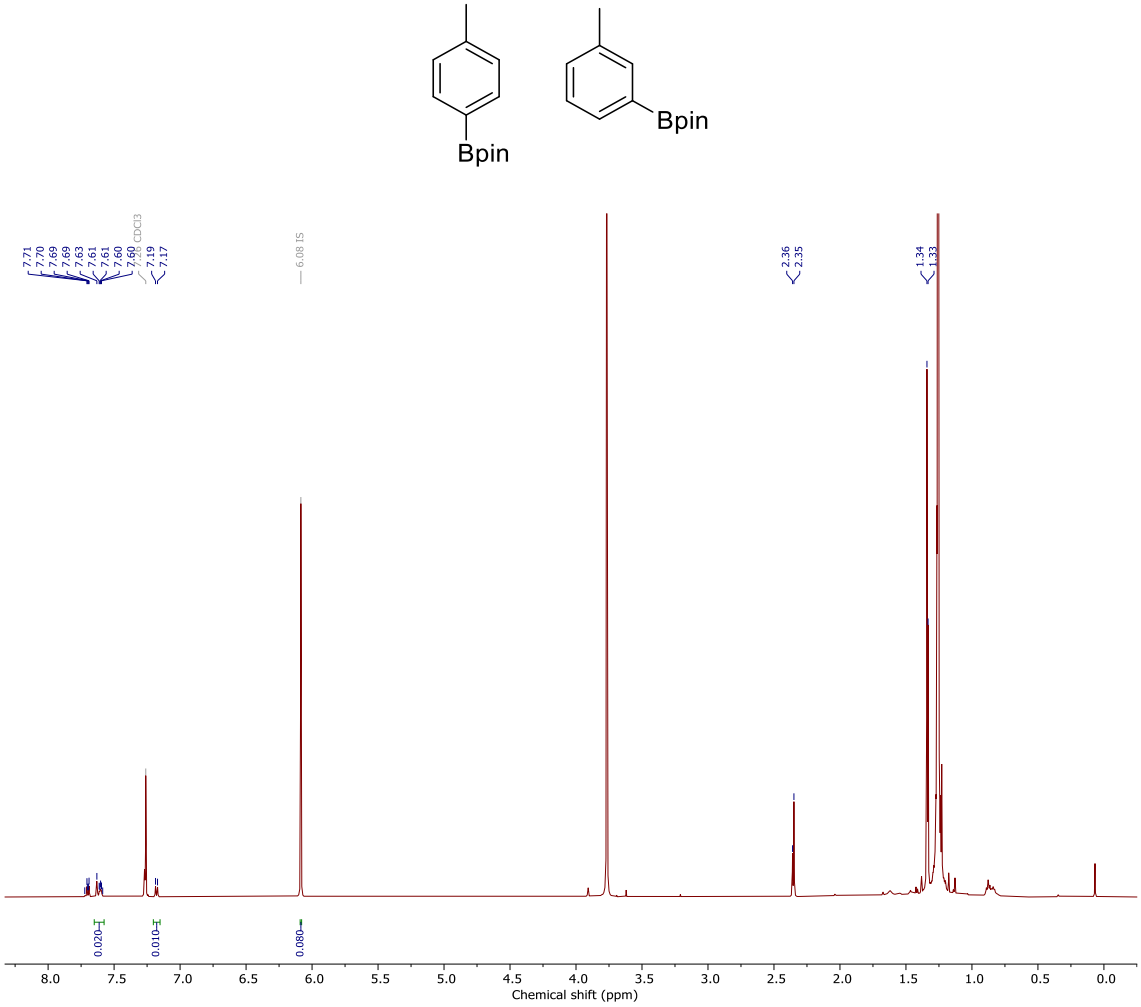

^{13}C NMR (126 MHz, $CDCl_3$) Spectrum of the crude reaction mixture of (4,4,5,5-tetramethyl-1,3,2-dioxaborole)toluene

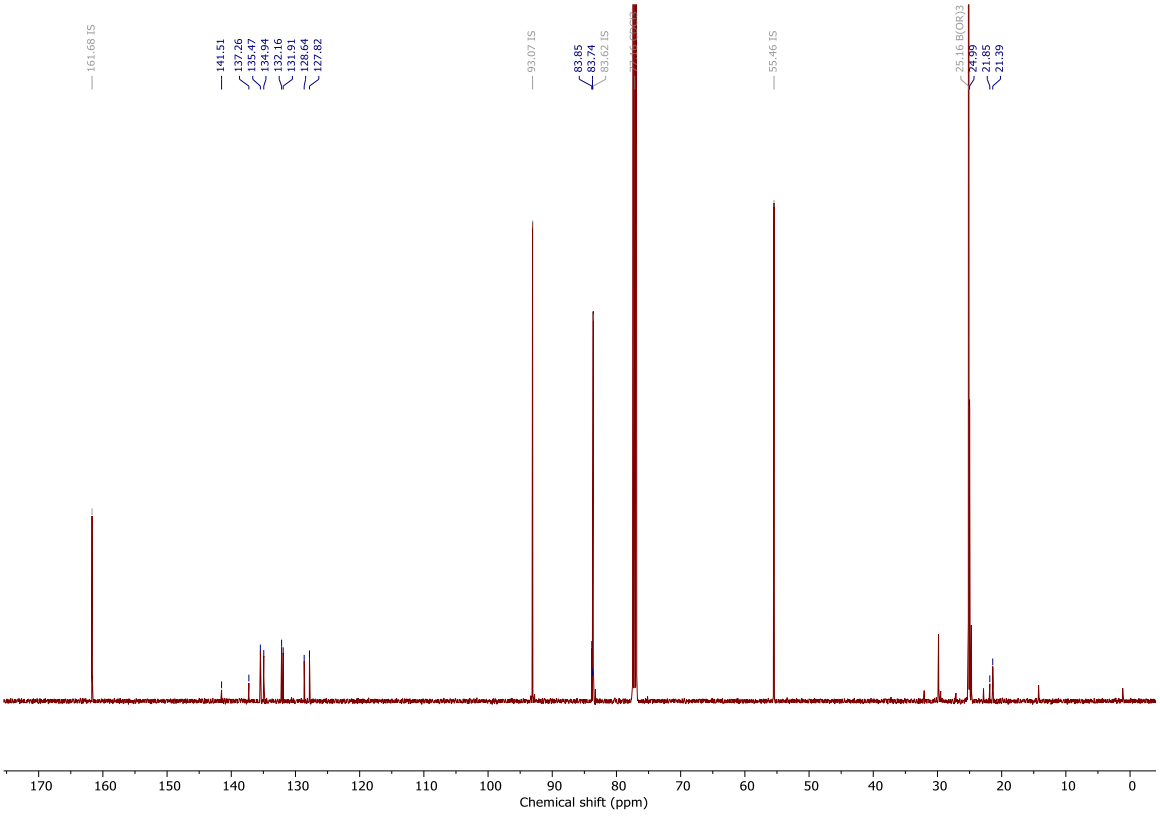

5.4.18. Synthesis and characterization of 5-(4,4,5,5-Tetramethyl-1,3,2-dioxaborole)-1,3-dimethoxybenzene

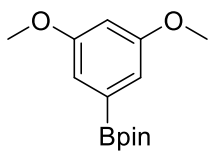

According to the general procedure, potassium *tert*-butoxide (23 mg, 0.24 mmol), bis(pinacolato)diboron (58 mg, 0.24 mmol), [dmpeMn(CO)$_3$Br] (7.4 mg, 0.02 mmol), and 1,3-dimethoxybenzene (26 mL, 0.2 mmol) in anhydrous MTBE (0.5 mL) were reacted. The crude product was purified by flash column chromatography (Teledyne ISCO CombiFlash NextGen 300+, 12 g, 40 mL min^{-1}, hexane/ethyl acetate 10:1) to give 5-(4,4,5,5-tetramethyl-1,3,2-dioxaborole)-1,3-dimethoxybenzene as an amorphous colourless solid (15 mg, 0.06 mmol, 28%). ^{1}H NMR: (500 MHz, $CDCl_3$) 6.95 (d, J = 2.4 Hz, 2H), 6.57 (t, J = 2.4 Hz, 1H), 3.81 (s, 6H), 1.34 (s, 12H). ^{11}B NMR: (160 MHz, $CDCl_3$) 30.9. ^{13}C NMR: (126 MHz, $CDCl_3$) 160.6, 111.8, 104.7, 84.0, 55.6, 25.0.

^{1}H NMR (500 MHz, $CDCl_3$) Spectrum of 5-(4,4,5,5-tetramethyl-1,3,2-dioxaborole)-1,3-dimethoxybenzene

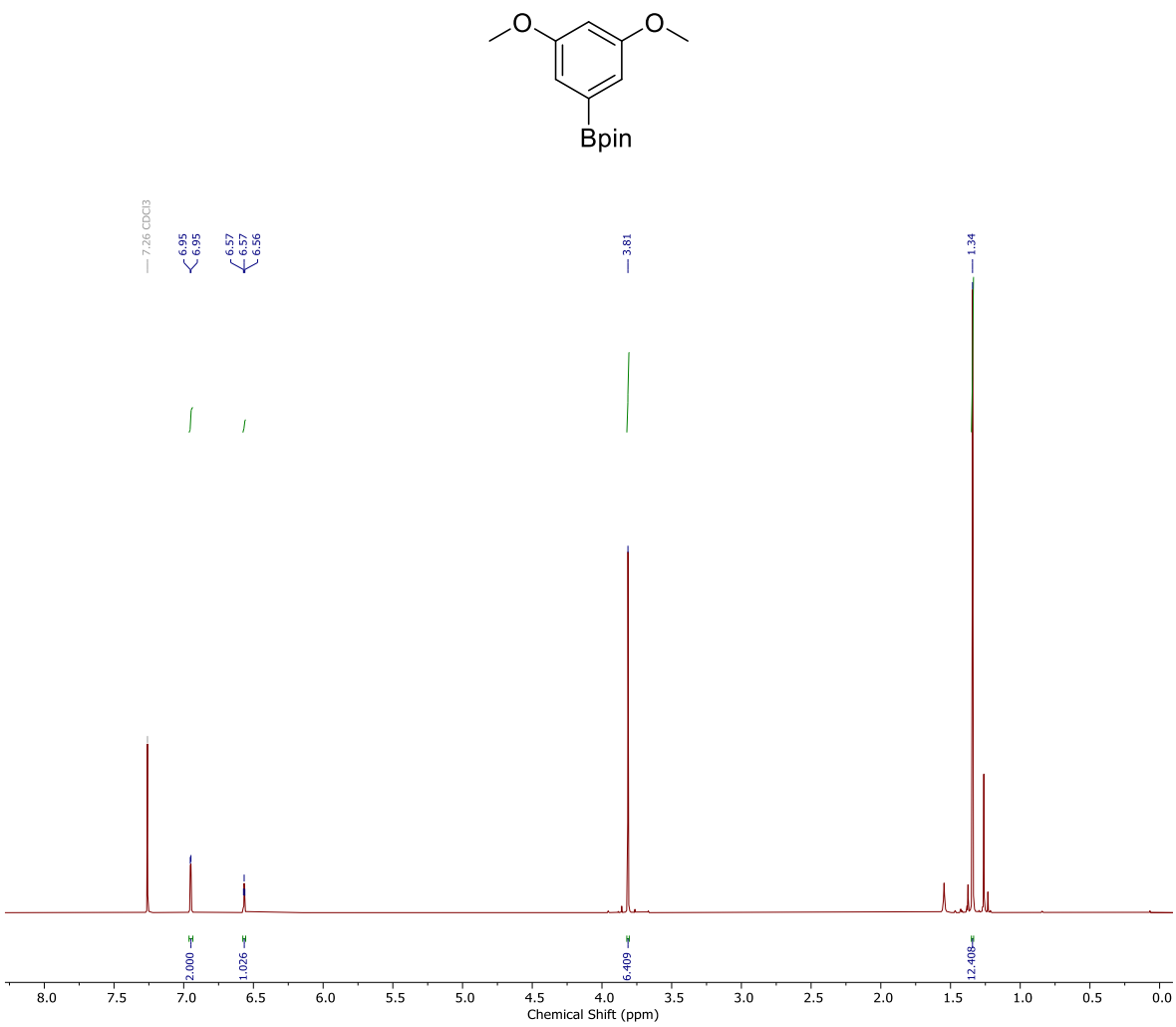

^{11}B NMR (160 MHz, $CDCl_3$) Spectrum of 5-(4,4,5,5-tetramethyl-1,3,2-dioxaborole)-1,3-dimethoxybenzene

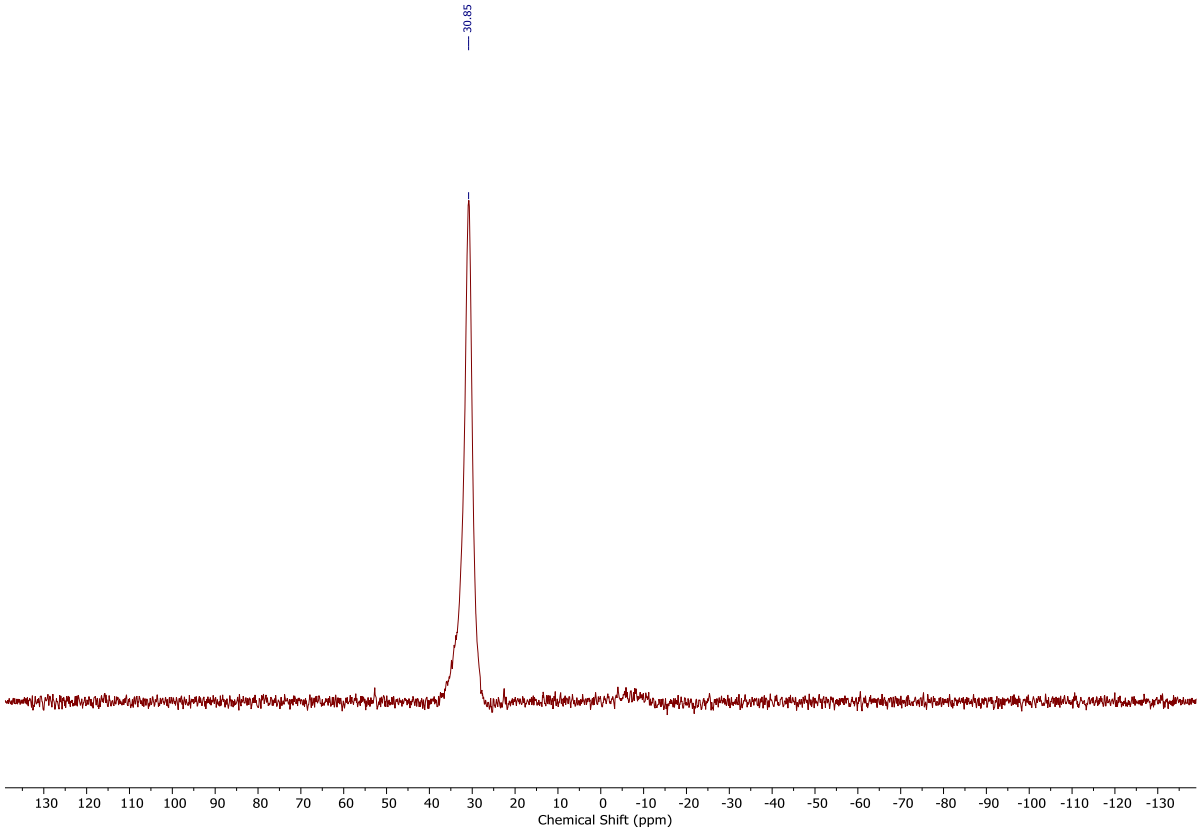

^{13}C NMR (126 MHz, $CDCl_3$) Spectrum of 5-(4,4,5,5-tetramethyl-1,3,2-dioxaborole)-1,3-dimethoxybenzene

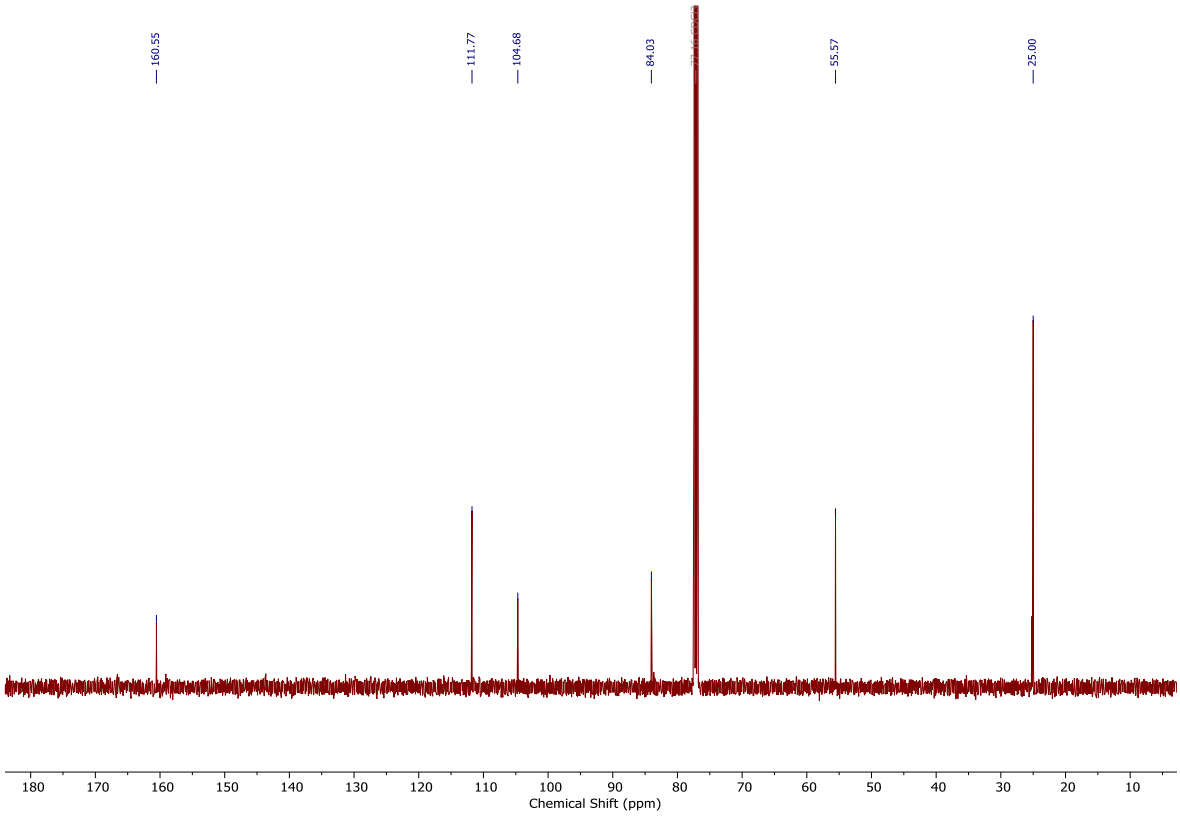

5.4.19. Synthesis and characterization of (4,4,5,5-Tetramethyl-1,3,2-dioxaborole)trifluorotoluene and 3,5-bis(4,4,5,5- tetramethyl-1,3,2-dioxaborole)trifluorotoluene

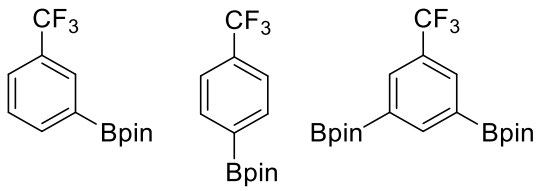

According to the general procedure, potassium *tert*-butoxide (23 mg, 0.24 mmol), bis(pinacolato)diboron (58 mg, 0.24 mmol), [dmpeMn(CO)$_3$Br] (7.4 mg, 0.02 mmol), and trifluorotoluene (25 mL, 0.2 mmol) in anhydrous MTBE (0.5 mL) were reacted to give (4,4,5,5-tetramethyl-1,3,2-dioxaborole)trifluorotoluene and 3,5-bis(4,4,5,5-tetramethyl-1,3,2-dioxaborole)trifluorotoluene in a 45:45:10 3-:4-:3,5-bis ratio (55%) as determined by ^{1}H NMR spectroscopy of the crude reaction mixture. The crude product was purified by flash column chromatography (Teledyne ISCO CombiFlash NextGen 300+, 12 g, 40 mL min^{-1}, hexane/ethyl acetate 10:1) to give (4,4,5,5-tetramethyl-1,3,2-dioxaborole)trifluorotoluene as a colourless oil in a 77:23 3-:4- ratio (14 mg, 0.05 mmol, 25%) and 3,5-bis(4,4,5,5-tetramethyl-1,3,2- dioxaborole)trifluorotoluene as an amorphous colourless solid (4 mg, 0.01 mmol, 5%). Total isolated yield (3-:4-:3,5-bis) = 30%.

3-(4,4,5,5-Tetramethyl-1,3,2-dioxaborole)trifluorotoluene: ^{1}H NMR: (500 MHz, $CDCl_3$) 8.06 (s, 1H), 7.97 (d, J = 7.5 Hz, 1H), 7.70 (m, 1H), 7.50 – 7.47 (m, 1H), 1.36 (s, 12H). ^{11}B NMR: (160 MHz, $CDCl_3$) 30.6. ^{19}F NMR: (470 MHz, $CDCl_3$) −62.6 (s).

4-(4,4,5,5-Tetramethyl-1,3,2-dioxaborole)trifluorotoluene: ^{1}H NMR: (500 MHz, $CDCl_3$) 7.91 (d, J = 7.7 Hz, 2H), 7.61 (d, J = 7.7 Hz, 2H), 1.36 (s, 12H). ^{11}B NMR: (160 MHz, $CDCl_3$) 30.6. ^{19}F NMR: (470 MHz, $CDCl_3$) −63.0 (s).

3,5-Bis(4,4,5,5-Tetramethyl-1,3,2-dioxaborole)trifluorotoluene: ^{1}H NMR: (500 MHz, $CDCl_3$) 8.41 (s, 1H), 8.13 (s, 2H), 1.35 (s, 24H). ^{11}B NMR: (160 MHz, $CDCl_3$) 30.6. ^{13}C NMR: (126 MHz, $CDCl_3$) 144.4, 134.1, 84.4, 25.0. ^{19}F NMR: (470 MHz, $CDCl_3$) −62.5 (s).

^{1}H NMR (500 MHz, $CDCl_3$) Spectrum of (4,4,5,5-tetramethyl-1,3,2-dioxaborole)trifluorotoluene

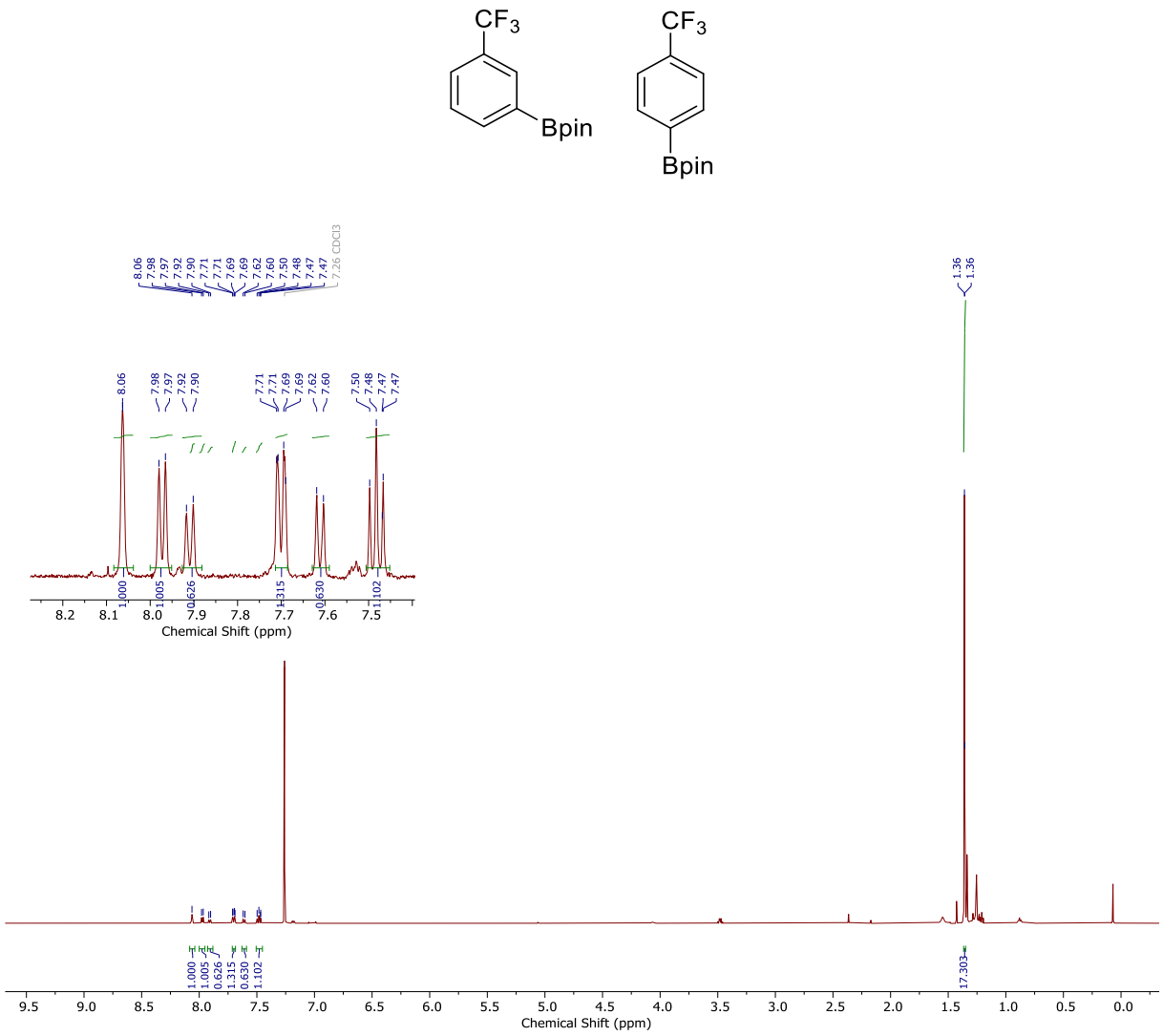

^{11}B NMR (160 MHz, $CDCl_3$) Spectrum of (4,4,5,5-tetramethyl-1,3,2-dioxaborole)trifluorotoluene

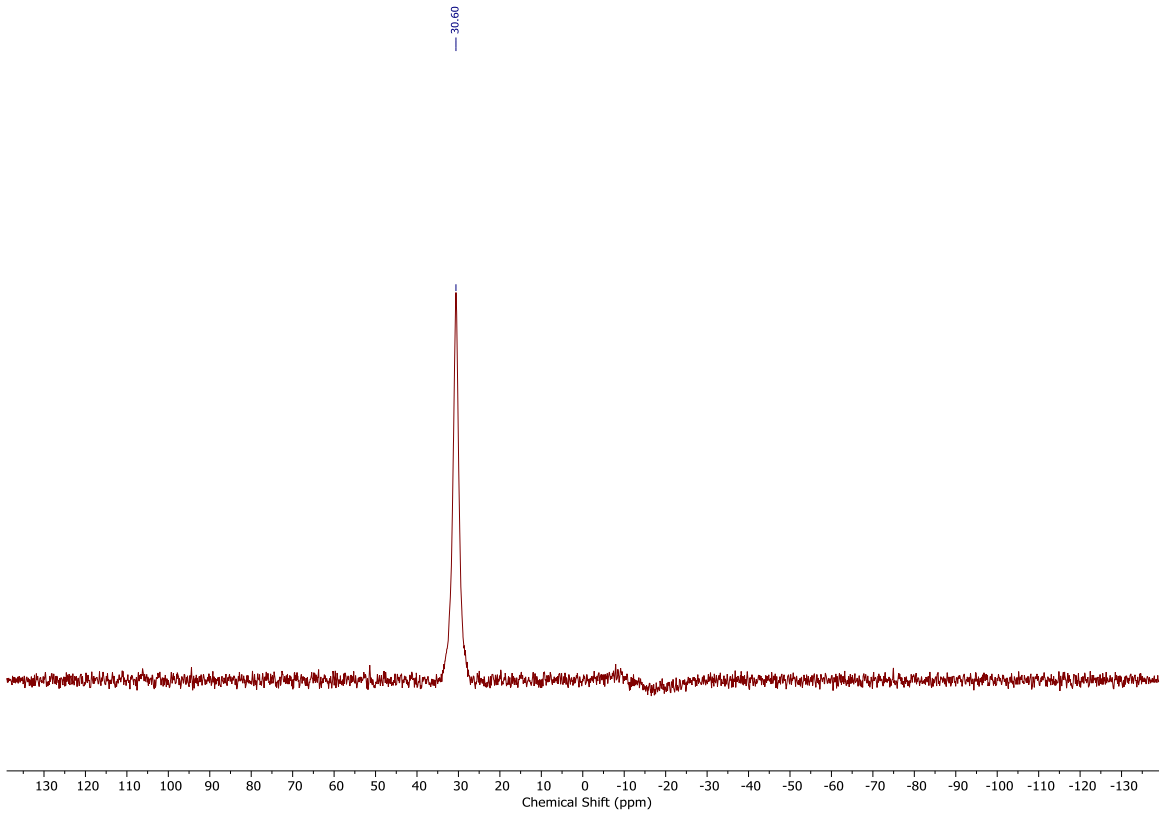

^{19}F NMR (470 MHz, $CDCl_3$) Spectrum of (4,4,5,5-tetramethyl-1,3,2-dioxaborole)trifluorotoluene

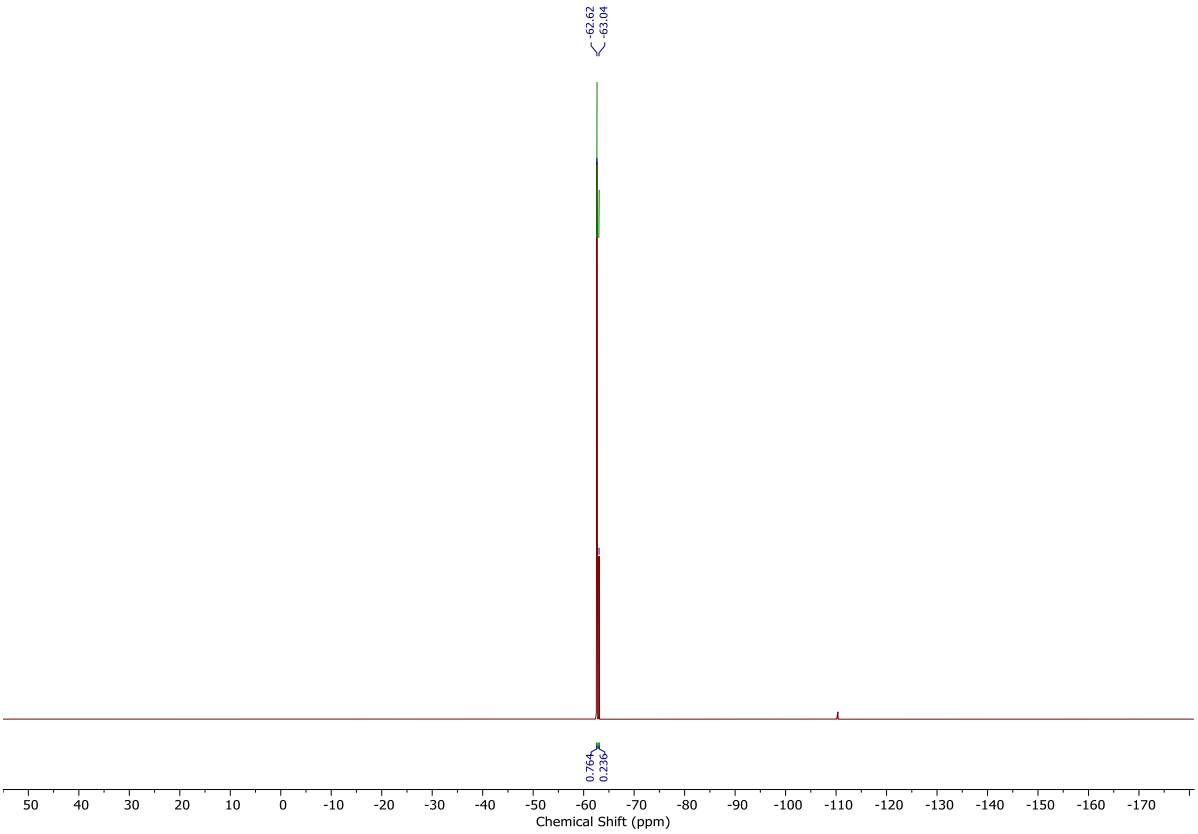

^{1}H NMR (500 MHz, $CDCl_3$) Spectrum of 3,5-bis(4,4,5,5-tetramethyl-1,3,2-dioxaborole)trifluorotoluene

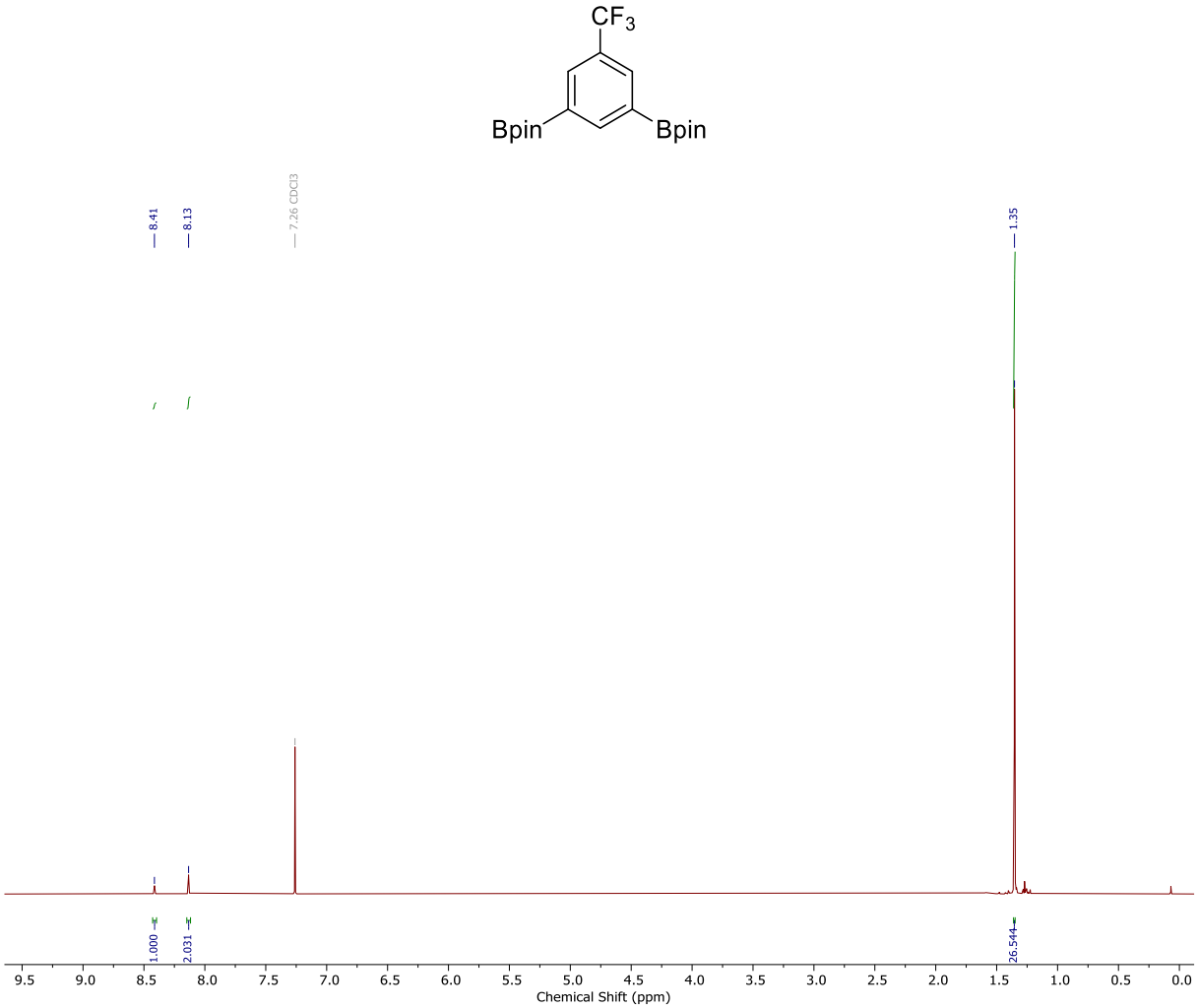

^{11}B NMR (160 MHz, $CDCl_3$) Spectrum of 3,5-bis(4,4,5,5-tetramethyl-1,3,2-dioxaborole)trifluorotoluene

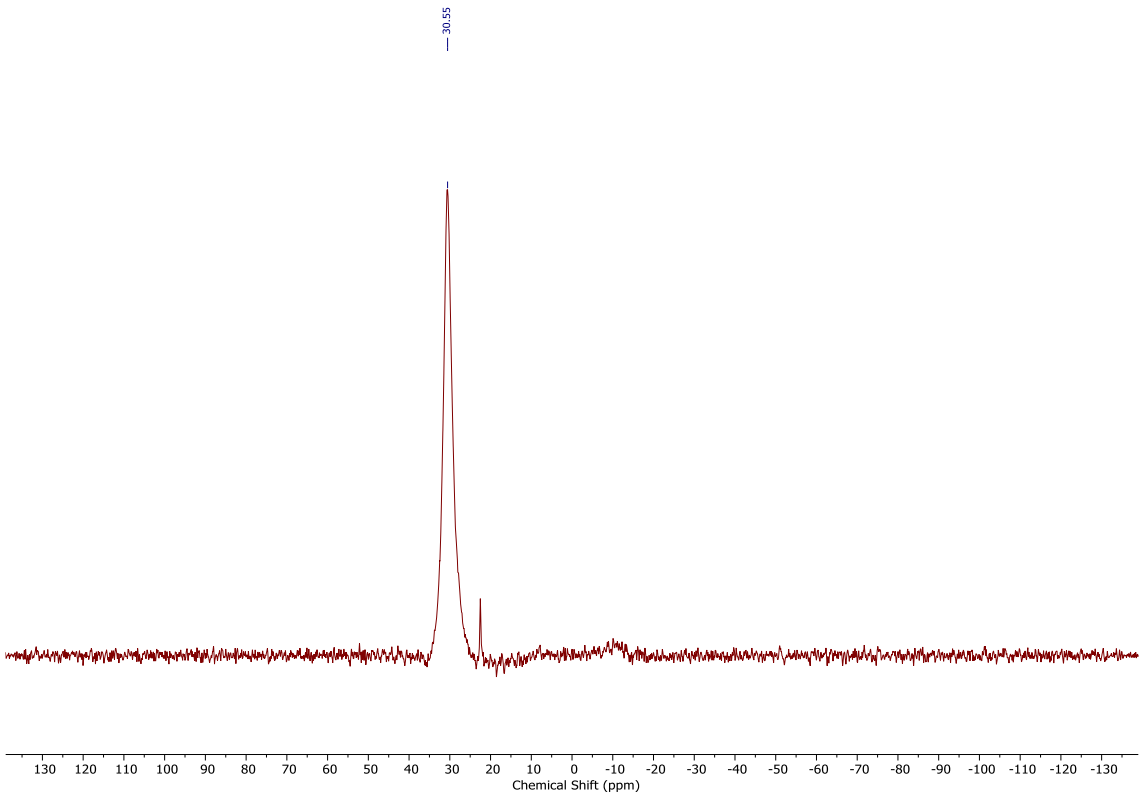

^{13}C NMR (126 MHz, $CDCl_3$) Spectrum of 3,5-bis(4,4,5,5-tetramethyl-1,3,2-dioxaborole)trifluorotoluene

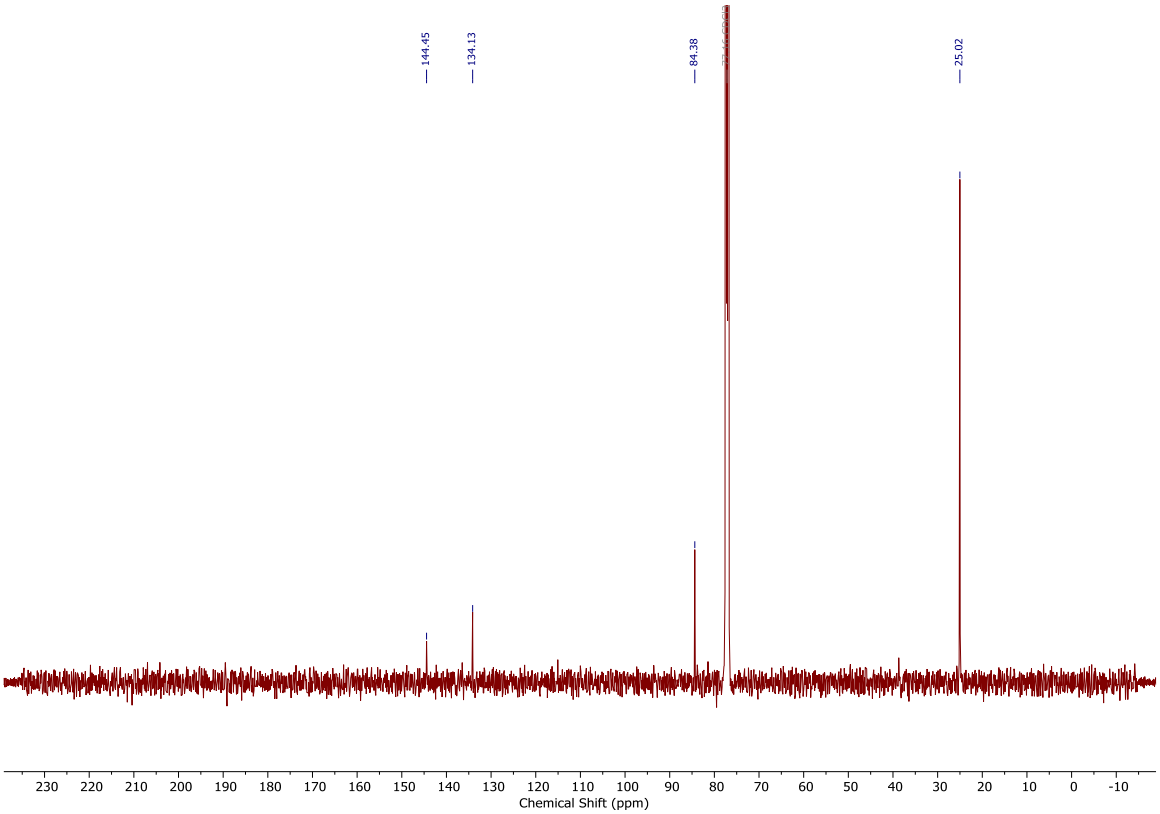

^{19}F NMR (470 MHz, $CDCl_3$) Spectrum of 3,5-bis(4,4,5,5-tetramethyl-1,3,2-dioxaborole)trifluorotoluene

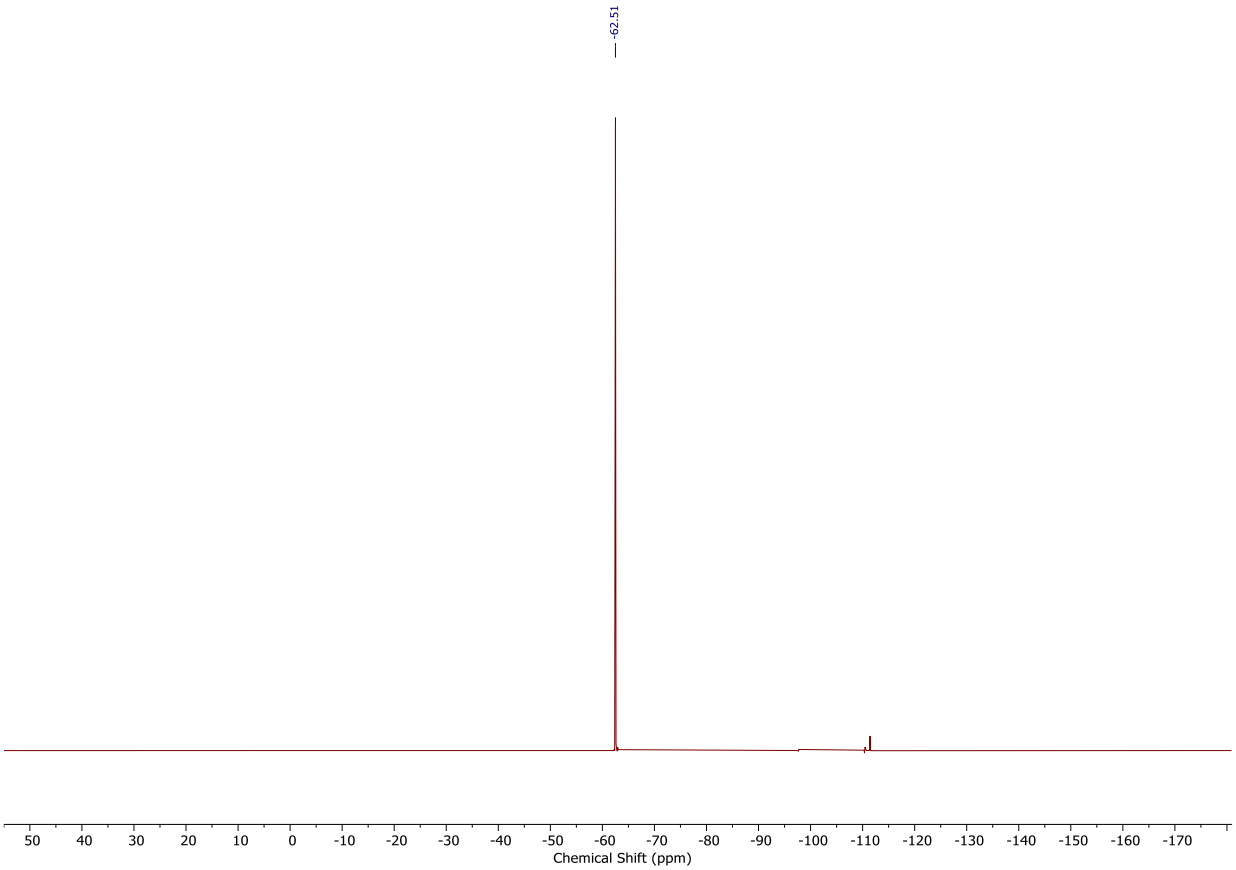

5.4.20. Synthesis and characterization of 6-(4,4,5,5-Tetramethyl-1,3,2-dioxaborole)-3-methylfluorobenzene and 5-(4,4,5,5-tetramethyl-1,3,2-dioxaborole)-3-methylfluorobenzene

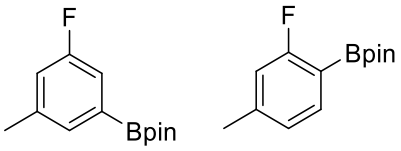

According to the general procedure, potassium *tert*-butoxide (23 mg, 0.24 mmol), bis(pinacolato)diboron (58 mg, 0.24 mmol), [dmpeMn(CO)$_3$Br] (7.4 mg, 0.02 mmol), and 3-methylfluorobenzene (22 mL, 0.2 mmol) in anhydrous MTBE (0.5 mL) were reacted. The crude product was purified by flash column chromatography (Teledyne ISCO CombiFlash NextGen 300+, 12 g, 40 mL min^{-1}, hexane/ethyl acetate 10:1) to give an inseparable mixture of 6-(4,4,5,5-Tetramethyl-1,3,2-dioxaborole)-3-methylfluorobenzene and 5-(4,4,5,5-tetramethyl-1,3,2-dioxaborole)-3- methylfluorobenzene in a 73:27 6-:5- ratio as a colourless oil (19 mg, 0.07 mmol, 35%). Product fractions contained inseparable amounts of borylated toluene products.

6-(4,4,5,5-Tetramethyl-1,3,2-dioxaborole)-3-methylfluorobenzene: ^{1}H NMR: (500 MHz, $CDCl_3$) 7.64 – 7.58 (m, 1H), 6.96 – 6.92 (m, 1H), 6.87 – 6.82 (m, 1H), 2.35 (s, 3H), 1.35 (s, 12H). ^{11}B NMR: (160 MHz, $CDCl_3$) 30.2. ^{13}C NMR: (126 MHz, $CDCl_3$) 167.5 (d, J = 250.6 Hz), 144.5 (d, J = 8.9 Hz), 136.8 (d, J = 8.6 Hz), 124.6 (d, J = 2.9 Hz), 116.0 (d, J = 23.7 Hz), 83.9, 25.0, 21.6 (d, J = 1.9 Hz). ^{19}F NMR: (470 MHz, $CDCl_3$) −103.8 (s).

5-(4,4,5,5-Tetramethyl-1,3,2-dioxaborole)-3-methylfluorobenzene: ^{1}H NMR: (500 MHz, $CDCl_3$) 7.41 – 7.37 (m, 1H), 7.29 – 7.26 (m, 1H), 6.98 – 6.96 (m, 1H), 2.36 (s, 3H), 1.34 (s, 12H). ^{11}B NMR: (160 MHz, $CDCl_3$) 30.2. ^{13}C NMR: (126 MHz, $CDCl_3$) 162.7 (d, J = 246.3 Hz), 140.0 (d, J = 7.0 Hz), 131.1 (d, J = 2.5 Hz), 119.0 (d, J = 21.0 Hz), 118.0 (d, J = 19.2 Hz), 84.2, 25.0, 21.2 (d, J = 1.9 Hz). ^{19}F NMR: (470 MHz, $CDCl_3$) −115.4 (t, J = 9.4 Hz).

^{1}H NMR (500 MHz, $CDCl_3$) Spectrum of 6-(4,4,5,5-Tetramethyl-1,3,2-dioxaborole)-3-methylfluorobenzene and 5-(4,4,5,5-tetramethyl-1,3,2-dioxaborole)-3- methylfluorobenzene

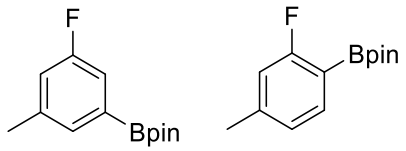

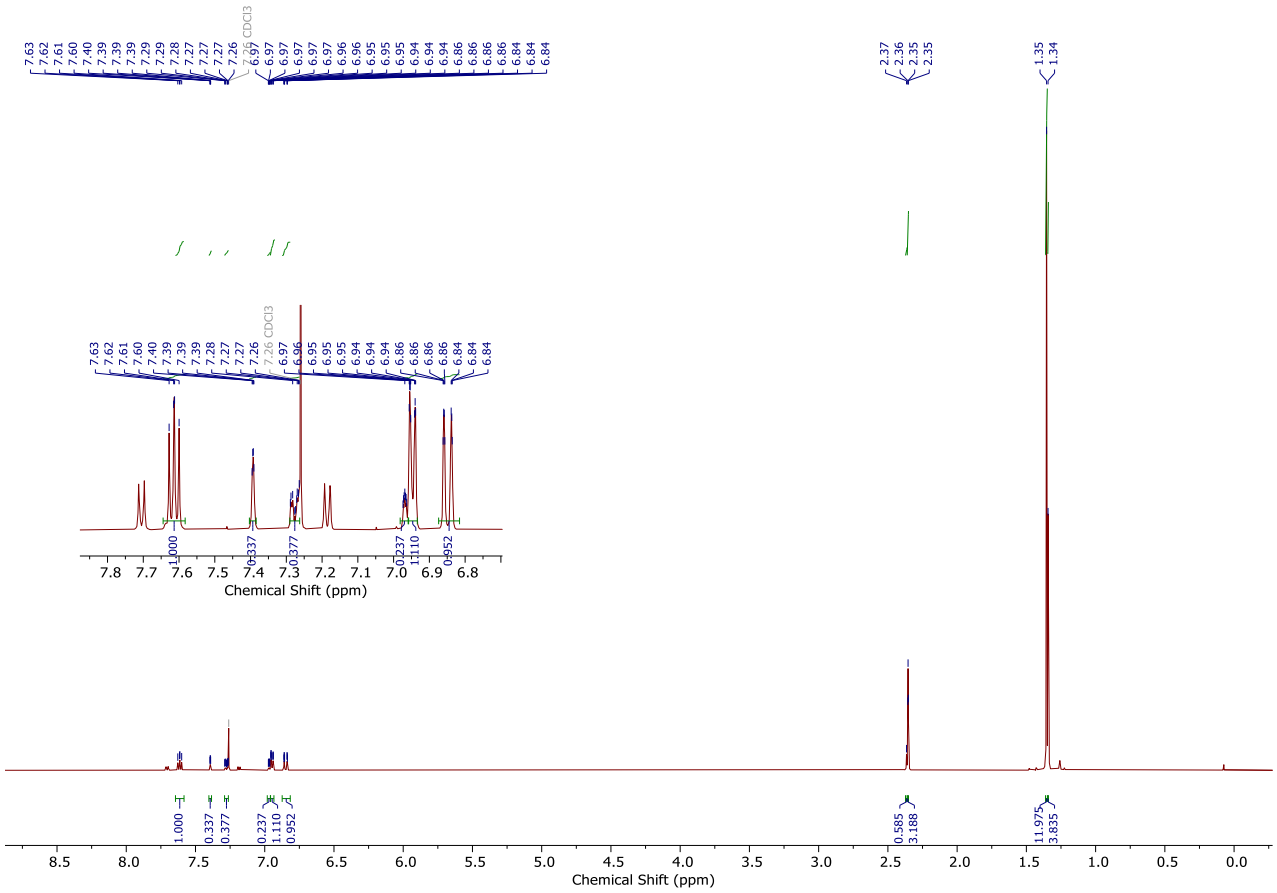

^{11}B NMR (160 MHz, $CDCl_3$) Spectrum of 6-(4,4,5,5-Tetramethyl-1,3,2-dioxaborole)-3-methylfluorobenzene and 5-(4,4,5,5-tetramethyl-1,3,2-dioxaborole)-3- methylfluorobenzene

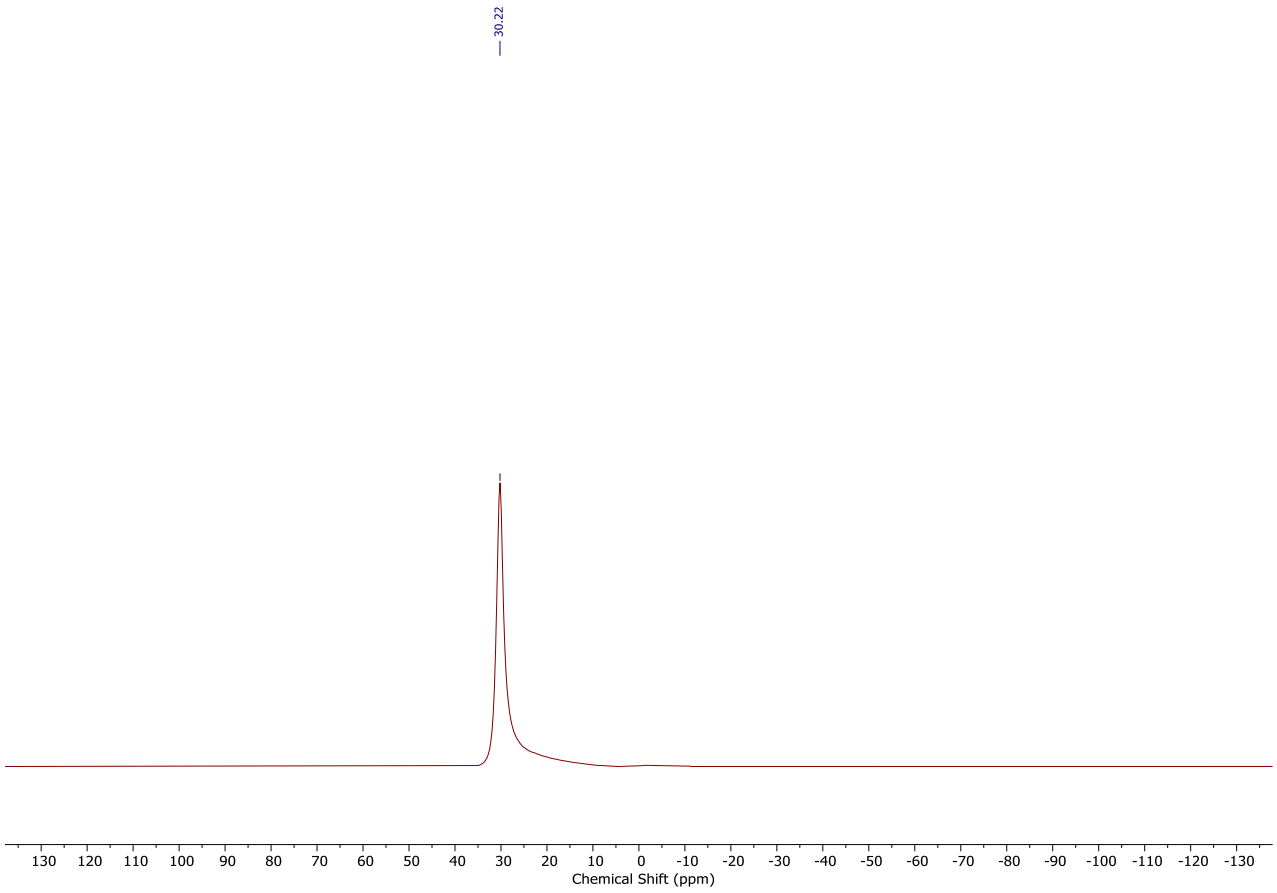

^{13}C NMR (126 MHz, $CDCl_3$) Spectrum of 6-(4,4,5,5-Tetramethyl-1,3,2-dioxaborole)-3-methylfluorobenzene and 5-(4,4,5,5-tetramethyl-1,3,2-dioxaborole)-3- methylfluorobenzene

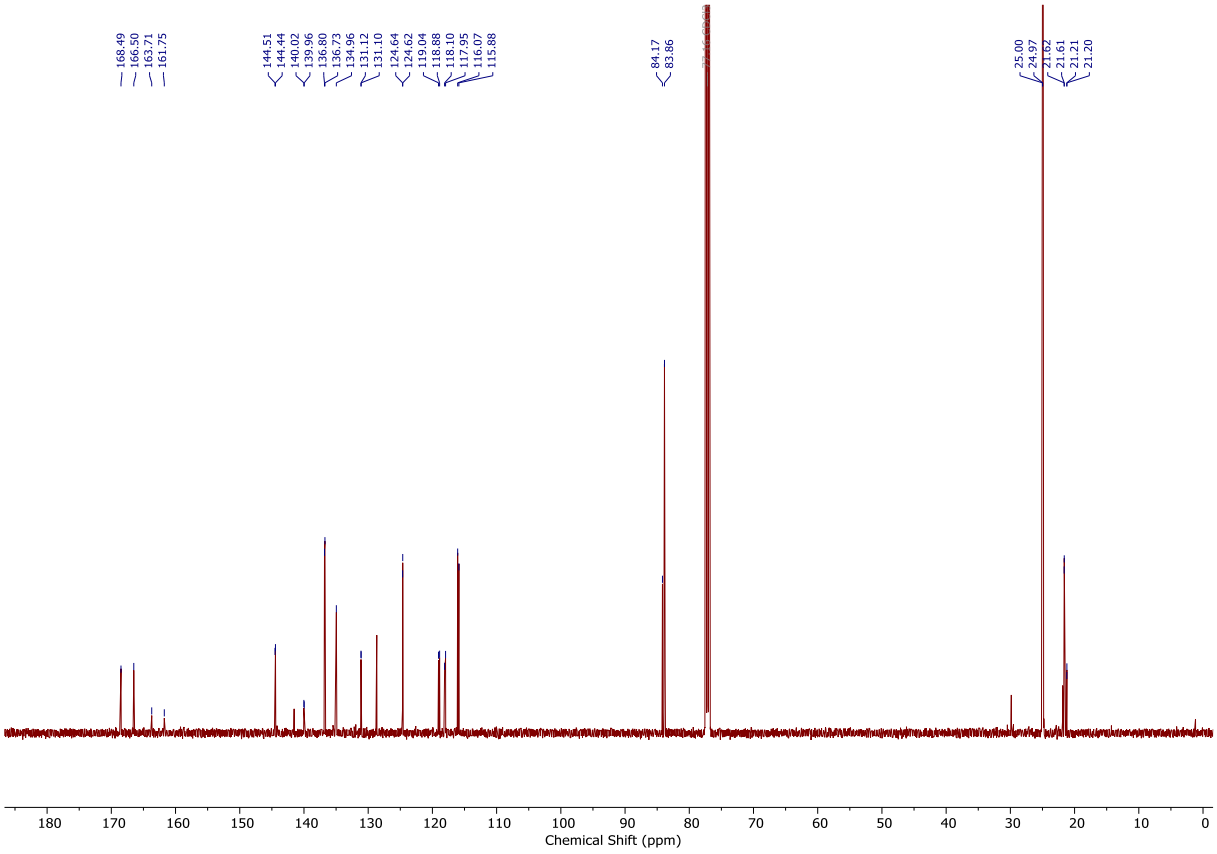

^{19}F NMR (470 MHz, $CDCl_3$) Spectrum of 6-(4,4,5,5-Tetramethyl-1,3,2-dioxaborole)-3-methylfluorobenzene and 5-(4,4,5,5-tetramethyl-1,3,2-dioxaborole)-3- methylfluorobenzene

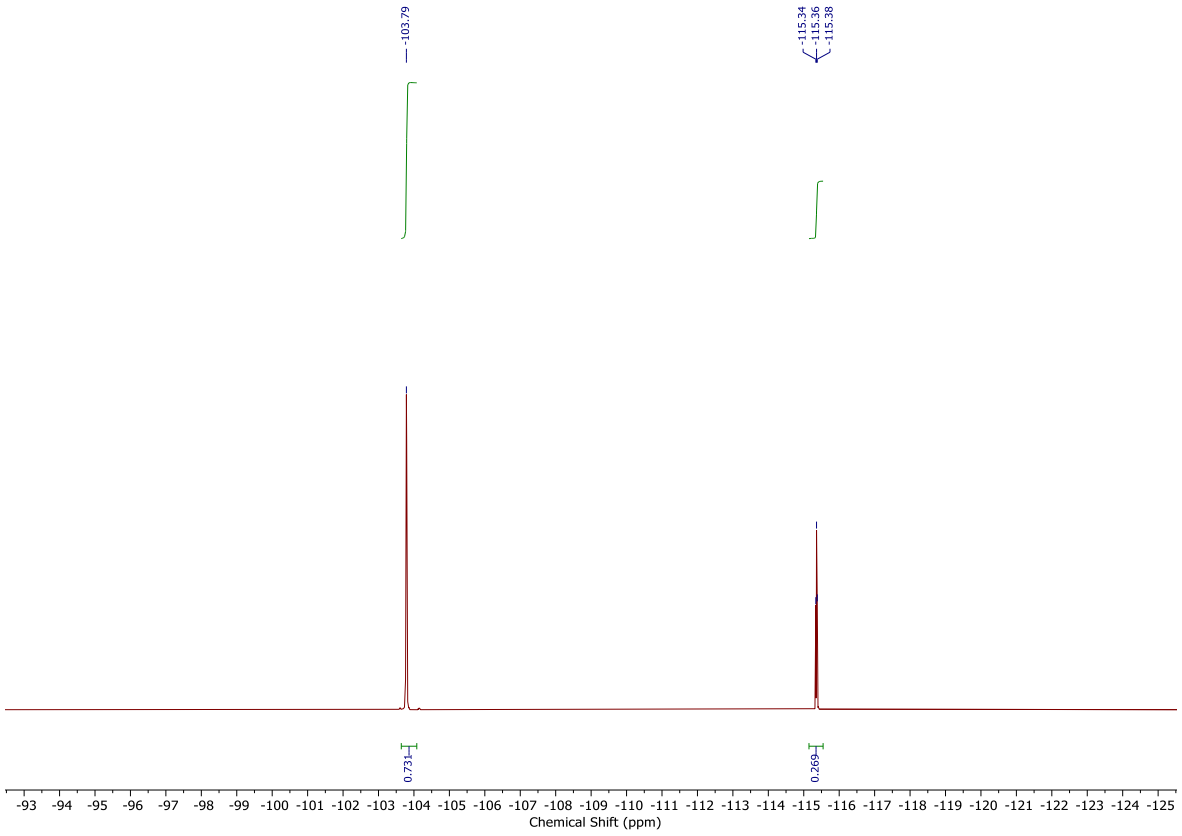

5.4.21. Synthesis and characterization of 2-(4,4,5,5-Tetramethyl-1,3,2-dioxaborole)-4-methylfluorobenzene

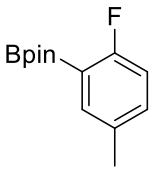

According to the general procedure, potassium *tert*-butoxide (23 mg, 0.24 mmol), bis(pinacolato)diboron (58 mg, 0.24 mmol), [dmpeMn(CO)$_3$Br] (7.4 mg, 0.02 mmol), and 4-methylfluorobenzene (22 mL, 0.2 mmol) in anhydrous MTBE (0.5 mL) were reacted. The crude product was purified by flash column chromatography (Teledyne ISCO CombiFlash NextGen 300+, 12 g, 40 mL min^{-1}, hexane/ethyl acetate 10:1) to give 2-(4,4,5,5-tetramethyl-1,3,2-dioxaborole)-4-methylfluorobenzene as a colourless oil (17 mg, 0.05 mmol, 27%). Product fractions contained inseparable amounts of borylated toluene products. ^{1}H NMR: (500 MHz, $CDCl_3$) 7.52 (dd, *J* = 5.6, 2.3 Hz, 1H), 7.23 – 7.19 (m, 1H), 6.91 (app. t, *J* = 8.8 Hz, 1H), 2.31 (d, J = 0.9 Hz, 3H), 1.36 (s, 12H). ^{11}B NMR: (160 MHz, $CDCl_3$) 30.2. ^{13}C NMR: (126 MHz, $CDCl_3$) 165.6 (d, *J* = 248.0 Hz), 137.1 (d, *J* = 7.9 Hz), 133.9 (d, *J* = 8.5 Hz), 132.1 (d, *J* = 31.5 Hz), 115.1 (d, *J* = 24.0 Hz), 84.0, 25.0, 20.6. ^{19}F NMR: (470 MHz, $CDCl_3$) −108.3 (dt, *J* = 9.9, 5.5 Hz).

^{1}H NMR (500 MHz, $CDCl_3$) Spectrum of 2-(4,4,5,5-tetramethyl-1,3,2-dioxaborole)-4-methylfluorobenzene

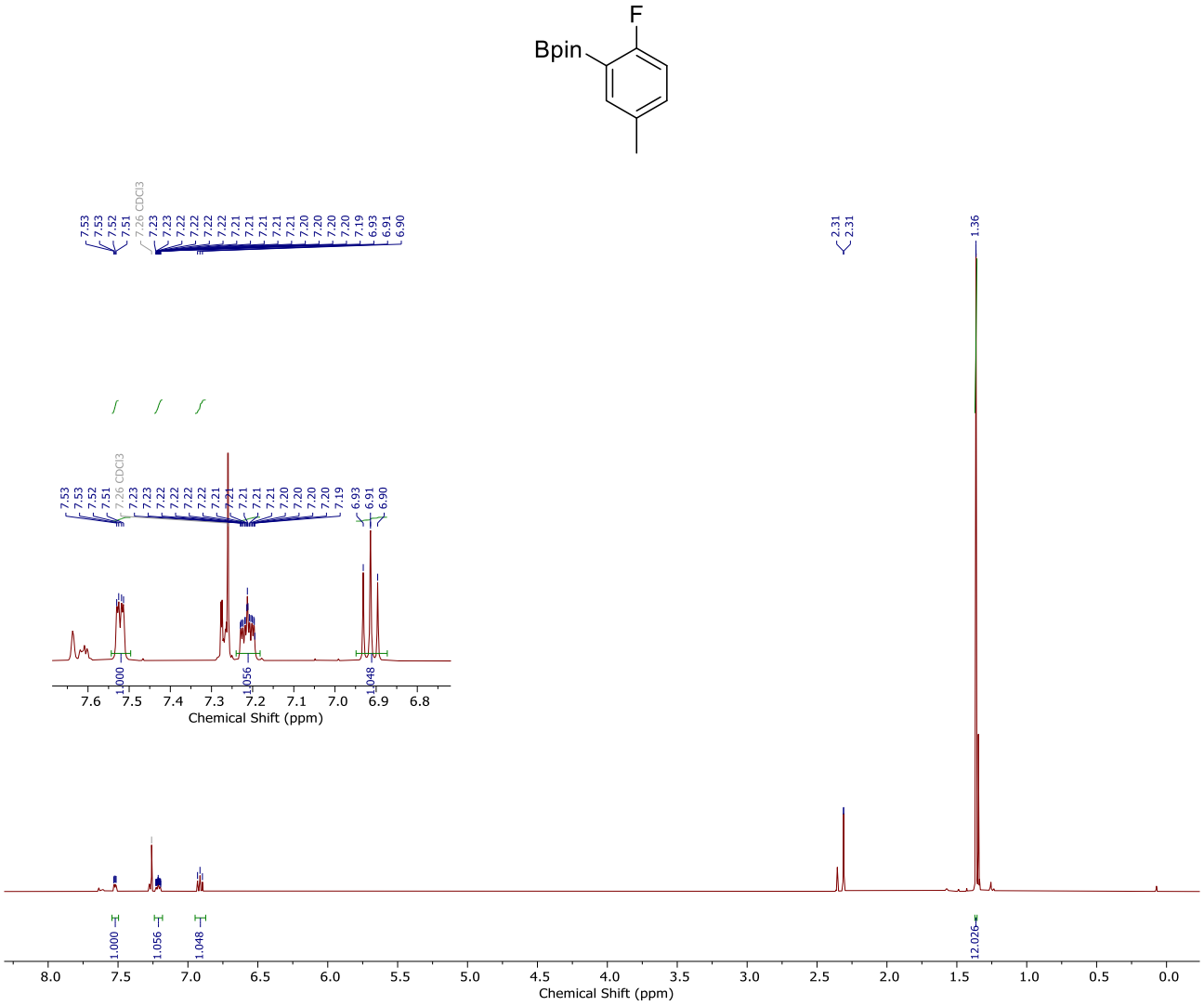

^{11}B NMR (160 MHz, $CDCl_3$) Spectrum of 2-(4,4,5,5-tetramethyl-1,3,2-dioxaborole)-4-methylfluorobenzene

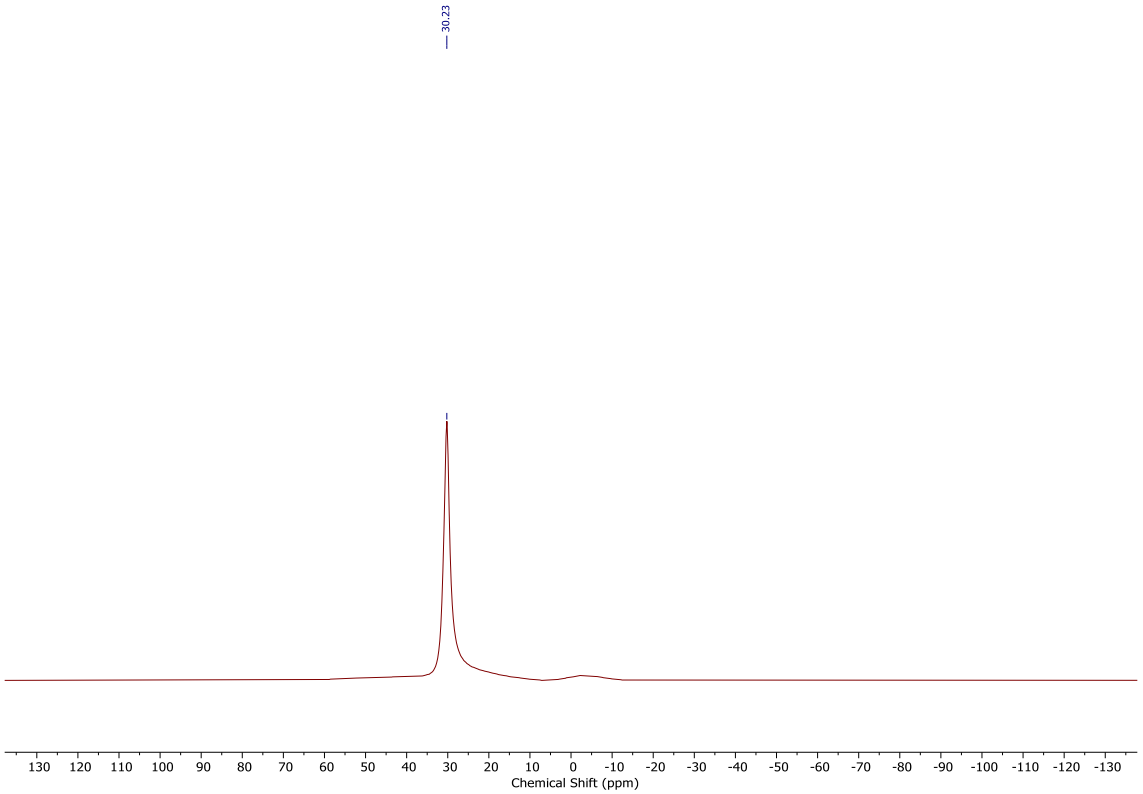

^{13}C NMR (126 MHz, $CDCl_3$) Spectrum of 2-(4,4,5,5-tetramethyl-1,3,2-dioxaborole)-4-methylfluorobenzene

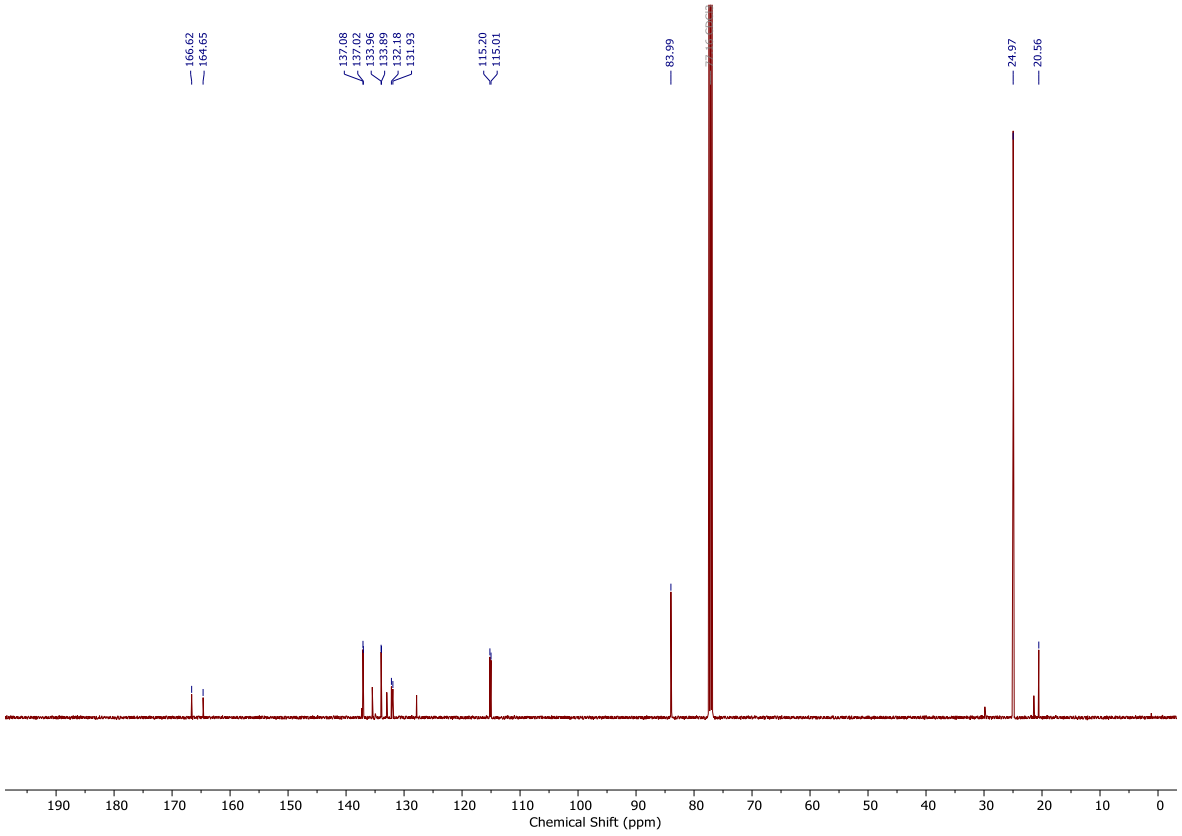

^{19}F NMR (470 MHz, $CDCl_3$) Spectrum of 2-(4,4,5,5-tetramethyl-1,3,2-dioxaborole)-4-methylfluorobenzene

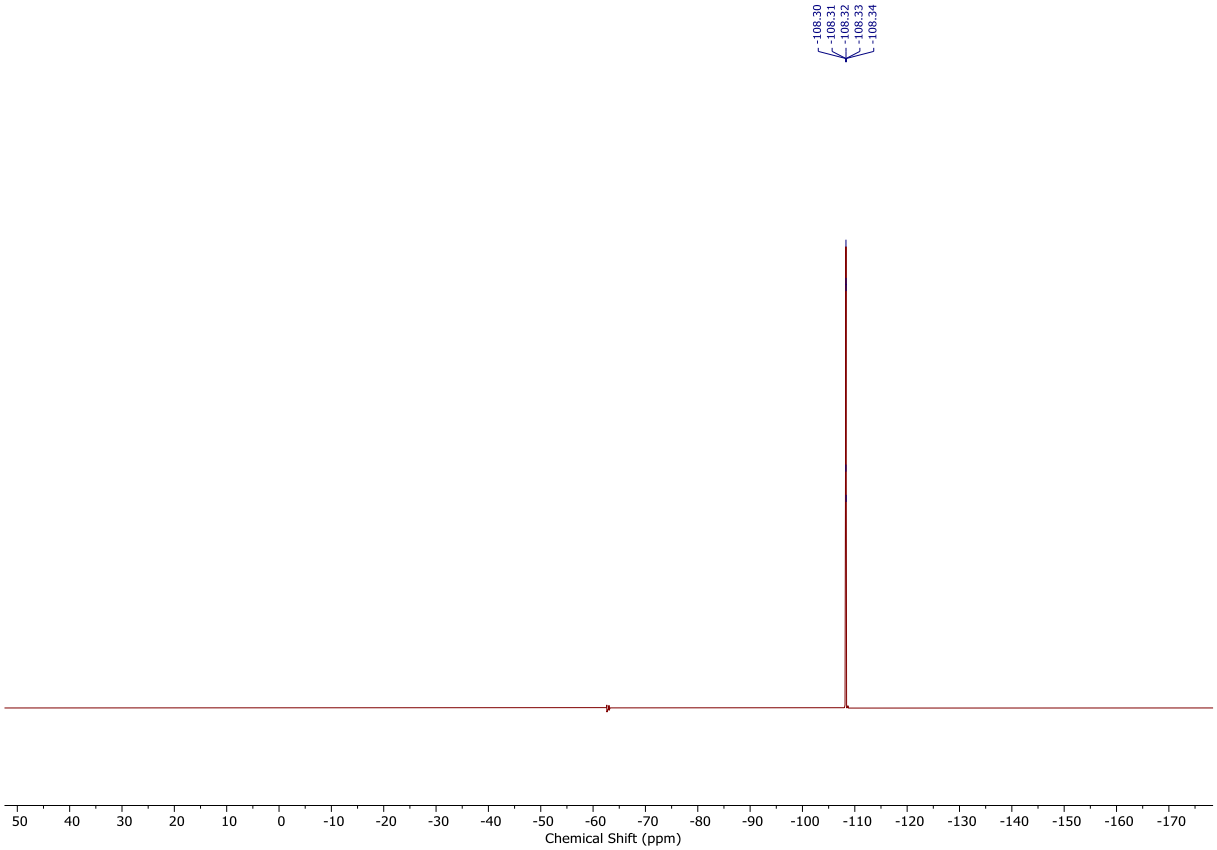

5.5. Bibliography

1. Sheldon, R. A., Arends, I. & Hanefeld, U. *Green Chemistry and Catalysis*. (Wiley VCH, 2007).
2. Tang, H. *et al.* Platinum-group metals: Demand, supply, applications and their recycling from spent automotive catalysts. *J. Environ. Chem. Eng.* **11**, 110237 (2023).
3. Wheelhouse, K. M. P., Webster, R. L. & Beutner, G. L. Advances and Applications in Catalysis with Earth-Abundant Metals. *Org. Process Res. Dev.* **27**, 1157–1159 (2023).
4. Kaplaneris, N. *et al.* Chemodivergent manganese-catalyzed C–H activation: modular synthesis of fluorogenic probes. *Nat. Commun.* **12**, 1–9 (2021).
5. Kuninobu, Y., Nishina, Y., Takeuchi, T. & Takai, K. Manganese-Catalyzed Insertion of Aldehydes into a C - H Bond. *Angew. Chemie - Int. Ed.* **46**, 6518–6520 (2007).
6. Rej, S., Amos, S. G. E. & Kleij, A. W. Photochemical C − H Borylation in Organic Synthesis. *ACS Catal.* **15**, 1753–1770 (2025).
7. Hartwig, J. F. Borylation and Silylation of C-H Bonds: A Platform for Diverse C-H Bond Functionalizations. *Acc. Chem. Res.* **45**, 864–873 (2012).
8. Di, V. *et al.* Mild Iridium-Catalyzed Borylation of Arenes . High Turnover Numbers , Room Temperature Reactions , and Isolation of a Potential Intermediate. *J. Am. Chem. Soc.* **124**, 390–391 (2002).
9. Borylation, C. C. H., Obligacion, J. V, Semproni, S. P. & Chirik, P. J. Cobalt-Catalyzed C − H Borylation. *J. Am. Chem. Soc.* **136**, 4133–4136 (2014).
10. Britton, L. *et al.* Iron-catalysed alkene and heteroarene H/D exchange by reversible protonation of iron-hydride intermediates. *Chem. Sci.* **13**, 10291–10298 (2022).
11. Su, X. *et al.* Nickel-catalyzed, silyl-directed, *ortho*-borylation of arenes via an unusual Ni(II)/Ni(IV) catalytic cycle. *Nat. Commun.* **15**, (2024).
12. Chen, H. & Hartwig, J. F. Catalytic, Regiospecific End-Functionalization of Alkanes: Rhenium-Catalyzed Borylation under Photochemical Conditions. *Angew. Chemie - Int. Ed.* **38**, 3391–3393 (1999).
13. Britton, L. *et al.* Manganese-Catalyzed C(sp2)-H Borylation of Furan and Thiophene Derivatives. *ACS Catal.* **11**, 6857–6864 (2021).
14. Dombray, T. *et al.* Iron-catalyzed C-H borylation of arenes. *J. Am. Chem. Soc.* **137**, 4062–4065 (2015).
15. Bonet, A., Pubill-Ulldemolins, C., Bo, C., Gulyás, H. & Fernández, E. Transition-metal-free diboration reaction by activation of diboron compounds with simple lewis bases. *Angew. Chemie - Int. Ed.* **50**, 7158–7161 (2011).

16. Docherty, J. H., Peng, J., Dominey, A. P. & Thomas, S. P. Activation and discovery of Earth-abundant metal catalysts using sodium *tert*-butoxide. *Nat. Chem.* **9**, 595–600 (2017).

17. Alder, C. M. *et al.* Updating and further expanding GSK's solvent sustainability guide. *Green Chem.* **18**, 3879–3890 (2016).

18. Britton, L., Docherty, J. H., Nichol, G. S., Dominey, A. P. & Thomas, S. P. Iron-Catalysed C(sp^2)-H Borylation with Expanded Functional Group Tolerance. *Chinese J. Chem.* **40**, 2875–2881 (2022).

19. Hartwig, J. F. Regioselectivity of the borylation of alkanes and arenes. *Chem. Soc. Rev.* **40**, 1992–2002 (2011).

20. Jayasundara, C. R. K. *et al.* Cobalt-Catalyzed C–H Borylation of Alkyl Arenes and Heteroarenes Including the First Selective Borylations of Secondary Benzylic C–H Bonds. *Organometallics* **37**, 1567–1574 (2018).

21. Qiu, D. *et al.* Synthesis of Pinacol Arylboronates from Aromatic Amines: A Metal-Free Transformation. *J. Org. Chem.* **78**, 1923–1933 (2013).

22. Mfuh, A. M. *et al.* Additive- and Metal-Free, Predictably 1,2- and 1,3-Regioselective, Photoinduced Dual C − H/C − X Borylation of Haloarenes. *J. Am. Che* **138**, 8408–8411 (2016).

23. Zhu, C. & Yamane, M. Transition-Metal-Free Borylation of Aryltriazene Mediated by BF3 . OEt2. *Org. Lett.* **14**, 4560–4563 (2012).

24. Kinuta, H., Tobisu, M. & Chatani, N. Rhodium-Catalyzed Borylation of Aryl 2 - Pyridyl Ethers through Cleavage of the Carbon − Oxygen Bond: Borylative Removal of the Directing Group. *J. Am. Chem. Soc.* **137**, 1593–1600 (2015).

25. Esteruelas, M. A., Olivan, M. & Vélez, A. POP − Rhodium-Promoted C − H and B − H Bond Activation and C − B Bond Formation. *Organometallics* **34**, 1911–1924 (2015).

26. Yin, Q., Klare, H. F. T. & Oestreich, M. Catalytic Friedel – Crafts C - H Borylation of Electron-Rich Arenes : Dramatic Rate Acceleration by Added Alkenes. *Angew. Chemie - Int. Ed.* **56**, 3712–3717 (2017).

27. Liu, W., Yang, X., Gao, Y. & Li, C.-J. Simple and E fficient Generation of Aryl Radicals from Aryl Tri fl ates : Synthesis of Aryl Boronates and Aryl Iodides at Room Temperature. *J. Am. Chem. Soc.* **139**, 8621–8627 (2017).

Chapter 6. Conclusions and perspectives

In conclusion, this doctoral research has been carried out within the strategic framework of the Rome Technopole Innovation Ecosystem, contributing to the broader mission of developing sustainable functional materials and translating them into environmentally responsible technological solutions. By operating at the intersection of materials chemistry, sensor development, and green process design, the work aligns with the objectives of Spoke 1, Flagship 1, which aims to bridge fundamental research and technological innovation that combine high performance with environmental responsibility.

Through the integration of the principles of Green Chemistry with the design of functional materials and sensing platforms, the thesis aims to demonstrate how sustainability can be effectively embedded into applied chemical research, from molecular synthesis to device fabrication and application.

Addressing this challenge requires a holistic approach that explicitly incorporates the green paradigm, including waste prevention, energy efficiency, catalysis, and the use of renewable or abundant materials, into material selection, synthetic methodology, device fabrication, operational lifetime, and end-of-life management.

A central aspect of this work has been the adoption of a sustainable-by-design approach to the development of functional organic and metallomacrocyclic materials for environmental sensing. This class of compounds are particularly attractive due to their extended π-conjugated macrocycle, chemical robustness, and tunable redox properties. Rather than focusing solely on analytical performance, the research emphasizes the importance of considering the environmental footprint of the entire process, including synthesis, processing, and device fabrication.

In this regard, the implementation of the Twelve Principles of Green Chemistry has guided the development of synthetic strategies aimed at minimizing waste production, improving atom economy, and reducing energy consumption. The use of one-pot

procedures and greener reaction media has demonstrated that complex functional materials, such as metallophthalocyanines, can be obtained through efficient and environmentally conscious synthetic routes, without compromising their structural integrity or functional properties.

Building upon this sustainable synthetic framework, the thesis explores the use of functional water-soluble phthalocyanines as active materials for the straightforward fabrication of electrochemical sensors for catechol detection. Through appropriate functionalization, the phthalocyanine derivatives investigated in this work exhibit good solubility in aqueous media, enabling their processing through environmentally friendly deposition techniques (**Figure 1**).

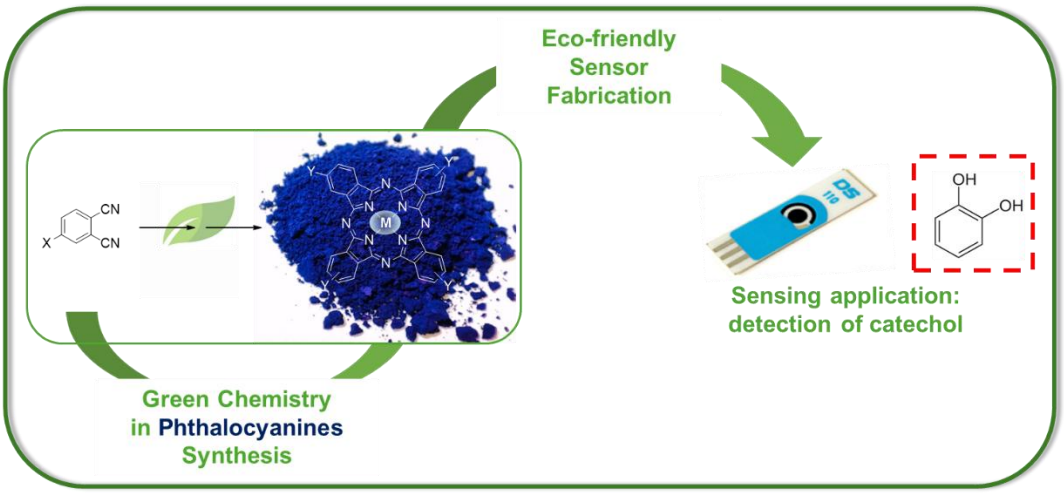

Figure 1. Schematic representation of the main study of this doctoral thesis.

The immobilization of a PEGylated copper phthalocyanine (4-PEGCuPc) onto screen-printed electrodes was achieved through a simple drop-casting procedure using fully aqueous solutions. Despite the simplicity of this approach, the resulting modified electrodes displayed efficient electrochemical detection of catechol. In particular, the new phthalocyanine-based sensor enabled catechol oxidation at a relatively low potential and

providing stable and reproducible responses over repeated washing cycles. Remarkably, reliable electrochemical signals were maintained even after one hundred washing steps, highlighting the strong adhesion and robustness of the deposited molecular layer.

The exploration of the electrochemical behavior of other PEGylated phthalocyanine derivatives suggests that catechol detection arises from a mediated electron-transfer process involving both the central metal ion and the extended π-conjugated macrocycle of the phthalocyanine. While the coordinated metal appears to enhance catalytic activity and facilitate electron transfer, the measurable activity observed for the metal-free derivative indicates that the macrocyclic ligand itself contributes significantly to the sensing mechanism, possibly through ligand-centered redox processes.

From a broader perspective, the results obtained in this thesis demonstrate that high-performance electrochemical sensors can be fabricated through extremely simple, accessible, and sustainable procedures. Unlike some previously reported phthalocyanine-based sensing platforms, the sensors developed in this work operate efficiently using only the phthalocyanine complexes deposited from aqueous solution. The possibility of achieving reliable catechol detection through such a straightforward fabrication strategy without any pretreatment of the electrode surface represents an important step toward the development of environmentally responsible sensing technologies that can be easily reproduced without specialized instrumentation.

Beyond the specific case study of phthalocyanine-based sensors, the work presented in this thesis emphasizes the importance of integrating sustainability metrics into the evaluation of new materials and devices. Analytical performance alone is no longer sufficient as the sole criterion for technological advancement. Instead, parameters such as fabrication simplicity, reusability, and environmental impact must also be considered.

By adopting this broader perspective, the thesis contributes to redefining how functional materials and sensing technologies should be designed and assessed in the context of sustainable innovation.

The thesis also included work carried out during the time at the University of Edinburgh, focused on the development of a sustainable optical sensor for metal detection. In particular, the study addressed the design and evaluation of a sensing system capable of detecting metal ions both in solution and on a solid support in the form of paper-based test strips. Special attention was devoted to the sustainability of the entire process, from the synthesis of the molecular sensing material to the fabrication of the final device. In this context, the use of paper as a substrate represents an attractive platform due to its low cost, ease of fabrication, and reduced environmental impact, enabling the development of simple and accessible sensing tools for the detection of copper.

Finally, during the research period abroad, the sustainability-oriented approach of this thesis was further extended to the field of catalysis. In particular, the investigation of catalytic systems based on Earth-abundant elements addressed one of the key challenges of modern chemical research: reducing the reliance on scarce and expensive Platinum Group Metals. This aspect of the work further reinforces the central role of catalysis within Green Chemistry and highlights how the development of sustainable catalytic methodologies can complement advances in materials science and sensing technologies. Furthermore, it gave me the invaluable opportunity to advance my research on sustainable catalysis, further fueling my ambition to continue working in this field.

Future research could focus on the long-term stability and reusability of the sensing devices. Although the drop-cast phthalocyanine layers demonstrated remarkable robustness under repeated washing cycles, systematic investigations on operational lifetime, regeneration protocols, and performance under real environmental conditions, as well as on a deeper understanding of the sensing mechanism and the factors governing device operation, would further validate their practical applicability for continuous monitoring applications.

From a sustainability perspective, particular attention should also be devoted to the end-of-life management of the sensors. Future work could explore strategies for the recovery and recycling of the sensing platforms after use, including the regeneration of the electrode

surface after use. The development of simple procedures for sensor refurbishment or material recycling would significantly enhance the overall sustainability of the devices and contribute to the implementation of circular approaches in sensor technology.

In addition, the integration of the developed sensing materials into alternative platforms, such as flexible substrates, or paper-based analytical systems, could open new opportunities for low-cost and portable environmental monitoring. In this context, combining electrochemical sensing with optical or colorimetric detection strategies may enable the development of multifunctional sensing systems capable of providing complementary analytical information.

Finally, the sustainable synthetic strategies explored in this thesis could be extended to the preparation of other functional macrocycles and highly promising derivatives. Expanding this approach may contribute to the development of new environmentally responsible materials for applications not only in sensing but also in catalysis, energy conversion, and environmental remediation.

Acknowledgements

I started my PhD journey a bit differently from many students, after already spending time as a research fellow at the CNR. I was more motivated than ever to earn this title and pursue a career as a scientific researcher, so I gave it my all and always did my best, because I was fully aware of the opportunity I had in my hands. Now that I've finally reached this milestone, I feel incredibly grateful to all the people who supported me and helped me get here with enthusiasm and energy.

First, I would like to thank my supervisors, Dr. Gloria Zanotti and Dr. Mattea Castrovilli, for their guidance and expertise over these three years, I've learned so much from you. A special thank you also goes to Prof. Antonella Cartoni, who never stopped believing in me during the most difficult moments and always encouraged me to move forward. I know I've been a very dynamic and sometimes demanding PhD student, always eager to explore new ideas, take on new challenges, and share the results of my work around the world. Thank you for never holding me back whenever I said: "I saw this really interesting conference, it has some great speakers… actually, I already prepared the abstract, can I show it to you? Pleaase?" Curiosity, enthusiasm and the desire to understand the mechanisms behind what surrounds us have always been my driving force. I was incredibly proud that my thesis work formed the foundation of the Mainstream project, that was selected for funding under the European Water4All 2024 call, and I'm confident it will lead to further success under the guidance of Dr. Noemi Colozza, with whom I had the pleasure of working.

A very special thank you goes to Prof. Stephen Thomas, Steve, whom I had the honour to work with for eight months during my time abroad at the University of Edinburgh. You were much more than a supervisor, you were a true mentor. You always trusted me, supported me through difficult moments (the imine synthesis was tough!), and your "Go for it!" every time I proposed a new experiment during group meetings became my life mantra. The opportunity to attend the Cambridge conference to present the results we

achieved was incredibly inspiring, and I will always be grateful for it. You are a source of inspiration, and I truly hope we will have the chance to work together again in the future.

Beyond work, I've been incredibly lucky to receive support from many people who are part of my personal life (and some also of my professional one).

First, Venanzio, my "partner in lab" and in real life, who supported me with patience and calm in every moment. We shared both the struggles and the joys of organic chemistry, low yields in early experiments, sleepless nights reading newly published papers and writing our own. You were truly indispensable: from changing test tubes during column chromatography to helping troubleshoot experiments and even dealing with a washing machine or dishwasher at home, you were always by my side, beyond what anyone could expect. You've been an incredible guide and, as I always tell you because it is true, you are a brilliant organic chemist.

Then my family, my parents, my sister, and my amazing grandparents, who always found the time to listen to all my stories about experiments, conferences, and travels. Even when you didn't understand anything about nucleophilic attacks, reaction intermediates, or purification techniques ("Columns? You mean like temple columns?"), you always showed me unconditional love and support, even across long distances. I will always remember with affection my grandfather following my conference travels on his atlas from home. I would also like to thank my uncles, aunts, and cousins, both younger and older, including Martina, Marianna, Alessia, Leonardo, Chiara, Michele, who have always supported me and been close to me throughout this journey.

It's also time to thank my scientist friends Denise, Giuliana, Veronica, and Giorgio, with whom I shared both research challenges and many beers, maybe one day we'll work together at the interface between chemistry and biology! Thanks also to my longtime friends, Elena and Lorenzo, and their partners, who have always been part of the important moments of my life, including this one.

A big thank you also goes to the entire Thomas group, who welcomed me like a family and made me feel at home in the wonderful setting of Scotland. It was a pleasure working with all of you and sharing so many moments together. I will never forget our trips to St. Andrews and Glasgow to attend seminars by MacMillan and Hartwig, or the "Italian gelato" you made me try in St. Andrews, not exactly the same, but still good! Not to mention the surprise party you organized for my 30th birthday and the pasta at Ciao Roma… next time you want to have "carbonara pasta" you're all my guests in Rome!

A heartfelt thank you also to the amazing administrative staff in Montelibretti, whose smiles brightened many long and tough days, always ready to offer coffee and snacks. The pocket coffees that Lory used to leave on my desk were always such a sweet surprise. Thanks also to Paolo, with whom I shared many long walks when I needed to clear my mind.

I am truly grateful to have experienced unforgettable moments during my PhD: holding Prof. MacMillan's 2021 Nobel Prize medal and chatting with him about my Master's thesis, which was entirely based on his research; traveling to Cambridge and enjoying the over five-hour train journey back along the stunning east coast of the UK; attending countless conferences and meeting inspiring scientists such as Prof. Aggarwal, Prof. Arnold (Nobel Prize in Chemistry 2018), and Prof. Catellani; collaborating with researchers from different institutions, and working on exciting chemical challenges such as MOFs investigation, CO_2 reduction, and complex synthetic problems, as well as participating in outreach activities and research events. I also had the opportunity to present my research in extraordinary places, including giving a talk at the Hall of Globes in the Egyptian Museum of Turin and presenting a poster at a conference at Niagara Falls, something a PhD student doesn't easily forget.

I close this chapter with deep gratitude, and now that I'm finishing this project, I'm already excited to dive into the next one life has in store for me, and as the Scots say in Gaelic: "Slàinte!".